Loughborough University

BEHAVIOUR OF R.C. BEAMS UPGRADED WITH EXTERNALLY BONDED STEEL OR FRP PLATES

by

Mahmoud Abdel Hamed Hassanen, BSc., MSc.

A Doctoral Thesis
Submitted in partial fulfilment of the requirements for the award of the
Degree of Doctor of Philosophy of the
Loughborough University

June 2000

ABSTRACT

The structural behaviour of simply supported reinforced concrete (R.C.) beams strengthened in flexure by externally bonded steel or fibre reinforced plastic (FRP) plates has been investigated. A novel theoretical model coupled with simple (hence, practical) procedure(s) for designing such beams against premature plate peeling failure has been developed. The theoretical model and the design procedures have been validated by an extensive number (169) of mainly large-scale test data (using steel or FRP plates) from other sources. The effects of variations in the magnitude of Young's modulus for FRP plates on the potential changes in the flexural ultimate load of R.C. beams with externally bonded FRP plates, in the absence and/or presence of plate peeling, have been investigated in some detail with the theoretical predictions of various failure loads and associated modes of failure supported by an extensive number of test results from other sources. Moreover, brief theoretical parametric studies for other first order composite beam design parameters have also been carried out in order to clarify the effects of variations in such parameters on the predicted modes of failure.

It has been shown (both, theoretically and by using large scale experimental data) that the load bearing capacity for a plated beam could (under certain circumstances) be significantly lower than even that for the corresponding unplated beam with the mode of failure being of an undesirable brittle nature. Such brittle failures can obviously have serious implications in practice, where this method has been used extensively for upgrading both bridges and buildings in a number of countries, with the design calculations very often not having properly accounted for the possible occurrence of premature plate peeling phenomenon, especially when FRP plates have been used. Further work in this area included a quantitative theoretical insight into the effect of pre-cracking of the beams (under service conditions) on the ultimate plate peeling load.

A critical quantitative examination of a number of previously available theoretical models, as proposed by others, has also been carried out, and some of these models for predicting the plate peeling failure of R.C. beams have been shown to suffer from rather serious shortcomings.

ACKNOWLEDGEMENTS

The author would like to express his gratitude and appreciation to his supervisor Professor M. Raoof for his sincere guidance, invaluable advice, and stimulating supervision during the course of development of this thesis and the entire period of the research programme.

The author wishes to extend his gratitude to his family and his wife for their understanding, continuous encouragement, and support throughout the different stages of this work.

TABLE OF CONTENTS

LIST OF FIGURES

LIST OF TABLES

NOTATION

a	Distance from where the plate is terminated and the support; Depth of equivalent concrete stress block
A_e	The concrete stretched area
A_p	Plate cross-section area
A_s	Cross-section area of tensile bars
A_s'	Cross-section area of compression bars
b, b_c	Width of the beam
b_1, b_b, b_p	Width of the externally bonded plate
b_a	Average width of the adhesive layer
B	Width of the externally bonded plate
$C_{R1} C_{R2}$	Normal stress indicator
d	Distance between the C.G. of the embedded tension bars and the top of the section
d'	Distance between the compression bars and the top of the section
d_a	Average thickness of the adhesive layer
d_d	Total depth of the beam cross-section
d_p	Plate thickness
D	Distance between the bonded plate and the top of the section
E_a	Young's modulus of the adhesive material
$E_{(a)}$	Minimum value of modulus of elasticity for the FRP plate for the $-R-$ mode of failure
$E_{(A)}$	Minimum value of modulus of elasticity for the FRP plate for the $-RP$ mode of failure
$E_{(b)}$	Minimum value of modulus of elasticity for the FRP plate for the $---$ mode of failure, associated with the plate peeling behaviour

$E_{(B)}$	Minimum value of modulus of elasticity for the FRP plate for the $--P$ mode of failure (under-reinforced plated section)
E_c	Modulus of elasticity for concrete
$E_{(C)}$	Minimum value of modulus of elasticity for the FRP plate for the $C--$ mode of failure
$E_{(d)}$	Minimum value of modulus of elasticity for the FRP plate for the $---$ mode of failure, associated with the full bond behaviour
$E_{(D)}$	Minimum value of modulus of elasticity for the FRP plate for the $--P$ mode of failure (over-reinforced plated section)
$(EI)_b$	Flexural rigidity of the beam
$(EI)_{cp}$	Flexural rigidity of the cracked plated beam
$(EI)_s$	Flexural rigidity of the steel plate
E_p, E_{Po}, E_{p1}, E_{p2}	Modulus of elasticity for the FRP plate
E_s	Young's modulus for the steel plate
f_a	Maximum axial peeling stress
f_c	Concrete compressive stress, maximum curvature peeling stress
f_{cu}	Concrete cube strength
f_{cz}	Concrete compression stress at a distance z from the neutral axis
f_p	Plate axial stress, steel yield stress, FRP ultimate strength
f_{pu}	FRP plate ultimate strength
f_{py}	Yield strength for the steel plate
f_s	Axial stress or yield strength for the tensile bars
f'_s	Axial stress in the compression bars
f_t	Tensile strength of concrete

f_t'	Tensile splitting strength of concrete
f_{sy}, f_y	Yield strength of main (embedded) tensile reinforcement
F_a	Force normal to the plate
F_c	Total compression force
F_{cc1}, F_{cc2}	Concrete compression force corresponding to the parabolic and uniform stress distributions, respectively
F_{co}, F_{c1}, F_{c2}, F_{c3}, F_{c4}, F_{cc}	Total concrete compression force
F_{ct}, F_{ct1}, F_{ct2}	Tension force in concrete
F_o	Shear force acting on the section of the beam located at the end of the plate
F_p, F_{po}	Plate axial tensile force
F_s, F_{so}	Axial force in the tensile bars
F_s'	Axial force in the compression bars
F_t, F_T	Total tensile force
G_a	Shear modulus of the adhesive material
h	Depth of Neutral axis, distance from the neutral axis of the beam to the plate
h_1	Half the total depth of assumed (effective) region of concrete in tension
h'	Net depth of concrete cover
h_p	Distance between the C.G. of the externally bonded plate and the top fiber of the concrete section
h_s	Distance between the C.G. of the embedded tension bars and the top of the section
I	Second moment of area of the concrete section.
I_A	Second moment of area of the concrete tooth between two adjacent stabilised cracks

I_p	Second moment of area of the steel (or FRP) transformed section.
k	Adjusting factor for the shear links' strength
K_n	Normal stiffness of the adhesive material
K_s	Shear stiffness of the adhesive material
K_{SF}	Ratio of actual/nominal shear reinforcement strength
K_T	$=(A_s f_y + A_p f_{pu})$
l_{max}	Maximum stabilised crack spacings in an unplated R.C. beam
l_{min}	Minimum stabilised crack spacings in an unplated R.C. beam
l^p_{max}	Maximum stabilised crack spacings in the beam with externally bonded plates
l^p_{min}	Minimum stabilised crack spacings in the beam with externally bonded plate
L	Depth of the tooth which acts as a cantilever (equal to stabilised crack spacing), total span of the simply supported beam
L_c	Distance from the support to the nearest end of the plate
L_o	Distance between the external load nearest to the support and the support
L_p	Effective length of the externally bonded plate within the shear span
L^1_p	Length of the externally bonded plate within the shear span between where it terminates and the point of application of the point load nearest to the support
L_{p-1}	Length of the externally bonded plate within the shear span between where it terminates and the point of application of the point load nearest to the support
L_{p-2}	Estimated effective length of the externally bonded plate within the shear span
M	Bending moment
M_c	Moment resulting from the concrete compressive stresses, total compression moment

M_{cc1}, M_{cc2}	Concrete compression moment corresponding to the parabolic and uniform stress distributions, respectively
M_{exp}	Experimental moment
M_{lower}	Lower bound theoretical ultimate plate peeling moment
M_{min}	Flexural ultimate moment of an unplated R.C. beam with partial material safety factors set equal to unity
M_o	Bending moment acting on the section of the beam located at the end of the plate
M_p	Moment at the end of the plate causing peeling
M_{peel}	Ultimate plate peeling moment, lower bound theoretical plate peeling moment
$M_{peel-1,l}$	Theoretical lower bound value of plate peeling moment for an uncracked plated beam
$M_{peel-1,u}$	Theoretical upper bound value of plate peeling moment for an uncracked plated beam
$M_{peel-2,l}$	Theoretical lower bound value of plate peeling moment for a cracked plated beam
$M_{peel-2,u}$	Theoretical upper bound value of plate peeling moment for a cracked plated beam
M_{peel-i}	Accurate (predicted) lower bound plate peeling moment resulting from the iterative calculations
M_{peel-p}	Simplified lower bound plate peeling moment considering parabolic concrete strain-stress relationship
M_{peel-R}	Simplified lower bound plate peeling moment considering uniform concrete stress distribution
$M_{peel,l}$	Theoretical lower bound value of plate peeling moment
$M_{peel,u}$	Theoretical upper bound value of plate peeling moment
M_{pltd}	Ultimate moment capacity of a plated section according to BS8110
M_{pult}, M_{max}	Ultimate moment capacity of a plated section according to BS8110 with material partial safety factors set equal to unity

M_{RC}	Flexural ultimate moment of unplated R.C. beams with material partial safety factors included
M_{sp}	Predicted value of serviceability peeling moment
M_{up}	Predicted value of ultimate peeling moment
M_{upper}	Upper bound theoretical ultimate plate peeling moment
P	Beam load (at support)
P_a	Axial force in the plate
P_{expt}	Failure load
P_{flex}	Flexural capacity of a plated beam
s_1, s_2	Distance below the neutral axis
s_a	Ratio of the mean-to-maximum tensile peeling stress
s_c	Ratio of the mean-to-maximum tensile peeling stress
t, t_1, t_p	Plate thickness
u	Steel/concrete average bond strength
u_1	FRP/concrete average bond strength
u_{rp}	Moment ratio = M_{peel}/M_{pult}
V_c	Shear strength of the plain concrete section
V_{exp}	Experimental failure load (for plated beams)
V_p	Shear force at the end of the plate causing peeling
V_s	Shear strength of the beam due to shear links
V_u	Ultimate shear strength of unplated reinforced concrete beams
V_{uc}	Theoretical shear strength of an unplated concrete beam in the total absence of shear reinforcement
X	Depth ratio = y/d
X_{creep}	Increase in curvature due to creep after plating
X_p	Sum of curvatures at the end of the plate.

X_{pure}	Curvature which causes debonding
X_{short}	Curvature induced by the short-term loads after plating
X_{shrink}	Increases in curvature due to shrinkage after plating
y, y_a, y_A, y_{b1}, y_{b2}, y_B, y_{B1}, y_{B2}, y_C, y_d, y_D	Depth of neutral axis
y_0, y_3, y_4	Depth of neutral axis
y_{cp}	Approximate depth of neutral axis
z	Distance above the neutral axis
α	$=\sqrt{K_s/(E_p b_p d_p)}$
$\alpha_{f_{cu}}$	Fraction of the depth of the neutral axis $=\left[1+\frac{\beta}{\varepsilon_o}\left(\frac{E_c\beta}{6\times 0.67 f_{cu}}-\frac{2}{3}\right)\right]$
α_{pc}	Modular ratio $= E_p/E_c$
α_{sc}	Modular ratio $= E_s/E_c$
β	Concrete strain at the onset of peak stress
ε_1	Concrete strain at the onset of peak stress
ε_a	Plate axial strain
ε_c	Concrete strain, concrete strain at the top of the section
ε_{cz}	Concrete strain at a distance z from the neutral axis
ε_{ct}	Concrete tensile strain
ε_m	Concrete crushing strain
ε_o	Maximum concrete strain
ε_p, ε_{po}, ε_{p1}, ε_{p2}	Plate axial strain

ε_{pel}, ε_{pp}	Plate axial strain at premature plate peeling failure
ε_{py}	Yield strain (steel plate)
ε_{pu}	Ultimate strain (FRP plate)
ε_s, ε_{so}, ε_{s1}	Axial strain in the tensile bars
ε_s'	Axial strain in the compression bars
ε_{sy}	Yield strain in the tensile bars
ε_t	Concrete tensile strain associated with the tensile splitting strength
ε_{ue}	Plate axial strain at premature plate peeling failure
ε_z	Concrete strain at a distance z from the neutral axis
ϕ	Diameter of embedded reinforcing bars, curvature of the beam
γ_m	Material partial safety factor
γ_c	Material partial safety factor for concrete
γ_p	Material partial safety factor for FRP
γ_s	Material partial safety factor for steel
η_1	Strain ratio $= \dfrac{\beta}{\varepsilon_o}$
η_2	Strain ratio $= \left(1 - \dfrac{\beta}{\varepsilon_o}\right)$
η_b, η_e	Constants
ρ_p	Plate/beam cross-section area ratio $= A_p/bd$
ρ_s	Tension-bars/beam cross-section area ratio $= A_s/bd$
ρ_s'	Compression-bars/beam cross-section area ratio $= A_s'/bd$
σ_A	Maximum tensile stress at the extreme fibre of concrete tooth bending as a cantilever

σ_o	Approximate values of normal stresses within the adhesive layer located at the end of the plate
σ_s	Plate longitudinal tensile stress
$\sigma_{s(min)}$, $\sigma_{s(max)}$	Lower and upper bounds to the magnitude of plate longitudinal tensile stresses at the instance of peeling failure, respectively
$\sigma_{s-1(min)}$, $\sigma_{s-1(max)}$	Lower and upper bounds to the magnitude of plate longitudinal tensile stresses at the instance of peeling failure for uncracked beams, respectively
$\sigma_{s-2(min)}$, $\sigma_{s-2(max)}$	Lower and upper bounds to the magnitude of plate longitudinal tensile stresses at the instance of peeling failure for cracked beams, respectively
σ_u	Ultimate tensile stress for the FRP plate
σ_y	Yield strength of the reinforcing bars in tension
$\sum O_{bars}$	Total circumference of the main (embedded) tensile reinforcing bars
τ	Shear stress between the plate and concrete
τ_{min} , τ_{max}	Minimum and maximum values of shear stresses at the interface between concrete and the externally bonded plate, respectively
τ_o	Approximate magnitude of shear stresses within the adhesive layer located at the end of the plate

Chapter 1

PRELIMINARY REMARKS

Chapter 1

PRELIMINARY REMARKS

1.1 INTRODUCTION

A significant proportion of current expenditure in the United Kingdom, relating to repair and maintenance of existing structures, is directed towards maintenance and upgrading of its concrete infrastructure. Many of the bridges and other civil engineering structures are deteriorating world-wide, due to problems associated with corrosion of steel in reinforced concrete, and a large proportion of bridges are unsuitable for carrying current or projected traffic needs. In certain other countries (such as Egypt), such problems are much more acute, largely due to the lack of regular maintenance. Indeed, in such countries, it has only been in recent years that the urgent need for maintenance and upgrading of the infrastructure has been fully recognised.

The effects of environment (harsh climate, de-icing salts, seismic activity, etc.), the increase in both traffic volume and truck weights, and changes in the design codes which necessitate a re-evaluation of older structures, are factors which contribute to the infrastructure becoming either structurally deficient or functionally obsolete. Upgrading usually involves strengthening of existing members to carry higher ultimate loads and/or satisfy more stringent serviceability requirements. Provided, rapid, effective, and simple upgrading methods are available, strengthening of existing structures becomes both environmentally and also economically preferable to demolition and rebuilding.

With the development of strong epoxy adhesives back in the 1960's, bonding external steel or fibre reinforced plastic (FRP) plates to the tension side of reinforced concrete beams, Figure 1.1, has proved very attractive for increasing the flexural strength of beams and/or slabs: such externally bonded plates supplement the area of internal tension reinforcement and are, indeed, more effective (in terms of bending resistance) than the reinforcing bars, because the plates are located at a maximum possible distance from the centroid of the concrete compressive stress block.

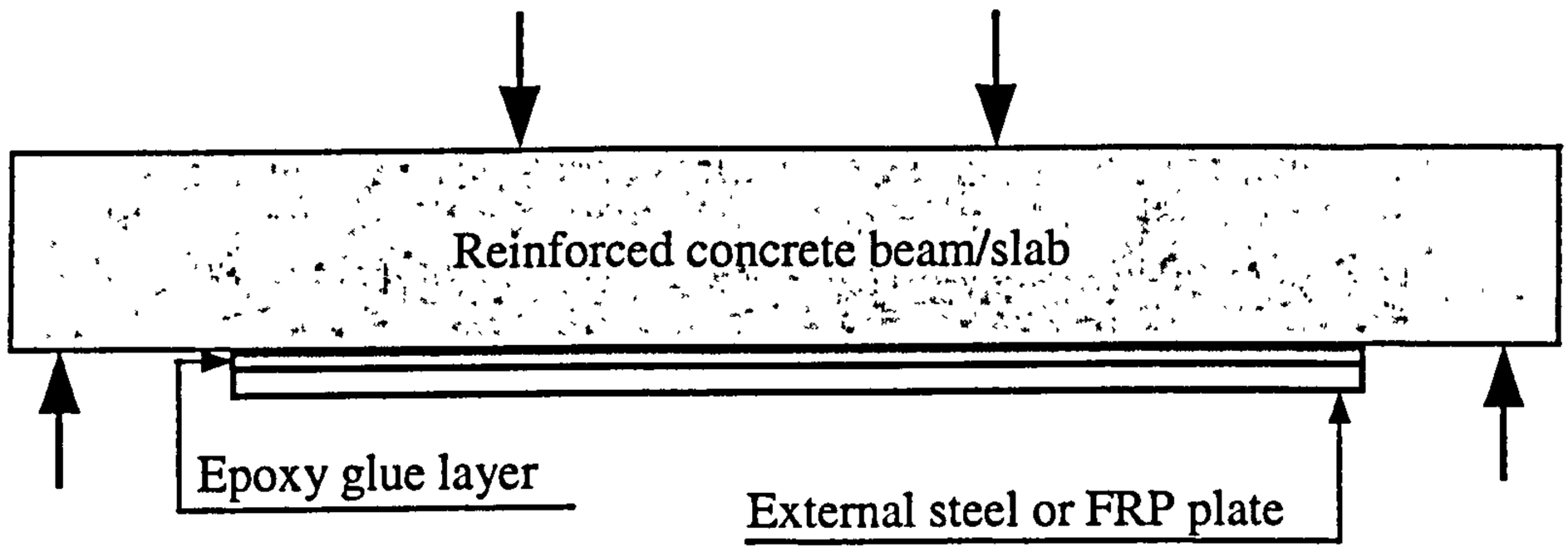

Fig. 1.1 Reinforced concrete beam strengthened with externally bonded steel/FRP plate.

The external plate bonding technique offers certain advantages when compared with other strengthening techniques and has, indeed, been extensively used in practice for both buildings and bridges, in a large number of countries (Oehlers (1992)). The work can be carried out relatively simply and quickly, even while the structure is still in use, and its application causes minimal changes in the member dimensions (including overhead clearance) and negligible increases in the self-weight. It also does not alter the configuration of the structure. Plates bonded to the tension side of reinforced concrete beams can be used to improve performance under service loads, by, for example, reducing cracking or deflections, and increase ultimate load in flexure. The plated member can carry the live load or live and dead load if propping is used.

As far as using externally bonded steel plate is concerned, it does, however, have some disadvantages when compared with using FRP plates as, for example, pointed out by Meier and his associates at Swiss Federal Laboratories for Materials Testing and Research (EMPA). These include difficulty in transportation and handling the heavy steel plates at the installation site, the possibility of corrosion at the steel/adhesive joint interface, the problem of forming clean butt joints between the relatively short lengths of commercially available plates, and expensive false work to hold the plates in position during adhesive curing. These difficulties have, in recent years, led to research into the potential use of the very light weight FRP plates as external reinforcement to replace the use of mild steel plates in practice. Such FRP materials have previously been used in, for example, aircraft and space industry: plates fabricated from these materials are characterised by their high strength to weight ratio, outstanding corrosion resistance, and, unlike steel plates which are available with limited lengths, they may be delivered on site in rolls of up to, say, 300 m in length. Furthermore, the FRP plates are formable and can be bonded to curved and irregular surfaces. However, FRP plates are currently about 10 times more expensive than the steel used up to date which may pose some doubts on economical grounds, for their use in civil engineering applications. In addition, their use poses the increased possibility of brittle failure modes. However, as pointed out by Meier and Kaiser (1991), for example, in a typical strengthening application, steel material cost may only be about, say, 20% of the total cost, versus 80% for the labour cost, with the relative ease of handling the FRP plates reducing the labour costs drastically, hence, making their use in structural applications, perhaps, an economically viable option. One thing is for sure; research on the structural properties of reinforced concrete

beams strengthened by external FRP plates has (in recent years) been conducted with vigour in a number of institutions world-wide, and there is currently an ever increasing number of related publications appearing in the public domain. However, the vast majority of these publications are of a purely experimental nature, with a pressing need for the development of theoretical models which clearly identify various structural aspects of this external plate/concrete composite beam construction. In other words, many unresolved problems still remain in this area.

1.2 PREMATURE PLATE PEELING FAILURE

Reinforced concrete beams and slabs strengthened by external plates are usually designed for flexure on the basis of conventional ultimate load procedures such as, for example, those recommended by the British Standard BS8110 (1985), assuming full bond between concrete and the plate up to ultimate load, and using the plane section bending assumption and a concrete stress block at failure. However, as repeatedly reported in the literature, the designer should also check that premature anchorage failure (Figure 1.2) caused by peeling and debonding of the plate at its end, in a brittle fashion, does not occur prior to the beam achieving its full flexural strength. The premature failure mode shown in Figure 1.2 involves the plate and concrete cover becoming separated as a unit, from underside of the main reinforcing bars, which is the most commonly reported type of plate peeling phenomena. There is also the possibility of plate peeling off at the plate/glue or concrete/glue interfaces: with the strong nature of currently available epoxy glues, such failure modes are not common and if they happen, it is usually attributed to bad workmanship (Oehlers (1989)).

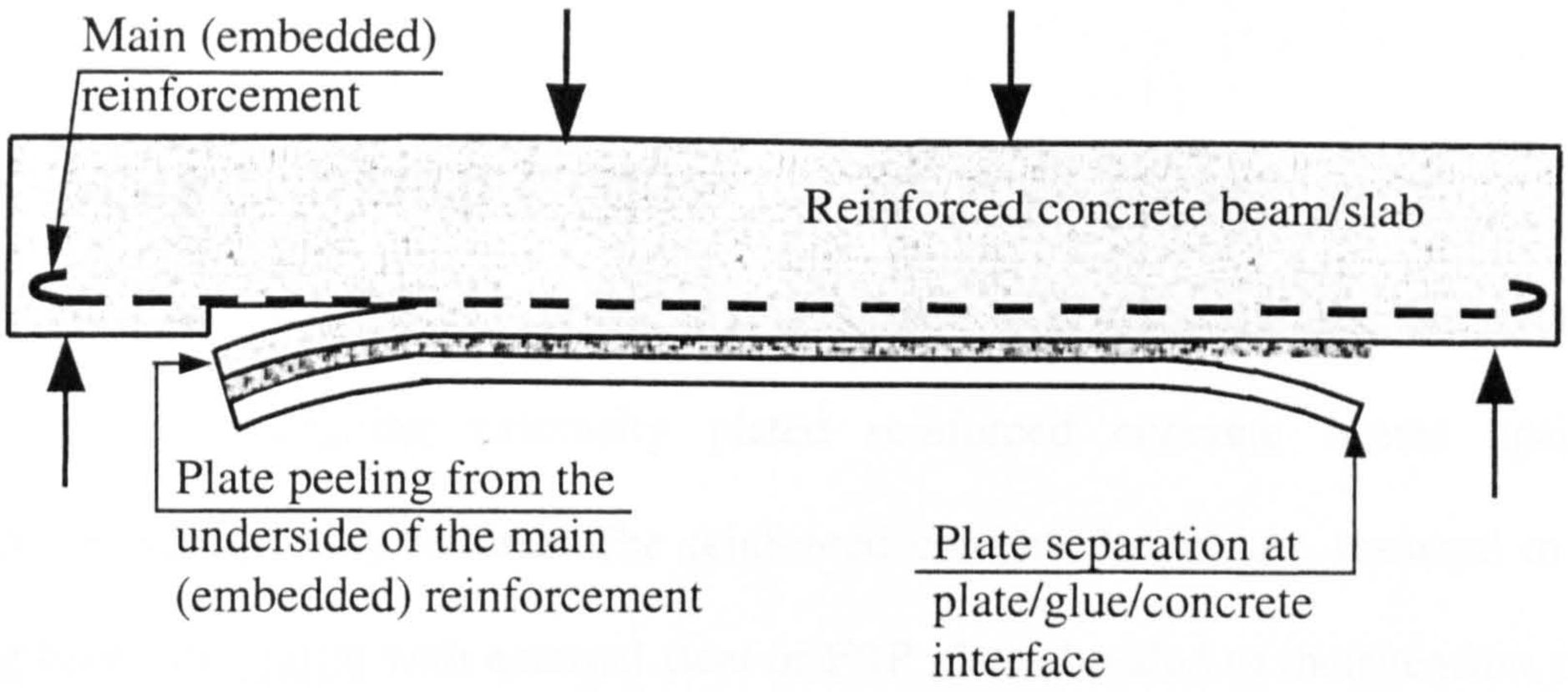

Fig. 1.2 Possible types of premature plate peeling failure.

The research in this thesis mainly focuses on the problem of premature plate peeling failure in which the concrete cover together with the external plate are peeled-off from underside of the main (embedded) tension reinforcement. This mode of failure is usually of a brittle nature, and happens at loads lower than those predicted by the design recommendations based on various codes of practice which have originally been developed for only concrete beams with internal reinforcement. So far, there is no design procedures recommended by any of the codes of practice which address the design of externally plated reinforced concrete beams or slabs against premature plate peeling failures. Meanwhile, none of the previously available methods of analysis in the public domain has been sufficiently reliable for general use in practice: these will be critically examined later on in this thesis. Over the last thirty years, rather extensive experimental parametric studies have been carried out by researchers in various institutions, world-wide. Due to the complexity of the problem, however, a great deal of disagreements exist among the findings based on such purely experimental parametric studies, and, to date, the researchers cannot even agree among themselves as to which beam design parameters are, indeed, the first order (i.e. controlling) ones, once one addresses the problem of premature plate peeling failures: a critical study of their findings will also be presented later on.

1.3 AIMS AND OBJECTIVES

The primary aim of the work reported in this thesis is to develop a simple but reliable procedure for designing externally plated reinforced concrete beams against premature plate peeling failures. The reinforced concrete beams are assumed to be strengthened in flexure with external steel or FRP plates bonded to their tension side with the plates glued to either pre-cracked or uncracked (i.e. as cast) specimens. The following objectives were set at the onset of the work:

1- Extending and further verifying the model originally developed by Raoof and Zhang for predicting premature plate peeling failures. The extended model should be able to handle beams plated with either steel or FRP plates with the original reinforced concrete beam being either cracked or uncracked prior to the application of the external plates.

2- Identifying all the possible modes of failure associated with plated beams, and developing associated theoretical models, the predictions of which are to be compared with the previously reported experimental modes of failure in the literature.

3- Identifying the main parameters which affect the behaviour of plated beams even in the absence of premature plate failures, and quantifying the effect of variations in these parameters on each mode of failure on an individual basis – even those modes of failure associated with which the plate remains fully bonded to concrete up to the ultimate load will be considered.

4- Determining the critical values of such main parameters which trigger initiation of such alternative modes of failure, covering a wide range of material properties especially in relation to FRP plates.

5- Deriving formulae, based on such key parameters, for designing the plated beams, which should be simple but of general applicability and, hence, of value to busy practising engineers.

1.4 METHODOLOGY AND ORGANISATION OF THE THESIS

In order to accomplish the above objectives, a detailed programme of work was devised to ensure effective and reliable routes to be followed in the course of this research. In what follows, a general outline of the various chapters in this thesis will be presented: the final outcome (as presented in detail in subsequent chapters) is believed to have met all the main objectives which were set at the onset of the work: Figure 1.3 presents a guide chart for the contents of this thesis, including:

1- Extensive and critical review of the available experimental data relating to the problem at hand. This review will save considerable time and effort, avoiding the otherwise necessity of carrying out extensive experimental work: it will secure a large number of experimental results covering a wide range of parameters as carried out by a number of independent institutions. Such valuable test data is obviously difficult to obtain by one research group or within one Ph.D. programme (considering the time and resource constraints). The review includes not only the gathering of raw experimental data but also a critical examination of the observations and conclusions made by different research groups. This information will later be used to assess the validity of different analytical models as proposed by others and also the presently proposed model. Using such information, the commonly reported modes of failure are studied, and a complete theoretical description for all the possible

modes of failure relating to plated beams will, subsequently, be developed. This review is presented in Chapter 2.

2- Critical examination of the previously available methods of analysis relating to plate peeling failure will also be carried out: this will be presented in Chapter 3. This study will include a discussion of the basic assumptions, plus details of the derivations. Such previously recommended formulae will be used to produce numerical data to be checked against the available (but independent) experimental results as gathered in the experimental review (reported in Chapter 2). Such a critical examination will serve to clarify the general (or otherwise) reliability of the most widely cited models and, in addition, will help the present work to identify the most suitable assumptions to be adopted for the presently proposed methods of analysis.

3- Guided by the above critical examination, a theoretical model for analysing the externally plated reinforced concrete beams will be developed. This will be coupled with a numerical procedure in order to handle the iterative analysis, and to produce numerical data which will, subsequently, be compared with experimental results. Details of the presently proposed analytical model are presented in Chapter 4, while the computer programme is included in appendix A.

4- All the possible modes of failure associated with externally plated beams in the presence and/or absence of premature plate peeling failures will be identified. Full derivations of the formulae and the associated conditions for these modes will be presented in Chapter 5.

5- A crucial material parameter for the FRP plate (i.e. its modulus of elasticity) will be selected to perform comprehensive theoretical parametric studies to

throw some light on its effect on the behaviour of the plated beams as regards their various associated modes of failure. Chapter 6 presents details of such a study.

6- In Chapter 7, the critical values of modulus of elasticity for the externally bonded FRP plate which control the initiation of a number of widely different modes of failure will be derived theoretically, with the final numerical results checked against the available experimental data from various sources. Parametric sub-studies for the other key parameters will also be carried out in order to clarify their effect on the initiation of different modes of failure.

7- Focusing on the behaviour of plated beams failing in the premature plate peeling modes, and guided by the outcome of parametric studies, certain assumptions will be made enabling one to obtain the stresses and strains in the critical plated beam section via simple formulations. Chapter 8 presents details of such simple formulations which are amenable to hand calculations, using a pocket calculator, and using which, the depth of the neutral axis and, hence, the flexural load bearing capacity of the plated beam may be predicted. The final numerical results based on such simple formulations will then be compared with the corresponding results based on the considerably lengthier iterative method which necessitates the use of a computer programme. The final output of the simple formulations will also be checked against experimental results, where very encouraging correlations have been found, hence, confirming the general validity of the simplified approach for use in practice.

8- Finally, in Chapter 9, a summary of the research work carried out in this thesis will be presented in some detail, and the main conclusions will be highlighted. Recommendations will also be made for future research.

Chapter 1

Preliminary Remarks

Background to the research. Problem definition. Aims and objectives. Methodology and thesis organisation.

Chapter 2

Experimental Review

Review of the relevant experimental results, observations and conclusions. Data base for 169 specimens is built-up which will be used for later verifications.

Chapter 3

Critical Examinations

Approximate analysis, approaches of limiting normal or shear stresses in the adhesive, limiting curvature and peeling stresses, limiting tension stress in the concrete cover, and other approaches. Experimental results used to check various models.

Chapter 4

Proposed Method of Analysis

A purely empirical method examined. Proposed model for FRP plates. Model developed for pre-loaded beams prior to plating. Model verified against independent test results. Model examined by experimental parametric studies. Computer programme outlined with the assumptions mentioned.

Chapter 5

Modes of failure for Plated Beams

Identifying and fully describing the eight possible modes of failure of plated beams. Derivation of the force and moment equilibrium equations for each mode.

Chapter 6

Effect of Modulus of Elasticity of the Plate

Examining the effect of changes in the plate Young's modulus on the different eight modes. Progress of changes in failure modes with changes in the Young's modulus, and, hence, identifying different types of plated beam characteristics.

Chapter 7

Critical Values of Young's Modulus, E_p, for the Plate

Derivation of the critical values of E_p associated with different modes of failure. Classification and description of the different types of plated beam behaviour. Numerical results compared with experimental data. Parametric studies for the key parameters.

Chapter 8

Simple Design Procedures

Development of a simplified method to predict the depth of neutral axis and to propose a simple formula to calculate the premature plate peeling moment. Proposed design procedures verified against experimental results.

Chapter 9

Summary and Conclusions

Summary and conclusions of the work, and recommendations for future research.

Fig. 1.3 Guide to the thesis

Chapter 2

UPGRADING OF REINFORCED CONCRETE BEAMS - EXPERIMENTAL REVIEW

Chapter 2

UPGRADING OF REINFORCED CONCRETE BEAMS - EXPERIMENTAL REVIEW

2.1 INTRODUCTION

In this chapter, a review of literature will be presented which relates to the experimental studies associated with reinforced concrete beams strengthened by gluing external plates to their tension sides. A review of the published theoretical studies relating to this problem, on the other hand, will be presented in the next chapter which will, in turn, include a critical examination of the most promising available theoretical models for the plate peeling problem.

It is, perhaps, worth mentioning that, unlike steel structures, repair and upgrading of reinforced concrete structures is generally more involved and needs well experienced designers and specialists for design and detailing in addition to well trained and skilled teams for execution. Different strengthening techniques have (in fairly recent years) been developed and utilised in practice depending on the structural system and the given situation (such as site conditions, traffic flow, etc.). The external pre-stressing technique, additional supports, etc., have in the past been used, with varying degrees of success, to strengthen structural elements. With the development of strong adhesives back in the 1960's, the plate-bonding technique has proved to be an attractive option. With the introduction of new composite materials such as fibre reinforced plastics (FRP), such upgrading techniques are often used with advantages over other types of strengthening methods. As mentioned previously, the plate-bonding method for reinforced concrete beams and slabs is easy to apply in practice

and does not, for example, significantly alter the shape, weight, or the size of the structural element. In most cases, it may be carried out while the structure is still in use, with minimum disruptions to, say, traffic flow.

Over the last twenty years, a large number of experimental studies relating to this technique (with either FRP or steel plates) have been reported in the literature, with the majority of the experimental studies concentrating on the behaviour of simply supported beams under symmetrical four-point loading.

2.2 EXPERIMENTAL REVIEW

2.2.1 Composite plates

Saadatmanesh *et al.* (1991) experimentally studied rectangular and T-beams strengthened by gluing external glass fibre reinforced plastic (GFRP) plates to the tension sides of simply supported beams subjected to symmetrical four-point loading. Five externally plated rectangular and one T-beams were tested. The test specimens were all of large scale with a width of 205 mm and a depth of 455 mm, while having a clear span of 4570 mm. The flange width for the T-beam was 610 mm, while its thickness was 75 mm. The strengthening plates were of the GFRP type, with a width of 152 mm and a thickness of 6 mm, while their total length was 4260 mm. One of the rectangular beams was under-designed for shear (according to ACI-318), while the rest of the beams were designed so that shear failure did not occur, with the flexural behaviour controlling the final failure mode. One of the rectangular beams (which was designed against shear failure) was also externally pre-stressed by cambering it prior

to the GFRP plate being bonded to its tension side, in order to observe the effect of external pre-stressing.

These authors measured the load versus axial strains in the GFRP plates, and steel rebars, plus the bending strains at the extreme compression fibre of concrete. Load versus mid-span deflection measurements were also taken. It is interesting to note that the beam which was not designed against shear failure did not develop major shear cracks, and the failure was as a result of concrete crushing on the compression side in the absence of any premature plate peeling. The beams which were designed against shear failure, on the other hand, suffered from plate peeling either within the adhesive layer or with the concrete cover ripping-off prior to the concrete crushing within the maximum moment section.

It was also reported that brittle premature concrete cover ripping-off (initiated at the end of the plate) occurred in the beam which had been cambered (i.e. externally pre-stressed). A plate separation mode of failure occurred in an un-cambered beam associated with which yielding of the embedded bars also took place.

In general, their results indicated that the flexural strength of reinforced concrete beams may significantly be increased by gluing GFRP plates to their tension face. It was also reported that epoxy bonded plates improved the cracking characteristics of the beams by delaying the formation of visible cracks, and reducing crack widths at higher load levels.

Sharif *et al.* (1994) experimentally studied the behaviour of initially loaded reinforced concrete beams to 85 percent of their ultimate flexural capacity, and subsequent strengthening of the beams with different types of fibreglass reinforced plastic (FRP) plates.

Ten small-scale rectangular reinforced concrete beams with overall dimensions of 150x150x1280 mm and a clear span of 1180 mm were tested. The internal reinforcement ratio was chosen so as to ensure under-reinforced flexural behaviour. The beams were over-designed (by more than 200 percent) in shear to avoid a brittle shear failure in view of the expected increases in the failure load in the presence of external plates. The ultimate load bearing capacity of the unplated beam was determined from a loading to failure test on a control beam, and the pre-loading behaviour was determined from another control beam which had been loaded up to a central deflection of 10 mm (corresponding to 85 percent of the ultimate capacity of the associated control beam), unloaded and, then, reloaded to failure. They reported a similar behaviour up to failure for both control beams.

To investigate the occurrence of plate peeling failure (initiated at the plate curtailment zone) due to the high concentration of shear and peeling stresses, and to ensure occurrence of a ductile mode of failure, a range of plate thicknesses and different types of anchoring schemes were used. Bolts in the vicinity of the ends of the plates, side plates within the shear span, and I-jacket plates were all used to provide the desired end anchorage.

The results of their study indicated that the flexural strength of plated beams is, indeed, increased, and the ductile behaviour of the strengthened beams is inversely dependent on the plate thickness.

It was interesting to note that although using external plates to strengthen the beams improved their flexural load bearing capacity, doubling the plate thickness did not lead to any further improvements in the flexural load bearing capacity. Furthermore, using much thicker plates was found to reduce the enhancement in the flexural capacity for the un-anchored beams associated with which the premature type of plate failure (i.e. plate separation) was reported to take place.

Their results showed insignificant increases in the beam flexural capacity when anchor bolts were used for medium plate thicknesses. Moreover, the rates of increase in the flexural capacity were found to diminish, when thicker plates were bonded to the beams. It was reported that although using bolts eliminated the occurrence of plate separation, it caused the formation of diagonal tension cracks leading to failure. It should be noted that the shear strength of the upgraded beams with anchor bolts was estimated to be 1.5 times their flexural strength, however, the ultimate failure generally occurred at a load level equivalent to 60-65 percent of the beam shear strength. For the medium thickness plates, adding side plates improved the ductility, and developed the full flexural strength, while for the thicker plates neither of these beam characteristics were found to have been improved with the plate peeling being found to be the dominant failure mechanism.

Their results also showed that, in general, thicker plates caused brittle premature failure even when anchor bolts or side plates were used. However, using I-jacket plates was found to lead to a higher ductility index with the full development of flexural strength: in such cases, failure was due to crushing of concrete in compression within the constant moment zone under symmetrical four-point loading.

In another experimental study by Ritchie *et al.* (1991), composite plates reinforced with different types of fibre reinforcement plastics such as glass, carbon, and aramid were used to externally reinforce concrete beams by gluing the plates to their soffits and testing them to failure. In addition, some beams were reinforced with external steel plates. The purpose of these tests was again to study the effectiveness of the external strengthening of reinforced concrete beams with FRP and steel plates.

Their test program included 16 reinforced concrete beams of 152 mm width, 304 mm depth, and 2440 mm clear span. Two beams were strengthened with steel plates, while the rest were upgraded with different types of FRP plates. The overall lengths of the plates differed from one beam to another: four beams had plates extended from one support to the other support, and certain beams were also reinforced with side plates at the location of plate curtailment, while in other cases, the beams were upgraded with angle shaped plates.

In the absence of end anchorages, plate peeling failures were reported not to occur within the maximum moment region but were initiated at the end of the plates within the shear span. In an attempt to shift the location and the mode of failure as well as to increase the ultimate load capacity of the beam, these researchers introduced four

alternative modifications. In the first case, unequal leg fibreglass angle was used at the end of the plate, with the longer leg being in an upside position, which led to a higher load capacity but the failure mode was not found to have been altered. In the second case, full-height FRP plates were bonded to the sides of the beam in the vicinity of the end of the plate and, then, were connected to the plate (at the soffit) by using bonded fibreglass angles. This scheme led to a higher load capacity and successfully altered the failure mode for one beam, while in the other beam, where the angle connection to the plate failed, the failure mode was not altered. In their third scheme, they replaced the plate with a pair of angles bonded along the underside of the beam, but the failure mode was not found to alter and this was inferred to be due to the use of insufficient upside leg length. Finally, the extension of the plates from one support to the other support was adopted: this technique was reported to be very effective in terms of increasing the load capacity and in changing the final failure mode.

Their investigation indicated that using FRP plates increased (within their experimental range) the overall flexural stiffness from 17 to 99 percent, and the ultimate strength of the beams by 40 to 97 percent. Significant improvements in the crack patterns were reported, which were found to change from several widely spaced and relatively large cracks to the desirable situation whereby many more closely spaced and narrower cracks were formed. To avoid the occurrence of premature failure mode initiated at the end of the plate, it was recommended that one should reduce the average anchorage stresses, by extending the plates towards the support(s), in preference to using other types of plate end anchorage systems. In spite of using different types of FRP plates with different fibre orientations, their findings about the practical implications of using different FRP materials were largely inconclusive.

In a preliminary experimental parametric study aimed at identifying the main parameters affecting the plated beam behaviour, Garden *et al.* (1996) tested small scale beams reinforced with carbon fibre reinforced polymer (CRP) plates. The cross-section dimensions were 100x100 mm with a clear span of 900 mm. To ensure the occurrence of flexural failures, the beams were internally under-reinforced with a tensile steel percentage ratio of 1.0. The plates had width/thickness ratios ranging from 45.0 (45/1) to 180.0 (90/0.5) with an intermediate value of 92.8 (67/0.7) while the overall plate cross section area was kept constant. The simply supported beams were tested under symmetrical four-point loading with the distances between the external point loads being varied, from one test to another, in order to study the effect of the shear span/depth ratio: this ratio was considered to express the plate anchor length as the overall lengths of the plates were kept constant for all the beams. Moreover, through extending certain plates to the supports, such plates were anchored at their ends by using the external force acting from the point support(s). The axial strains in the plates at their end, at the sections under the point loads, and at the mid-span were all monitored. In addition, bending strains at selected locations of the beams were measured as were deflections at the mid-span.

In their discussion of the results, it was pointed out that the shear cracks were not found to be wide due to the presence of sufficient shear reinforcement, and that the failures were accompanied by separation of concrete cover from the underside of internal main reinforcement. The beams with low shear span/depth ratios failed with concrete cover separation occurring across the whole width of the beam when the wide (i.e. 90 mm width) plates were used, while, for the narrower plates, the width of

separated portion of concrete cover was less than the width of the beam at the end of the plate but these approached the full width of the beam as one moved towards the mid-span. Beams with large shear span/depth ratios were found to fail with the width of separated portion of concrete cover being equal to the width of the plate all along the beam. The failure was reported to happen at only one end of the plate, and was never found to simultaneously happen at both its ends.

It was concluded that for externally plated beams, and in the absence of premature plate peeling failures, the overall bending stiffness throughout the loading range to failure was increased with an associated significant loss of ductility. It was also reported that the ultimate loads and deflections at failure were relatively high for those beams with plates extended to their ends, with the reactions from the supports providing increased end anchorages.

For a constant cross-section area of the plate, the failure load was, in general, reported to be reduced with reductions in the width of the plate and/or increases in the plate thickness for either the beams with anchored plates or where no end anchorages were provided. The load-deflection curves were reported to be similar for both the beams with and without end anchorages up to the yielding of internal reinforcement: beyond the yielding of embedded bars, however, the plated beams with end anchorages were found to be stiffer in bending.

When compared to the corresponding control (unplated) beams, greater incremental increases in the ultimate moments over the initial yield moments were found. The measured bending strains along the beams showed that the plate axial strains were

compatible with the bending strains in concrete while, at the mid-span, plane sections were reported not to have remained plane (due to the presence of large cracks in the concrete in tension). Moreover, they reported lower neutral axis depths associated with the plated beams (i.e. larger concrete compression blocks), compared to the corresponding unplated beams.

The measured tensile strains at the end of the plates versus external loads were reported not to have been increased by significant margins until the failure loads were approached. Plate axial strains within the shear spans were found to be more symmetrical about the mid-span for those beams with a high shear span/depth ratio, while the strains were greater in the shear span where failure happened. In all cases, remarkable reductions were reported in the magnitudes of the plate axial strains upon failure initiated at the end of the plate, once plate separation had occurred with associated relaxation.

In a later publication (Garden *et al.* (1997)), more details regarding the material characteristics, beam configurations, and test results for tests conducted by Garden and his associates were reported.

Garden (1997) extended his programme of research to cases when large scale beams with lengths from 2200 to 4500 mm were tested. The advantage of providing anchorage at the ends of the plate was demonstrated to be greatest for low shear span/depth ratios, preventing or delaying the occurrence of plate peeling.

Garden's studies also included the use of pre-stressed plates which were claimed to improve the composite action between the beam and the plate for low shear span/depth ratios. It was noted that improvements in the serviceability loads can be expected in the presence of plate pre-stressing. Moreover, the magnitude of ultimate load was found to depend on the mode of failure, also being related to the shear span/depth ratio and the initial level of plate pre-stress.

The long term effects of environmental durability were also experimentally investigated, and it was concluded that deterioration of the adhesive mechanical properties is not necessarily translated into reduced structural performance of the plated member. The experimental study of the response to cyclic loading showed that the concrete cracking characteristics, which give rise to plated beam failures under static loading, may be expected to occur under a lower maximum load if the load is applied cyclically. However, at the serviceability load level, it was concluded that fatigue loading is not expected to cause overall failure, and that the maximum values of stresses in the internal reinforcement, located in the vicinity of the concrete cracks, are reduced due to external plating.

The flexural response of the plated beams to externally applied loads was modelled using a simple analytical approach which was then applied to beams with both non-- pre-stressed and also pre-stressed plates. The unsatisfactory correlations between experimental and numerical results were attributed to the poor representation of concrete flexural cracking inherent in the ABAQUS finite element program. Various previously proposed analytical methods for analysing the separation of steel plates

from reinforced concrete beams were also critically examined, and were found, in general, to be inappropriate for obtaining accurate results.

In a private communication, Hollaway (1997) provided the present author with some more details regarding the measured plate axial strains at the point of application of the external loads for some selected beams from the above research programme: these results (as discussed later) proved to be very useful for developing the plate peeling model (when FRP plates are used) in this thesis.

Quantrill *et al.* (1996:A) carried out an experimental parametric study on small scale beams externally plated with either glass fibre reinforced plastics (GFRP) or carbon fibre reinforced plastics (CRP). Their experimental parametric study covered a wide range of plate parameters such as area, width/thickness, material, and the method of anchoring the ends of the plate.

In these series of tests, ten beams were tested with typical dimensions of 100x100 mm and a clear span of 900 mm, with under-reinforced tension steel ratio of 1.0%, while the plate dimensions were varied.

One control (unplated) beam and nine plated beams were tested as simply supported specimens under symmetrical four point-point loading with the two external point loads being 300 mm apart. Four of the beams were reinforced with GFRP and five with CRP plates. One of those reinforced with GFRP was provided with plate end anchorages in the form of steel clamps, and the other three beams had no plate end anchorages. While the end of the plate in only one of those reinforced with CRP was

not anchored, one was anchored by steel clamps, two anchored by extending the plate up to the supports, and one was provided with GFRP angles at the end of the plate. Except for those which were extended up to the supports, the plates were terminated 20 mm away from either support. Their theoretical results were compared with test data, and certain conclusions (to be discussed in Chapter 3) were drawn.

Quantrill *et al.* (1996:B) continued their study by testing more of similar types of beams but with externally bonded GFRP plates. Eleven beams were tested with two unplated control specimens. All the plates were terminated 20 mm away from the supports, except for one beam in which the plate was terminated 150 mm from the support with no plate end anchorage provided. The plate cross-sections were kept the same with 80 mm width and 1.2 mm thickness, and two different batches of concrete were used with concrete cube strengths of 70 and 42 MPa. Two of the beams in the second batch (with a cube strength of 42 MPa) were provided with side plates, with a height of 50 mm and length of 150 mm, in order to provide the plate with end anchorages: one of the beams was steel clamped, and the other one was provided with GFRP angles - the rest of the beams were not provided with any plate end anchorages. Moreover, none of the beams in the first batch were provided with any end anchorages. The test results were presented in terms of experimental failure modes and ultimate loads. As in their previous work, the experimental data were compared with their analytical results, and certain conclusions were drawn - their analytical method will be discussed later (in Chapter 3).

In an experimental parametric study aimed at examining the influence of the FRP plates on the failure mechanisms, ductility, and overall bending stiffness of the

upgraded beams, Triantafillou *et al.* (1992) tested (to failure) seven small scale beams strengthened with FRP plates. They also tested one unplated beam as a control specimen. The beams were designed with the only change relating to the plate cross-section dimensions, in order to study the effect of the plate area on the behaviour of the composite beam. The beams were small scale specimens with a width of 76 mm, depth of 127 mm, and length of 1350 mm, internally reinforced with 2 steel bars of 4.6 mm diameter (i.e. steel percentage ratio of 0.38 %). The externally plated beams were strengthened with unidirectional CFRP plates with a length of 1070 mm, being tested as simply supported with an effective span of 1220 mm. The plates had a very high ultimate strength of 1450 MPa, and a high Young's modulus of 186,000 GPa. The test specimens were loaded to failure under symmetrical four-point loading, with a shear span of 457.5 mm, and a spacing of 305 mm between the external point loads.

For low ratios of plate/concrete area, their results showed that the most probable mode of failure is the plate rupture, provided that the original unplated reinforced concrete beam is under-reinforced. For relatively higher ratios of plate-to-concrete area, the failures happened due to plate debonding, with the FRP plate peeling-off. In general, it was reported that strengthening of concrete beams with externally bonded composite sheets is a feasible way of increasing the load-carrying capacity and overall flexural stiffness of existing structures. However, the need was emphasised for performing further detailed studies, prior to applying this technique in practice: it was argued that one needs to address certain additional issues, such as the behaviour under sustained loading, fatigue, thermal and humidity cycling, and the fact was underlined that the FRP-adhesive system has a very low fire resistance unless the burning rate of the

plastic materials is reduced by either using additives or by chemical modification of the polymer chains.

These authors also carried out analytical studies in order to analyse the collapse mechanisms, and used some of the test results to calibrate their analytical model. Their analytical work will be discussed later in Chapter 3.

2.2.2 Steel plates

To investigate the problem of premature plate peeling in reinforced concrete beams externally reinforced with steel plates, Oehlers and Moran (1990) proposed a semi--empirical model, using results based on 57 beams as tested by Moran (1988), and Moloney (1986). Fortunately, by and large, full details for the test data, relating to which so many loading and design parameters were varied, were reported.

In 49 beams, the plates were terminated within the constant moment region of the simply supported beams subjected to symmetrical four-point loading, while only 8 beams were tested with the plates extended to the shear span. Some of these beams were precracked prior to the application of external steel plates, certain others were pre-cracked and then pre-cambered during the upgrading, while a certain number of external plates were pre-curved before gluing them to the beam in order to induce pre-stressing.

The beams were tested with their clear span being varied from 1650 to 2500 mm. The width of the beams was either 120 or 125 mm, while their depth varied from 150 to

240 mm. The plate thickness was varied from 2 to 15 mm, while the concrete cover varied from 10 to 50 mm, and the width of the plates was chosen so as to cover the whole width of the beams except for a minor number of the beams where the widths of the plates varied from 25 mm to 100 mm. Based on a semi-empirical approach, a method was proposed for predicting the premature plate peeling loads. Their method will be discussed in some detail later, while plenty of use will be made of their test results in the subsequent chapters in this thesis.

Oehlers (1992) continued his previous studies by carrying out more tests on plated beams, with the tests including 26 specimens which were externally strengthened with steel plates: in the vast majority of these tests, the plates were extended to the shear span (only two of the beams had plates terminated within the constant moment region). All these specimens had the same dimensions and configurations with the exception of the lengths for those plates which were extended to the shear span. Moreover, slightly different concrete cube strengths were achieved. In some of these beams, shear reinforcement in the form of vertical stirrups were used, while others were left without any shear reinforcement. A typical width of the beams was 130 mm with a depth of 170 mm. The plates had thicknesses of 5 mm with widths of 130 mm to cover the whole width of the beams. The spans of the beams were not quoted in Oehlers' paper, although the distances of the external point load(s) from support(s), and the plate termination locations (as a distance from the support) were given, and these were varied from one beam to another.

These tests showed that external shear and flexural forces may (for a given beam design) cause the occurrence of plate peeling prior to the beam reaching its design

ultimate load. In some cases, the failure load was found to be even lower than that expected for the corresponding unplated beam. A semi-empirical design procedure was, then, proposed by Oehlers, which was based on the so-obtained experimental results. Oehlers concluded that the debonding initiated at the ends of the plate due to shear forces is not influenced by the presence of stirrups, and depends on the formation of diagonal shear cracks, the magnitude of which is given as that of the shear strength for an unplated beam in the absence of any stirrups. Accordingly, it was suggested that limiting the shear flow at the steel plate-concrete interface will not prevent the occurrence of plate debonding. A strong interaction was found between what was claimed to be debonding due to shear and flexural forces. Such an interaction was quantified by employing a curve fitting exercise using the test results. Guided by the test results, Oehlers concluded that such plate strengthening systems are best suited for the strengthening of reinforced concrete slabs rather than reinforced concrete beams, although it was suggested that this technique enhances the serviceability requirements for both types of such elements.

In a later publication, Oehlers *et al.* (1998) reported an experimental study on a series of continuous reinforced concrete beams strengthened with steel plates glued to their tension faces in addition to their vertical sides. Oehlers and his associates also used the method proposed by Lue (1993) to develop a design procedure using such a set of test results. The side plates were positioned so as to prevent the occurrence of plate shear peeling failure. A study of continuous beams for any load combination or distribution or changes in the cross-section properties is of considerable practical importance.

Jones *et al.* (1980) carried out three series of tests to investigate the influence of the glue thickness, plate lapping, multiple plates, and of pre-cracking prior to plate bonding, on the composite behaviour of concrete beams strengthened with steel plates.

Their experimental work included testing unplated (control) plain (internally un-reinforced) concrete beams, plain concrete beams reinforced only with external steel plates, unplated (control) reinforced concrete beams, and reinforced concrete beams with steel plates glued to their tension faces. The beams were all of small scale, and two types of epoxy glue were used for each beam design.

The first series of tests was on plain concrete beams and included eight beams out of which two were of the unplated (control) type. Two beams were tested with the adhesive thickness varying linearly along the beam. Four beams had constant adhesive thicknesses, with two of these specimens not provided with any shear reinforcement while the rest of the beams in this series were reinforced against shear at the supports to avoid shear failure outside the plated length. The beams were tested under three-point loading. The beam dimensions were 150x150x710 mm with a clear span of 610 mm, and the plate dimensions were l00x1.0x500 mm.

The second series included ten unreinforced beams (i.e. without embedded main tensile steel bars) with limited shear reinforcement within the portion of the beam between the end of the plates and the supports. The beam cross-sectional dimensions were 100x150 mm, and they had a total length of 1200 mm with a clear span of 1100

mm. Four beams were not plated, and the rest were externally reinforced with plates of dimensions 75x1.0x1000 mm. All the beams were tested under three-point loading.

The third series consisted of 16 internally reinforced beams with the same overall dimensions as those in the second series. All these under-reinforced beams were internally reinforced in flexure using high strength deformed bars with a steel percentage ratio of 0.75%. Most of these beams were provided with shear reinforcement (stirrups) near their ends. To study the effect of the glue thickness, the average adhesive thickness for these beams was varied from 1.6 to 8.0 mm. While, in general, the beams in this series were tested under three-point loading, a group of four beams were tested using symmetrical four-point loading in order to study the change in the mode of failure by varying the external load configurations. In most cases, single plates of dimensions 80x1.6xl000 mm were used and terminated 50 mm away from the supports. However, a group of these beams was provided with double plates or half plates which were joined together with a splice plate in order to study the effect of plate lapping and use of multiple plates. To check the effect of concrete pre-cracking, one beam was pre-loaded prior to bonding of the external plate.

By analysing the test results, it was concluded that using external reinforcement in the form of steel plates glued to the tension face of plain or reinforced concrete beams will affect the structural behaviour by increasing the elastic range, and delaying the initiation of the first visual cracks, hence, increasing the serviceability loads. Moreover, it was concluded that gluing external plates increases the flexural stiffness at all load levels, and, consequently, reduces beam deflections at the corresponding external loads. It was concluded that the ultimate flexural capacity is generally

enhanced, and the ductility at flexural failure would be increased once one uses external plates. For a given load, it was suggested that, in the presence of full composite action, the tensile bending strains in the concrete will be reduced when compared with the corresponding unplated beams.

In addition, the results of their study showed that, for a constant plate area, the stiffness of the beam increased with increases in the glue thickness, with a negligible associated effect on the magnitude of ultimate strength. Similarly, for a constant glue thickness, the stiffness of the beams and their ultimate strength were found to increase with increasing plate area, but the mode of failure was found to change from flexural to combined flexural-shear. The steel plates failed by yielding, and subsequent crushing of concrete within the compression zones was found to take place. It was shown that pre-cracking prior to plate bonding slightly reduces the flexural stiffness, whilst plate lapping increases the magnitude of flexural stiffness to the corresponding levels associated with un-cracked plated beams. Bending strain measurements showed that plane sections very nearly remain plane throughout loading.

Regarding the use of more than one plate and/or lapping of the plates for strengthening and/or stiffening pre-cracked or un-cracked reinforced concrete beams, it was suggested that such external plate bonding arrangements may be carried out efficiently and successfully, and that the external plate bonding method is sufficiently reliable for use in practice.

Jones *et al.* (1982) carried out tests on internally reinforced concrete beams, rather than the previously mentioned plain concrete specimens, in order to study the

behaviour of the internally under- and over-reinforced sections when strengthened with external steel plates glued to either their tension or compression side.

Eight beams were cast: five were under-reinforced with a percentage steel ratio of 1.2%, and three were of the over-reinforced type with a percentage steel ratio of 6.76%. All these beams had the same overall dimensions, and were identically reinforced for shear in order to ensure that failure would occur in the flexural mode. Two beams (one under-reinforced and the other one over-reinforced) were left unplated as control specimens. The other beams were externally reinforced using mild steel plates with a width of 80 mm, which were terminated 50 mm away from the supports, and a constant glue thickness of 3.0 mm was used. The plates used for the over-reinforced beams had a thickness of 5.0 mm, and were glued to the tension face for one of the test specimens while, for the second beam, the plate was glued to the compression face. Plates with different thicknesses were externally bonded to the under-reinforced beams with their thickness varying from 1.5 to 10.0 mm. In the case of the under-reinforced beams, the plates were invariably glued to the tension face. Typical beam dimensions were 100x150 mm. The beams were tested as simply supported under symmetrical four-point loading, with a clear span of 2250 mm. The measurements included variations against the external loads of concrete strains at the compression face and over the sides, embedded bar axial strains, plate axial strains, vertical deflection at mid-span and under the external point loads, plus the longitudinal displacements at the end of the plate.

For two of the under-reinforced plated beams, the modes of failure were reported to have involved yielding of the embedded steel bars and external plates prior to the

crushing of concrete in compression, with limited plate separation under the point load just after crushing of concrete. The other under-reinforced beams with larger plate thicknesses (5 and 10 mm) were reported to have failed with neither the steel elements yielding nor concrete crushing but suffered from plate separation at one end of the plate (plate peeling failure). The two over-reinforced plated beams (with the external plates glued to either tension or compression faces) both failed due to plate separation.

Their results demonstrated a general reduction in the average crack widths by using external plates and by increasing the plate thickness (up to a certain limit), within the range of service loads, for both under- and over-reinforced beams. However, increasing the plate thickness beyond a certain limit was found to have an insignificant effect regarding the size of crack widths although it was found to change the overall behaviour of the beam at failure which was then of a brittle nature. Regarding the crack spacings, it was reported to be generally not influenced by plating in relation to both the ultimate loads and the loads within the serviceability range.

As regards the mid-span deflections, the test results, in general, showed a significant reduction for both the under-reinforced and also the over-reinforced plated specimens. The deflection was found to be reduced with increases in the plate thickness.

Measured concrete bending strains showed that (to a large extent) for plated beams under low levels of external loads, plane sections remained plane after bending (prior to the yielding of steel). It was noticed that, for similar levels of external loads, increasing the plate thickness (i.e. area) reduces the overall section bending strains.

The axial strains in the steel bars and in the plates (at the plate mid-span) were found to reach the yield condition for under-reinforced beams strengthened with thin plates and that, in general, the steel strains were found to be reduced with increasing cross-section area of the external plate.

Regarding the slippage at the end of the plate, larger and multiple slips were measured for the over-reinforced beam compared with the corresponding under-reinforced specimens which had the same plate dimensions. It was noticed that the interface shear stresses for the under-reinforced beams which were plated with thinner plates were lower in magnitude than those for similar beams with thicker plates, while, for the beams with considerably thicker plates, the interface shear stresses were not found to change significantly with increasing thickness of the plates (i.e. plate cross-section area).

Bearing in mind the small number of tests performed to investigate the influence of various parameters, one should exercise caution in drawing any definite conclusions from such a brief study. However, their main conclusions may be summarised as follows:

- Up to failure by either yielding of steel or plate separation, composite action between the reinforced concrete beam and the steel plate was achieved.
- The plates increased the ultimate strengths of the original (unplated) beams in all cases. Thicker plates generally had a greater effect, but the mode of failure changed from yielding to separation as the plate thickness was increased. The maximum increase in strength for the under-reinforced beams was over 100%. For

the over-reinforced beams, a 44% increase in ultimate load was achieved with a tension plate and a 22% increase with a compression plate.

- The plates increased the bending stiffness of the beams with associated decreases in deflection and rotation. Thicker plates, again, had a proportionately greater effect.
- The appearance of the first visible crack was delayed by the presence of external plates on the tension face. For under-reinforced beams, the delay was insignificant, but for over-reinforced beams, the first cracking load was increased by a factor of four.
- Generally, for beams with relatively thin plates, the application of external plates had little effect on the spacing of cracks, but this was not the case for the beams with very thick plates.
- Plates applied to the tension face of beams reduced the crack heights and widths, and thicker plates had the greatest effect.
- For tension plated beams, plate separation occurred when the interface shear stress reached a limiting value of about 2.15 N/mm^2. Plate separation was through the concrete adjacent to the glue layer and was accompanied by low angle cracks up to the level of reinforcement.

Jones *et al.* (1988) also carried out more tests on steel plated beams. Seven rectangular reinforced concrete beams strengthened by epoxy-bonded steel plates, and one control (unplated) beam were tested. The beams were simply supported over a span of 2300 mm, with external loads applied at the third points. The test specimens were externally reinforced with 2200 mm long mild steel plates which had a width of 125 mm. The beams were internally reinforced with high yield deformed bars, and had

3.2% internal reinforcement ratio. Sufficient shear reinforcement was used in order to avoid shear failure. Typical beam cross-section dimensions were 155x225 mm.

Various plating and end anchoring schemes were used. One beam was provided with a constant thickness (6 mm) plate, while another one was similarly plated but with 4 M6 anchor bolts at both ends of the plate. Two plates with a thickness of 3 mm were glued to a beam with the outer plate terminated at the mid length of the part of the second plate in the shear span. A similar plated beam was provided with 6 M6 anchor bolts at both extended ends of the plate. Two beams were provided with 6 mm thickness plates, one of them was anchored at each end of the plate, with two short angles (250 mm length) of unequal legs (l30x60 mm), and the other was provided with two short angles (250 mm) at one end of the plate and two long angles (770 mm) to nearly cover the whole shear span; these angles also had unequal legs (100x50 mm). The seventh beam was strengthened with a plate along which the thickness varied from 6 to 2 mm.

Compared to the failure load for the control beam, three beams had failure loads lower than that for the unplated beam: in other words, the external plating not only did not strengthen, but rather, weakened the beams. This was associated with the occurrence of plate separation for the three beams which had no plate anchorages; namely: the beam with one 6 mm thick plate, the beam with double 3 mm thick plates (outer terminated), and the beam with a tapered 6/2 mm thick plate.

For the beams with plate end anchorages in the form of bolts, there was nearly full composite action up to the corresponding unplated failure load (for the control beam) when the debonding happened. Following plate debonding, it was noticed that the

bolts prevented occurrence of complete plate separation, and the beams were able to carry higher loads. As the load was increased, more plate debonding took place, and some tearing actions occurred in the region close to the bolts. Total failure eventually took place by crushing of concrete within the constant moment region, without yielding of the plates. The failure load was about 5-8% higher than that of the failure load for the unplated (control) beam.

Beams anchored with angles at their ends failed after yielding of the plate subsequent to crushing of concrete within the constant moment region. The failure load was about 35% higher than the failure load for the unplated (control) beam.

Regarding the ductility of plated beams, when compared to that of the unplated specimens, using the load-deflection records it was shown that the beams without plate end anchorages were less ductile than the corresponding unplated beam(s), while the beams with plate end anchorages had the same ductility as the unplated (control) beam(s).

An interesting observation by these authors was that the use of bolts did not prevent occurrence of plate debonding, but prevented complete plate separation and increased the strength by only 8% over that of the unplated beam. It was concluded that the anchored plates with the angles were the most effective ones, producing yielding of the tensile plates and achieving the full theoretical strengths above the failure load of unplated beams.

In addition, it was reported that the specific details of plate end anchorage systems had no effect on the deflection performance in the service load regime, and that all the plated beams had approximately the same stiffness equivalent to that of the cracked plated section which had about 60% greater ultimate load than the corresponding unplated beams. The rate of plate strain and stress build-up within the plate anchorage zone was found to increase as the plate thickness was reduced, and very high interface bond stresses were reported within that zone in the vicinity of the plate ends, with a limiting value of plate end stresses approximately equal to $\sqrt{2 \times \text{tensile cylinder splitting strength of concrete}}$.

Another experimental study relating to the provision of end anchorages to externally bonded steel plates was reported by Jansze *et al.* (1996). These authors investigated the influence of plate bonded length and the use of a bolt to provide plate end anchorage. Reinforced concrete beams with cross section of 100x200 mm and a steel percentage ratio of 0.5% in conjunction with shear reinforcement in the form of 6 mm diameter links at 75 mm spacing were tested. Two reference beams were tested under symmetrical four-point loading with an effective span of 2400 mm - i.e. a shear span of 800 mm. One of the reference beams was not plated, while the other one had external steel plates with a thickness of 5 mm covering the whole 100 mm width of the beam. The plate was terminated 100 mm away from either support. The reference plated beam was found to fail by plate separation with flexural capacity having increased by a factor of 2.2 over that of the corresponding unplated reference beam.

Using specimens with a span of 800 mm but with plates clamped and the whole assembly configured to obtain the statically equivalent loading conditions as that of the reference (simply supported) plated beam, three plated specimens were tested with plates terminated by 100, 200 and 300 mm away from the support in order to study the effect of the plate length. As the terminated end of the plates moved closer to the support, significant increases in the beam load bearing capacity were achieved, but the final failure modes were found to be of a brittle nature. It was shown that a shorter length of the external plates significantly reduced the so-obtained ultimate loads. However, the maximum load was found to increase if the bonded plate was (at its end) anchored by a pre-stressed bolt.

To generate a more ductile mode of failure, and to study the effect of using bolts to provide extra plate end anchorage, different schemes of bolting were used. In one case, a 10 mm diameter bolt was used to anchor the end of the plate without exerting any tensile forces (i.e. pre-stressing) on the bolt. Under such conditions, the beam's load bearing capacity was slightly increased as the bolt acted as a kind of extra reinforcement crossing the separation (horizontal) crack. Similar diameter bolts with different pre-stressing forces were, then, used to generate a compression force on the adhesive layer as a preventative means against plate separation. Two different pre-stressing forces (namely, 10 and 25 kN) were used on the bolts. Generally, the initial overall flexural stiffness was not found to have been affected by the plate bolting, up to the initiation stages of the plate separation. Even when the plate separation cracks were initiated, the bolts were found to prevent total collapse of the specimens. In all the pre-stressed bolted plates, plate separation was found to occur at the interface between the epoxy glue and concrete which is totally different from the plate

separation mechanism within the concrete cover at the level of internal reinforcement which was the mechanism of plate peeling associated with the unbolted plates.

It was concluded that using pre-stressed bolts to anchor the end of the plate not only increased the load bearing capacity of the beam, but also changed the mechanism of plate separation failure from a brittle concrete cover rip-off to a more ductile type of failure at the interface between the concrete and the epoxy glue. In a preliminary study of the effect of cyclic loading on the behaviour of plated beams, it was concluded that (within their experimental range) the plate anchorage capacity was not sensitive to repeated loading.

Swamy *et al.* (1987) presented a comprehensive set of test data relating to the effect of glued steel plates on the first cracking load, general cracking behaviour, structural deformations, serviceability loads, and ultimate strength of reinforced concrete beams strengthened with steel plates bonded to their tension face. In total, twenty beams were tested with cross section dimensions of 155x255 mm, and the specimens were 2500 mm long. The beams were reinforced for flexure with an internal steel percentage ratio of 2.76%. The shear spans were provided with 6 mm diameter links at 75 mm spacing. The beams were tested as simply supported with a clear span of 2300 mm. They were loaded at the third points. The externally bonded steel plates were 2200 mm long.

In general, three different glue thicknesses equal to 1.5, 3, and 6 mm were used and, for each glue thickness, three different plate thicknesses were chosen (1.5, 3, and 6 mm). All the plates had a constant width of 125 mm. Some beams were strengthened

with more than one plate either as an additional one or by lapping to another at either mid-span or at the point loads at the supports. Certain beams were pre-loaded, cracked, and unloaded before the plates were bonded externally. The thickness for the adhesive was varied from 3 to 8 mm along the length of one beam. One beam had V notches induced in its tension face (at the external point loads) in order to produce points of stress concentration. Two beams were not plated and were used as control specimens, but one of them was provided with adhesive with a thickness of 3 mm in the absence of any external plate.

It was concluded that the addition of glued steel plates to reinforced concrete beams can substantially increase their flexural stiffness, reduce cracking and structural deformations at all load levels, and contribute to a modest increase in their ultimate flexural capacity. The restraining effect of the glue and the plate could be observed even on first cracking, and when the glue alone was present. The reduction in cracking and deformations were found to increase with increasing the plate and the glue thicknesses.

From a structural point of view, it was concluded that the stiffening effect was far more influential in reducing the axial strains in the reinforcing bars and the steel plate than in reducing deflections. Thus, the glued plates contributed more to controlling the cracking rather than the deflections. The structural effect of glued plate was also argued to be much greater than when the area of reinforcing bars had been increased by the same amount as that of the plate. The net effect of the reduced structural deformations is that the serviceability loads are substantially increased by the stiffening action of the external plates. Lapped plates, pre-cracking prior to plating,

variable glue thickness, and the presence of stress concentrations in the adhesive, were all found to have no adverse effect on the structural behaviour of the plated beams. It was argued that provided appropriate glues were chosen and adequate precautions were taken in the gluing procedure, the composite behaviour could be preserved up to failure. Moreover, the glued plates were found to increase the ultimate flexural capacity by 10 to 15 %, and this was argued to be satisfactorily predicted by the current ultimate limit state design procedures. These authors, however, recommended certain limitations on the plate width/thickness ratio, beyond which premature brittle shear/bond failure may occur without achieving the full flexural strength accompanied with the desired ductility.

Two tentative design criteria for plated beams were, therefore, proposed in order to ensure occurrence of their full flexural capacity and ductility at failure: firstly, the plate width/thickness ratio was recommended not to be less than 50; secondly, the neutral axis depth was suggested not to be greater than 0.4 times the effective depth.

In another experimental study to examine the applicability of the plate bonding technique to strengthen structurally damaged reinforced concrete, Swamy *et al.* (1989) conducted laboratory tests on nine beams with rectangular cross-sections. Their main objective was to study the structural implications of applying external plates to reinforced concrete beams that had already been loaded and had significantly cracked, and also the effect of external bonding of the plates when the beams were under load and were substantially cracked. For the latter case, seven beams were plated on their tension faces using glue of 1.5 mm thickness and steel plates with dimensions 1.5x125 mm and a length of 2200 mm. The other two beams were not plated: one was

manufactured with only a 3 mm glue thickness, and the other with no glue (to be used as a control beam). All these specimens were tested as simply supported with a clear span of 2300 mm, and were loaded at the third points. All these beams were identical in size (155x255x2500 mm), internally reinforced for flexure using steel bars with a steel percentage ratio of 2.76%, and were provided with 6 mm diameter shear links at 75 mm spacing within both of the shear spans in order to avoid shear failure.

Based on the value of the experimental ultimate flexural load capacity of the unplated control beam, two sets composed of three beams in each set, were loaded by different extents and were, then, tested when plated to simulate the repair process while the structure is in different conditions of use. In the first series, the beams were loaded at the age of 28 days to 30%, 50% and 70% of their ultimate load, and then strengthened using external plates while loaded. The external loads were sustained for 14 days subsequent to which the beams were tested to failure at an age of 42 days. In the second series, three beams were pre-loaded to the same loads as in the first series at the same age, unloaded, and were, then, strengthened with a similar set of external plates. They were, then, tested to failure at an age of 42 days.

As regards the test results for the beams initially loaded up to 70% of their ultimate flexural strength (which were either strengthened after unloading or while loaded), it was concluded that the epoxy resin adhesive ensures full composite action of structurally damaged reinforced concrete beams strengthened by externally bonded steel plates, and such a strengthening procedure results in increased stiffness and strength. Moreover, a flexible epoxy system was recommended to ensure that the adhesive layer does not crack prior to the beam failure, and, therefore, acts not only as

a stress transfer agent but also as a full participant in the structural resistance of the composite section.

As these beams were severely cracked prior to strengthening, and for the specimens which were strengthened while unloaded, it was concluded that the specific method of strengthening had no practically significant effect on the flexural behaviour of plated beams. The restraining effect of the plates on the existing cracks was, however, found to be more pronounced when the load was increased beyond the original pre-loading value. It was noticed that damaged beams, strengthened while under very high loads, showed deformations and crack widths slightly larger than those of the control beam plated when in an undamaged condition. But despite the increases in creep deformations during the epoxy curing, these deformations and crack widths were found to be less than those of the unplated (control) beam. Thus, it was suggested that plating severely damaged beams under load is structurally efficient and can restore a structural member to stiffness and strength conditions, perhaps, even better than the original undamaged beam. It was suggested that, when strengthening is carried out under external loads, the yield strain and plastic properties of the plates should be chosen in such a way as to enable the full structural exploitation of the added plates, even though they become active only beyond the applied pre-loads. With the increases in stiffness and strength borne in mind, it was mentioned that the external steel plates are able to restrain the opening of the tensile cracks and allow a high stress transfer within the cracks, resulting in an improved performance of concrete in the tension zone. Thus, a higher overall beam stiffness was suggested to be achieved by strengthening even damaged beams, compared to conventional (internal) reinforcement designed to achieve the same performance.

Regarding the plate peeling failure, Martins and Guimaräes (1996) carried out an experimental study on large (full scale) beams. They tested six beams with an effective span of 4800 mm and a 1200 mm long cantilever with a rectangular cross-section of 150x600 mm. Four of the tested beams were reinforced using thin plates with a thickness of 3.34 mm, while, the other two beams were reinforced with additional external rebars grouted with high resistance mortar to form a cage-like with overall cross-section dimensions of 200x700mm.

Their final conclusions placed much emphasis on the need for practically convenient devices to ensure plate end anchorage stability. It was stressed that, even in the case of glue failure, the existence of good anchorage devices will cause the beam to behave as a layered beam without bond between the materials which, as they described, is perfectly possible and acceptable as a guarantee for ductility of the beam. Fastening the plates to concrete was suggested as to be the most efficient and simple way to anchor such plates. Using external stirrups to press the plates against the concrete surface during the glue hardening period was advocated in order to avoid air bubbles, though it was admitted that this was more difficult to apply in practice.

Despite the availability of the extensive and wide ranging experimental studies in relation to various characteristics of externally strengthened reinforced concrete beams, there is, however, very limited data currently available in the public domain on the long-term performance and durability characteristics of these elements. This is of particular practical importance in terms of the long-term effectiveness of epoxy resin adhesives. In a series of publications, Calder (1979-1989) reported the results of

exposure tests on un-reinforced (plain) concrete beams of dimensions 102x102x508 mm, strengthened with external mild steel plates with dimensions 38x3x508 mm, which were loaded centrally. These tests were subsequently extended to include another series of beams with overall dimensions 150x250x3500 mm which were strengthened with external mild steel plates of dimensions 85x3x2800 mm. Two different epoxy resins (types I and II) were used to bond the plates to the beams in the second series: half the number of these beams were loaded in such a way as to produce cracking in the concrete prior to plating, and the other half of the test specimens were loaded centrally after plating. The beams were kept under external load for up to 8 years. Light corrosion was observed at the plate-resin interface of the beams bonded with resin type I, and the structural performance of these beams was not believed to have been adversely affected by the 8 year exposure period. Premature failure of the beams with plates bonded using resin type II led to the conclusion that this type of resin was of an inappropriate nature for such applications.

A comprehensive experimental programme on the structural behaviour of beams with externally bonded steel plates was undertaken by Swamy *et al.* (1995) who initially left reinforced concrete beams exposed in an industrial (polluted) area for periods of 11 to 12 years, following which the specimens were loaded to failure. The main variables in this study included the thickness of the adhesive layer, number of steel plates, presence and location of plate laps, and the loading regime (i.e. some were only stacked as unloaded, while others were kept under load). During the exposure period, the test specimens were purposely left exposed directly and continuously without any maintenance whatsoever, and were subjected to air, water, snow, and wind to pass through and circulate around them. No attempt were made to clean the beams or

remove the accumulated natural debris and remnants of water, snow or ice. Eight beams were kept under sustained load in specially designed creep test rigs and the other 13 were left unloaded. The loaded beams in the sustained loading rigs were simply supported over an effective span of 2300 mm, and loaded at the third points for the whole exposure period and, then, they were unloaded immediately before testing to failure. All the beams were identical in size and internal steel reinforcement. The beams with overall dimensions 155x255x2500 mm were reinforced with 3x20 mm diameter bars (2.76% flexural reinforcement ratio), and were provided with adequate shear reinforcement according to the British Standard: the shear spans had 6 mm diameter links at 75 mm centre to centre. The plates were bonded to the tension face of the reinforced concrete beams, and consisted of three main plating categories. The first category consisted of ten beams which were each reinforced with a single continuous plate. The second category consisted of six beams which had a jointed single plate system with lap plates at one or more locations. The third category consisted of five beams which had two layers of plates throughout their length.

One beam was tested after 18 months of exposure to give an idea about the short-term exposure, and a similar beam, but from another set, was tested after 28 days: this beam was used as a reference (control) plated beam for non-exposed behaviour. In their theoretical predictions of the failure load, full interaction between the plate and the beam was assumed, and the actual material properties at the time of the tests were used in their theoretical analysis (which was based on BS8110 (1985) with the material partial safety factors removed). Their durability study led to the following conclusions

- The overall condition and structural performance of the plated beams was very satisfactory despite the complete lack of maintenance during the 11-12 year exposure period.
- Deflections and crack widths at service load levels of beams tested after exposure were similar to or less than those of the control plated beam.
- Failure loads of the plated beams after exposure were 1% to 29% higher than the failure load of the equivalent short-term control plated beam.
- The extent of corrosion arising from the exposure, and its effect on structural performance, varied markedly with the plating system. As a result, failure in some of the exposed beams occurred in modes other than the originally anticipated flexural yielding, although most of the beams showed a good degree of ductility at failure and failed at loads in excess of 90% of the theoretical failure load for the plated beams (allowance being made for the increased concrete strength).
- Beams with a single continuous plate showed (on average) no adverse effect due to exposure, and these beams carried a higher load (by some 10%) than the theoretical prediction.
- Beams with a jointed single-layer plate system with lap plates at one or more positions showed some corrosion between the plates. These beams suffered from shear failure or lap bond failure, resulting in concrete anchorage zone failure at the joint. However, the failure loads were reduced by only 3 to 4% below the theoretical value.
- In beams with two layers of plates throughout their length, there were areas of corrosion between the outer and the inner plates in some of the beams, and these

specimens showed reduced failure loads by 5-6% when compared with the control beam (possibly because of the reduced plate width/thickness ratio).

- The plating system proved to be very tolerant to even fairly large areas of corrosion, and no deterioration in structural performance occurred other than in those cases of very severe plate corrosion.

- Great care was urged in attending to details in the plate bonding system, and in the application and maintenance of a protective system in vulnerable areas such as interfaces between the plate layers, corners, and ends of the plates.

- Since the anchorage zone appeared to be particularly vulnerable to deterioration, the provision of end U-shaped anchor plates was strongly recommended (wherever possible) even if they were theoretically not taken into account. Alternatively, in a continuous soffit (e.g. slabs), the use of anchor bolts was recommended.

- In beams with multiple-plates, the design rules relating to acceptable plate width/thickness ratio were suggested to be strictly observed for the total range of plate thicknesses.

- It was finally concluded that with careful detailing and adequate maintenance, the use of a plate bonding system for strengthening and rehabilitating concrete structures can be durable and reliable, and may be carried out with confidence.

2.3 CONCLUSION

The literature on the experimental studies relating to reinforced concrete beams strengthened with externally bonded steel and/or fibre reinforced plastic (FRP) plates has been reviewed in considerable detail. In a number of areas, it is evident that there is an undue amount of repetition and imprecise conclusions. Details of the individual

experiments have nevertheless been presented in view of the fact that a considerable number of test results will be used in the subsequent chapters (Chapters 3, 4, 7, and 8) for verifying different aspects of the theoretical works of others in addition to the present work. The experimental work, reported by others, has covered many aspects such as the effect of plate and beam dimensions, external loading configurations, characteristics of the materials involved, and the schemes of plating, on the plated beams' structural performance such as ultimate strength, flexural stiffness, serviceability, cracking, durability, and fatigue strength. Depending on the extent of completeness of the published data, certain geometrical and material data from different sources are given in Table (2.1) for beams plated with external FRP plates, and in Table (2.2) for beams with steel plates: these include the basic data regarding the beam configurations, dimensions and strength of materials. In the following, a summery may be presented for the common conclusions by various researchers

1- Regarding the ultimate strength, using external plates generally increases the load bearing capacity of the plated beam, provided that the thickness of the plate (i.e. the cross-section area) does not exceed a certain limit.

2- Regarding the mode of failure, it is concluded that extending the ends of the plate to the supports, avoiding thick plates, and using appropriate anchorage at the ends of the plate, may ensure largely ductile behaviour at failure.

3- Regarding the flexural stiffness, in general, external plating improves the cracking behaviour by reducing the crack widths and spacing. It also delays formation of initial cracks, increases the flexural stiffness and the level of service loads.

4- Strengthening of the beams with external plates has by and large been successful in terms of durability and resistance to harsh outdoor weather conditions.

5- At the serviceability load levels, it is concluded that fatigue loading is not expected to cause failure, and the maximum values of axial stresses in the internal reinforcement, located in the vicinity of the concrete cracks, are reduced in the presence of external plating.

6- Increasing the thickness of the plate has been found to tend to cause brittle failure and in some cases would reduce the load bearing capacity to such levels which are lower than the unplated beam capacity. The same conclusion is applicable in relation to the cross-section area of the plate.

Table 2.1 - Various geometrical and material parameters for the reinforced concrete beams upgraded with external FRP plates.

Beam	Beam dimensions		Compression bars			Tension bars			Net cover h' (mm)	h_1 (mm)	Concrete		Steel bars		Plate		Shear span L_ω (mm)	L_p (mm)	Plate	
	Width b, (mm)	Depth (mm)	No.	Φ (mm)	Cover (mm)	No.	Φ (mm)	Cover (mm)			f_{cu} MPa	E_c GPa	f_y MPa	E_s GPa	Width b_p (mm)	Thickness t_p (mm)			f_p MPa	E_p GPa
H-A1b	100	100	2	6	15	3	6	15	12	15	70	35	440	210	80	1.2	300	280	1078.9	49
H-A1c	100	100	2	6	15	3	6	15	12	15	70	35	440	210	80	1.2	300	280	1078	49
H-A2b	100	100	2	6	15	3	6	15	12	15	42	35	440	210	80	1.2	300	280	1078	49
H-A2c	100	100	2	6	15	3	6	15	12	15	42	35	440	210	80	1.2	300	280	1078	49
H-A2d	100	100	2	6	15	3	6	15	12	15	42	35	440	210	80	1.2	300	280	1078	49
H-A2e	100	100	2	6	15	3	6	15	12	15	42	35	440	210	80	1.2	300	280	1078	49
H-A2f	100	100	2	6	15	3	6	15	12	15	42	35	440	210	80	1.2	300	280	1078.5	49
H-A2g	100	100	2	6	15	3	6	15	12	15	42	35	440	210	80	1.2	300	150	1078	49
H-A2h	100	100	2	6	15	3	6	15	12	15	42	35	440	210	80	1.2	300	280	1078	49
H-B2	100	100	2	6	15	3	6	15	12	15	53	34	440	215	80	1.2	300	280	1078	49
H-B3	100	100	2	6	15	3	6	15	12	15	53	34	440	215	30	1.2	300	280	1078	49
H-B4	100	100	2	6	15	3	6	15	12	15	53	34	440	215	60	1.6	300	280	1078	49
H-B5	100	100	2	6	15	3	6	15	12	15	53	34	440	215	80	1.2	300	280	1078	49
H-B6	100	100	2	6	15	3	6	15	12	15	53	34	440	215	80	1.2	300	280	987	118.5
H-B7	100	100	2	6	15	3	6	15	12	15	53	34	440	215	80	1.2	300	300	987	118.5
H-B8	100	100	2	6	15	3	6	15	12	15	53	34	440	215	80	1.2	300	280	987	118.5
H-B9	100	100	2	6	15	3	6	15	12	15	53	34	440	215	80	1.2	300	280	987	118.5
H-B10	100	100	2	6	15	3	6	15	12	15	53	34	440	215	65	1.2	300	300	987	118.5

Table 2.1 - Continued

Beam	Beam dimensions		Compression bars			Tension bars			Net cover h' (mm)	h_1 (mm)	Concrete		Steel bars		Plate		Shear span L_ω (mm)	L_p (mm)	Plate	
	Width b, (mm)	Depth (mm)	No.	Φ (mm)	Cover (mm)	No.	Φ (mm)	Cover (mm)			f_{cu} MPa	E_c GPa	f_y MPa	E_s GPa	Width b_p (mm)	Thickness t_p (mm)			f_p MPa	E_p GPa
H-1Au	100	100	2	6	16	3	6	16	13	16	59.1	33.5	436	215	90	0.5	300	299	1273	111
H-2Au	100	100	2	6	16	3	6	16	13	16	59.1	33.5	436	215	90	0.5	340	339	1273	111
H-3Au	100	100	2	6	16	3	6	16	13	16	59.1	33.5	436	215	90	0.5	400	399	1273	111
H-2Aa	100	100	2	6	16	3	6	16	13	16	59.1	33.5	436	215	90	0.5	340	339	1273	111
H-2A2a	100	100	2	6	16	3	6	16	13	16	59.1	33.5	436	215	90	0.5	340	339	1273	111
H-2A3a	100	100	2	6	16	3	6	16	13	16	59.1	33.5	436	215	90	0.5	340	339	1273	111
H-1Bu	100	100	2	6	16	3	6	16	13	16	59.1	33.5	436	215	65	0.7	300	299	1273	111
H-1B2u	100	100	2	6	16	3	6	16	13	16	59.1	33.5	436	215	65	0.7	300	299	1273	111
H-2Bu	100	100	2	6	16	3	6	16	13	16	59.1	33.5	436	215	65	0.7	340	339	1273	111
H-3Bu	100	100	2	6	16	3	6	16	13	16	59.1	33.5	436	215	65	0.7	400	399	1273	111
H-2Ba	100	100	2	6	16	3	6	16	13	16	59.1	33.5	436	215	65	0.7	340	339	1273	111
H-2B2a	100	100	2	6	16	3	6	16	13	16	59.1	33.5	436	215	65	0.7	340	339	1273	111
H-1Cu	100	100	2	6	16	3	6	16	13	16	59.1	33.5	436	215	45	1.0	300	299	1273	111
H-2Cu	100	100	2	6	16	3	6	16	13	16	59.1	33.5	436	215	45	1.0	340	339	1273	111
H-3Cu	100	100	2	6	16	3	6	16	13	16	59.1	33.5	436	215	45	1.0	400	399	1273	111
H-2Ca	100	100	2	6	16	3	6	16	13	16	59.1	33.5	436	215	45	1.0	340	339	1273	111
CC	205	455	2	13	55	2	13	55	48.5	55	43.8	29.7	456	200	152	6.0	1983	1828	400	37.2
AA	205	455	2	13	55	3	25	55	42.5	55	43.8	29.7	456	200	152	6.0	1983	1828	400	37.2
BB	205	455	2	13	55	2	25	55	42.5	55	43.8	29.7	456	200	152	6.0	1983	1828	400	37.2
DD	205	455	2	13	55	2	25	55	42.5	55	43.8	29.7	456	200	152	6.0	1983	1828	400	37.2

Table 2.1 - Continued

Beam	Beam dimensions		Compression bars			Tension bars			Net cover	h_1	Concrete		Steel bars		Plate		Shear span	L_p	Plate	
	Width b, (mm)	Depth (mm)	No.	Φ (mm)	Cover (mm)	No.	Φ (mm)	Cover (mm)	h' (mm)	(mm)	f_{cu} MPa	E_c GPa	f_y MPa	E_s GPa	Width b_p, (mm)	Thickness t_p, (mm)	L_ω (mm)	(mm)	f_p MPa	E_p GPa
C	152	305	0	0	1	2	12.7	54	47.6	54	49.7	22.8	413.8	200	152	4.8	915	711	160.7	11.7
D	152	305	0	0	1	2	12.7	54	47.6	54	49.7	22.8	413.8	200	151	4.8	915	711	160.7	11.7
E	152	305	0	0	1	2	12.7	54	47.6	54	53.7	25.5	413.8	200	153	4.8	915	656	160.7	11.7
F	152	305	0	0	1	2	12.7	54	47.6	54	49.7	22.8	413.8	200	153	9.5	915	693	160.7	11.7
G	152	305	0	0	1	2	12.7	54	47.6	54	53.7	25.5	413.8	200	152	4.2	915	914	184.1	10.3
H	152	305	0	0	1	2	12.7	54	47.6	54	53.7	25.5	413.8	200	152	9.3	915	711	241.4	20.7
I	152	305	0	0	1	2	12.7	54	47.6	54	49.7	22.8	413.8	192	150	4.1	915	711	319.3	27.6
J	152	305	0	0	1	2	12.7	54	47.6	54	49.7	22.8	413.8	198	152	3.2	915	584	590.3	30.3
K	152	305	0	0	1	2	12.7	54	47.6	54	53.7	25.5	413.8	200	152	3.2	915	584	590.3	30.3
L	152	305	0	0	1	2	12.7	54	47.6	54	49.7	22.8	413.8	200	152	1.3	915	914	613.8	54.5
M	152	305	0	0	1	2	12.7	54	47.6	54	53.7	25.5	413.8	200	152	1.3	915	914	1489.7	117.9
N	152	305	0	0	1	2	12.7	54	47.6	54	49.7	22.8	413.8	200	153	6.4	915	610	1172.4	72.4
F-P1	150	150	2	6	36	2	10	36	31	36	47.1	27	450	200	100	1.0	393	318	170	14.9
F-P2	150	150	2	6	36	2	10	36	31	36	47.1	27	450	200	100	2.0	393	318	170	14.9
F-P3	150	150	2	6	36	2	10	36	31	36	47.1	27	450	200	100	3.0	393	318	170	14.9
F-P2B	150	150	2	6	36	2	10	36	31	36	47.1	27	450	200	100	2.0	393	318	170	14.9
F-P3B	150	150	2	6	36	2	10	36	31	36	47.1	27	450	200	100	3.0	393	318	170	14.9
F-P2BW	150	150	2	6	36	2	10	36	31	36	47.1	27	450	200	100	2.0	393	318	170	14.9
F-P3BW	150	150	2	6	36	2	10	36	31	36	47.1	27	450	200	100	3.0	393	318	170	14.9
F-P3J	150	150	2	6	36	2	10	36	31	36	47.1	27	450	200	100	3.0	393	343	170	14.9

Table 2.2 - Various geometrical and material parameters for the reinforced concrete beams upgraded with external STEEL plates.

Beam	Beam dimensions		Compression bars			Tension bars			Net cover h' (mm)	h_1 (mm)	Concrete		Steel bars		Plate		Shear span L_∞ (mm)	L_p (mm)	Plate	
	Width b, (mm)	Depth (mm)	No.	Φ (mm)	Cover (mm)	No.	Φ (mm)	Cover (mm)			f_{cu} MPa	E_c GPa	f_y MPa	E_s GPa	Width b_p (mm)	Thickness t_p (mm)			f_p MPa	E_p GPa
URB5	100	150	0	0	1	2	10	20	15	20	67.4	35.8	530	200	80	10.0	750	700	240	200
B1	150	150	0	0	1	2	10	30	25	30	47.1	27.3	414	200	100	3.0	400	350	276	200
C11	100	150	0	0	1	2	8	25	21	25	93	40	490	200	80	1.6	250	200	175	200
C12	100	150	0	0	1	2	8	25	21	25	93	40	490	200	80	1.6	365	315	175	200
MF1	150	150	0	0	1	2	12	30	24	30	49.9	27.8	414	200	100	3.0	400	350	264	200
FRB5	150	150	0	0	1	2	10	30	25	30	47.1	27.3	414	200	100	2.0	400	350	276	200
URB4	100	150	0	0	1	2	10	20	15	20	67.4	35.8	530	200	80	5.0	750	700	217.5	200
F31	155	255	0	0	1	3	20	35	25	35	57.9	32	432	200	125	6.0	767	717	291	200
205	155	255	0	0	1	3	20	35	25	35	72.3	36	470	200	125	6.0	767	717	248	200
209	155	255	0	0	1	3	20	35	25	35	72.3	36	470	200	125	6.0	767	717	248	200
218	155	255	0	0	1	3	20	35	25	35	72.3	36	470	200	125	6.0	767	717	248	200
204	155	255	0	0	1	3	20	35	25	35	72.3	36	470	200	125	3.0	767	717	258	200
208	155	255	0	0	1	3	20	35	25	35	72.3	36	470	200	125	3.0	767	717	258	200
217	155	255	0	0	1	3	20	35	25	35	72.3	36	470	200	125	3.0	767	717	258	200
203	155	255	0	0	1	3	20	35	25	35	72.3	36	470	200	125	1.5	767	717	236	200
C3	100	150	0	0	1	2	8	25	21	25	93	40	490	200	80	1.6	550	500	175	200
C5	100	150	0	0	1	2	8	25	21	25	93	40	490	200	80	1.6	550	500	175	200

Table 2.2 - Continued.

Beam	Beam dimensions		Compression bars			Tension bars			Net cover	h_1 (mm)	Concrete		Steel bars		Plate		Shear span	L_p (mm)	Plate	
	Width b, (mm)	Depth (mm)	No.	Φ (mm)	Cover (mm)	No.	Φ (mm)	Cover (mm)	h' (mm)		f_{cu} MPa	E_c GPa	f_y MPa	E_s GPa	Width b_p, (mm)	Thickness t_p, (mm)	L_{av} (mm)		f_p MPa	E_p GPa
C7	100	150	0	0	1	2	8	25	21	25	93	40	490	200	80	1.6	550	500	175	200
C16	100	150	0	0	1	2	8	25	21	25	93	40	490	200	80	1.6	550	500	175	200
FRB2	150	150	0	0	1	2	10	30	25	30	47.1	27.3	414	200	100	1.0	400	350	276	200
URB2	100	150	0	0	1	2	10	20	15	20	67.4	35.8	530	192	80	1.5	750	700	216.6	192
B10	150	150	0	0	1	2	10	30	25	30	47.1	27.3	414	200	100	1.5	400	350	276	200
URB3	100	150	0	0	1	2	10	20	15	20	104	44.4	530	198	80	3.0	750	700	263	198
F11	155	255	0	0	1	3	20	35	25	35	56.6	32	430	200	125	1.5	767	717	240	200
207	155	255	0	0	1	3	20	35	25	35	72.3	36	470	200	125	1.5	767	717	236	200
216	155	255	0	0	1	3	20	35	25	35	72.3	36	470	200	125	1.5	767	717	236	200
O	152	305	0	0	1	2	12.7	54	47.6	54	53.7	25.5	413.8	200	153	2.6	915	711	206.9	200
P	152	305	0	0	1	2	12.7	54	47.6	54	53.7	25.5	413.8	200	150	2.5	915	914	206.9	200
1/2/S	130	175	2	10	30	2	16	28	20	28	52.5	22	444	210	130	5.0	550	450	272	210
1/2/N	130	175	2	10	30	2	16	28	20	28	52.5	22	444	210	130	5.0	550	400	272	210
1/3/S	130	175	2	10	30	2	16	28	20	28	52.5	22	444	210	130	5.0	550	300	272	210
1/3/N	130	175	2	10	30	2	16	28	20	28	52.5	22	444	210	130	5.0	550	150	272	210
1/4/S	130	175	2	10	30	2	16	28	20	28	52.5	22	444	210	130	5.0	550	500	272	210
2/1/S	130	175	2	10	30	2	16	28	20	28	57	29	444	210	130	5.0	550	475	272	210
2/1/N	130	175	2	10	30	2	16	28	20	28	57	29	444	210	130	5.0	550	250	272	210
2/2/N	130	175	2	10	30	2	16	28	20	28	57	29	444	210	130	5.0	550	250	272	210

Table 2.2 - Continued.

Beam	Beam dimensions		Compression bars			Tension bars			Net cover	h_1 (mm)	Concrete		Steel bars		Plate		Shear span	L_p (mm)	Plate	
	Width b_s (mm)	Depth (mm)	No.	Φ (mm)	Cover (mm)	No.	Φ (mm)	Cover (mm)	h' (mm)		f_{cu} MPa	E_c GPa	f_y MPa	E_s GPa	Width b_p (mm)	Thickness t_p (mm)	L_{cp} (mm)		f_p MPa	E_p GPa
2/2/S	130	175	2	10	30	2	16	28	20	28	57	29	444	210	130	5.0	550	475	272	210
2/3/N	130	175	2	10	30	2	16	28	20	28	57	29	444	210	130	5.0	550	250	272	210
2/3/S	130	175	2	10	30	2	16	28	20	28	57	29	444	210	130	5.0	550	475	272	210
2/4/N	130	175	2	10	30	2	16	28	20	28	57	29	444	210	130	5.0	550	250	272	210
2/4/S	130	175	2	10	30	2	16	28	20	28	57	29	444	210	130	5.0	550	475	272	210
5/1/N	130	175	2	10	30	2	16	28	20	28	59	29	444	210	130	5.0	550	150	272	210
5/1/S	130	175	2	10	30	2	16	28	20	28	59	29	444	210	130	5.0	550	400	272	210
6/1/-	130	175	2	10	30	2	16	28	20	28	63	30	444	210	130	5.0	925	300	272	210
6/2/-	130	175	2	10	30	2	16	28	20	28	63	30	444	210	130	5.0	925	300	272	210
6/3/-	130	175	2	10	30	2	16	28	20	28	63	30	444	210	130	5.0	1125	300	272	210
6/4/-	130	175	2	10	30	2	16	28	20	28	63	30	444	210	130	5.0	1225	400	272	210
7/1/N	130	175	2	10	30	2	16	28	20	28	59	32	444	210	130	5.0	1400	400	272	210
7/1/S	130	175	2	10	30	2	16	28	20	28	59	32	444	210	130	5.0	1400	400	272	210
8/1/N	130	175	2	10	30	2	16	28	20	28	47	27	444	210	130	5.0	1700	400	272	210
8/1/S	130	175	2	10	30	2	16	28	20	28	47	27	444	210	130	5.0	1700	400	272	210
1/1/N*	130	175	2	10	30	2	16	28	20	28	52.5	22	444	210	130	5.0	550	549	272	210
7/2/*	130	175	2	10	30	2	16	28	20	28	59	32	444	210	130	5.0	1000	999	272	210
8/2/*	130	175	2	10	30	2	16	28	20	28	47	27	444	210	130	5.0	775	774	272	210

Table 2.2 - Continued.

Beam	Beam dimensions		Compression bars			Tension bars			Net cover h' (mm)	h_1 (mm)	Concrete		Steel bars		Plate		Shear span L_∞ (mm)	L_p (mm)	Plate	
	Width b, (mm)	Depth (mm)	No.	Φ (mm)	Cover (mm)	No.	Φ (mm)	Cover (mm)			f_{cu} MPa	E_c GPa	f_y MPa	E_s GPa	Width b_p, (mm)	Thickness t_p, (mm)			f_p MPa	E_p GPa
1/1	125	150	2	12	36	2	16	38	30	38	48	28	444	210	125	3.0	NA	NA	272	210
1/2	125	150	2	12	36	2	16	38	30	38	48	28	444	210	125	3.0	NA	NA	272	210
2/1	125	150	2	12	26	2	16	28	20	28	34	25	444	210	125	5.0	NA	NA	272	210
2/2	125	150	2	12	26	2	16	28	20	28	34	25	444	210	125	5.0	NA	NA	272	210
3/1	125	150	2	12	26	2	16	28	20	28	28	28	444	210	125	3.0	NA	NA	272	210
3/2	125	150	2	12	26	2	16	28	20	28	28	28	444	210	125	3.0	NA	NA	272	210
3/3	125	150	2	12	26	2	16	28	20	28	28	28	444	210	125	3.0	NA	NA	272	210
3/4	125	150	2	12	26	2	16	28	20	28	28	28	444	210	125	3.0	NA	NA	272	210
4/1	125	150	2	12	26	2	16	28	20	28	45	25	444	210	125	5.0	NA	NA	272	210
4/2	125	150	2	12	26	2	16	28	20	28	45	25	444	210	125	5.0	NA	NA	272	210
4/3	125	150	2	12	26	2	16	28	20	28	44	26	444	210	125	5.0	NA	NA	272	210
4/4	125	150	2	12	26	2	16	28	20	28	44	26	444	210	125	5.0	NA	NA	272	210
5/1	125	150	2	12	26	2	16	28	20	28	44	30	444	210	125	5.0	NA	NA	272	210
5/2	125	150	2	12	26	2	16	28	20	28	44	30	444	210	125	5.0	NA	NA	272	210
5/3	125	150	2	12	26	2	16	28	20	28	43	27	444	210	125	5.0	NA	NA	272	210
5/4	125	150	2	12	26	2	16	28	20	28	43	27	444	210	125	5.0	NA	NA	272	210
6/1	125	150	2	12	26	2	16	28	20	28	36	29	444	210	125	5.0	NA	NA	272	210
6/2	125	150	2	12	26	2	16	28	20	28	36	29	444	210	125	5.0	NA	NA	272	210

Table 2.2 - Continued.

Beam	Beam dimensions		Compression bars			Tension bars			Net cover	h_1 (mm)	Concrete		Steel bars		Plate		Shear span	L_p (mm)	Plate	
	Width b, (mm)	Depth (mm)	No.	Φ (mm)	Cover (mm)	No.	Φ (mm)	Cover (mm)	h' (mm)		f_{cu} MPa	E_c GPa	f_y MPa	E_s GPa	Width b_p (mm)	Thickness t_p (mm)	L_ω (mm)		f_p MPa	E_p GPa
6/3	125	150	2	12	26	2	16	28	20	28	36	23	444	210	125	5.0	NA	NA	272	210
6/4	125	150	2	12	26	2	16	28	20	28	36	23	444	210	125	5.0	NA	NA	272	210
7/1	120	200	2	12	26	2	16	28	20	28	35	33	444	210	120	5.0	NA	NA	272	210
7/2	120	200	2	12	26	2	16	28	20	28	35	33	444	210	120	5.0	NA	NA	272	210
7/3	120	200	2	12	26	2	16	28	20	28	34	28	444	210	120	5.0	NA	NA	272	210
7/4	120	200	2	12	26	2	16	28	20	28	34	28	444	210	120	5.0	NA	NA	272	210
8/1	120	200	2	12	26	2	16	28	20	28	37	37	444	210	120	5.0	NA	NA	272	210
8/2	120	200	2	12	26	2	16	28	20	28	37	37	444	210	120	5.0	NA	NA	272	210
8/3	120	200	2	12	26	2	16	28	20	28	35	24	444	210	120	5.0	NA	NA	272	210
8/4	120	200	2	12	26	2	16	28	20	28	35	24	444	210	120	5.0	NA	NA	272	210
9/1	125	150	2	12	26	2	16	28	20	28	38	23	444	210	125	3.0	NA	NA	272	210
9/2	125	150	2	12	26	2	16	28	20	28	38	23	444	210	125	3.0	NA	NA	272	210
9/3	125	150	2	12	26	2	16	28	20	28	29	23	444	210	125	3.0	NA	NA	272	210
9/4	125	150	2	12	26	2	16	28	20	28	29	23	444	210	125	3.0	NA	NA	272	210
10/1	120	180	2	12	26	2	16	28	20	28	33	26	444	210	120	10.0	NA	NA	272	210
10/2	120	180	2	12	26	2	16	28	20	28	33	26	444	210	120	10.0	NA	NA	272	210
10/3	120	180	2	12	26	2	16	28	20	28	37	23	444	210	120	6.5	NA	NA	272	210
10/4	120	180	2	12	26	2	16	28	20	28	37	23	444	210	120	6.5	NA	NA	272	210
11/1	120	180	2	12	26	2	16	28	20	28	34	26	444	210	120	3.0	NA	NA	272	210
11/2	120	180	2	12	26	2	16	28	20	28	34	26	444	210	120	3.0	NA	NA	272	210

Table 2.2 - Continued.

Beam	Beam dimensions		Compression bars			Tension bars			Net cover	h_1 (mm)	Concrete		Steel bars		Plate		Shear span	L_p (mm)	Plate	
	Width b, (mm)	Depth (mm)	No.	Φ (mm)	Cover (mm)	No.	Φ (mm)	Cover (mm)	h' (mm)		f_{cu} MPa	E_c GPa	f_y MPa	E_s GPa	Width b_p (mm)	Thickness t_p (mm)	L_ω (mm)		f_p MPa	E_p GPa
11/3	120	180	2	12	26	2	16	28	20	28	36	32	444	210	120	15.0	NA	NA	272	210
11/4	120	180	2	12	26	2	16	28	20	28	36	32	444	210	120	15.0	NA	NA	272	210
12/1	120	180	2	12	26	2	16	28	20	28	30	23	444	210	100	10.0	NA	NA	272	210
12/2	120	180	2	12	26	2	16	28	20	28	30	23	444	210	50	10.0	NA	NA	272	210
12/3	120	180	2	12	26	2	16	28	20	28	36	32	444	210	25	10.0	NA	NA	272	210
12/4	120	180	2	12	26	2	16	28	20	28	36	32	444	210	75	10.0	NA	NA	272	210
13/6	120	200	2	12	16	2	16	18	10	18	42	21	444	210	120	5.0	NA	NA	272	210
13/7	120	240	2	12	16	2	16	18	10	18	41	22	444	210	120	5.0	NA	NA	272	210
13/9	120	160	2	12	16	2	16	18	10	18	46	25	444	210	120	2.0	NA	NA	272	210
13/10	120	160	2	12	16	2	16	18	10	18	46	25	444	210	120	2.0	NA	NA	272	210
13/11	120	160	2	12	16	2	16	18	10	18	35	26	444	210	120	5.0	NA	NA	272	210
13/13	120	160	2	12	36	2	16	38	30	38	37	20	444	210	120	2.0	NA	NA	272	210
13/14	120	160	2	12	36	2	16	38	30	38	37	20	444	210	120	5.0	NA	NA	272	210
13/15	120	160	2	12	36	2	20	40	30	40	33	22	444	210	120	2.0	NA	NA	272	210
13/16	120	160	2	12	36	2	20	40	30	40	33	22	444	210	120	5.0	NA	NA	272	210
13/17	120	160	2	12	56	2	16	58	50	58	43	24	444	210	120	6.0	NA	NA	272	210
13/18	120	160	2	12	56	2	16	58	50	58	43	24	444	210	120	2.0	NA	NA	272	210
13/19	120	160	2	10	35	2	12	36	30	36	43	21	444	210	120	2.0	NA	NA	272	210
13/20	120	160	2	10	35	2	12	36	30	36	43	21	444	210	120	5.0	NA	NA	272	210

Chapter 3

CRITICAL EXAMINATION OF VARIOUS METHODS FOR PREDICTING THE PLATE PEELING LOAD

Chapter 3

CRITICAL EXAMINATION OF VARIOUS METHODS FOR PREDICTING THE PLATE PEELING LOAD

3.1 INTRODUCTION

In this chapter, a critical examination of various methods for the prediction of plate peeling failure in reinforced concrete beams strengthened/upgraded with external plates will be carried out. Attention will be devoted to examining the most promising methods in some detail, while certain other approaches will also be briefly reviewed. The predictions of so-examined methods will be checked against a wide range of experimental data previously reported by others as discussed in Chapter 2.

The most promising methods are developed by Zhang *et al.* (1995), Sharif *et al.* (1994), Baluch *et al.* (1995) and Oehlers and Moran (1990). The method developed by Zhang *et al.* (1995) will be shown to predict safe values for the plate peeling capacity of uncracked reinforced concrete beams strengthened with external steel plates and, in particular, it enables one to identify the first order beam design parameters which control the plate peeling phenomenon.

In a number of cases, the analytical methods are based on the approximate analysis of shear and normal stresses within the adhesive layer of the plated reinforced concrete beams as proposed by Roberts (1989) and Roberts and Haji-Kazemi (1989); this method will, therefore, be presented first followed by a detailed review of other available models.

3.2 APPROXIMATE ANALYSIS OF SHEAR AND NORMAL STRESSES WITHIN THE ADHESIVE LAYER

Roberts (1988, 1989) and Roberts and Haji-Kazemi (1989) have presented a purely theoretical (and approximate) analysis for predicting the magnitudes of shear and normal stresses within the adhesive layer located between the reinforced concrete beam and the external plate. To simplify the derivations, the process was divided into three stages. During the first stage, the stresses were determined assuming presence of full composite action between the concrete beam and the external steel plate. In the course of the second and third stages, the model was modified to take the actual boundary conditions at the ends of the steel plate into account. The complete solution was, then, obtained by superposition.

A number of simplifying assumptions was made in order to obtain a relatively simple solution. One simplifying assumption (related to the second and third stages) was that the steel plate is bonded to a rigid concrete beam, neglecting the effect of flexibility in the concrete. Another assumption was that the curvatures (at the end of the plate) of both the concrete beam and the steel plate were equal and, hence, the global straining actions in that location were assumed to be distributed between the steel plate and the concrete beam, in proportion to their section stiffnesses.

For a beam with geometrical details as shown in Figures 3.1 and 3.2, the governing differential equations were derived and solved, employing reasonable boundary conditions. One of the assumed boundary conditions was that the relative displacements between the steel plate and the rigid concrete beam, are decreased in magnitude as one moves away from one end of the plate and approaches the other

end; gradually tending to zero. Obviously (due to the symmetry of the problem), this reduction in relative displacements is expected not to continue up to the other end, as there will also exist similar trends of changes in displacements being initiated at the other end of the plate. To cater for this, the mirror image of the problem was considered in the solution procedure, with each term in the equations (which was related to the far end of the plate) being expressed as that corresponding to the nearest end.

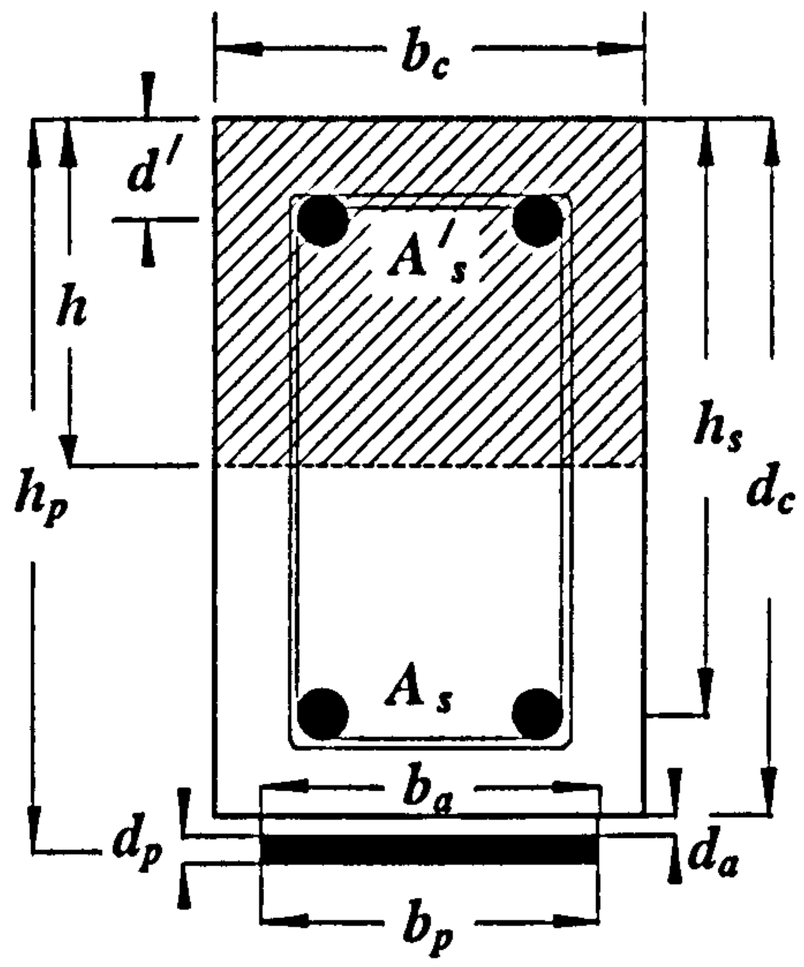

Fig. 3.1 Typical cross-section of plated reinforced concrete beams .

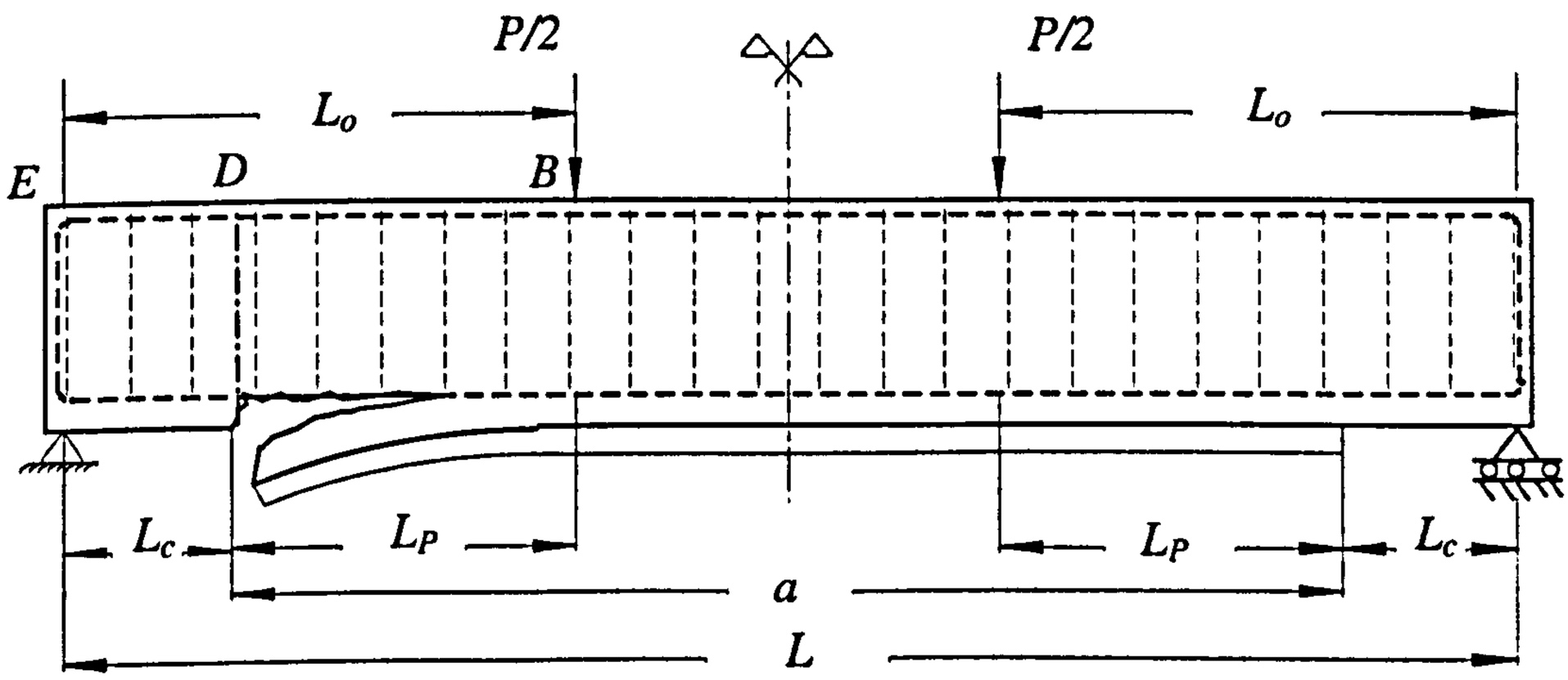

Fig. 3.2 A typical plate peeling failure for a reinforced concrete beam upgraded with externally bonded plate.

A further simplification was made which involved assuming $\cosh \alpha a = \sinh \alpha a$, where a is the length of the plate as in Figure 3.2 and $\alpha = \sqrt{K_s / (E_p b_p d_p)}$, with K_s and E_p representing the shear stiffness of the adhesive and the modulus of elasticity of the bonded plate, respectively, and b_p and d_p denoting the plate width and thickness, respectively.

The approximate magnitude of shear stresses within the adhesive layer located at the end of the plate, τ_o, was, then, found to be given by the following:

$$\tau_o = \left(F_o + \left(\frac{K_s}{E_p b_p d_p}\right)^{1/2} M_o \right) \frac{b_p d_p}{I b_a} (h_p - h) \tag{3.1}$$

with the approximate values of normal stresses at this same location, σ_o, given by

$$\begin{aligned} \sigma_o &= \tau_o d_p \left\{ \frac{K_n}{4 E_p I_p} \right\}^{1/4} \\ &= \left\{ \frac{K_n}{4 E_p I_p} \right\}^{1/4} \left(F_o + \left(\frac{K_s}{E_p b_p d_p}\right)^{1/2} M_o \right) \frac{b_p d_p^2}{I b_a} (h_p - h) \end{aligned} \tag{3.2}$$

where, F_o and M_o are the shear force and the bending moment, respectively, acting on the section of the beam located at the end of the plate, K_n is the normal stiffness of the adhesive. K_n and K_s are given by $K_n = E_a b_a / d_a$ and $K_s = G_a b_a / d_a$ with E_a and G_a being the Young's and shear moduli of the adhesive material, respectively. b_a and d_a denote the width and the thickness of the adhesive layer, respectively, with h_p and h representing the depth of the centre of gravity of the plate and the concrete stress block in compression (as measured from the top fibre of concrete section), respectively.

To check the accuracy of this approximate method, Roberts compared the so- obtained results with the corresponding ones based on a so-called more accurate theoretical analysis as proposed elsewhere (Roberts *et al.* (1989)) in which the analysis was based on the partial interaction theory. The comparisons between these two alternative methods indicated that the proposed approximate solution may underestimate the magnitudes of stress concentrations by up to 30% and such differences were attributed to the approximation made in the first stage of the analysis which assumed the presence of full composite action between the concrete beam and the externally bonded steel plate. To improve the accuracy of the approximate results, it was recommended that one should replace the global moment at the end of the plate, in the above equations, by the moment at a certain distance from the end of the plate in the direction of the applied point load. This recommended distance was proposed to be equal to half the sum of the depths of the beam and the plate (i.e. $=(d_p+d_c)/2$), which resulted in a more satisfactory correlation with certain test data as reported by Jones *et al.* (1988), and also with the results based on the other (more rigorous) theoretical solution as developed by Roberts and Haji-Kazemi (1989).

3.3 PLATE PEELING ANALYSIS

Due to the rather complicated nature of the plate peeling problem, it has largely not been possible (in previous literature) to deal with this issue in a comprehensive way by considering the simultaneous combinations of shear and flexural stresses. Most of the theoretical research in this area has only focused (for simplicity) on either the shear or flexural behaviour in isolation. In this section, various available analytical

methods relating to either shear or flexural behaviour will be briefly discussed. The available models may be categorised into three main approaches.

The first approach is based on using the approximate analysis for calculating the normal and shear stresses within the adhesive layer at the end of the plate (as developed by Roberts (1989)), and, then trying to either limit the shear stresses within the adhesive layer, as presented by Sharif *et al.* (1994), or adjust the capacity of the shear reinforcement of the plated beam according to the level of the normal stresses within the adhesive layer, as suggested by Baluch *et al.* (1995).

Another (second) approach is based on limiting the peeling stresses in such a way that the curvature peeling stresses of the plated beam do not exceed the tensile strength of concrete in plated beams subjected to pure flexural loads, or limiting the load bearing capacity so as not to exceed the shear capacity for the plain concrete beam experiencing pure shear: such an approach was presented by Oehlers and Moran (1990) and Oehlers (1992).

The third approach introduced by Zhang *et al.* (1995) is based on limiting the tensile stresses in the cracked concrete cover to be lower in magnitude than the tensile strength of concrete. In view of the central role that this last model plays in the present thesis, its various features will be explained in some detail later on in this chapter.

3.3.1 Approach of Limiting the Normal and/or Shear Stresses in the Adhesive Layer

Based on the approximate expressions for normal and shear stresses located at the end of the plate as developed by Roberts (1989), fairly recently Baluch *et al.* (1995) claimed that they have identified the most important design parameters that play a primary role in connection with shear or concrete rip-off failure which invariably has been reported to happen with the plate peeling off from the tension side of reinforced concrete beams while the plate remains attached to the concrete cover and peeling occurs at the underside of the main (embedded) tensile bars.

In their paper, these authors argued that changes in the mode of failure for the externally plated beams are greatly influenced by the plate thickness and classified the various modes of failure into four types as in the following:

(1) The flexure failure mode: this flexure dominated mode is characterised by extensive yielding of the internal reinforcement and the external plate, deep intrusion of flexural cracks and crushing of concrete in the compression zone (this mode of failure is equivalent to the mode ***CR-*** as discussed in Chapter 5).

(2) The plate separation mode: this mode is characterised by the premature separation of the plate at the concrete-glue-plate interface, initiated at the zone of plate curtailment. Separation leads to a reduced bonded plate length with ultimate failure resulting from the formation of a diagonal crack proceeding from the inward delimitation at the plate/concrete interface to the point of loading (this is equivalent to the mode - - - as discussed in Chapter 5).

(3) Shear mode of failure: this is characterised by horizontal tearing of concrete cover, initiated at the location of plate curtailment. The interface remains

intact, with the crack passing through the concrete below the level of main internal reinforcement. This horizontal crack proceeds upwards to the point of external loading in a steep vertical ascent (this is equivalent to the mode - - -).

(4) Flexure/Shear-Hybrid mode of failure: here, there is yielding of the internal reinforcement and the external plate prior to total beam failure, with actual failure being precipitated by the horizontal tearing of concrete cover below the level of internal reinforcement (this is equivalent to the mode -*R*- as discussed in Chapter 5).

Using test data reported by Jones *et al.* (1980, 1982), Charif (1983), and Swamy *et al.* (1987) in the United Kingdom, and by Munawar (1992) in Saudi Arabia, these authors developed a semi-empirical expression that enabled one (as they put it) to check the efficiency of the stirrups for use in the design for plated reinforced concrete beams.

They showed that the ultimate load for certain plated reinforced concrete beams failing in shear is overestimated by the ACI expression for shear strength of even unplated reinforced concrete beams, because, as they argued, crack profile renders stirrups ineffective. Moreover, in their work, the premature failure was inferred to be due to the lack of efficiency of the stirrups: this lack of efficiency was, then, correlated with a parameter called the normal stress indicator $C_{R1}C_{R2}$. The value of this normal stress indicator was obtained using the approximate expressions for predicting the magnitude of normal stress within the adhesive layer at the location of plate curtailment as originally developed by Roberts (Ref. Equation (3.2)), divided by the applied shear force, i.e. $C_{R1}C_{R2} = \sigma_o / F_o$, where

$$C_{R1}C_{R2} = \left\{\frac{K_n}{4E_pI_p}\right\}^{1/4}\left(1+\left(\frac{K_s}{E_pb_pd_p}\right)^{1/2}L_C\right)\frac{b_pd_p^2}{Ib_a}(h_p-h) \qquad (3.3)$$

In the above, $L_C = M_o/F_o =$ distance from the support to the nearest end of the plate. Accordingly, they suggested that the ACI expression for shear strength of unplated reinforced concrete beams is not safe for use in connection with certain plated beams and should be modified. More specifically, it was assumed that the modification should be applied only to the part of shear strength due to the presence of shear links, V_s.

Assuming that the shear strength of the plain concrete section, V_c, (as calculated by the expression suggested by ACI) is fully utilised, these authors calculated what they called the actual shear strength of shear links by subtracting the nominal shear strength of the plain concrete, V_c, from the actual failure loads, P_{expt}, (as obtained by tests) for 26 test results as reported by others.

By plotting the so-obtained values of the ratio of actual/nominal shear reinforcement strength, K_{SF}, against the corresponding normal stress indicator $C_{R1}C_{R2}\times10^6$, a correlation was found between these two parameters and an exponentially decaying curve was fitted to the data points, suggesting an empirical expression which predicts the value of an adjusting factor k for the shear reinforcement strength as given by

$$k = 2.4e^{(-0.08C_{R1}C_{R2}x10^6)} \qquad (3.4)$$

where $K_{SF} = (0.5P_{expt} - V_C)/V_S$

The suggested adjusted ACI-formula for the overall ultimate shear strength, V_u, relating to the plated beams was, then, given as

$$V_u = V_c + kV_s \tag{3.5}$$

According to this method, the capacity of the beam is determined by the lower value of their ACI-formula-adjusted shear load, V_u, and the flexural load, P_{flex}, based on ACI recommendations, with the calculation for flexural strength assuming presence of full bond between the external plate and concrete with both the steel plate and the embedded steel bars reaching yield while the concrete in compression reaches the maximum crushing strain. Based on this method, the predicted failure load and mode of failure will correspond to the lower value of the shear and/or flexural loads.

Though developed for steel plates, Sharif *et al.* (1994) adopted the same approximate expressions for predicting the shear and normal stresses as derived by Roberts (1989), to predict the plate separation load for reinforced concrete beams upgraded with FRP plates after the unplated beams were preloaded to 85% of their ultimate strength. In their analysis, Equation (3.1) was used to calculate the load on the beam assuming that the limiting value of shear strength within the adhesive layer $\tau_o = 3.5$ MPa. However, the failure load was calculated considering the critical stresses at a constant distance $(d_p + d_c)/2$ from the support, assuming that the plate separates due to the presence of excessive shear stresses within the adhesive layer. Moreover, these authors calculated the flexural capacity of the beam, adopting the ACI ultimate strength method, using an iterative technique that assumed presence of full bond between the plate and concrete.

Although these authors claimed satisfactory agreement between their predictions based on such a theoretical approach and their test data, later detailed critical examination of their numerical results strongly suggested an oversight in their calculations: their subsequently corrected numerical results (presented later in this chapter) were found to be grossly different from both their corresponding test and theoretical results.

3.3.1.1 Critical Examination

The first method as developed by Baluch *et al.* (1995) introduces a predictor equation which, as they claim, can determine the load bearing capacity for a reinforced concrete beam externally reinforced with a steel plate glued to its tension side.

As explained early on in this chapter, these authors have suggested that using the ACI expression for calculating the shear capacity of unplated beams is not safe when it is used for certain plated beams and, hence, have introduced an adjusting factor for the shear capacity provided by the shear reinforcement. This adjusting factor is applied to the part of the beam shear capacity which is related to the shear reinforcement and the total (modified) shear capacity of the plated beam is the summation of the adjusted capacity due to shear reinforcement and the shear capacity of the plain concrete section. The overall beam capacity and the expected mode of failure, then, are determined by choosing the lower value of either the full bond flexural capacity for the plated beam (as calculated by the ACI code of practice) or the so-obtained modified shear capacity, whichever is smaller.

To check the reliability of this model, two types of checks will be carried out next: the first involves reviewing the numerical data as published by the authors.

The individual steps described in their paper (to develop the empirical expression for the adjusting factor) were carefully followed, using the same input data and the same formulae as used by the authors. Surprisingly, it was found that their reported numerical results were neither accurate nor were they consistent, and the individual parameters as presently recalculated from the curve fitting exercise, were not found to match their previously published values. Table (3.1) and Figure 3.3 show both the modified analysis by the present author and the incorrect published data as it appeared in the original paper. In view of the large number of parameters involved in this semi-empirical approach, it has not been possible to determine as to what has exactly gone wrong in the authors' original work. One may, nevertheless, suggest that the most likely reason for the error in their calculations relates to the mistakes in the way the moment of inertia of the transformed section was originally calculated. The underlying reason for such a suggestion will be clarified through a critical examination of the method developed by Sharif *et al.* (1994) which will be discussed later on in this section.

Furthermore, to check the general reliability of their model, this technique has been applied to some other (different) experimental results to predict the failure load and mode of failure for beams with other design parameters. To this end, 26 test data as previously published by Oehlers (1992) have been used. The results are presented in Table (3.2) with the final outcome as follows:

1- The modes of failure predicted by this method for the majority of the beams (i.e. 24 out of 26) were found to be of the shear failure type while according to the reported experimental observations, only 7 beams failed due to shear (these appear in bold letters in the last column of Table (3.2)).

2- The predicted minimum (i.e. the lower of flexural and adjusted shear capacities) total failure load, $2P$, for 9 beams was higher than the experimental total failure load, P_{expt} : the predictions were, therefore, unsafe. The adjusted shear capacities for these 9 beams were based on the parameter V_c as the adjusting factor K for all these specimens was found to be equal to zero. In other words, the actual failure loads, $P_{expt}/2$, were lower than both the plated beam flexural capacity, $P_{flex}/2$, and also the shear capacity for the plain concrete section, V_c.

3- The range of the predicted total failure loads (equal to the total external load on the beam = $2P$) for all the beams was relatively narrow (from 50.3 kN to 58.6 kN) despite the obvious great varieties of the beam spans and plate lengths. On account of the largely different beam and load configurations, the experimental total failure load, P_{expt} , varied (as expected) from 29.6 to 92.2 kN.

The authors' model is based on correlations between the reduction of the shear reinforcement capacity as influenced by the normal stress in the adhesive layer in-between the plate and the concrete beam. In practice, however, the normal stress in the adhesive layer is transferred to the concrete beam directly through the concrete cover with the cover obviously lying outside the concrete section confined by the shear reinforcement. Indeed, it is unlikely that the normal (peeling) stress in the adhesive layer affects or, indeed, reduces the contribution from the shear

reinforcement. As demonstrated by the experimental results, such predictions of the failure load are lower than even the shear capacity of the plain concrete section that completely neglects the shear reinforcement capacity. This assumption is not believed to be justified and it is highly unlikely that there exists a link between the reductions in the shear strength of the shear links and the normal stress within the adhesive layer.

Finally, for certain beams, neither the ACI flexural full bond bearing load nor, indeed, the ACI shear load predictions for a plain concrete section provided a safe value (when compared to the experimental failure load): the suggested failure mode classification in their model is also not satisfactory and, in view of our largely incomplete knowledge of shear in concrete, such speculative suggestions are fraught with uncertainties and far from convincing. In conclusion, this model is not considered to be a reliable one for design purposes.

A detailed examination of the previously reported work by Sharif *et al.* (1994), which is also based on the approximate theoretical solutions of Roberts (1989), will also demonstrate that there has been an oversight in their proposed model and that it suffers from major shortcomings. Their numerical results have been found not to be accurate, and, once corrected by the present author, their predicted failure loads were found to be substantially higher in magnitude than the theoretical flexural capacity for all their beam designs (with these having been based on the ACI recommendations and assuming full bond between concrete and plate up to the ultimate load). Their numerically corrected results plus their experimental and the incorrect analytical results are presented in Table (3.3). Here, their corrected predictions of load bearing capacities are all higher in magnitude than the corresponding experimental data for all

the beams some of which failed due to plate separation. It should also be noted that in certain cases, these beams (with external FRP plates) had plate end anchorages.

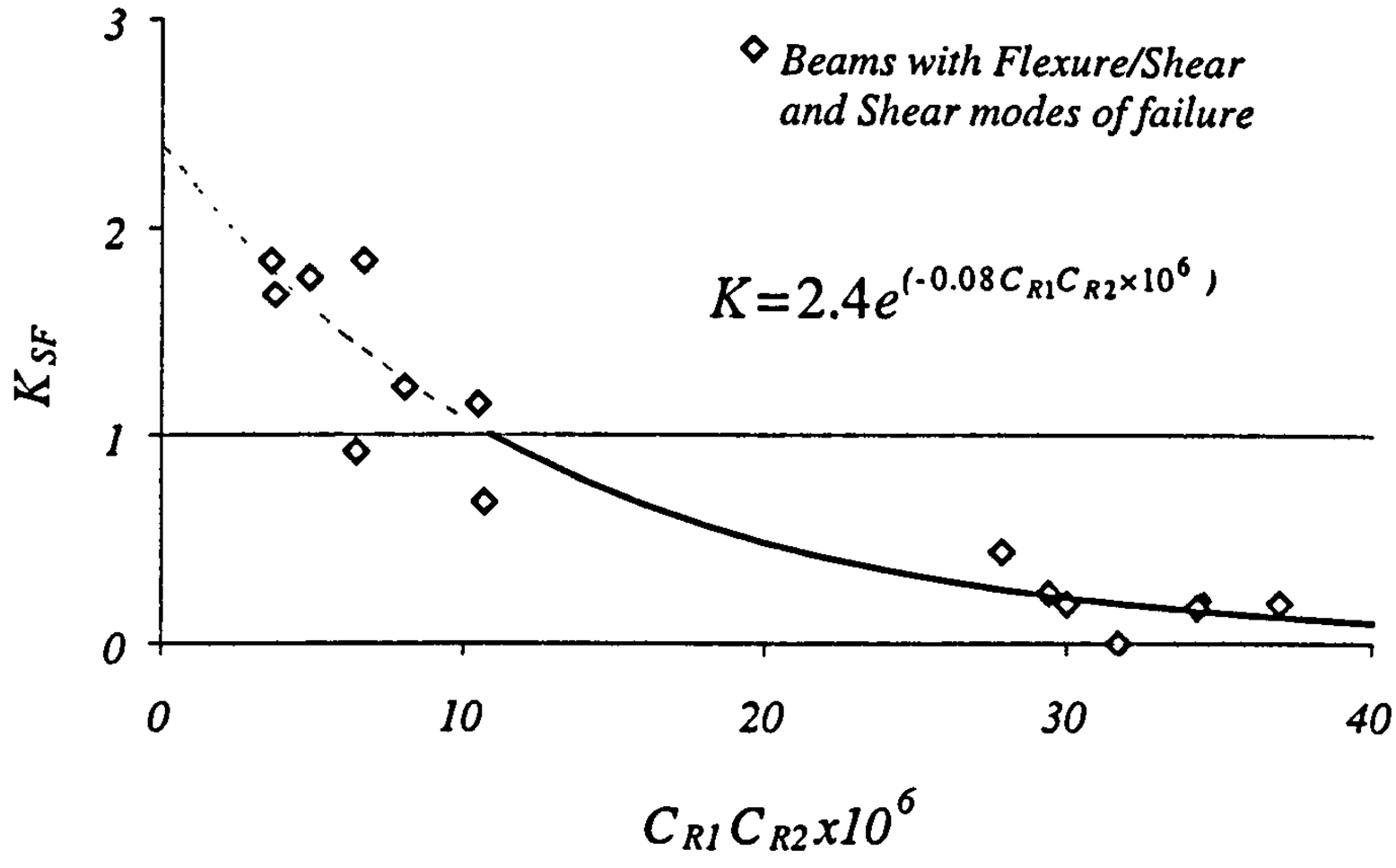

(a)

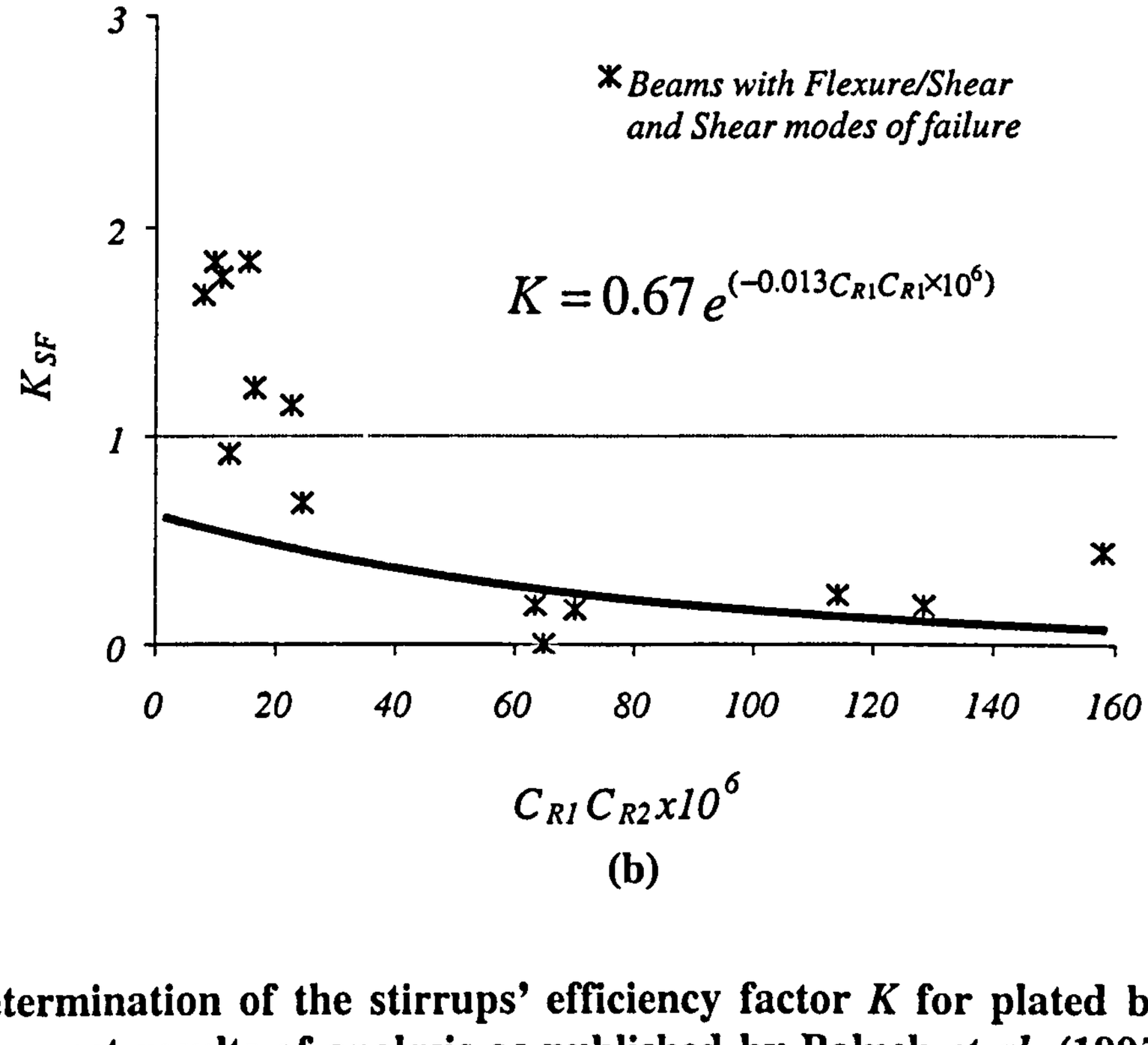

(b)

Fig. 3.3 Determination of the stirrups' efficiency factor *K* for plated beams: (a) incorrect results of analysis as published by Baluch *et al.* (1995), (b) the presently corrected version of the results.

Beam Title	Experimental Load P_{expt} (kN)	ACI-318			K_{SF} $\frac{0.5 P_{expt} - V_C}{V_S}$	Baluch's incorrect parameters		Corrected parameters	
		P_{Flex} (kN)	V_C (kN)	V_S (kN)		$C_{R1}C_{R2}x10^6$	K	$C_{R1}C_{R2}x10^6$	K
URB5	53.2	87.7	18.5	43.1	0.19	37.4	0.12	128.5	0.13
B1	58.0	91.2	21.0	46.8	0.17	37.4	0.12	70.0	0.13
C11	65.0	73.3	19.6	29.0	0.44	34.7	0.12	158.0	0.27
C12	65.0	50.2	19.6	29.0	0.44	27.8	0.15	158.0	0.09
MF1	45.0	102.3	22.7	46.8	0.00	27.8	0.26	64.9	0.09
FRB5	60.0	73.7	21.0	46.8	0.19	31.7	0.26	63.4	0.29
URB4	57.6	56.5	18.5	43.1	0.24	29.9	0.19	114.1	0.29
F31	182.0	298.0	54.4	53.7	0.68	29.3	0.22	24.5	0.15
205	213.0	312.3	58.9	41.5	1.15	10.7	0.23	22.6	0.49
209	220.0	313.0	58.9	41.5	1.23	10.6	1.02	16.4	0.50
218	194.0	314.5	58.9	41.5	0.92	8.2	1.03	12.2	0.54
204	270.0	269.4	58.9	41.5	1.83	6.5	1.25	15.4	0.57
208	264.0	269.7	58.9	41.5	1.76	6.7	1.43	10.8	0.55
217	257.0	270.5	58.9	41.5	1.68	5.1	1.40	7.9	0.58
203	270.0	243.2	58.9	41.5	1.83	3.9	1.60	9.7	0.60

Table 3.1 Evaluation of K and K_{SF}: incorrect published results of Baluch *et al.* (1995), and the subsequently corrected data in the present work.

Beam Title	Experimental load *P_{expt} (kN)	ACI-318 **P_{flex} (kN)	V_C (kN)	V_S (kN)	^2V_U (kN)	K_{SF}= $\frac{0.5 P_{expt} V_C}{V_S}$	Baluch's parameters C_{R1}	C_{R2}	K	Adjusted Shear Capacity ^^2V_{AU} (kN)	Predicted Failure load 2P (kN)	Failure mode
1/1/N	82.0	161.4	27.3	0	54.7	NA	4.13E-05	0.61	0.315	54.7	54.7	safe-Shear
1/2/S	59.4	161.4	27.3	0	54.7	NA	1.48E-04	0.61	0.002	54.7	54.7	safe-Shear
1/2/N	65.0	161.4	27.3	0	54.7	NA	2.02E-04	0.61	0.000	54.7	54.7	safe-Shear
1/3/S	83.2	161.4	27.3	0	54.7	NA	3.09E-04	0.61	0.000	54.7	54.7	safe-Shear
1/3/N	69.2	161.4	27.3	0	54.7	NA	4.70E-04	0.61	0.000	54.7	54.7	safe-Shear
1/4/S	82.0	161.4	27.3	0	54.7	NA	9.40E-05	0.61	0.024	54.7	54.7	safe-Shear
2/1/N	88.0	165.3	28.2	0	56.4	NA	3.54E-04	0.61	0.000	56.4	56.4	safe-Shear
2/1/S	80.2	165.3	28.2	0	56.4	NA	1.18E-04	0.61	0.007	56.4	56.4	safe-Shear
2/2/N	87.6	165.3	28.2	28.0	112.4	0.56	3.54E-04	0.61	0.000	56.4	56.4	safe-Shear
2/2/S	87.6	165.3	28.2	28.0	112.4	0.56	1.18E-04	0.61	0.007	56.8	56.8	safe-Shear
2/3/N	89.8	165.3	28.2	56.6	169.7	0.29	3.54E-04	0.61	0.000	56.4	56.4	safe-Shear
2/3/S	90.4	165.3	28.2	56.6	169.7	0.30	1.18E-04	0.61	0.007	57.2	57.2	safe-Shear
2/4/N	92.2	165.3	28.2	94.4	245.2	0.19	3.54E-04	0.61	0.000	56.4	56.4	safe-Shear
2/4/S	89.8	165.3	28.2	94.4	245.2	0.18	1.18E-04	0.61	0.007	57.8	57.8	safe-Shear
5/1/N	91.8	166.8	28.6	94.4	246.0	0.18	4.59E-04	0.61	0.000	57.2	57.2	safe-Shear
5/1/S	87.8	166.8	28.6	94.4	246.0	0.16	1.97E-04	0.61	0.000	57.2	57.2	safe-Shear
6/1/-	50.0	100.9	29.3	0	58.6	NA	6.93E-04	0.61	0.000	58.6	58.6	Unsafe-Shear
6/2/-	51.0	100.9	29.3	0	58.6	NA	6.93E-04	0.61	0.000	58.6	58.6	Unsafe-Shear
6/3/-	42.8	82.9	29.3	0	58.6	NA	9.02E-04	0.61	0.000	58.6	58.6	Unsafe-Shear
6/4/-	42.2	76.2	29.3	0	58.6	NA	9.02E-04	0.61	0.000	58.6	58.6	Unsafe-Shear
7/1/N	34.0	65.5	28.6	0	57.2	NA	1.08E-03	0.61	0.000	57.2	57.2	Unsafe-Shear
7/1/S	35.0	65.5	28.6	0	57.2	NA	1.08E-03	0.61	0.000	57.2	57.2	Unsafe-Shear
7/2/*	47.6	91.8	28.6	0	57.2	NA	3.99E-05	0.61	0.337	57.2	57.2	Unsafe-Shear
8/1/N	29.4	50.3	26.2	0	52.5	NA	1.41E-03	0.61	0.000	52.5	50.3	Unsafe-Flexure
8/1/S	29.6	50.3	26.2	0	52.5	NA	1.41E-03	0.61	0.000	52.5	50.3	Unsafe-Flexure
8/2/*	64.0	110.4	26.2	0	52.5	NA	4.05E-05	0.61	0.327	52.5	52.5	safe-Shear

Table 3.2 Results based on Baluch *et al.* 's original (uncorrected) theory applied to Oehlers' test data (1992).

*P_{expt} : Total external load on the beam = 2 X point loads

**P_{flex} : 2 X Ultimate flexural load on the critical beam section

^$2V_U$ = 2 X Total shear capacity = 2 X (V_C+V_S)

^^$2V_{AU}$ = 2 X Total adjusted shear capacity = 2 X (V_C+KV_S)

A comparison of their analytical (incorrect) results with the experimental loads, demonstrates that their method failed to predict a safe failure load in more than 25% of the cases, while failing to predict the correct mode of failure for more than 50% of the test results. An examination of their presently corrected theoretical results and their subsequent comparison with their experimental data, on the other hand, shows that for each beam category, the so-obtained predicted plate separation loads are higher than the corresponding experimental failure loads in addition to the flexural load relating to most of the beams (i.e. their subsequently corrected premature failure load predictions are invariably unconservative).

Beam title	Experimental ultimate load (*kN*) and mode of failure		Analytical results (*kN*)		
			ACI Flexural strength	Load based on plate separation	
				Incorrect results after Sharif *et al.*	Presently corrected results
P1	67	Flexural by rupturing of the plate	66	100	143.3
P2	68	Plate separation	80	77	103.1
P2B	65	Diagonal tension crack			
P2BW	78	Flexural by crushing of concrete			
P3	66	Plate separation	80	65	86.4
P3B	73	Diagonal tension crack			
P3BW	72	Horizontal and vertical crack around wing			
P3J	82	Flexural by crushing of concrete			

Table 3.3 Experimental and analytical data after Sharif *et al.* (1994) compared with the presently corrected results.

Sharif *et al.* (1994) have given a numerical example (in an appendix in their paper) which presents, in some detail, their method of calculating the plate peeling load: a careful examination of their calculations does, indeed, provide the clue as to where the mistake has occurred. They have calculated the moment of inertia of the fully composite transformed (equivalent) sections, I , wrongly and this is believed to be at least partly the source of error in their work. In that numerical example, their calculated incorrect value for I is $1.59x10^7\ mm^4$ while the corresponding correct value as calculated by the present author is $2.08x10^7\ mm^4$. It is, perhaps, worth mentioning that most of the authors for Baluch *et al.*'s (1995) paper have also contributed to Sharif *et al.*'s (1994) paper which was also shown to suffer from numerical mistakes, and it is likely that the same mistake relating to the moment of inertia for a transformed section has also been made in this second paper.

Moreover, although it was specified (in the original derivations by Roberts (1989)) that the critical location of the stress concentration is to be at a distance $(d_p+d_c)/2$ from the end of the plate, Baluch *et al.* (1995) (in their application of Roberts' method) have mistakenly calculated the shear stress in the adhesive layer at a distance $(d_p+d_c)/2$ from the support. In addition, Baluch *et al.* (1995) assumed that the plate separation failure happens when the shear stress in the adhesive layer reaches a certain value ($\tau_o = 3.5$ MPa) ignoring that the plate separation failure invariably happens by plate peeling away (with the plate and concrete cover separating as a unit) rather than plate debonding at the steel/glue/concrete interface where the normal stresses within the adhesive layer are probably the more appropriate type of stresses to be considered. Indeed, the theoretical normal stress equation developed by Roberts

(1989) is more relevant to the plate debonding problem at the steel/glue/concrete interface rather than the plate peeling phenomenon of the type where the plate and concrete cover peel off as a unit from underside of the main (embedded) tensile reinforcement. In conclusion, it may, therefore, be concluded that the method presented by Sharif *et al.* (1994) is not a reliable one and is fraught with uncertainties.

3.3.2 Approach of Limiting the Axial and Curvature Peeling Stresses

Oehlers and Moran (1990), derived a simple semi-empirical expression to determine the moment at which plate peeling starts within the serviceability limit state, and the flexural moment that causes complete separation of the plate at the ultimate limit state. Their derivations needed experimental calibrations in order to determine the values of some critical parameters, in their model, and to select the most appropriate way to calculate the magnitude of flexural rigidity which was to be used in their expressions. The plate peeling failure was assumed to be due to the presence of excessive peeling stresses. The influence of two different types of peeling stresses was considered: axial peeling stresses due to the axial strain in the plate, and curvature peeling stresses due to the curvature of the reinforced concrete beam.

The derivation was initially based on the basic assumptions that the plated beam is isotropic and uncracked and that the plated section is subjected to pure flexural loads only. Obviously, these last two assumptions are not generally applicable to the upgrading of reinforced concrete beams under normal conditions of loading, however, it was mentioned that, using the experimental results, the model may be calibrated in

order to override the assumption of an uncracked beam. On the other hand, it was argued that flexural cracking of the concrete beam has opposite effects on the assumed two underlying causes of plate peeling, as flexural cracking increases the curvature but (at the same time) reduces the bending strains in concrete. To ensure that the peeling forces, which were assumed to act normal to the plate/concrete interface, depend only on the plate thickness, it was assumed that the plate thickness is much less than the depth of the beam which is a reasonable assumption for normal practice.

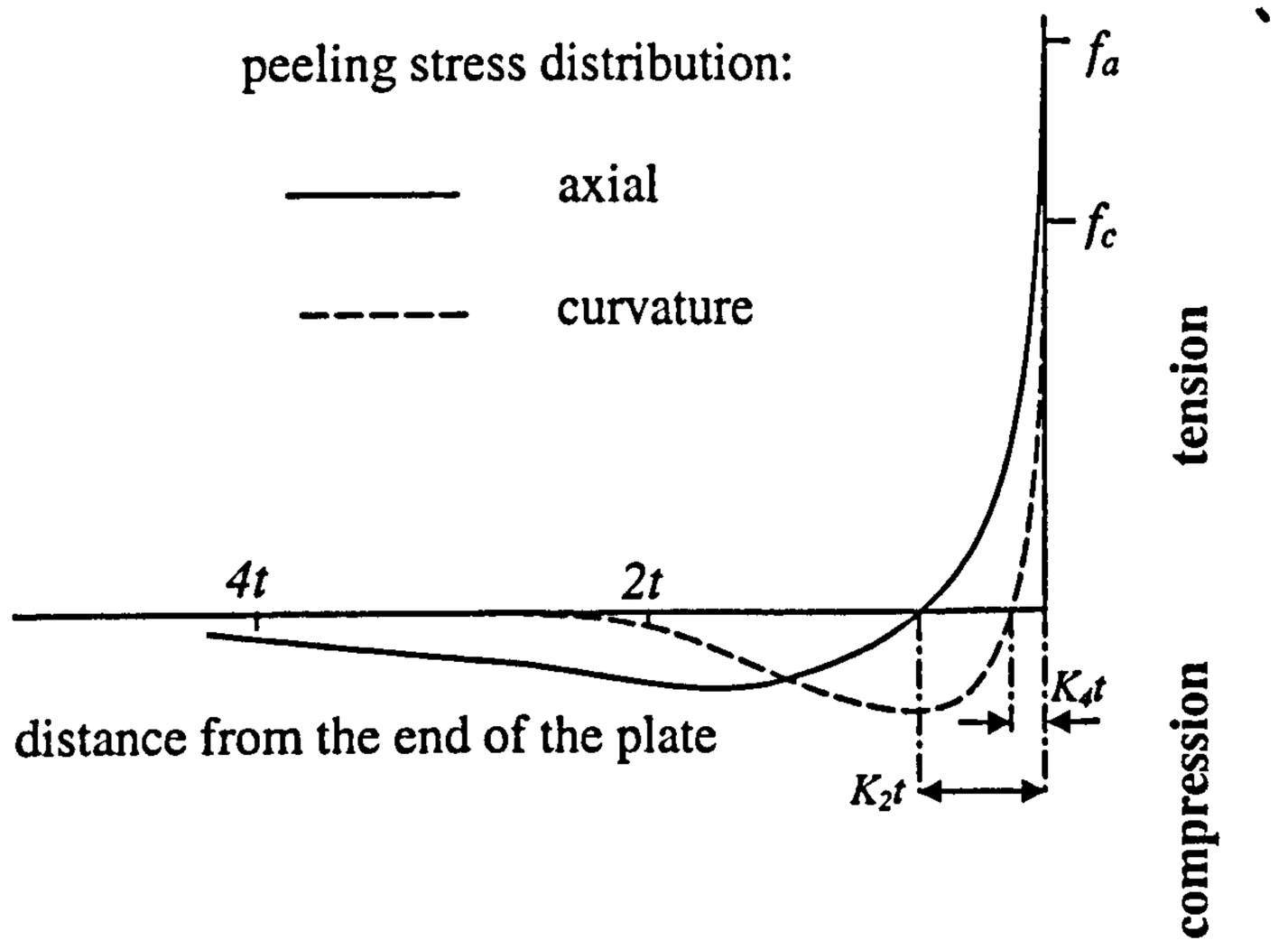

Fig. 3.4 Flexural peeling stresses across the interface.

To get an idea about the distributions of both the plate axial and curvature peeling stresses, these authors used a finite element analysis. The results based on such a preliminary analysis showed that both of the plate peeling stress distributions have the same general shape but extend over different lengths of the plate with the maximum tensile stress positions being coincident at the end of the plate, Figure 3.4 (after Oehlers *et al.* (1990)). The forces acting on the beam and the plate are shown in

Figure 3.5 (after Oehlers *et al.* (1990)). Different expressions were derived for estimating the plate axial and curvature peeling stresses: these are discussed next.

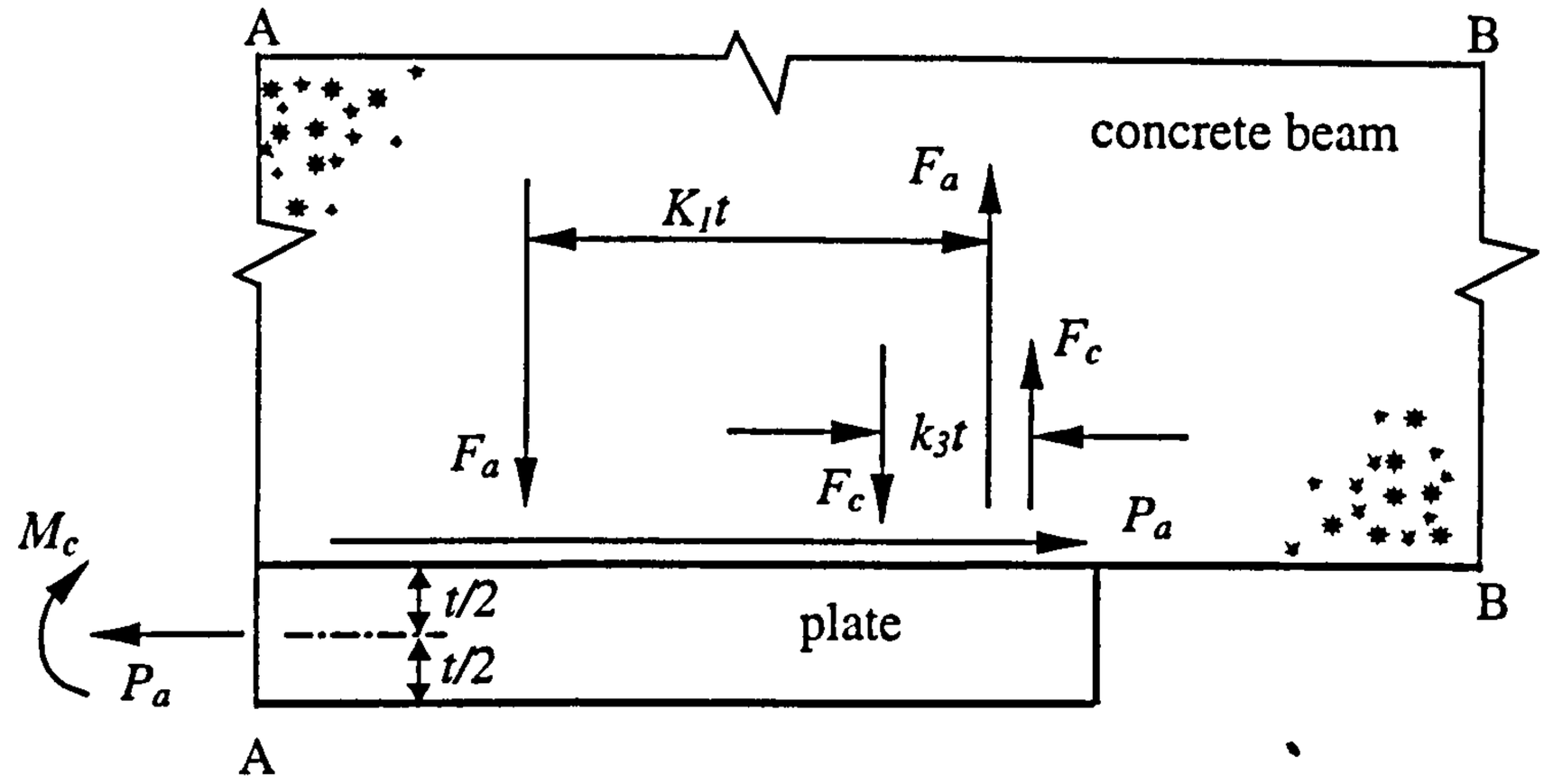

Fig. 3.5 Flexural peeling forces.

It is, perhaps, worth noting that all the analytical and numerical solutions as previously reported by Goland and Reissner (1994), Cornell (1953), Adams and Peppiatt (1964), Allman (1977), Crocombe and Adams (1981), and Adams and Wake (1984) for the shear and normal or peeling stresses in adhesive joints, subjected to bending and axial forces, indicate the characteristics and the general trend shown in Figure 3.6.

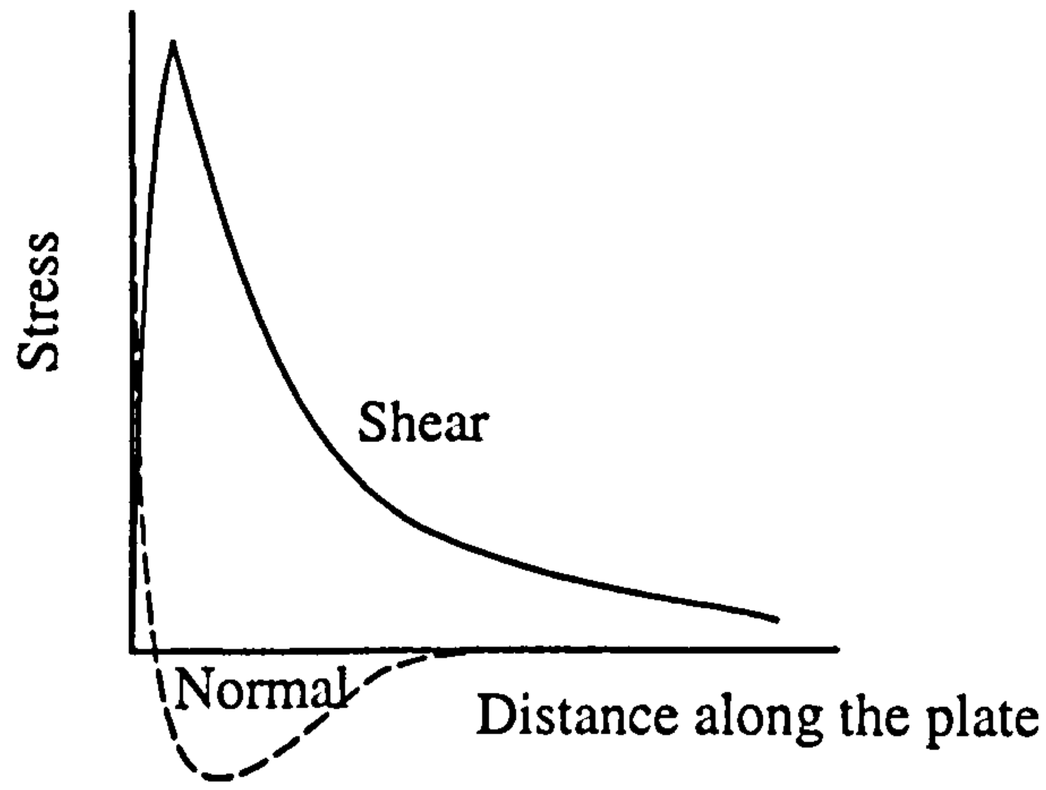

Fig. 3.6 Shear and normal stresses at end of adhesive layer.

3.3.2.1 Axial Peeling Stress

The maximum peeling stress, f_a in Figure 3.4, that is induced by an axial plate strain, ε_a, is determined from the equilibrium of the forces P_a and F_a in Figure 3.5

$$P_a t = 2 F_a k_1 \tag{3.6}$$

Substituting for $P_a = E_s \varepsilon_a b_b t$, where E_s = Young's modulus for the steel plate, and b_b = the width of the plate, and also substituting for $F_a = s_a k_2 t b_b f_a$, where s_a = the ratio of the mean-to-maximum tensile peeling stress in the region $k_2 t$ in Figure 3.4, with $\varepsilon_a = h\phi$, where ϕ = the curvature of the beam, and h = the distance from the neutral axis of the beam to the plate; leads to the following expression

$$f_a = k_a E_s h \phi \tag{3.7}$$

where, $k_a = (2 k_1 k_2 s_a)^{-1}$

3.3.2.2 Curvature Peeling Stress

The maximum peeling stress, f_c, in Figure 3.4, that is induced by the curvature ϕ in the plate, is determined from equilibrium of forces P_a and F_a in Figure 3.5

$$M_c = F_c k_3 t \tag{3.8}$$

Substituting for $M_c = (EI)_s \phi$, where $(EI)_s$ = the flexural rigidity of the steel plate, and using $F_c = s_c k_4 t b_p f_c$ gives

$$f_c = k_c E_s t \phi \tag{3.9}$$

where, $k_c = (12 k_3 k_4 s_c)^{-1}$, and s_c = the ratio of the mean-to-maximum tensile peeling stress in the region $k_4 t$ in Figure 3.5.

3.3.2.3 Flexural Peeling Strength

As the positions of f_a and f_c coincide, the peeling cracks will occur when the sum of these two stresses reaches the tensile strength of concrete, f_t:

$$f_t = f_a + f_c \tag{3.10}$$

Substituting into Equation (3.10), the previously derived values of f_a, f_c, and $\phi = M_p/(EI)_b$, where M_p = the moment at the end of the plate that will cause peeling, with $(EI)_b$ = the flexural rigidity of the beam, results in the following expression for predicting the peeling strength:

$$M_p = \frac{(EI)_b f_t}{k_c E_s t + k_a E_s h} \tag{3.11}$$

Initially, the values of k_a and k_c were obtained using an isotropic finite element analysis and both of these parameters were found to have values around 0.7, and (as it has been assumed that $h >> t$) it is expected that the axial strain effect is at least an order of magnitude greater than the curvature effect, hence, it was suggested that ε_a should govern the peeling load. It was, however, argued that, in real life, the problem is further complicated by the flexural cracking which causes large local variations in the bending strains in concrete, large local variations in the curvature along the beam, and, hence, large local variations in the flexural rigidity. To take such variations in practice into account, these authors used the experimental results of Moran (1988)

and Moloney (1986) (44 and 13 tests, respectively) in order to experimentally determine the most appropriate values of k_a and k_c and also establish the most realistic method for determining the flexural rigidity of the beam $(EI)_b$, plus the influence of other factors such as pre-cracking and pre-cambering of the reinforced concrete beam or pre-stressing of the plate prior to gluing.

Details of the test data are already described in Chapter 2. These authors noticed that the experimental strengths are not consistent with the predictions of the equations relating to the behaviour of plated beams (which will be derived later) with the plates having a width less than that of the concrete beam and for those beams with plates terminated within the shear span: the test data relating to such beams were, therefore, excluded from their regression analysis. Moreover, by selecting the method which gives the minimum scatter, the cracked flexural rigidity for plated beams was suggested to be more appropriate than those for cracked unplated, uncracked plated and uncracked unplated cases, exhibiting a relatively lower scatter factor. Using the test results for the remaining 49 plated beams, and using their corresponding values of cracked flexural rigidities, Oehlers and his associate determined the values of the parameters k_a and k_c using linear regression analysis, and, surprisingly, found these to be equal to 0.0083 and 0.603, respectively. Although the value of 0.603 for k_c is relatively close to the figure of 0.7 as previously determined using the isotropic analysis, the so-obtained value of k_a was very small, suggesting that the effect of the axial peeling stress, and strain, is negligible when flexural cracking is catered for. The value of the parameter k_c was suggested to be equal to 0.474 if the effect of the plate

axial strain is ignored and, hence, the predicted value of ultimate peeling moment, M_{up}, was suggested to be given by the following

$$M_{up} = \frac{(EI)_{cp} f_t}{0.474 E_s t} \tag{3.12}$$

where, $(EI)_{cp}$ = the flexural rigidity of cracked plated beam, with a coefficient of variation equal to 0.283 which suggests a significant degree of scatter in the results.

The same type of approach was also adopted for the serviceability limit state, and the theoretical peeling moment, M_{sp}, for such cases was found to be given by the following:

$$M_{sp} = \frac{(EI)_{cp} f_t}{0.827 E_s t} \tag{3.13}$$

Using the above equation for predicting the ultimate peeling moment of plated beams, M_{up}, these authors also suggested that one can predict the ultimate plate peeling moment for plated beams for other conditions such as pre-cracked, pre-cambered, and pre-loaded beams. In other words, it was suggested that these conditions have no practically significant effect on the strength of plated beams. Guided by the test results, it was reported that beams plated over part of their width have strengths higher than those plated across their full width. Unexpectedly, it was noticed that, for the same plate thickness, reducing the plate width increases the ultimate strength of the plated beam. In fact, the strength of the beam was found to be increased with reductions in the cross-section area of the external plate.

Although they claimed that their method is also applicable to plated beams subjected to combinations of shear and flexure, these authors excluded (from their analysis) the test results for plated beams, in which shear diagonal cracking had occurred.

The above semi-empirical model was developed for the plated sections subjected to pure bending only and in practice the beams are usually subjected to both flexure and shear: in a later publication, Oehlers (1992), therefore, extended the aforementioned analysis to cover cases when the beams had their external plates terminated within the shear span. The experimental results for symmetrical four-point loading cases with the tests carried out on 26 simply supported plated beams (as discussed in Chapter 2) were, therefore, used to develop an appropriate design procedure against plate peeling failure, when the end of the plate is subjected to both shear and flexural loads.

A careful examination of the experimental results indicated that plate peeling failures had occurred at almost the same levels of external loads regardless of the amount of shear reinforcement even when shear links were completely absent and, hence, it was concluded that the plate peeling strength of a beam is controlled (and may be predicted) only by the theoretical shear strength of the corresponding unplated concrete beam in the total absence of shear reinforcement, V_{uc}. For cases when the plated beam is subjected to pure flexural forces, on the other hand, the beam's plate peeling strength was assumed to be solely controlled by the ultimate peeling moment, M_{up}, as previously derived by Oehlers and Moran.(1990), and fully discussed before. In view of the fact that the external plates are usually extended to the shear span where a combination of shear and flexural loads are imposed at the end of the plate,

the test data was used in an interaction diagram, presenting variations of M_p/M_{up} against changes in V_p/V_{uc}, where M_p and V_p are the applied moment and the shear force, respectively, at the end of the plate, where plate peeling was invariably initiated. Based on this interaction diagram, Figure 3.7, the failure envelope with a slop of minus one through the mean of the experimental values was plotted with the governing relationship being of the following form

$$\frac{M_p}{M_{up}} + \frac{V_p}{V_{uc}} \leq 1.17 \qquad (3.14)$$

It was, then, suggested that, as a simple procedure for the design of plated beams or one-way slabs, one should use the characteristic values of the ultimate peeling moment, M_{up}, which may be predicted using the following

$$M_{up} = \frac{(EI)_{cp} f_t}{0.9 E_s t} \qquad (3.15)$$

with the characteristic or nominal value of the shear strength for the member in the total absence of shear reinforcement in the form of links V_{uc} to be estimated using the design formulations given in any limit state code of practice, depending on national or international standards.

Based on the same approach, Oehlers *et al.* (1998) extended their analysis to include the effect of other practical factors such as creep and shrinkage which affect the curvature (and, hence, the peeling stress) of the plated beam. Considering the ultimate peeling moment, M_{up}, as a property of the plated section, the above relationship defining the failure envelope was re-written as

$$\frac{X_p}{X_{pure}} + \frac{V_p}{V_{uc}} \leq 1.17 \qquad (3.16)$$

where, X_{pure} is the curvature to cause debonding if the beam section, at the end of the plate, is subjected to pure flexural load, and X_p is the sum of curvatures at the end of the plate. The sum of curvatures consists of the curvature induced by the short-term loads after plating, X_{short}, and the increase in curvature due to creep after plating, X_{creep}, in addition to the increases in curvature due to shrinkage after plating, X_{shrink}.

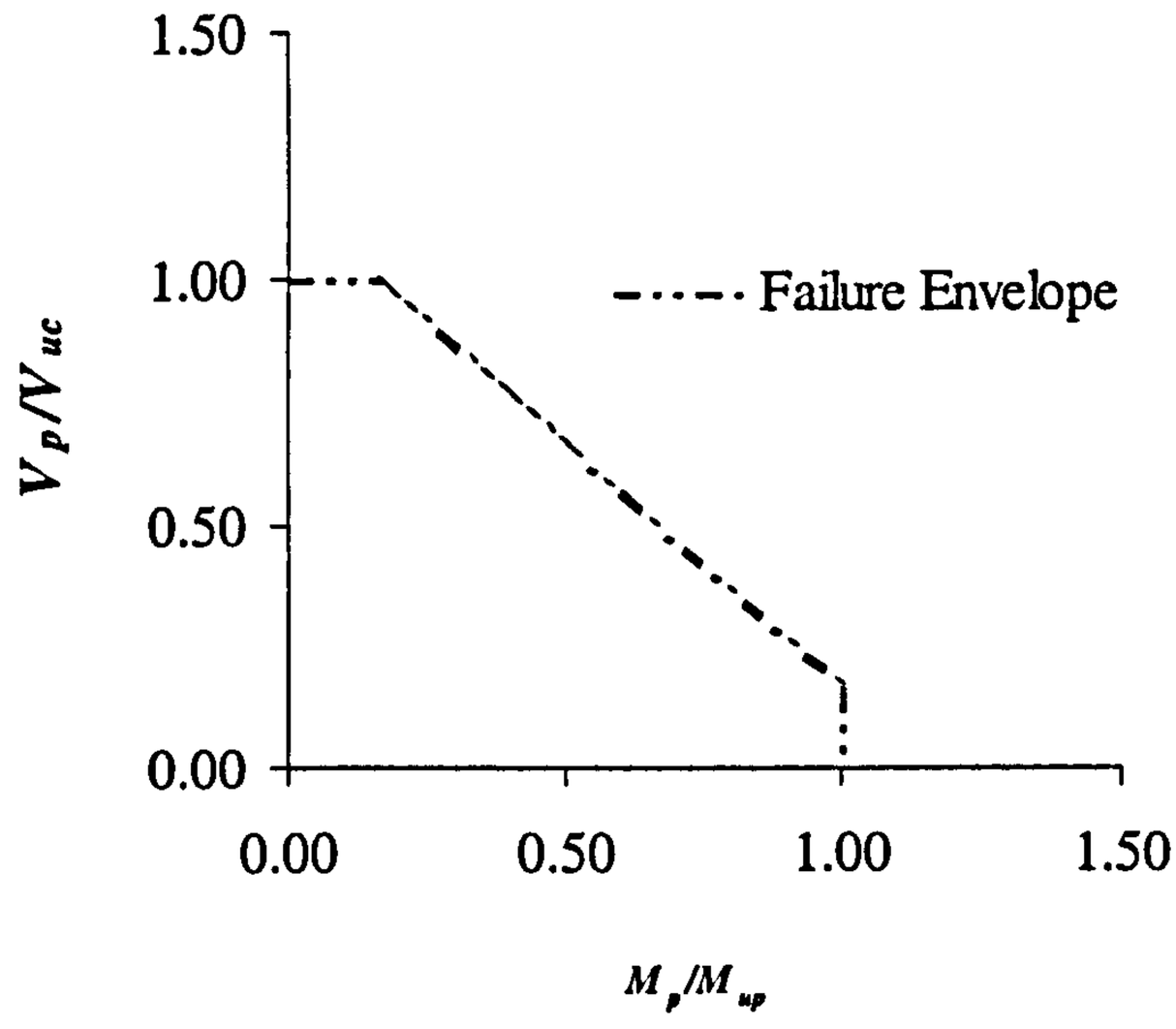

Fig. 3.7 Force and moment interaction diagram at the end of the plate.

It was emphasised that the sum of curvatures X_p is the curvature in the tension-face of the plate, equal in magnitude to that of the curvature induced in the beam after plating: X_{pure} does not include the curvature present in the beam prior to plating. As the parameter V_{uc}, on the other hand, represents the shear capacity of the unplated beam which is characterised by the formation of diagonal shear cracks, the term V_p

represents the total shear load regardless of the prior loading conditions or the method of construction (i.e. whether propped or un-propped): it was suggested that it is the formation of the diagonal crack which in part causes shear peeling as quantified in the equation defining the failure envelop.

3.3.2.4 Critical Examination

The primary assumptions in this approach (regarding the axial and curvature peeling stresses as the causes of peeling failure) are more reasonable when compared with the previously discussed models by the group at King Fahad University in Saudi Arabia. However, a careful examination of the detailed derivations in conjunction with the final design equation(s) suggests that this model also suffers from certain shortcomings and is far from exact. The main points of concern are the proposed interaction relationship for design, the effect of the width of the plate, and the effect of the flexural cracking either in beams which have been precracked prior to plating or for those cases where the external steel plates have been bonded to uncracked (i.e. as cast) reinforced concrete beams: in what follows, these issues will be discussed in some detail.

3.3.2.4.1 The Interaction Relationship

As concluded by many researchers, using external plates to strengthen reinforced concrete beams increases both the serviceability and also the ultimate load bearing capacities in the absence of premature plate peeling failures. The common recommendation by various researchers is to avoid occurrence of plate peeling failures (despite their disagreements about the final values of load bearing capacities),

by extending the plate as far as is practically possible towards the supports, and reducing the thickness of the plate by as much as possible.

Theoretically, if the ends of the externally bonded plate are extended to the supports, and if the plate is very thin, the load bearing capacity is expected to be equal to the full bond capacity of the plated beam. Increasing the thickness of the plate will increase the load bearing capacity until, for a certain (large enough) plate thickness, premature plate peeling failure is initiated leading to reductions in the ultimate load with this becoming (sometimes) even less than that of the corresponding original (unplated) specimen – Refer Chapters 4 and 7.

A careful study of the simple interaction relationship presented by Oehlers (1992) which is meant to predict the maximum possible combination of moment and shear forces at the end of the plate suggests that the capacity of the specimen is assumed to be limited by the shear capacity of the corresponding unplated beam, hence, taking no account of the contribution from the shear links regardless of the thickness of the plate or the extension of the plate within the shear span to the support. In Equation (3.14), it is clear that the plate peeling is expected to initiate at a load V_p which is, indeed, lower than that of shear capacity of a plain concrete beam (i.e. the one with no shear links).

It should be noted that for an average R.C. beam (even with minimum internal shear reinforcement), the shear reinforcement makes a considerable contribution to the total shear capacity. For example, for beam designs reported by Baluch *et al.* (1995), the shear capacity due to the shear links, V_s, is calculated to lie between 70 to 232% of the

shear capacity for the corresponding plain concrete, V_c, while the contribution from shear links is found to vary from 99 to 335% for those beams which were tested by Oehlers (1992), Table (3.4). In other words, according to Oehlers' design method, the load bearing capacity of the plated beam never exceeds a fraction of the load bearing capacity for the corresponding unplated (original) reinforced concrete beam: this contradicts the widely reported and practically successful upgrading cases by others who have reported fairly substantial increases in the ultimate load in the presence of external plates.

The above observation suggests that the interaction equation proposed by Oehlers may considerably underestimate the beam load capacity and gives substantially reduced values for the design load of plated beams with the predicted values sometimes being even lower than those for the corresponding unplated beams.

3.3.2.4.2 Effect of Plate Width and Peeling Stress Distributions in Concrete

In Oehlers' model, the plate peeling stresses (resulting from the axial peeling stress and curvature effects in the plate) are calculated at the level of adhesive layer and not at the location where the plate/concrete cover peeling is expected to happen (which is just under the main reinforcing bars). The distribution (or flow) of these stresses from the adhesive layer to the critical location just under the main (embedded) reinforcement has not been considered. Indeed, it may be argued that Oehlers' model would be more suitable for estimating the load bearing capacity relating to the plate separation at the glue interface between the plate and concrete.

Beam title	ACI-318		V_S/V_C %
	V_C (kN)	V_S (kN)	
URB5	18.5	43.1	232
B1	21.0	46.8	223
C11	19.6	29.0	148
C12	19.6	29.0	148
MF1	22.7	46.8	206
FRB5	21.0	46.8	223
URB4	18.5	43.1	232
F31	54.4	53.7	99
205	58.9	41.5	70
209	58.9	41.5	70
218	58.9	41.5	70
204	58.9	41.5	70
208	58.9	41.5	70
217	58.9	41.5	70
203	58.9	41.5	70
C3	19.6	29.0	148
C5	19.6	29.0	148
C7	19.6	29.0	148
C16	19.6	29.0	148
FRB2	21.0	46.8	223
URB2	18.5	43.1	232
B10	21.0	46.8	223
URB3	22.3	43.1	193
F11	54.0	53.7	100
207	58.9	41.5	70
216	58.9	41.5	70
2/2/N	28.2	28.0	99
2/2/S	28.2	28.0	99
2/3/N	28.2	56.6	201
2/3/S	28.2	56.6	201
2/4/N	28.2	94.4	335
2/4/S	28.2	94.4	335
5/1/N	28.6	94.4	330
5/1/S	28.6	94.4	330

Table 3.4 Components of shear capacity of reinforced concrete beams used in the work of Baluch *et al.* (1995) and Oehlers (1992).

The effect of this approximation is probably more significant for beams which have external plate widths smaller than the total width of the beams because the associated area over which the peeling forces act at the underside of main embedded reinforcement (where the peeling-off takes place) is wider than the contact area at the adhesive level. Obviously, this effect becomes more pronounced with increases in the thickness of the concrete cover. Because the re-distribution of the such stresses reduces the level of stresses at the underside of the main reinforcement where plate peeling takes place, one would expect the actual load capacity of the plated beam to be higher than the corresponding predicted one (as such redistribution of stresses are not considered). In fact, these authors (Oehlers and Moran (1990)) have reported higher experimental load bearing capacities than the corresponding predicted ones, based on their statistical analysis, for those beams with plate widths less than the overall width of the beam which supports the present argument. In their work, Oehlers and Moran (1990) excluded the results for such beams from their statistical analysis in order to achieve an apparently more satisfactory calibration. Their model is, therefore, only applicable to those plated beams with plates covering the whole width of the beam and fails to cater for cases when the ratio of the width of the plate to the width of the beam is less than one.

3.3.2.4.3 Effect of the Flexural Cracking

The finite element analysis carried out by Oehlers and Moran (1990) showed that the significance of the plate axial strain is at least an order of magnitude greater than that of the curvature effect. However, their experimental calibration, surprisingly, showed that this effect is at least two orders of magnitude smaller than the effect of curvature

which suggests that the significance of the curvature stress is raised by three orders of magnitude (through the experimental observations) and, hence, in the peeling problem, the plate axial stress has a relatively negligible effect (compared to the curvature).

These authors justified such contradictions between the theoretical isotropic analysis and the experimental observations by attributing the cause of such discrepancies to the ever presence of flexural cracking which was assumed not to be present in their isotropic analysis. It was argued that flexural cracking causes large local variations in the direct bending strains in concrete associated with which are large local variations in the beam curvature and, hence, substantial local variations in the flexural rigidity can exist in practice. This is in direct contrast to the basic assumption in the theoretical model developed by Zhang *et al.* (1995), the predictions of which have been supported by a very large number of test data relating to beams with widely varying design details (including all the test data of Oehlers and Moran (1990) and Oehlers (1992)) to be discussed later. Indeed, in Raoof and Zhang's model, the plate axial strain is assumed to be the controlling parameter with the curvature effects being of hardly any significance.

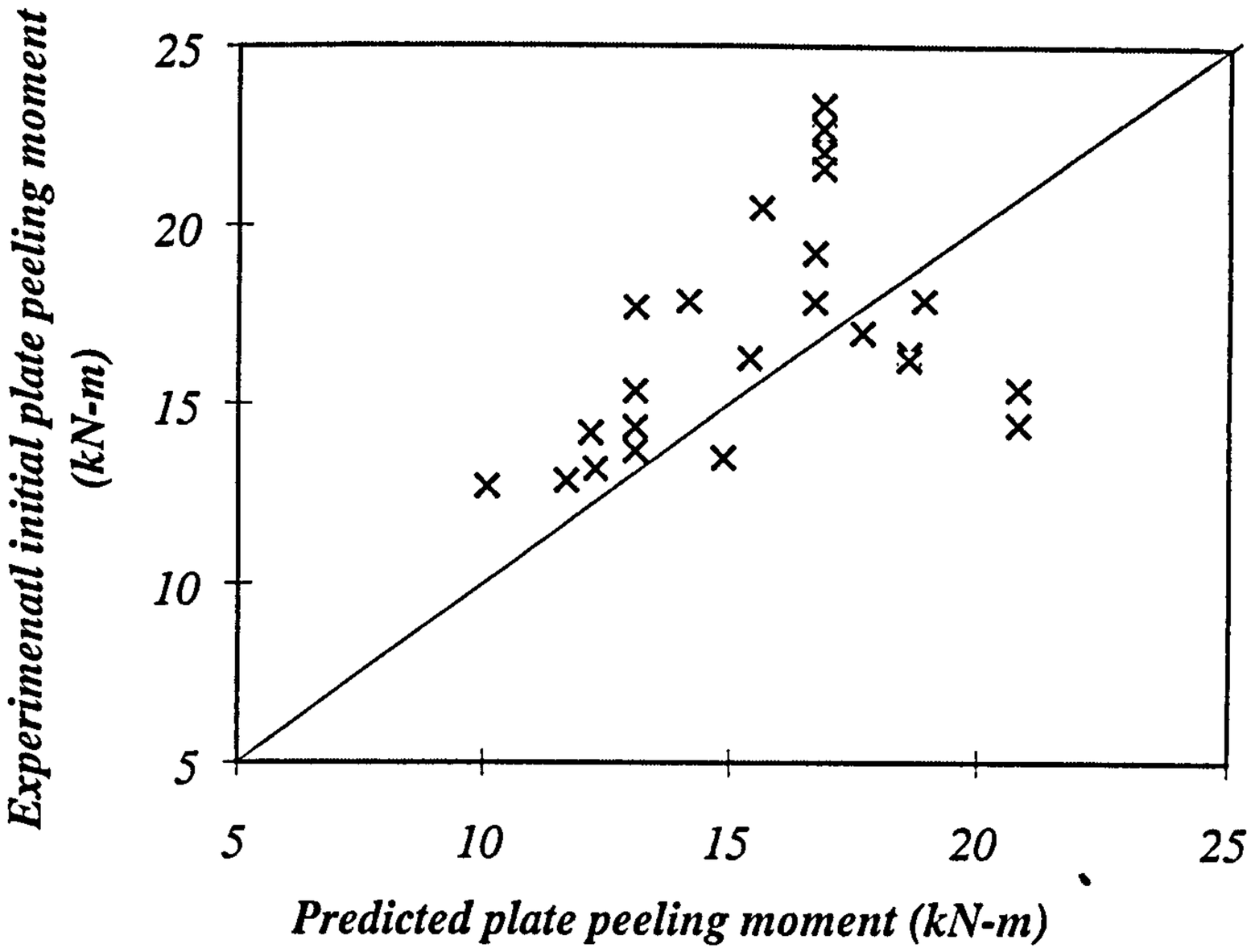

(a)

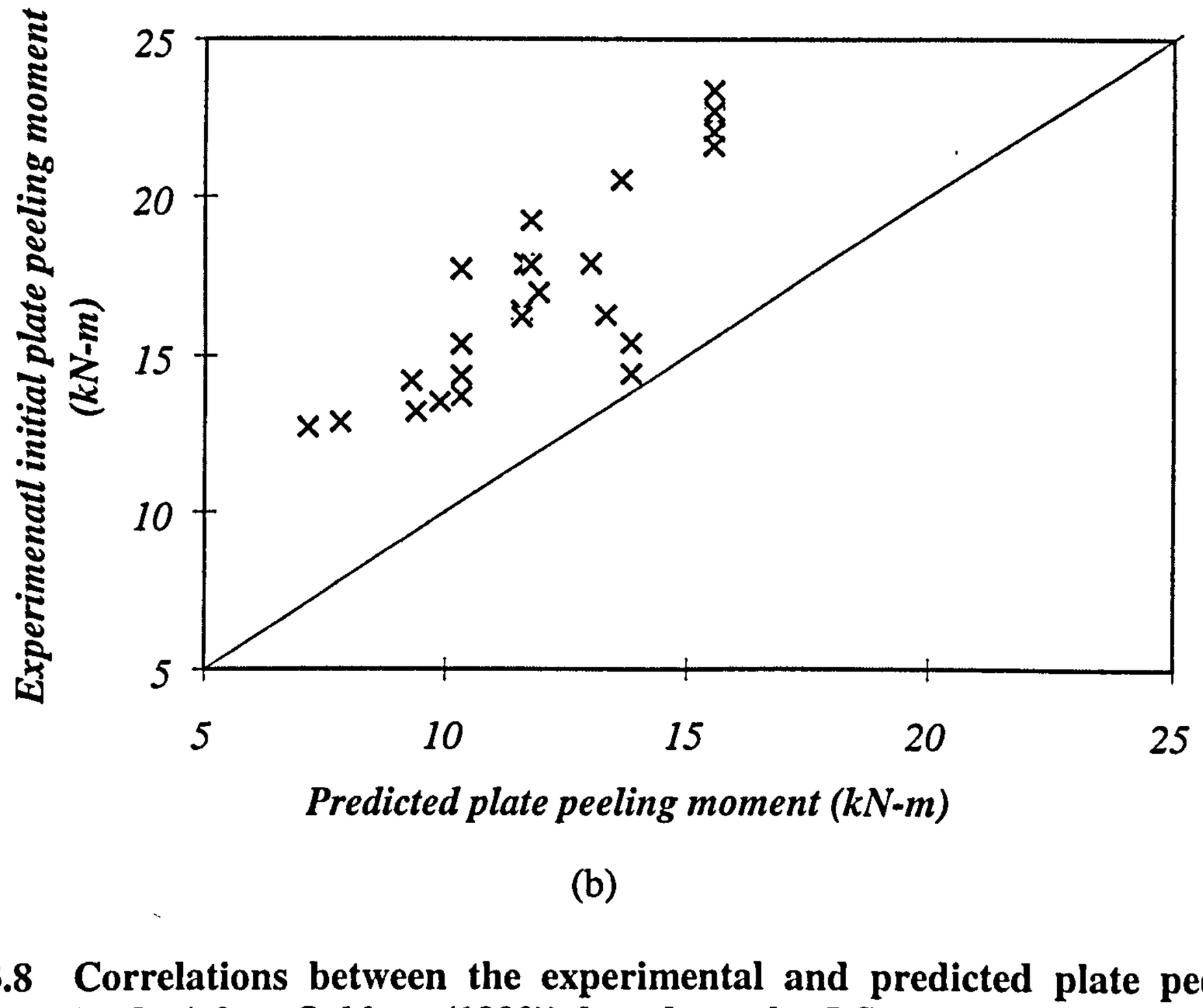

(b)

Fig. 3.8 Correlations between the experimental and predicted plate peeling loads (after Oehlers (1992)) based on the BS8110 (1985) method of calculating the shear strength: (a) mean values for M_{up}, (b) characteristic values for M_{up}.

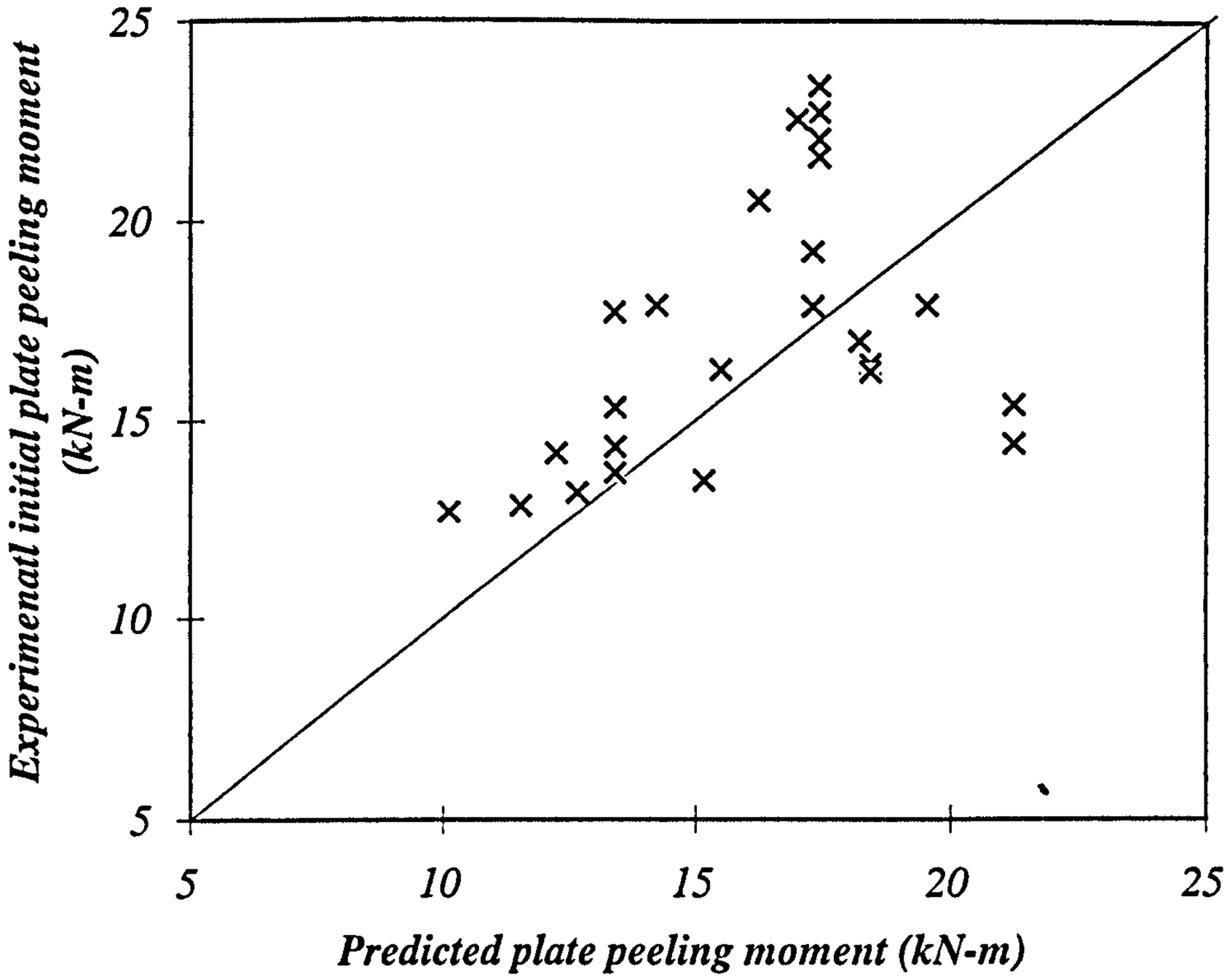

(a)

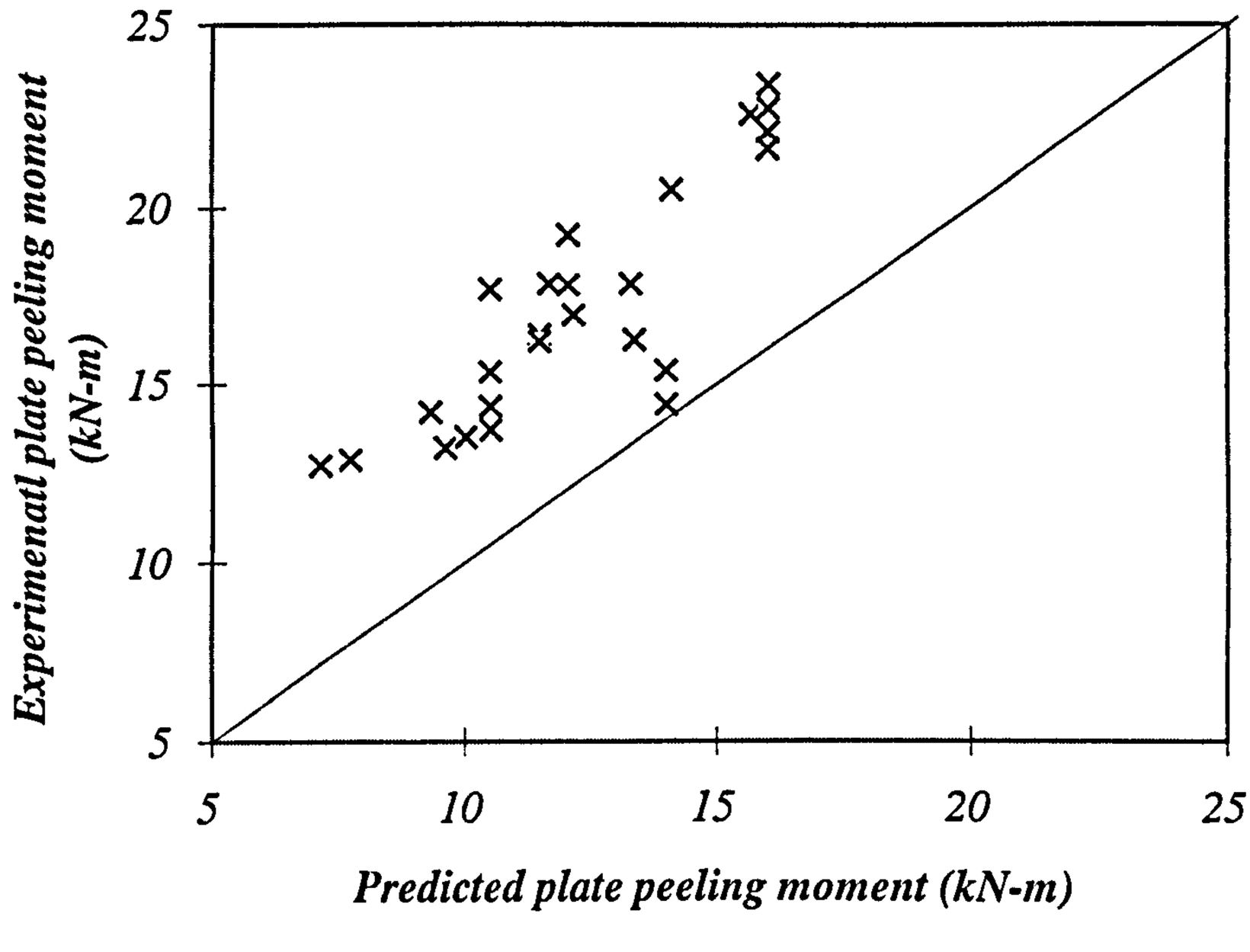

(b)

Fig. 3.9 **Correlations between the experimental and predicted plate peeling loads (after Oehlers (1992)) based on the Australian Standard (1988:A & B) method of calculating the shear strength: (a) mean values for M_{up}, (b) characteristic values for M_{up}.**

A final point, regarding this method, is related to the concept of trying to predict a single (i.e. unique) value for the plate-peeling load for a plated beam. Careful examination of the proposed design procedure by Oehlers (1992) suggests a very wide degree of scatter for the experimental results even for nominally similar beams: Figures 3.8, 3.9 and 3.10 show the very wide scatter of their experimental data when plotted against their predicted plate peeling moments. Here, Figures 3.8 and 3.9 present the correlations between the experimental and the predicted plate peeling moments based on the formulae recommended by BS8110 (1985) and the Australian Standard (1988:A) and (1988:B), respectively, for calculating the ultimate shear capacity of the unplated beam, V_{uc}. The predicted values of peeling loads based on the mean and characteristic values of the ultimate peeling moment M_{up} are presented in parts (a) and (b) of Figures 3.8 and 3.9, respectively. In these figures, the values of the mean M_{up} are calculated by using Equation (3.12), and the characteristic values of M_{up} are based on Equation (3.15), with the predicted peeling load calculated using the interaction Equation (3.14). In Figure 3.10, even with the values of M_{up} and V_{uc} being obtained from actual (experimental) results, nominally similar beams are found to exhibit significant scatters (note that for the plots in Figure 3.10, Equation (3.15) for M_{up} or the code recommendations for V_{uc} have not been used).

Oehlers' semi-empirical model fails to correctly identify the most important beam design parameters, and its predictions (although safe in most cases) are overly conservative for practical applications. As discussed next, its prediction of a unique solution is also questionable.

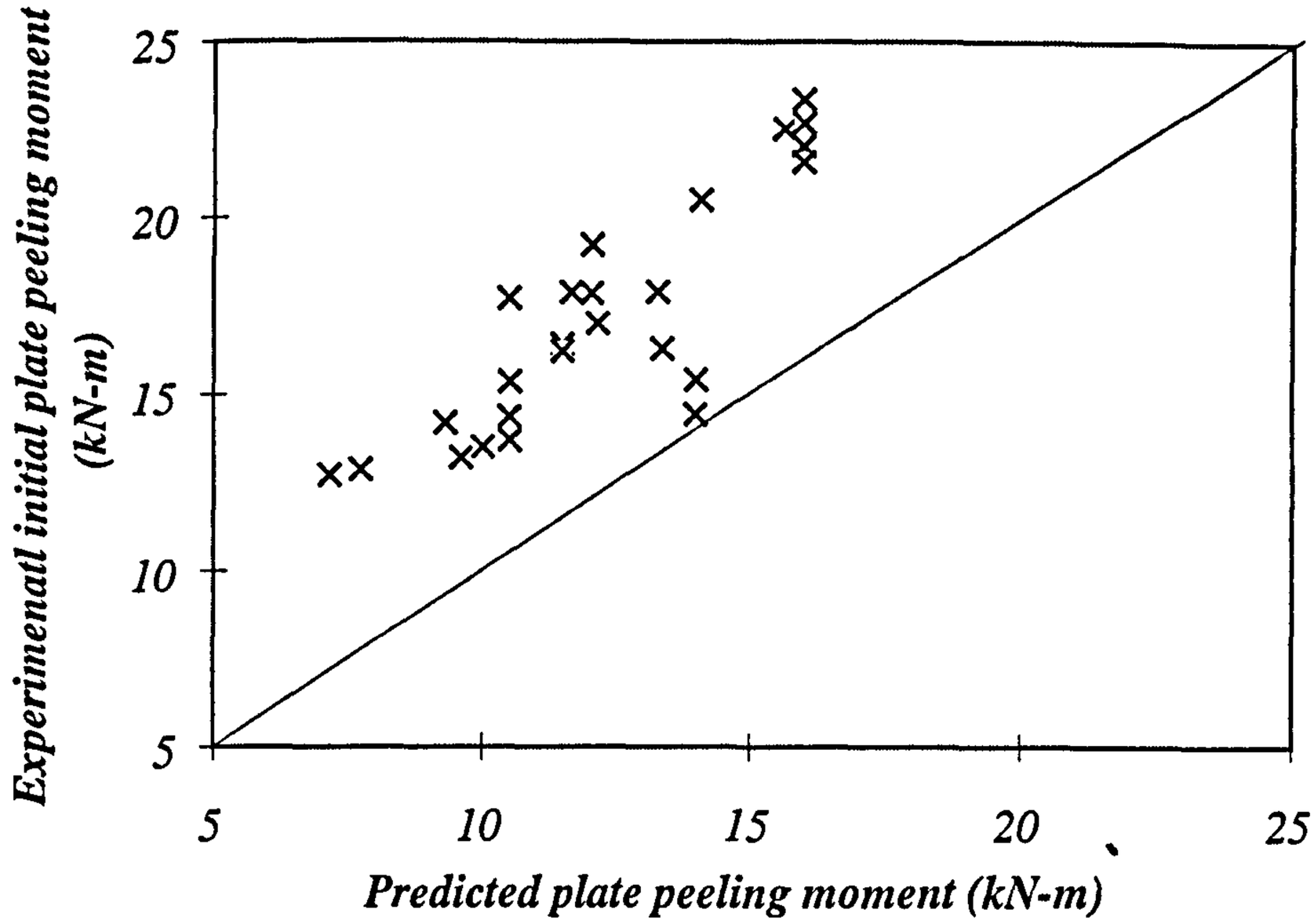

Fig. 3.10 Correlations between the experimental and predicted plate peeling moment (after Oehlers (1992)) based on experimental values of M_{up} and V_{uc} from control beams.

3.3.3 Approach of Limiting the Tensile Stresses within Concrete Cover

In this approach, the tensile stresses in the concrete cover, located at the end of the plate, are limited by the magnitude of concrete tensile strength and the plate peeling phenomena is assumed to be controlled by the spacings of stabilised cracks within the concrete cover zone.

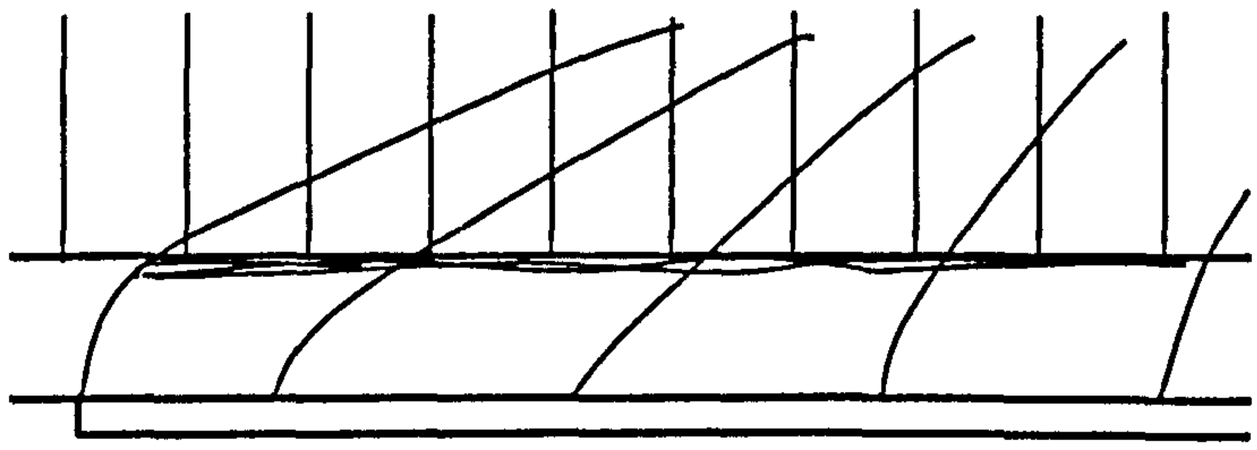

Fig. 3.11 Pattern of concrete cracking associated with plate peeling failure.

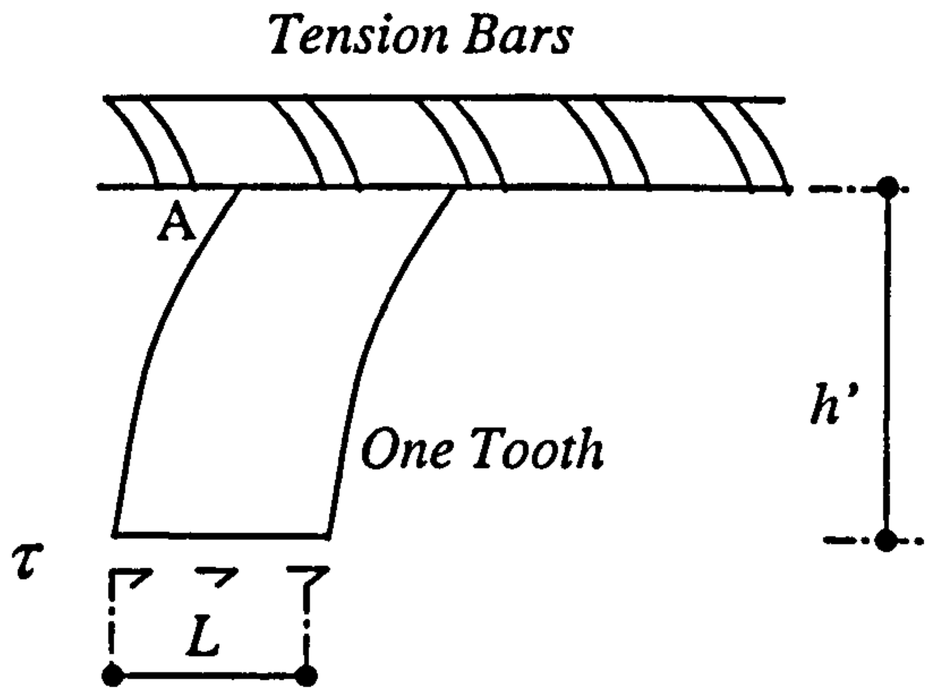

Fig. 3.12 Behaviour of an individual tooth within the concrete cover.

3.3.3.1 Assumed Mode of Failure and Flexural Crack Spacing

Zhang , Raoof and Wood (1995), and Raoof and Zhang (1997) suggested a mode of failure, Figure 3.11, which is controlled by the characteristics of the individual teeth in between adjacent cracks within the concrete cover and forms the basis of the proposed theoretical model which very much depends on the size of stabilised crack spacings. An extension of the classical theory of cracking after Watstein and Parsons (1943) was used for calculating the minimum and maximum stabilised crack spacings, $l^p_{\min}$ and $l^p_{\max}$, respectively, in the case of a reinforced concrete beam with an externally bonded plate, where

$$l^p_{\min} = \frac{A_e f'_t}{u(\sum O_{bars} + b_1)} \tag{3.17}$$

and

$$l^p_{\max} = 2l^p_{\min} \tag{3.18}$$

In the above, u = steel/concrete average bond strength, f'_t = tensile strength of concrete, $\sum O_{bars}$ = the total perimeter of the tension (reinforcing) bars, b_1 = width of

the externally bonded plate, and A_e = the assumed area of concrete in tension, Figure 3.13.

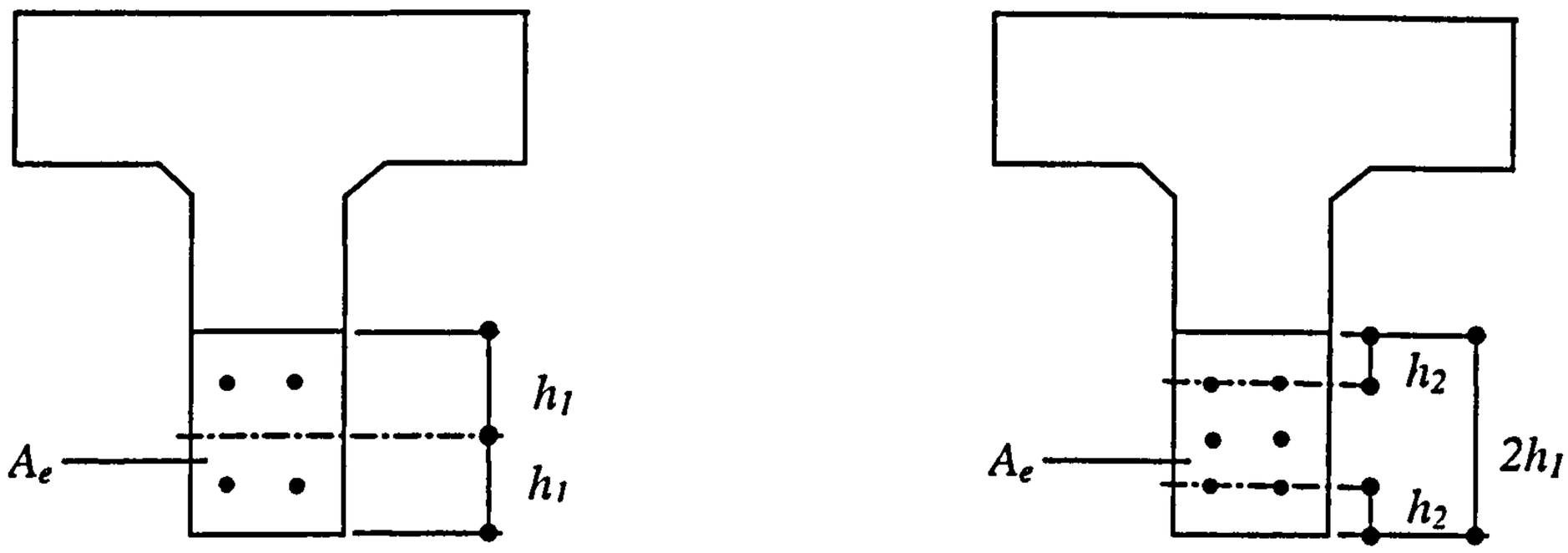

(b) Uniform distribution of reinforcing bars

(a) Non-uniform distribution of reinforcing bars

Fig. 3.13 Assumed concrete region in tension.

3.3.3.2 Estimation of Plate Peeling Failure

Consider the behaviour of an individual plain concrete tooth formed between two adjacent cracks (within the concrete cover) deforming like a cantilever under the action of lateral shear stresses τ applied at the interface between the steel plate and concrete beam (or one-way slab), Figure 3.12. Ignoring the interactions between neighbouring teeth, the tensile stress at point A in Figure 3.12, σ_A, reaches the concrete tensile strength, f_t', for the largely brittle plate peeling failure to initiate - i.e. at the critical state: $\sigma_A = f_t'$. Assuming elastic behaviour for the structural deformations of an isolated tooth up to failure, it may reasonably be assumed that (although, to be more exact, in practice the concrete tooth is likely to act more like a deep beam)

$$\sigma_A = \frac{M_A(L/2)}{I_A} \tag{3.19}$$

where, $I_A = b\,L^3/12$, and

$$M_A = \tau L b_1 h' \tag{3.20}$$

In the above, b_1 = width of the steel plate, b = width of the beam, τ = shear stress at the interface between the concrete and the steel plate, L = depth of the cantilever, and h' = net height of the concrete cover (= length of the cantilever). It, then, follows that

$$\sigma_A = \frac{6\tau h'}{L}\frac{b_1}{b} \tag{3.21}$$

At the instant of plate peeling failure (i.e. when $\sigma_A = f_t'$), therefore, Equation (3.21) gives

$$\tau = \frac{f_t' L}{6h'}\frac{b}{b_1} \tag{3.22}$$

From Equation (3.22), it appears that the ultimate shear stress sustained by an individual tooth is proportional to stabilised crack spacing, L. Following the arguments in the previous section on crack spacing, the minimum and maximum stabilised crack spacings are $l_{\min}^p$ and $l_{\max}^p$, respectively, as given by Equations (3.17) and (3.18). It, then, follows that from Equations (3.17), (3.18) and (3.22), the upper and lower bounds to shear stress $\tau_{\max}$ and $\tau_{\min}$, respectively, are

$$\tau_{\max} = \frac{f_t' l_{\min}^p}{3h'}\frac{b}{b_1} \tag{3.23}$$

and

$$\tau_{\min} = \frac{f_t' l_{\min}^p}{6h'}\frac{b}{b_1} \tag{3.24}$$

Within the region D-B in Figure 3.2, the shear stress, τ, is balanced by the axial stress in the steel plate, σ_s, so that at the location under the point load nearest to the support (i.e. at a distance L_p^1 from where the plate is terminated):

$$\sigma_s = \frac{\tau L_p}{t} \tag{3.25}$$

where L_p = effective length of the steel plate in the shear span over which equivalent shear stresses at the plate/concrete interface may be assumed to remain uniform, and t = plate thickness. The magnitude of effective length, L_p, is given by the lower value of the actual length of plate within the critical shear span in Figure 3.2, L_p^1, and the value of L_p^2 as calculated from the following Equations - whichever is smaller (Raoof and Zhang, (1997))

$$L_p^2 = l_{\min}^p \left(21 - 0.25 l_{\min}^p\right) \quad , \quad l_{\min}^p \leq 72 \tag{3.26}$$

$$L_p^2 = 3 l_{\min}^p \quad , \quad l_{\min}^p > 72 \tag{3.27}$$

In the case of a beam under symmetrical four-point loading with the plate positioned within the constant moment zone (where it terminates) the value of effective L_p in Equation (3.25) may be obtained by only using Equations (3.26) or (3.27). The majority of tests reported by Oehlers and Moran (1990) were, indeed, of such a configuration and the correlations between theoretical upper and lower bound solutions and this set of experimental data as reported by Raoof and Zhang (1997) are based on the estimates of effective L_p as obtained from Equations (3.26) and (3.27).

Using Equations (3.17), (3.23), (3.24), and (3.25), therefore, the lower bound to steel plate direct tensile stresses, $\sigma_{s(\min)}$, is

$$\sigma_{s(\min)} = \frac{A_e \left(f_t'\right)^2 L_p}{6 h' t u \left(\sum O_{bars} + b_1\right)} \frac{b}{b_1} \tag{3.28}$$

The upper bound to σ_s, on the other hand, (noting that $\tau_{s(\max)} = 2\tau_{s(\min)}$) is given as

$$\sigma_{s(\max)} = 2\sigma_{s(\min)} \tag{3.29}$$

The effective area of concrete in tension, A_e, is calculated from Figure 3.13 (Nawy, 1992)

$$A_e = 2 h_1 b \tag{3.30}$$

Assuming that $u = 0.28\sqrt{f_{cu}}$ (Mosley, 1990), where f_{cu} = concrete cube strength, and the cylinder splitting tensile strength $f_t' = 0.36\sqrt{f_{cu}}$ (after BS8110), with the units of f_{cu} and f_t' in MPa. Equation (3.28) may be written as

$$\sigma_{s(\min)} = 0.154 \frac{L_p h_1 b^2 \sqrt{f_{cu}}}{h' b_1 t \left(\sum O_{bars} + b_1\right)} \tag{3.31}$$

With the magnitudes of $\sigma_{s(\min)}$ and $\sigma_{s(\max)} = 2\sigma_{s(\min)}$ directly under the point load nearest to the support estimated, it is, then, straight-forward to predict the corresponding lower and upper bounds to the peeling bending moment at this location: this may be done by using the traditional simple bending theory with the assumption of plane-section bending as fully explained elsewhere (Zhang *et al.* (1995)), with the influence of tensile stresses below the neutral axis taken into account (Raoof and Zhang (1997)).

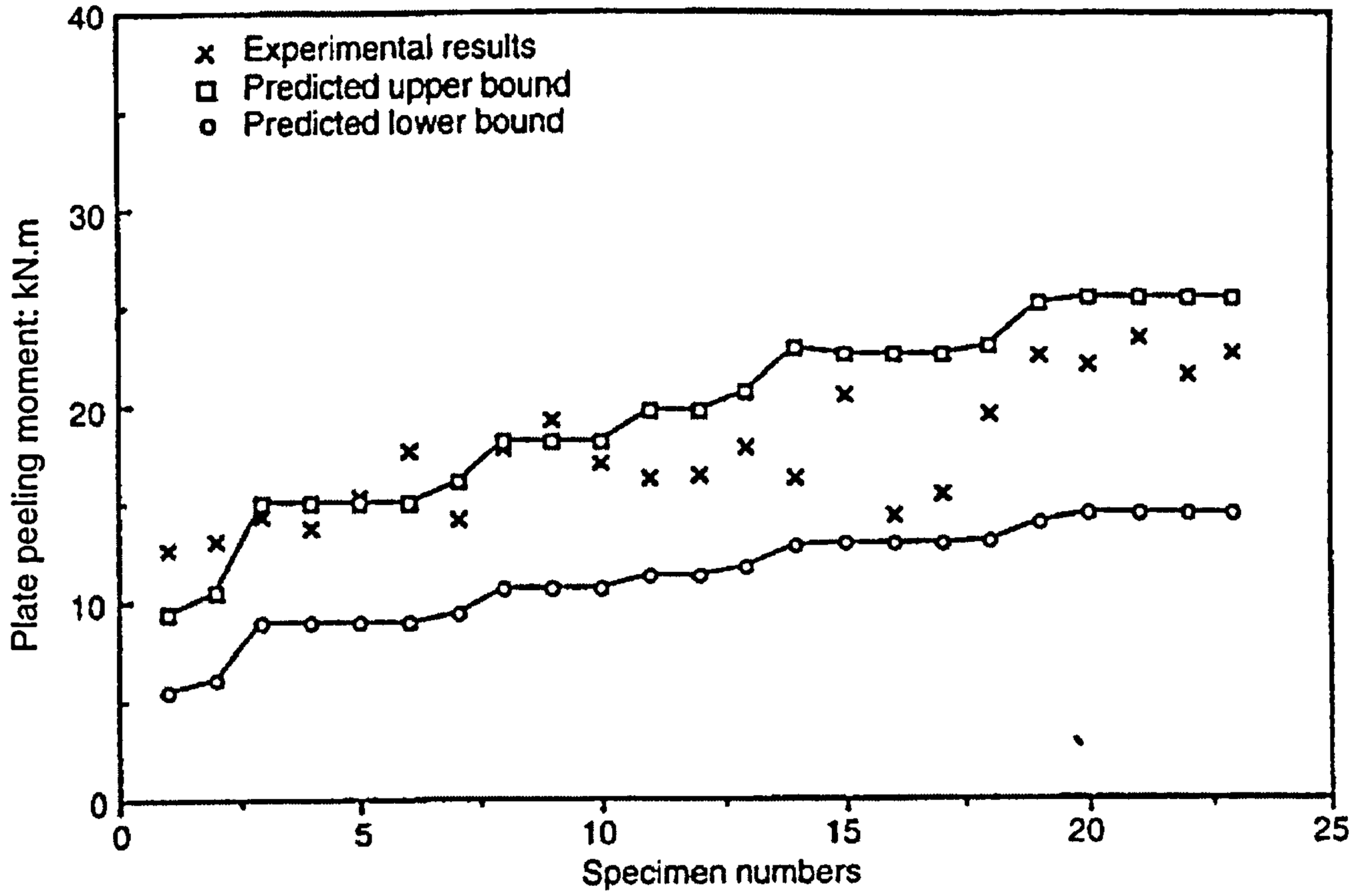

Fig. 3.14 Correlations between the theoretical upper and lower bound solutions of Raoof and Zhang (1997) and experimental data after Oehlers (1992).

Using the above procedure, then, the theoretical upper and lower bounds of the initial peeling bending moments for all the test results of Oehlers and Moran (1990) and Oehlers (1992) have been calculated, and these are compared with experimental data in Figures 3.14 and 3.15 (after Raoof and Zhang (1997)): the presently proposed theory is found to provide very encouraging bounding solutions to such a set of extensive large scale test data relating to 83 individual beams. Most importantly, it was argued that owing to large variations (by a factor of, say, 2) in spacings of stabilised cracks (and, hence, the width of a tooth within the concrete cover) in practice, wide scatter is to be expected in the test data from even closely controlled experiments. It was, therefore, concluded that due to this inherent property of the problem, a lower/upper bound theoretical approach is the most appropriate one to

adopt with the lower bound solution being the suitable (i.e. safe) one for design purposes. In view of the absence of a unique solution, therefore, the previous practice among various researchers of carrying out experimental parametric studies was shown to be fraught with difficulties and uncertainties with the wide scatter problem making any conclusive deductions based on purely experimental comparisons very difficult if at all possible.

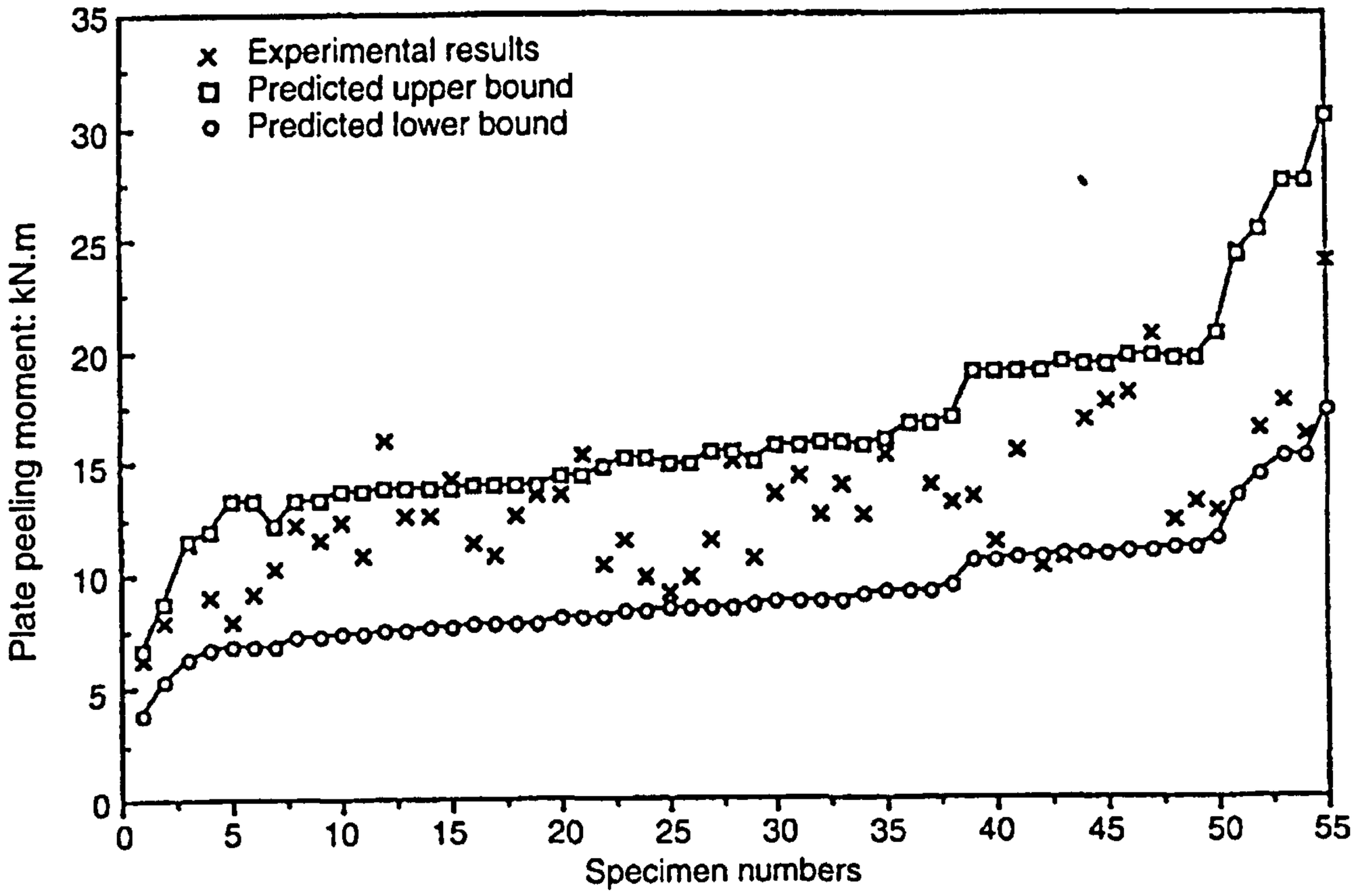

Fig. 3.15 Correlations between the theoretical upper and lower bound solutions of Raoof and Zhang (1997) and experimental data after Oehlers and Moran(1990).

Raoof and Zhang (1997) also used non-linear finite element method to demonstrate the significant influence of the ratio of plate area to the total area of main embedded (tensile) reinforcement on the ultimate flexural load of reinforced concrete beams with external steel plates in the presence of full bond between the plate and concrete up to the ultimate load. Changes in the flexural stiffness in the presence of external

plates bonded to under- or over-reinforced concrete beams but in the absence of premature plate peeling failures up to the ultimate load were also investigated by Raoof and Zhang (1997), using non-linear finite element method: it was shown that inclusion of external steel plates leads to practically significant increases in the overall flexural stiffness of the composite beams such as those tested by Jones *et al.* (1982) with the increases in the flexural stiffness being more pronounced for under-reinforced beams. Moreover, using non-linear finite element method, these authors showed that even in the presence of full bond between the external plate and concrete up to the ultimate load, there are noticeable deviations from the plane-section bending, with R.C. beam's cross-section experiencing significant distortions. Based on test data and numerical studies, however, it was demonstrated that despite such deviations from the classical (i.e. plane-section bending) methods of ultimate limit state design as recommended by various codes of practice, such traditional methods may still be used in practice to provide reasonably accurate estimates of the ultimate flexural load bearing capacity for externally plated beams.

3.3.3.3 Critical Examination

The method of Raoof and his associates certainly looks promising and (in what follows) its various aspects will be checked against a large body of test data as reported by others.

Neglecting the curvature peeling stresses of the beam and assuming that the axial plate stress is the controlling one regarding the premature plate peeling forms one of the basic assumptions in this model: this assumption has been proven to be a

reasonable one by the isotropic analysis previously reported by Oehlers and Moran (1990) in which these authors have shown that the effect of axial plate peeling stresses is at least one order of magnitude greater than that due to the effect of the beam curvature.

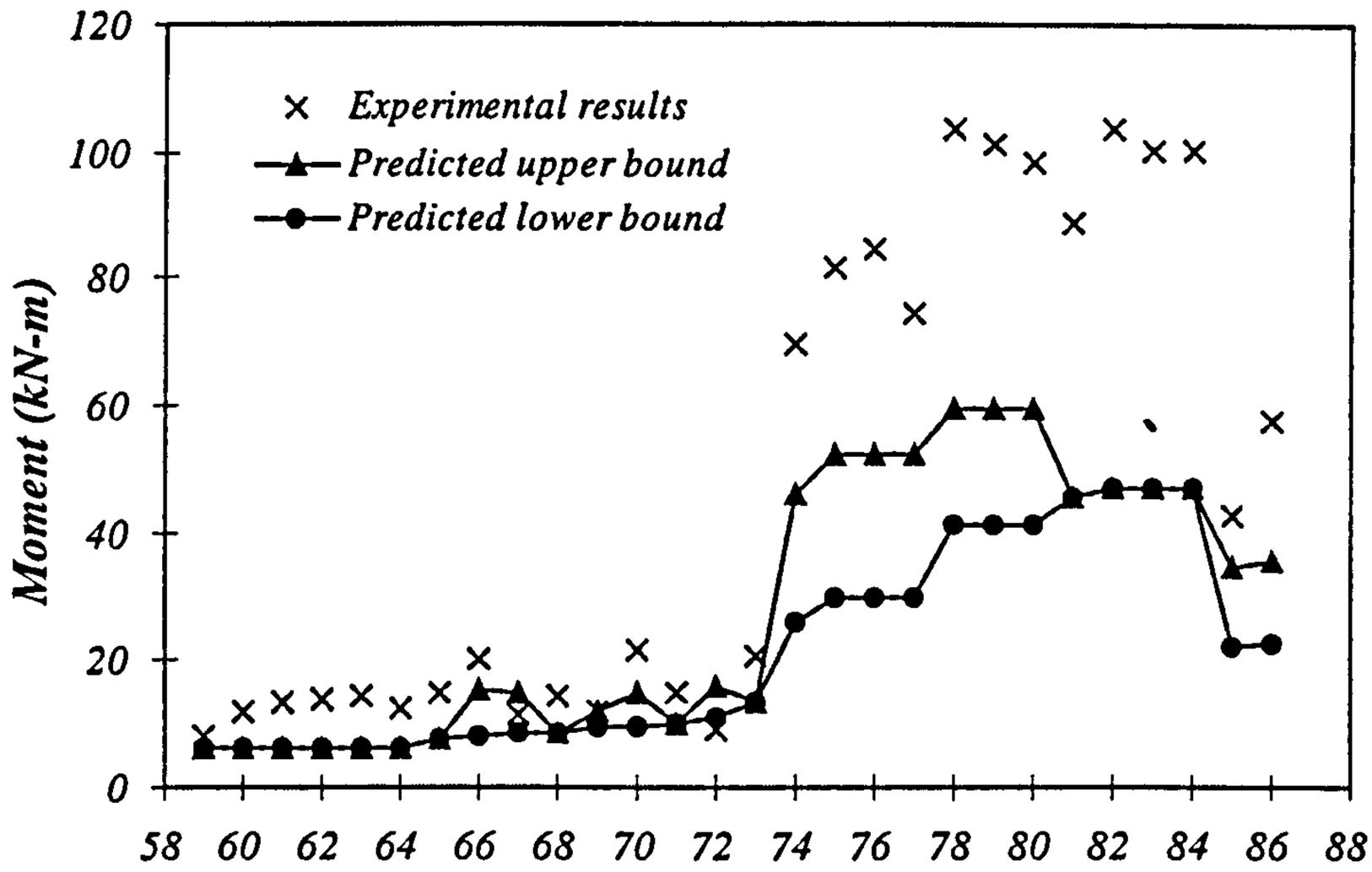

Fig. 3.16 Correlations between the upper and lower bound theoretical predictions of peeling bending moment of Raoof and Zhang and test data after Baluch *et al.* (1995) and Ritchie *et al.* (1991).

The second cautionary point relates to their assumed behaviour of the concrete tooth in-between two adjacent cracks which was taken to follow Bernolli's assumption of plane section bending despite the usual large depth of the cantilever compared to its arm. This potential shortcoming of their model has, however, been catered for by employing certain calibration factors relating to what Raoof and Zhang called the effective length of the critical section of the plate located within the shear span to be discussed fully later on in this thesis.

Raoof and Zhang's neglect of the transverse deformations in the adhesive layer is, on the other hand, believed not to significantly affect the accuracy of their model unless the thickness of the adhesive layer is relatively large with very low values of shear modulus for the adhesive material which is not the usual case in practice.

In this thesis, Raoof and Zhang's model will be checked against further (i.e. more extensive) experimental results, as reported by others, relating not only to steel but also FRP plated beams, in order to verify its reliability for general use in practice. A computer programme has been developed to calculate lower/upper bound theoretical peeling capacities of the plated beams: some details of this programme and the final numerical results are reported in Chapter 4. The experimental results from a large body of references as cited by Baluch *et al.* (1995), plus the test data of Ritchie *et al.* (1991), Oehlers (1992), and Oehlers and Moran (1990) have, indeed, been found to correlate well with the predicted lower/upper bound solutions of this model: these are shown in Figures 3.14, 3.15 and 3.16, which suggest that despite the wide variations of beam design details, this method predicts a safe (lower bound) peeling load capacity. Details of the calculations regarding the predicted moments are fully covered in Chapter 4. With this model verified, it will then be extended to cover other aspects of the problem: this includes studies on beams which have been pre-cracked prior to strengthening by external plates, and beams upgraded with external FRP plates. Details of such extensions of the model are also reported in Chapter 4.

3.3.4 Other Approaches

Ritchie *et al.* (1991) adopted an iterative method, as originally developed by Geymayer (1968), to predict the stiffness and the maximum strength in bending of plated beams. The external plate was assumed to be fully bonded to the concrete beam throughout the numerical iterations which were terminated by either the plate rupturing or the plate acting effectively (i.e. in full composite action with concrete) up to the maximum beam strength. The iterative method assumed initial values for the magnitudes of bending strain in the top fibre of concrete and the depth of neutral axis and, then, calculated total tension and compression forces to check equilibrium. If needed, the initially assumed depth of neutral axis was changed until the equilibrium condition was satisfied. Once this was achieved, the moment about the neutral axis was determined, and the curvature calculated, with the deflection and slope of the beam estimated, using the finite difference method. The maximum strength of the beam was assumed to have been reached, when either the externally bonded FRP plate was fractured or the moment was reduced with increases in the magnitude of bending strain at the top fibre of concrete. The ACI limiting value of 0.003 for the maximum concrete compressive strain was not adhered to, but the actually measured material properties were used. The so-obtained theoretical results were, then, compared with the experimental data relating to tests carried out on 16 beams, out of which 14 were plated (Ref. Chapter 2). Although their theoretical load-deflection curves were found to be stiffer than the corresponding experimental curves, there were fairly good correlations between the experimental and predicted load-deflection curves. However, in the majority of cases, the experimental failure was not found to occur within the maximum moment region as predicted by the theoretical model. Moreover, out of the 14 tested plated beams, the theoretical failure load for only 1

beam provided a conservative answer, with the predictions for the other 13 beams being larger than the experimental failure load: this was believed to be as a result of assuming full bond between the plate and concrete, and not considering other possible modes of failure.

Wei An *et al.* (1991), reported analytical models, based on the compatibility of deformations and equilibrium of forces, to approximate the behaviour of R.C. beams externally reinforced with epoxy-bonded fibre composite plates. These authors assumed full transfer of forces from the composite plate to the concrete beam. It was shown that the composite plate bonded to the tension side of the beam increases the stiffness, the yield moment, and the ultimate moment of the beam, and reduces the curvature at failure. Their theoretical parametric studies indicated that the technique of strengthening the existing concrete beams with epoxy-bonded composite plates is particularly effective in reinforced concrete beams with a relatively low internal steel reinforcement percentage ratio. Moreover, it was argued that although increases in the compressive strength of concrete did not appreciably increase the ultimate moment of under-reinforced and unplated beams, in the presence of external composite plates, increases in the concrete compressive strength could lead to practically significant increases in the ultimate moment of the section.

In an analytical study, focusing on the behaviour of side plated beams with the side plates anchored using steel bolts, Oehlers and Ahmed (1996) proposed a model based on full and also partial-shear connection, using a rigid-plastic procedure, for determining the increases in the shear and flexural strength of side-plated reinforced concrete beams. It was shown that both the shear and also the flexural strengths may

be increased, and the deflections and crack widths are reduced by using bolted steel side plates. It should be pointed out that, in certain cases, a reinforced concrete beam upgraded in flexure by only gluing an external plate to its tension side may not have the shear strength to carry the load that the increased flexural capacity would permit, and, hence, external shear reinforcement (in the form of, for example, external plates bonded and/or bolted to the sides of the beam) would be required: the work of Oehlers and Ahmed (1996) obviously addressed this issue regarding which there remains a number of unresolved problems. This aspect of the plated beams is, however, outside the scope of the present thesis which only concentrates on various structural characteristics of reinforced concrete beams upgraded by gluing steel or fibre reinforced plastic (FRP) plates to their soffits, in order to strengthen them in flexure.

3.4 DISCUSSION AND CONCLUSIONS

In this chapter, the salient features of a number of previously reported analytical and/or semi-empirical models for predicting various structural characteristics of reinforced concrete beams upgraded by gluing steel or FRP plates to their tension side has been presented. Critical quantitative examinations of the previously reported models of Baluch, Sharif, Oehlers, and Raoof and Zhang have been undertaken in order to identify their potential advantages and/or shortcomings. Further experimental verifications of the model proposed by Raoof and Zhang, have been carried out, using test data reported by others. It is concluded that, contrary to all the other models, the model which was reported by Zhang and Raoof is, indeed, a promising one from the prospective of a safe prediction for the plate peeling load and regarding the basic

assumptions of their theory. In addition, this model has the highly desirable feature of enabling one to easily identify the first order design parameters which affect the plate peeling phenomenon.

In a number of areas, unresolved issues have been identified, and these will be critically addressed in the following chapters which include detailed studies as follows:

1- The effect of pre-cracking of the plated reinforced concrete beams on the upper/lower bound predictions of plate peeling load as predicted by Raoof and Zhang's model (which was originally developed for uncracked beams prior to plating) will be critically examined. Further insights will also be given regarding certain practical implications of this model.

2- Using test data recently reported by the group at Surrey University, Raoof and Zhang's model (which was originally developed for external steel plates) will be extended to predict upper/lower bounds to the values of plate peeling moments in those cases when FRP (as opposed to steel) plates are used for upgrading reinforced concrete beams in flexure.

3- Using the model of Raoof and Zhang, a theoretical parametric study will be carried out in order to identify the influence of various beam design parameters on the magnitude of plate peeling moment.

4- A detailed study will be carried out in order to identify all the possible flexural modes of failure for R.C. beams strengthened with either external steel or FRP plates. In particular, various characteristics of each of these failure modes will be studied in a quantitative fashion.

5- The effect of variations in the magnitude of Young's modulus for FRP plates on potential changes in the flexural ultimate load of reinforced concrete beams upgraded with externally bonded FRP plates, in the absence and/or presence of plate peeling, will be investigated in some detail, with the theoretical predictions of various failure loads and associated modes of failure supported by an extensive set of test results from other sources.

6- Finally, simple formulations (amenable to hand calculations, using a pocket calculator) will be recommended for designing reinforced concrete beams, with either external steel or FRP plates, against occurrence of premature plate peeling failure which should prove of value to busy practising engineers.

Chapter 4

PREDICTION OF PLATE PEELING FAILURE

Chapter 4

PREDICTION OF PLATE PEELING FAILURE

4.1 INTRODUCTION

In this chapter, certain unresolved issues relating to premature plate peeling phenomenon will be critically addressed. A semi-empirical model will be developed for predicting the peeling failure of FRP plated reinforced concrete (R.C.) beams. Moreover, the question of pre-cracking of the beam prior to upgrading it with externally bonded steel plates will be addressed in some detail. Previous experimental studies have largely used uncracked laboratory specimens to which external plates have been bonded with the upgraded beams tested to failure, and little attention has been devoted to the real life situations where the R.C. beams in actual structures (under service conditions) are already cracked to some degree. The purpose of the present study is to clarify as to whether or not testing uncracked R.C. beams provides conservative answers for the practical conditions, and to provide a reasonable quantitative theoretical insight into the problem.

In the following sections, it will also be demonstrated that, unlike steel plated beams, purely empirical approaches based on limiting the ratio of plate width/thickness do not always ensure safety against premature plate peeling failure for R.C. beams upgraded with external FRP plates.

4.2 CASES TO BE EXAMINED

Despite the extensive experimental studies available in the literature that focus on the so-called most influential parameters affecting the plated beam behaviour, there is no theory which deals with all of the primary parameters in a systematic fashion. The previously reported formulations are largely either purely empirical or semi-empirical in nature and have invariably ignored the effect of certain first order beam design parameter(s). For example, many tests have been carried out to study the effect of pre-loading prior to external plating which is quite an important factor as it represents the practical situations associated with repair works in which the structures have already been in use for some time and, hence, are cracked prior to strengthening. However, the final results have invariably been inconclusive. Similarly, the previous semi-empirical models (originally developed for steel plated beams) are unable to properly model the effects of different types of plate material. The theory developed by Zhang *et al.* (1995), however, has the potential for further development to cover such aspects of the problem. Certain issues which are in need of further development and/or clarification are as follows:

1- As the original theory of Zhang *et al.* (1995) was developed for beams strengthened with external steel plates, there is a need to extend it to cover those cases with external FRP plates as this type of plate material is emerging with advantages over steel and is a promising one to be used extensively for future strengthening applications. Experimental results for beams strengthened with FRP plates will be used to determine the effective length of the plate located within the shear span, adopting alternative (but reasonable) values of bond strength between the FRP plate and concrete.

2- The vast majority of strengthening works which use external plates are carried out on R.C. beams which have already been in use. Any experience of pre-loading (even due to self-weight) leaves the flexural element(s) with some sort of cracking. It is, therefore, of prime importance to examine the influence of pre-cracking in flexural elements which are to be upgraded with externally bonded steel/FRP plates.

4.3 A PURELY EMPIRICAL METHOD

Figure 4.1 presents plots of M_{exp}/M_{pult} against the ratio of the width of the plate, b, to its corresponding thickness t (i.e. b/t), for a total number of 94 simply supported R.C. beams, upgraded with externally bonded steel plates, using test data after Ritchie *et al.* (1991), Baluch *et al.* (1995), Oehlers (1992), and Oehlers and Moran (1990), where M_{exp} is the experimental ultimate plate peeling moment, and M_{pult} is the ultimate flexural moment of the plated beam according to BS8110 (1985) with material partial safety factors set equal to unity. All the beam specimens were experimentally found to suffer from premature plate peeling failure, and, as shown in Figure 4.1, the values of M_{exp}/M_{pult} for all the beam specimens (apart from only two cases) are less than 1.0 - i.e. full bond between the plate and concrete up to the beams' ultimate load (associated with which the steel plate will, according to the traditional design approaches, yield) was not maintained.

It is, however, interesting to note that the limiting value of $b/t = 60$ may (as a simple empirical bounding value) be established from the plots in Figure 4.1: in other words, as a simple preliminary design approach, in order to avoid occurrence of premature

plate peeling failures, the width to thickness ratio, b/t, of bonded steel plates should not be less than 60. This limiting value of $b/t = 60$ is the same as that previously recommended by McDonald (1982) who based his tentative recommendations on somewhat limited number of test results in contrast to the present study which is based on a rather extensive set of data relating to test results for simply supported beams covering a wide range of beam design parameters.

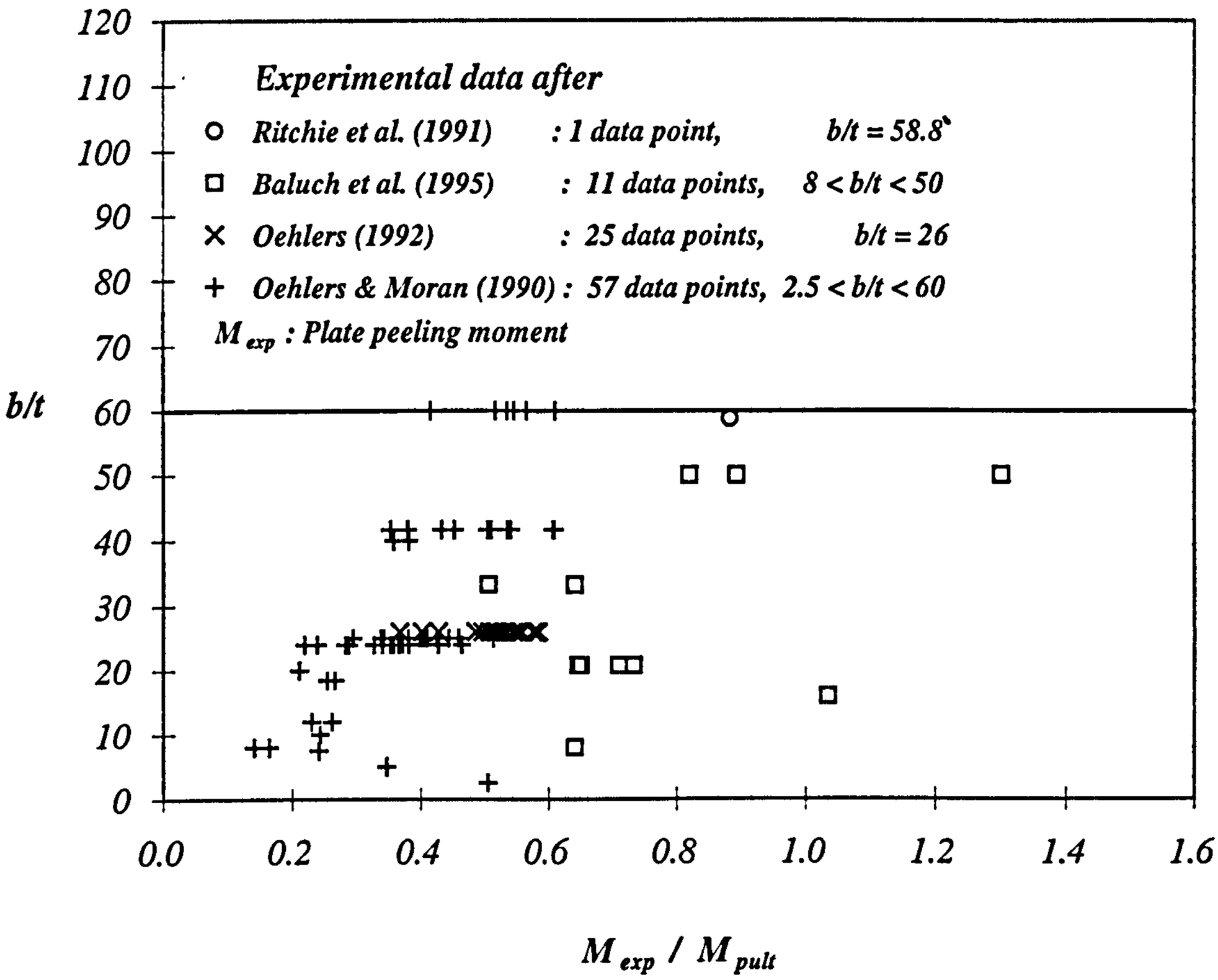

Fig. 4.1 Influence of steel plate width/thickness ratio on plate peeling failure for cases when premature plate peeling has occurred.

It is, perhaps, worth noting that the corresponding recommended limit suggested by Swamy *et al.* (1987), who only used very limited number of test data, is $b/t = 50$. On the other hand, Figure 4.2 presents plots of b/t versus M_{exp}/M_{pult} with the experimental results after Ritchie *et al.* (1991) and Baluch *et al.* (1995) again relating

to reinforced concrete beams upgraded by gluing steel plates to their soffits. All the experimental results, M_{exp}, relate to cases when the external steel plate remained fully bonded to concrete up to the ultimate (failure) load with non of the 15 test specimens suffering from occurrence of premature plate peeling failures: the values of M_{exp}/M_{pult} are (as a whole) greater than 1.0 over the wide range $26 < b/t \leq 100$. Eleven of the test specimens from Baluch *et al.* (1995) failed in flexure, while the other four test specimens failed in shear. It is, then, obvious that for even the values of $b/t < 60$, occurrence of premature plate failure is not definite, and there must be other first order design parameters such as the cross-section area of the plate (as discussed later in this chapter) which control this phenomena. Moreover, as it is the case with most purely empirical methods, the range of values for the design parameters used associated with test specimens leading to plots such as those in Figure 4.1, are unlikely to have covered all the possible practical ranges of controlling design parameters and, in certain instances (not covered by the corresponding tests), one may be faced with the breakdown of this purely empirical method. The value of a reliable theoretical model such as the one to be reported is, then, obvious: using such a model, one is able to carry out extensive theoretical parametric studies at reasonable cost and effort and, hence, identify the first order beam design parameters with reasonable confidence. Once identified, these parameters may be controlled in a systematic fashion for efficient and reliable design purposes.

Finally, Figure 4.3 presents similar plots of b/t versus M_{exp}/M_{pult}, for a total number of 18 simply supported R.C. beams which were (unlike the plots in Figures. 4.1 and 4.2 which correspond to steel plated R.C. beams) strengthened in flexure by external bonding of fibre reinforced plastic (FRP) plates: the test data presented in Figure 4.3

are after Quantrill *et al.* (1996), Saadatmanesh *et al.* (1991), and Ritchie *et al.* (1991), with all the beams suffering from premature plate peeling failures - i.e. $M_{exp}/M_{pult} < 1.0$.

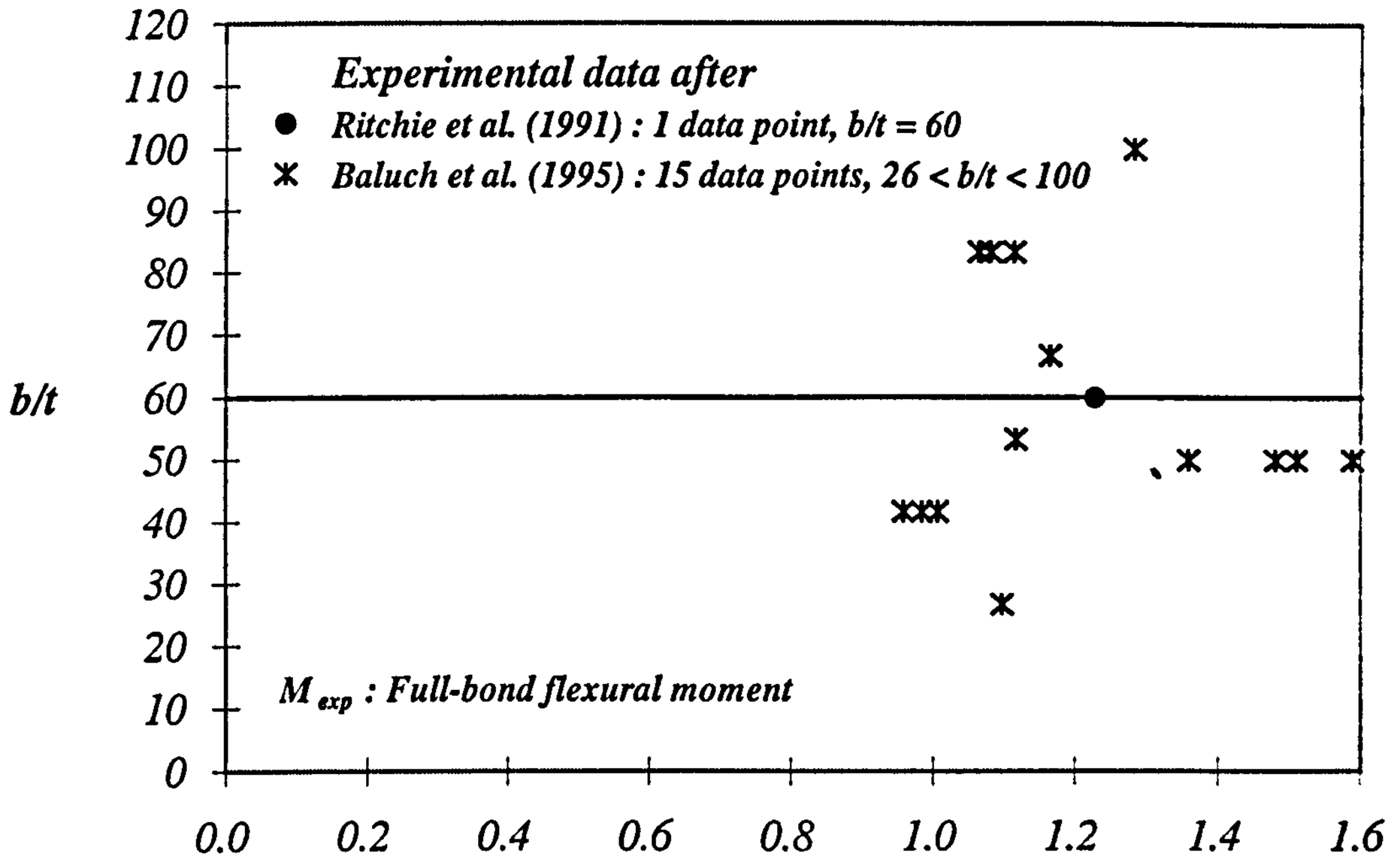

Fig. 4.2 Influence of steel plate width/thickness ratio on failure load for cases when premature peeling failure did not occur.

An examination of the results in Figure 4.3, however, suggests that, unlike externally bonded steel plates, even for the ratios of b/t greater than 60, premature FRP plate peeling failures can, indeed, happen and one is not able to sensibly suggest a simple empirical limiting value of b/t for design against FRP plate peeling. This is believed to be (at least partly) due to the very large variations in the values of Young's modulus, E_p, and ultimate tensile strength, σ_u, associated with FRP plates as currently available on the market: for the test data presented in Figure 4.3, $10.3 \le E_p \le 118.5\ GPa$ and $160.7 \le \sigma_u \le 1490\ MPa$. Unlike FRP plates, the values of Young's modulus for steel plates are very nearly constant, with their associated

magnitudes of yield (or ultimate strength) lying within a fairly narrow range, which enable one to come up with a constant empirical limiting value of $b/t = 60$ for preliminary design purposes.

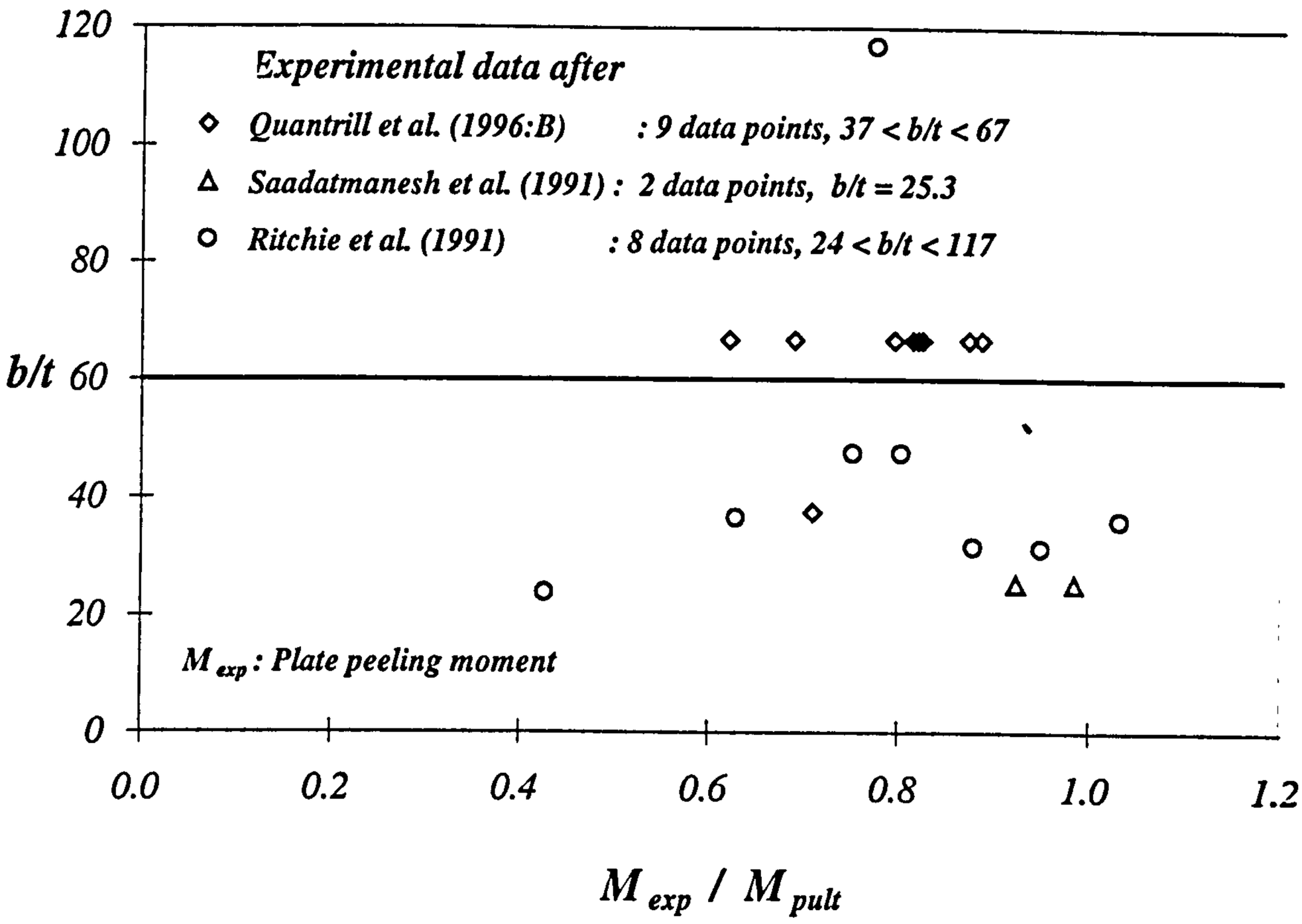

Fig. 4.3 Influence of FRP plate width/thickness ratio on plate peeling failure.

4.4 EXTENSION OF THE THEORETICAL MODEL TO FRP PLATES

Raoof and Zhang's (1997) theoretical model was originally developed for reinforced concrete beams strengthened by externally bonded steel plates with the extensive large scale experimental support for this model already presented in Chapter 3. The other case of practical interest relates to externally bonded FRP plates which is to be discussed in what follows, and is based on an extended version of Raoof and Zhang's peeling model. A close examination of Equations (3.17) to (3.31) in Chapter 3 suggests that the necessary modification to the theoretical model, when applied to this

alternative plating material, involves replacing the semi-empirical Equations (3.26) and (3.27) with the alternative ones applicable to cases when FRP plates are used. Moreover, there are uncertainties regarding the choice of an appropriate value for the bond strength, u_1, between FRP plates and concrete, with the value of parameter u_1 needed as an input into a modified version of Equation (3.28), which is

$$\sigma_{s(\min)} = \frac{A_e\ (f_t')^2\ L_P}{6h't\ (u\sum 0_{bars} + u_1 b_1)}\frac{b}{b_1} \qquad (4.1)$$

where, $u =$ bond strength between the embedded steel bars and concrete, $u = 0.28\sqrt{f_{cu}}$ (after Mosley and Bungey (1990)), and $u_1 =$ bond strength between the FRP plate (with a width equal to b_1) and concrete. Obviously, for cases when external steel plates are used $u_1 = u = 0.28\sqrt{f_{cu}}$, as implicit in Equation (3.31). Unfortunately, to the best of present author's knowledge, no equivalent simple relationship for determining the value of u_1 has been reported in the literature for cases when FRP (as opposed to steel) plates are used and, in this respect, the subject is still in its infancy. The ever presence of a thin layer of strong epoxy glue between the FRP plate and concrete will also further complicate the matter. Moreover, due to the inherent nature of concrete as a material, wide scatter is to be expected in practice, in any empirical method adopted for determining the parameter u_1 (or indeed, u), over the practical range of concrete strengths and mix designs.

In passing, however, it is, perhaps, worth mentioning that as reported by Ritchie *et al.* (1991), by using a full-length plate, one of the plates with 26-kip strength was fractured within the constant moment region (under symmetrical four-point loading) at an average bond stress of about 120 psi (= 0.83 N/mm^2): these authors, then, suggested a limiting average bond stress, u_1, between FRP plate and concrete for their

beams of about 110 to 120 psi (= 0.76 to 0.83 N/mm^2). The very tentative nature of their suggested value for u_1 should be born in mind. It is also, perhaps, worth mentioning that the values of allowable shear stresses as recommended in BS5400 (1990), part 4, for grade 40 concrete or stronger is 0.8 N/mm^2 with this allowable ultimate shear stress relating to constructions in which two concrete surfaces, one in situ and one pre-cast, act compositely. The closeness of the tentative value of 0.8 N/mm^2 for ultimate shear stress between FRP plates and concrete as recommended by Ritchie *et al.* (1991) and also the figure of 0.8 N/mm^2 for two concrete surfaces as recommended by BS5400 (1990) is interesting. In the absence of any more conclusive results, the figure of 0.8 N/mm^2 may be taken as a very rough (perhaps, lower bound) value for the bond strength between FRP plates and concrete, u_1, and this will be used as a double check on the final results based on alternative assumed values of u_1, as discussed next.

As previously mentioned, an extended version of the original theoretical model reported by Zhang *et al.* (1995) was developed by Raoof and Zhang (1997) for predicting the steel plate peeling moment which removed certain limitations imposed by the original version of the model. Unlike the original version which (for sufficiently short lengths of the plate within the shear span) assumed a uniform distribution of shear stresses between the steel plate and concrete over the whole portion of the plate within the critical shear span where plate peeling occurred, the extended semi-empirical version enabled one to cater for the more general cases when the portion of the steel plate within the critical shear span (where it terminates) can be as long as is desired: under such conditions, it is reasonable to assume that non-uniform variations of shear stresses over the steel plate/concrete interface can exist

which may be modelled by the concept of effective length, L_p (similar to Equations (3.26) and (3.27) in Chapter 3), with the effective length being defined as the equivalent length of the plate within the critical shear span along which a state of uniform shear stresses may be assumed. For the present purposes, using a method similar to that previously reported for steel plates, alternative semi-empirical equations based on test data reported by others will be developed which are applicable to FRP plates: rearranging Equation (4.1), with A_e given by

$$A_e = 2h_1 b$$

and $f_t^{'} = 0.36\sqrt{f_{cu}}$, one gets

$$L_p = \frac{\sigma_s h' b_1 t\,(u\sum 0_{bars} + u_1 b_1)}{0.0431 h_1 b^2 f_{cu}} \frac{1}{1.5} \qquad (4.2)$$

where, the axial tensile stresses in the plate lie between $\sigma_{s(\min)}$ and $\sigma_{s(\max)} = 2\sigma_{s(\min)}$, and, following Raoof and Zhang (1997), one may reasonably assume that the average σ_s in Equation (4.1) is equal to 1.5 $\sigma_{s(\min)}$: hence the factor 1.5 in Equation (4.2). All the terms in Equation (4.2) are as defined in the relevant section in Chapter 3. Using test data relating to the value of the plate axial stress, σ_s, directly under the point load nearest to the support, then, the value of effective L_p for any given beam design may be obtained by Equation (4.2).

Recently, Hollaway and his associates (Hollaway (1997) and Garden *et al.* (1997)) obtained test data relating to the critical plate axial strain, ε_{ue} (at plate peeling failure), directly under the point load nearest to the support, of 13 simply supported R.C. beams having a span of 1000 mm with external FRP plates bonded to their soffits. All these beams were loaded to failure under symmetrical four-point loading, and exhibited premature plate peeling failures. Table (4.1) presents various

geometrical and material properties for these beams with the information for the nine beams *S1-S9* after Hollaway (1997), and the data for the other four beams being after Garden *et al.* (1997). The effective length, L_p, for all the beams of Garden *et al.* (1997) and Hollaway (1997) may, then, simply be obtained by using Equation (4.2) in conjunction with the experimental data for the elastic strains ε_{ue} as given in Table (4.1), and assuming $\sigma = E_p \varepsilon_{ue}$, where E_p = Young's modulus for FRP; once appropriate values for the bond strength, u_1, are chosen.

Following the earlier discussions in this section, the value of u_1 remains (at least for the present) rather uncertain. However, in view of a number of other uncertainties in the model such as the usual wide scatter problem associated with certain concrete material properties such as its cube and tensile strengths, f_{cu} and $f_t^{'}$, respectively, which are needed as an input into the model, plus the simplifying assumption of plane-section bending implicit in Equation (3.19) in Chapter 3 (although, as mentioned before, in practice the concrete tooth is likely to act more like a deep beam with significant deviations from the plane-section behaviour), and finally, the semi-empirical method to be used for determining the values of effective lengths, L_p, (which follow next), one may, in the absence of any other reliable information, reasonably assume $u_1 = u = 0.28\sqrt{f_{cu}}$ - i.e. the bond strength between FRP plates and concrete, u_1, may be estimated using the same relationship as that reported by Mosley and Bungey (1990) for determining the bond strength between the embedded steel bars and concrete, u. In other words, by calibrating the model against test data (by way of the semi-empirical approach for determining the effective L_p), one may

reasonably cater for a number of, perhaps, inevitable practical uncertainties surrounding the problem. Once a semi-empirical method is established for determining the effective length, L_p, the theoretical predictions may, then, be checked against other **independent** test data (which have not originally been used for calibrating the model) in order to check the general reliability of the proposed model: indeed, as discussed in the next section, such an independent check of the proposed model has been found to result in encouraging correlations between theory and test data reported by others, hence, confirming the practical soundness of various underlying assumptions in the proposed model.

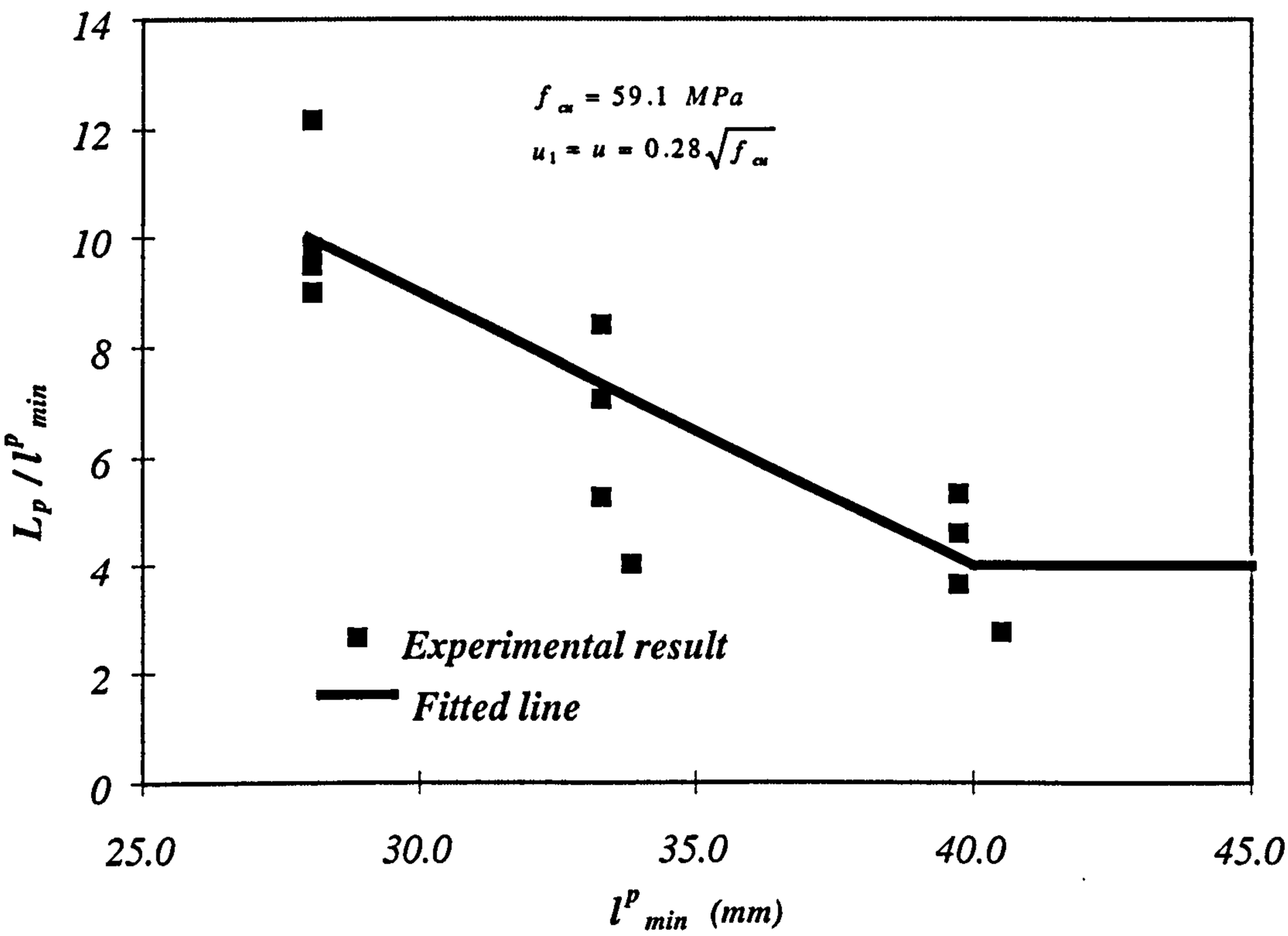

Fig. 4.4 **Determination of FRP plate effective length, L_p, assuming $u_1 = u = 0.28\sqrt{f_{cu}}$.**

Bearing the above in mind, it is, then, possible to plot variations of $L_p/l^p_{\min}$ against $l^p_{\min}$ as shown in Figure 4.4, where $l^p_{\min}$ and $l^p_{\max}$ = estimated minimum and maximum

stabilised crack spacings, respectively, as given by Equations (4.3) and (4.4) below (with their various terms as defined previously) which assume $u_1 = u = 0.28\sqrt{f_{cu}}$, and the parameter L_p is determined by using Equation (4.2) (again, assuming $u_1 = u = 0.28\sqrt{f_{cu}}$) in conjunction with the plate axial strain measurements, ε_{ue}, (and, hence, stresses $\sigma_s = E_p \varepsilon_{ue}$) at plate peeling failure from Hollaway (1997) and Garden *et al.* (1997) as given in Table (4.1).

$$l^p_{\min} = \frac{A_e f_t^{'}}{u(\sum O_{bars} + b_1)} \qquad (4.3)$$

and

$$l^p_{\max} = 2l^p_{\min} \qquad (4.4)$$

The fitted line through the semi-empirical data points in Figure 4.4 is defined by the following equations:

$$L_p = l^p_{\min}.(24.0 - 0.5 l^p_{\min}) \quad , \quad l^p_{\min} \le 40.0 \qquad (4.5)$$

$$L_p = 4.0 l^p_{\min} \quad , \quad l^p_{\min} > 40.0 \qquad (4.6)$$

The rather tentative nature of Equation (4.6) should, however, be noted at once: for $l^p_{\min} > 40.0$, no experimental data is currently available, and this equation is proposed as guided by the work of Raoof and Zhang (1997) on steel plated beams. There is clearly a need for experimental data relating to cases when $l^p_{\min} > 40.0$.

The above equations, then, provide a simple means of estimating reasonable values for the effective length of the FRP plate within the critical shear span, L_p, to be used in Equation (4.7) (see the derivation of Equation (3.31) in Chapter 3): the correct L_p

is the lower value of L_p as calculated from Equations (4.5) and (4.6), L_{p-1}, and the actual length of the plate as shown in Figure 3.2 in Chapter 3, L_{p-2} (whichever is smaller). Obviously, if the plate is only positioned within the constant moment zone, the value of L_p in Equation (4.7) (given below) may only be estimated by using Equations (4.5) and (4.6). With the above borne in mind, one can predict $\sigma_{s(\min)}$ from

$$\sigma_{s(\min)} = \frac{L_p h_1 b^2 \sqrt{f_{cu}}}{h' b_1 t (\sum O_{bars} + b_1)} \qquad \textbf{(4.7a)}$$

and

$$\sigma_{s(\max)} = 2\sigma_{s(\min)} \qquad \textbf{(4.7b)}$$

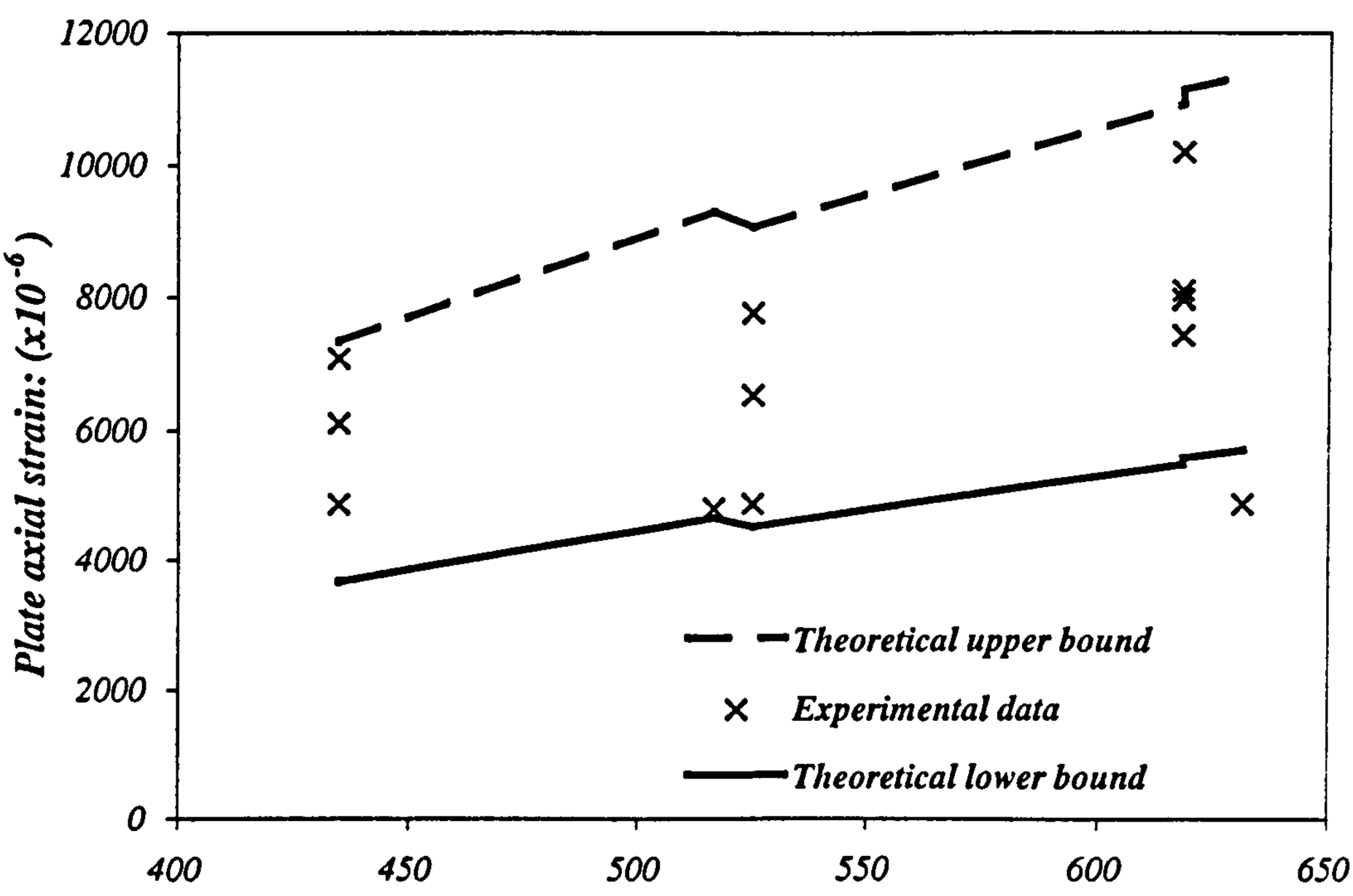

Fig. 4.5 **Variation of FRP plate axial strains with changes in the theoretical values of minimum plate axial stresses - test data after Hollaway (1997) and Garden *et al.* (1997).**

At first glance, the scatter of experimental data points about the mean fitted line in Figure 4.4, may perhaps, appear as rather too much. It must at once be noted, however, that due to large variations (by a factor of, say, 2) in the spacings of stabilised cracks in practice, a unique solution for the parameter L_p probably does not exist, and similar large variations of L_p for even a given beam design are to be expected in practice. As reported by Raoof and Zhang (1997), a theoretical approach based on either linearly elastic or non-linear interaction of the plate with concrete, aimed at determining the magnitude of an effective L_p, over which the plate/concrete shear stresses may be assumed to be constant, is, on the other hand, fraught with difficulties. These authors argued that even the application of formulations for the complex non-linear Finite Element technique which may either use the smeared, discrete or mixed smeared/discrete crack modelling is (in the present state of art) highly unlikely to lead to more meaningful answers than those using the very simple proposed semi-empirical method based on the plots of Figure 4.4. In this context, it is instructive to examine the plots in Figure 4.5; here, the experimentally determined plate axial strains are plotted against the theoretical values of minimum plate axial stresses, $\sigma_{s(\min)}$, as determined by Equation (4.7a), with the values of L_p in this equation determined by Equations (4.5) and (4.6). The test data in Figure 4.5 are all after Hollaway (1997) and Garden *et al.* (1997) and relate to the beams under symmetrical four-point loading in which the plates were extended to the shear span. It is interesting to note that (apart from only one data point) the test data lie within the region between the upper and lower bound theoretical lines. Only one data point falls below the theoretical lower bound line, and even this is (for all practical purposes) very close to the lower bound line which thus provides one with a reasonable degree of confidence in that the use of a fitted mean line to the test data in Figure 4.4 has

resulted in a semi-empirical formulation (or calibration) which leads to sensible lower and upper bound solutions for the critical axial stresses in the plates at peeling failure. However, it should be noted that unless one checks the same semi-empirical formulations against a much wider set of large scale test data, one cannot assume the proposed semi-empirical formulations to be of general applicability.

In the following section, the numerical results based on the above semi-empirical model will be checked against test data for a wide range of beam designs, from various sources, to demonstrate its general applicability.

4.5 CORRELATIONS BETWEEN THEORY AND TEST DATA

Figure 4.6 presents the correlations between upper and lower bound theoretical predictions of plate peeling moment and test data after Quantrill *et al.* (1996:A), Quantrill *et al.* (1996:B) and Garden *et al.* (1997).

Similar to all the other theoretical results presented in this section, a bi-linear (elasto-plastic) axial stress-strain relationship as recommended by the British Standard, BS8110 (1985), has been assumed for the embedded steel bars, while the FRP plate is assumed to be linearly elastic with a brittle fracture at ultimate axial load. The total number of test data points in Figure 4.6 is 34, all of which are **independent** of the 13 test data points originally used for calibrating the proposed model (i.e. deriving the semi-empirical Equations (4.5) and (4.6)), so that the correlations between theory and test data in Figure 4.6 provide an **independent** check of the general applicability of the proposed model.

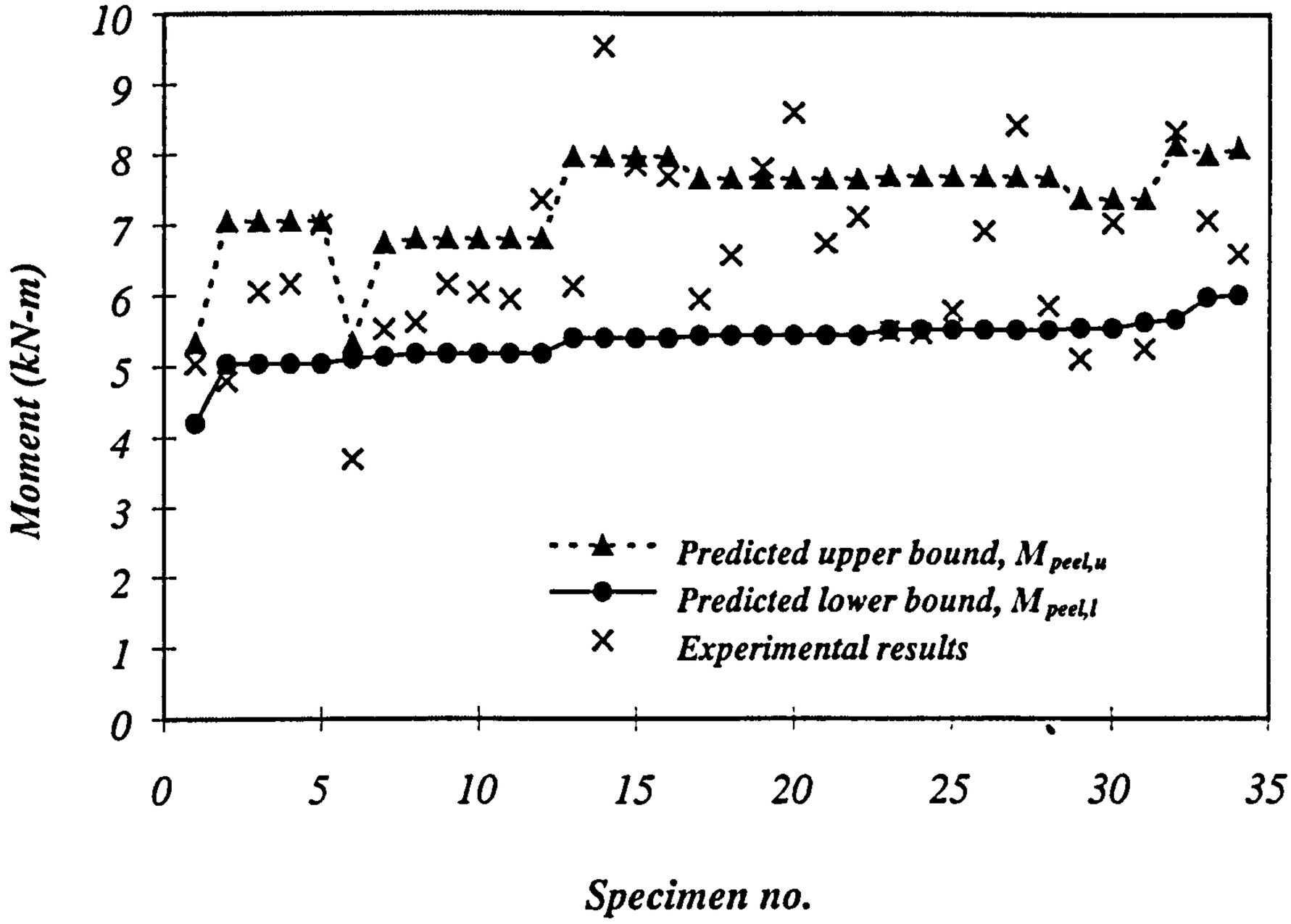

Fig. 4.6 Correlations between upper and lower bound theoretical predictions of FRP plate peeling moment and test data after Quantrill *et al.* (1996:A), Quantrill *et al.* (1996:B) and Garden *et al.* (1997).

The test data in Figure 4.6 are expressed as bending moment at premature FRP plate peeling failure with the bending moment corresponding to the beam section directly under the point load nearest to the support. It is important for the theoretical predictions of the bending moment, which are based on the concept of effective length as given by Equations (4.5) and (4.6), to take concrete tensile stresses below the neutral axis into account: such concrete tensile stresses must be taken into account in view of the sometimes very low values of axial stresses in the FRP plates, at the critical instance of premature plate peeling failure, with the net tensile force in concrete, then, becoming significant in magnitude when compared with the total tensile force in the FRP plate. An examination of the results in Figure 4.6 suggest that the test data reasonably lie in-between the upper and lower bound theoretical predictions with the lower bound predictions providing a safe solution in almost all

cases apart from one case (i.e. specimen number 6) where the test data is significantly lower than the corresponding theoretical lower bound solution. This is believed to be due to the rather small-scale of the beam specimens tested by Hollaway and his associates, with the beams only having a span of 1000 mm with a reinforcement concrete cover of only 16 mm (i.e. $h' = 13\,\text{mm}$), while the coarse aggregate used in their concrete mix was of 10 mm maximum size with the largest fine aggregate being 5 mm: although (as suggested by the good correlations between theoretical bounding predictions and this set of extensive test data which cover a wide range of beam design parameters) these small scale specimens are (as a whole) believed to have been carefully manufactured, adhering to closely controlled manufacturing tolerances, there may nevertheless have been some out of straightness imperfections in the 6 mm diameter steel reinforcing bars. Bearing in mind the prime (controlling) influence of the parameter h' in the model, a concrete cover of only 16 mm in the presence of such large aggregates coupled with the possible out of straightness imperfections of the reinforcing bars for the test result relating to specimen number 6 may be the responsible factors for this particular experimental result to be of a suspect nature and probably unreliable.

Similar correlations between the theoretical bounding solutions and (this time) large scale test data are, on the other hand, presented in Figures 4.7 and 4.8, where the test data in Figure 4.7 is after Saadatmanesh and Ehsani (1991:I), while the test data from Ritchie *et al.* (1991) is used for the plots in Figure 4.8. In particular, the reinforced concrete beams tested by Saadatmanesh and Ehsani (1991:I) had a very large clear span of 4570 mm. The beam specimens tested by Ritchie *et al.* (1991) had a clear

span of 2400 mm. The theoretical lower bound solution is found to provide a safe answer in all cases in Figures 4.7 and 4.8.

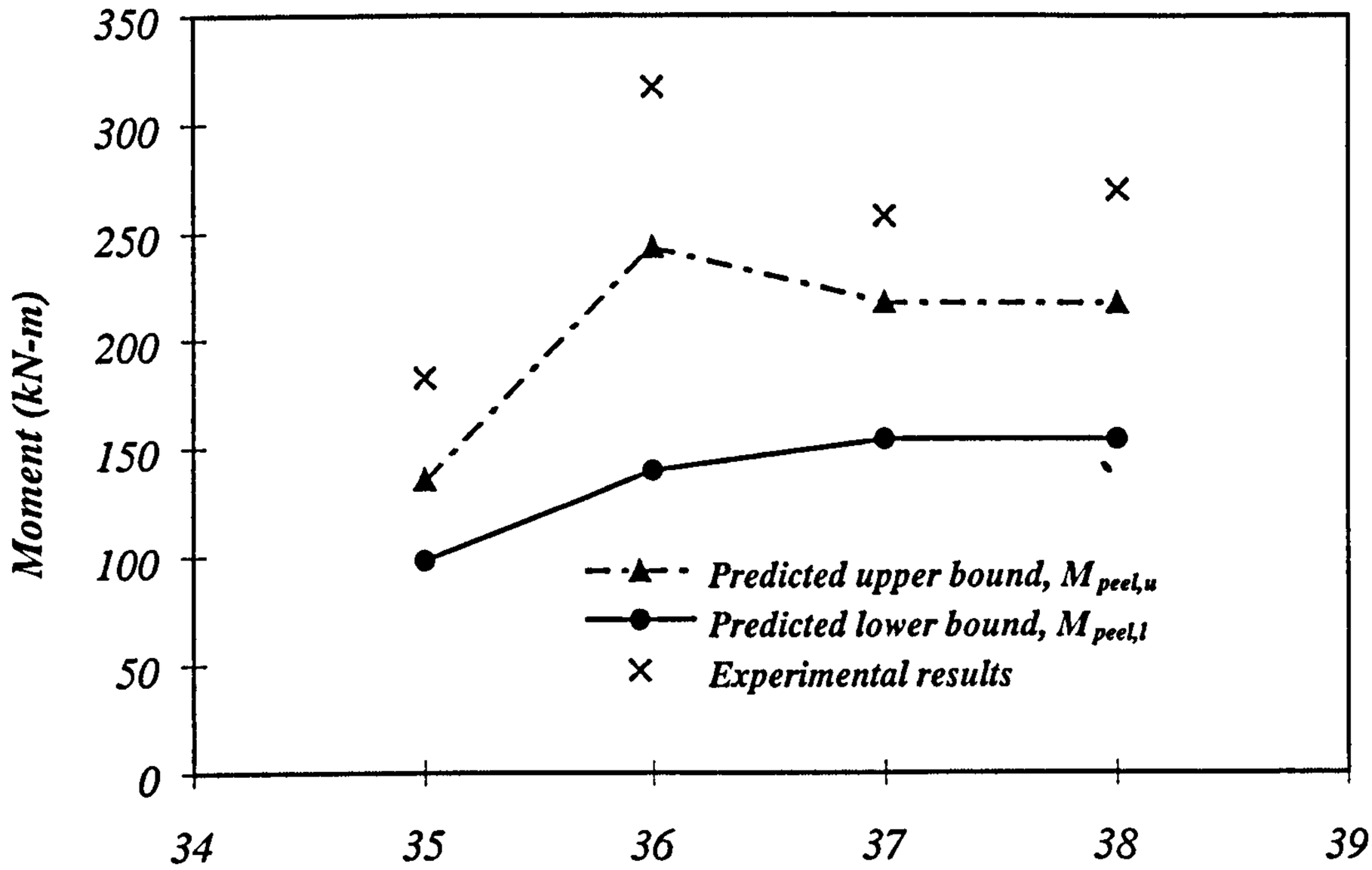

Fig. 4.7 Correlations between upper and lower bound theoretical predictions of FRP plate peeling moment and test data after Saadatmanesh *et al.* (1991).

Finally, in Figure 4.9, the theoretical upper and lower bounds for the premature FRP plate peeling bending moments are found to be equal in magnitude with $\sigma_{s(max)} = \sigma_{s(min)} = \sigma_u$ for all the beams tested by Sharif *et al* (1994): the correlations between theoretical predictions and the corresponding test data are found to be encouraging.

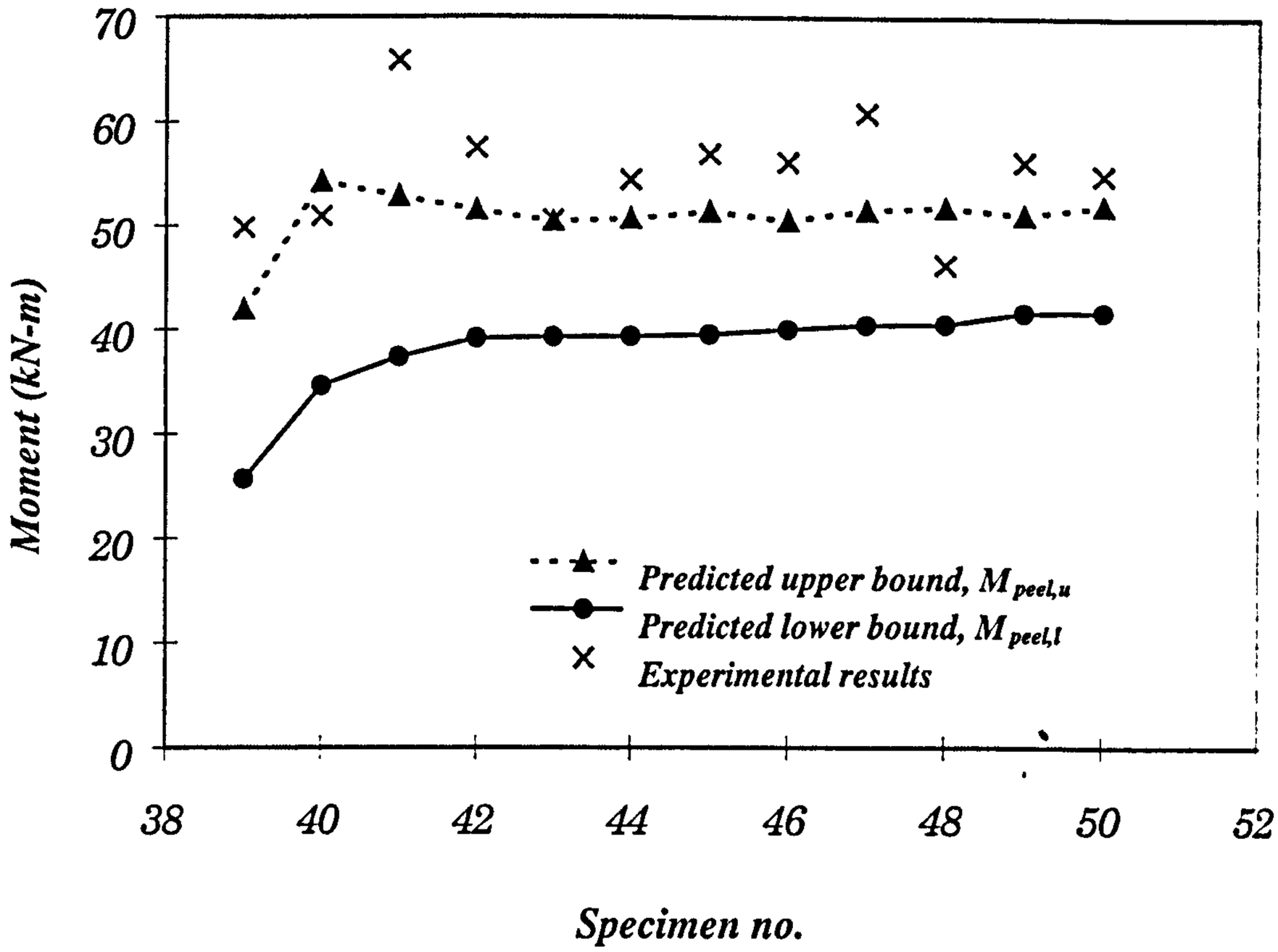

Fig. 4.8 Correlations between upper and lower bound theoretical predictions of FRP plate peeling moment and test data after Ritchie *et al.* (1991).

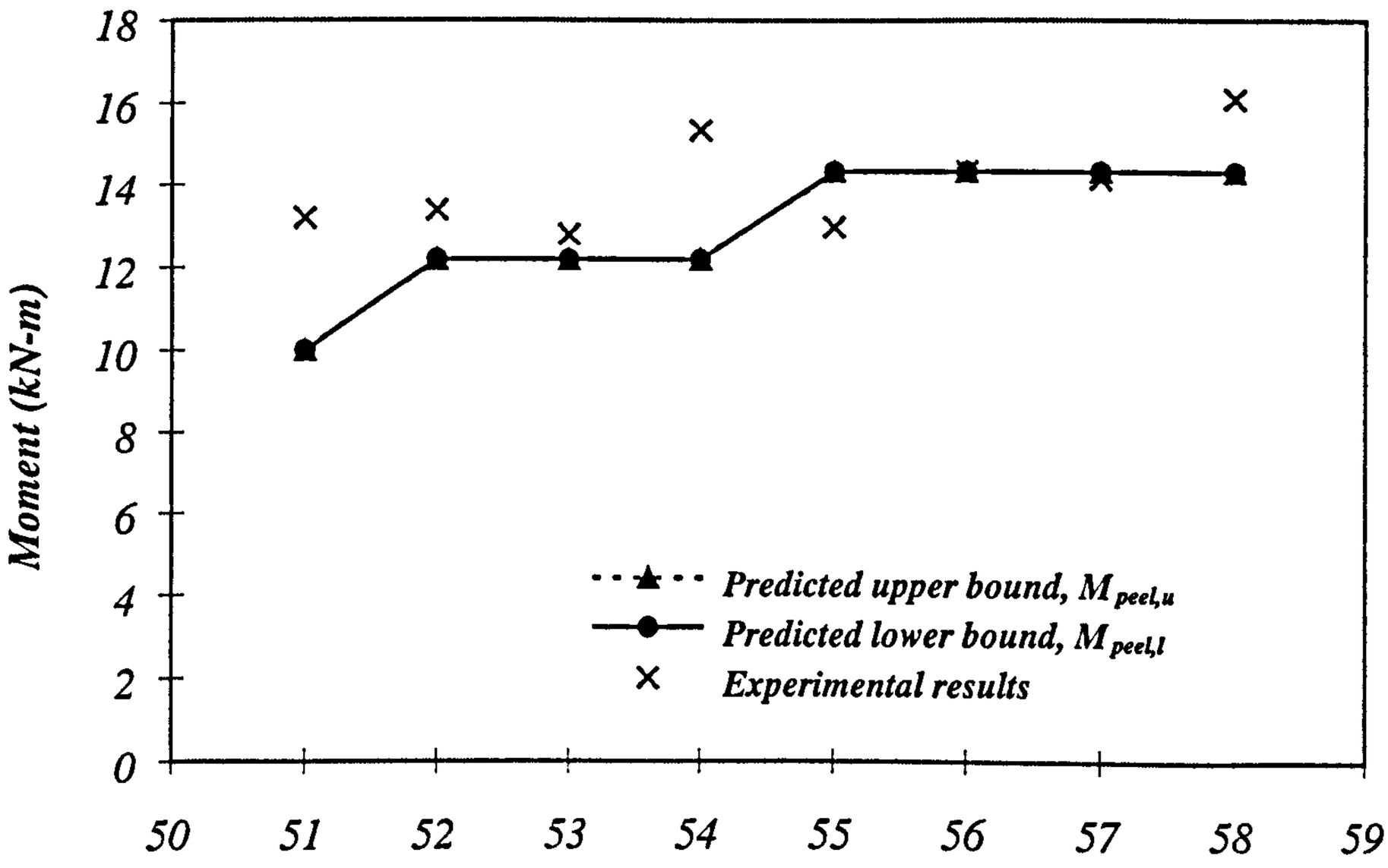

Fig. 4.9 Correlations between upper and lower bound theoretical predictions of FRP plate peeling moment and test data after Sharif *et al.* (1994).

To identify the underlying reason as to why certain experimental data points lie above the theoretical upper bound to plate peeling moment in Figures 4.7, 4.8, and 4.9, a careful study of the test results of Oehlers (1992) is instructive. Oehlers (1992) has fortunately reported both the initial and also the ultimate values of premature plate peeling loads for beams strengthened with external steel plate. There is significant differences between the experimentally determined values of the premature plate peeling ultimate moments (at which total collapse occurs) and those which correspond to the initiation of premature plate peeling for Oehlers' beams which had plates terminated within the shear span.

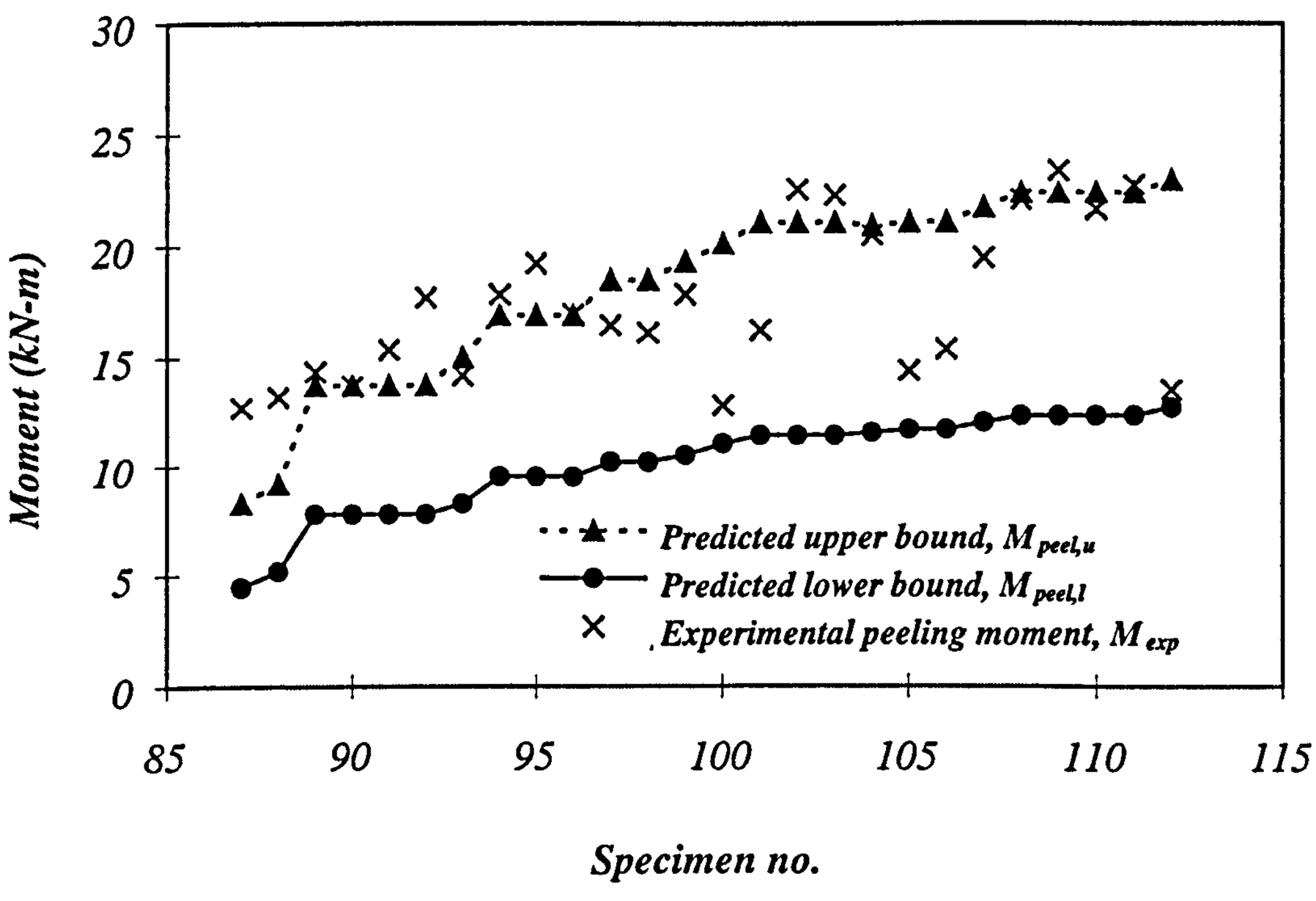

Fig. 4.10 Correlations between upper and lower bound theoretical predictions of steel plate peeling moment and test data relating to initial plate peeling moment after Oehlers (1992).

Plots in Figures 4.10 and 4.11 show the correlations between upper and lower bound theoretical predictions and test data relating to the initial plate peeling moments and

the ultimate peeling moments, respectively. It is particularly noteworthy that the test data points of ultimate peeling moments in Figure 4.11 are located significantly above the theoretical upper bound line while the test data points of the initial plate peeling moments, in general, lie within the lower and upper bounds with the lower bound in both plots providing a safe prediction against plate peeling failure. It is, then, concluded that, in certain cases, the plate peeling ultimate moments are higher than the theoretical upper bound as the theory was originally developed to predict fully brittle upper and lower bounds for the plate peeling moments and can not handle presence of any (although practically not very significant) degree of ductility in the plate peeling process.

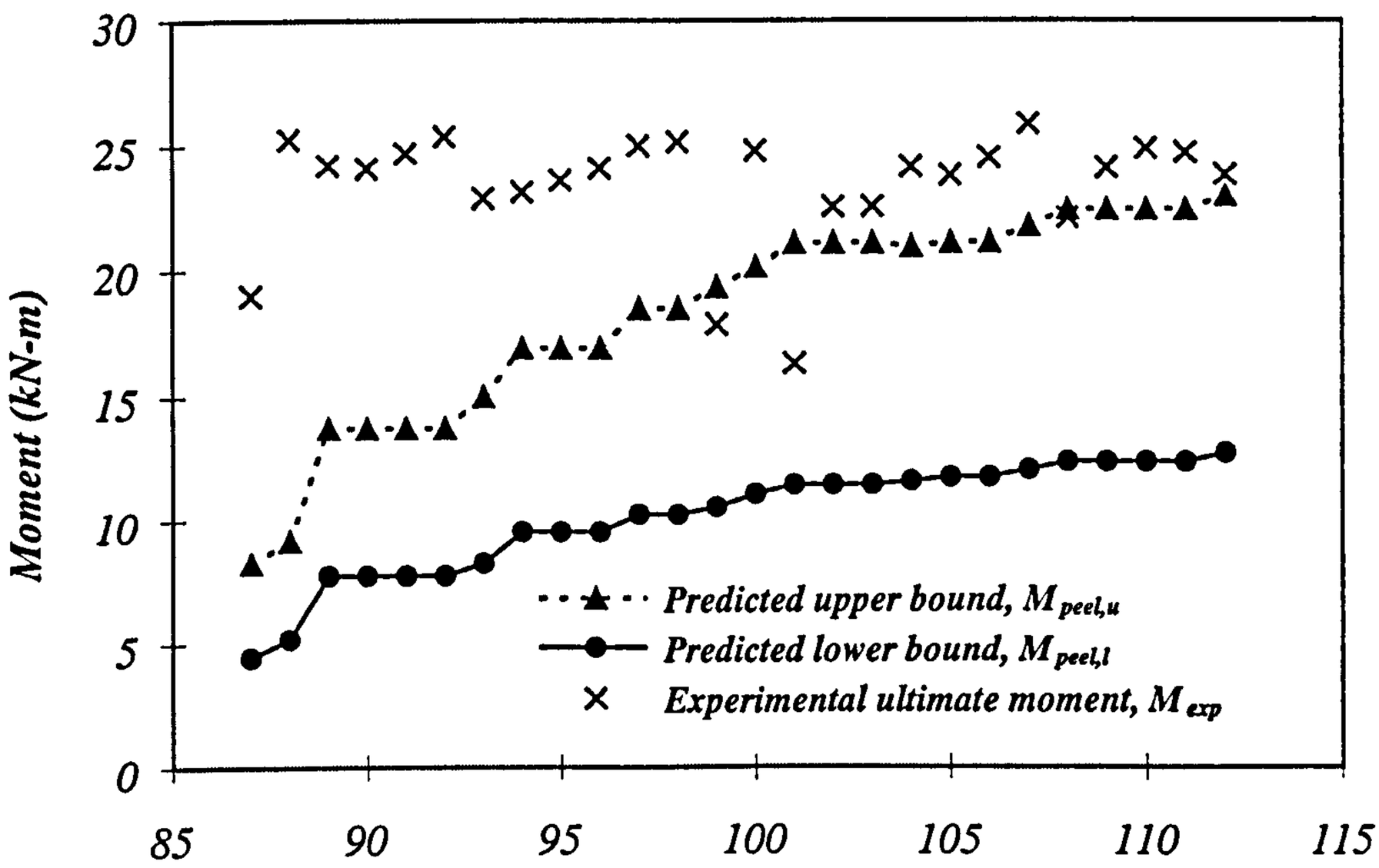

Fig. 4.11 Correlations between upper and lower bound theoretical predictions of steel plate peeling moment and test data relating to ultimate plate peeling moment after Oehlers (1992).

Unfortunately, no such detailed description of experimental results as of Oehlers (1992) have been reported by Saadatmanesh and Ehsani (1991) and Ritchie *et al.*

(1991): this, then, may be the underlying reason for a number of test data in Figures 4.7 and 4.8 lying above the theoretical upper bound solutions with these experimental results probably relating to the ultimate plate peeling moments, although (considering the usual inherent variability of concrete as a material) particularly the test data in Figure 4.7 are (as a whole) quite close to the corresponding upper bound solutions and the theoretical predictions are not believed to be too conservative for practical purposes. Moreover, in certain cases (particularly relating to the test data after Ritchie *et al.* (1991)) the test specimens had plate end anchorage arrangements which delay the occurrence of plate peeling and, hence, could have well increased the level of plate peeling load to be higher than the theoretical upper bound.

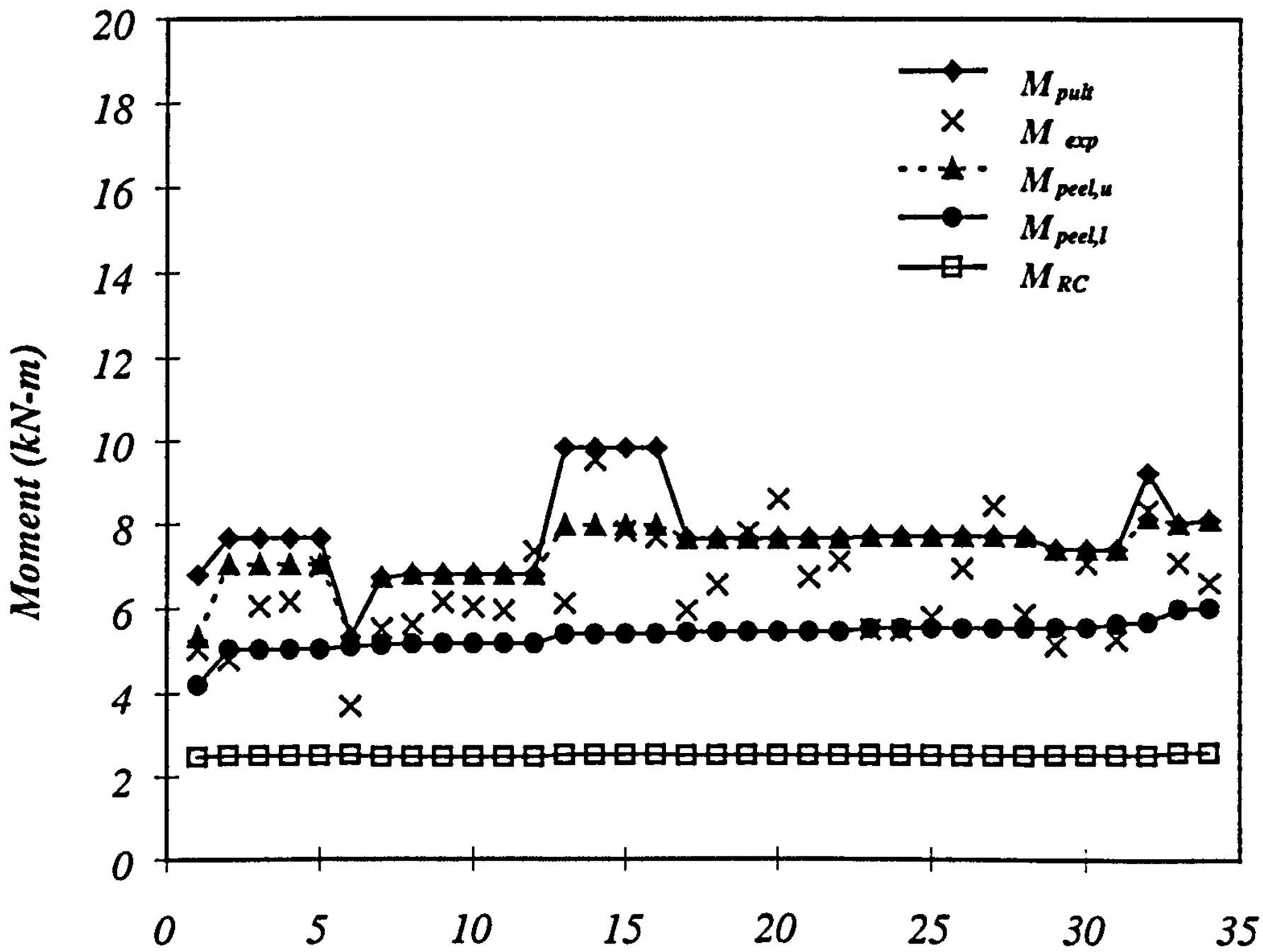

Fig. 4.12 **Comparison of plated and unplated ultimate bending moments, M_{pult} and M_{RC}, respectively, with FRP plate peeling moments: beam designs after Quantrill *et al.* (1996:A), Quantrill *et al.* (1996:B) and Garden *et al.* (1997).**

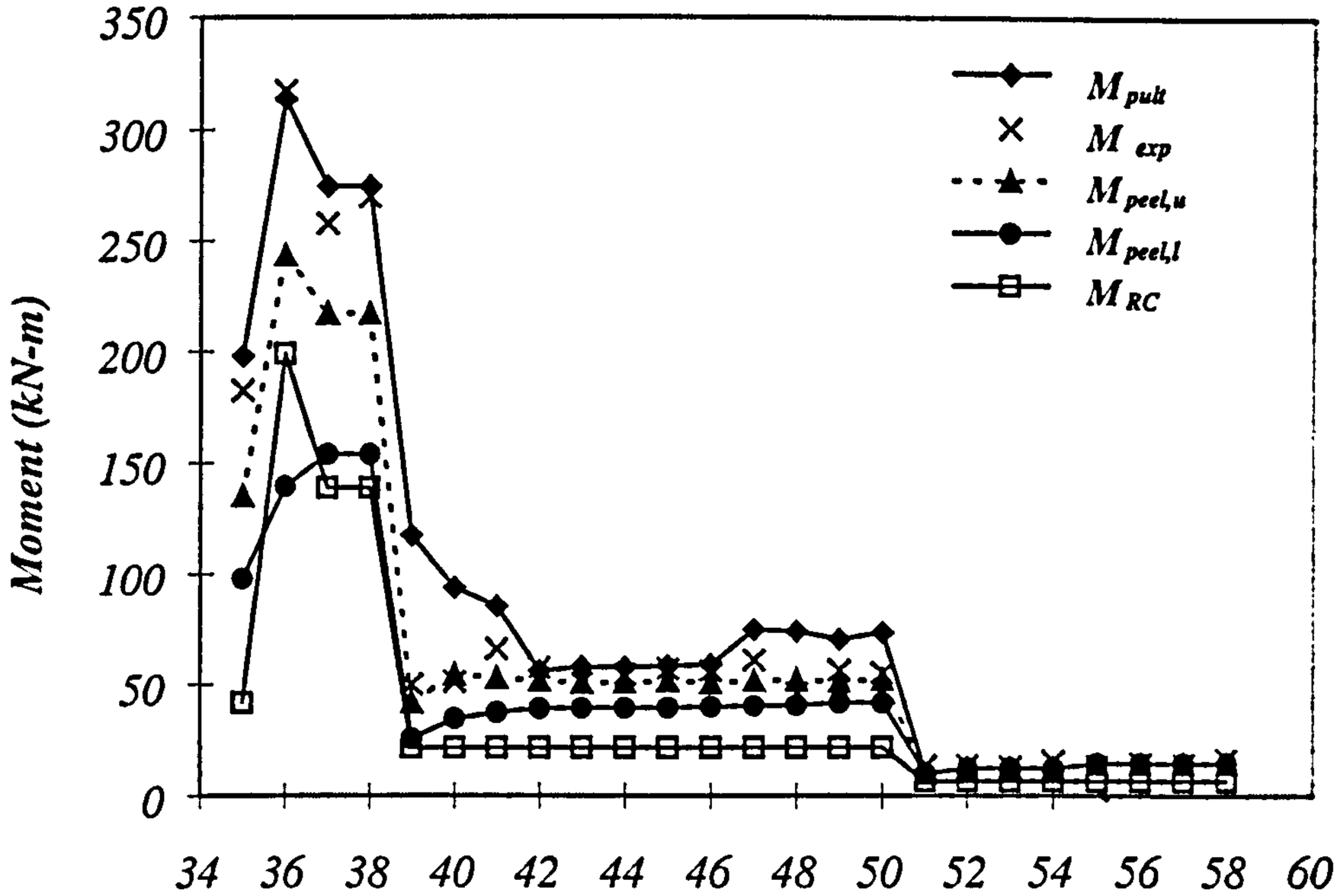

Fig. 4.13 **Comparison of plated and unplated ultimate bending moments, M_{pult} and M_{RC}, respectively, with FRP plate peeling moments: beam designs after Saadatmanesh *et al.* (1991), Ritchie *et al.* (1991) and Sharif *et al.* (1994).**

From the above encouraging experimental support for the present theory, covering a wide range of beam design parameters, with the test data as obtained from a number of **independent** sources, it is concluded that the basic underlying assumptions used in developing the model are all reasonable ones. Tables (4.2) and (4.3) give the full set of numerical data used for producing Figures 4.6 to 4.9 in addition to certain other geometrical and numerical properties corresponding to each beam design with FRP plates, while Table (4.4) gives the corresponding numerical data used for producing Figures 4.10 and 4.11 which is related to beams with steel plates. In these tables, the specimens have been grouped according to the ascending values of theoretical lower bound plate peeling moments, $M_{peel,l}$, which is meant to make the plots more presentable with specimen numbers varying from 1 to 58 in Tables (4.2) and (4.3),

and from 87 to 112 in Table (4.4), which is different from the original labelling designations of Saadatmanesh and Ehsani (1991), Ritchie *et al.* (1991), Sharif *et al.* (1994), Quantrill *et al.* (1996:A), Quantrill *et al.* (1996:B), Garden *et al.* (1997), and Oehlers (1992), with these also quoted in the tables for completeness.

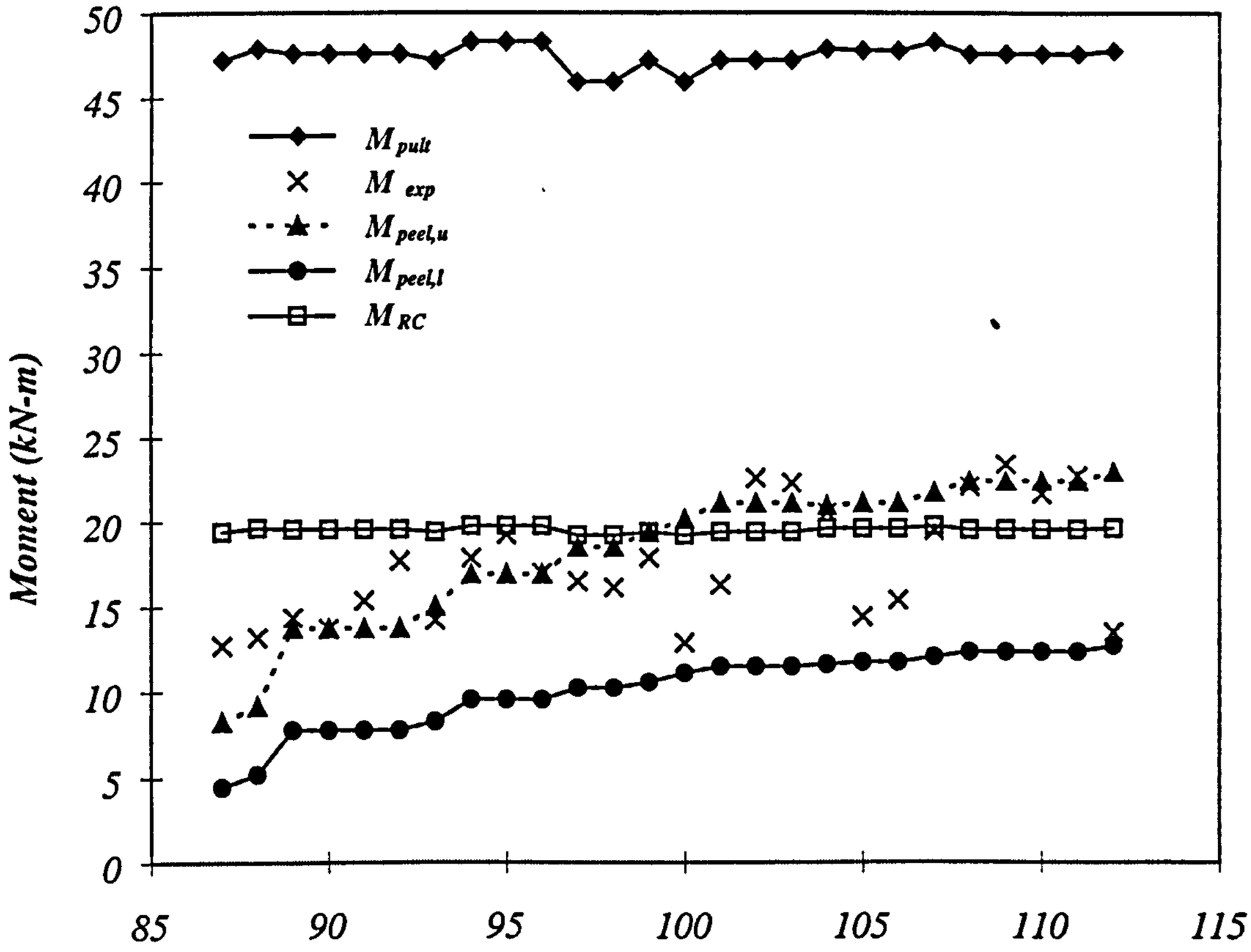

Fig. 4.14 Comparison of plated and unplated ultimate bending moments, M_{pult} and M_{RC}, respectively, with steel plate peeling moments: beam designs after Oehlers (1992).

Values of the parameters M_{pult} and M_{RC} for each beam design are also included in Tables (4.3), (4.3) and (4.4), where M_{pult} = ultimate bending moment of plated beam assuming full bond between the plate and concrete up to the failure load according to BS8110 (1985) with the material partial safety factors set equal to unity, and

M_{RC} = ultimate bending moment of unplated beam according to BS8110 (1985) with the material partial safely factors included in the calculations.

Figures 4.12 and 4.13 compare plots of M_{pult}, M_{RC}, M_{exp}, $M_{peel,u}$, and $M_{peel,l}$, for beams 1-34 after Quantrill *et al.* (1996:A), Quantrill *et al.* (1996:B), and Garden *et al.* (1997), and beams 35-58 after Saadatmanesh and Ehsani (1991), Ritchie *et al.* (1991), and Sharif *et al.* (1994). A careful examination of the values of M_{RC} and $M_{peel,l}$ relating to specimen 36 as presented in Figure 4.13 is interesting: for this specimen, M_{RC} is greater than the corresponding $M_{peel,l}$. Similar observations are made in Figure 4.14 in connection with simply supported R.C. beams strengthened by gluing steel plates to their soffits where, for the vast majority of the 26 large scale beam specimens tested by Oehlers (1992), values of M_{RC} are found to be substantially higher than both the corresponding theoretical values of $M_{peel,u}$ (let alone $M_{peel,l}$) and also their associated values of experimental initial peeling moment, M_{exp}.

One may argue, however, that the reported premature failures might have been due to insufficient shear capacity of the plated beams. By careful examination of the modes of failure for the beams tested by Oehlers (1992), for example, it is found that only 8 specimens out of the 26 tested beams failed in shear: this, then, leads to the conclusion that the premature failure was not (at least for most cases) due to lack of shear capacity. Moreover, in order to further confirm this, the shear capacity of the unplated beams as calculated according to ACI-318 (1983) are compared with the actual failure loads of the plated beams in Table (4.5). This table also includes the reported experimentally observed failure modes. Table (4.5) presents some numerical data in which, based on the reported material and geometrical data, the shear capacity

of the unplated beam, V_u (according to the ACI-318 (1983)) for 9 cases is found to be higher than the actual failure load, V_{exp}, for the corresponding plated beams, hence, confirming that the failure, in general, has not been due to the presence of insufficient shear capacity and the plate peeling capacity has, indeed, been the underlying cause of failure. In conclusion, therefore, bonding external steel and/or FRP plates to reinforced concrete beams in order to strengthen them in flexure may (if one does not guard against premature plate peeling failures) reduce their flexural ultimate strength! Such largely brittle failures can obviously have serious implications in practice where the plate bonding technique has been used extensively for upgrading both bridges and buildings in a number of countries.

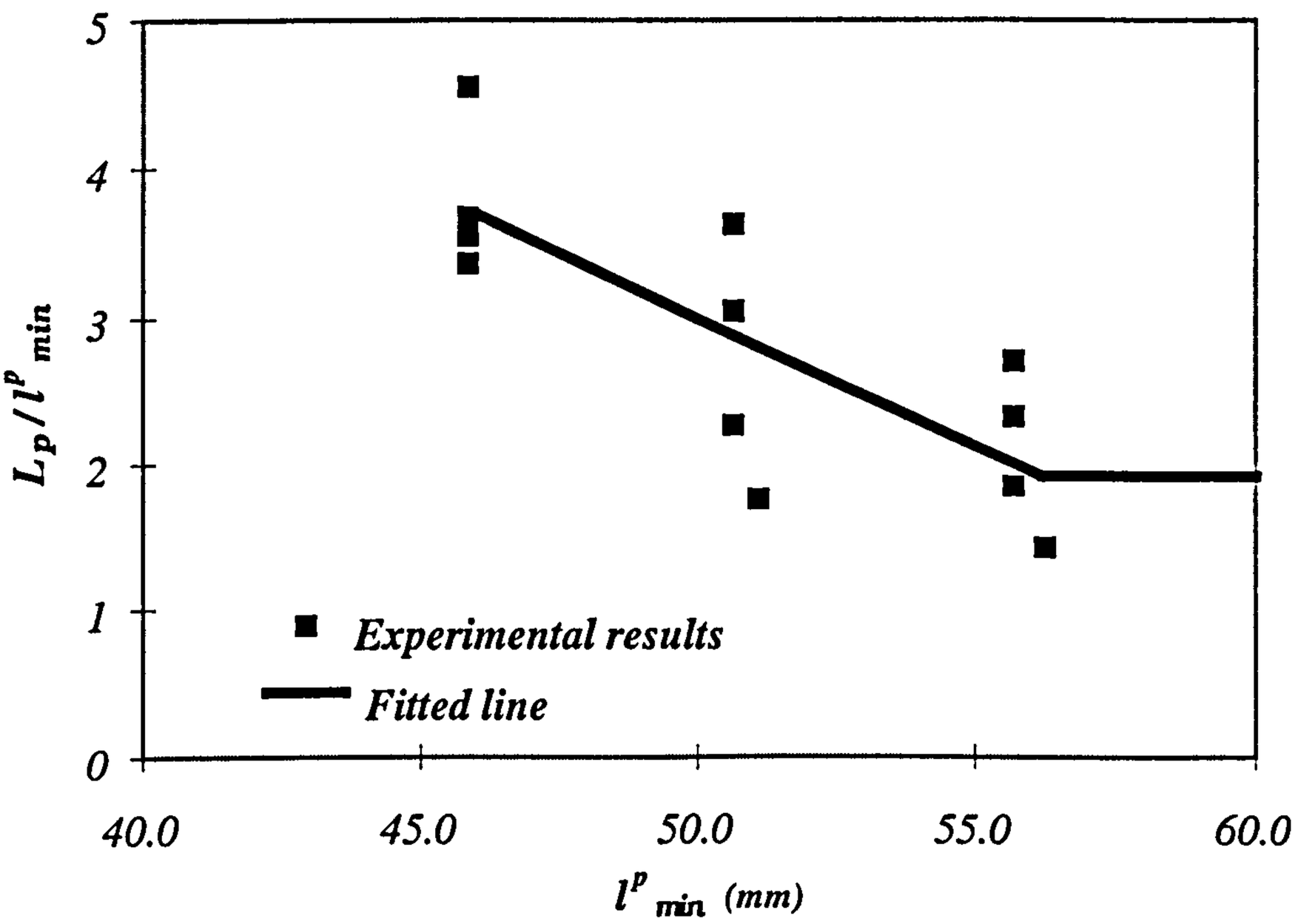

Fig. 4.15 Determination of FRP plate effective length, L_p, assuming $u_1 = 0.8\,N/mm^2$ and $u = 0.28\sqrt{f_{cu}}$.

Finally, in order to clarify the implications of assuming $u_1 = u = 0.28\sqrt{f_{cu}}$ implicit in the plots of Figure 4.4 (and, hence, semi-empirical Equations (4.5) and (4.6)), Figure

4.15 presents plots of $L_p/l^p_{\min}$ against $l^p_{\min}$ for all the beam specimens in Table (4.1) with the provision that the results presented in Figure 4.15 are based on the assumption in Equation (4.2) that $u_1 = 0.8\,N/mm^2$ and $u = 0.28\sqrt{f_{cu}}$. The fitted lines through the semi-empirical data points in Figure 4.15 are defined by the following

$$L_p = l^p_{\min}.(11.6 - 0.17\,l^p_{\min}) \quad , \quad l^p_{\min} \le 56.5 \qquad (4.8)$$

and

$$L_p = 2.0\,l^p_{\min} \quad , \quad l^p_{\min} > 56.5 \qquad (4.9)$$

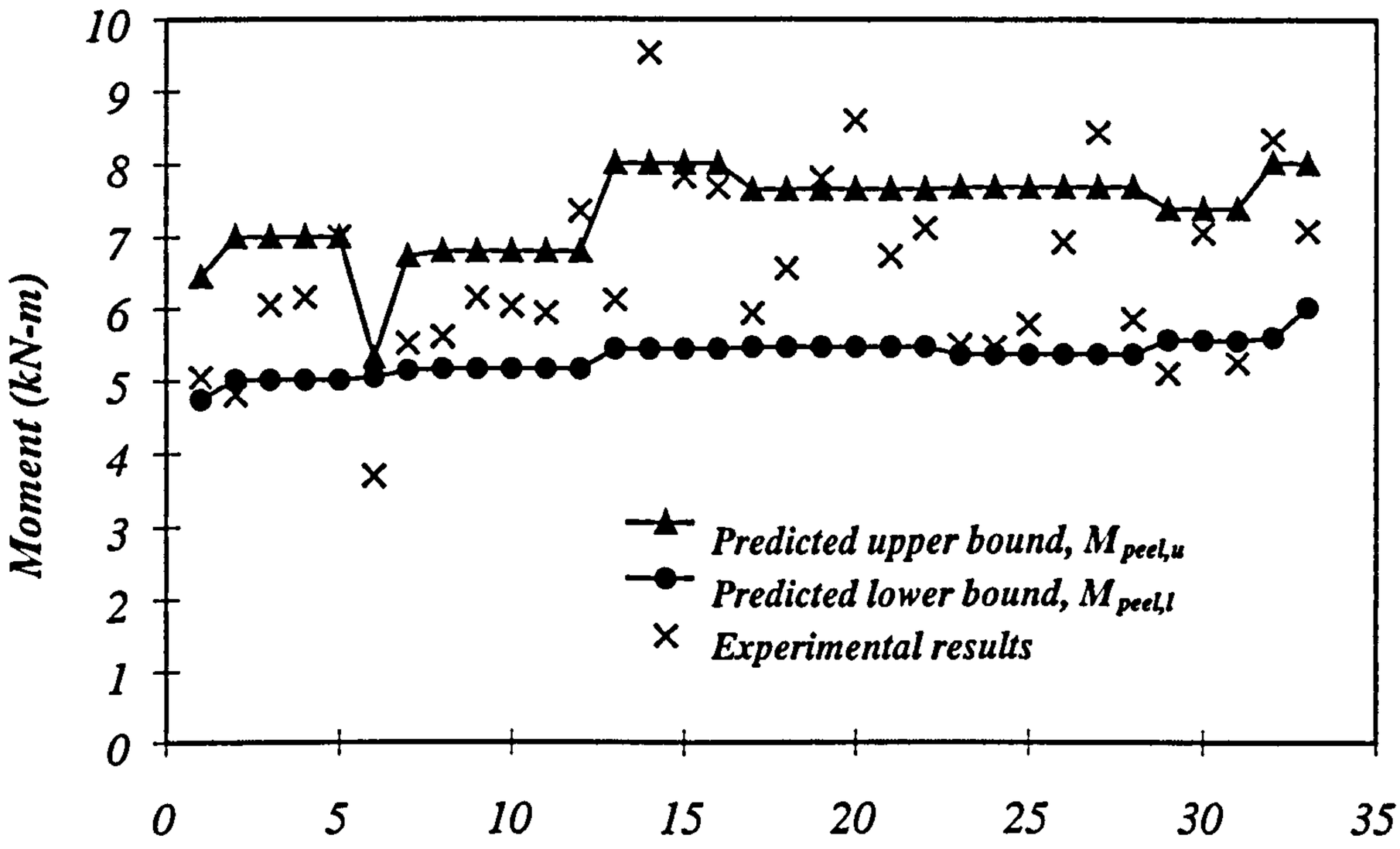

Fig. 4.16 **Correlations between upper and lower bound theoretical predictions of FRP plate peeling moment (assuming $u_1 = 0.8\,N/mm^2$ and $u = 0.28\sqrt{f_{cu}}$) and test data after Quantrill *et al.* (1996:A), Quantrill *et al.* (1996:B) and Garden *et al.* (1997).**

In other words, such alternative values of u_1 lead to different relations (i.e. Equations (4.8) and (4.9)) to Equations (4.5) and (4.6). Using Equations (4.8) and (4.9), new estimates of theoretical $M_{peel,u}$ and $M_{peel,l}$, may, then, be obtained for all the beam

designs of Quantrill *et al.* (1996:A), Quantrill *et al.* (1996:B), and Garden *et al.* (1997), and these are compared with the corresponding experimental plate peeling moments, M_{exp}, in Figure 4.16. Comparing the plots as presented in Figure 4.16 with the alternative plots in Figure 4.6 (which relate to these same beams but assume $u_1 = u = 0.28\sqrt{f_{cu}}$) strongly suggest the largely insignificant influence of the exact value chosen for the parameter u_1 (within reasonable limits $0.8 \leq u \leq 0.28\sqrt{f_{cu}}$) on the theoretical predictions of $M_{peel,u}$ and $M_{peel,l}$, provided that the appropriate forms of semi-empirical equations are used for estimating the values of effective L_p with such equations being a function of the assumed value for u_1.

4.6 EFFECT OF PRE-CRACKING

As discussed earlier, previous (largely experimental) studies have (in the vast majority of cases) used uncracked (i.e. as cast) R.C. beam specimens to which external steel (or FRP) plates have been bonded prior to testing the beams to failure, with little attention devoted to the real life situations where R.C. beams in actual structures (under service conditions) are already cracked to some degree. In view of the central role that crack spacings play as regards the premature plate peeling failure (as discussed earlier), then, the question arises as to whether the test results from uncracked specimens provide a safe (i.e. conservative) answer for the real life conditions. Moreover, due to the inherent wide scatter problem in the test data from even the same beam designs, by comparing the test results from uncracked and pre-cracked specimens (which are otherwise nominally identical), one is unlikely to come up with any conclusive deductions with the wide scatter problem making experimental comparisons (i.e. experimental parametric studies) fraught with difficulties. The present model,

however, enables one to study the pre-cracking phenomenon in a reasonable way, and makes it possible to gain a rational quantitative theoretical insight into the problem.

As discussed earlier, the minimum and maximum stabilised crack spacings in R.C. beams in the presence of external plates are given by Equations (4.3) and (4.4). In the extreme case, on the other hand, when no externally bonded plate is present, the stabilised crack spacings are given by the following equations (Watstein and Parsons (1943))

$$l_{\min} = \frac{A_e f_t^{'}}{u \sum 0_{bars}} \tag{4.10}$$

$$l_{\max} = 2\, l_{\min} \tag{4.11}$$

In other words, the only difference between Equations (4.3) and (4.10) is that the term representing the plate width, b_1, in the denominator of Equation (4.3) is omitted in Equation (4.10). An examination of Equations (4.3) and (4.4), on the one hand, and Equations (4.10) and (4.11), on the other, then, suggests that addition of externally bonded plates will lead to a reduction in the magnitudes of minimum and maximum stabilised crack spacings in R.C. beams. This observation, provides the clue for identifying the difference in the magnitudes of the plate peeling moments in uncracked and pre-cracked beams.

As discussed in some detail earlier (Chapter 3), the plate peeling moment is controlled by the structural behaviour of the teeth formed in-between adjacent stabilised cracks. It, then, follows that the difference between the magnitudes of plate peeling moments in pre-cracked and/or uncracked R.C. beams is directly related to the size of their

associated critical concrete teeth as determined by their patterns of stabilised crack spacings. In the relatively simpler case of an uncracked plated R.C. beam, the sizes of minimum and maximum crack spacings, l^{p}_{min} and l^{p}_{max}, respectively, may be estimated using Equations (4.3) and (4.4). In the case of plated pre-cracked beams, on the other hand, it may reasonably be assumed that (provided, under service conditions, the unplated R.C. beam has been loaded with its reinforcing tensile bars not reaching yield) the associated stabilised crack spacings lie in between two extreme conditions: (a) stabilised crack spacings, l_{min} and l_{max}, as determined by Equations (4.10) and (4.11), respectively; and (b) stabilised crack spacings, l^{p}_{min} and l^{p}_{max}, as determined by Equations (4.3) and (4.4), respectively, with the actual size of crack spacings lying in-between these limiting conditions. For a pre-cracked beam, one may calculate the limits to plate peeling moment firstly by using Equation (4.12), which is based on l^{p}_{min} as determined by Equation (4.3) (as derived in Chapter 3) with $\sigma_{s\text{-}1(max)} = 2\sigma_{s\text{-}1(min)}$ which is associated with the uncracked section, where

$$\sigma_{s-1(min)} = 0.154 \frac{L_p h_1 b^2 \sqrt{f_{cu}}}{h' b_1 t(\sum 0_{bars} + b_1)} \qquad (4.12)$$

and, secondly, Equation (4.13), based on l_{min}, may be used for determining $\sigma_{s\text{-}2(max)} = 2\sigma_{s\text{-}2(min)}$, which is associated with the cracked section, where

$$\sigma_{s-2(min)} = 0.154 \frac{L_p h_1 b^2 \sqrt{f_{cu}}}{h' b_1 t \sum 0_{bars}} \qquad (4.13)$$

The safe solution will, then, be the lowest value of plate peeling moments as determined by the above two alternative approaches for determining the upper and lower bounds for the magnitudes of plate direct stresses in both uncracked and also pre-cracked beams.

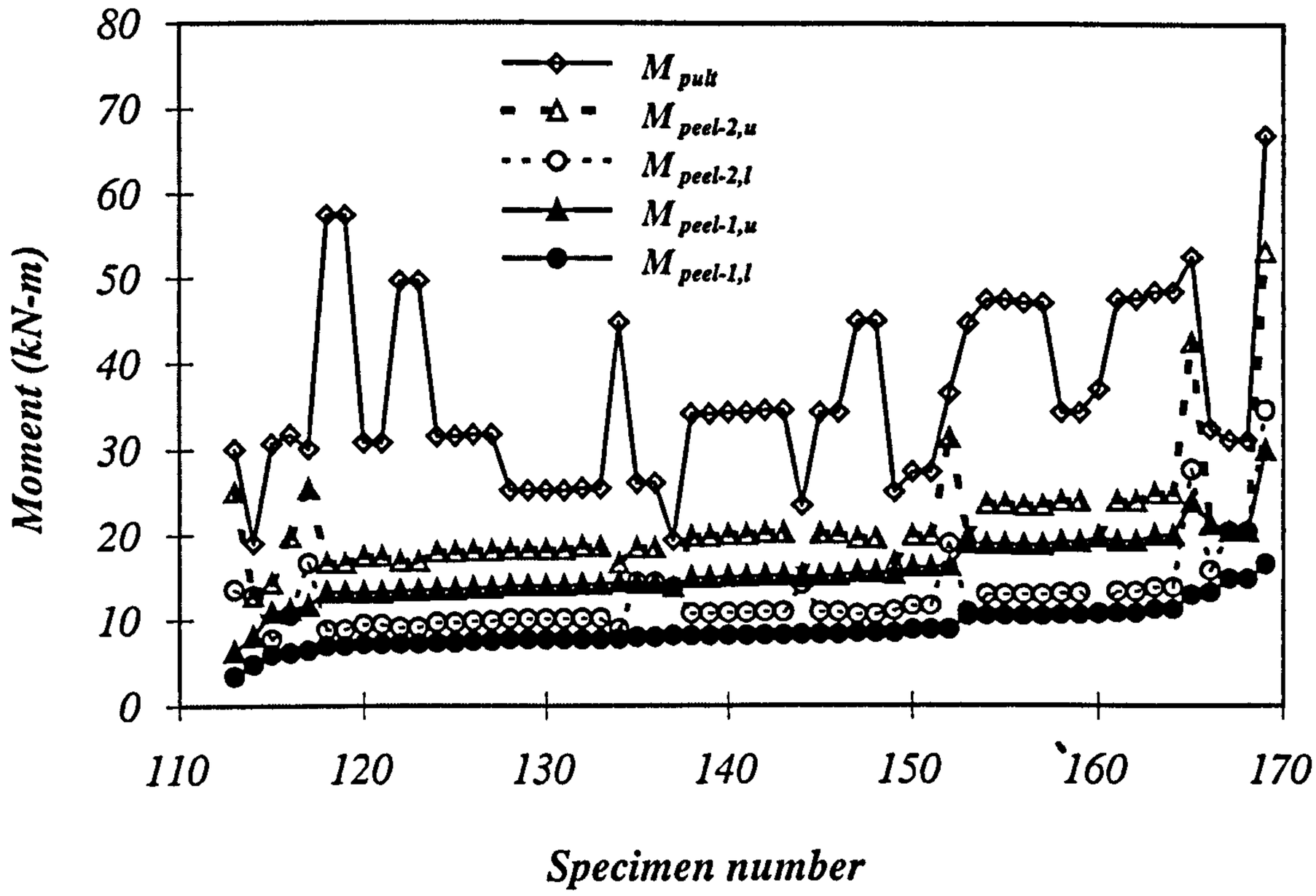

Fig. 4.17 **Theoretical comparison of the peeling moments in pre-cracked and uncracked specimens using beam designs after Oehlers and Moran (1990).**

Figures 4.17, 4.18 are produced using the above procedure: Figure 4.17 is based on the 57 beam designs used by Oehlers and Moran (1990), and Figure 4.18 relates to the 26 beam designs used by Oehlers (1992), where Oehlers and Moran (1990) and Oehlers (1992) adopted a very wide range of beam design parameters. In both Figures 4.17 and 4.18, the following estimates of flexural moments are presented for each beam design: absolute maximum bending moment for the plated section, M_{pult}, based on BS8110 (1985) as defined previously (with material partial safety factors set equal to unity); upper and lower bound plate peeling moments for uncracked sections based on estimates of $\sigma_{s\text{-}1(min)}$ and $\sigma_{s\text{-}1(max)}$ (as given by Equation (4.12)), $M_{peel-1,u}$ and $M_{peel-1,l}$, respectively; and, finally, the upper and lower bound plate peeling moments

based on estimate of $\sigma_{s\text{-}2(min)}$ and $\sigma_{s\text{-}2(max)}$ as given by Equation (4.13), $M_{peel-2,u}$ and $M_{peel-2,l}$, respectively.

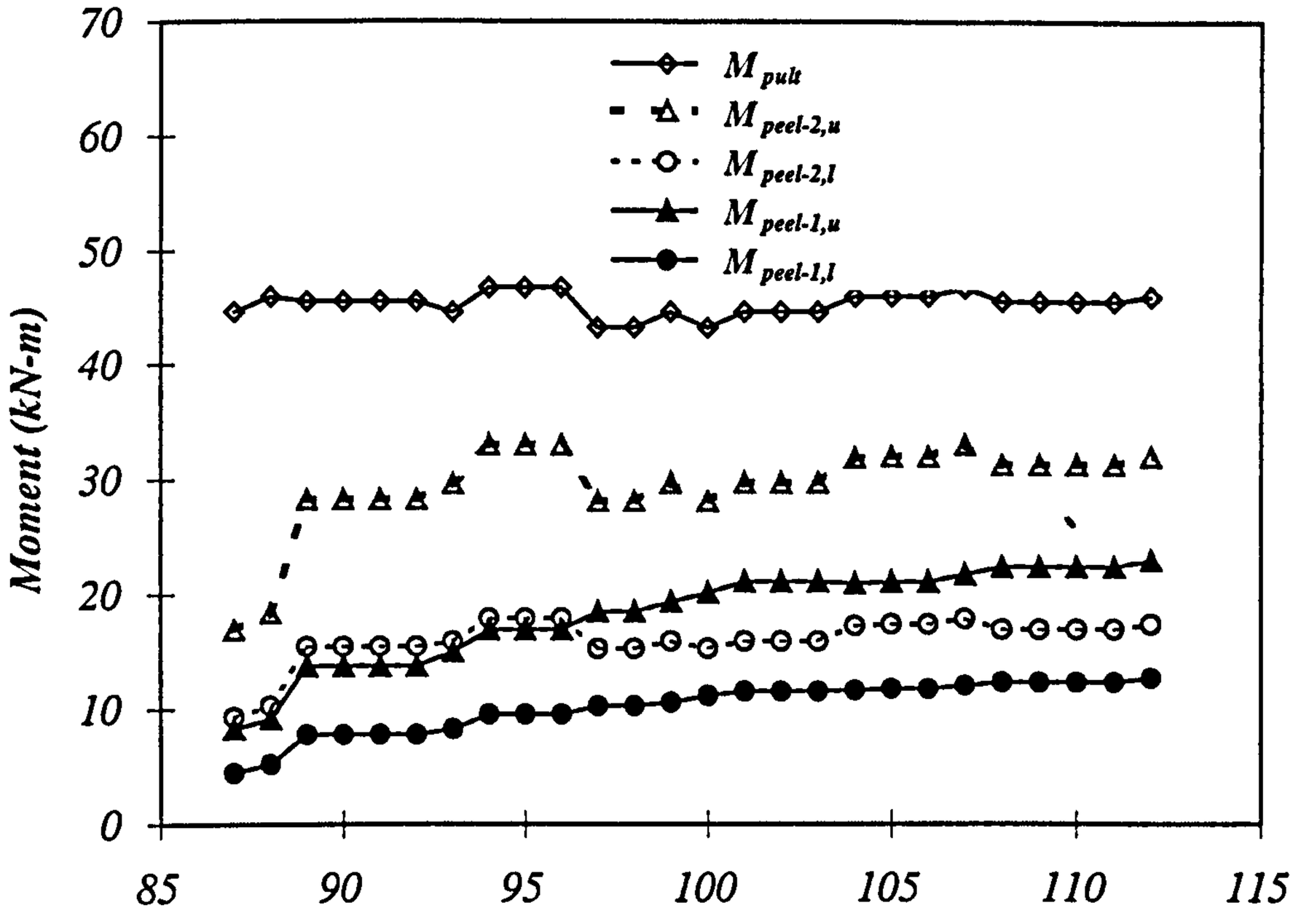

Fig. 4.18 Theoretical comparison of the peeling moments in pre-cracked and uncracked specimens using beam designs after Oehlers (1992).

Similarly, Figure 4.19 is produced using the same procedure and is based on the 26 beam designs reported by Baluch *et al.* (1995), and the 2 beam designs used by Ritchie *et al.* (1991), covering a very wide range of beam design parameters.

It is interesting to note that for all the 111 specimens covered in Figures 4.17, 4.18 and 4.19, the safest (i.e. most conservative) solution is invariably that of $M_{peel-1,l}$ - i.e. the lower bound plate peeling moment for an uncracked section. It may, then, be reasonably concluded that the previous practice among various researchers is, perhaps, a conservative approach and the so-obtained test data on uncracked beams

may, indeed, be used for deriving reasonably safe solutions for use in practice. Finally, Tables (4.6), (4.7), and (4.8) present the values of M_{pult}, $M_{peel-1,u}$ and $M_{peel-1,l}$, and $M_{peel-2,u}$ and $M_{peel-2,l}$, for each of the specimens using associated designated specimen numbers 59 to 86, 87 to 112 and also 113 to 169, with the results for specimens 113-169 in Table (4.8) (after Oehlers and Moran (1990)) presented in Figure 4.17, the data for specimens 87-112 in Table (4.7) (after Oehlers (1992)) plotted in Figure 4.18, and the data for specimens 59-86 in Table (4.8) shown in Figure 4.19, where the latter data is after Baluch *et al.* (1995) (specimens 59-84) and Ritchie *et al.* (1991) (specimens 85-86).

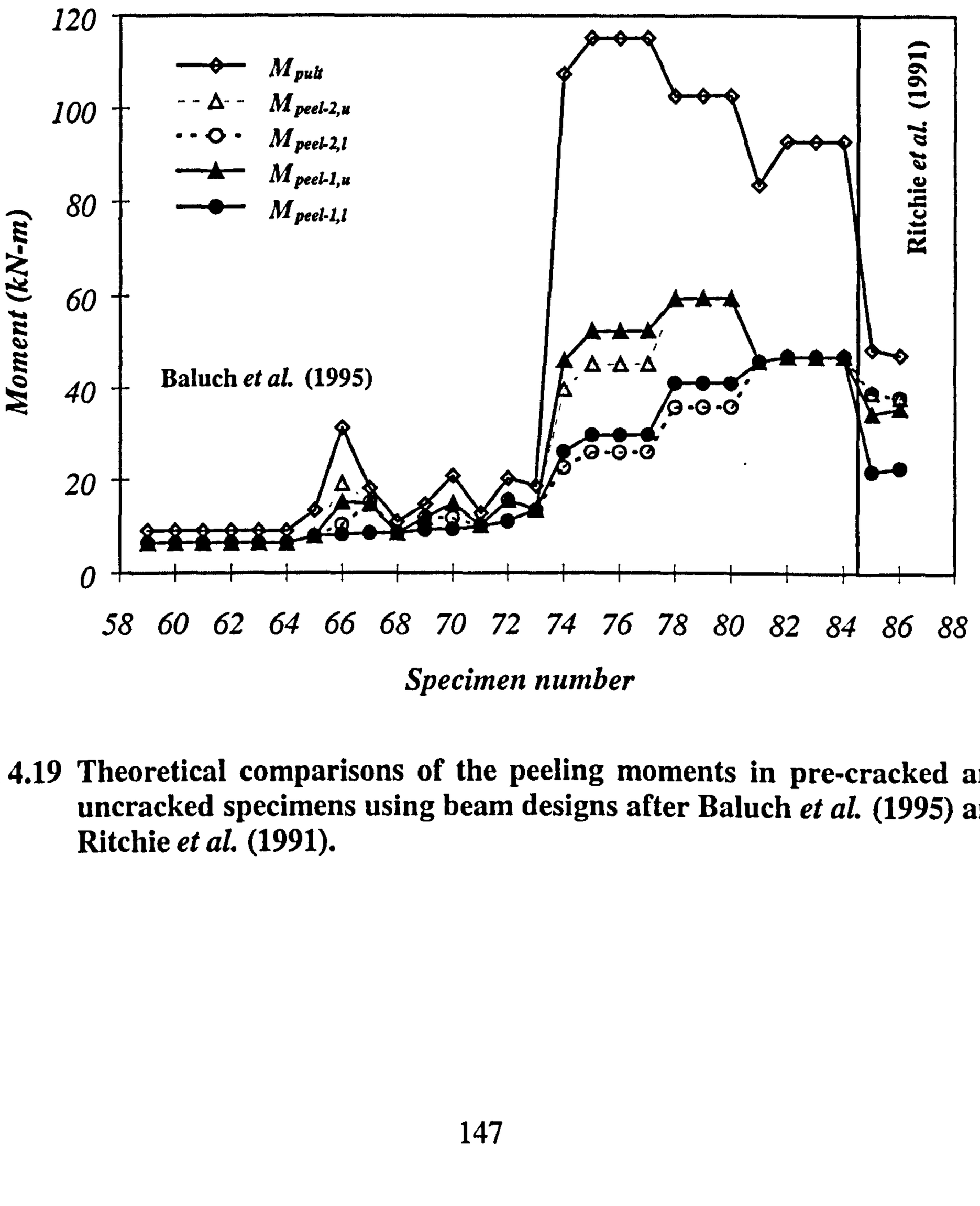

Fig. 4.19 Theoretical comparisons of the peeling moments in pre-cracked and uncracked specimens using beam designs after Baluch *et al.* (1995) and Ritchie *et al.* (1991).

4.6.1 Experimental Support

In what follows, the extensive large-scale test data after Oehlers and Moran (1990) will be used to provide experimental support for certain theoretical predictions. In their tests, Oehlers and Moran (1990) reported results for 57 large-scale R.C. beams with externally bonded steel plates glued to their soffits, covering a wide range of design parameters. The simply supported length of the beams varied from 1650 mm to 2500 mm, their depth from 150 mm to 240 mm, and the reinforcement cover from 10 mm to 50 mm, the plate thickness from 2.0 mm to 15.0 mm, the length of the plate from 600 mm to 1400 mm, and the width of the beam was either 120 mm or 125 mm. The top reinforcement diameter was either 10 or 12 mm, and the diameter of bottom reinforcement varied from 12 mm to 20 mm. In the majority of cases, straight plates were glued to uncracked and unstressed R.C. beams and the plates covered the full width of the beams, i.e. $b_1 = b$. Exceptions to this were: series 12 (with four beams) where b_1/b was varied; series 6 and 9 (with four beams in each series) where the plates were pre-curved in order to induce pre-stresses at the ends on plating; series 3 and 4 (with four beams in each series) where the R.C. beams were pre-cracked prior to gluing; and series 5, where the beams were pre-cambered and pre-cracked prior to gluing; as might occur in practice. All the specimens were tested with the plates terminated within the constant moment regions under symmetrical four-point loading except in series 7 and 8 (with four beams in each series) which were designed with the plates terminating within the shear span with varying ratios of external shear/moment imposed at the ends of the plates where plate peeling failures were invariably found to initiate in the beam specimens.

The very encouraging experimental support for the upper and lower bound theoretical predictions relating to all the beams tested by Oehlers(1992) have already been shown in Figure 4.14. For the present purposes, more emphasis will be placed on the correlations between the predictions of present theory and test data of Oehlers and Moran (1990) as regards the general trends of variations in the plate peeling moment with changes in the values of specific beam design parameters. The numerical data relating to the following discussions are also included in Table (4.8).

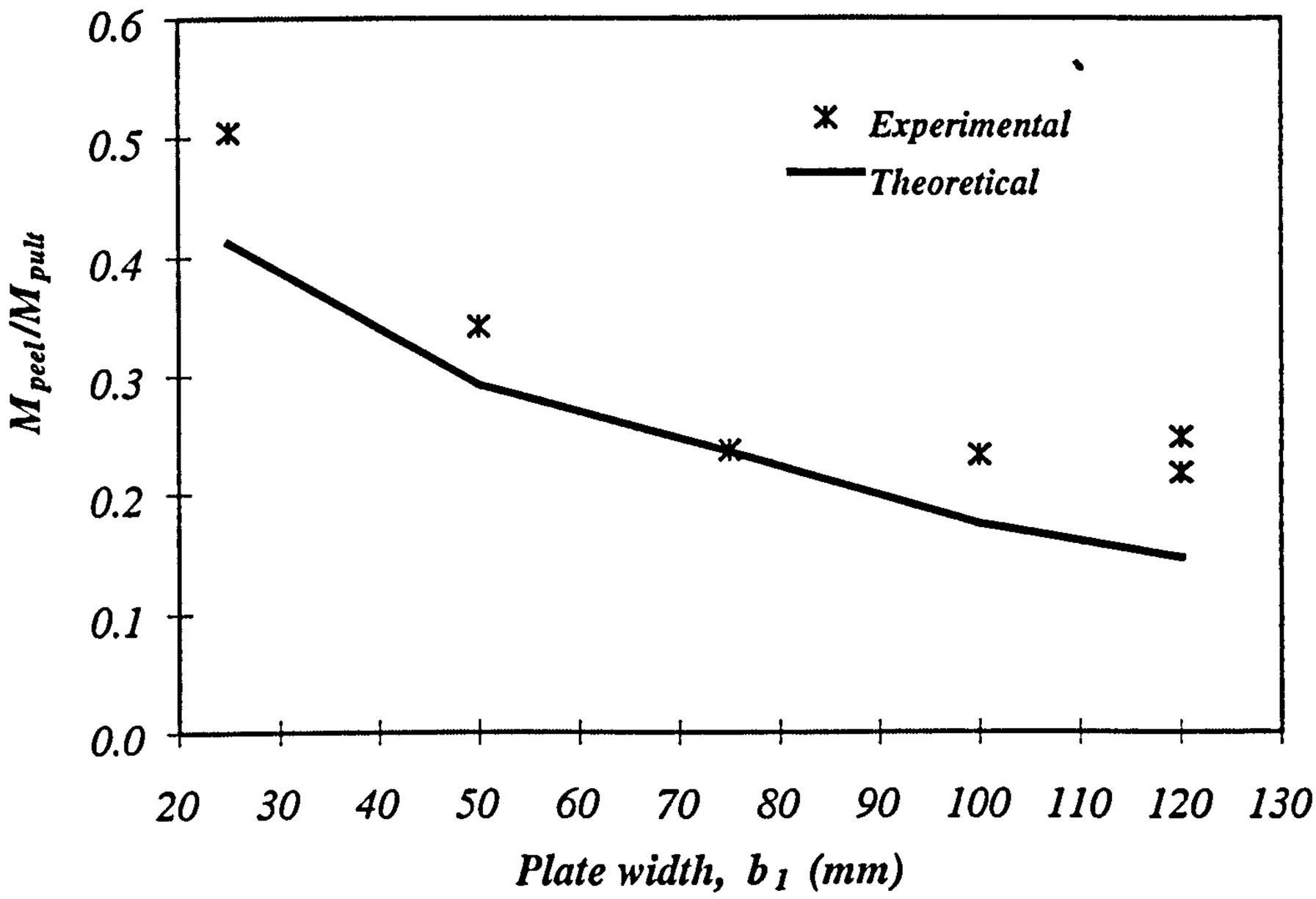

Fig. 4.20 Effect of plate width, b_1, on the plate peeling moment – comparison of test data after Oehlers and Moran (1990) and theory.

Figure 4.20 presents the correlations between the test data of Oehlers and Moran (1990) and theoretical lower bound predictions of plate peeling moment, M_{peel}, relating to variations of the plate peeling moment with changes in plate width for uncracked plated R.C. specimens 10/1-2 and 12/1-4, where the first number denotes the series number with the following numbers referring to the number of beams considered (i.e. beams 10/1 and 10/2 for the first set, series 10, and 12/1, 12/2, 12/3

and 12/4 from series 12). In all cases, the plate thicknesses were kept constant equal to 10 mm with the widths of the beams set equal to 120 mm. To avoid the scatter due to slight variations in the concrete cube strength, f_{cu}, all the theoretical and test data relating to the plate peeling moment have been non-dimensionalised with respect to the absolute maximum moment, M_{pult}, as calculated according to the British code BS8110 (1985), with material partial safety factors set equal to unity. As shown in the plots in Figure 4.20, the theory successfully predicts the general trend of variations between M_{peel}/M_{pult} and the plate width, with the theoretical lower bound solution predicting a safe solution in all cases. Both the theoretical and the corresponding experimental results in the same figure indicate that increasing the plate width (while keeping the plate thickness constant) reduces the efficiency of the plated beam as expressed in terms of the ratio of the plate peeling moment to the corresponding moment capacity of the plated beam with fully bonded plate, M_{peel}/M_{pult}.

The effect of changes in the plate thickness on the magnitude of the plate peeling moment, M_{peel}, is shown in Figure 4.21 where test data of Oehlers and Moran (1990) for series 10 and 11 (with 4 beams in each series) is used to provide support for the lower bound theoretical predictions relating to uncracked plated beams with all the steel plates having the same width as the beams equal to 120 mm Both the theoretical and the corresponding experimental results in Figure 4.21 indicate that increasing the plate thickness (while keeping the plate width constant) reduces the efficiency of plated beam as expressed in terms of the ratio of the plate peeling moment to the corresponding moment capacity of the plated beam with fully bonded plate, M_{peel}/M_{pult}.

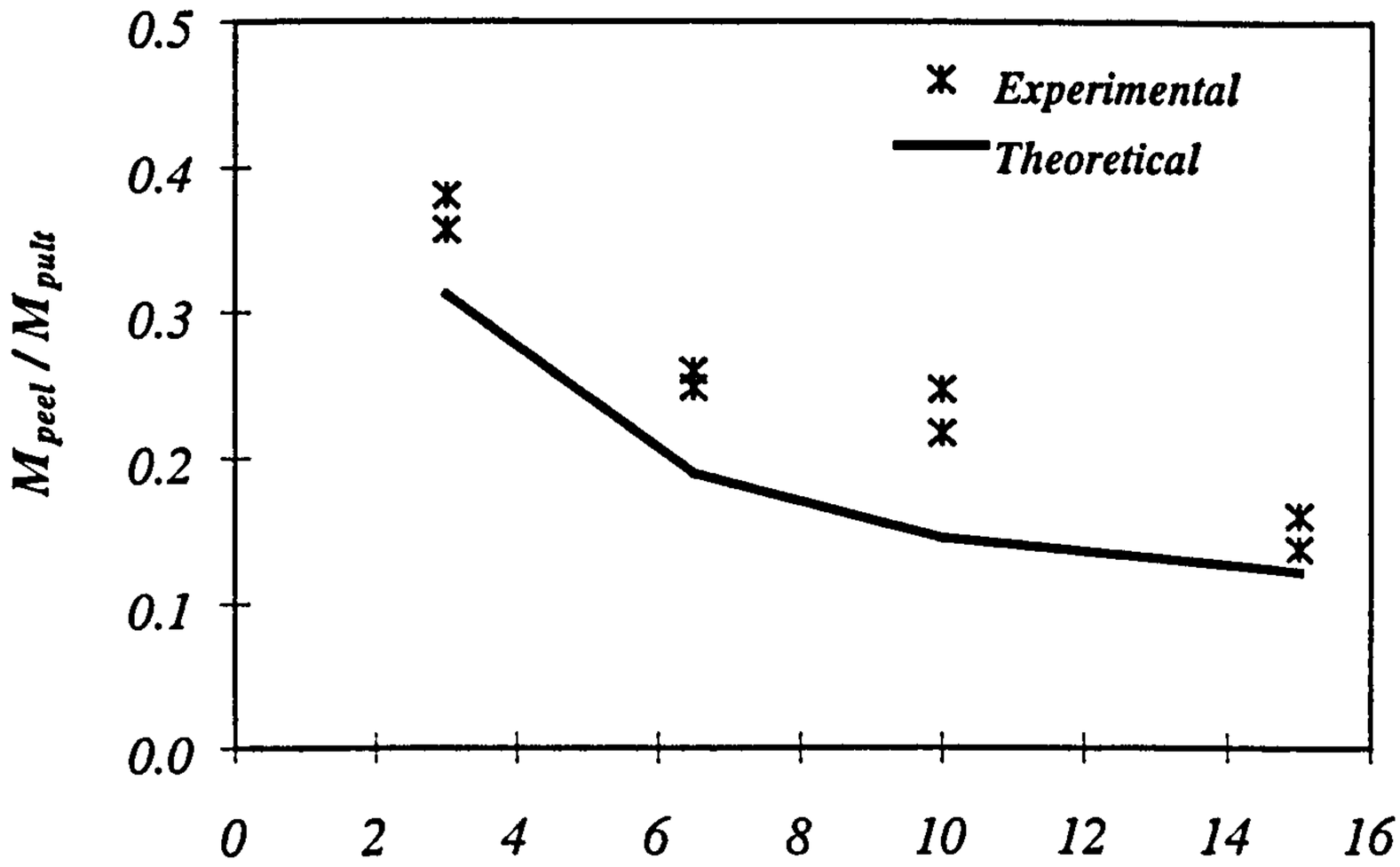

Fig. 4.21 Effect of plate width, *t*, on the plate peeling moment – comparison of test data after Oehlers and Moran (1990) and theory.

It is particularly noteworthy that the above reported reductions in the predicted ratio M_{peel}/M_{pult} and its corresponding test data, as shown in Figures 4.20 and 4.21, is accompanied with matching reductions in the values of the theoretical and experimental plate peeling moments. It, then, shows that increasing the area of the external bonded plate (either by increasing the plate thickness, width, or both) reduces not only the efficiency of the plated beam (expressed by the M_{peel}/M_{pult} ratio) but also reduces the corresponding absolute plate peeling moment.

Figure 4.22 presents variations of experimental and also lower bound theoretical predictions of plate peeling moment (non-dimensionalised with respect to M_{pult}) with changes in the ratio of plate width/plate thickness, with the test data relating to the beams of series 10, 11, and 12 of Oehlers and Moran (1990) including four beams in each series: yet again the correlations between the test data and theory are very

encouraging. Notice that all the plated test specimens in Figure 4.22 were uncracked with the test specimens having plate thicknesses, t, ranging from 3.0 to 10.0 mm, and varying widths of plates with other beam design parameters kept nominally constant. It is noticeable in Figure 4.22 that although the theoretical plate peeling moment provides a safe prediction and is always lower than the experimental results, no general trend may be identified in connection with changes in the plate peeling moment with increases in the plate width/thickness ratio. A careful study of the results presented in Figures 4.20, 4.21, and 4.22, however, indicates that it is the area of the plate rather than the plate width, thickness, or width/thickness ratio, which is the primary factor controlling the magnitude of plate peeling moment. Moreover, it may be concluded that increasing the total area of the externally bonded plate would reduce the load bearing capacity of the plated beam with the higher possibility of the brittle premature plate peeling failure to occur. This conclusion will be clarified further in the course of the theoretical study reported in Chapter 6: it will be proven that increasing the area of the plate may lead to an over-reinforced type of plated beam even for under-reinforced unplated beams and, hence, may result in a brittle type of failure at a lower load bearing capacity.

The data presented in Tables (4.7) and (4.8) are also meant to throw some experimental and related theoretical light into the effect of pre-cracking on the plate peeling moment (non-dimensionalised with respect to M_{pult}). The test data after Oehlers and Moran (1990) relating to the beams 1-4 in series 4 (i.e. 4/1-4) were pre-cracked prior to bonding steel plates to their soffits, and beams 2/1 and 2/2 had nominally identical design parameters to the beams of series 4 with the exception that beams 2/1-2 were both uncracked. An examination of the results in Table (4.8)

suggests that for the 6 beams tested, comparing the presented test data M_{exp}/M_{pult} from series 2 with those of series 4 does not provide any clue as regards the effect of pre-cracking on the magnitude of M_{exp}/M_{pult}, with the scatter in the test data masking any possible differences. Both, the theoretical uncracked and pre-cracked lower bound solutions $M_{peel-1,1}/M_{pult}$ and $M_{peel-2,1}/M_{pult}$, respectively, on the other hand, are found to provide safe answers with the predictions of $M_{peel-1,1}/M_{pult}$ for beams 4/1-4 and 2/1-2 being less than the corresponding theoretical estimations of $M_{peel-2,1}/M_{pult}$.

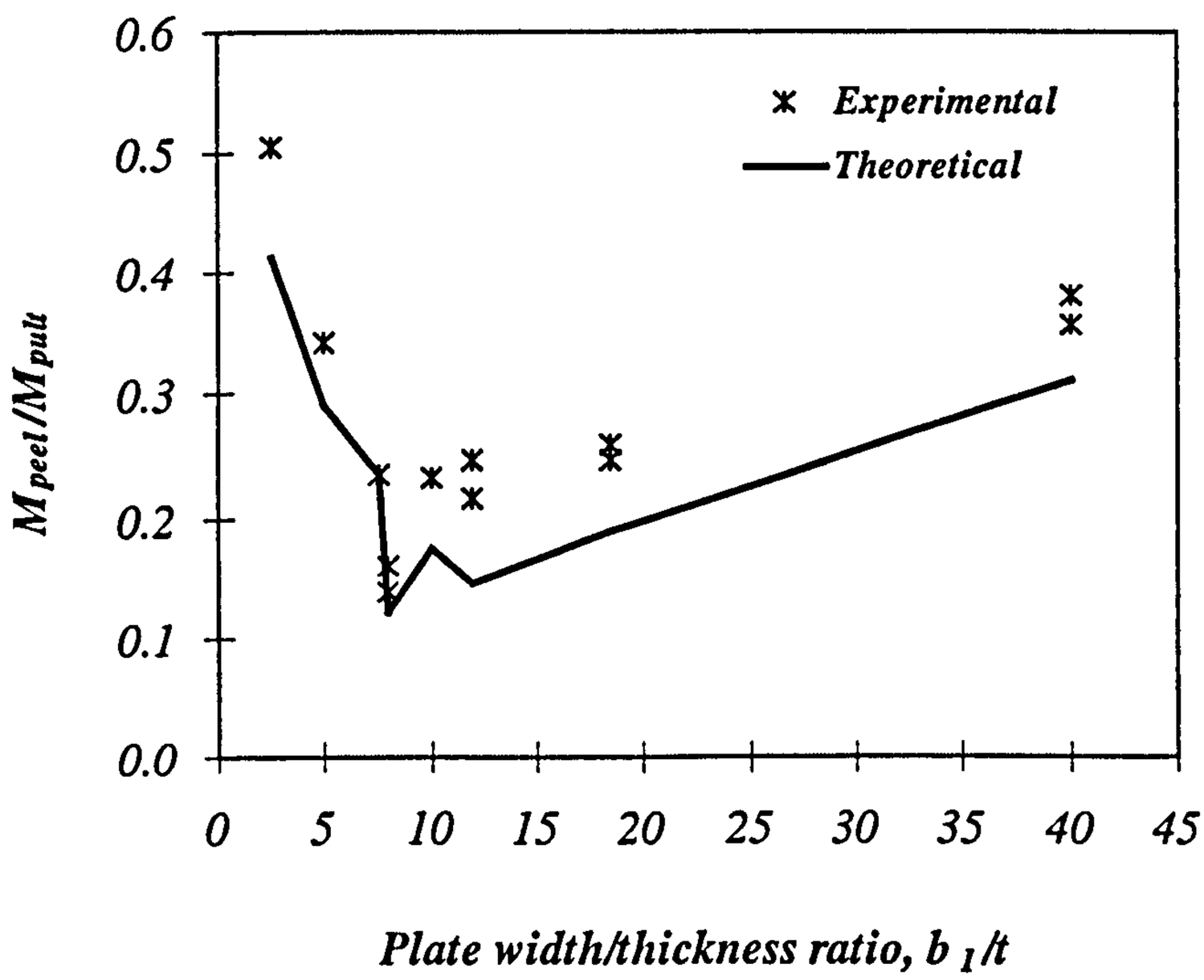

Fig. 4.22 **Effect of plate width/thickness, b_1/t, on the plate peeling moment – comparison of test data after Oehlers and Moran (1990) and theory.**

The effect of plate curving (prestressing) in the case of group 6/1-4 where the plates were pre-curved in the course of the experiments in order to induce pre-stresses at the ends on plating, as reported in Oehlers and Moran (1990), may be deducted from the data in Table (4.8). In this same Table are also included the test data relating to the

non-dimensionalised plate peeling moments, M_{exp}/M_{pult} of uncracked specimens 2/1-2 which (otherwise) had nominally identical design parameters to all the four beams of series 6. An examination of such non-dimensionalised results in Table (4.8) relating to M_{exp}/M_{pult} suggest some significant scatter in the test data relating to the four beams of series 6 which all had the same geometrical and material design parameters with two of its test data exceeding the corresponding values of M_{exp}/M_{pult} for the uncracked beams 2/1-2 and the other two test data points giving the same values of M_{exp}/M_{pult} as the beam 2/1. It is encouraging that the theoretical predictions of $M_{peel-1,l}/M_{pult}$ (for uncracked sections) for beams 6/1-4 and 2/1-2 are found to provide a conservative solution to all the associated non-dimensionalised test data relating to beams 6/1-4 and 2/1-2.

Table (4.8) also presents the test data relating to M_{exp}/M_{pult} for 4 nominally identical beams 9/1-4 which had pre-curved plates, in conjunction with the corresponding M_{exp}/M_{pult} test data for the 4 beams in series 3 (i.e. 3/1-4) which were pre-cracked but (otherwise) had nominally identical construction details to the beams 9/1-4. Again, significant scatter is observed in the test data relating to M_{exp}/M_{pult} of beams 9/1-4 and 3/1-4 with their associated lower bound theoretical predictions for uncracked section, $M_{peel-1,l}/M_{pult}$ (or, indeed, $M_{peel-2,l}/M_{pult}$), offering conservative solutions.

In addition, Table (4.8) presents the test results in terms of M_{exp}/M_{pult} for the beams in series 5 (i.e. beams 5/1-4) where the beams were pre-cracked and pre-cambered

prior to gluing, as might occur in practice. In this Table are also included the test data for the uncracked beams 2/1-2 which (otherwise) had nominally identical design parameters to the beams 5/1-4. Again, significant scatter is observed in the test results (under nominally identical conditions) for the four beams, 5/1-4, and when compared to the experimental results for beams 2/1-2, deriving any conclusive deductions based on purely experimental comparisons becomes difficult. It is encouraging that the corresponding non-dimensionalised theoretical lower bound predictions for uncracked sections, $M_{peel-1,l}/M_{pult}$, are found to offer conservative answers in all cases relating to M_{exp}/M_{pult} for beams 5/1-4 and 2/1-2.

Finally, Table (4.8) compares the four test results as regards M_{exp}/M_{pult} for beams 5/1-4 (which, as mentioned in the above, were pre-cracked and pre-cambered) and corresponding experimental values of M_{exp}/M_{pult} for the beams 4/1-4 which were pre-cracked but (otherwise) had nominally identical design parameters to the beams 5/1-4. Yet again, no definite conclusions may be drawn by comparing such non-dimensionalised test data in Table (4.8), which are found to suffer from a significant degree of scatter. However, the non-dimensionalised lower bound theoretical estimates $M_{peel-2,l}/M_{pult}$ are found to provide a safe solution to all the associated non-dimensionalised experimental data in Table (4.8) relating to the beams 5/1-4 and 4/14.

Bearing the above observations in mind, it may be concluded that, in view of the inherent wide scatter problem associated with the plate peeling phenomenon in practice, use of purely experimental data for investigating the influence of various

beam design parameters and/or plating techniques (i.e. purely experimental parametric studies) is, even under closely controlled laboratory conditions, unlikely to lead to any conclusive deductions: such purely empirical approaches are fraught with difficulties and uncertainties. In view of the absence of a unique solution, therefore, the presently developed version of lower/upper bound model which is based on an extended version of the model suggested by Raoof and Zhang (1997) should prove useful in this context, with the lower bound formulations being the appropriate ones for design purposes, relating to a wide range of beam design parameters and steel and/or FRP plating techniques.

4.7 COMPUTER PROGRAMME

As most of the published results are concerned with the ultimate failure load/moment and very few sources present the direct axial stresses (or strains) in the externally bonded plates, the need arises to develop a computer programme to predict the flexural load bearing capacity of the plated beam in terms of moments at the instant of plate peeling failures. The computer programme used throughout this research was written to fulfil these needs with certain added features (for further analysis of data).

The computer programme predicts the theoretical upper and lower bound plate peeling moments for the plated R.C. beam corresponding to the maximum and minimum axial stresses in the external plate. It considers the pre-loading conditions (i.e. pre- or uncracked conditions) prior to plating, and it can cater for various material characteristics for the plate. The programme handles the stress-strain relationships for concrete as in Figure 4.23a, FRP as in Figure 4.23b and steel with the option that the tensile stresses in concrete may be ignored (or included) if desired.

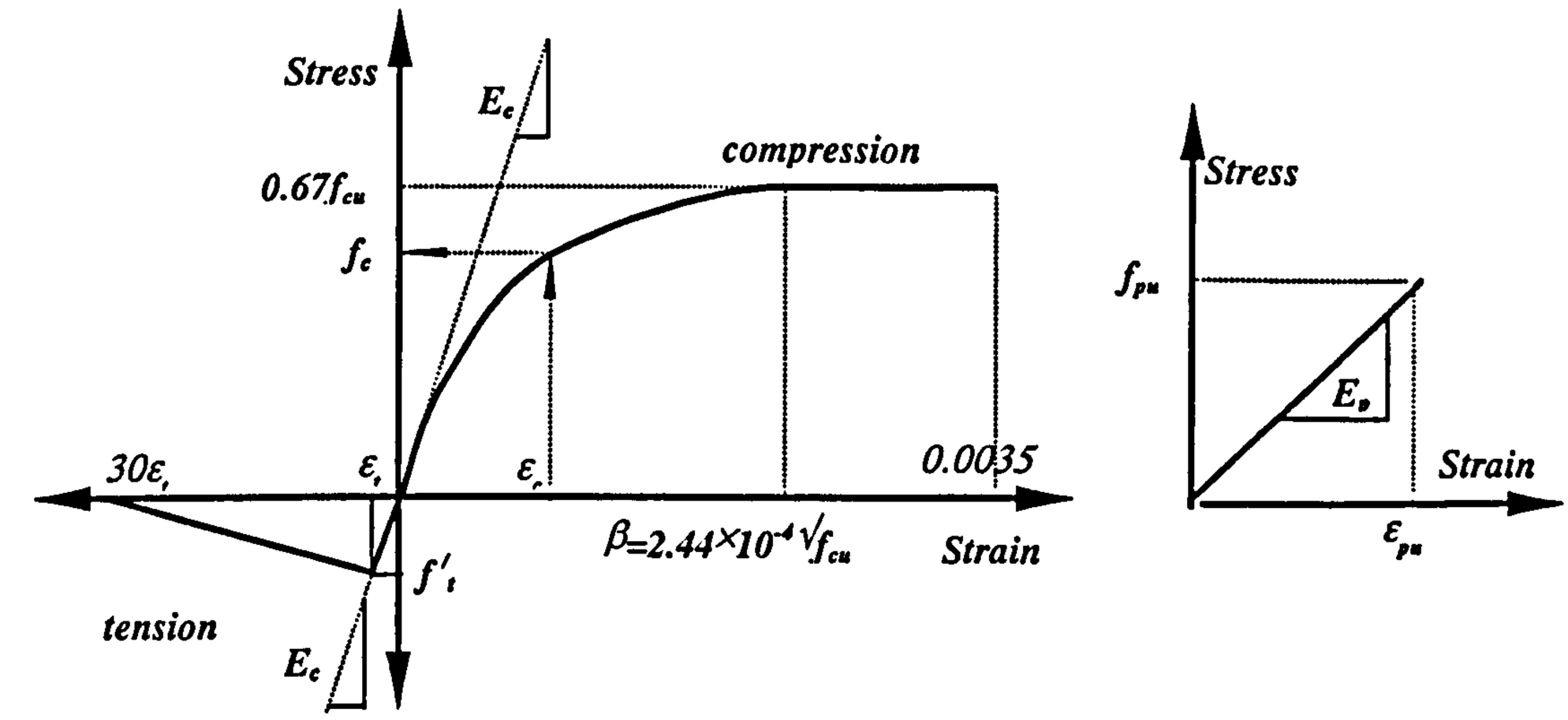

(a) (b)

Fig. 4.23 Stress-strain relationship: (a) for concrete after BS8110 (1985), (b) for FRP material.

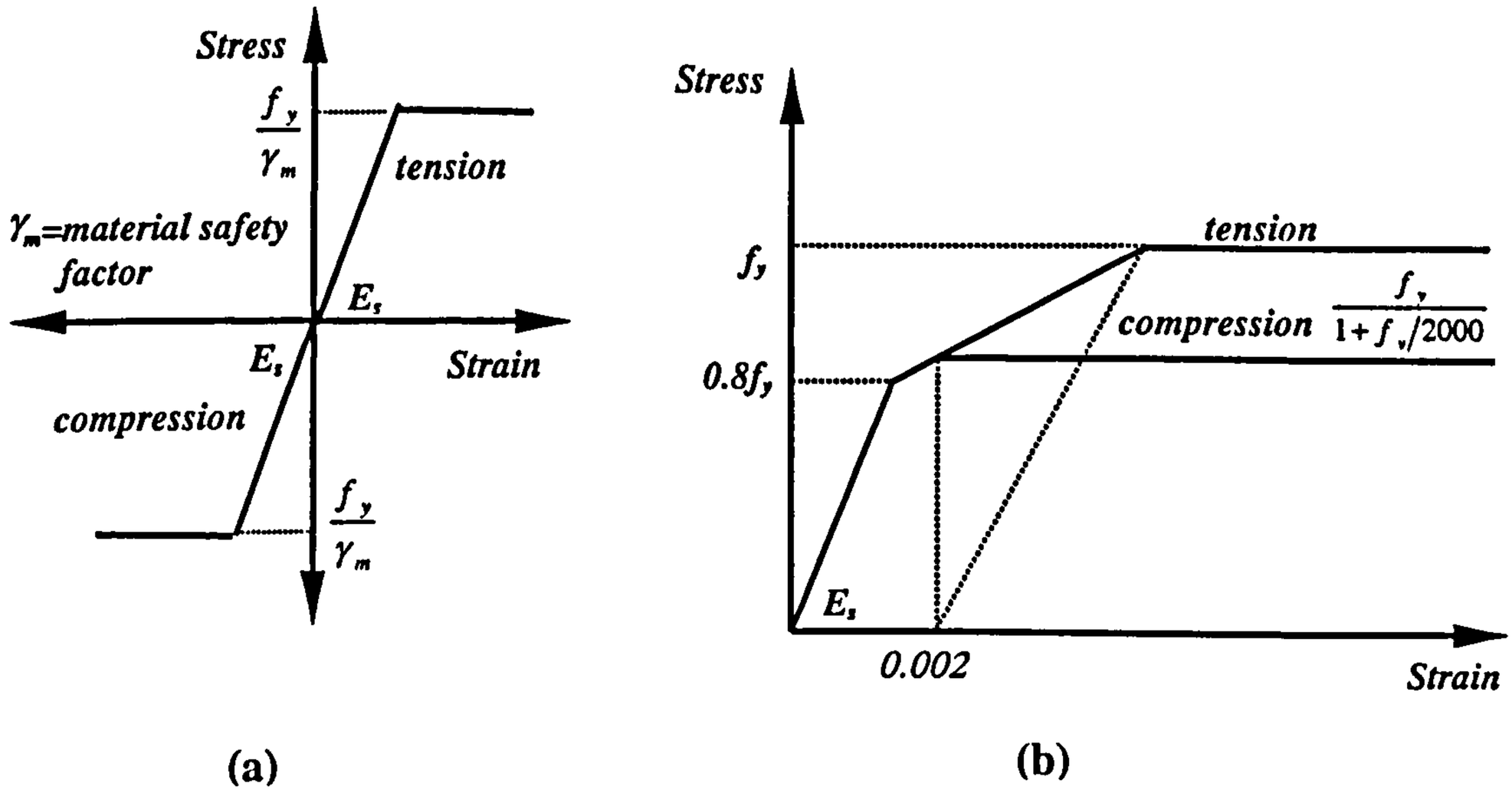

(a) (b)

Fig. 4.24 Stress-strain relationship for steel: (a) bi-linear after BS8110 (1985), (b) tri-linear after BS5400 (1990).

Both bi-linear (elastic-perfectly plastic) and/or tri-linear relationships, Figures 4.24a and 4.24b, respectively, for the steel material (bars and/or plates) can be handled.

Different types of bond stresses between the plate and concrete beam may also be selected. The material partial safety factors may be included or omitted as desired. Although the numerical analysis throughout the programme generally follows the recommendations of BS8110 (1985) and/or BS5400 (1990), details of the strain compatibility throughout the cross-section of the plated beam are catered for, and a numerical integration technique is used in order to calculate the section forces with an iterative method implemented for achieving the force equilibrium.

The full list of the computer programme which is written in FORTRAN-77 (release 9.0) for HP-UX system with its sub-programmes is presented in appendix A. Appendix A also presents the algorithm for the programme in addition to the numerical techniques adopted.

4.8 CONCLUSIONS

Following the previously reported (Chapters 2 and 3) critical review of available literature on external FRP plate bonding technique, certain major gaps were identified in the state of knowledge. This chapter reports a semi-empirical model backed by extensive large and small scale test data from a number of independent sources, covering a wide range of beam design parameters, for predicting the upper and also lower bounds to premature FRP plate peeling moments of R.C. beams strengthened in flexure by externally bonded FRP plates. The proposed model is an extended version of the one developed by Raoof and Zhang, with the original version applicable to cases when steel (as opposed to FRP) is used as the plating material. The presently developed model deals with R.C. beams strengthened with steel/FRP plates and enables one to study the pre-loading conditions of the beam prior to the application of

external FRP and/or steel plates. The model depends on the spacings of stabilised cracks in the concrete cover zone, and in view of large variations (by a factor of, say, 2) in spacings of such cracks in practice, it is argued that a unique solution for the premature FRP and/or steel plate peeling moment does not exist and, hence, one has to resort to theoretical bounding solutions with these being different from upper/lower bounds in the sense used in, for example, plastic analysis of frames.

In total, 58 individual test data for FRP plated beams, and 111 individual test results relating to steel plated beams (as reported by others) have been found to support the theoretical bounding solutions: this, then, provides ample evidence for the general applicability of the proposed model for use in practice. It is particularly noteworthy that out of the 169 individual test data, only in connection with <u>one</u> test result has the model been found not to provide a safe (lower bound) solution with this individual test result being believed to be of a suspect nature. Moreover, it has been shown (particularly in the case of steel plated beams) that the premature plate peeling moment may in certain cases be significantly lower than the associated flexural ultimate moment of unplated R.C. beam which has been designed according to, for example, BS8110 (1985) even when (unlike the corresponding calculations for the externally plated beam) material partial safety factors are included in the calculations for the unplated beam. In other words, it is noteworthy that adding externally bonded plates to R.C. beams in order to strengthen them in flexure <u>may</u> (if one does not guard against premature plate peeling failure) <u>reduce</u> their flexural ultimate load. Such largely brittle failures can obviously have serious implications in practice where this method has been used extensively for strengthening both bridges and buildings in a number of countries.

Based on extensive test data, it has also been demonstrated that in the case of externally bonded steel plates to R.C. beams, by keeping the plate width to thickness ratio above 60, one may, as a simple preliminary design approach, avoid occurrence of premature plate peeling failures. No such simple empirical bounding value for the plate width to thickness ratio, however, has been shown to exist in relation to cases when externally bonded FRP plates (which unlike steel plates are available with a wide range of ultimate strengths and Young's moduli) are used, hence, the pressing need for a generally applicable and reliable model such as the one presently proposed.

This chapter also addresses the question of pre-cracking in R.C. beams prior to bonding steel plates to their soffits and testing them to failure. It is theoretically shown that the previous practice by most researchers who have tested uncracked (i.e. as cast) plated R.C. beams to investigate the influence of various beam design parameters on the plate peeling moment, is, perhaps, a conservative approach and the so-obtained test data on uncracked beams may reasonably safely be used for predicting the behaviour of R.C. beams in actual structures which (under service conditions) are invariably pre-cracked to some degree.

Finally, using a rather comprehensive set of large scale test data (from other sources), encouraging support has been provided for certain aspects of theoretical predictions as regards the influence of various beam design parameters on the magnitude of plate peeling moment. In particular, it is shown that in view of the inherent wide scatter problem associated with the plate peeling phenomenon in practice, purely experimental parametric studies for investigating the influence of various beam design

parameters and/or plating techniques on the plate peeling moment are, even under closely controlled laboratory conditions, unlikely to lead to any conclusive deductions, and such purely empirical approaches are fraught with uncertainties.

In conclusion, the lower/upper bound semi-empirical model presented in this chapter is believed to be of general applicability and its lower bound (i.e. conservative) predictions are the appropriate ones to be used for design purposes

Beam	Beam Dimensions		Compression Bars			Tension Bars			h'	h_1	f_{cu}	Steel Bars		Plate Dimensions		L_o	E_p	ε_{ue}
	Width, b (mm)	Depth (mm)	No.	Diameter (mm)	Cover (mm)	No.	Diameter (mm)	Cover (mm)	(mm)	(mm)	(MPa)	f_y (MPa)	E_s (MPa)	Width, b_1 (mm)	Thickness, t (mm)	(mm)	(MPa)	($x10^{-6}$)
$1B_u$	100	100	2	6	16	3	6	16	13	16	59.1	436	215000	65	0.70	300	111000	4850
$1C_u$	100	100	2	6	16	3	6	16	13	16	59.1	436	215000	45	1.00	300	111000	4800
$2A_u$	100	100	2	6	16	3	6	16	13	16	59.1	436	215000	90	0.50	340	111000	7950
$2A_{3a}$	100	100	2	6	16	3	6	16	13	16	59.1	436	215000	90	0.50	340	111000	10200
S1	100	100	2	6	16	3	6	16	13	16	59.1	436	215000	90	0.50	300	112973	7414
S2	100	100	2	6	16	3	6	16	13	16	59.1	436	215000	67	0.82	300	116068	4870
S3	100	100	2	6	16	3	6	16	13	16	59.1	436	215000	47	1.13	300	118389	4856
S4	100	100	2	6	16	3	6	16	13	16	59.1	436	215000	90	0.50	340	112994	8088
S5	100	100	2	6	16	3	6	16	13	16	59.1	436	215000	67	0.82	340	115986	6538
S6	100	100	2	6	16	3	6	16	13	16	59.1	436	215000	47	1.13	340	118666	7094
S7	100	100	2	6	16	3	6	16	13	16	59.1	436	215000	90	0.50	400	113018	7971
S8	100	100	2	6	16	3	6	16	13	16	59.1	436	215000	67	0.82	400	116063	7772
S9	100	100	2	6	16	3	6	16	13	16	59.1	436	215000	47	1.13	400	118448	6107

Table 4.1 **Various geometrical and material parameters plus experimental values of ε_{ue} for the R.C. beams tested by Hollaway and his associates (Hollaway (1997) and Garden *et al.* (1997)).**

Specimen Number		M_{pult}	M_{exp}	$M_{peel,l}$	$M_{peel,u}$	M_{RC}	*Plate*		$\frac{b_1}{t}$	f_{cu}	$\frac{M_{exp}}{M_{pult}}$	$\frac{M_{peel,l}}{M_{pult}}$
Present	*Original*	*(kN-m)*	*(kN-m)*	*(kN-m)*	*(kN-m)*	*(kN-m)*	*Width b_1, (mm)*	*Thickness t, (mm)*		*(N/mm^2)*		
1	*A2g*	6.80	5.04	4.20	5.33	2.48	80	1.2	66.7	42.0	0.74	0.62
2	*$1C_u$*	7.67	4.80	5.04	7.05	2.51	45	1.0	45.0	59.1	0.63	0.66
3	*$2C_u$*	7.67	6.05	5.04	7.05	2.51	45	1.0	45.0	59.1	0.79	0.66
4	*$3C_u$*	7.67	6.16	5.04	7.05	2.51	45	1.0	45.0	59.1	0.80	0.66
5	*$2C_a$*	7.67	7.00	5.04	7.05	2.51	45	1.0	45.0	59.1	0.91	0.66
6	*B3*	5.32	3.69	5.11	5.32	2.53	30	1.2	25.0	53.0	0.69	0.96
7	*A2b*	6.73	5.52	5.14	6.73	2.48	80	1.2	66.7	42.0	0.82	0.76
8	*A2c*	6.80	5.61	5.17	6.80	2.48	80	1.2	66.7	42.0	0.83	0.76
9	*A2d*	6.80	6.15	5.17	6.80	2.48	80	1.2	66.7	42.0	0.90	0.76
10	*A2e*	6.80	6.03	5.17	6.80	2.48	80	1.2	66.7	42.0	0.89	0.76
11	*A2f*	6.80	5.94	5.17	6.80	2.48	80	1.2	66.7	42.0	0.87	0.76
12	*A2h*	6.80	7.35	5.17	6.80	2.48	80	1.2	66.7	42.0	1.08	0.76
13	*B6*	9.84	6.12	5.39	7.96	2.53	80	1.2	66.7	53.0	0.62	0.55
14	*B7*	9.84	9.54	5.39	7.96	2.53	80	1.2	66.7	53.0	0.97	0.55
15	*B8*	9.84	7.83	5.39	7.96	2.53	80	1.2	66.7	53.0	0.80	0.55
16	*B9*	9.84	7.68	5.39	7.96	2.53	80	1.2	66.7	53.0	0.78	0.55
17	*$1A_u$*	7.65	5.94	5.43	7.65	2.51	90	0.5	180.0	59.1	0.78	0.71

Table 4.2 Values of various parameters for beam specimens after Quantrill *et al.* (1996:A), Quantrill *et al.* (1996:B), and Garden (1997).

Specimen Number		M_{pult}	M_{exp}	$M_{peel,l}$	$M_{peel,u}$	M_{RC}	Plate		$\frac{b_1}{t}$	f_{cu}	$\frac{M_{exp}}{M_{pult}}$	$\frac{M_{peel,l}}{M_{pult}}$
Present	Original	(kN-m)	(kN-m)	(kN-m)	(kN-m)	(kN-m)	Width b_1, (mm)	Thickness t, (mm)		(N/mm^2)		
18	$2A_u$	7.65	6.56	5.43	7.65	2.51	90	0.5	180.0	59.1	0.86	0.71
19	$3A_u$	7.65	7.80	5.43	7.65	2.51	90	0.5	180.0	59.1	1.02	0.71
20	$2A_a$	7.65	8.60	5.43	7.65	2.51	90	0.5	180.0	59.1	1.12	0.71
21	$2A_{2a}$	7.65	6.73	5.43	7.65	2.51	90	0.5	180.0	59.1	0.88	0.71
22	$2A_{3a}$	7.65	7.11	5.43	7.65	2.51	90	0.5	180.0	59.1	0.93	0.71
23	$1B_u$	7.69	5.49	5.51	7.69	2.51	65	0.7	92.9	59.1	0.71	0.72
24	$1B_{2u}$	7.69	5.46	5.51	7.69	2.51	65	0.7	92.9	59.1	0.71	0.72
25	$2B_u$	7.69	5.78	5.51	7.69	2.51	65	0.7	92.9	59.1	0.75	0.72
26	$3B_u$	7.69	6.92	5.51	7.69	2.51	65	0.7	92.9	59.1	0.90	0.72
27	$2B_a$	7.69	8.43	5.51	7.69	2.51	65	0.7	92.9	59.1	1.10	0.72
28	$2B_{2a}$	7.69	5.85	5.51	7.69	2.51	65	0.7	92.9	59.1	0.76	0.72
29	B2	7.38	5.10	5.54	7.38	2.53	80	1.2	66.7	53.0	0.69	0.75
30	B5	7.38	7.05	5.54	7.38	2.53	80	1.2	66.7	53.0	0.96	0.75
31	B4	7.39	5.25	5.63	7.39	2.53	60	1.6	37.5	53.0	0.71	0.76
32	B10	9.22	8.34	5.67	8.15	2.53	65	1.2	54.2	53.0	0.90	0.61
33	A1b	8.01	7.08	5.98	8.01	2.60	80	1.2	66.7	70.0	0.88	0.75
34	A1c	8.10	6.60	6.01	8.10	2.60	80	1.2	66.7	70.0	0.81	0.74

Table 4.2 Continued.

Specimen Number		M_{pult}	M_{exp}	$M_{peel,l}$	$M_{peel,u}$	M_{RC}	Plate		$\frac{b_1}{t}$	f_{cu}	$\frac{M_{exp}}{M_{pult}}$	$\frac{M_{peel,l}}{M_{pult}}$
Present	*Original*	*(kN-m)*	*(kN-m)*	*(kN-m)*	*(kN-m)*	*(kN-m)*	*Width b_1, (mm)*	*Thickness t, (mm)*		*(N/mm^2)*		
35	*CC*	197.91	182.44	98.14	135.44	41.79	152	6.0	25.3	43.8	0.92	0.50
36	*AA*	313.71	317.28	139.68	243.23	198.92	152	6.0	25.3	43.8	1.01	0.45
37	*BB*	274.49	257.79	153.84	217.00	139.09	152	6.0	25.3	43.8	0.94	0.56
38	*DD*	274.49	269.69	153.84	217.00	139.09	152	6.0	25.3	43.8	0.98	0.56
39	*N*	117.52	49.87	25.69	41.89	21.63	153	6.4	23.9	49.7	0.42	0.22
40	*H*	93.75	50.97	34.59	54.31	21.72	152	9.3	16.3	53.7	0.54	0.37
41	*M*	85.39	65.88	37.35	52.90	21.72	152	1.3	116.9	53.7	0.77	0.44
42	*G*	56.03	57.55	39.18	51.59	21.72	152	4.2	36.2	53.7	1.03	0.70
43	*C*	57.82	50.69	39.34	50.59	21.63	152	4.8	31.7	49.7	0.88	0.68
44	*D*	57.62	54.53	39.41	50.79	21.63	151	4.8	31.5	49.7	0.95	0.68
45	*E*	58.34	57.00	39.56	51.50	21.72	153	4.8	31.9	53.7	0.98	0.68
46	*L*	58.77	56.18	40.03	50.63	21.63	152	1.3	116.9	49.7	0.96	0.68
47	*F*	74.73	60.85	40.47	51.55	21.63	153	9.5	16.1	49.7	0.81	0.54
48	*I*	73.91	46.30	40.55	51.85	21.63	150	4.1	36.6	49.7	0.63	0.55
49	*J*	70.37	56.27	41.72	51.15	21.63	152	3.2	47.5	49.7	0.80	0.59
50	*K*	73.36	54.99	41.79	52.07	21.72	152	3.2	47.5	53.7	0.75	0.57
51	*P1*	9.99	13.17	9.99	9.99	6.58	100	1.0	100.0	47.1	1.32	1.00
52	*P2*	12.17	13.36	12.17	12.17	6.58	100	2.0	50.0	47.1	1.10	1.00
53	*P2B*	12.17	12.77	12.17	12.17	6.58	100	2.0	50.0	47.1	1.05	1.00
54	*P2BW*	12.17	15.33	12.17	12.17	6.58	100	2.0	50.0	47.1	1.26	1.00
55	*P3*	14.33	12.97	14.33	14.33	6.58	100	3.0	33.3	47.1	0.91	1.00
56	*P3B*	14.33	14.34	14.33	14.33	6.58	100	3.0	33.3	47.1	1.00	1.00
57	*P3BW*	14.33	14.15	14.33	14.33	6.58	100	3.0	33.3	47.1	0.99	1.00
58	*P3J*	14.33	16.11	14.33	14.33	6.58	100	3.0	33.3	47.1	1.12	1.00

Table 4.3 **Values of various parameters for beam specimens after Saadatmanesh *et al.* (1991), Ritchie *et al.* (1991), and Sharif *et. al.* (1994).**

Specimen Number		M_{pult}	M_{exp}	$M_{peel,l}$	$M_{peel,u}$	M_{RC}	Plate		$\frac{b_1}{t}$	f_{cu}	$\frac{M_{exp}}{M_{pult}}$	$\frac{M_{peel,l}}{M_{pult}}$
Present	Original	(kN-m)	(kN-m)	(kN-m)	(kN-m)	(kN-m)	Width b_1, (mm)	Thickness t, (mm)		(N/mm^2)		
87	1/3/N	47.22	19.03	4.46	8.27	19.40	130	5.0	26.0	52.5	0.40	0.09
88	5/1/N	47.88	25.25	5.20	9.17	19.62	130	5.0	26.0	59.0	0.53	0.11
89	2/1/N	47.61	24.20	7.78	13.73	19.55	130	5.0	26.0	57.0	0.51	0.16
90	2/2/N	47.61	24.09	7.78	13.73	19.55	130	5.0	26.0	57.0	0.51	0.16
91	2/3/N	47.61	24.70	7.78	13.73	19.55	130	5.0	26.0	57.0	0.52	0.16
92	2/4/N	47.61	25.36	7.78	13.73	19.55	130	5.0	26.0	57.0	0.53	0.16
93	1/3/S	47.22	22.88	8.27	15.00	19.40	130	5.0	26.0	52.5	0.48	0.18
94	6/1/-	48.30	23.13	9.53	16.93	19.74	130	5.0	26.0	63.0	0.48	0.20
95	6/2/-	48.30	23.59	9.53	16.93	19.74	130	5.0	26.0	63.0	0.49	0.20
96	6/3/-	48.30	24.08	9.53	16.93	19.74	130	5.0	26.0	63.0	0.50	0.20
97	8/1/N	45.96	24.99	10.24	18.50	19.20	130	5.0	26.0	47.0	0.54	0.22
98	8/1/S	45.96	25.16	10.24	18.50	19.20	130	5.0	26.0	47.0	0.55	0.22
99	1/2/N	47.22	17.88	10.56	19.34	19.40	130	5.0	26.0	52.5	0.38	0.22
100	8/2/*	45.96	24.80	11.10	20.14	19.20	130	5.0	26.0	47.0	0.54	0.24
101	1/2/S	47.22	16.34	11.47	21.09	19.40	130	5.0	26.0	52.5	0.35	0.24
102	1/4/S	47.22	22.55	11.47	21.09	19.40	130	5.0	26.0	52.5	0.48	0.24
103	1/1/N*	47.22	22.55	11.47	21.09	19.40	130	5.0	26.0	52.5	0.48	0.24
104	5/1/S	47.88	24.15	11.61	20.94	19.62	130	5.0	26.0	59.0	0.50	0.24
105	7/1/N	47.80	23.80	11.74	21.09	19.62	130	5.0	26.0	59.0	0.50	0.25
106	7/1/S	47.80	24.50	11.74	21.09	19.62	130	5.0	26.0	59.0	0.51	0.25
107	6/4/-	48.30	25.85	12.05	21.72	19.74	130	5.0	26.0	63.0	0.54	0.25
108	2/1/S	47.61	22.06	12.35	22.38	19.55	130	5.0	26.0	57.0	0.46	0.26
109	2/2/S	47.61	24.09	12.35	22.38	19.55	130	5.0	26.0	57.0	0.51	0.26
110	2/3/S	47.61	24.86	12.35	22.38	19.55	130	5.0	26.0	57.0	0.52	0.26
111	2/4/S	47.61	24.70	12.35	22.38	19.55	130	5.0	26.0	57.0	0.52	0.26
112	7/2/*	47.80	23.80	12.71	22.94	19.62	130	5.0	26.0	59.0	0.50	0.27

Table 4.4 Values of various parameters for beam specimens after Oehlers (1992).

Beam title	*ACI unplated predicted shear capacity V_u (kN)*	*Actual failure load for plated beam V_{exp} (kN)*	*Reported mode of failure*
1/1/N	27.3	41.0	Shear
1/2/S	27.3	29.7	Shear
1/2/N	27.3	32.5	Shear
1/3/S	27.3	41.6	Shear
1/3/N	27.3	34.6	Shear
1/4/S	27.3	41.0	Shear
2/1/N	28.2	44.0	Flexural
2/1/S	28.2	40.1	Shear
2/2/N	**56.2**	**43.8**	**Flexural**
2/2/S	**56.2**	**43.8**	**Flexural**
2/3/N	**84.8**	**44.9**	**Flexural**
2/3/S	**84.8**	**45.2**	**Flexural**
2/4/N	**122.6**	**46.1**	**Flexural**
2/4/S	**122.6**	**44.9**	**Flexural**
5/1/N	**123.0**	**45.9**	**Flexural**
5/1/S	**123.0**	**43.9**	**Flexural**
6/1/-	**29.3**	**25.0**	**Flexural**
6/2/-	**29.3**	**25.5**	**Flexural**
6/3/-	**29.3**	**21.4**	**Flexural**
6/4/-	**29.3**	**21.1**	**Flexural**
7/1/N	**28.6**	**17.0**	**-**
7/1/S	**28.6**	**17.5**	**Flexural**
7/2/*	**28.6**	**23.8**	**Flexural**
8/1/N	**26.2**	**14.7**	**-**
8/1/S	**26.2**	**14.8**	**Flexural**
*8/2/**	26.2	32.0	Flexural

Table 4.5 **Comparisons between the actual failure load and mode of failure for the plated beams and the predicted shear capacity of the corresponding unplated beams for beam designs after Oehlers (1992).**

Specimen Number		M_{pult}	M_{exp}	$M_{peel\text{-}1,l}$	$M_{peel\text{-}1,u}$	$M_{peel\text{-}2,l}$	$M_{peel\text{-}2,u}$	M_{RC}	Plate		$\frac{b_1}{t}$	f_{cu}	$\frac{M_{exp}}{M_{pult}}$	$\frac{M_{peel\text{-}1,l}}{M_{pult}}$	$\frac{M_{peel\text{-}2,l}}{M_{pult}}$
Present	Original	(kN-m)	(kN-m)	(kN-m)	(kN-m)	(kN-m)	(kN-m)	(kN-m)	Width b_1, (mm)	Thick. t, (mm)		(N/mm^2)			
59	C11	9.14	8.13	6.44	6.44	6.44	6.44	5.13	80	1.6	50.0	93.0	0.89	0.70	0.70
60	C12	9.14	11.86	6.44	6.44	6.44	6.44	5.13	80	1.6	50.0	93.0	1.30	0.70	0.70
61	C3	9.14	13.48	6.44	6.44	6.44	6.44	5.13	80	1.6	50.0	93.0	1.47	0.70	0.70
62	C5	9.14	13.75	6.44	6.44	6.44	6.44	5.13	80	1.6	50.0	93.0	1.50	0.70	0.70
63	C7	9.14	14.47	6.44	6.44	6.44	6.44	5.13	80	1.6	50.0	93.0	1.58	0.70	0.70
64	C16	9.14	12.38	6.44	6.44	6.44	6.44	5.13	80	1.6	50.0	93.0	1.35	0.70	0.70
65	URB2	13.44	15.00	7.92	7.92	7.92	7.92	8.53	80	1.5	53.3	67.4	1.12	0.59	0.59
66	URB5	31.31	19.95	8.29	15.26	10.36	19.22	8.53	80	10	8.0	67.4	0.64	0.26	0.33
67	B1	18.17	11.60	8.57	14.82	15.14	15.14	6.27	100	3	33.3	47.1	0.64	0.47	0.83
68	FRB2	11.10	14.20	8.67	8.67	8.67	8.67	6.27	100	1	100.0	47.1	1.28	0.78	0.78
69	FRB5	14.70	12.00	9.39	11.93	11.93	11.93	6.27	100	2	50.0	47.1	0.82	0.64	0.81
70	URB4	20.96	21.60	9.51	14.95	11.80	14.95	8.53	80	5	16.0	67.4	1.03	0.45	0.56
71	B10	12.91	15.00	10.11	10.31	10.31	10.31	6.27	100	1.5	66.7	47.1	1.16	0.78	0.80
72	MF1	20.39	9.00	11.08	15.61	15.61	15.61	8.77	100	3	33.3	49.9	0.44	0.54	0.77
73	URB3	18.85	20.63	13.54	13.54	13.54	13.54	8.83	80	3	26.7	103.5	1.09	0.72	0.72
74	F31	107.49	69.80	26.15	46.23	22.80	39.92	62.00	125	6	20.8	57.9	0.65	0.24	0.21
75	205	115.25	81.69	29.81	52.52	26.04	45.38	69.61	125	6	20.8	72.3	0.71	0.26	0.23
76	209	115.25	84.37	29.81	52.52	26.04	45.38	69.61	125	6	20.8	72.3	0.73	0.26	0.23
77	218	115.25	74.40	29.81	52.52	26.04	45.38	69.61	125	6	20.8	72.3	0.65	0.26	0.23
78	204	102.86	103.55	41.12	59.43	35.83	59.43	69.61	125	3	41.7	72.3	1.01	0.40	0.35
79	208	102.86	101.24	41.12	59.43	35.83	59.43	69.61	125	3	41.7	72.3	0.98	0.40	0.35
80	217	102.86	98.56	41.12	59.43	35.83	59.43	69.61	125	3	41.7	72.3	0.96	0.40	0.35
81	F11	83.55	88.97	45.81	45.81	45.81	45.81	61.44	125	1.5	83.3	56.6	1.06	0.55	0.55
82	203	92.91	103.55	46.91	46.91	46.91	46.91	69.61	125	1.5	83.3	72.3	1.11	0.50	0.50
83	207	92.91	100.48	46.91	46.91	46.91	46.91	69.61	125	1.5	83.3	72.3	1.08	0.50	0.50
84	216	92.91	100.48	46.91	46.91	46.91	46.91	69.61	125	1.5	83.3	72.3	1.08	0.50	0.50
85	O	48.50	42.73	21.87	34.49	39.03	39.03	21.72	153	2.6	58.8	53.7	0.88	0.45	0.80
86	P	47.20	57.83	22.56	35.62	37.91	37.91	21.72	150	2.5	60.0	53.7	1.23	0.48	0.80

Table 4.6 Values of various parameters for beam specimens after Baluch *et al.* (1995), and Ritchie *et al.* (1991).

Specimen Number		M_{pult}	$*M_{exp}$	$M_{peel\text{-}1,l}$	$M_{peel\text{-}1,u}$	$M_{peel\text{-}2,l}$	$M_{peel\text{-}2,u}$	M_{RC}	Plate		$\frac{b_1}{t}$	f_{cu}	$\frac{M_{exp}}{M_{pult}}$	$\frac{M_{peel\text{-}1,l}}{M_{pult}}$	$\frac{M_{peel\text{-}2,l}}{M_{pult}}$
Present	Original	(kN-m)	(kN-m)	(kN-m)	(kN-m)	(kN-m)	(kN-m)	(kN-m)	Width b_1, (mm)	Thick. t, (mm)		(N/mm^2)			
87	1/3/N	44.64	19.03	4.46	8.27	9.29	16.92	19.40	130	5	26.0	52.5	0.43	0.10	0.21
88	5/1/N	45.98	25.25	5.20	9.17	10.25	18.36	19.62	130	5	26.0	59.0	0.55	0.11	0.22
89	2/1/N	45.58	24.20	7.78	13.73	15.42	28.29	19.55	130	5	26.0	57.0	0.53	0.17	0.34
90	2/2/N	45.58	24.09	7.78	13.73	15.42	28.29	19.55	130	5	26.0	57.0	0.53	0.17	0.34
91	2/3/N	45.58	24.70	7.78	13.73	15.42	28.29	19.55	130	5	26.0	57.0	0.54	0.17	0.34
92	2/4/N	45.58	25.36	7.78	13.73	15.42	28.29	19.55	130	5	26.0	57.0	0.56	0.17	0.34
93	1/3/S	44.64	22.88	8.27	15.00	15.88	29.66	19.40	130	5	26.0	52.5	0.51	0.19	0.36
94	6/1/-	46.76	23.13	9.53	16.93	17.91	33.00	19.74	130	5	26.0	63.0	0.49	0.20	0.38
95	6/2/-	46.76	23.59	9.53	16.93	17.91	33.00	19.74	130	5	26.0	63.0	0.50	0.20	0.38
96	6/3/-	46.76	24.08	9.53	16.93	17.91	33.00	19.74	130	5	26.0	63.0	0.51	0.20	0.38
97	8/1/N	43.27	24.99	10.24	18.50	15.25	28.09	19.20	130	5	26.0	47.0	0.58	0.24	0.35
98	8/1/S	43.27	25.16	10.24	18.50	15.25	28.09	19.20	130	5	26.0	47.0	0.58	0.24	0.35
99	1/2/N	44.64	17.88	10.56	19.34	15.88	29.66	19.40	130	5	26.0	52.5	0.40	0.24	0.36
100	8/2/*	43.27	24.80	11.10	20.14	15.25	28.09	19.20	130	5	26.0	47.0	0.57	0.26	0.35
101	1/2/S	44.64	16.34	11.47	21.09	15.88	29.66	19.40	130	5	26.0	52.5	0.37	0.26	0.36
102	1/4/S	44.64	22.55	11.47	21.09	15.88	29.66	19.40	130	5	26.0	52.5	0.51	0.26	0.36
103	1/1/N*	44.64	22.55	11.47	21.09	15.88	29.66	19.40	130	5	26.0	52.5	0.51	0.26	0.36
104	5/1/S	45.98	24.15	11.61	20.94	17.26	31.82	19.62	130	5	26.0	59.0	0.53	0.25	0.38
105	7/1/N	46.04	23.80	11.74	21.09	17.41	31.94	19.62	130	5	26.0	59.0	0.52	0.25	0.38
106	7/1/S	46.04	24.50	11.74	21.09	17.41	31.94	19.62	130	5	26.0	59.0	0.53	0.25	0.38
107	6/4/-	46.76	25.85	12.05	21.72	17.91	33.00	19.74	130	5	26.0	63.0	0.55	0.26	0.38
108	2/1/S	45.58	22.06	12.35	22.38	16.96	31.24	19.55	130	5	26.0	57.0	0.48	0.27	0.37
109	2/2/S	45.58	24.09	12.35	22.38	16.96	31.24	19.55	130	5	26.0	57.0	0.53	0.27	0.37
110	2/3/S	45.58	24.86	12.35	22.38	16.96	31.24	19.55	130	5	26.0	57.0	0.55	0.27	0.37
111	2/4/S	45.58	24.70	12.35	22.38	16.96	31.24	19.55	130	5	26.0	57.0	0.54	0.27	0.37
112	7/2/*	46.04	23.80	12.71	22.94	17.41	31.94	19.62	130	5	26.0	59.0	0.52	0.28	0.38

Table 4.7 Values of various parameters for beam specimens tested by Oehlers (1992),

*** M_{exp} = experimental ultimate plate peeling moment.**

Specimen Number		M_{pult}	M_{exp}	$M_{peel\text{-}1,l}$	$M_{peel\text{-}1,u}$	$M_{peel\text{-}2,l}$	$M_{peel\text{-}2,u}$	M_{RC}	Plate		$\frac{b_1}{t}$	f_{cu}	$\frac{M_{exp}}{M_{pult}}$	$\frac{M_{peel\text{-}1,l}}{M_{pult}}$	$\frac{M_{peel\text{-}2,l}}{M_{pult}}$
Present	Original	(kN-m)	(kN-m)	(kN-m)	(kN-m)	(kN-m)	(kN-m)	(kN-m)	Width b_1, (mm)	Thick. t, (mm)		(N/mm^2)			
113	13/17	30.05	6.30	3.47	6.31	13.48	25.12	10.71	120	6	20.0	43.0	0.21	0.12	0.45
114	13/18	19.06	7.90	4.82	8.10	12.79	12.79	10.71	120	2	60.0	43.0	0.41	0.25	0.67
115	13/16	30.71	11.40	5.96	10.89	7.76	14.30	17.97	120	5	24.0	33.0	0.37	0.19	0.25
116	13/14	31.73	9.00	6.14	11.23	10.60	19.82	14.46	120	5	24.0	37.0	0.28	0.19	0.33
117	13/20	30.14	10.20	6.44	11.69	16.63	25.44	9.16	120	5	24.0	43.0	0.34	0.21	0.55
118	11/3	57.43	7.90	7.02	13.26	8.87	16.72	19.95	120	15	8.0	36.0	0.14	0.12	0.15
119	11/4	57.43	9.20	7.02	13.26	8.87	16.72	19.95	120	15	8.0	36.0	0.16	0.12	0.15
120	2/1	30.86	12.20	7.20	13.21	9.46	17.50	15.29	125	5	25.0	34.0	0.40	0.23	0.31
121	2/2	30.86	11.50	7.20	13.21	9.46	17.50	15.29	125	5	25.0	34.0	0.37	0.23	0.31
122	10/1	49.70	12.30	7.23	13.46	9.08	16.92	19.87	120	10	12.0	33.0	0.25	0.15	0.18
123	10/2	49.70	10.80	7.23	13.46	9.08	16.92	19.87	120	10	12.0	33.0	0.22	0.15	0.18
124	6/3	31.55	12.60	7.35	13.54	9.67	17.99	15.35	125	5	25.0	36.0	0.40	0.23	0.31
125	6/4	31.55	14.20	7.35	13.54	9.67	17.99	15.35	125	5	25.0	36.0	0.45	0.23	0.31
126	6/1	31.74	16.00	7.54	13.74	9.87	18.16	15.34	125	5	25.0	36.0	0.50	0.24	0.31
127	6/2	31.74	12.60	7.54	13.74	9.87	18.16	15.34	125	5	25.0	36.0	0.40	0.24	0.31
128	3/1	25.30	11.30	7.76	14.00	10.12	18.31	15.08	125	3	41.7	28.0	0.45	0.31	0.40
129	3/2	25.30	10.80	7.76	14.00	10.12	18.31	15.08	125	3	41.7	28.0	0.43	0.31	0.40
130	3/3	25.30	12.60	7.76	14.00	10.12	18.31	15.08	125	3	41.7	28.0	0.50	0.31	0.40
131	3/4	25.30	13.50	7.76	14.00	10.12	18.31	15.08	125	3	41.7	28.0	0.53	0.31	0.40
132	9/3	25.53	13.50	7.76	14.14	10.16	18.64	15.13	125	3	41.7	29.0	0.53	0.30	0.40
133	9/4	25.53	15.30	7.76	14.14	10.16	18.64	15.13	125	3	41.7	29.0	0.60	0.30	0.40

Table 4.8 Values of various parameters for beam specimens tested be Oehlers and Moran (1990).

Specimen Number		M_{pult}	M_{exp}	$M_{peel\text{-}1,l}$	$M_{peel\text{-}1,u}$	$M_{peel\text{-}2,l}$	$M_{peel\text{-}2,u}$	M_{RC}	Plate		$\frac{b_1}{t}$	f_{cu}	$\frac{M_{exp}}{M_{pult}}$	$\frac{M_{peel-1,l}}{M_{pult}}$	$\frac{M_{peel-2,l}}{M_{pult}}$
Present	Original	(kN-m)	(kN-m)	(kN-m)	(kN-m)	(kN-m)	(kN-m)	(kN-m)	Width b_1, (mm)	Thick. t, (mm)		(N/mm^2)			
134	12/1	44.78	10.40	7.79	14.47	8.93	16.63	19.78	100	10	10.0	30.0	0.23	0.17	0.20
135	1/1	26.15	9.20	7.98	14.28	14.43	18.50	13.46	125	3	41.7	48.0	0.35	0.31	0.55
136	1/2	26.15	9.90	7.98	14.28	14.43	18.50	13.46	125	3	41.7	48.0	0.38	0.31	0.55
137	13/19	19.46	10.60	8.18	13.87	13.87	13.87	9.16	120	2	60.0	43.0	0.54	0.42	0.71
138	5/3	34.15	11.50	8.19	15.01	10.75	19.90	15.54	125	5	25.0	43.0	0.34	0.24	0.31
139	5/4	34.15	9.90	8.19	15.01	10.75	19.90	15.54	125	5	25.0	43.0	0.29	0.24	0.31
140	4/3	34.37	13.50	8.26	15.15	10.84	20.11	15.57	125	5	25.0	44.0	0.39	0.24	0.32
141	4/4	34.37	14.40	8.26	15.15	10.84	20.11	15.57	125	5	25.0	44.0	0.42	0.24	0.32
142	4/1	34.59	12.60	8.32	15.30	10.93	20.33	15.60	125	5	25.0	45.0	0.36	0.24	0.32
143	4/2	34.59	14.00	8.32	15.30	10.93	20.33	15.60	125	5	25.0	45.0	0.40	0.24	0.32
144	13/13	23.58	12.60	8.34	15.08	14.24	15.43	14.46	120	2	60.0	37.0	0.53	0.35	0.60
145	5/1	34.37	11.50	8.39	15.29	10.97	20.24	15.57	125	5	25.0	44.0	0.33	0.24	0.32
146	5/2	34.37	15.10	8.39	15.29	10.97	20.24	15.57	125	5	25.0	44.0	0.44	0.24	0.32
147	10/3	45.04	11.20	8.54	15.68	10.64	19.69	20.00	120	6.5	18.5	37.0	0.25	0.19	0.24
148	10/4	45.04	11.70	8.54	15.68	10.64	19.69	20.00	120	6.5	18.5	37.0	0.26	0.19	0.24
149	13/15	25.19	15.30	8.55	15.48	11.08	16.96	17.97	120	2	60.0	33.0	0.61	0.34	0.44
150	9/1	27.52	16.70	8.93	16.35	11.70	20.06	15.41	125	3	41.7	38.0	0.61	0.32	0.43
151	9/2	27.52	14.00	8.93	16.35	11.70	20.06	15.41	125	3	41.7	38.0	0.51	0.32	0.43
152	13/11	36.62	13.10	8.94	16.45	19.04	31.39	19.41	120	5	24.0	35.0	0.36	0.24	0.52
153	12/4	44.82	10.60	10.54	19.17	11.00	20.05	19.95	75	10	7.5	36.0	0.24	0.24	0.25

Table 4.8 Continued.

Specimen Number		M_{pult}	M_{exp}	$M_{peel\text{-}1,\,l}$	$M_{peel\text{-}1,\,u}$	$M_{peel\text{-}2,\,l}$	$M_{peel\text{-}2,\,u}$	M_{RC}	Plate		$\frac{b_1}{t}$	f_{cu}	$\frac{M_{exp}}{M_{pult}}$	$\frac{M_{peel\text{-}1,l}}{M_{pult}}$	$\frac{M_{peel\text{-}2,l}}{M_{pult}}$
Present	*Original*	*(kN-m)*	*(kN-m)*	*(kN-m)*	*(kN-m)*	*(kN-m)*	*(kN-m)*	*(kN-m)*	*Width b_1, (mm)*	*Thick. t, (mm)*		*(N/mm^2)*			
154	*8/3*	47.62	13.40	10.58	19.06	13.07	23.82	23.04	120	5	24.0	35.0	0.28	0.22	0.27
155	*8/4*	47.62	11.30	10.58	19.06	13.07	23.82	23.04	120	5	24.0	35.0	0.24	0.22	0.27
156	*7/3*	47.25	15.40	10.60	18.95	13.05	23.62	23.00	120	5	24.0	34.0	0.33	0.22	0.28
157	*7/4*	47.25	10.30	10.60	18.95	13.05	23.62	23.00	120	5	24.0	34.0	0.22	0.22	0.28
158	*11/1*	34.44	12.30	10.75	19.34	13.27	24.13	19.90	120	3	40.0	34.0	0.36	0.31	0.39
159	*11/2*	34.44	13.10	10.75	19.34	13.27	24.13	19.90	120	3	40.0	34.0	0.38	0.31	0.39
160	*12/2*	37.14	12.70	10.86	19.90	10.97	20.10	19.78	50	10	5.0	30.0	0.34	0.29	0.30
161	*7/1*	47.71	16.80	10.94	19.43	13.43	24.17	23.02	120	5	24.0	35.0	0.35	0.23	0.28
162	*7/2*	47.71	17.60	10.94	19.43	13.43	24.17	23.02	120	5	24.0	35.0	0.37	0.23	0.28
163	*8/1*	48.55	18.00	11.38	20.14	13.95	25.03	23.08	120	5	24.0	37.0	0.37	0.23	0.29
164	*8/2*	48.55	20.70	11.38	20.14	13.95	25.03	23.08	120	5	24.0	37.0	0.43	0.23	0.29
165	*13/6*	52.71	24.40	13.11	24.03	27.81	42.67	25.82	120	5	24.0	42.0	0.46	0.25	0.53
166	*12/3*	32.51	16.40	13.40	21.46	15.94	21.46	19.95	25	10	2.5	36.0	0.50	0.41	0.49
167	*13/9*	31.18	17.60	15.01	20.60	20.60	20.60	19.68	120	2	60.0	46.0	0.56	0.48	0.66
168	*13/10*	31.18	16.10	15.01	20.60	20.60	20.60	19.68	120	2	60.0	46.0	0.52	0.48	0.66
169	*13/7*	66.98	23.90	16.68	30.04	34.66	53.33	32.01	120	5	24.0	41.0	0.36	0.25	0.52

Table 4.8 Continued.

Chapter 5

FLEXURAL FAILURE MODES FOR THE EXTERNALLY PLATED BEAMS

Chapter 5

FLEXURAL FAILURE MODES FOR THE EXTERNALLY PLATED BEAMS

5.1 INTRODUCTION

The purpose of this chapter is to address all the possible modes of failure which are likely to occur in connection with reinforced concrete beams upgraded with externally bonded steel/FRP plates glued to their soffit (tensile side). The different types of beam-plate interaction phenomena and the related composite beam load carrying capacities will be discussed in some detail in the next chapter.

5.2 PLATED BEAM FLEXURAL CAPACITIES

In view of the fact that the external plate is not (similar to the internal steel bars) monolithic with the concrete, the interaction between the plate and concrete will not be as strong as it is in the case of the internal steel bars.

The external plates are usually glued to the tensile side of the beams by using a strong adhesive. There is no direct contact between the concrete and the plate and the latter is not confined by the concrete. In view of these conditions, the plate may not remain fully bonded to the beam up to its full flexural capacity.

In what follows, the term 'full bond flexural capacity' refers to the load carrying capacity of the beam when the externally bonded plate remains fully bonded to concrete up to the ultimate load, with plane sections remaining plane over all the

beam sections. In the presence of full bond, the external plate will act in a similar fashion to the embedded steel bars and, then, the strain compatibility and equilibrium conditions for forces and moments over all the beam sections will be similar in form for both the plate and the embedded bars. Under such conditions, at least one maximum moment section exists, and the beam will eventually reach its full load carrying capacity at that section: the beam's flexural load bearing capacity will, then, be referred as the full bond capacity.

There are, however, certain other modes of failure which are premature in nature and, hence, reduce the plated beam's load bearing capacity below that of the full bond capacity. These undesirable modes of failure occur, for example, due to separation and slippage at the steel/concrete interface, or due to the plate/concrete cover ripping off (peeling). The plate separation occurs either between the plate and the adhesive layer, or between the concrete and the adhesive layer. The plate peeling phenomenon, on the other hand, is always initiated at the end of the plate with concrete cover peeling at the underside level of the internal (embedded) reinforcing steel bars with the plate and concrete cover, as a unit, splitting away from the beam.

There are currently a number of research projects world-wide which address the question of enhancing the bond between the plate and concrete, and avoiding the occurrence of plate peeling, using many techniques such as end anchoring, side plating, etc.. By using strong adhesives, and adopting more sensible glue application techniques, it has (in certain cases) been found that the plate separation problem at the glue line can be avoided. The plate/concrete peeling failure, however, still poses an

obstacle in the way to achieve the full bond capacity for the externally plated reinforced concrete beams.

When the plate does not interact fully with the reinforced concrete beam up to the ultimate load (i.e. premature failure occurs), the load bearing capacity of the composite beam will be referred to as the 'partial bond capacity', and the beam's failure may happen outside the maximum moment zone: this may be due to premature failure within the adhesive material or, can, indeed, happen in the concrete cover.

As discussed in the previous chapters, partial bond (peeling) behaviour is largely controlled by the tensile strength of concrete. In the present work, it is assumed that estimates of the tensile stresses at the critical location within the concrete cover may be based on the stabilised crack formation theory within the concrete cover which, due to the complicated nature of the problem, embodies an upper (maximum) and a lower (minimum) limit on the spacings of stabilised flexural cracks.

The axial force carried by the plate which is responsible for the presence of such tensile stresses in the concrete cover, depends on the spacings between two adjacent stabilised cracks, the effective length of the plate, the width of the beam, the thickness of the concrete cover, and the concrete tensile strength. The crack spacings are the most uncertain factors in practice, and have a wide range of values varying from a minimum to a maximum limit.

Considering that there generally exist two largely different minimum and maximum values for the axial plate stresses, the plated beam will have two corresponding

limiting values of load bearing capacities (i.e. flexural moments): these correspond to cases when the axial plate stress reaches its minimum (for the lower partial bond capacity) or its maximum (for the upper partial bond capacity).

In what follows, the estimates of flexural beam capacities will be based on the following assumptions:

1- plane sections remain plane after bending, and

2- the stress-strain relationships for steel and concrete as recommended by the BS5400 (1990) and BS8110 (1985) (wherever appropriate), will be used.

Moreover, the strain compatibility along the plated beam sections, and the equilibrium of forces and moments will be considered: these results will, then, be used in the subsequent chapters in order to throw some light on the changes of the modes of failure as influenced by variations in, for example, the magnitude of the modulus of elasticity for the FRP plate material (within current manufacturing limits).

The material partial safety factors which are used in the following formulations relating to the flexural beam capacity, follow those recommended by the codes of practice, and are assumed to be 1.0 in certain cases while in other instances (wherever appropriate) those recommended by the British code BS8110 (1985) will be used.

According to BS8110 (1985), the material partial safety factor of 1.15 is used for the steel plates and the reinforcing bars, while for the concrete, a material partial safety factor of 1.5 is assumed. The material partial safety factor for the FRP used as the plating medium (in the absence of any code recommendations) is (for the present

purposes) chosen as that for steel (i.e. 1.15): this is in view of the high quality control usually adopted in producing composite materials..

The full bond capacities relate to the moments M_{pult} and M_{min} for the plated and unplated sections, respectively: these moments will be calculated using material partial safety factors of 1.0. In addition, the plated and unplated beam moments M_{plated} and M_{RC}, respectively, are (in what follows) calculated according to the BS8110 (1985) recommendations using the material partial safety factors as recommended by BS8110 (1985).

The partial bond capacities relate to the lower bound moment, M_{lower}, and the upper bound moment, M_{upper}. The assumed material partial safety factors for these two limiting premature flexural moments will be taken to be equal to 1.0.

5.3 THE EXPECTED MODES OF FAILURE

As regards the failure characteristics of reinforced concrete beams, the flexural modes of failure may be classified as either ductile (where the failure happens after the internal bars have yielded associated with which are large deformations and curvatures), or brittle, where the failure occurs without any warning and no significant associated beam overall deformations, and in the absence of yielding of the embedded bars.

Failure of plated beams may either be due to over-stressing (or over-straining) in the brittle elements such as compressive or tensile failure of concrete, and rupture of FRP

plate, or it may be due to failure of the ductile materials such the internal steel bars and/or the steel plates which may be strained far beyond their initial yield points, up to total failure (i.e. rupture).

Brittle materials such as the FRP or concrete can not carry any load when strained to their elastic limits and fail suddenly, while the ductile materials such as reinforcing steel bars or steel plates continue to carry the yield load subsequent to being strained to the initiation of yield, whereby their corresponding load level very nearly remains unchanged with increasing levels of imposed axial strains.

Unplated beams have only one type of brittle material (i.e. concrete). Their brittle mode happens when the maximum concrete strain, ε_m, reaches the crushing value (e.g. $\varepsilon_m = 0.0035$ in BS8110 (1985)), while the steel bars never reach the yield point. Their ductile mode of failure, on the other hand, happens if the concrete is crushed after the bars have yielded and, in such cases, the beam experiences large overall deformations and curvatures.

In contrast to unplated reinforced concrete beams, the externally plated beams have up to three different types of brittle elements (i.e. crushing of concrete, rupture of FRP plate, and failure of concrete in tension initiated at the end of the plate): it then follows (at least theoretically) that, for plated beams, there are up to eight different possible flexural modes of failure.

Since the steel plates are of a ductile type, certain number of these eight modes of failure will not occur in the case of composite beams which are reinforced with external steel plates, and will only be applicable to those beams which are upgraded using externally bonded brittle FRP plates.

Similarly, because the FRP plates and concrete are both brittle, a certain number of the failure modes which correspond to simultaneous over-straining of both the concrete in compression and the FRP plate in tension, are extremely unlikely to occur in practice. The reason being that these two brittle materials are unlikely to fail together at the same instance, and (most probably) only one of them will be the controlling factor for the theoretical ultimate failure. Such brittle modes of failure, in which the concrete and the plate would fail simultaneously, are not considered here when addressing the behaviour of beams which are externally reinforced with only FRP plates and are assumed to be applicable only to those beams with external steel plates.

In the case of beams with external steel or FRP plates, ductile failure modes are assumed to occur only if the internal steel reinforcing bars reach yield. Their failure mode will be described as brittle if the axial stresses in the steel bars, at the instant of beam's total collapse, are lower in magnitude than that of yield stress for steel.

In summary, the load carrying capacity of the beam will be classified as a partial bond capacity due to premature plate peeling failure, if the concrete in tension within the cover, is the controlling factor for the failure mode, while it will be classified as full

bond capacity, if the failure is controlled by either the crushing of concrete or the rupture of FRP plate at the maximum moment section.

The possible eight modes of failure for the externally plated beams may, thus, be listed as in the following, with the element which controls the final failure in each mode underlined: (the symbols ***C***, ***R*** or ***P*** refer to Concrete, Rebar, or Plate, respectively)

1- *Crushed concrete*, unyielded bars and unruptured/unyielded plate ***C- -,***

2- *Crushed concrete*, unyielded bars and yielded plate ***C-P,***

3- *Crushed concrete*, yielded bars and unruptured/unyielded plate ***CR-,***

4- *Crushed concrete*, yielded bars and plate ***CRP,***

5- Uncrushed concrete, yielded bars and *ruptured plate* ***-RP,***

6- Uncrushed concrete, unyielded bars and *ruptured plate* ***- -P,***

7- *Peeled end plate*, yielded bars and unruptured/unyielded plate ***-R-***, and

8- *Peeled end plate*, unyielded bars and unruptured/unyielded plate ***- - -.***

Table (5.1) lists all the theoretically assumed modes of failure for the beams upgraded with either external steel or FRP plates, classified according to the type of the bond (full/partial bond capacity), and the ductile or brittle nature of failure mode.

The stress and strain distributions corresponding to each of the above failure modes, and the associated equations of equilibrium are addressed in some detail in what follows. In the present work, tension in concrete will be neglected for simplicity, as its effect is of relatively minor importance compared to the other tensile forces in the

reinforcing bars and the external plate. For the present purposes, the simply supported beam is assumed to be subjected to symmetrical four-point loading.

<table>
<tr><th rowspan="2">Capacity</th><th rowspan="2">Ductility</th><th colspan="2">Beam externally reinforced with</th></tr>
<tr><th>FRP plate</th><th>Steel plate</th></tr>
<tr><td rowspan="5">Full bond capacity</td><td rowspan="2">Ductile modes</td><td colspan="2">CR-</td></tr>
<tr><td></td><td>CRP</td></tr>
<tr><td rowspan="3">Brittle modes</td><td>-RP</td><td></td></tr>
<tr><td colspan="2">C- -</td></tr>
<tr><td></td><td>C-P</td></tr>
<tr><td rowspan="2">Partial bond capacity</td><td>Ductile modes</td><td colspan="2">-R-</td></tr>
<tr><td>Brittle modes</td><td colspan="2">- - -</td></tr>
</table>

Table 5.1 Modes of failure for beams upgraded with external plates.

5.3.1 Failure Mode *C- -*

This mode corresponds to cases when, the brittle failure is due to concrete crushing ($\varepsilon_o = \varepsilon_m = 0.0035$) at the maximum moment section (i.e. between the external point loads), while the stress in the embedded bars is lower than the steel yield stress ($f_s < f_y$), and the axial plate stress is lower than either the FRP ultimate strength or the steel yield stress ($f_p < f_{pu}$ or $f_p < f_y$) - see Figure 5.1.

The failure will happen suddenly, following the crushing of concrete at the top surface of the beam. In this mode, the beam capacity is classified as full bond capacity, and this type of failure may occur in the beams reinforced with either steel or FRP plates.

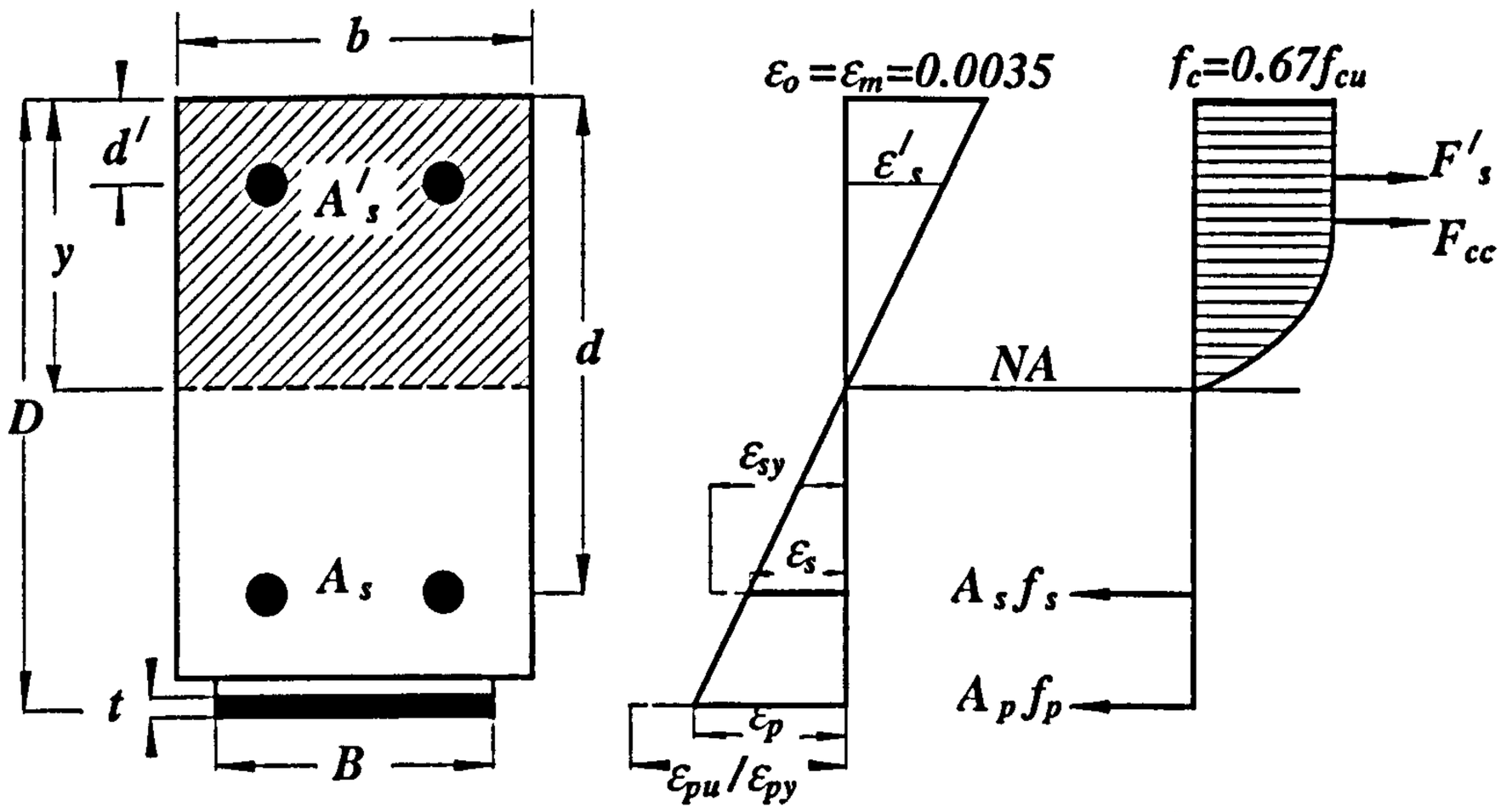

Fig. 5.1 Mode *C*- -: Section strains, stresses, and dimensions.

From Figure 5.1, the following may be derived:

$$\frac{\varepsilon_p}{D-y} = \frac{\varepsilon_s}{d-y} = \frac{\varepsilon_s'}{y-d'} = \frac{\varepsilon_o}{y}$$

$$\varepsilon_s = \varepsilon_o \frac{d-y}{y} \text{ and } \varepsilon_p = \varepsilon_o \frac{D-y}{y}$$

From the equilibrium condition, $F_c = F_t$

where, $F_t = F_s + F_p$,

$$F_s = A_s.E_s\varepsilon_s = A_s.E_s\varepsilon_o \frac{d-y}{y},$$

$$F_p = A_pE_p\varepsilon_p = A_pE_p\varepsilon_o \frac{D-y}{y}$$

and, the total compression force, F_c, as derived in Appendix B (Equation B.51), is

$$F_c = A_s'E_s\varepsilon_o\left(\frac{y-d'}{y}\right) + 0.67 f_{cu}\, yb\alpha_{f_{cu}}$$

where, $\alpha_{f_{cu}} = \left[1 + \frac{\eta_b\sqrt{f_{cu}}}{\varepsilon_o}\left(\frac{\eta_e\eta_b}{4} - \frac{2}{3}\right)\right]$, $E_c = \eta_e\sqrt{f_{cu}}$ and $\beta = \eta_b\sqrt{f_{cu}}$

with, $\eta_b = 2.44 \times 10^{-4}$, $\varepsilon_o = \varepsilon_m = 0.0035$, and if the concrete modulus of elasticity is not determined experimentally, one may assume (according to the BS5400 (1990)) $\eta_e = 5.5$.

The above equilibrium equation will, then, lead to the following:

$$A_s E_s \varepsilon_o \frac{d-y}{y} + A_p E_p \varepsilon_o \frac{D-y}{y} = A_s' E_s \varepsilon_o \left(\frac{y-d'}{y} \right) + 0.67 f_{cu} y b \alpha_{f_{cu}} \qquad (5.1)$$

5.3.2 Failure Mode *C-P*

This case corresponds to the brittle failure due to crushing of concrete ($\varepsilon_o = \varepsilon_m = 0.0035$) at the maximum moment section, while the stresses in the embedded bars are lower than the steel yield ($f_s < f_y$), but the attached steel plate has yielded (i.e. $\varepsilon_p > \varepsilon_{py}$ and $f_p = f_{py}$) - see Figure 5.2. The final failure will happen suddenly, following the concrete crushing at the top surface of the beam.

In this mode, the composite beam has full bond capacity. It should be noted that this case is assumed not occur when the plate material is FRP, as, in such cases, the final failure is highly unlikely to simultaneously happen in both the concrete and the FRP plate.

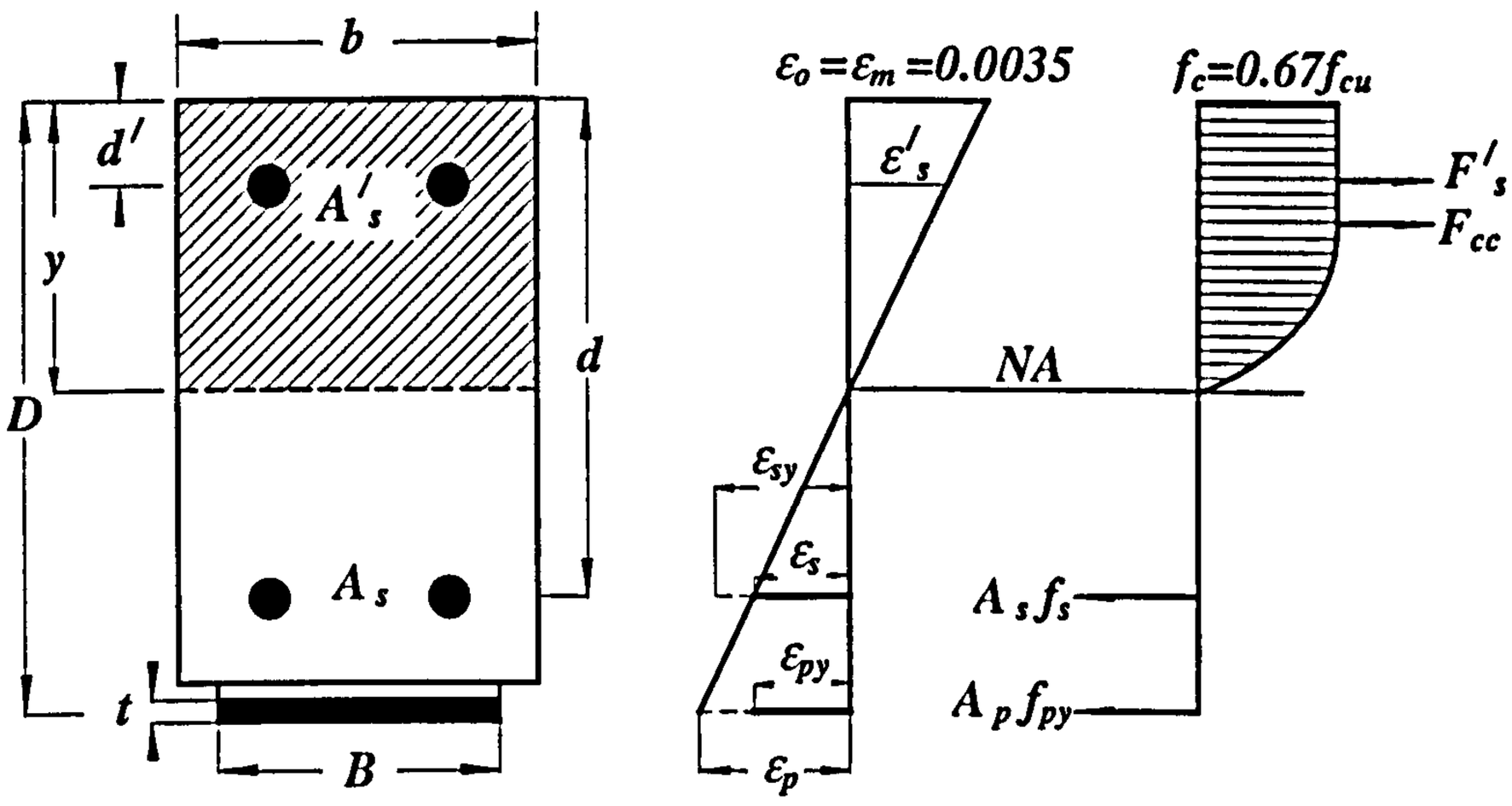

Fig. 5.2 Mode *C-P*: Section strains, stresses, and dimènsions.

The equilibrium equation for this mode may be derived following the same procedure as that used for the previous mode *C-* - (Equation (5.1)), with the only difference being that the tensile force acting on the external steel plate, F_p, will be

$$F_p = A_p f_{py}$$

Equation (5.1) may, then, be replaced by

$$A_s E_s \varepsilon_o \frac{d-y}{y} + A_p f_{py} = A_s' E_s \varepsilon_o \left(\frac{y-d'}{y} \right) + 0.67 f_{cu} y b \alpha_{f_{cu}} \qquad (5.2)$$

5.3.3 Failure Mode *CR-*

In this mode, ductile failure is due to crushing of concrete ($\varepsilon_o = \varepsilon_m = 0.0035$) at the maximum moment section subsequent to the bars yielding (i.e. $\varepsilon_s > \varepsilon_y$ and $f_s = f_y$), and the axial plate stress is lower than either the FRP ultimate strength or the steel yield strength ($f_p < f_{pu}$ or $f_p < f_y$) - see Figure 5.3.

The final failure will happen after large overall beam curvatures and deformations, associated with propagation of the cracks on the tension side, and subsequent crushing of concrete at the top surface of the beam. In this mode, the load bearing behaviour of the beam is classified as the full bond capacity, and this type of failure can occur in beams upgraded with either steel or FRP plates.

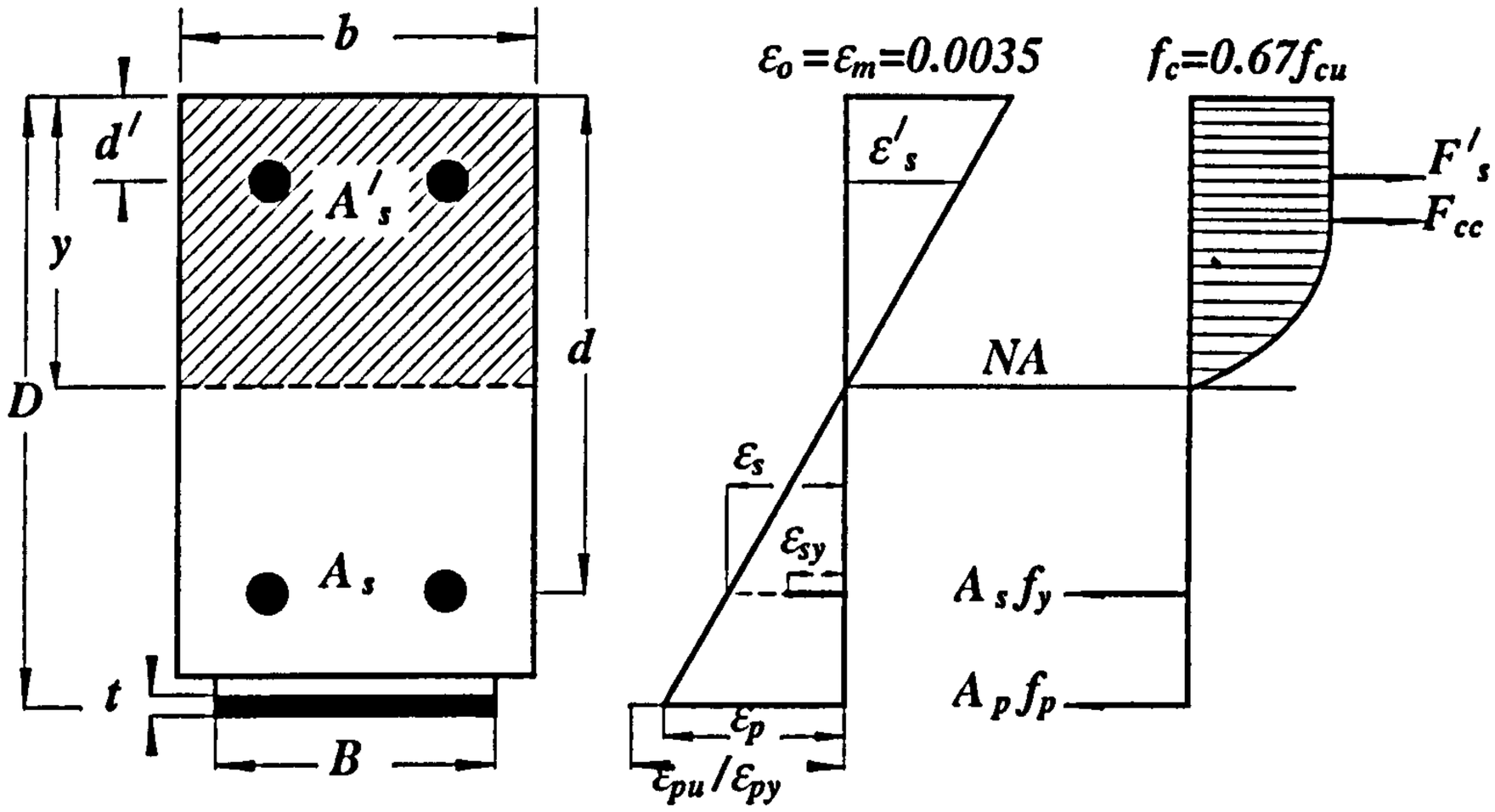

Fig. 5.3 Mode *CR-*: Section strains, stresses, and dimensions.

The equilibrium equation for this mode may be derived following the same procedure as that for the previous mode *C- -* (Equation 5.1), with the only difference being that the tensile force acting on the internal reinforcing bars, F_s, will, then, be

$$F_s = A_s . f_y$$

which leads to

$$A_s f_y + A_p E_p \varepsilon_o \frac{D-y}{y} = A'_s E_s \varepsilon_o \left(\frac{y-d'}{y} \right) + 0.67 f_{cu} y b \alpha_{f_{cu}} \qquad \textbf{(5.3)}$$

5.3.4 Failure Mode *CRP*

In this case of ductile failure, crushing of concrete ($\varepsilon_o = \varepsilon_m = 0.0035$) at the maximum moment section is associated with yielding of the embedded bars and the attached steel plate (i.e. $\varepsilon_s > \varepsilon_y$ and $f_s = f_y$) - see Figure 5.4.

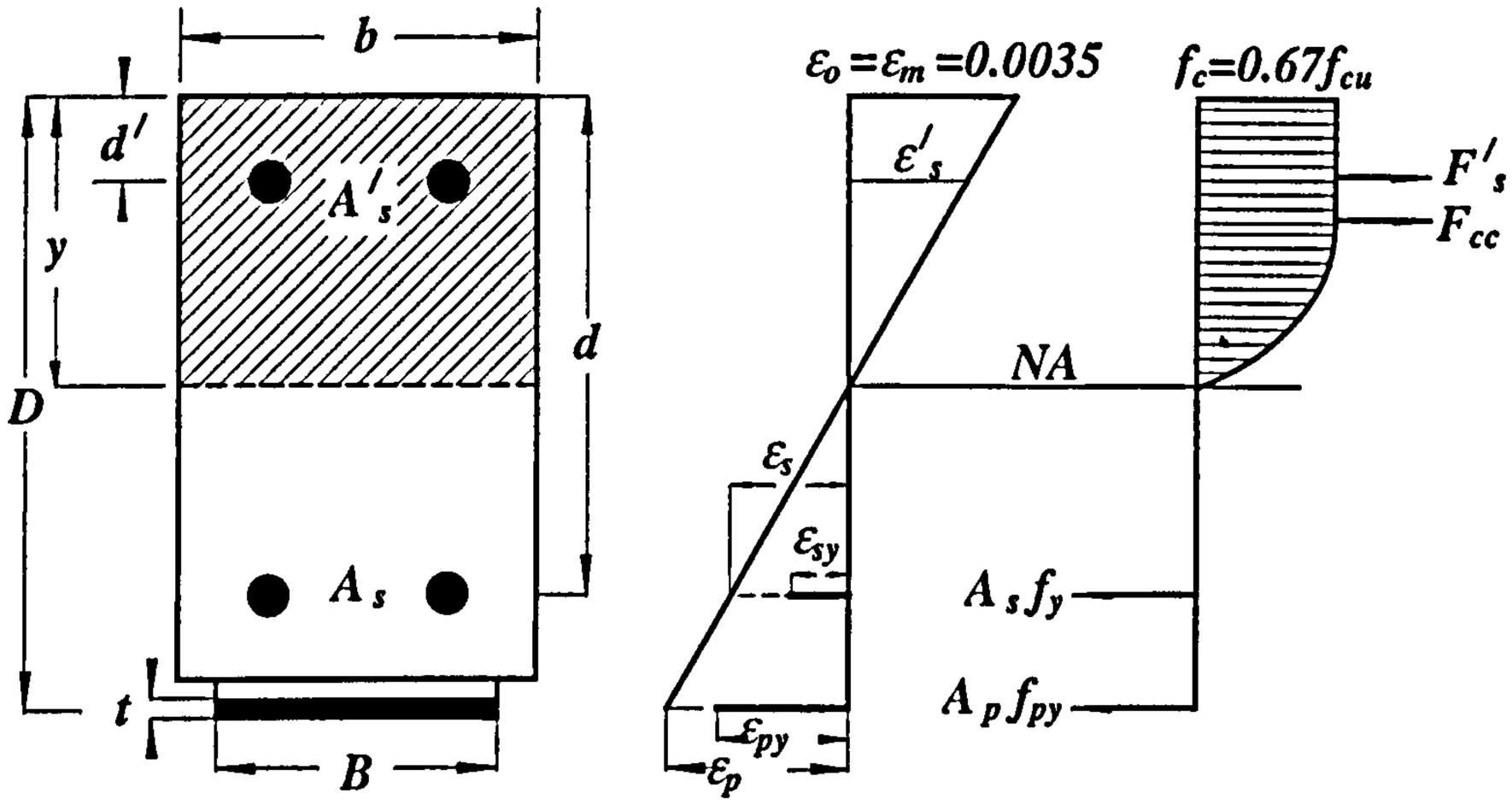

Fig. 5.4 Mode *CRP*: Section strains, stresses, and dimensions.

The final failure will happen with large overall changes in curvatures and deformations, with the propagation of the cracks within the tension side of the specimen (with the plate having yielded), and subsequent crushing of concrete at the top surface of the beam. In this mode, the beam load bearing capacity is classified as the full bond capacity with full utilisation of all the section materials. It should be noted that this case is highly unlikely to occur when FRP plates are used, as the failure is extremely improbable to simultaneously occur in both the concrete and the FRP plate.

The equilibrium equation for this mode may be derived following the same procedure as that used for the mode *C-* - (Equation 5.1), with the provision that, in this case, the value of tensile forces acting on the internal reinforcing bars, F_s, and the external steel plate, F_p, will be

$F_s = A_s.f_y$ and $F_p = A_p f_{py}$

which lead to Equation (5.1) being re-written as

$$A_s f_y + A_p f_{pu} = A_s' E_s \varepsilon_o \left(\frac{y - d'}{y} \right) + 0.67 f_{cu} y b \alpha_{f_{cu}} \qquad (5.4)$$

5.3.5 Failure Mode -*RP*

In this ductile mode of failure, the FRP plate ruptures (i.e. $\varepsilon_p = \varepsilon_{pu}$ and $f_p = f_{pu}$) within the maximum moment zone, while the internal bars have yielded (i.e. $\varepsilon_s > \varepsilon_y$ and $f_s = f_y$), but the maximum concrete strain is not large enough to cause crushing of concrete ($\varepsilon_o = \varepsilon_m = 0.0035$) - see Figure 5.5.

The final failure will happen following the development of large curvatures and deformations at the tension side of the beam, and after the rupture of FRP. In this mode, the load bearing capacity of the beam is classified as full bond capacity. It should, however, be noted that this mode of beam failure will not occur when ductile steel plates are used. Due to the concrete not crushing, there are two possible cases to be studied associated with the maximum concrete strain-stress distribution.

The first case relates to instances when the maximum concrete compressive stress is less than the crushing value ($=0.67 f_{cu}$) and the concrete stress distribution is of a

parabolic form (i.e. $\varepsilon_o \leq \beta$, where $\beta = 2.44 \times 10^{-4} \sqrt{f_{cu}}$), see Figure 5.5, (Case 1), using which the total compression force, F_c, may be expressed by the following equation (as derived in Appendix B (Equation (B.52))

$$F_c = A'_s E_s \varepsilon_p \left(\frac{y - d'}{D - y} \right) + \frac{bE_c}{2} \left(\frac{\varepsilon_p}{D - y} \right) y^2 + \frac{bK_1}{3} \left(\frac{\varepsilon_p}{D - y} \right)^2 y^3$$

where

$$K_1 = \frac{0.67 f_{cu} - E_c \beta}{\beta^2}$$

and, the tension forces are

$F_s = A_s f_y$ and $F_p = A_p f_{pu}$

By applying the force equilibrium condition

$F_c = F_t = F_s + F_p$, then

$$A_s f_y + A_p f_{pu} = A'_s E_s \varepsilon_p \left(\frac{y - d'}{D - y} \right) + \frac{bE_c}{2} \left(\frac{\varepsilon_p}{D - y} \right) y^2 + \frac{bK_1}{3} \left(\frac{\varepsilon_p}{D - y} \right)^2 y^3 \qquad \textbf{(5.5)}$$

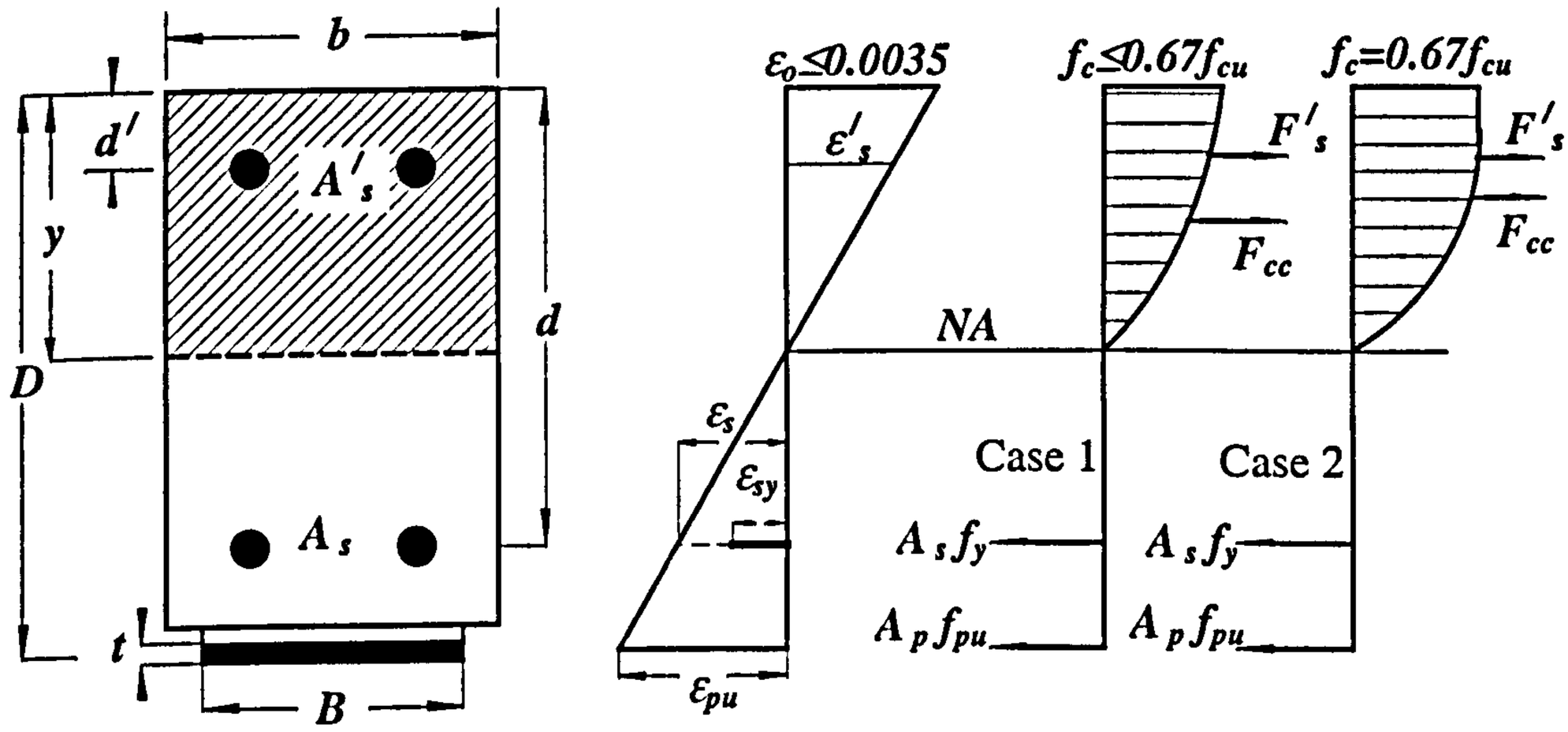

Fig. 5.5 Mode -*RP*: Section strains, stresses, and dimensions.

Relating the above equation to the axial strains in the embedded steel bars, ε_s, one gets

$$A_s f_y + A_p f_{pu} = A_s' E_s \varepsilon_s \left(\frac{y-d'}{d-y}\right) + \frac{bE_c}{2}\left(\frac{\varepsilon_s}{d-y}\right) y^2 + \frac{bK_1}{3}\left(\frac{\varepsilon_s}{d-y}\right)^2 y^3 \qquad (5.6)$$

The second case relates to instances when the maximum concrete compressive stress reaches the highest possible value ($=0.67 f_{cu}$), with the maximum concrete strain, ε_o, being higher than β but not large enough to cause crushing of concrete (i.e. $\beta \le \varepsilon_o < \varepsilon_m = 0.0035$). In this case, the compression stress distribution is a combination of parabolic and linear distributions as shown in the Figure 5.5 (Case 2): the total compression force, F_c, may, then, be expressed by Equation (B.54) as derived in Appendix B, - i.e.

$$F_c = A_s' E_s \varepsilon_p \left(\frac{y-d'}{D-y}\right) + 0.67 f_{cu} b \left(y + \frac{\beta}{\varepsilon_p} y - \frac{\beta}{\varepsilon_p} D \right) + \frac{bE_c}{2}\frac{\beta^2}{\varepsilon_p}(D-y) + \frac{bK_1}{3}\frac{\beta^3}{\varepsilon_p}(D-y)$$

and by applying the equilibrium condition $F_c = F_t = F_s + F_p$

where, $F_s = A_s f_y$, and $F_p = A_p f_{pu}$

one gets

$$A_s f_y + A_p f_{pu} = A_s' E_s \varepsilon_p \left(\frac{y-d'}{D-y}\right) + 0.67 f_{cu} b \left(y + \frac{\beta}{\varepsilon_p} y - \frac{\beta}{\varepsilon_p} D \right) + \frac{bE_c}{2}\frac{\beta^2}{\varepsilon_p}(D-y) + \frac{bK_1}{3}\frac{\beta^3}{\varepsilon_p}(D-y) \qquad (5.7)$$

By multiplying both sides by ε_p, Equation (5.7) may be re-written as

$$A_s f_y \varepsilon_p + A_p f_{pu} \varepsilon_p = A_s' E_s \varepsilon_p^2 \left(\frac{y-d'}{D-y}\right) + 0.67 f_{cu} b \left[y\,\varepsilon_p - \beta(D-y) \right] + \frac{bE_c}{2}\beta^2(D-y) + \frac{bK_1}{3}\beta^3(D-y) \qquad (5.8)$$

and, relating the above equation to the axial strains in the embedded bars, ε_s, one finally arrives at the following:

$$A_s f_y \varepsilon_s + A_p f_{pu} \varepsilon_s = A_s' E_s \varepsilon_s^2 \left(\frac{y - d'}{d - y} \right) + 0.67 f_{cu} b [y\varepsilon_s - \beta(d - y)] + \frac{bE_c}{2} \beta^2 (d - y) + \frac{bK_1}{3} \beta^3 (d - y) \quad \textbf{(5.9)}$$

5.3.6 Failure Mode - *-P*

This case relates to the brittle failure due to FRP plate rupture (i.e. $\varepsilon_p = \varepsilon_{pu}$ and $f_p = f_{pu}$) at the maximum moment zone, while the embedded steel bars have not yielded (i.e. $\varepsilon_s < \varepsilon_y$ and $f_s < f_y$), and the maximum concrete strain is not large enough to cause total crushing of concrete (i.e. $\varepsilon_o < \varepsilon_m = 0.0035$) - see Figure 5.6.

The final failure will happen suddenly, without any prior warning. In this mode, the load bearing capacity of the beam is classified as full bond capacity. It should, however, be noted that this mode will not occur when ductile steel plates are used. As in the previous mode of failure, there are two cases to be considered as regards the value of maximum concrete strain (or stress) distribution.

For both cases, the previously derived equations for the ***-RP*** mode may still be used with the provision that the axial force in the embedded bars, F_s, may, then, be expressed as

$$F_s = A_s E_s \varepsilon_s \text{ or } F_s = A_s E_s \varepsilon_p \left(\frac{d - y}{D - y} \right)$$

and, the equilibrium equation for Case 1 will be

$$A_s E_s \varepsilon_p (d-y)(D-y) + A_p f_{pu} (D-y)^2 = A'_s E_s \varepsilon_p \left(y - d'\right)(D-y) + \frac{bE_c}{2} \varepsilon_p (D-y) y^2 + \frac{bK_1}{3} \varepsilon_p^2 y^3 \quad \textbf{(5.10)}$$

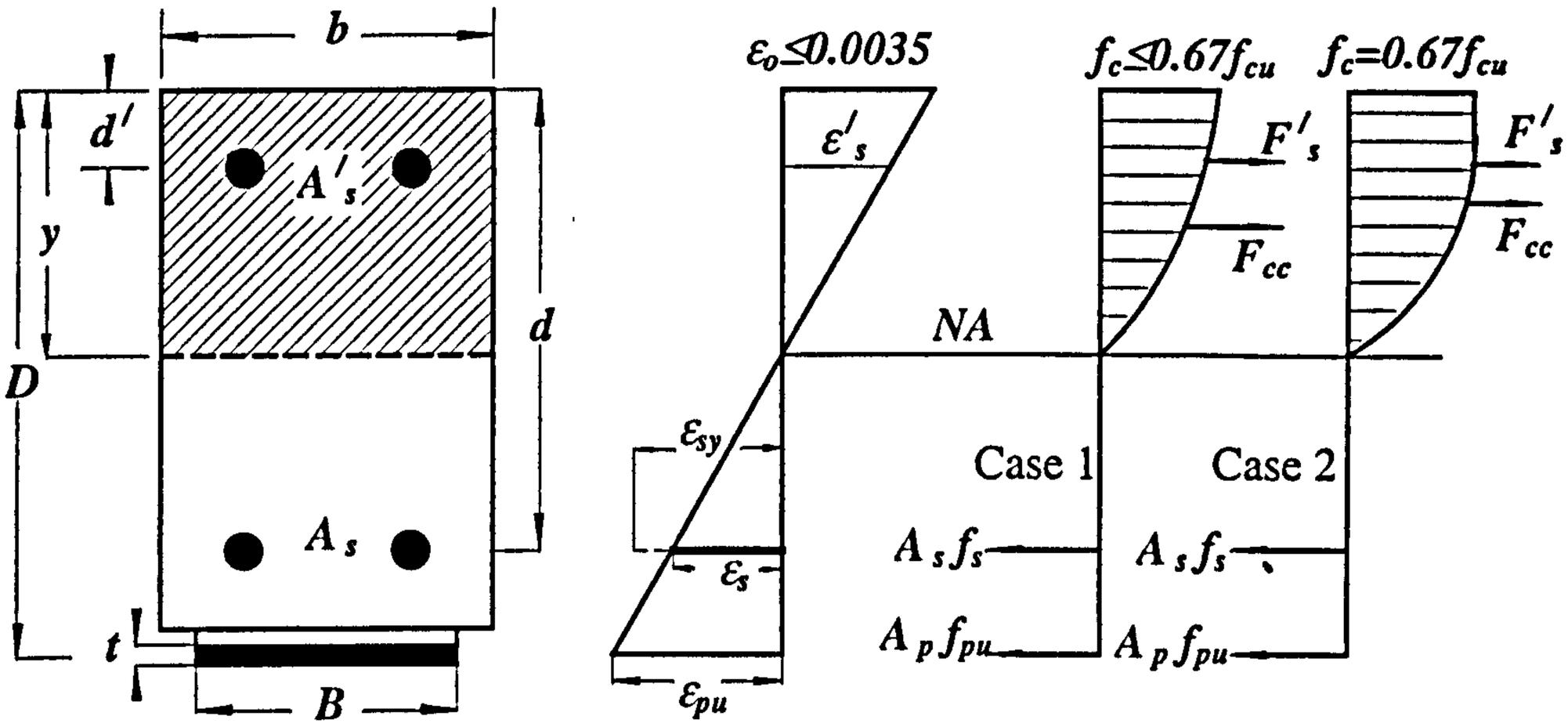

Fig. 5.6 Mode - -*P*: Section strains, stresses, and dimensions.

If one relates the above equation to the axial strains in the embedded bars, ε_s, one arrives at the following

$$A_s E_s \varepsilon_s (d-y)^2 + A_p f_{pu} (d-y)^2 = A'_s E_s \varepsilon_s \left(y - d'\right)(d-y) + \frac{bK_1}{3} \varepsilon_s^2 y^3 + \frac{bE_c}{2} \varepsilon_s (d-y) y^2 \quad \textbf{(5.11)}$$

Applying the same procedure as that adopted for Case 2, then, the equilibrium equation will be

$$A_s E_s \varepsilon_p^2 \frac{d-y}{D-y} + A_p f_{pu} \varepsilon_p = A'_s E_s \varepsilon_p^2 \left(\frac{y-d'}{D-y}\right) + 0.67 f_{cu} by \left[\varepsilon_p - \beta(D-y)\right] + \frac{bE_c}{2} \beta^2 (D-y) + \frac{bK_1}{3} \beta^3 (D-y) \quad \textbf{(5.12)}$$

or, in terms of the axial strains in the embedded steel bars:

$$A_s E_s \varepsilon_s^2 + A_p f_{pu} \varepsilon_s = A_s' E_s \varepsilon_s^2 \left(\frac{y - d'}{d - y} \right) + 0.67 f_{cu} b \left[y\varepsilon_s - \beta(d - y) \right] + \frac{bE_c}{2} \beta^2 (d - y) + \frac{bK_1}{3} \beta^3 (d - y) \quad \textbf{(5.13)}$$

5.3.7 Failure Mode -*R*-

This corresponds to a ductile mode of failure due to the concrete cover ripping off (i.e. plate peeling), where $f_p = \sigma_s$, associated with which the embedded bars are yielded (i.e. $\varepsilon_s > \varepsilon_y$ and $f_s > f_y$), but the maximum compressive strain in concrete is not large enough to lead to total crushing of concrete ($\varepsilon_o < 0.0035$) - see Figure 5.7. The final failure will happen subsequent to the development of large curvatures and deformations at the tension side of the beam, and after the plate with concrete cover have peeled off, as a unit, from underside of the beam. According to the stabilised crack formation theory, the critical plate peeling stress, σ_s, may vary by a factor of two. In this mode, the load bearing capacity of the beam is classified as partial bond capacity.

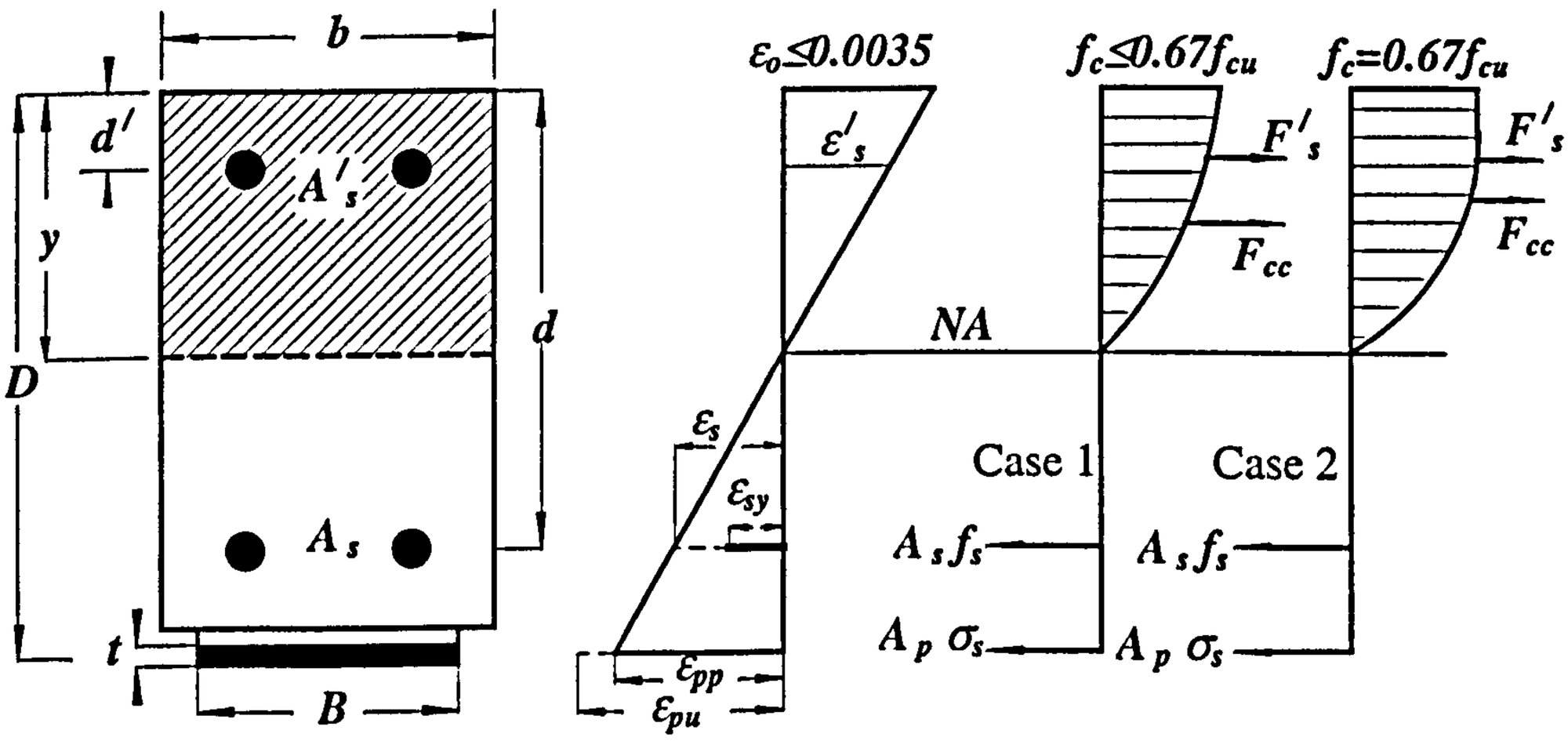

Fig. 5.7 Mode -*R*-: Section strains, stresses, and dimensions.

As the concrete will not be totally crushed, similar to the two previously discussed modes of failure, there are two possible cases for the maximum concrete strain-stress distribution to be studied. In both cases, the equilibrium equations already derived for the ***-RP*** mode may still be used with the provision that one should also consider the changes in tensile forces in the external plate, F_p, which will, then, be limited by the values of minimum or maximum axial plate peeling stress, σ_s - i.e.

$$F_p = A_p \sigma_s$$

This leads to the equilibrium equation for Case 1 to be

$$A_s.f_y(D-y)^2 + A_p.\sigma_s(D-y)^2 = A_s' E_s \varepsilon_p (y-d')(D-y) + \frac{bK_1}{3}\varepsilon_p^2 y^3 + \frac{bE_c}{2}\varepsilon_p (D-y)y^2 \qquad \textbf{(5.14)}$$

Relating the above equation to the axial strains in the embedded bars, ε_s, it may, then, be written as

$$A_s f_y (d-y)^2 + A_p \sigma_s (d-y)^2 = A_s' E_s \varepsilon_s \left(y-d'\right)(d-y) + \frac{bE_c}{2}\varepsilon_s (d-y)y^2 + \frac{bK_1}{3}\varepsilon_s^2 y^3 \qquad \textbf{(5.15)}$$

Following the same procedure as that for Case 2, the equilibrium equation will be

$$A_s f_y \varepsilon_p + A_p \sigma_s \varepsilon_p = A_s' E_s \varepsilon_p^2 \left(\frac{y-d'}{D-y}\right) + 0.67 f_{cu} b\left[y\varepsilon_p - \beta(D-y)\right] + \frac{bE_c}{2}\beta^2(D-y) + \frac{bK_1}{3}\beta^3(D-y) \qquad \textbf{(5.16)}$$

and, relating the above equation to the axial strains in the embedded bars, ε_s, one gets

$$A_s.f_y\varepsilon_s + A_p.\sigma_s\varepsilon_s = A_s' E_s \varepsilon_s^2 \frac{y-d'}{d-y} + 0.67 f_{cu} b\left[y\varepsilon_s - \beta(d-y)\right] + \frac{bE_c}{2}\beta^2(d-y) + \frac{bK_1}{3}\beta^3(d-y) \qquad \textbf{(5.17)}$$

5.3.8 Failure Mode - - -

In this mode of brittle failure due to the concrete cover ripping off (i.e. plate peeling), where $f_p = \sigma_s$, the bars have not yielded (i.e. $\varepsilon_s < \varepsilon_y$ and $f_s < f_y$), and the magnitude of maximum concrete strain is not large enough to make the concrete in compression undergo crushing ($\varepsilon_o < 0.0035$) - see Figure 5.8.

The failure will happen suddenly, with the concrete cover and plate peeling, as a unit, from the tensile side of the beam. According to the stabilised crack formation theory, the critical plate peeling stress, σ_s, can vary by a factor of two. In this mode, the load bearing capacity of the beam is classified as partial bond capacity.

As the concrete will not be totally crushed, similar to the two previously discussed modes of failure, there exists two possible cases for the distributions of maximum concrete strains (or stresses) to be studied.

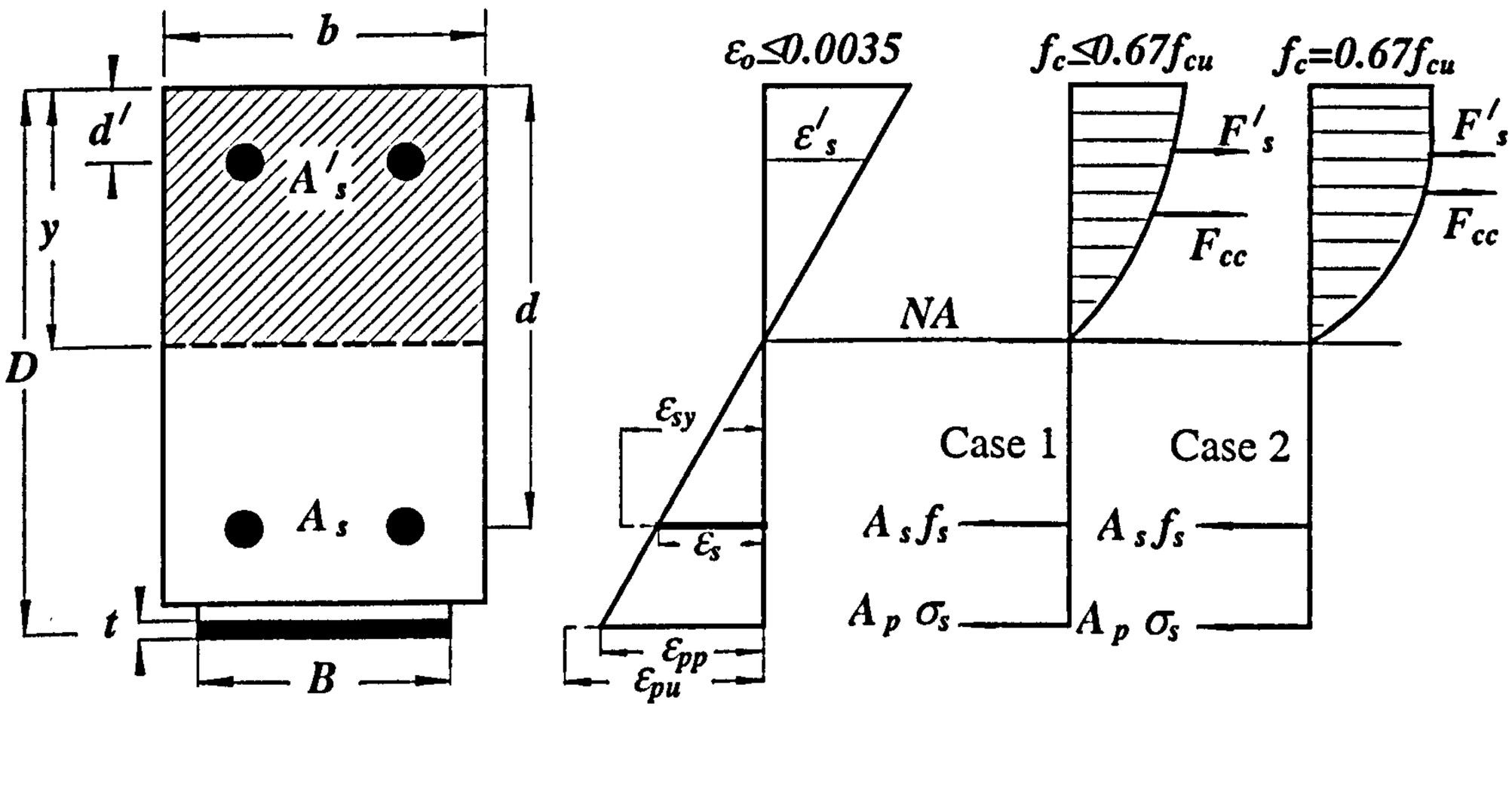

Fig. 5.8 Mode - - -: Section strains, stresses, and dimensions.

For both cases, the equilibrium equations derived for the ***-RP*** mode may still be used with the provision that changes in the axial force of the external plate, F_p, will be limited by the minimum or the maximum values of axial plate peeling stress, σ_s, and the tensile force in the embedded steel bars, f_s, will not reach the yield point - i.e.

$$F_p = A_p\sigma_s \text{ and } F_s = A_sE_s\varepsilon_s \text{ or } F_s = A_s.E_s\varepsilon_p\left(\frac{d-y}{D-y}\right)$$

which leads to the equilibrium equation for Case 1

$$A_s.E_s\varepsilon_p(d-y)(D-y)+A_p.\sigma_s(D-y)^2 = A_s'E_s\varepsilon_p(y-d')(D-y)+ \frac{bE_c}{2}\varepsilon_p(D-y)y^2+\frac{bK_1}{3}\varepsilon_p^2y^3 \quad \textbf{(5.18)}$$

If one relates the above equation to the axial strains in the embedded bars, ε_s, it may be re-written as

$$A_sE_s\varepsilon_s(d-y)^2+A_p\,\sigma_s(d-y)^2 = A_s'E_s\,\varepsilon_s\left(y-d'\right)(d-y)+\frac{bE_c}{2}\varepsilon_s(d-y)y^2+ \frac{bK_1}{3}\varepsilon_s^2y^3 \quad \textbf{(5.19)}$$

Applying the same procedure as that for the Case 2, then, the equilibrium equation will be

$$A_sE_s\varepsilon_p^2\left(\frac{d-y}{D-y}\right)+A_p\,\sigma_s\,\varepsilon_p = A_s'E_s\,\varepsilon_p^2\left(\frac{y-d'}{D-y}\right)+0.67f_{cu}b\left[y\varepsilon_p-\beta(D-y)\right]+ \frac{bE_c}{2}\beta^2(D-y)+\frac{bK_1}{3}\beta^3(D-y) \quad \textbf{(5.20)}$$

or, once it is expressed in terms of the embedded steel bar strains:

$$A_sE_s\varepsilon_s^2+A_p\,\sigma_s\,\varepsilon_s = A_s'E_s\,\varepsilon_s^2\left(\frac{y-d'}{d-y}\right)+0.67f_{cu}b\left[y\varepsilon_s-\beta(d-y)\right]+ \frac{bE_c}{2}\beta^2(d-y)+\frac{bK_1}{3}\beta^3(d-y) \quad \textbf{(5.21)}$$

5.4 CONCLUSIONS

The equilibrium and compatibility equations for all the eight possible modes of failure associated with steel/FRP plated beams have been developed. These will be used in the next chapter for formulating solutions for the theoretical predictions of the various characteristics of all the possible modes of failure as a function of changes in the magnitude of the modulus of elasticity for FRP plates (within current manufacturing limits).

Chapter 6

EFFECT OF THE MODULUS OF ELASTICITY FOR THE FRP PLATE ON THE PLATED BEAM FLEXURAL LOAD CAPACITIES AND MODES OF FAILURE

Chapter 6

EFFECT OF THE MODULUS OF ELASTICITY FOR THE FRP PLATE ON THE PLATED BEAM FLEXURAL LOAD CAPACITIES AND MODES OF FAILURE

6.1 GENERAL

The purpose of this chapter is to present a study which explains the effect of variations in the magnitude of the modulus of elasticity, E_p, for the external FRP plate bonded to reinforced concrete beams, on the modes of failure for the composite beam with a detailed account of section stress and strain distributions, plus the resulting beam flexural load capacities.

Only the two types of failure modes (i.e. CRP and $C-P$ - as described in Chapter 5) which are only relevant to cases when steel plates are used, will not be considered here. The reason being that, unlike the FRP materials which are currently available with a wide range of moduli of elasticity, the steel materials used for plating generally possess a very narrow range of elastic moduli: this suggests that there is no need to extend the study to those modes of failure which exclusively occur in connection with steel as the plating material.

In what follows, it is assumed that the unplated beams are all under-reinforced. The failure mode for such unplated beams is, therefore, assumed to be ductile, and that the ratio of the area of embedded steel bars to the effective concrete area allows the bars to reach yield, prior to the final failure occurring by crushing of concrete.

6.2 EFFECT OF THE PLATE MODULUS OF ELASTICITY ON THE BEHAVIOUR OF PLATED BEAM

In the following sections, the influence of variations in the plate modulus of elasticity on the plated beam behaviour will be discussed individually for each of the related six modes of failure.

For the sake of simplification, with no significant loss of accuracy, the derivations in this chapter ignore the resistance of concrete in tension. The practical implications of this simplifying assumption will, however, be discussed at the end of this chapter (section 6.2.5), and it will be shown that this is a practically reasonable assumption.

6.2.1 Failure Mode CR-

In this full bond and ductile mode of failure, the equilibrium equation for section forces (Equation (5.3)), as derived in Chapter 5, will be used to investigate the effect of varying the magnitude of plate modulus of elasticity, where

$$A_s f_y + A_p E_p \varepsilon_o \left(\frac{D-y}{y} \right) = A_s' E_s \varepsilon_o \left(\frac{y-d'}{y} \right) + 0.67 f_{cu}\, yb\alpha_{f_{cu}} \qquad \textbf{(6.1)}$$

and

$$\alpha_{f\,cu} = \left[1 + \frac{\beta}{\varepsilon_o} \left(\frac{E_c \beta}{6 \times 0.67 f_{cu}} - \frac{2}{3} \right) \right],$$

It should be noted that, by definition, $\alpha_{f\,cu}$ is a fraction of the depth of the neutral axis and, hence, $0 < \alpha_{f\,cu} < 1$ (i.e. a positive value).

Multiplying by y one gets

$$A_s f_y y + A_p E_p \varepsilon_o (D - y) = A'_s E_s \varepsilon_o (y - d') + 0.67 f_{cu} y^2 b \alpha_{f_{cu}}$$

by differentiating with respect to E_p, then,

$$A_s f_y \frac{dy}{dE_p} + A_p \varepsilon_o (D - y) - A_p \varepsilon_o E_p \frac{dy}{dE_p} = A'_s E_s \varepsilon_o \frac{dy}{dE_p} + 2 \times 0.67 f_{cu} yb \alpha_{f_{cu}} \frac{dy}{dE_p} \quad (6.2)$$

$$\frac{dy}{dE_p}\left(A'_s E_s \varepsilon_o + 2 \times 0.67 f_{cu} yb \alpha_{f_{cu}} + A_p \varepsilon_o E_p - A_s f_y\right) = A_p \varepsilon_o (D - y) \quad (6.3)$$

but from Equation (6.1), one gets

$$A_s f_y = A'_s E_s \varepsilon_o \left(\frac{y - d'}{y}\right) + 0.67 f_{cu} yb \alpha_{f_{cu}} - A_p E_p \varepsilon_o \left(\frac{D - y}{y}\right)$$

Equation (6.3) will, then, be

$$\frac{dy}{dE_p}\left(A'_s E_s \varepsilon_o \frac{d'}{y} + 0.67 f_{cu} yb \alpha_{f_{cu}} + A_p \varepsilon_o E_p \frac{D}{y}\right) = A_p \varepsilon_o (D - y)$$

which may be rearranged in the following form

$$\frac{dy}{dE_p} = \frac{A_p \varepsilon_o (D - y)}{\left(A'_s E_s \varepsilon_o \frac{d'}{y} + 0.67 f_{cu} yb \alpha_{f_{cu}} + A_p \varepsilon_o E_p \frac{D}{y}\right)} = \frac{+ve}{+ve} \quad (6.4)$$

The above equation shows that positive (i.e. increasing) changes in the magnitude of plate modulus of elasticity, E_p, are accompanied by corresponding positive changes (i.e. increases) in the depth of neutral axis, y.

It has already been proven in Appendix B that, for a beam section with concrete in the crushing state, the total compression force will increase in magnitude by increases in the depth of neutral axis. This, in turn, leads to the total tension force on the beam section to be increased, to balance the compression force for equilibrium. Bearing in mind that the reinforcing steel bars in this mode of failure are in a state of yield and can not carry any more axial loads, one expects that such increases in the total tension

force will be carried by the externally bonded plate and, hence, the axial stresses in the FRP plate will be increased.

Since the maximum concrete strain in this mode (i.e. $CR-$) corresponds to the concrete crushing strain (i.e. it remains unchanged with any changes in the depth of neutral axis), it is, therefore, expected that increasing the depth of neutral axis from y_1 to y_2 will reduce the plate tensile strain from ε_{p1} to ε_{p2} - see Figure 6.1.

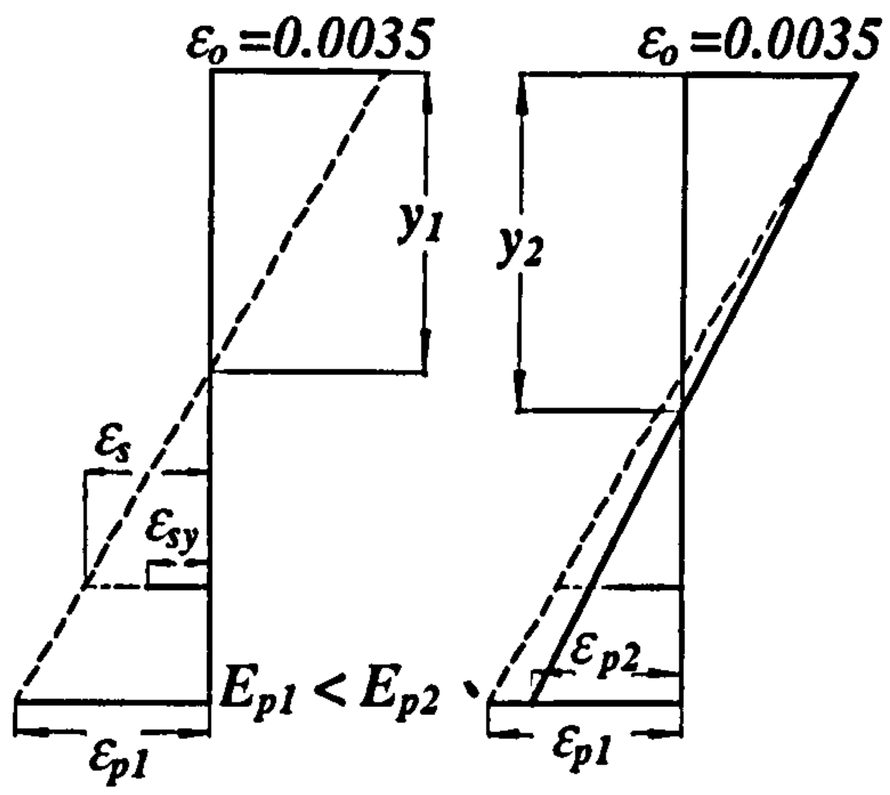

Fig. 6.1 Effect of increasing E_p on the section strains for the failure mode $CR-$.

From the above argument, it is clear that, despite the reductions in the plate tensile strain (with associated increases in the depth of neutral axis); the magnitude of tensile stress in the FRP plate will increase.

From Equation (6.5), which relates the plate axial stresses and strains to the modulus of elasticity, it may be concluded that the reason for increases in the plate tensile stress is due to the increases in the value of plate modulus of elasticity, which seems to have a greater influence than the corresponding effect due to reductions in the plate tensile strain:

$$\sigma_p = \varepsilon_p E_p \qquad (6.5)$$

Provided that the unplated section is under-reinforced, this mode of failure is the initial (i.e. primary) one, and is expected to happen at very low values of the plate modulus of elasticity. To prove this, let us assume an unplated section that fails by crushing of concrete after the internal reinforcing bars have yielded (i.e. ***CR*** mode). If the externally bonded FRP plate has a modulus of elasticity with an extremely low value (i.e. $E_p \cong 0$), then, the plate tensile stress, σ_p, and force, F_p, will be negligible in magnitude no matter what the value of the axial plate strain is (Equation (6.5)). In such cases, the changes in the magnitude of the total forces acting on the original unplated section will be minor, and the mode of failure will be the ***CR*** – one as the plate is not experiencing its ultimate stress and the concrete is in a crushing state with the embedded bars experiencing yielding.

From Appendix B (Equation (B.48)), the moment (due to the compression forces) about the neutral axis is

$$M_c = A'_s E_s \varepsilon_o \left(1 - \frac{d'}{y}\right)^2 y + \left[\frac{0.67 f_{cu}}{2} + \left(\frac{\beta}{\varepsilon_o}\right)^2 \left(\frac{E_c \beta}{12} - \frac{0.67 f_{cu}}{4}\right)\right] b y^2$$

and the beam's total flexural capacity, ***M***, will, then, be

$$M = A'_s E_s \varepsilon_o \left[y - 2d' + \frac{(d')^2}{y}\right] + \left[\frac{0.67 f_{cu}}{2} + \left(\frac{\beta^2}{\varepsilon_o}\right)\left(\frac{E_c \beta}{12} - \frac{0.67 f_{cu}}{4}\right)\right] b y^2 +$$

$$A_s f_y (d - y) + A_p E_p \varepsilon_o \frac{(D - y)^2}{y}$$

Differentiate the above equation with respect to E_p to determine the effect of increasing the plate modulus of elasticity on the beam's flexural load capacity

$$\frac{dM}{dE_p} = \frac{\partial M}{\partial y}\frac{\partial y}{\partial E_p}$$

where,

$$\frac{\partial y}{\partial E_p} = \frac{A_p \varepsilon_o (D-y)}{\left[A'_s E_s \varepsilon_o \left(\frac{d'}{y}\right) + 0.67 f_{cu} yb\alpha_{f_{cu}} + A_p \varepsilon_o E_p \left(\frac{D}{y}\right)\right]} = \frac{+ve}{+ve}$$

and

$$\frac{\partial M}{\partial y} = A'_s E_s \varepsilon_o \left[1 - \left(\frac{d'}{y}\right)^2\right] + \left[\frac{0.67 f_{cu}}{2} + \left(\frac{\beta^2}{\varepsilon_o}\right)\left(\frac{E_c \beta}{12} - \frac{0.67 f_{cu}}{4}\right)\right] 2by -$$

$$A_s f_y - A_p E_p \varepsilon_o \frac{2y(D-y) + (D-y)^2}{y^2}$$

For simplicity, use the recommended values by the BS8110 (1985) and BS5400 (1990) for β and E_c to get

$$\frac{\partial M}{\partial y} = A'_s E_s \varepsilon_o \left(1 - \frac{d'}{y}\right)\left(1 + \frac{d'}{y}\right) + 0.67 f_{cu} by \left[1 - \frac{1}{6}\left(\frac{\beta^2}{\varepsilon_o}\right)\right] -$$

$$A_s f_y - A_p E_p \varepsilon_o \left(\frac{D-y}{y}\right)\left(1 + \frac{D}{y}\right)$$

but Equation (6.1) may be rewritten as

$$A_s f_y + A_p E_p \varepsilon_o \left(\frac{D-y}{y}\right) = 0.67 f_{cu} yb \left[1 + \left(\frac{\beta}{\varepsilon_o}\right)\left(\frac{E_C \beta}{6 \times 0.67 f_{cu}} - \frac{2}{3}\right)\right] +$$

$$A'_s E_s \varepsilon_o \left(\frac{y - d'}{y}\right)$$

$$F_s + F_p = F'_s + 0.67 f_{cu} yb + 0.67 f_{cu} yb \left(\frac{\beta}{\varepsilon_o}\right)\left(\frac{E_c \beta}{4}\right) - \frac{2}{3} 0.67 f_{cu} yb \left(\frac{\beta}{\varepsilon_o}\right)$$

$$= F'_s + 0.67 f_{cu} yb + yb \left(\frac{\beta}{\varepsilon_o}\right)\left(\frac{E_c \beta}{6}\right) - \frac{2}{3} 0.67 f_{cu} yb \left(\frac{\beta}{\varepsilon_o}\right)$$

$$F_s + F_p - F'_s = 0.67 f_{cu} yb + yb \left(\frac{\beta}{\varepsilon_o}\right)\left(\frac{E_c \beta}{6} - \frac{2}{3} 0.67 f_{cu}\right)$$

$$= 0.67 f_{cu} yb + yb \left(\frac{\beta}{\varepsilon_o}\right)\left(\frac{0.67 f_{cu}}{3} - \frac{2x\, 0.67 f_{cu}}{3}\right)$$

$$= 0.67 f_{cu} yb \left(1 - \frac{\beta}{3\varepsilon_o}\right)$$

then

$$\frac{\partial M}{\partial y} = F_s'\left(1+\frac{d'}{y}\right)+0.67 f_{cu} by\left[1-\frac{1}{6}\left(\frac{\beta}{\varepsilon_o}\right)^2\right]-F_s-F_p\left(1+\frac{D}{y}\right)$$

$$= -\left(F_s+F_p-F_s'\right)+0.67 f_{cu} by\left[1-\frac{1}{6}\left(\frac{\beta}{\varepsilon_o}\right)^2\right]+\left(F_s'\frac{d'}{y}-F_p\frac{D}{y}\right)$$

$$= -0.67 f_{cu}\, yb\left(1-\frac{\beta}{3\varepsilon_o}\right)+0.67 f_{cu} by\left[1-\frac{1}{6}\left(\frac{\beta}{\varepsilon_o}\right)^2\right]+\left(F_s'\frac{d'}{y}-F_p\frac{D}{y}\right)$$

$$= 0.67 f_{cu}\, yb\frac{\beta}{3\varepsilon_o}\left(1-\frac{\beta}{2\varepsilon_o}\right)+\left(F_s'\frac{d'}{y}-F_p\frac{D}{y}\right)$$

$$\frac{dM}{dE_p} = \frac{\left[0.67 f_{cu}\, yb\frac{\beta}{3\varepsilon_o}\left(1-\frac{\beta}{2\varepsilon_o}\right)+\left(F_s'\frac{d'}{y}-F_p\frac{D}{y}\right)\right]A_p\varepsilon_o(D-y)}{\left(A_s' E_s\varepsilon_o\frac{d'}{y}+0.67 f_{cu}\, yb\alpha_{f_{cu}}+A_p\varepsilon_o E_p\frac{D}{y}\right)} \quad .$$

If one considers the values recommended by BS5400 (1990) for β and ε_o, the magnitude of the term $\left(1-\beta/2\varepsilon_o\right)$, in the above equation, is positive as long as the compressive strength of concrete is less than *820 kN/mm*^{2}, which is an extremely high concrete strength for general (practical) cases. The above equation may be re-written as follows

$$\frac{dM}{dE_p} = \frac{\left[0.67 f_{cu}\, yb\frac{\beta}{3\varepsilon_o}\left(1-\frac{\beta}{2\varepsilon_o}\right)+A_s' E_s\varepsilon_o\left(\frac{y-d'}{y}\right)\left(\frac{d'}{y}\right)-A_p E_p\varepsilon_o\left(\frac{D-y}{y}\right)\left(\frac{D}{y}\right)\right]A_p\varepsilon_o(D-y)}{\left(A_s' E_s\varepsilon_o\frac{d'}{y}+0.67 f_{cu}\, yb\alpha_{f_{cu}}+A_p\varepsilon_o E_p\frac{D}{y}\right)} \qquad \textbf{(6.6)}$$

Noting that this mode must be the primary mode associated with relatively low values of the plate modulus of elasticity, it is clear from the above Equation (6.6) that its outcome will be positive (as $E_p \cong 0$), meaning that the beam's flexural load capacity increases with increasing values of the plate modulus of elasticity. The remaining

point to clarify, then, is to find out as to what would happen if the value of E_p is not very small. To answer this question, re-write Equation (6.6) in the following form

$$\frac{dM}{dE_p} = \frac{\left[0.67 f_{cu}\, yb \frac{\beta}{3\varepsilon_o}\left(1-\frac{\beta}{2\varepsilon_o}\right) + A'_s E_s \varepsilon_o \left(\frac{y-d'}{y}\right)\left(\frac{d'}{y}\right) - Q\right] A_p \varepsilon_o (D-y)}{\left(A'_s E_s \varepsilon_o \frac{d'}{y} + 0.67 f_{cu}\, yb\alpha_{f_{cu}} + A_p \varepsilon_o E_p \frac{D}{y}\right)} \qquad (6.7)$$

where

$$Q = A_p E_p \varepsilon_o \left(\frac{D-y}{y}\right)\left(\frac{D}{y}\right)$$

By carefully checking all the parameters in the above equation, with increasing values of E_p (and, hence, with increasing associated values of y), the rate of change in M is found to be positive with positive changes in E_p, provided only that the term Q is reduced with such positive changes (i.e. increases) in E_p. By differentiating the term Q with respect to E_p, one arrives at the following:

$$\frac{dQ}{dE_p} = \frac{\partial Q}{\partial y}\frac{\partial y}{\partial E_p}$$

$$= A_p E_p \varepsilon_o D \frac{-y^2 - 2y(D-y)}{y^4} \frac{A_p \varepsilon_o (D-y)}{\left(A'_s E_s \varepsilon_o \frac{d'}{y} + 0.67 f_{cu}\, yb\alpha_{f_{cu}} + A_p \varepsilon_o E_p \frac{D}{y}\right)}$$

$$= \frac{E_p A_p^2 \varepsilon_o^2 (D-y)(y-2D)D}{y^3\left(A'_s E_s \varepsilon_o \frac{d'}{y} + 0.67 f_{cu}\, yb\alpha_{f_{cu}} + A_p \varepsilon_o E_p \frac{D}{y}\right)} = \frac{-ve}{+ve}$$

From the above, it is clear that the term Q in Equation (6.7) is reduced with increasing values of E_p, which suggests that the final result for the Equation (6.7) will always be positive: although the rate of increase may be reduced with increasing values of E_p, it will never become negative.

The preceding arguments suggest that the beam's flexural load capacity increases with any increases in the magnitude of plate modulus of elasticity as long as the failure mode remains to be $CR-$.

Unfortunately, in view of the complicated nature of the problem, the general trend for the flexural load capacity of a plated beam associated with the other modes of failure may not be determined in a formal mathematical way. In these circumstances, therefore, the effect of increases in the plate modulus of elasticity on changes in the flexural load capacity of plated beams, will be investigated through numerical studies on a wide range of beam configurations. Such studies will be presented at the end of the present chapter (section 6.4). Following such an approach for $CR-$ mode, for example, (though it has already been proven mathematically), it has been found that for all the cases studied, the beam's flexural load capacity increases with increasing values of the plate modulus of elasticity as long as this mode of failure is operative, hence, confirming the validity of the above mathematical derivations - see section 6.4 for the numerical results.

By increasing the value of E_p, the depth of neutral axis (NA), and the tensile stress in the plate both increase, while the tensile strains in the plate and the embedded bars decrease. Theoretically, the successor to this mode will either be the brittle mode $C--$ (if the reduction of the tensile strains in the embedded bars is sufficient to result for the bars to become unyielded), or the ductile modes $-RP$ or $-R-$ will take over (if the plate tensile stress is sufficiently increased in magnitude to first reach the ultimate strength or the peeling stress): there are many factors which may influence the behaviour of the section and determine as to which mode will be the one

to follow the primary mode $CR-$. Chapter 7 presents the appropriate methods, for determining the critical values of E_p at which the primary mode $CR-$ is changed to the successor mode, by calculating the critical values of E_p for initiating the successor modes (i.e. modes $C--$, $-RP$ & $-R-$), with the minimum of them corresponding to the maximum possible values of E_p for the primary mode $CR-$ to remain operative.

The increases in both the total compression and tension forces will increase the overall flexural moment of the beam about the neutral axis and, hence, the flexural load capacity of the beam will be increased: this is applicable to both the predicted values of absolute maximum moment, M_{max}, and also the plated moment, M_{pltd}. (M_{max} and M_{pltd} are defined in Appendix A).

It may, thus, be concluded that by increasing the modulus of elasticity for the plate, relating to a beam that fails in the ductile mode $CR-$, the following will apply:

1- an increase in the depth of neutral axis,

2- an increase in the compression forces in the concrete and the embedded compression bars,

3- an increase in the plate tensile stress and axial force with reductions in the plate tensile strain, without any changes occurring in the magnitude of axial forces in the yielded bars though their associated tensile strains will be reduced, and

4- an increase in flexural load capacities (i.e. $M_{max.}$ & M_{pltd}) of the composite beam.

This mode is the preferred one in practice, because it is ductile in nature with the material strengths for both the concrete and the internal steel bars in tension being fully utilised, although the FRP plate will not be fully stressed (i.e. to its ultimate strength). As mentioned in Chapter 5, both the FRP plate and the concrete may not be fully stressed at the same time (i.e. the mode ***CRP*** is highly unlikely to happen in practice when FRP plates are used) as both the concrete and the plate material are brittle, and the one (i.e. either concrete or FRP plate) which reaches the failure point first, will be the controlling factor for the occurrence of failure.

6.2.2 Failure Mode C- -

For this full bond brittle mode of failure, the equilibrium Equation (5.1), as derived in Chapter 5, will be used to investigate the effect of changing the plate modulus of elasticity:

$$A_s E_s \varepsilon_o \left(\frac{d-y}{y}\right) + A_p E_p \varepsilon_o \left(\frac{D-y}{y}\right) = A_s' E_s \varepsilon_o \left(\frac{y-d'}{y}\right) + 0.67 f_{cu}\, yb\alpha_{f_{cu}}$$

multiply the above equation by y to get

$$A_s E_s \varepsilon \left({}_o d - y\right) + A_p E_p \varepsilon_o (D-y) = \Lambda_s' E_s \varepsilon_o \left(y-d'\right) + 0.67 f_{cu}\, y^2 b\alpha_{f_{cu}}$$

differentiating with respect to E_p

$$-A_s E_s \varepsilon_o \frac{dy}{dE_p} + A_p \varepsilon_o (D-y) - A_p \varepsilon_o E_p \frac{dy}{dE_p} = A_s' E_s \varepsilon_o \frac{dy}{dE_p} + 2\times 0.67 f_{cu}\, yb\alpha_{f_{cu}} \frac{dy}{dE_p} \quad \textbf{(6.8)}$$

then

$$\frac{dy}{dE_p}\left(A_s' E_s \varepsilon_o + 2\times 0.67 f_{cu}\, yb\alpha_{f_{cu}} + A_s\, \varepsilon_o E_s + A_p \varepsilon_o E_p\right) = A_p \varepsilon_o (D-y)$$

which may be re-arranged as

$$\frac{dy}{dE_p} = \frac{A_p \varepsilon_o (D-y)}{\left(A'_s E_s \varepsilon_o + 2\times 0.67 f_{cu}\, yb\alpha_{f_{cu}} + A_s \varepsilon_o E_s + A_p \varepsilon_o E_p\right)} = \frac{+ve}{+ve}$$

The above equation shows that, for this brittle mode of failure, increasing the plate modulus of elasticity, E_p, will lead to increases in the depth of neutral axis y. As shown in Figure 6.2, increasing the depth of neutral axis, y, will reduce both the tensile strains in the embedded bars and the plate.

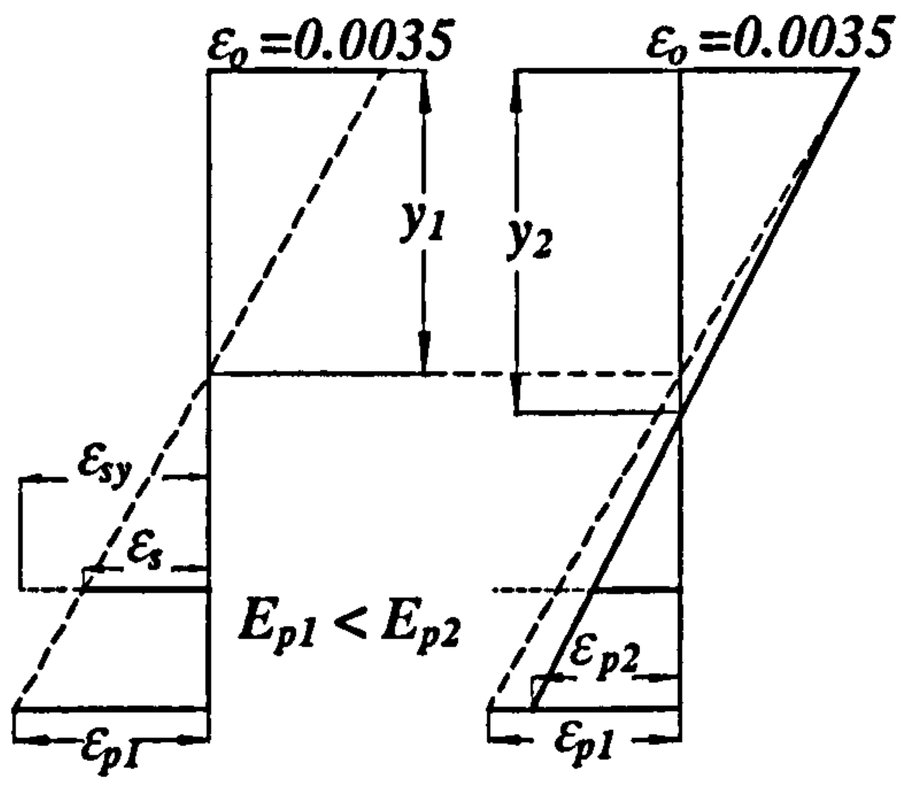

Fig. 6.2 Effect of increasing E_p on the section strains for the failure mode $C--$.

Since the embedded steel bars are assumed not to have yielded, then, any reductions in the tensile strains in the embedded bars lead to associated reductions in the magnitudes of axial stresses in the bars and, hence, the magnitudes of axial forces carried by them.

As previously proven in Appendix B (for a section with concrete in the crushing state), the total magnitude of compression force will increase as a result of increases in the depth of neutral axis. This, then, leads to the total tension force to be increased, in order to balance the forces acting on the section.

Considering the above, the tensile forces in the embedded bars will be reduced with the associated increases in the value of plate modulus of elasticity, and one expects that the resultant increase in the total tension force will, then, be carried only by the externally bonded plate: the tensile stress in the plate is, therefore, expected to be increased.

The increases in the magnitude of the plate tensile stress is accompanied with reductions in the magnitudes of plate tensile strains as increases in the values of plate modulus of elasticity take place - see Equation (6.5)

As demonstrated by the results of numerical studies on beam *N*, in Figure 6.69, (to be presented at the end of the present chapter in section 6.4), the simultaneous increases in both the total tension and compression forces lead to increases in the flexural load capacity of the composite beam.

It may, therefore, be concluded that by increasing the magnitudes of plate modulus of elasticity for a composite beam that fails in the brittle mode $C--$, the following hold true:

1- an increase in the depth of neutral axis,

2- an increase in the magnitudes of compression forces in the concrete and the embedded bars,

3- an increase in the plate tensile stress and, hence, its axial force, with an associated reduction in the plate's axial strain, and tensile strains and stresses in the embedded bars, and

4- an increase in flexural moment capacities (i.e. M_{max} & M_{plid}) of the composite beam.

It should be noted that, despite the increases in the load bearing capacity of the composite beam associated with increasing values of E_p, this mode of failure is a brittle one as the concrete is suddenly crushed in the absence of yielding of the embedded bars. In view of its brittle nature, this mode is not a preferred one in practice, despite the fact that its associated flexural load capacity increases with increases in the value of the modulus of elasticity for the plate, E_p.

As mentioned before, the predecessor to this mode is the $CR-$ mode of failure. Since the tensile stresses in the plate increase by increasing the magnitude of plate modulus of elasticity, then, there are two possibilities for the type of the successor mode to the $C--$ mode of failure. In the first case, the plate peeling stresses may be lower in magnitude than the plate ultimate strength and, hence, the successor mode will be the brittle one $---$, leading to a partial bond flexural load capacity. In the second case, the magnitude of plate ultimate strength may be lower than the magnitude of plate peeling stresses and, then, the successor mode will be the brittle one $--P$, leading to the associated full bond flexural capacity.

The next chapter (Chapter 7) introduces the method for calculating the minimum value of E_p required for this (i.e. $--P$) mode to be initiated, and the maximum values of E_p which can lead to the composite beam failing in such a mode.

6.2.3 Failure Modes $-RP$ and $-R-$

In these ductile modes of failure, crushing of concrete in compression will not be the direct cause of beam failure, but the total failure will be due to either the plate rupture (failure mode $-RP$), or the plate peeling (failure mode $-R-$), following (in both modes) yielding of the internal tensile bars.

The plate rupture (mode $-RP$) occurs when the tensile stresses in the plate reach the plate ultimate strength, while the maximum strain in concrete is not large enough to cause its crushing but the tensile strains in the embedded bars are sufficiently large to cause yielding of the bars and, hence, large beam overall deformations take place (mode $-RP$ with full bond capacity).

The plate peeling mode of failure (mode $-R-$ with partial bond capacity) takes place due to the failure of concrete in the beam's cover in tension, when the concrete tensile stresses within the cover reach the tensile strength of concrete, while the strains in both the concrete in compression and the plate at the maximum moment section are not large enough to cause the beam's overall failure but the tensile strains in the embedded steel bars are larger than the initial yield strain.

From a mathematical point of view, and unlike the previous $CR-$ and $C--$ modes of failure, determination of the changes of the depth of the neutral axis (for modes $-RP$ and $-R-$) due to increases in the plate modulus of elasticity E_p is a very difficult task. A comprehensive discussion for the effect of increasing the values of E_p will, hence, follow, which neglects the changes in the concrete tension to simplify the matters. At the end of this chapter (section 6.2.5), it will be argued that neglecting the

changes in the concrete tensile force does not influence the final conclusions in any practically significant way.

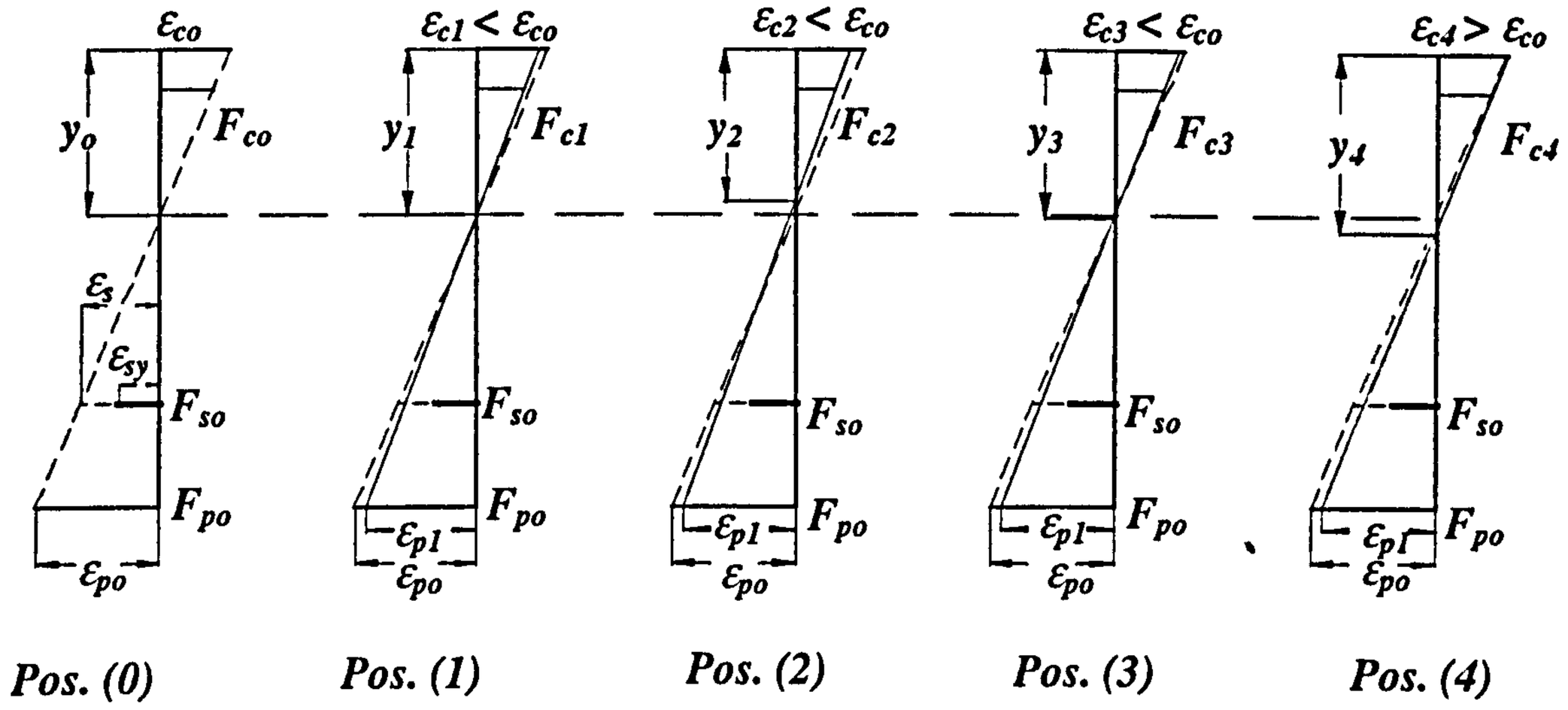

Fig. 6.3 Possible locations of the neutral axis for failure modes $-RP$ and $-R-$ as the value of E_p is increased.

In the modes $-RP$ and $-R-$, the tensile stresses in the plate are restricted in magnitude, and their values will not be changed by increasing the magnitude of E_p, because it is either the plate ultimate strength, f_{pu}, in mode $-RP$, or the plate peeling stress, σ_s (either its minimum or maximum) in mode $-R-$, which govern the beam's failure, and the axial force in the plate, F_{po}, will not in any way be affected by changes in the magnitude of E_p. The values of total force in the embedded tensile bars, F_{so}, will also not be changed, because the bars are in a state of yield. Increasing the values of E_p in these two modes of failure will not change the value of total tension forces and, hence, the values of total compression forces must also remain unchanged - i.e.

$$F_T = F_{po} + F_{so} = A_p f_{pu} + A_s f_y = constant \text{, mode } -RP$$

$$F_T = F_{po} + F_{so} = A_p \sigma_s + A_s f_y = constant \text{, mode } -R-$$

and

$$\varepsilon_{po} = \frac{f_{pu}}{E_{po}} \tag{6.9}$$

or

$$\varepsilon_{po} = \frac{\sigma_s}{E_{po}} \tag{6.10}$$

From Equations (6.9) and (6.10), increasing the value of E_{po} by δE_p will result in a reduction in the value of tensile strain in the plate from ε_{po} to ε_{p1}. Figure 6.3 shows the only four possible locations for the neutral axis if the magnitude of E_p is increased by δE_p.

$$\varepsilon_{p1} = \frac{f_{pu}}{E_{po} + \delta E_p} \text{ or } \varepsilon_{p1} = \frac{\sigma_s}{E_{po} + \delta E_p}$$

These possible four locations within the beam section for the neutral axis, *NA*, are as follows: Figure 6.3:

1- the *NA* depth, y_1, is not being changed by reducing the axial strain in the plate (Pos. 1): this reduces the strains in concrete in compression and the embedded compression bars with the area of concrete in compression being unchanged. The reduction in the compression strains will reduce the compression stresses and, hence, forces (i.e. $F_{c1} < F_{co}$), which will not be in balance with the constant tension forces (which are to remain unchanged). This position will not lead to the equilibrium conditions for the section forces to be satisfied.

2- the *NA* depth, y_2, will be reduced (Pos. 2): this reduces the strains in the compressed portion of beam section, and the values of stresses and forces will also be reduced. As in the previous case (i.e. case 1), the equilibrium conditions for forces will not be satisfied.

3- the *NA* depth, y_3, will be increased by just enough (Pos. 3) to enlarge the compressed area with the maximum concrete strain remaining less than the original strain ε_o so that the enlargement in the compressed area with the associated reduction in compression strains will result in no changes in the compression force: this, then, will be in balance with the constant tension forces, and lead to the force equilibrium condition being satisfied.

4- the *NA* depth, y_4, will be increased to the value which results in increases in the maximum concrete strain (Pos. 4) to be more than the ε_{co} (or even lower than ε_{co}), but with the result that the increases in the compressed area with the corresponding strains result in the compression force to be more than the tensile forces with the latter to remain unchanged. This situation does not satisfy the force equilibrium condition.

Out of the above four possibilities, it is clear that the depth of neutral axis should be increased with sufficient associated reductions in the maximum concrete strain, resulting in the total compression force to remain unchanged. Under such conditions, there will be a reduction of the section strains including those in the tension and compression steel bars and the concrete in tension. It will be proven later in this chapter, that the reduction in the tensile strains in concrete leads to increases in the concrete tensile forces and, hence, rules out the possibility of the first and second cases to occur.

Since the total tensile and compressive forces acting on the beam section in these modes of failure are almost constant, it is expected that the flexural load capacity of the composite beam will not be significantly affected by increasing the values of E_p as

far as these modes of failure (i.e. $-RP$ and $-R-$) are concerned. This has been confirmed by the final results based on the numerical studies on a large number of beam designs, as described later in the present chapter in section (6.4).

It may be concluded that increasing the plate modulus of elasticity will (for the failure modes $-RP$ and $-R-$):

1- increase the depth of neutral axis,

2- not change the magnitudes of total compression and tension forces,

3- reduce the axial strains in the embedded steel bars without changing their tensile stresses because the bars are yielded and the strains are already larger in magnitude, than the initiated yield strain,

4- reduce the plate tensile strains without changing its tensile stresses, and

5- not change the flexural load capacity of the beam.

The modes $-RP$ and $-R-$ are the preferred ones in practice, as they are of a ductile nature and the material strengths of the plate and the bars are fully utilised. Due to the higher moduli of elasticity for the plate and the larger areas of the concrete in compression and also in tension, the modes $-RP$ and $-R-$ are practically more desirable than the ductile mode $CR-$, in view of their higher stiffness while they have the same flexural load capacity as the $CR-$ mode.

As mentioned previously, the predecessor to modes $-RP$ and $-R-$ is the $CR-$ mode of failure. The continuous reduction in the magnitudes of tensile strains in the embedded bars and the plate with the increasing values of E_p lead to the tensile strains in the embedded bars (at a certain stage) to become lower than their initial yield value,

which suggests that the successor to mode $-RP$ will be the brittle mode $--P$ (full bond capacity), while the successor one to the mode $-R-$ will be the brittle mode $---$ (partial bond capacity).

A method for calculating the minimum values of E_p that is required for the modes $-RP$ and $-R-$ to be initiated is presented in the next chapter (Chapter 7).

6.2.4 Failure Modes $--P$ and $---$

In these brittle modes of failure, crushing of the concrete in compression will not be the direct cause of beam's failure (as it will not happen), but the failure will be due to either plate rupture or plate peeling: these will happen suddenly, in the absence of much noticeable overall beam deformations.

The plate rupture happens when the tensile stresses in the plate reach the plate ultimate strength, while neither the maximum concrete strain nor the tensile strains in the embedded bars are large enough to cause crushing of concrete or yielding of the bars, and give deformation warnings (mode $--P$ with full bond capacity). The plate peeling mode of failure (mode $---$ with partial bond capacity), on the other hand, happens as a result of the concrete failure in tension within the concrete cover when the tensile stresses, which are induced at the point of fixity to the teeth, reach the concrete tensile strength, while the axial strains in both the concrete in compression and the plate in tension, are not large enough to cause failure of any of them, and the tensile strains in the steel bars are less in value than the initial yield strain: a sudden brittle failure will, then, result.

To simplify the analysis, the tensile forces in concrete will be ignored, because the magnitude of such forces is very small and, hence, their effect is of insignificant practical implications: the implications of this assumption will be discussed in some detail later in this chapter in section 6.2.5.

In the failure modes $--P$ and $---$, the value of plate tensile stress is restricted to limited variations, and will not be changed by increasing the value of E_p, because it is equal to either the plate ultimate strength, f_{pu}, in the mode $--P$, or the plate peeling stresses, σ_s, in the mode $---$ (either the minimum (lower bound) or the maximum (upper bound) values). As the value of plate tensile stress remains unchanged, the axial strain in the plate is expected to be reduced in magnitude as a result of increasing the plate modulus of elasticity.

In these modes, the concrete in compression is not crushed and, hence, the value of maximum concrete strain is less than the crushing concrete strain (=*0.0035*). With the associated compression stress distribution over the beam section depending on the level of the maximum strain in concrete (as discussed in detail in Chapter 5), there are, therefore, only two cases to be studied.

The first case relates to when the magnitude of maximum concrete stress is less than $0.67f_{cu}$, and the compression stress distribution is of only a parabolic type (i.e. $\varepsilon_o \leq \beta$) as detailed in Chapter 5, where the following equilibrium Equation (6.11) applies - see its derivation in section 5.10:

$$A_s E_s (d-y)(D-y)\varepsilon_p + F_p (D-y)^2 = A'_s E_s \varepsilon_p \left(y-d'\right)(D-y) + \frac{bE_c}{2}\varepsilon_p (D-y)y^2 + \frac{bK_1}{3}\varepsilon_p^2 y^3 \quad (6.11)$$

If one assumes that the modulus of elasticity for the plate is to be increased to a very high value (i.e. $E_p \to \infty$), then, according to Equation (6.5), the axial strain in the plate will become very small (i.e. $\varepsilon_p \to 0$) in order for the plate tensile stress to remain unchanged. This assumption must obviously be verified to ensure that such assumed large increases in the value of modulus of elasticity will not cause modes $--P$ and $---$ to change to any other (different) ones. In fact, a later study of the changes in the modes of failure as included at the end of this chapter (plus discussions at the end of this section) show that each of the modes $--P$ and $---$ will not be followed by any other (alternative) mode, regardless of further increases in the value of plate modulus of elasticity.

Applying the above assumption to Equation (6.11), leads to $F_p(D-y)^2 \to 0$, and since $F_p \neq 0$, then, $(D-y) \to 0$: it may, then, be concluded that increasing the value of E_p will lead to increases in the depth of neutral axis, approaching D.

The second case to be studied relates to when the maximum compression stress in concrete, f_c, is equal to $0.67f_{cu}$, but the maximum strain in concrete is less than its crushing value (i.e. $\beta \leq \varepsilon_o < 0.0035$) with the concrete compression stress distribution being composed of parabolic and linear portions (i.e. distributions) as detailed in Chapter 5: the following equilibrium Equation (6.12) for section forces may, then, be written:

$$A_s E_s\left(\frac{d-y}{D-y}\right)\varepsilon_p^2 + A_p F_p \varepsilon_p = A_s' E_s \varepsilon_p^2\left(\frac{y-d'}{D-y}\right) + 0.67 f_{cu} b\left[y\varepsilon_p - \beta(D-y)\right] + \frac{bE_c}{2}\beta^2(D-y) + \frac{bK_1}{3}\beta^3(D-y) \quad \textbf{(6. 12)}$$

where

$$K_1 = \frac{0.67 f_{cu} - E_c \beta}{\beta^2}$$

In the above , if one assumes $E_p \to \infty$, then, $\varepsilon_p \to 0$, and Equation (6.12) leads to

$$-0.67 f_{cu} b\beta(D-y) + \frac{bE_c}{2}\beta^2(D-y) + \frac{bK_1}{3}\beta^3(D-y) = 0$$

$$(y-D)\left(0.67 f_{cu} b\beta - \frac{bE_c}{2}\beta^2 - \frac{bK_1}{3}\beta^3\right) = 0$$

$$(y-D)\left(\frac{2}{3}0.67 f_{cu} b\beta - \frac{bE_c}{6}\beta^2\right) = 0$$

$$(y-D)\left(2\times 0.67 f_{cu} - \frac{E_c\beta}{2}\ \frac{b\beta}{3}\right) = 0$$

Assuming $\beta = 2.44\times10^{-4}\sqrt{f_{cu}}$ and $E_c = 5500\sqrt{f_{cu}}$, as recommended by BS5400 (1990), then:

$$(y-D)0.67 f_{cu}\frac{b\beta}{3} = 0$$

However, since $0.67 f_{cu}\frac{b\beta}{3} \neq 0$, then D=y: in other words, increasing the plate modulus of elasticity to very high values increases the depth of neutral axis, y, with the upper (limiting) value of D, which is the depth to the centre of gravity of the externally bonded plate.

Following the discussions relating to the two above cases, it is clear that increasing the value of E_p for the plate (i.e. reducing the tensile strain in the plate) will always lead to increases in the depth of NA, and. accordingly, the total area of concrete in compression will be increased for those beams which fail with $--P$ or $---$ modes of failure, regardless of the level of the maximum concrete strain (which, for modes $--P$ and $---$, is always less than the limiting crushing strain).

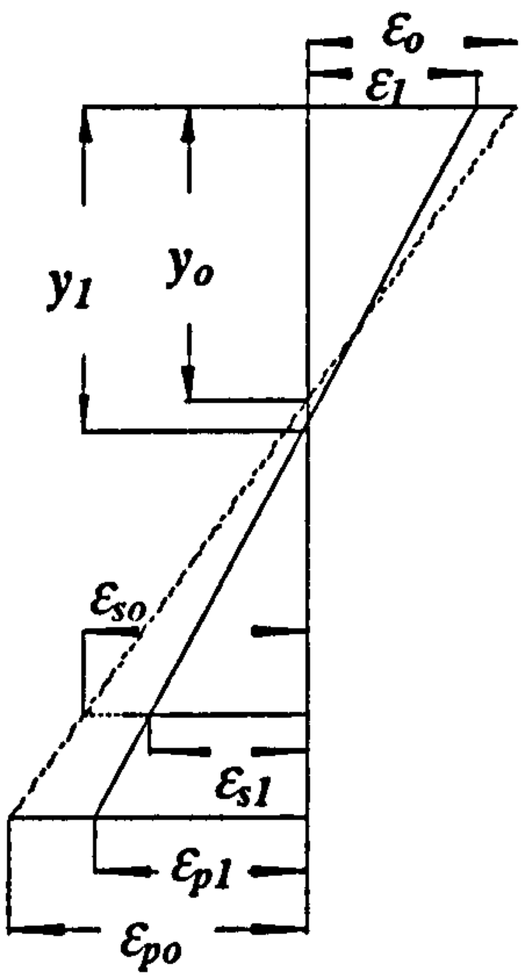

Fig. 6.4 Section strains, stresses for modes of failure $--P$ and $---$.

As shown in Figure 6.4, both the reduction in plate tensile strain and the increase in the depth of NA cause reductions in the magnitudes of tensile strains in the steel bars and, hence, cause a reduction in the value of total tension force on the beam section (note that the force in the plate is supposed to remain unchanged).

If the magnitude of tension force is reduced with increasing the value of E_p, while the concrete compression area is getting larger (as proved in the above, as a result of increases in the depth of neutral axis), then, the compression stresses and strains must be reduced in magnitude so that the total compression force acting on the beam

section is also reduced: the maximum strain in concrete ε_o must, therefore, also be reduced.

The reduction in both the tension and compression forces acting on the beam section lead to a reduction in the overall flexural load capacity of the beam. This conclusion is supported by the numerical results obtained using different beam designs as reported at the end of the present chapter.

It may, therefore, be concluded that increasing the plate modulus of elasticity for modes $--P$ and $---$ will result in

1- increases in the depth of neutral axis,

2- reductions in the maximum strains and stresses in concrete and the tensile strains in the internal steel bars plus the tensile strain in the plate - the axial stress in the plate will not be changed, and

3- reductions in the overall flexural load bearing capacity of the beam.

These mode (i.e. $--P$ and $---$) are not desirable ones in practice because of both their brittle nature and their associated reductions in the flexural load bearing capacity of the beam as a result of increases in the magnitude of the modulus of elasticity of the FRP material for the plates.

Because of the reductions in the compression strains in concrete and in the tensile strains in the embedded bars with increasing values of plate modulus of elasticity,

these failure modes will not be followed by any other (i.e. alternative) failure modes (with further increases in the plate modulus of elasticity).

For the full bond brittle mode $--P$, the predecessor modes of failure are either the brittle mode $C--$ (full bond flexural capacity), or the ductile mode $-RP$ (full bond flexural capacity).

For the partial bond brittle mode $---$, the predecessor modes of failure are either the brittle mode $C--$ (full bond flexural capacity), or the ductile mode $-R-$ (partial bond flexural capacity).

In general, therefore, increasing the value of E_p will, for all the six possible modes of failure, result in increases in the depth of neutral axis.

6.2.5 Implications of Neglecting the Concrete in Tension

Concrete resistance in the presence of tensile stresses is very low in magnitude. The concrete can resist the tensile stresses for only very low values of concrete strains. The concrete tensile stress-strain relationship as recommended by BS5400 (1990) is presented in Figure 6.5.

If the strain in concrete is higher than a certain value, the concrete will be cracked and will not carry any stresses across the cracks.

Let us start with the analysis for the modes associated with which crushing of concrete takes place (i.e. modes $CR-$ and $C--$). In the preceding analyses (with concrete in tension neglected), it was argued that increasing the plate modulus of elasticity will increase the depth of neutral axis for both of these modes, and that the magnitude of compression force tends to be increased in order to balance the increased tension force. There are only two possibilities to be considered regarding the influence of concrete in tension as the plate modulus of elasticity increases (i.e. as the axial strain in the plate is reduced). These possibilities relate to cases when the force due to the concrete in tension is either reduced or increased in magnitude. If the concrete tension force is reduced with increasing values of the plate modulus of elasticity (i.e. with reductions in the tensile strain in the plate), then, ignoring it must adversely affect the above derivations in cases when this reduction is large enough to be more than the previously discussed (and proven) increases in the plate axial force. If this is the case, the reduction in the overall tension force would result in a reduction in the compression force and, hence, the depth of neutral axis will be reduced: however, this contradicts the conclusion based on the above derivations as later on this chapter supported by the numerical results on a large number of beam designs which have taken the influence of concrete in tension into account.

In contrast, if the tension force in concrete is increased with increasing values of the plate modulus of elasticity, then, ignoring it will not affect the conclusions based on the preceding derivation, as including it will increase the total tension force on the beam section and, hence, will increase the magnitude of compression force to maintain force equilibrium, leading to increasing values of the depth of neutral axis. In other words, including the influence of concrete tension will lead to increases in the

depth of neutral axis, and support the conclusions based on the above derivations. It is also compatible with the results of numerical studies.

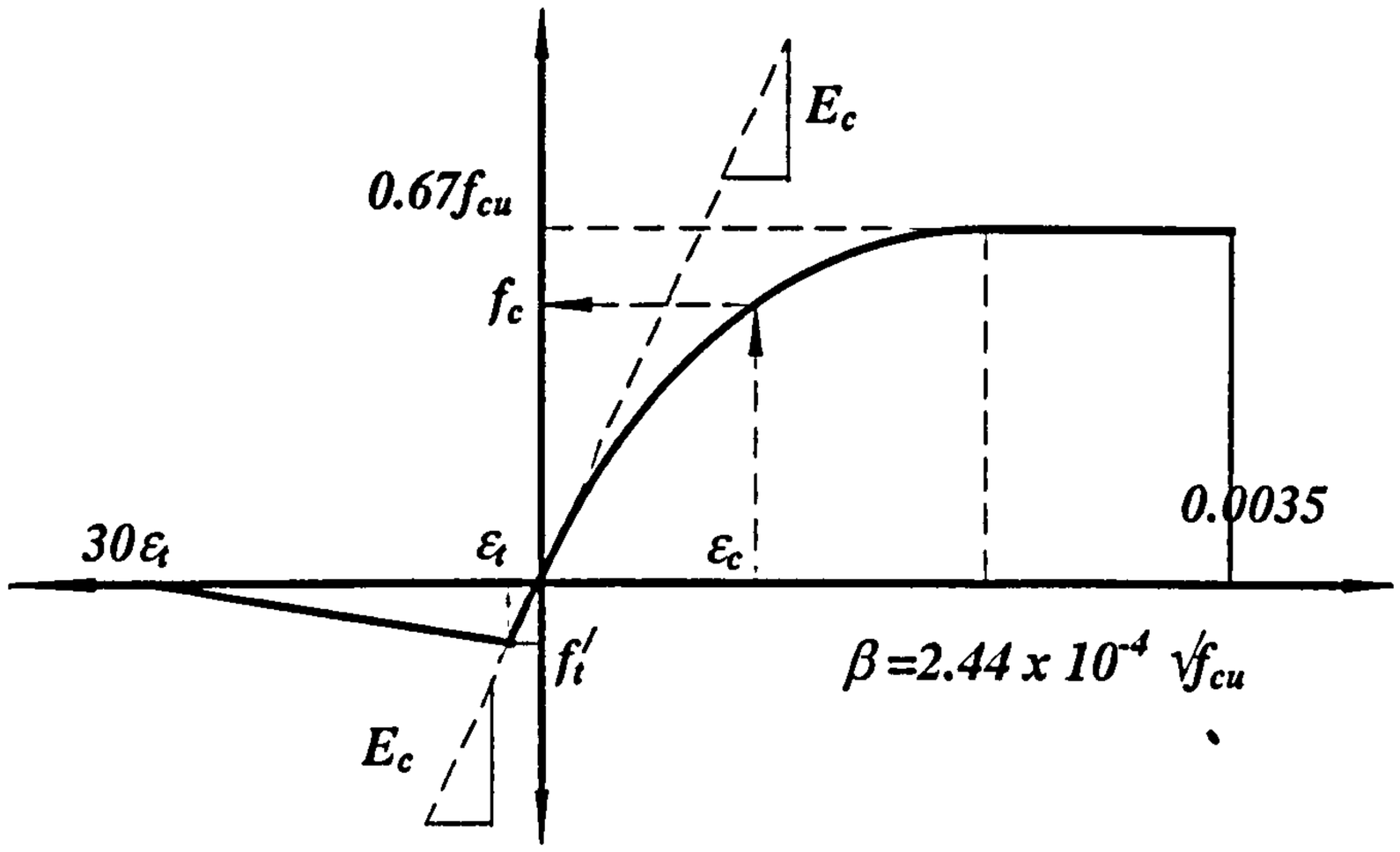

Fig. 6.5 Stress-strain relationship for concrete in compression and/or tension after BS5400 (1990).

The question now is as to whether the concrete tension force is increased or decreased with increasing values of the plate modulus of elasticity. To answer this question, let us consider Figure 6.6, where the plate modulus of elasticity is increased from E_{p1} to E_{p2} and, according to the arguments in the above, the depth of neutral axis will as a result increase from y_1 to y_2.

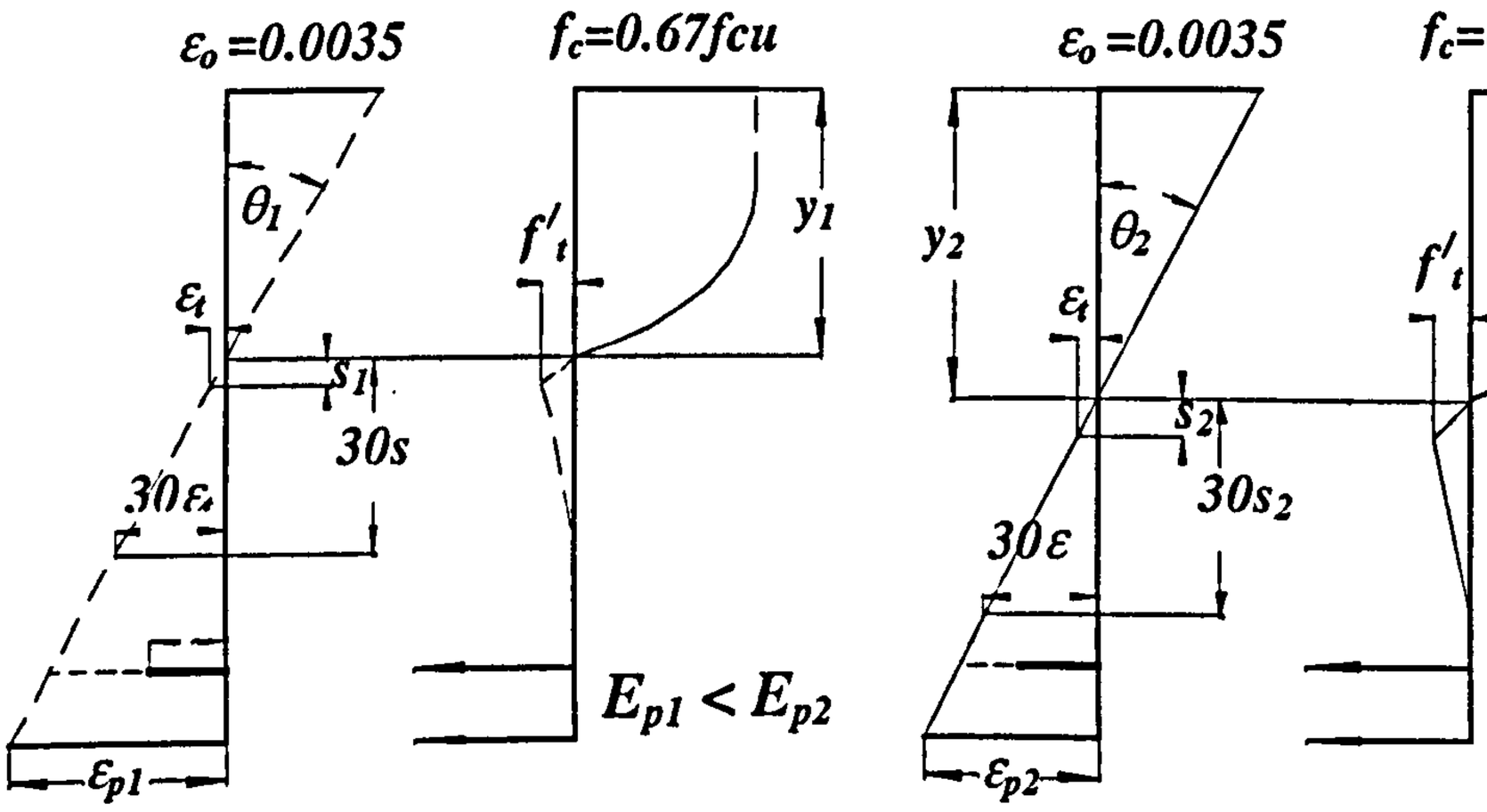

Fig. 6.6 Distribution of concrete tension stresses.

Since, in these two modes (i.e. $CR-$ and $C--$), the largest concrete strain is at its maximum possible values, then, the slope of the strain distribution plane within the beam cross-section will be reduced from θ_1 to θ_2 - see Figure 6.6. The tension concrete forces corresponding to E_{p1} and E_{p2} are F_{ct1} and F_{ct2}, respectively, and may be calculated as:

$$F_{ct1} = \frac{f_t'.b}{2}(30s_1) \text{ and } F_{ct2} = \frac{f_t'.b}{2}(30s_2) \qquad (6.13)$$

where, f_t' is the concrete tensile strength with the assumed value of $f_t' = 0.36\sqrt{f_{cu}}$ (according to the BS8110 (1985)) and

$$s_1 = \frac{\varepsilon_t}{\tan\theta_1} \quad \text{and} \quad s_2 = \frac{\varepsilon_t}{\tan\theta_2} \quad \text{where} \quad \varepsilon_t = \frac{f_t'}{E_c}$$

But $\theta_2 < \theta_1$ so that $s_2 > s_1$ and, hence, $F_{ct2} > F_{ct1}$

The above suggests that neglecting the concrete tension is not compatible with the outcome of the previously discussed derivations - i.e. the final conclusion for the two modes of failure $CR-$ and $C--$, whereby the increases in the depth of neutral axis are accompanied with increases in the total magnitudes of tension and compression forces.

Let us now study the totally opposite cases, whereby increases in the depth of neutral axis are accompanied with reductions in the total values of concrete compression and tension forces (i.e. modes $--P$ and $---$). If one considers the concrete force in tension in terms of the axial strain in the plate, and guided by Equation (6.13) with the concrete tensile strength given as $f_t' = 0.36\sqrt{f_{cu}}$, then

$$F_{ct} = \frac{30 f_t' b}{2}\left(\frac{D-y}{\varepsilon_p}\right)\frac{f_t'}{E_c} = \frac{15\left(f_t'\right)^2 b(D-y)}{\varepsilon_p E_c}$$

$$= \frac{1.944 f_{cu} b(D-y)}{\varepsilon_p E_c} = \frac{5.832 f_{cu}(D-y)}{\varepsilon_p E_c \beta}\left(\frac{b\beta}{3}\right)$$

where

$$\frac{\varepsilon_{ct}}{s} = \frac{\varepsilon_p}{D-y} \text{ and } \varepsilon_t = \frac{f_t'}{E_c}$$

Moreover, consider the concrete tension force in the equilibrium equation for these modes (i.e. Equation (6.12)), to get

$$A_s E_s\left(\frac{d-y}{D-y}\right)\varepsilon_p^2 + A_p F_p \varepsilon_p + \frac{5.832 f_{cu}(D-y)}{E_c \beta}\left(\frac{b\beta}{3}\right) = A_s' E_s \varepsilon_p^2\left(\frac{y-d'}{D-y}\right) + \quad \textbf{(6.14)}$$

$$0.67 f_{cu} b\left[y\varepsilon_p - \beta(D-y)\right] + \frac{bE_c}{2}\beta^2(D-y) + \frac{bK_1}{3}\beta^3(D-y)$$

with the plate axial strain approaching zero,

$$-0.67 f_{cu} b\beta(D-y) + \frac{bE_c}{2}\beta^2(D-y) + \frac{bK_1}{3}\beta^3(D-y) - \frac{5.832 f_{cu}(D-y)}{E_c \beta}\left(\frac{b\beta}{3}\right) = 0 \quad \textbf{(6.15)}$$

$$(y-D)\left[0.67 f_{cu} b\beta - \frac{bE_c}{2}\beta^2 - \frac{bK_1}{3}\beta^3 + \frac{5.832 f_{cu}}{E_c \beta}\left(\frac{b\beta}{3}\right)\right] = 0 \quad \textbf{(6.16)}$$

$$(y-D)\left[\frac{2}{3}(0.67 f_{cu} b\beta) - \frac{bE_c}{6}\beta^2 + \frac{5.832 f_{cu}}{E_c \beta}\left(\frac{b\beta}{3}\right)\right] = 0 \quad \textbf{(6.17)}$$

$$(y-D)\left(2 \times 0.67 f_{cu} - \frac{E_c \beta}{2} + \frac{5.832 f_{cu}}{E_c \beta}\right)\left(\frac{b\beta}{3}\right) = 0 \quad \textbf{(6.18)}$$

and, assuming $\beta = 2.44 \times 10^{-4}\sqrt{f_{cu}}$ with $E_c = 5500\sqrt{f_{cu}}$, as recommended by BS5400 (1990), then

$$(y-D)(0.67 f_{cu} + 4.35)\frac{b\beta}{3} = 0 \quad \textbf{(6.19)}$$

but since $(0.67 f_{cu} + 4.35)\ b\beta / 3 \neq 0$, then $D = y$: in other words, increasing the plate modulus of elasticity to a very high value increases the depth of neutral axis towards

the limiting value equal to the depth to the centre of gravity of the plate which is in line with the previous conclusion.

At this point, it is demonstrated that for the two opposite cases (i.e. the case when section forces are increased or reduced with increases in the values of plate modulus of elasticity), neglecting the tension force in concrete does not significantly affect the conclusions from previous analyses. It is expected that the same argument holds true for those cases whereby increases in the values of plate modulus of elasticity neither increases nor decreases the total forces in tension and compression (i.e. modes $-RP$ and $-R-$).

6.3 PROGRESS OF THE FAILURE MODES WITH INCREASING VALUES OF MODULUS OF ELASTICITY FOR THE PLATE

In this section (guided by the previous derivations), the progress in the variations of the modes of failure regarding plated beams, as influenced by increases in the FRP plate modulus of elasticity, will be discussed in a qualitative fashion, with further quantitative discussions presented in the next chapter.

Amongst other conclusions, it has been shown in the previous section (section 6.2) that for all the six FRP related modes of failure, increasing the plate modulus of elasticity will reduce the magnitudes of tensile strains in the plate and the embedded tensile bars, while it will increase the depth of neutral axis and the tensile stress in the plate (as long as the axial stress in the plate are less than the plate ultimate strength for

the full bond behaviour or less than the plate peeling stresses for the partial bond behaviour).

Moreover, it has been concluded that the flexural capacity of the plated beam will increase (with increases in the modulus of elasticity of the plate) if the failure mode is either $CR-$ or $C--$ and will decrease if the failure mode is $--P$ while there will be insignificant changes in the magnitude of the flexural capacity if the failure mode is $-RP$ (full bond behaviour). In addition, it has been concluded that the flexural capacity of the plated beam associated with the plate peeling behaviour will be reduced, with increases in the modulus of elasticity of the plate, if the mode of failure is $---$ while there will be insignificant changes associated with the mode $-R-$.

It is assumed that the unplated beam section is under-reinforced - i.e. the unplated section fails in a ductile manner due to crushing of concrete after the internal bars reach yield (mode CR).

Assuming that such an unplated beam has been strengthened by an externally bonded FRP plate with a very low modulus of elasticity (i.e. $E_p \cong 0.0$), the magnitude of both the axial stresses in the plate and the force carried by it will be negligible. This mode of failure will be $CR-$, as the axial stresses in the plate are extremely low in magnitude (and certainly lower than the plate peeling stresses and/or the plate ultimate strength), and the embedded bars have yielded, while the maximum concrete strain is equal to 0.0035 because the unplated beam is assumed to be an under-reinforced one.

Increasing the value of E_p for the FRP plate in the primary ductile mode $CR-$, will increase the axial stresses in the plate with such stresses being lower in magnitude than the plate ultimate strength, while the tensile strains in the embedded bars, which are higher in magnitude than the initial yield strain, will be reduced with the concrete crushing being the critical factor, causing failure at the maximum moment section where the maximum concrete strain continues to remain at the crushing strain equal to 0.0035 (according to the BS8110 (1985)).

This ductile mode of failure (i.e. $CR-$) will be changed to another failure mode, if one of the non-critical (till, then) elements (i.e. the tensile strains in the embedded bars, or the tensile stresses in the plate) become the controlling factors as regards beam's failure. Under such conditions, either the tensile strains in the embedded bars may become lower than the initial yield strain and the failure mode will, then, be the brittle mode $C--$ (with the concrete crushing controlling the failure), or the axial stresses in the plate may become the controlling factors for failure, in which case, the failure will not be due to the crushing of concrete and will instead be of a ductile nature - i.e. the failure mode $-RP$ will be initiated.

The axial stresses in the plate will become critical, if they reach the ultimate strength of the material for the FRP plate for the full bond behaviour, or if they become equal in magnitude to the minimum/maximum values of plate peeling stresses for the partial bond behaviour. For certain beam configurations, one and/or either of the plate peeling stresses may not be the critical factors, and such bounding values of plate stresses may be higher in magnitude than the plate ultimate strength. In such cases, the beam will not be in the partially bonded regime, and the full bond regime prevails.

Theoretically, by increasing the values of E_p, either ductile or brittle failure (i.e. the $-RP$ or $C--$ modes, respectively) take place, following the primary mode of failure $CR-$. These two types of general behaviour may be classified as either under-reinforced (ductile behaviour) or over-reinforced (brittle behaviour): the underlying reason for using such over- or under-reinforced classifications will be clarified in the next chapter (i.e. Chapter 7) where it is argued that the more the area of the externally bonded plate is, the higher will be the possibility for the brittle (i.e. over-reinforced) mode $C--$ to occur.

In view of the fact that so many design parameters influence the behaviour of a plated section, the following discussion will only present a qualitative description of the possible changes in the failure modes as the magnitude of the modulus of elasticity for the plate, E_p, is increased, with a quantitative treatment as regards the critical values of E_p associated with the mode transitions being addressed in some detail in Chapter 7.

6.3.1 Behaviour of Under-Reinforced Plated Beams

As regards the primary mode $CR-$, it is operative when (as E_p increases) the growing axial stress in the plate will eventually reach one of the critical values of plate stresses prior to the tensile strains in the embedded bars falling below the yielding strain: in this mode, the failure will continue to be ductile, and the sudden crushing of concrete does not happen.

Figure 6.7 presents the general pattern of behaviour for an under-reinforced plated beam as the magnitude of plate modulus of elasticity increases. At virtually a zero value for the plate modulus of elasticity (point O), the plate has no influence on the flexural capacity of the composite (i.e. plated) beam, and the flexural capacity will be the same as that of an unplated beam. Increasing the plate modulus of elasticity will increase the axial stresses in the plate and, hence, the flexural load capacity of the plated beam increases with the plate remaining fully bonded to concrete.

If the magnitude of axial stresses in the plate reach the minimum or maximum values of plate peeling stresses, then, the failure mode will be controlled by the ripping off of the cover, rather than the crushing of concrete, with the embedded bars experiencing yielding (ductile failure): under such conditions, the failure mode will be $-R-$, being initiated at the critical $E_{(a)}$ value (point a).

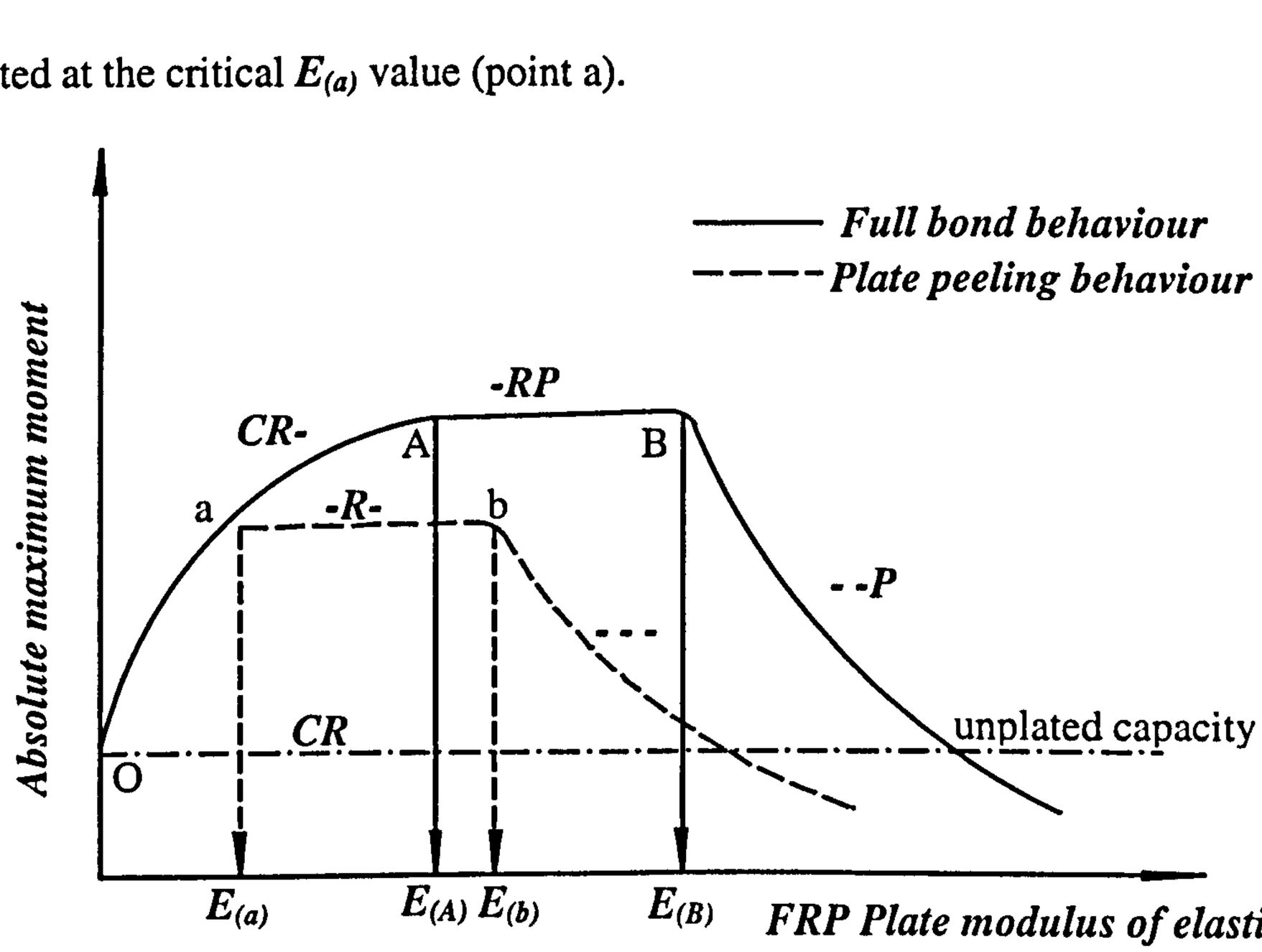

Fig. 6.7 Changes in the modes of failure associated with variations in the plate modulus of elasticity for under-reinforced plated beams.

Following the initiation of mode $-R-$, using externally bonded FRP plates with gradually higher moduli of elasticity causes a reduction in the tensile strains in the plate and the embedded bars, but does not significantly change the peeling flexural capacity of the beam. If the strains in the embedded bars are sufficiently reduced to be less than the initial yield strain, then, the failure mode will become the brittle mode $---$ at the critical $E_{(b)}$ value (point b), and this (i.e. $---$) failure mode will continue to be due to peeling of the plate – it is not ductile in nature. Any further increases in the values of E_p will further reduce the flexural capacity of the composite beam, with no further associated changes in the failure mode.

If the plated beam does not fail due to plate peeling (because either the magnitudes of plate peeling stresses are higher than the plate ultimate strength, or due to certain design arrangements such as mechanical anchoring to the end of the plate, which prevent the plate peeling to occur), then, the beam will continue to behave as a fully bonded one. In such cases, when (with increasing values of E_p) the tensile stresses in the plate reach the plate ultimate strength, the failure will be a ductile one due to the plate rupture at the maximum moment section (rather than it being caused by crushing of concrete) with the embedded bars experiencing yielding with the change in failure mode occurring at the critical value of $E_{(A)}$ (at point A) - the subsequent failure mode will be $-RP$.

Using plates with higher moduli of elasticity associated with the $-RP$ mode causes reductions in the magnitudes of tensile strains in the plate and the embedded bars, but does not significantly change the flexural load capacity of the plated beam. If the tensile strains in the embedded bars are sufficiently reduced to be less than the initial

yield strain, then, the beam failure mode will finally become the brittle one $--P$ at the critical value of $E_{(B)}$ (at point B) with the mode of failure continuing to be due to plate rupture. Any further increases in the values of E_p will reduce the flexural capacity of the beam but will not cause any further changes in the mode of failure.

6.3.2 Behaviour of Over-Reinforced Plated Beams

Figure 6.8 presents the general pattern of behaviour (in terms of changes in the failure modes) for an over-reinforced plated beam, as the values of plate moduli of elasticity are increased.

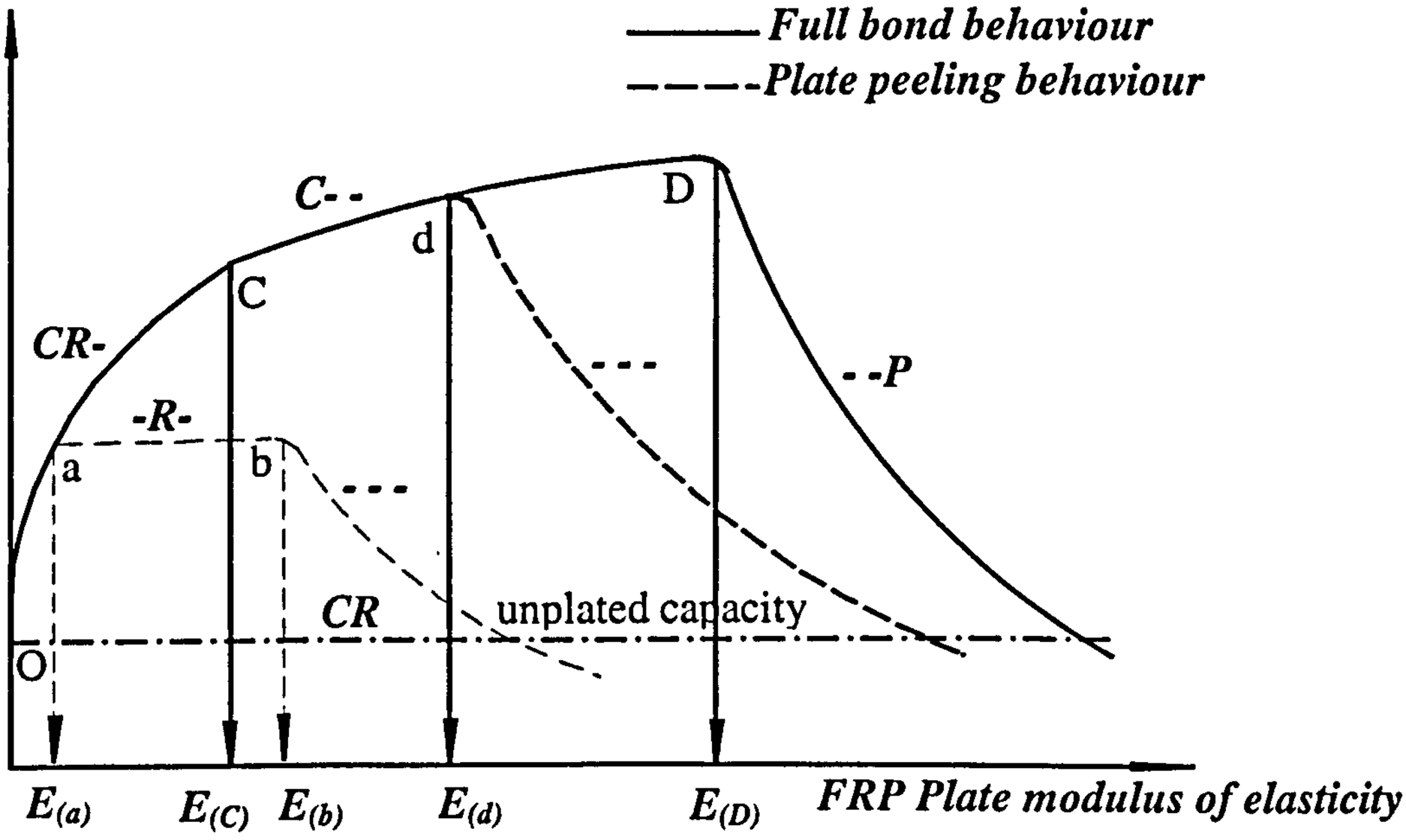

Fig. 6.8 Changes in the modes of failure associated with variations in the plate modulus of elasticity for over-reinforced plated beams.

For the primary mode $CR-$, with increasing values of modulus of elasticity for the plate, there will be gradual reductions in the magnitudes of tensile strains in the embedded bars, and when these strains become sufficiently small to be lower than the steel initial yield strain, prior to the simultaneously growing axial stress in the plate

reaching one of the critical plate stresses, then, the failure mode will be changed to the brittle one $C--$ due to the crushing of concrete at the maximum moment section, which occurs in the absence of large embedded bar deformations. This mode (i.e. $C--$) is similar to that of the over-reinforced unplated sections, and is initiated at the critical value of $E_{(C)}$ at point C in Figure 6.8.

Using plates with higher moduli of elasticity for the beams, which fail in the mode $C--$, leads to increasing values of tensile stresses in the plates and the flexural load capacity of the beam, and the composite beam will continue to behave as a full bonded element. With increasing values of E_p, if the axial stresses in the plate are sufficiently increased to reach that of plate peeling stress(es), then, the failure mode for the beam will be a brittle one $---$ at the critical value of $E_{(d)}$ (point d in Figure 6.8), with the failure being due to the end plate peeling rather than crushing of concrete. Any further increases in the value of E_p will further reduce the flexural load bearing capacity of the beam, with the mode of failure continuing to remain as $---$.

If with increasing values of E_p within the mode $C--$, the beam does not fail due to plate peeling because the plate peeling stresses are higher in magnitude than the plate ultimate strength or due to certain constructional arrangements (e.g. using bolts at the end of the plate as a mean of mechanical anchoring) which prevent the plate peeling to occur, then, the beam will continue to behave as a fully bonded element until the tensile stresses in the plate are sufficiently high to reach the plate ultimate strength and, then, the failure will be due to plate rupture at the maximum moment section rather than the crushing of concrete, with the failure mode being $--P$: this mode

will be initiated at the critical value of $E_{(D)}$ (point D). Any further increases in the magnitude of E_p will, then, lead to further reductions in the beam's flexural load capacity, with the mode $--P$ remaining unchanged for increasing values of E_p beyond $E_{(D)}$.

If the magnitudes of plate peeling stresses for an over-reinforced plated beam are relatively low, then, the partial bond behaviour might follow the alternative path $O-a-b$ in Figure 6.8, with the mode characteristics of the path $O-a-b$ in Figure 6.8 being similar to those of the partial bond $O-a-b$ path in Figure 6.7, which have already been fully discussed in the previous section and there is little point in repeating the story again.

6.4 NUMERICAL STUDIES

This section presents numerical studies to support the above arguments regarding the effect of variations in the modulus of elasticity for the externally bonded plate on various parameters of plated beams which were studied within the scope of the above analysis. Twenty-one beams were carefully selected to represent almost the whole set of the 58 reinforced concrete beams strengthened with external FRP plates (which were identified in the literature review with their details shown in Table 2.1). The range of values for the moduli of elasticity for the FRP plates chosen in this study, lies between 1 and 200 GPa .

Figures 6.9 to 6.30 show the effect of increases in the plate modulus of elasticity on the calculated values for the depth of neutral axis. From these figures, it is obvious

that (as previously discussed) increasing the plate modulus of elasticity increases the neutral axis depth for the plated section for all modes of failure (it will later be demonstrated in Figures 6.53 to 6.74 that the modes of failure associated with presently chosen FRP plated beams as influenced by the chosen range of moduli of elasticity cover the full range of possibilities).

Figures 6.31 to 6.52, on the other hand, show the effect of increasing the plate modulus of elasticity on the axial strains of the externally bonded FRP plates: for all the possible modes of failure, it is clear that increasing the plate modulus of elasticity reduces (by varying degrees) the values of axial strain in the FRP plate. This has also been one of the underlying assumptions for the previous derivations for all the possible modes of failure.

Finally, Figures 6.53 to 6.74 present the effect of increasing the plate modulus of elasticity, E_p, on the magnitudes of different flexural capacities for all the presently chosen FRP plated beams. These figures also present all the different possible modes of failure associated with each level of flexural load capacity over the full range of values for plate modulus of elasticity.

Careful examination of this set of figures (i.e. Figures 6.53 to 6.74) substantiates the underlying assumptions in the preceding sections:

1- At trivial values of E_p, all the plated section flexural capacities are equal to that for the corresponding unplated section.

2- The initial mode of failure for all the plated beams (i.e. at sufficiently low values of E_p) is the primary mode $CR-$ as shown in all these figures (though

this mode would either be followed by the successor mode at relatively small values of E_p, or would continue to be the cause of failure for still larger values of E_p).

3- With increases in E_p, the flexural capacity (full bond behaviour) of the plated beam increases if the failure mode is either the $CR-$ mode (as shown in all the figures) or the $C--$ mode (as shown in Figure 6.69 for beam *N*). For all those beams which experience the $--P$ and/or $---$ modes of failure, on the other hand, the flexural capacity of the plated beam is found to decrease with increases in E_p.

4- As previously suggested, there is insignificant changes in the flexural capacity (associated with variations in E_p) if the mode of failure is $-RP$ or $-R-$ (as demonstrated in almost all the plots).

5- In most cases, the sequence of changes in the modes of failure (with increases in E_p) is typical of that predicted for the under-reinforced sections as in Figure 6.7 - see, for example, Figures 6.60 to 6.63.

6- Moreover, the sequence of changes in the modes of failure for over-reinforced sections as shown in Figure 6.69 is similar to that presented in Figure 6.8. It should, however, be noted that the whole pattern is not shown for the full bond behaviour (i.e. M_{pult}) due to the restricted upper limit for the E_p-value in this study (i.e. 200 GPa) and the very large value (about 5047 GPa) of E_p which is needed for the initiation of the $--P$ mode which is expected to follow the $C--$ mode.

7- In certain cases, the peeling capacity for the plated beam may be less than the corresponding flexural capacity for even the associated unplated section (as

shown in many figures). This observation has also been previously reported in the literature although no explanations had previously been offered for such reductions in the beam capacity following the external plating. Moreover, in certain cases, the $--P$ capacity may, indeed, be less than that for the corresponding unplated section: beam ***F-P1*** is an example for such a case – Ref. Figure 6.70.

6.5 CONCLUSIONS

All the possible changes in the modes of failure, as a result of increases in the FRP modulus of elasticity for plated reinforced concrete beams have been addressed in some detail. A quantitative treatment of the critical values of the FRP modulus of elasticity causing various failure mode transitions (i.e. changes) will be presented in the next chapter.

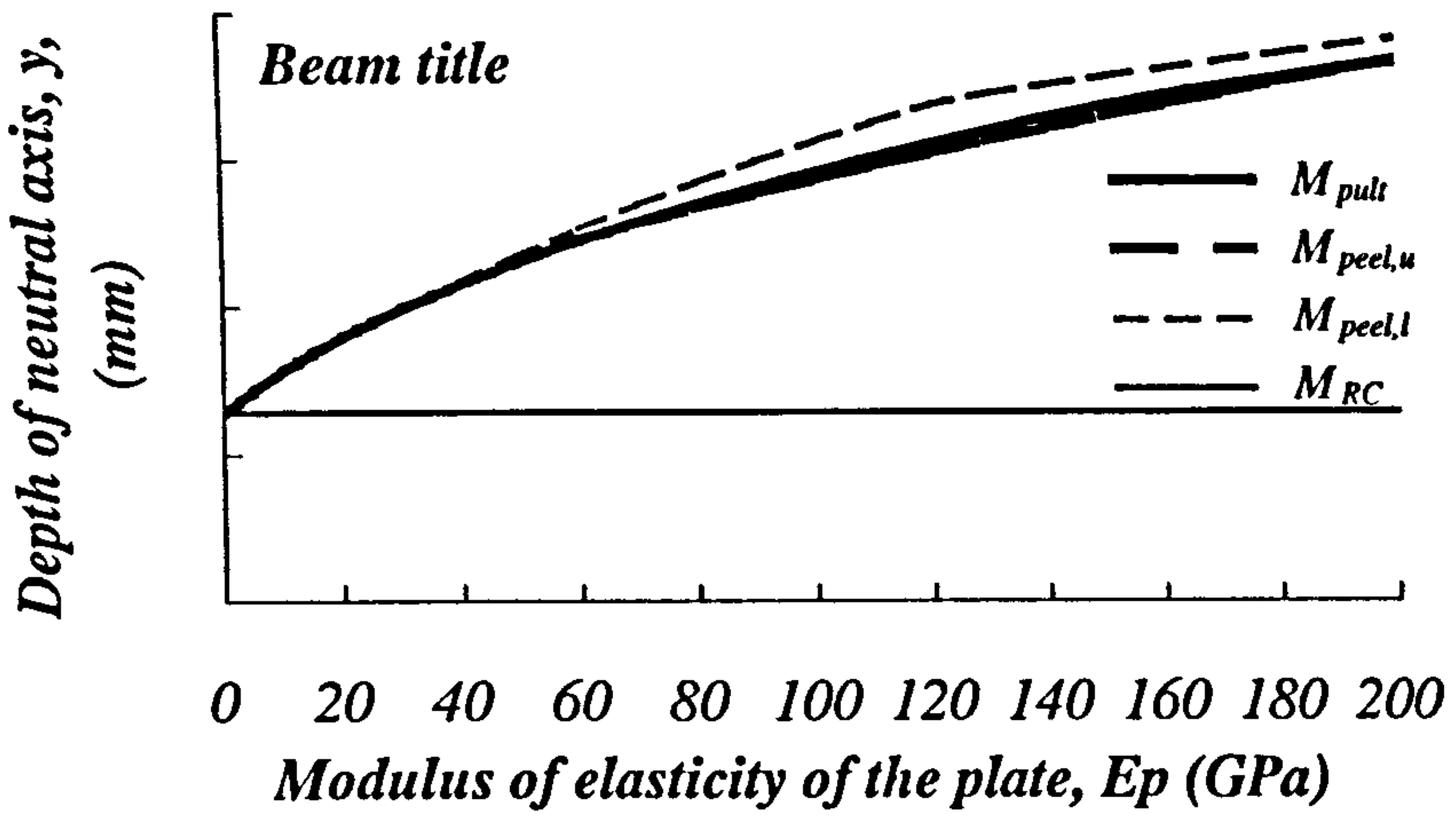

Fig. 6.9 Effect of increasing the plate modulus of elasticity, E_p, on the depth of neutral axis (typical legends for Figs 6.10 to 6.30).

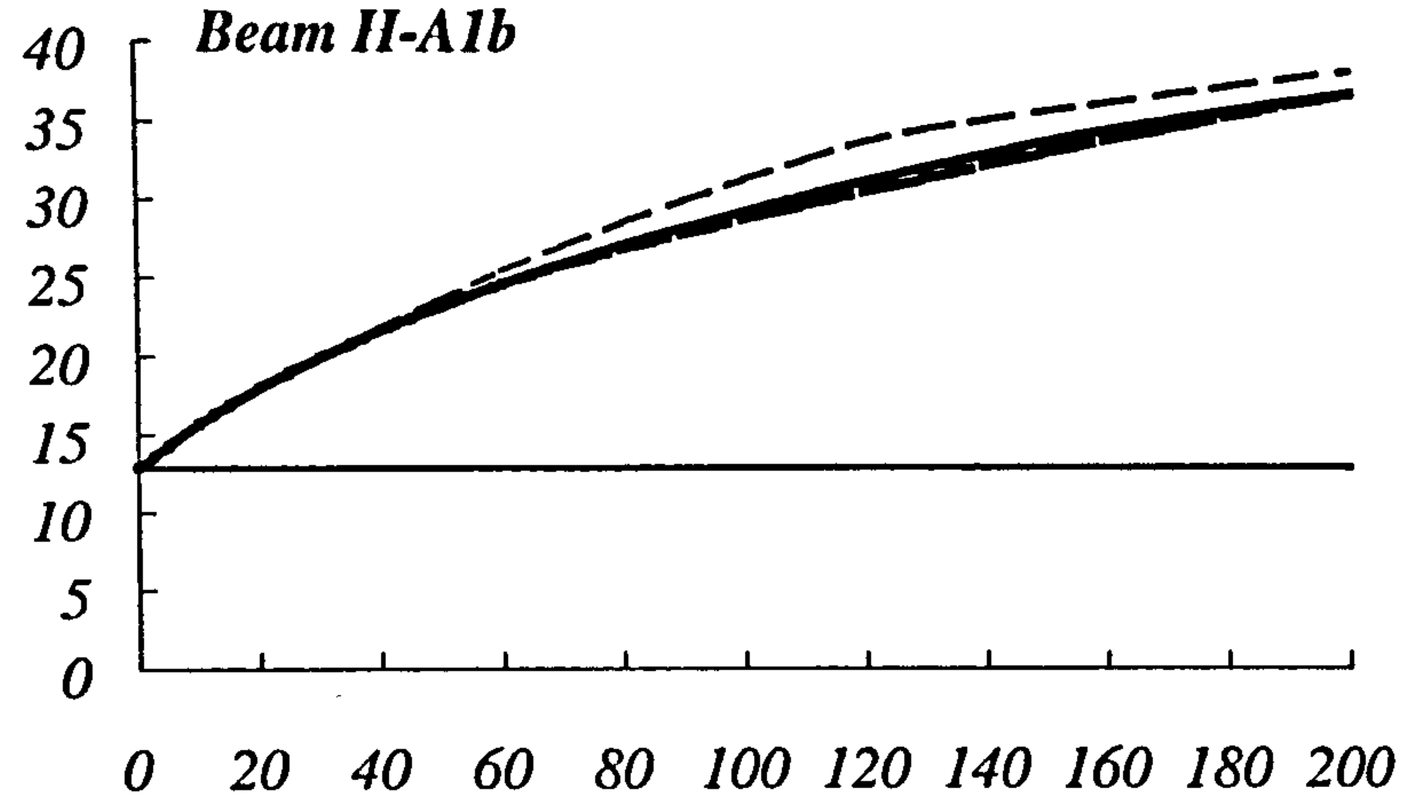

Fig. 6.10 Effect of E_p on the depth of neutral axis for beam *H-A1b*.

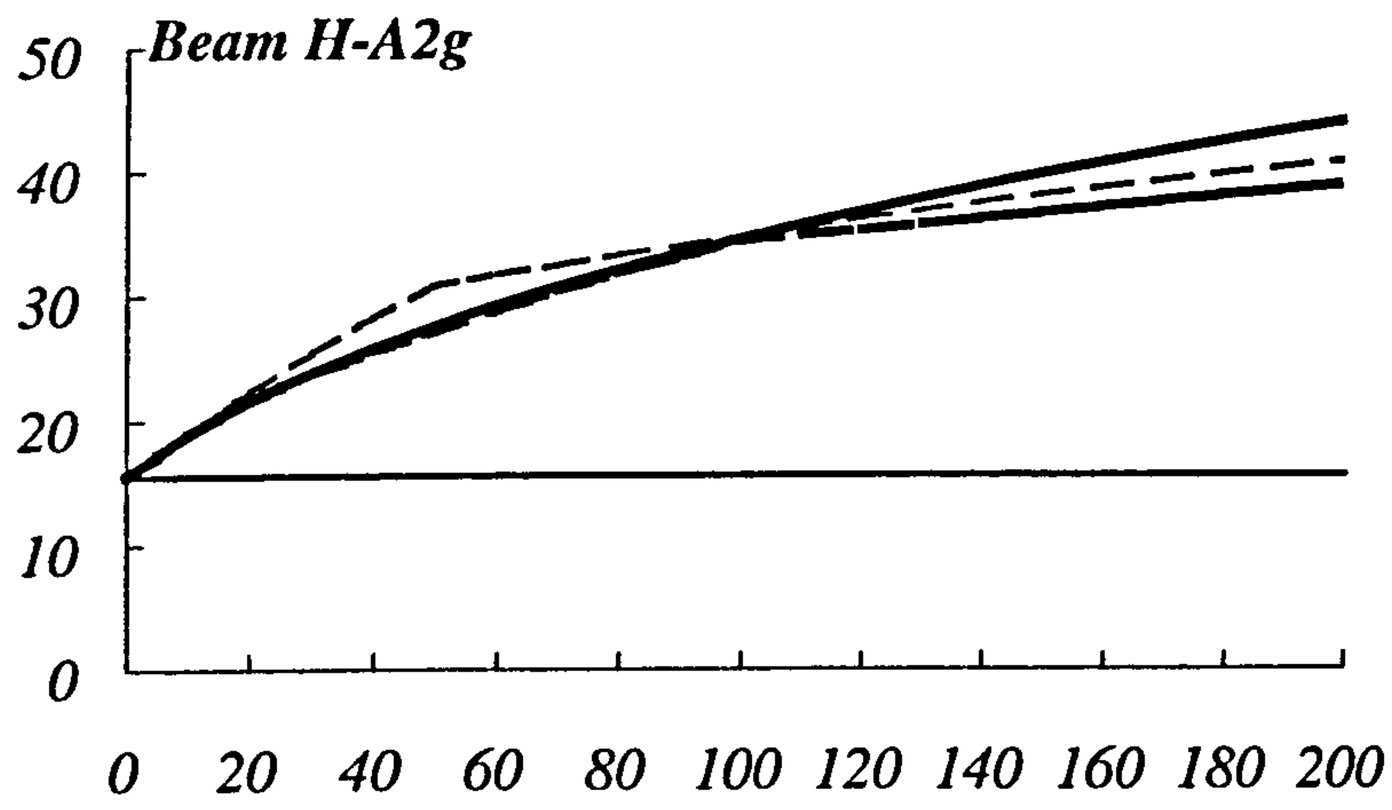

Fig. 6.11 Effect of E_p on the depth of neutral axis for beam *H-A2g*.

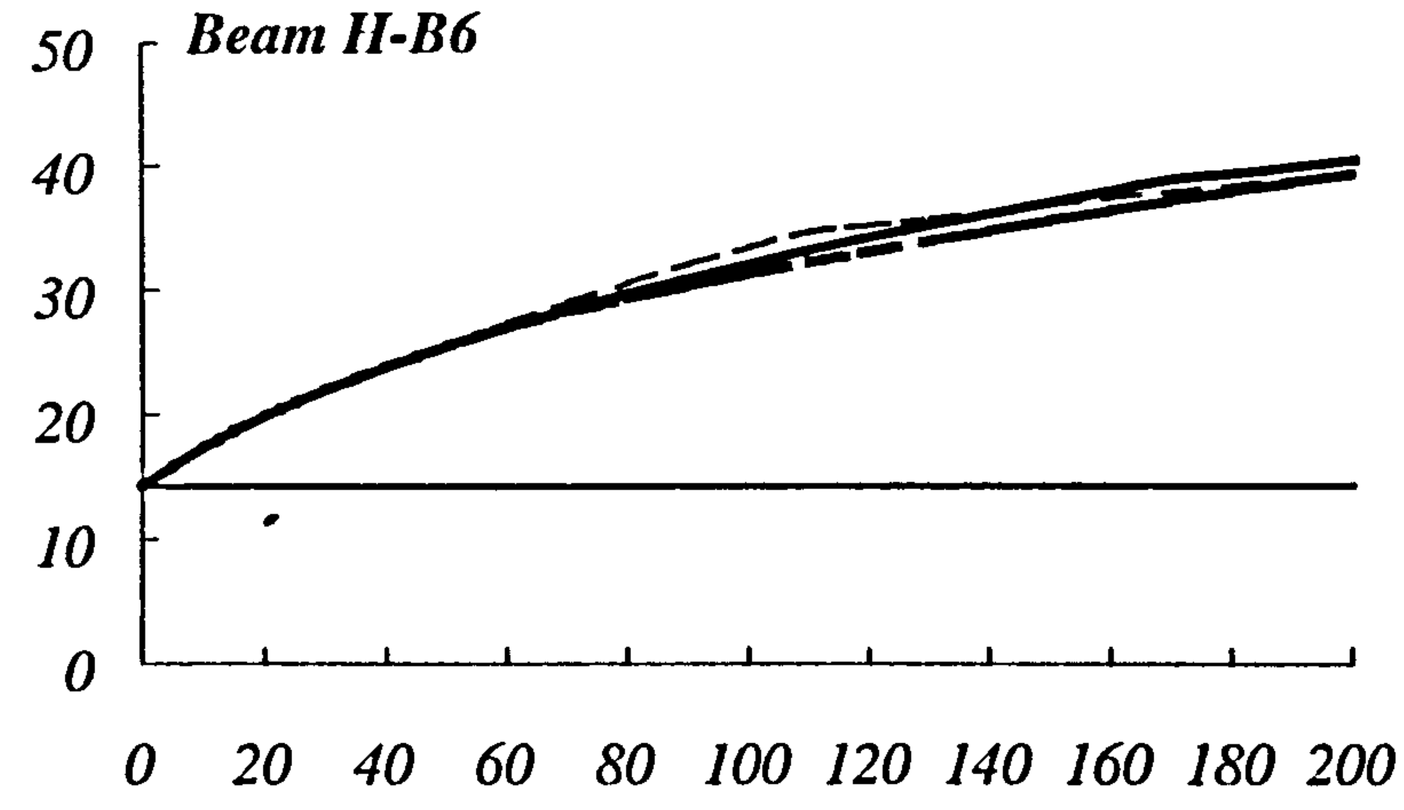

Fig. 6.12 Effect of E_p on the depth of neutral axis for beam *H-B6*.

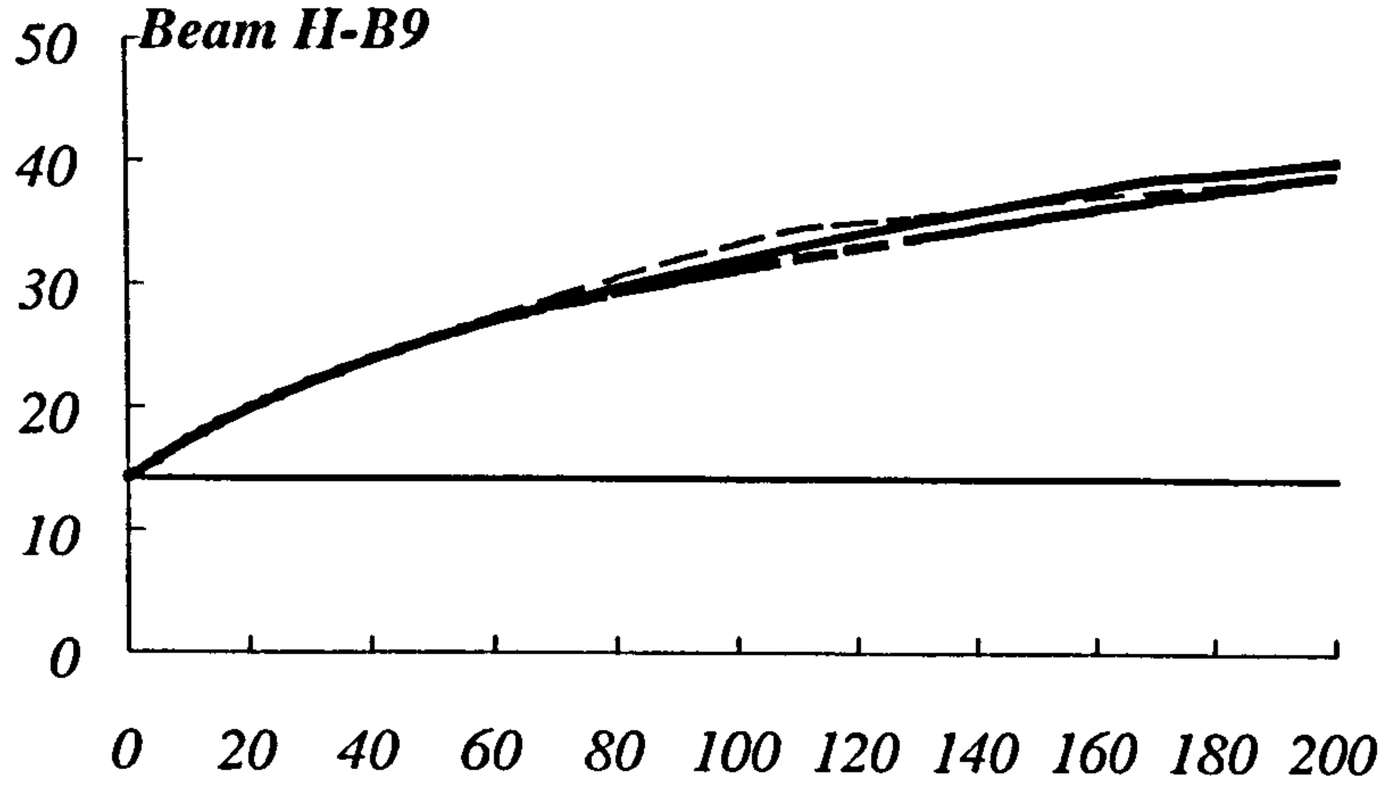

Fig. 6.13 Effect of E_p on the depth of neutral axis for beam *H-B9*.

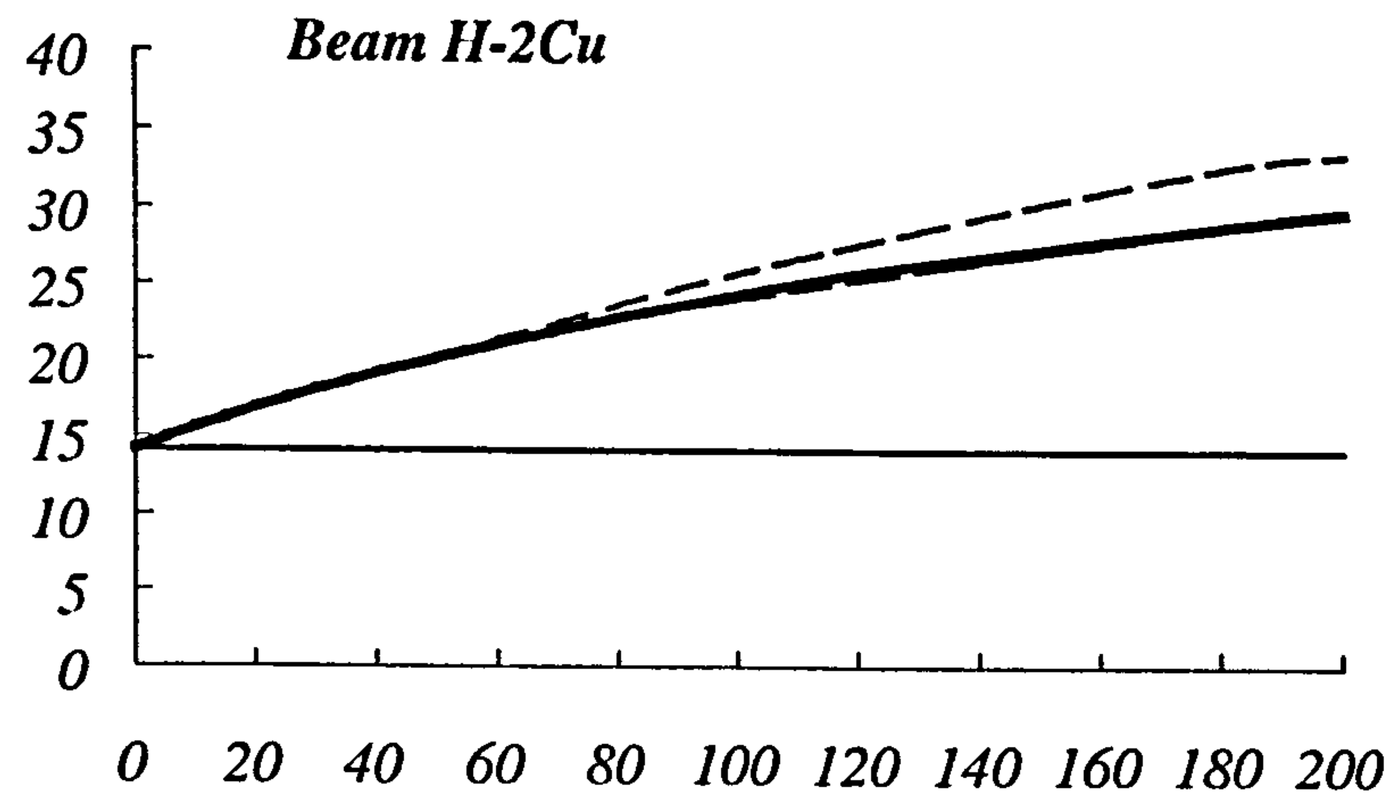

Fig. 6.14 Effect of E_p on the depth of neutral axis for beam *H-2Cu*.

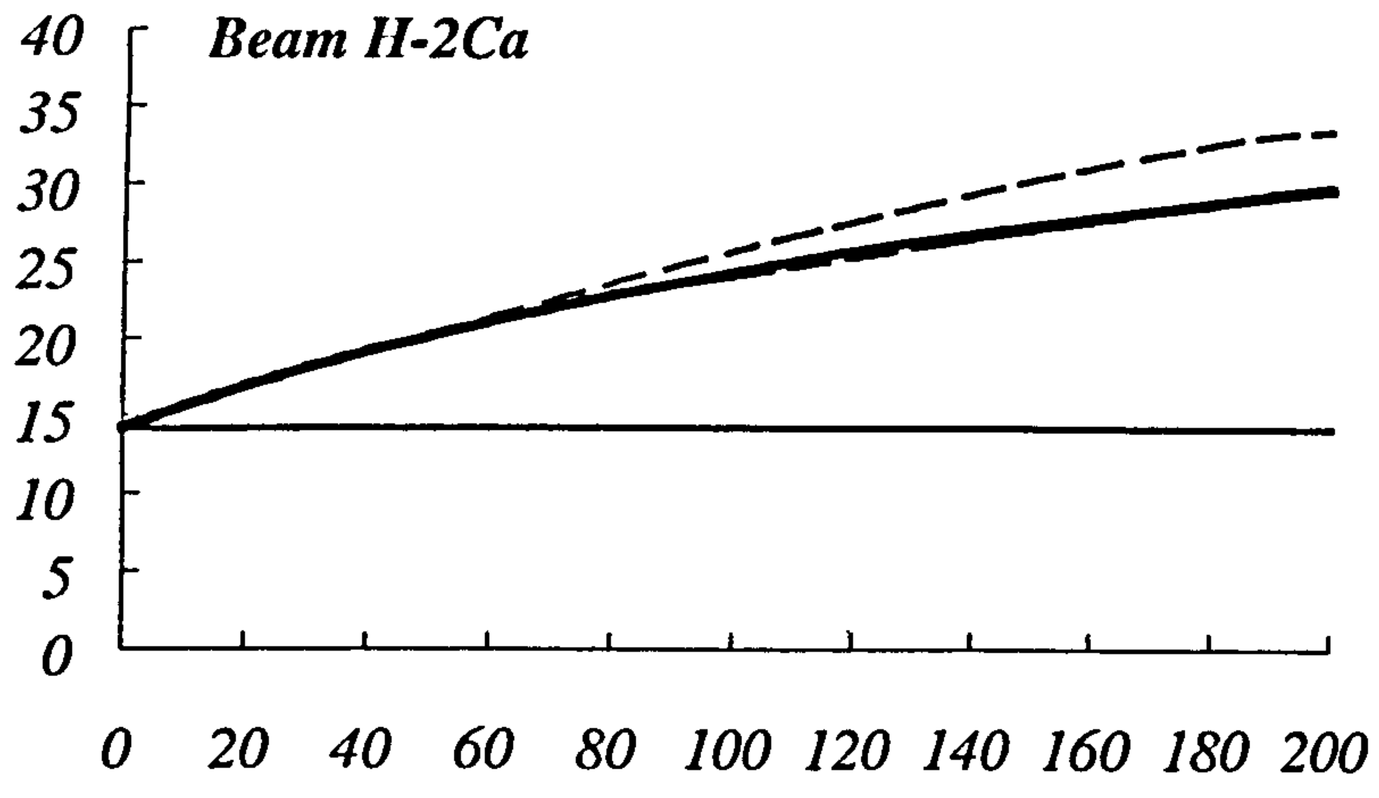

Fig. 6.15 Effect of E_p on the depth of neutral axis for beam *H-2Ca*.

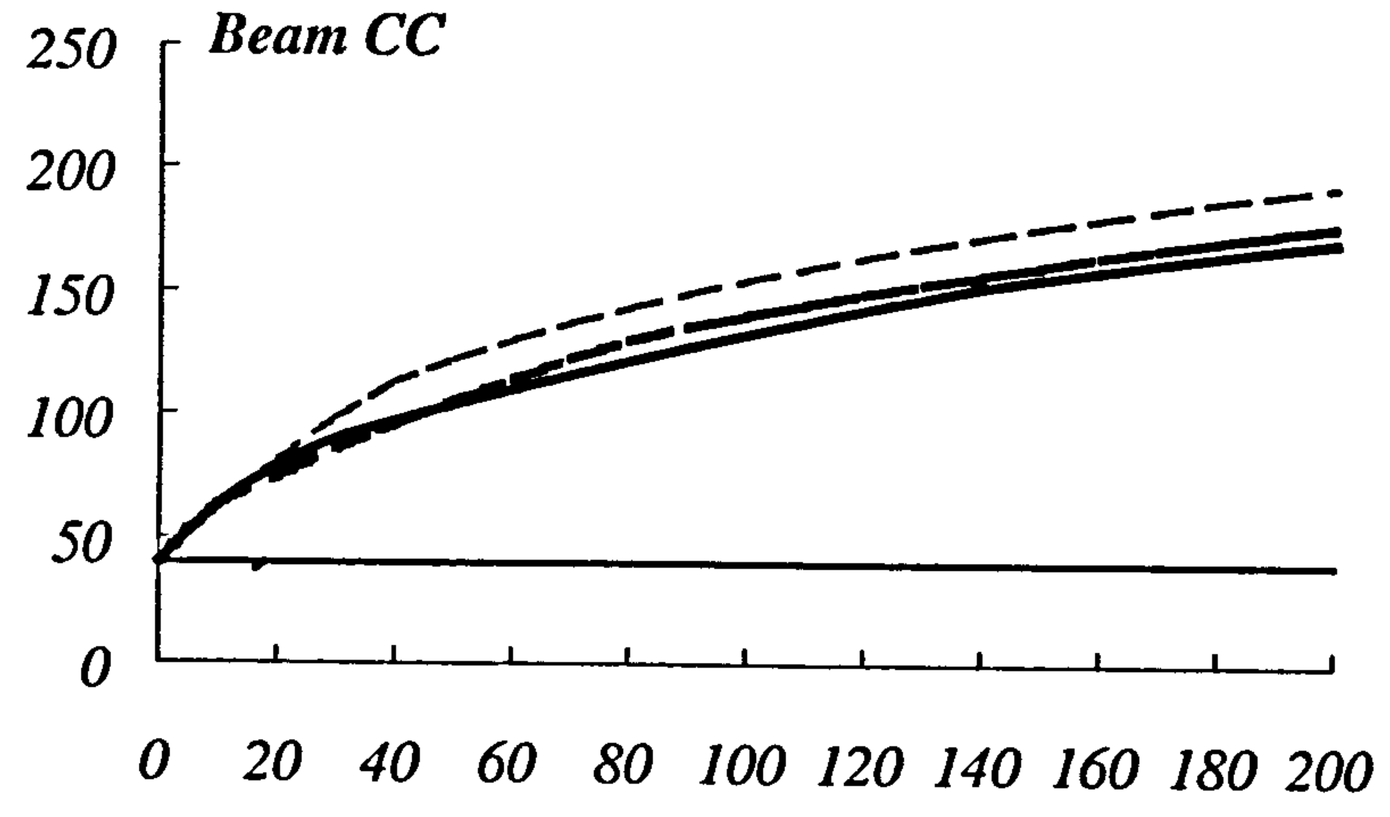

Fig. 6.16 Effect of E_p on the depth of neutral axis for beam *CC*.

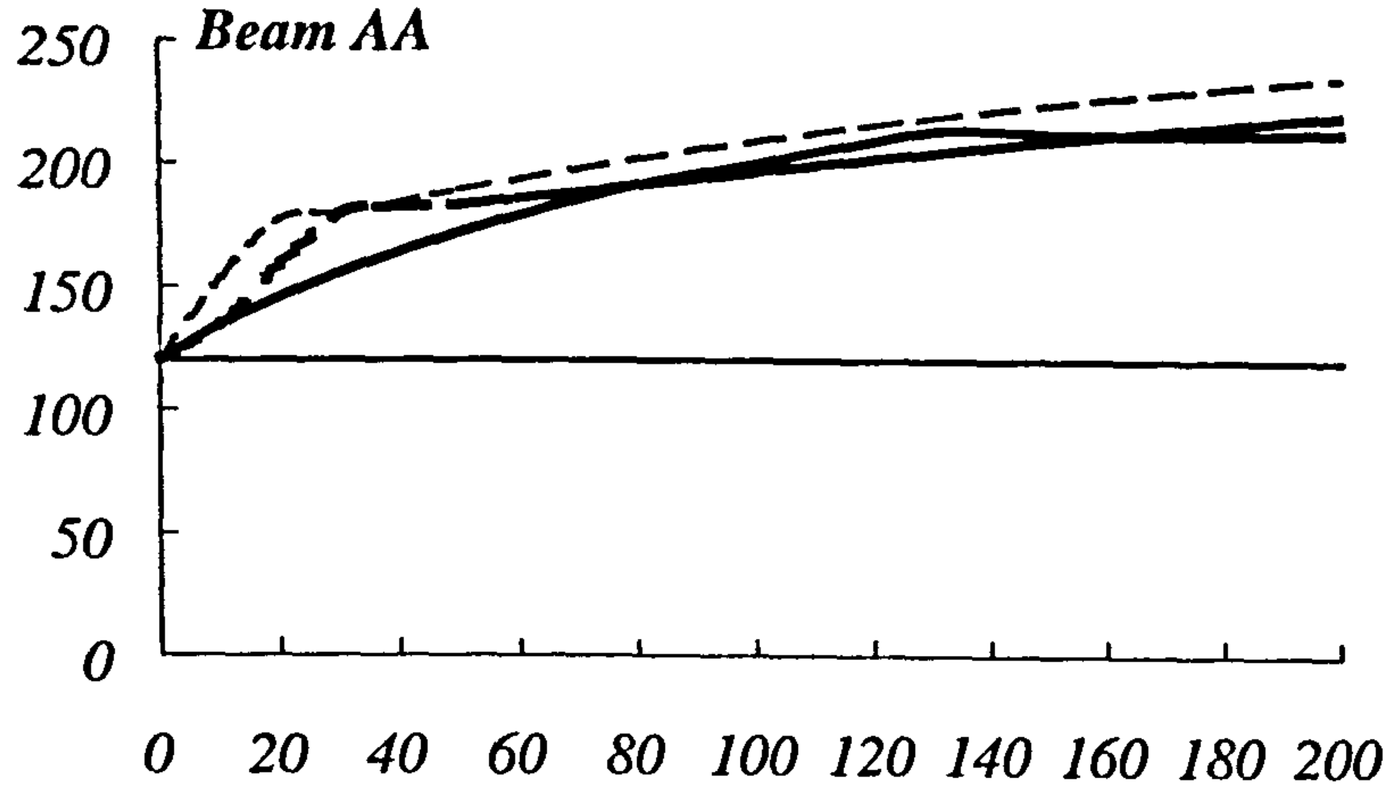

Fig. 6.17 Effect of E_p on the depth of neutral axis for beam *AA*.

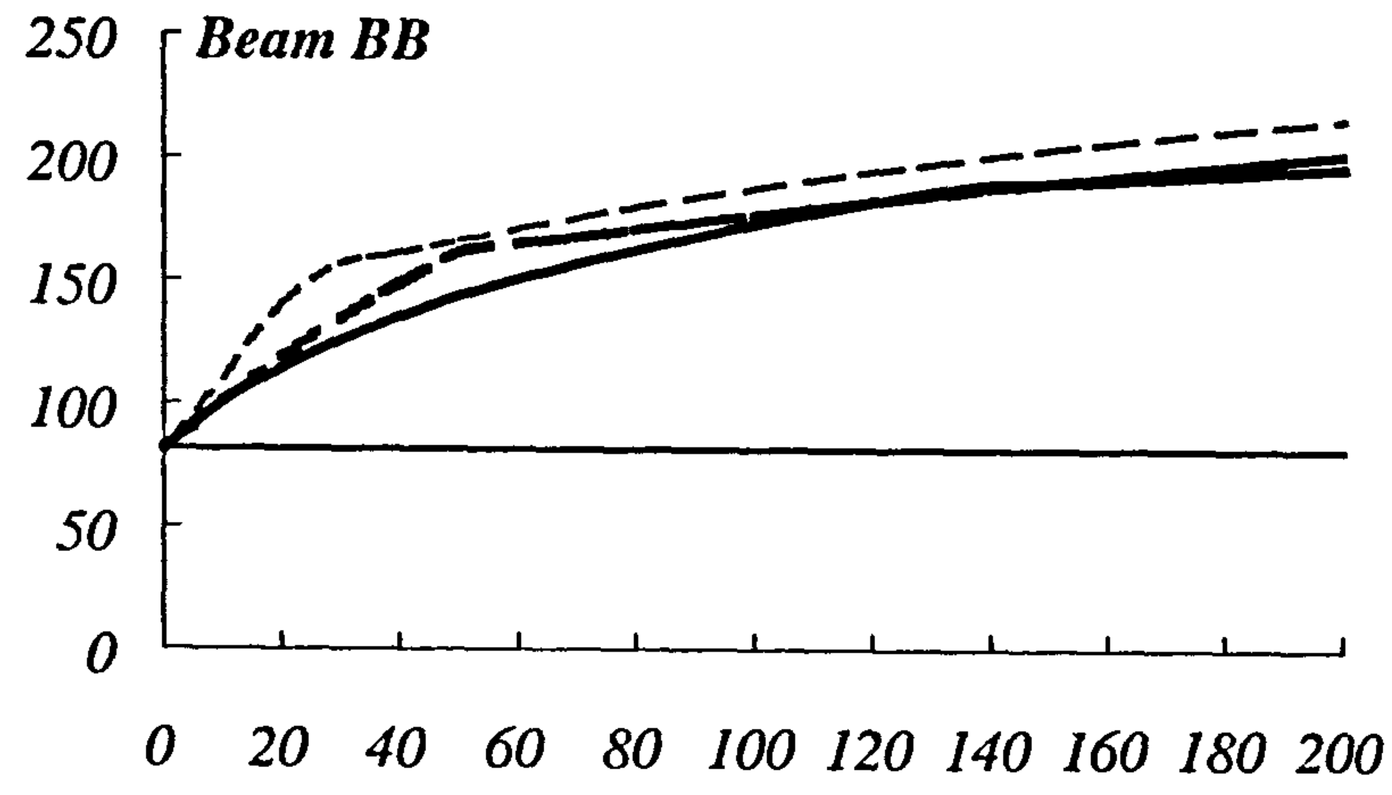

Fig. 6.18 Effect of E_p on the depth of neutral axis for beam *BB*.

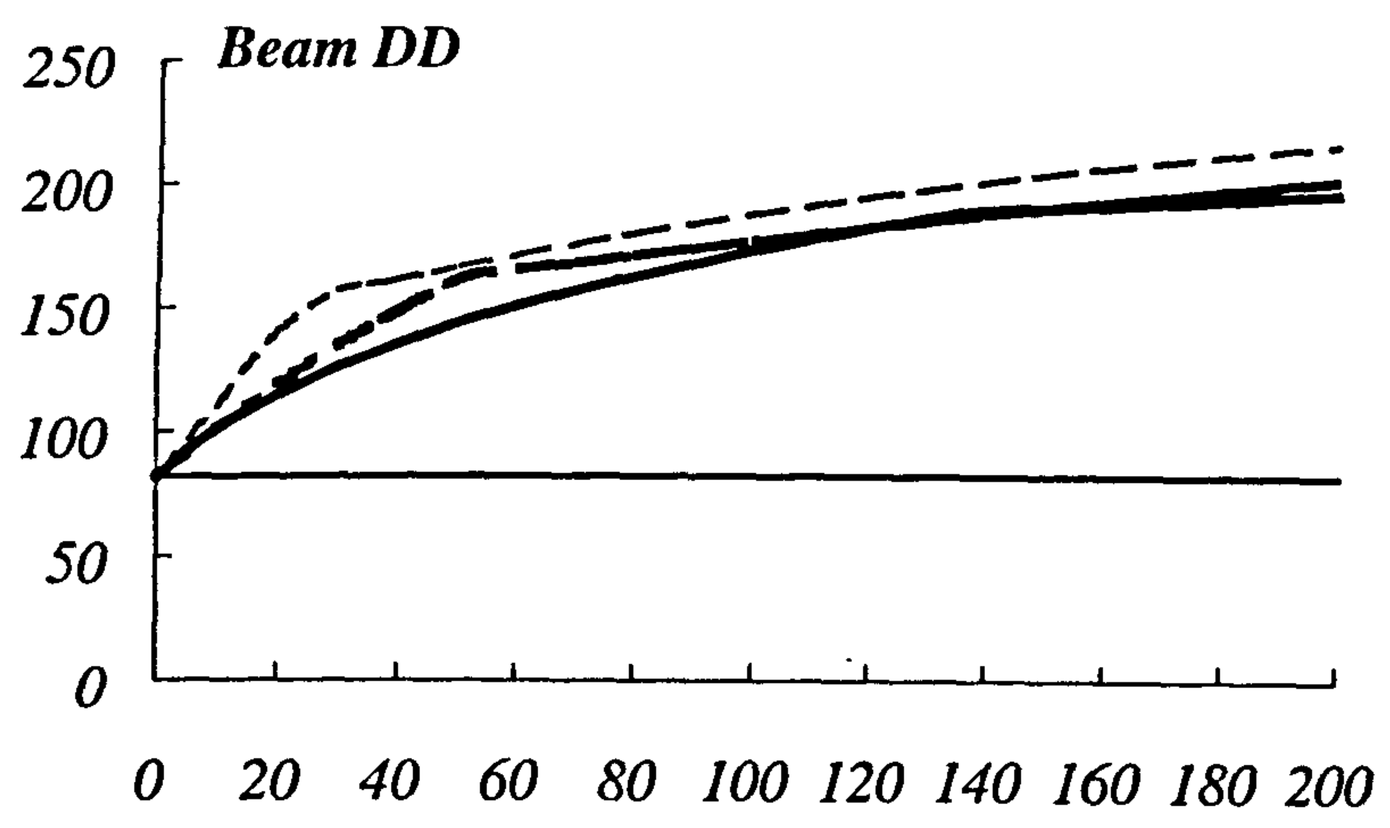

Fig. 6.19 Effect of E_p on the depth of neutral axis for beam *DD*.

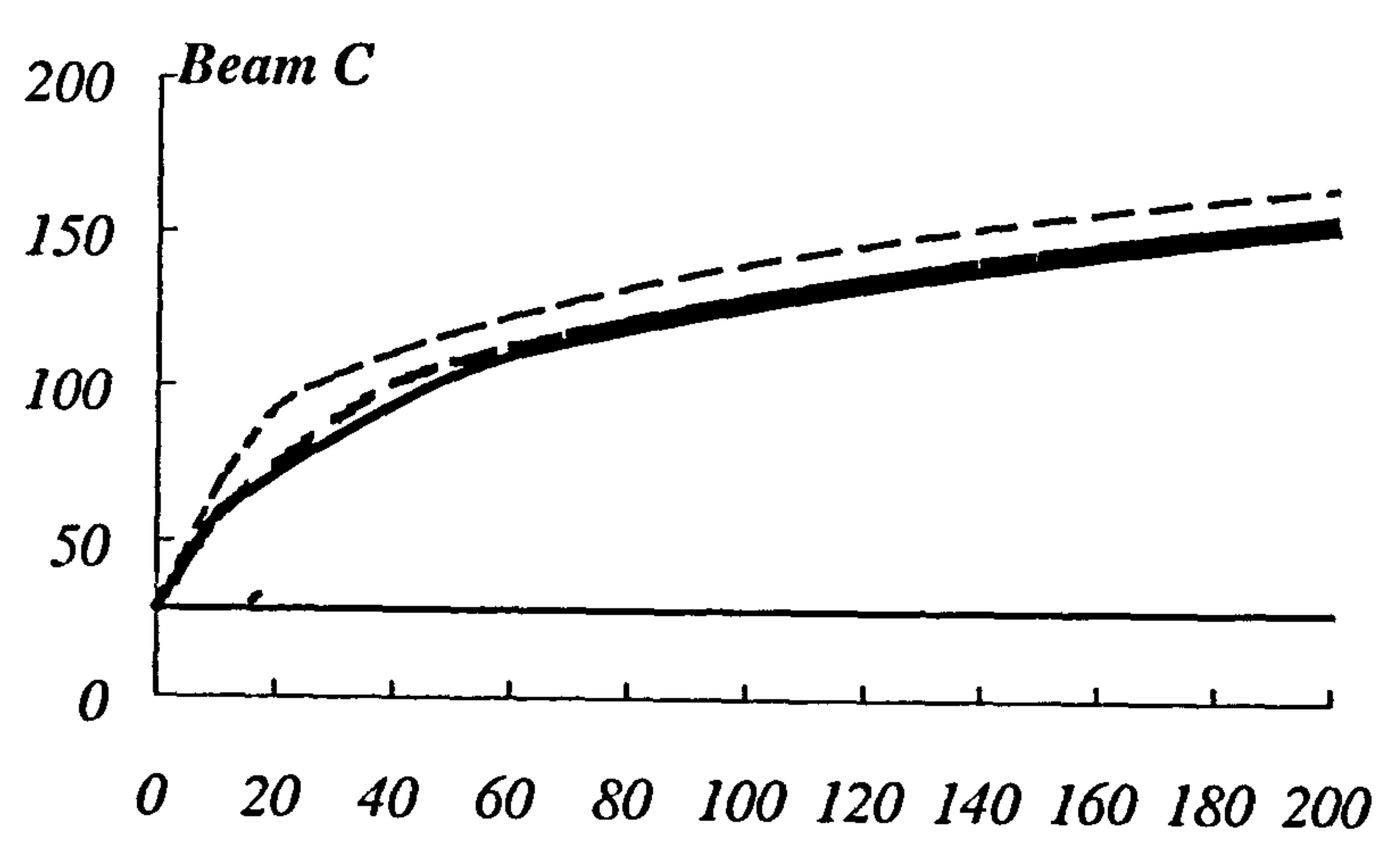

Fig. 6.20 Effect of E_p on the depth of neutral axis for beam *C*.

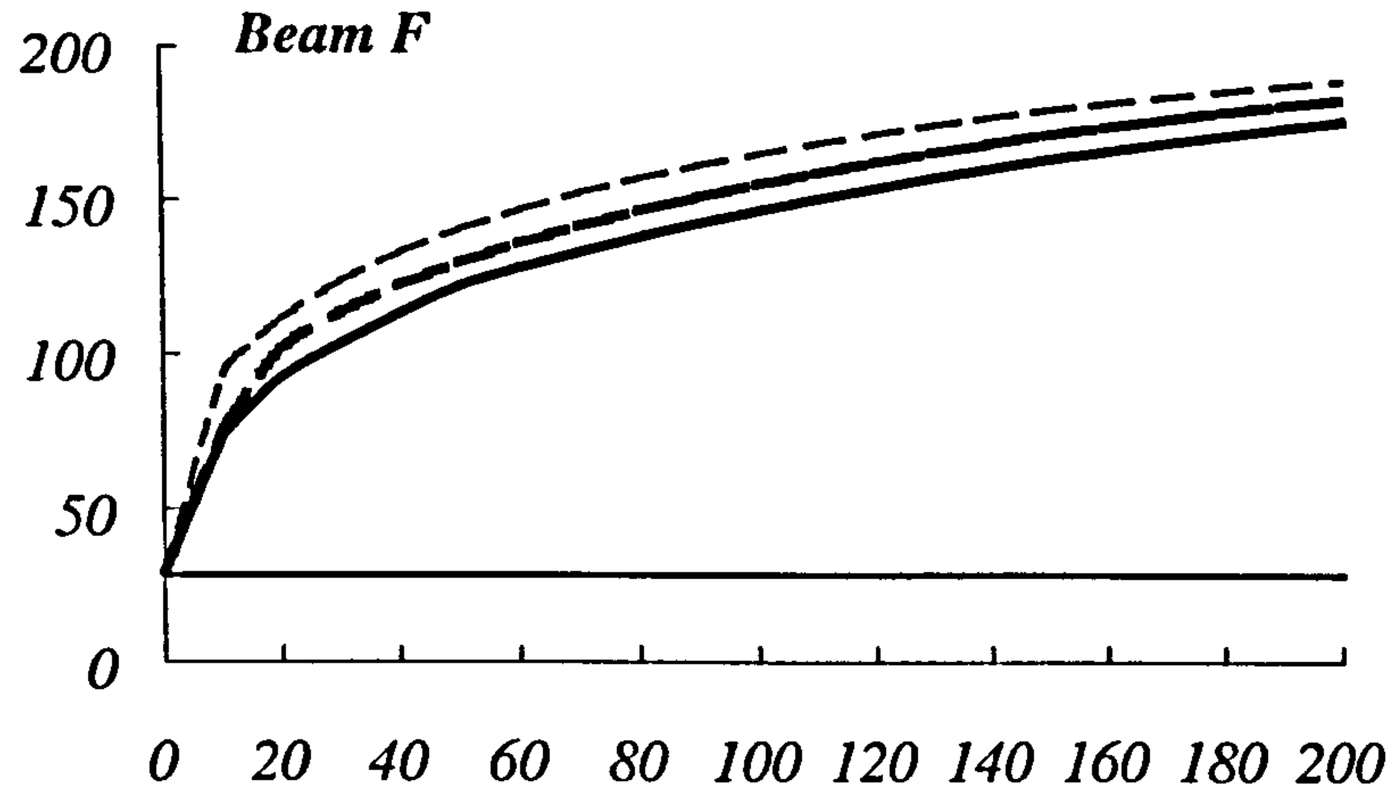

Fig. 6.21 Effect of E_p on the depth of neutral axis for beam *F*.

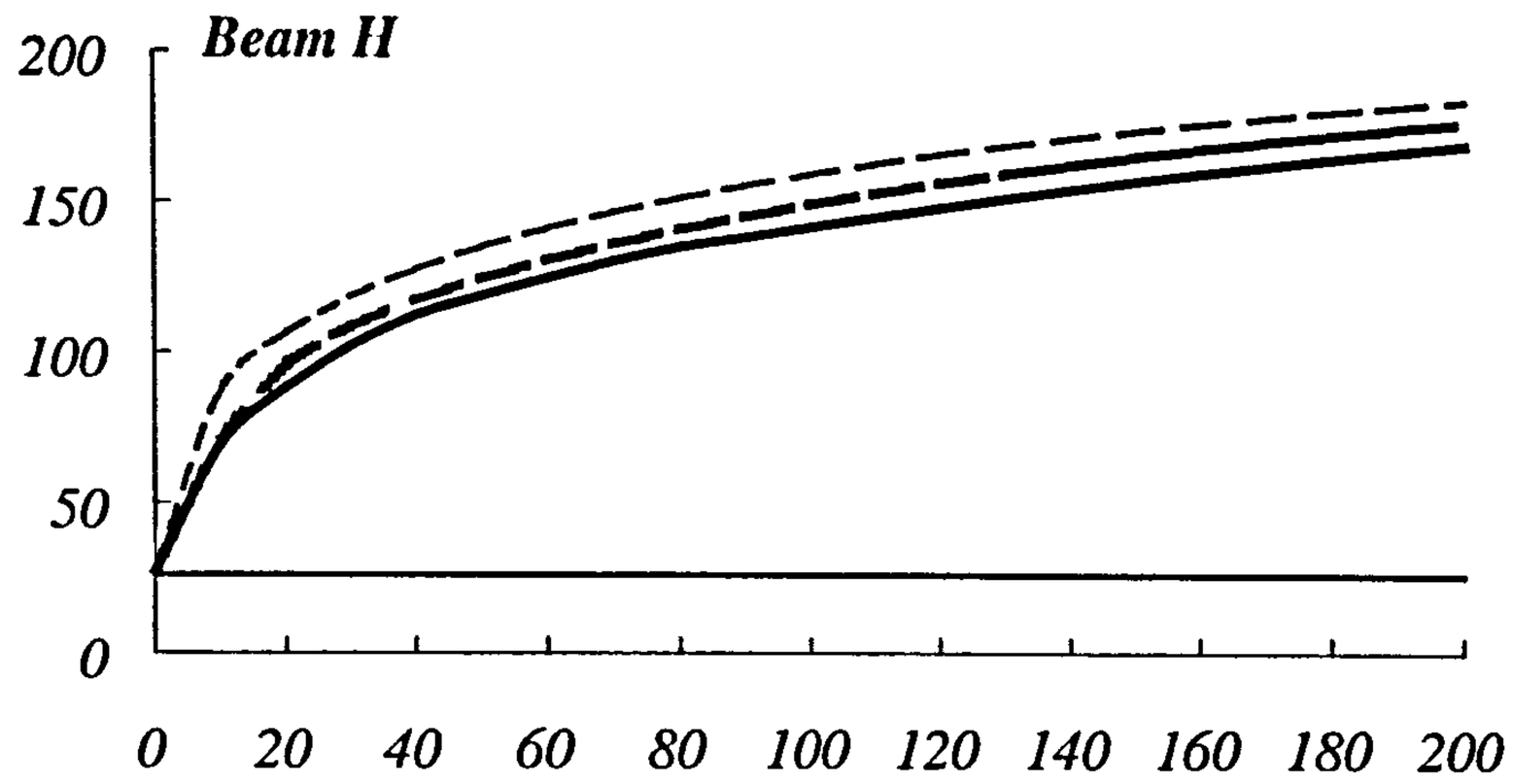

Fig. 6.22 Effect of E_p on the depth of neutral axis for beam *H*.

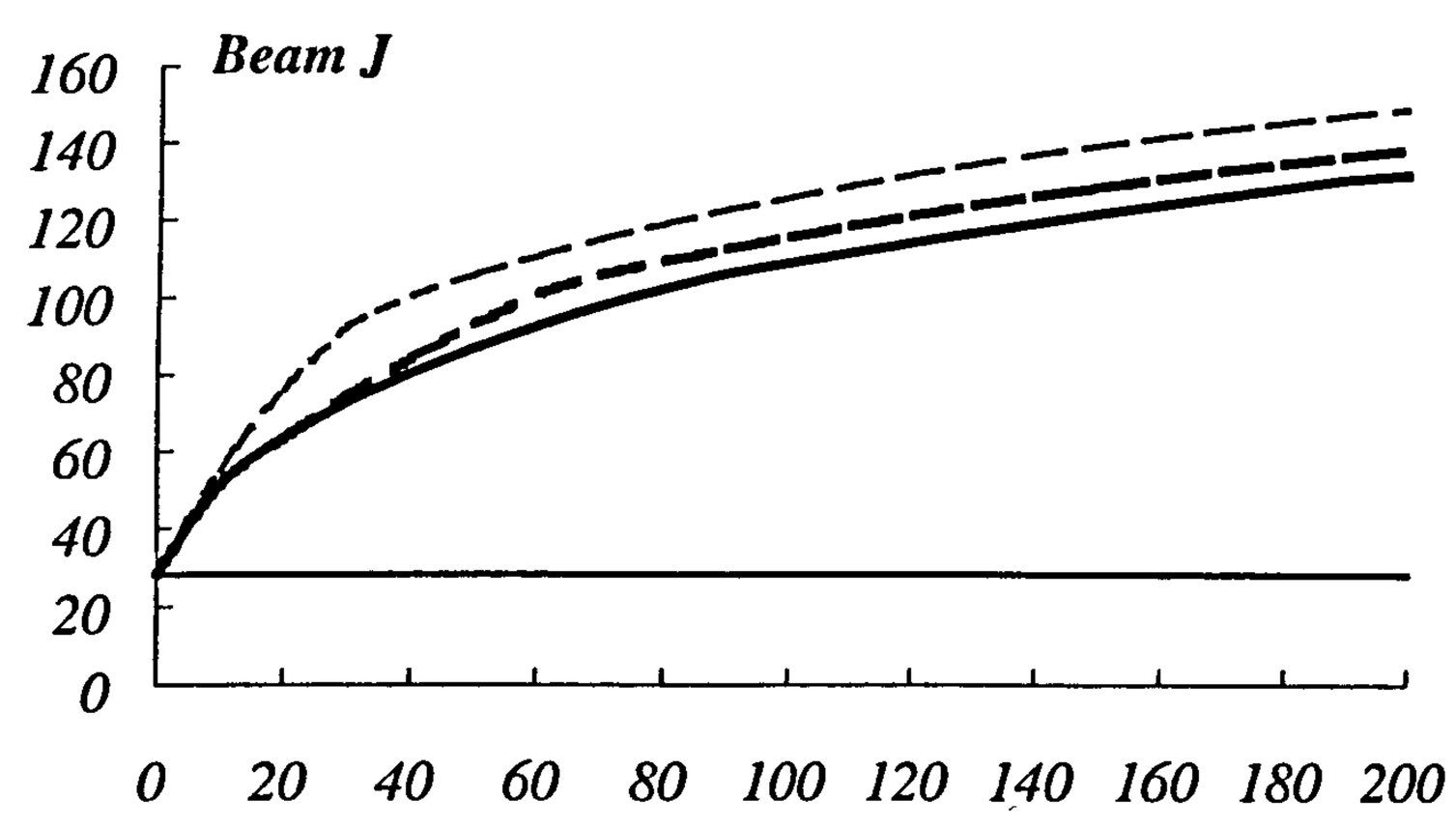

Fig. 6.23 Effect of E_p on the depth of neutral axis for beam *J*.

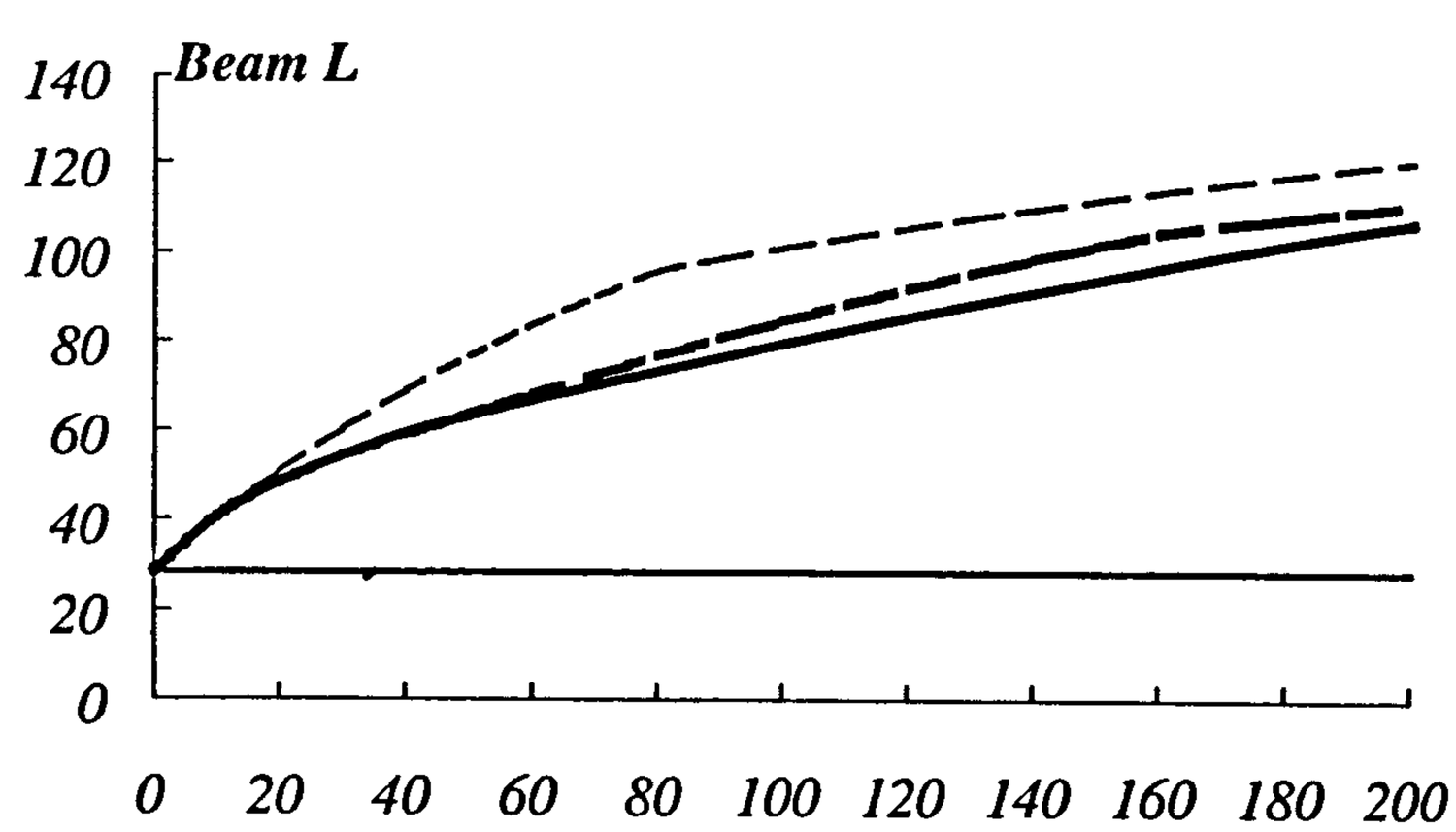

Fig. 6.24 Effect of E_p on the depth of neutral axis for beam *L*.

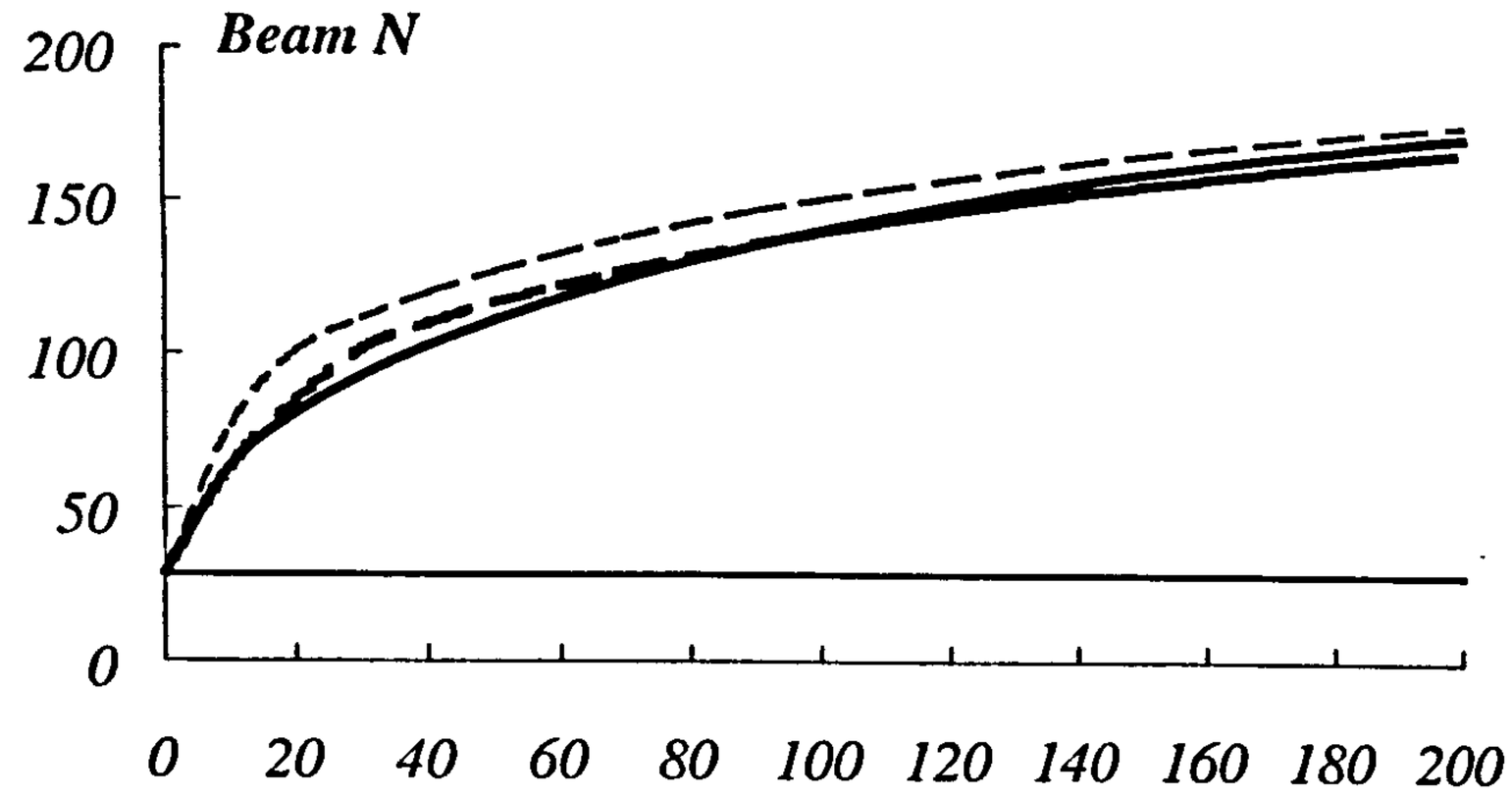

Fig. 6.25 Effect of E_p on the depth of neutral axis for beam *N*.

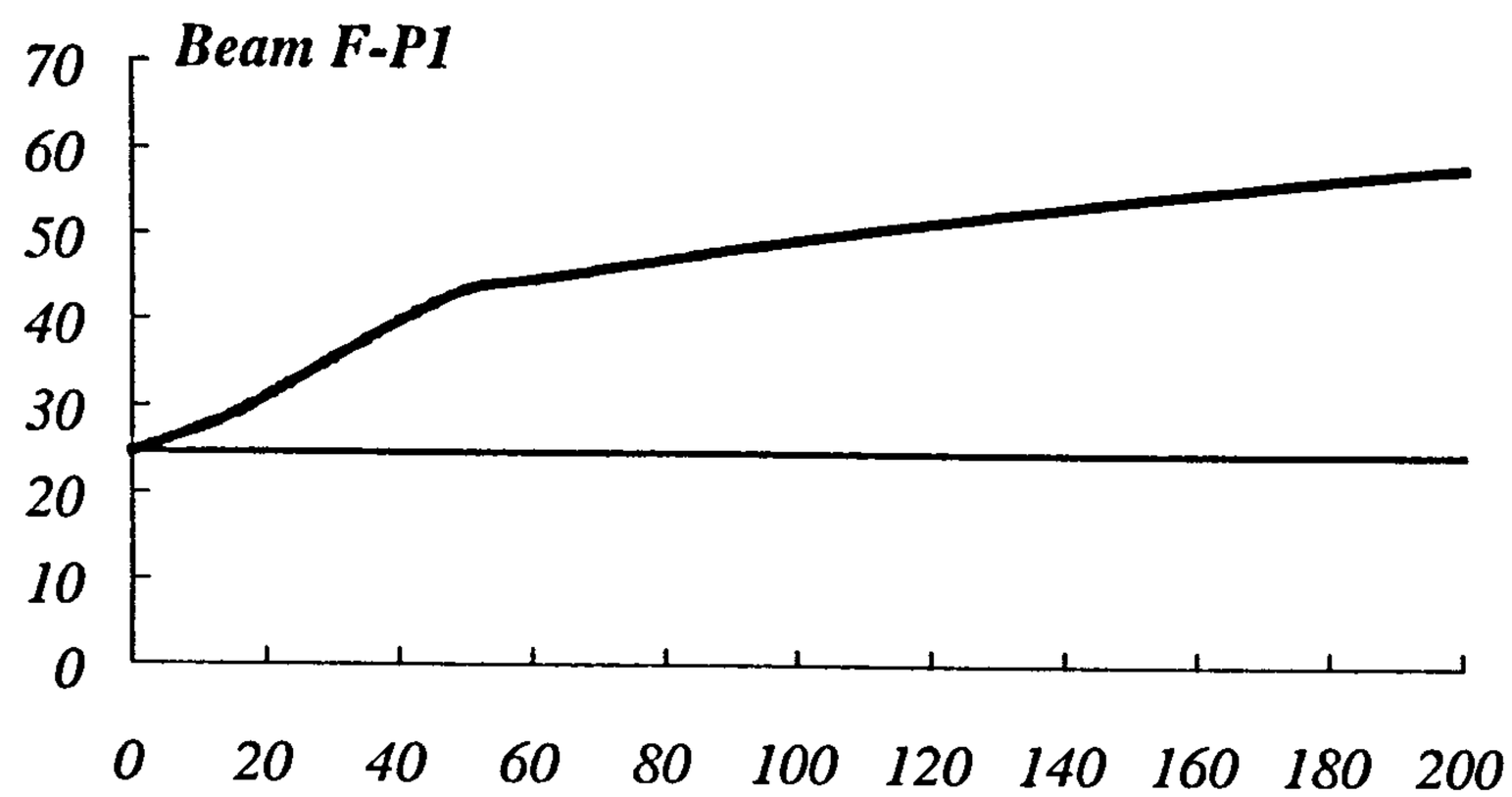

Fig. 6.26 Effect of E_p on the depth of neutral axis for beam *F-P1*.

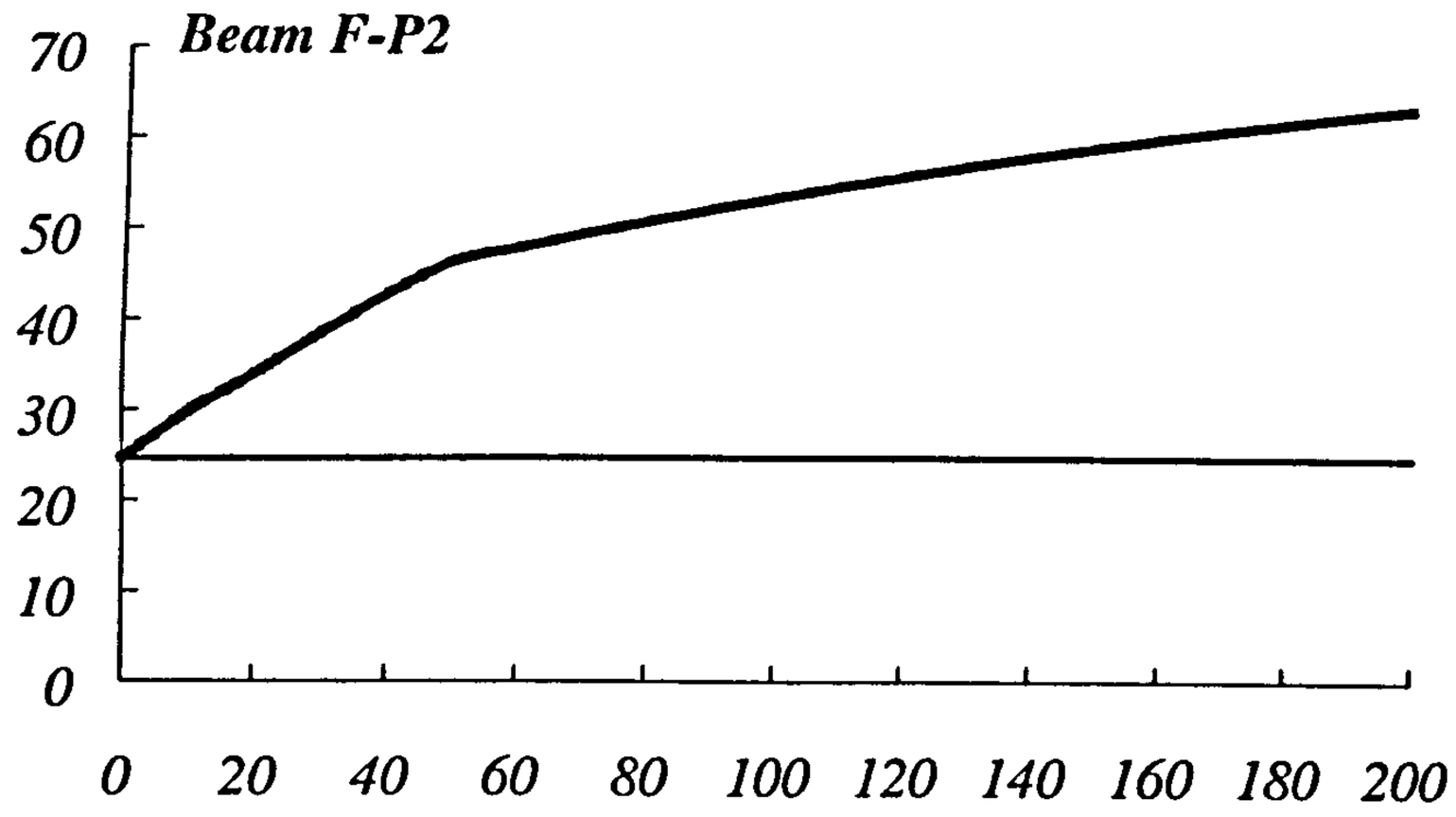

Fig. 6.27 Effect of E_p on the depth of neutral axis for beam *F-P2*.

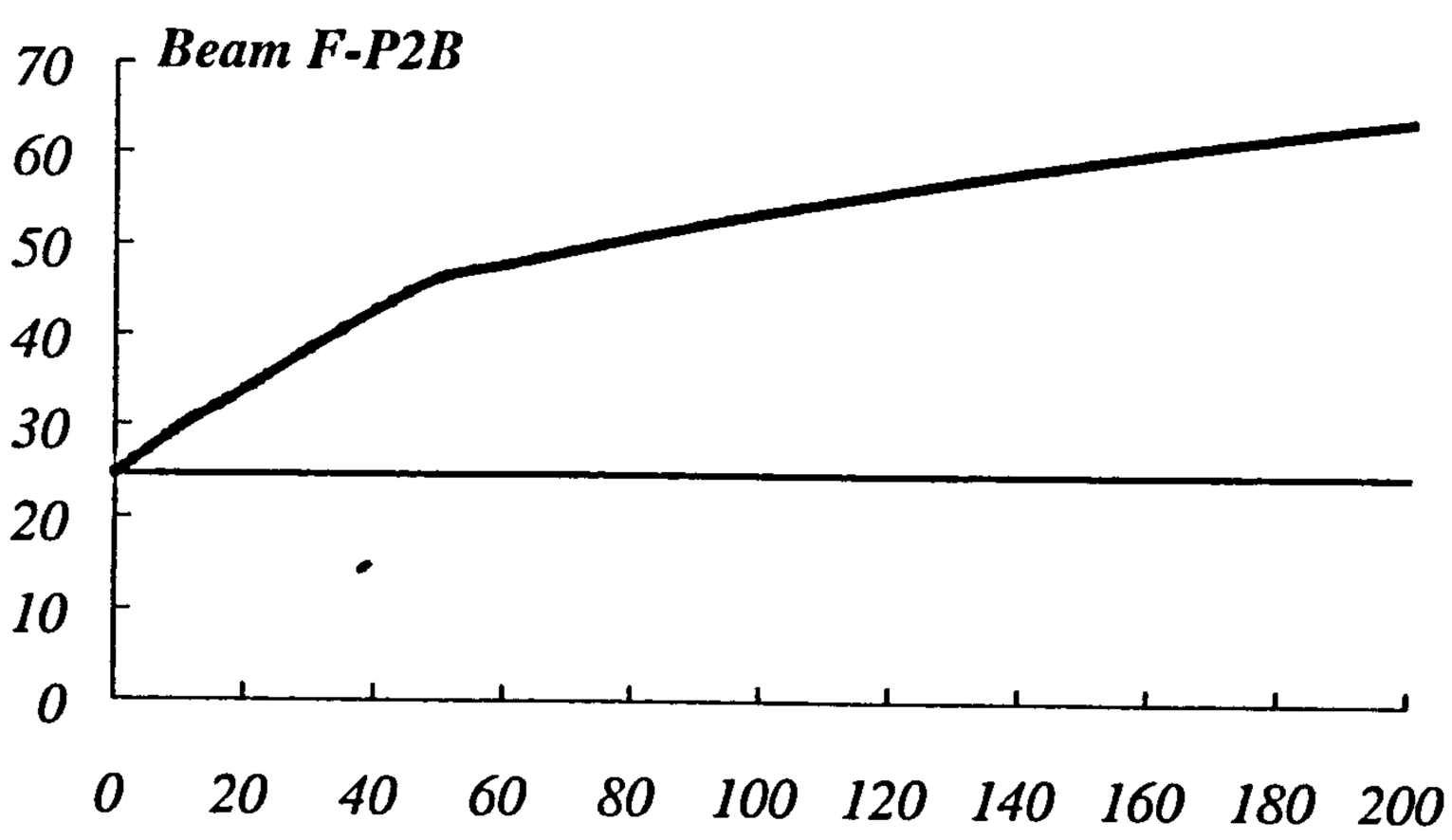

Fig. 6.28 Effect of E_p on the depth of neutral axis for beam *F-P2B*.

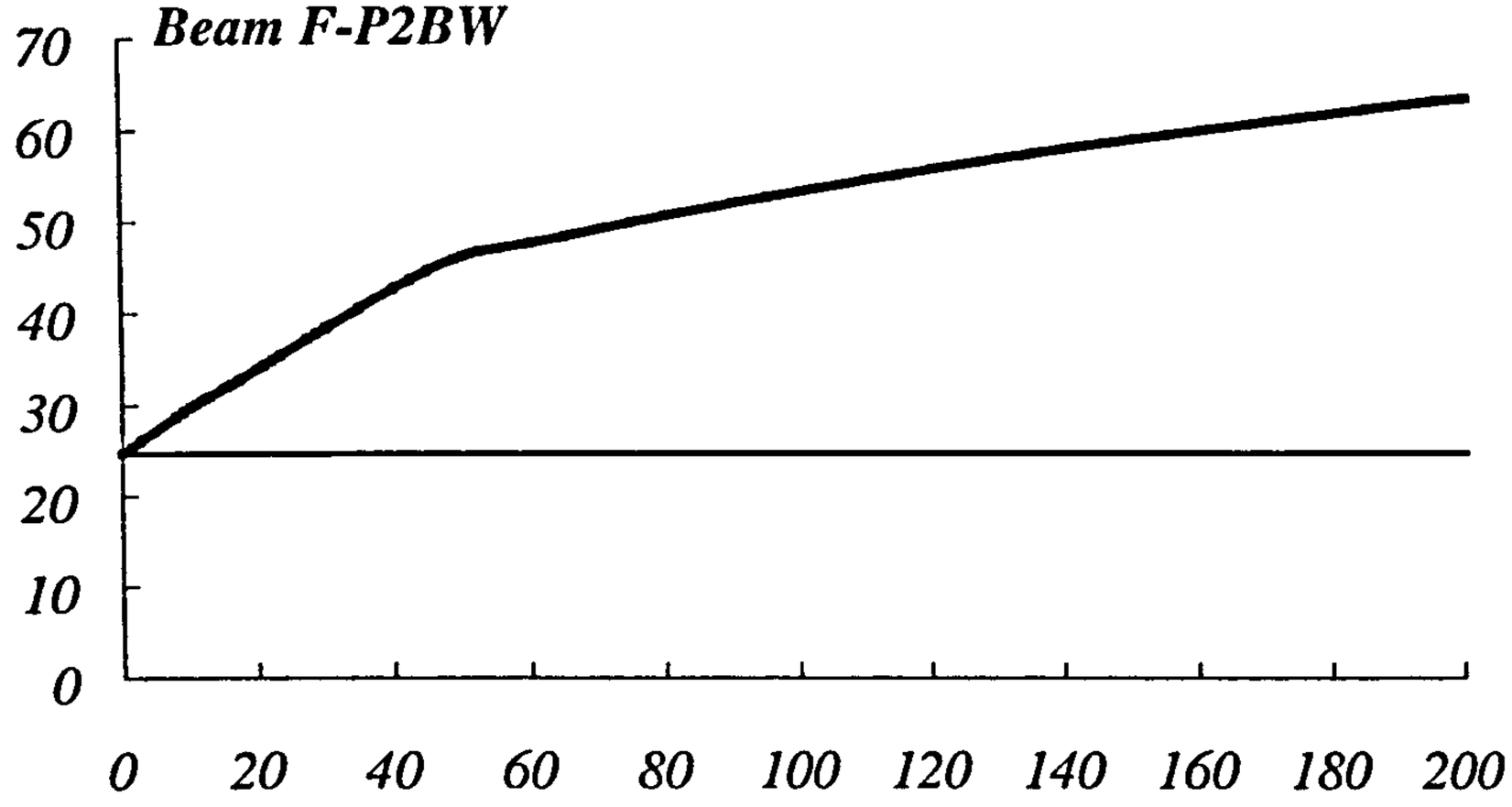

Fig. 6.29 Effect of E_p on the depth of neutral axis for beam *F-P2BW*.

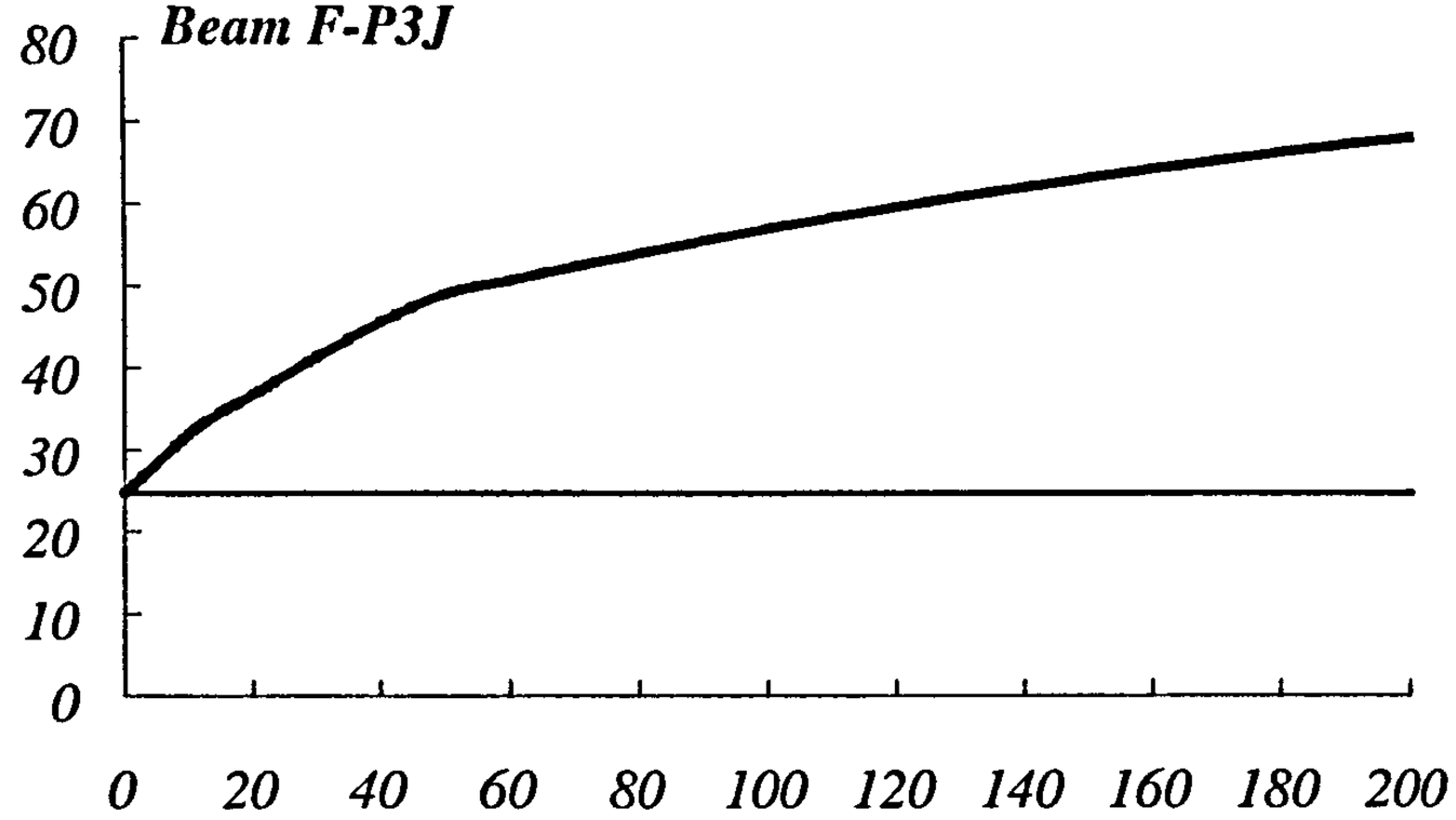

Fig. 6.30 Effect of E_p on the depth of neutral axis for beam *F-P3J*.

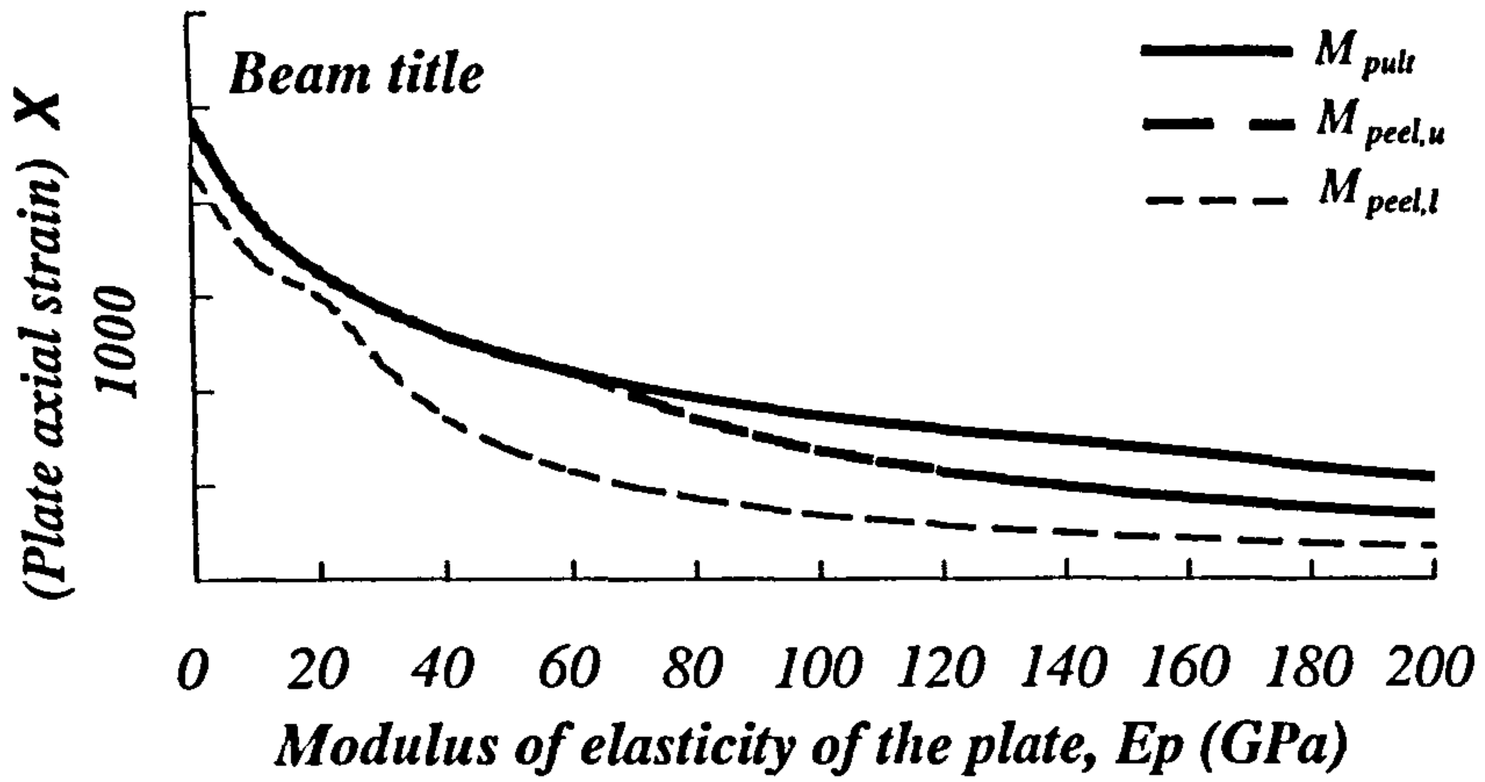

Fig. 6.31 Effect of increasing the plate modulus of elasticity, E_p, on the axial strain of the externally bonded plate (typical legends for Figs 6.32 to 6.52).

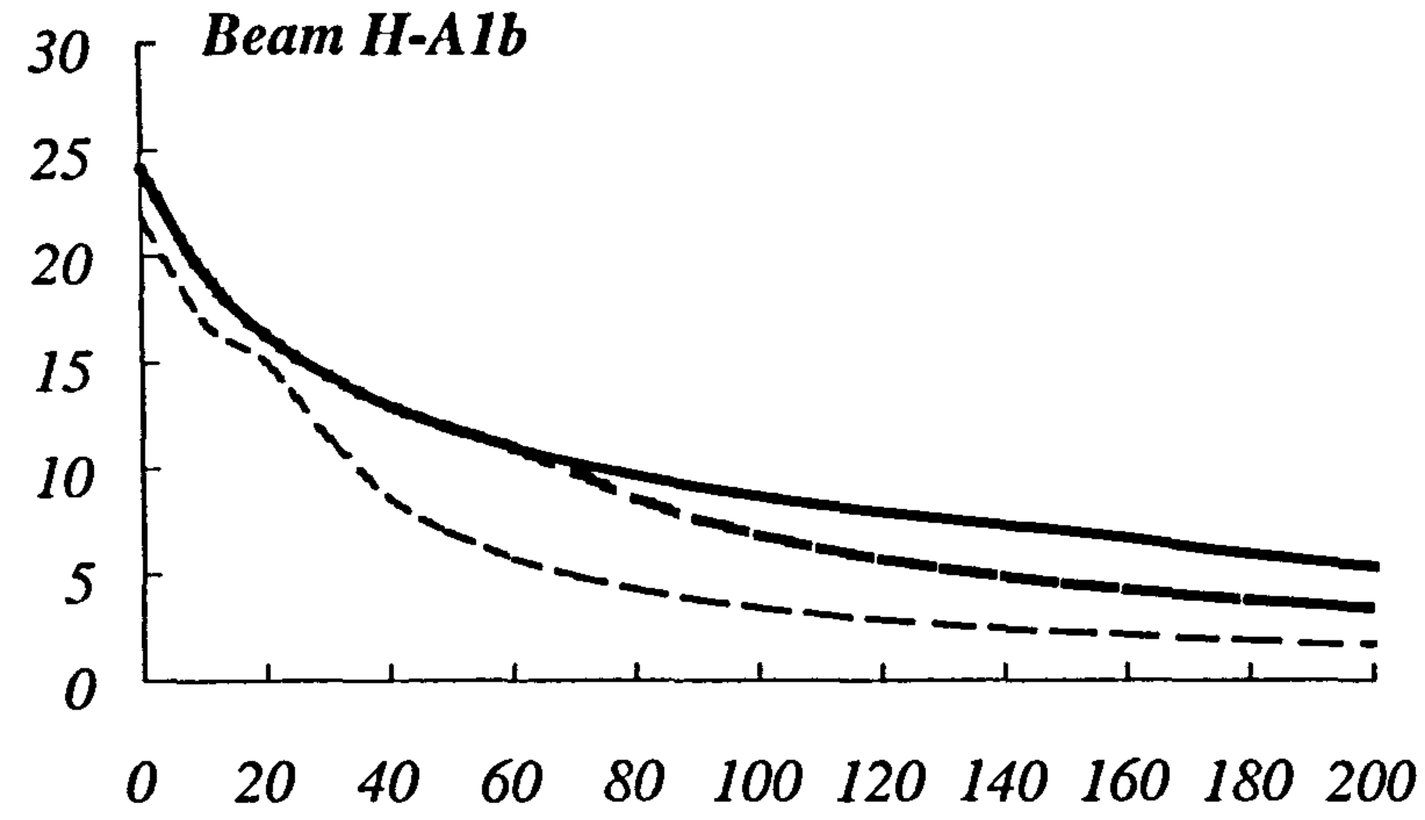

Fig. 6.32 Effect of E_p on the plate axial strain for beam *H-A1b*.

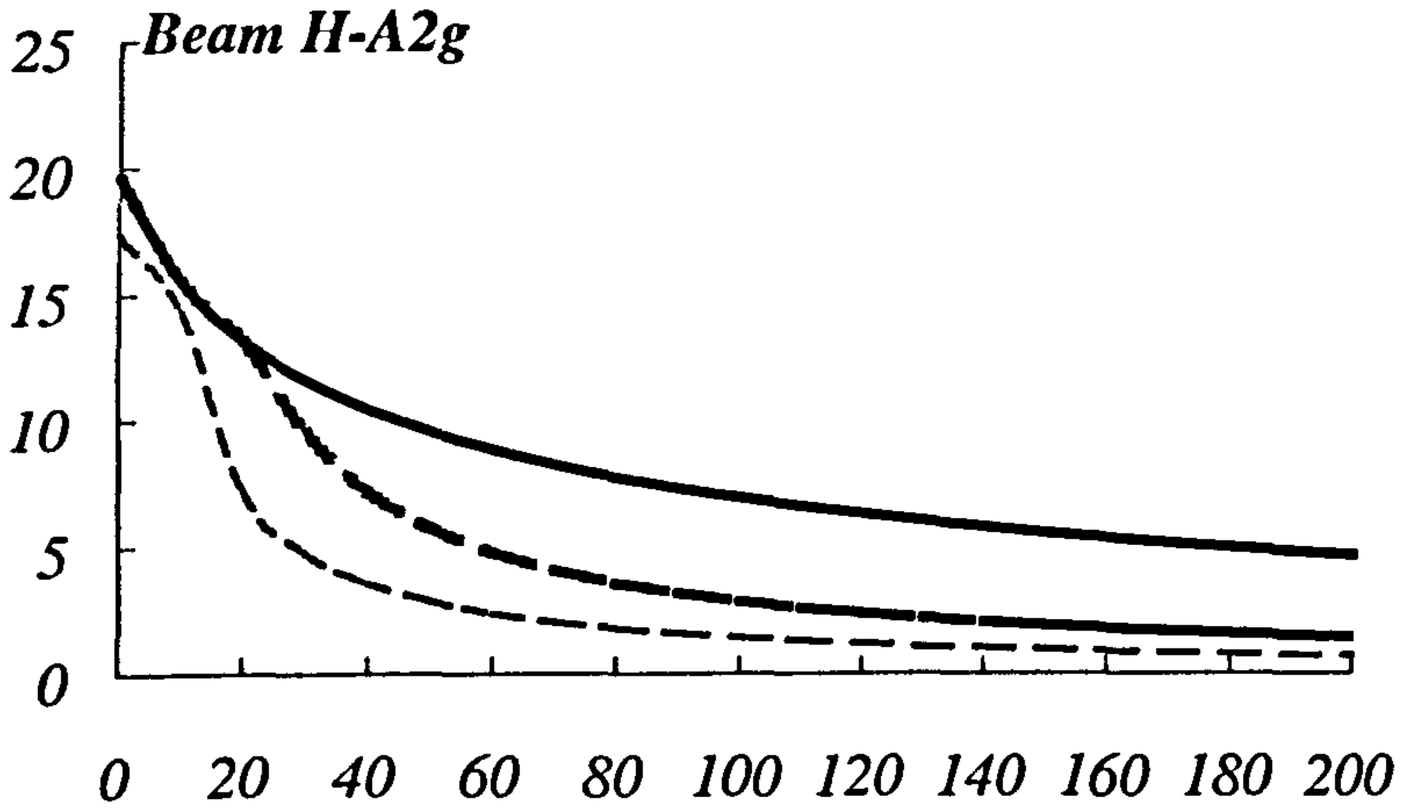

Fig. 6.33 Effect of E_p on the plate axial strain for beam *H-A2g*.

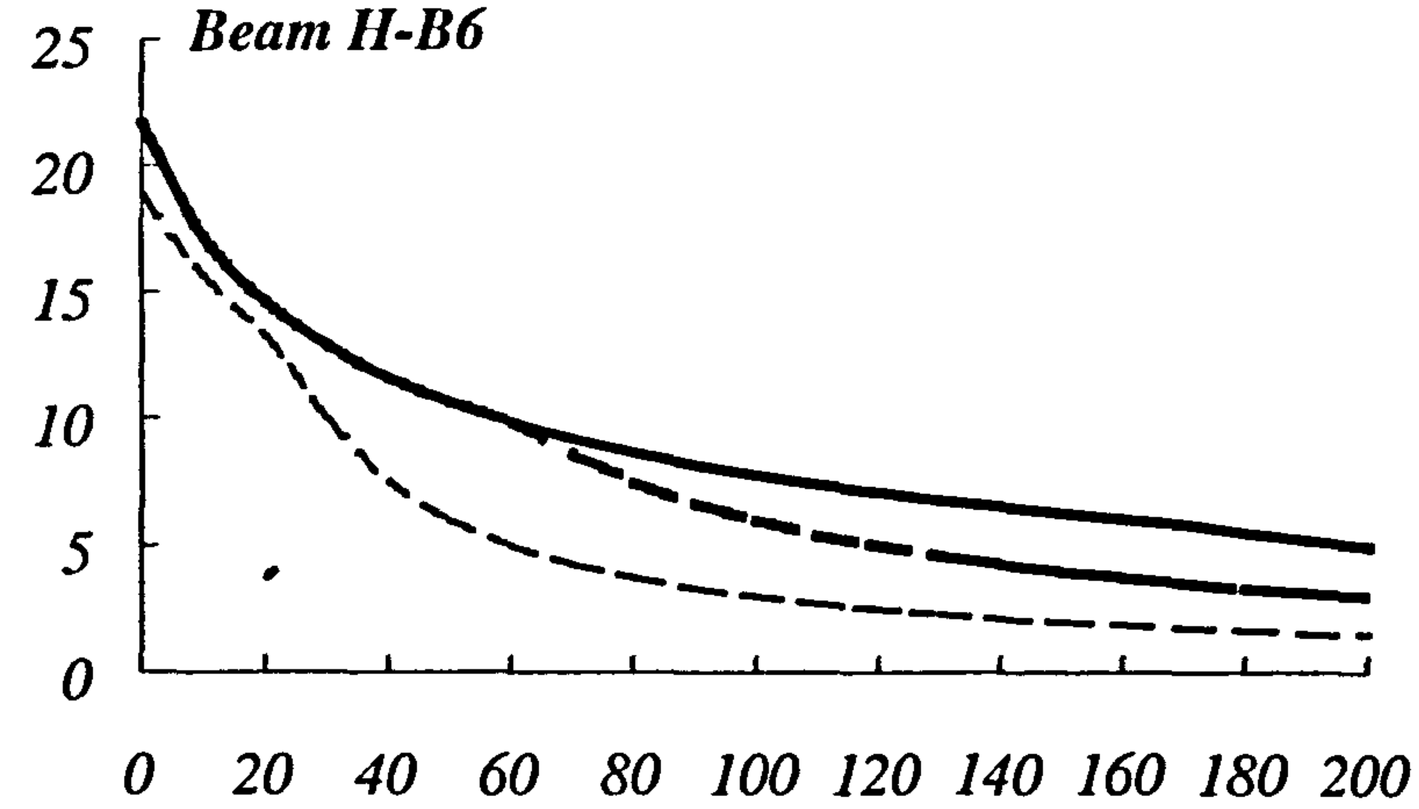

Fig. 6.34 Effect of E_p on the plate axial strain for beam *H-B6*.

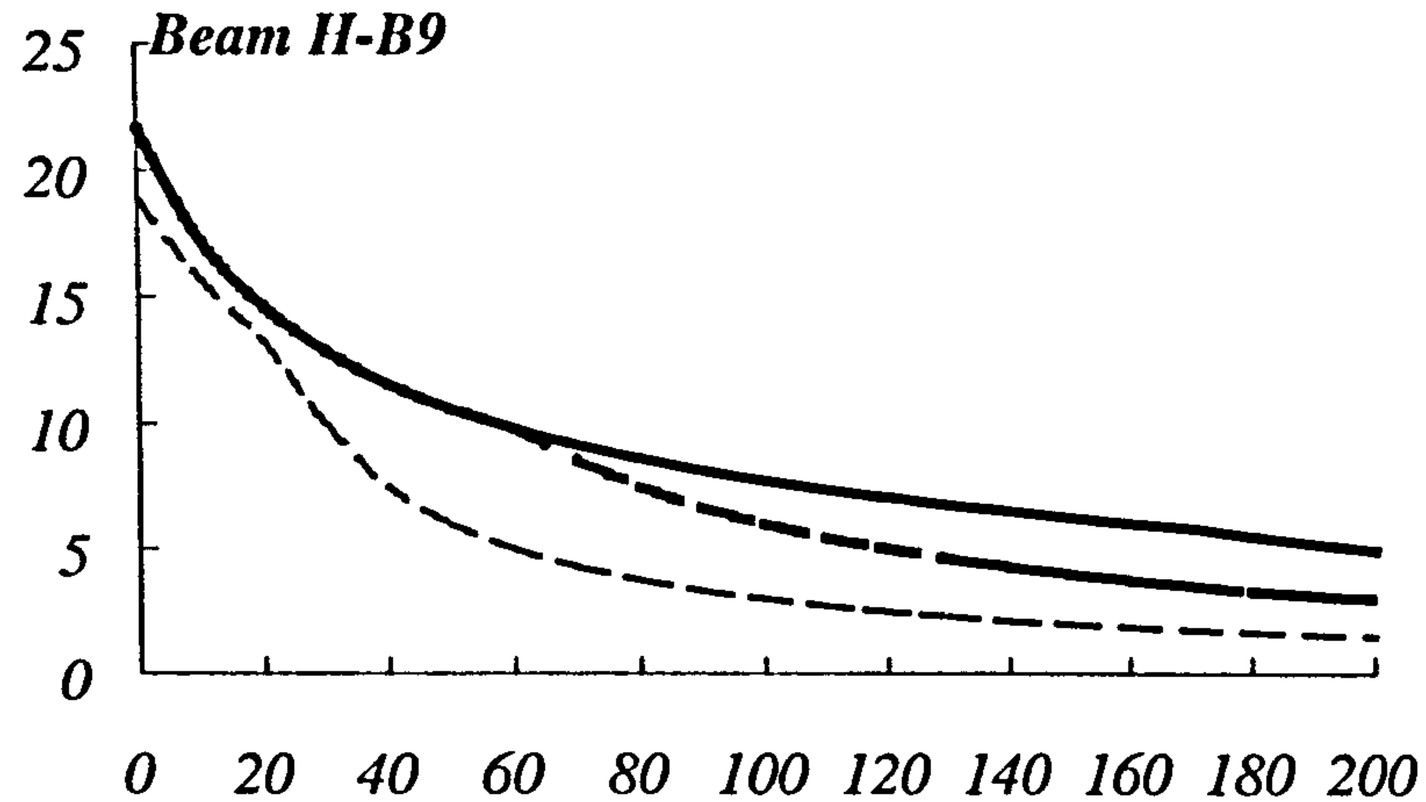

Fig. 6.35 Effect of E_p on the plate axial strain for beam *H-B9*.

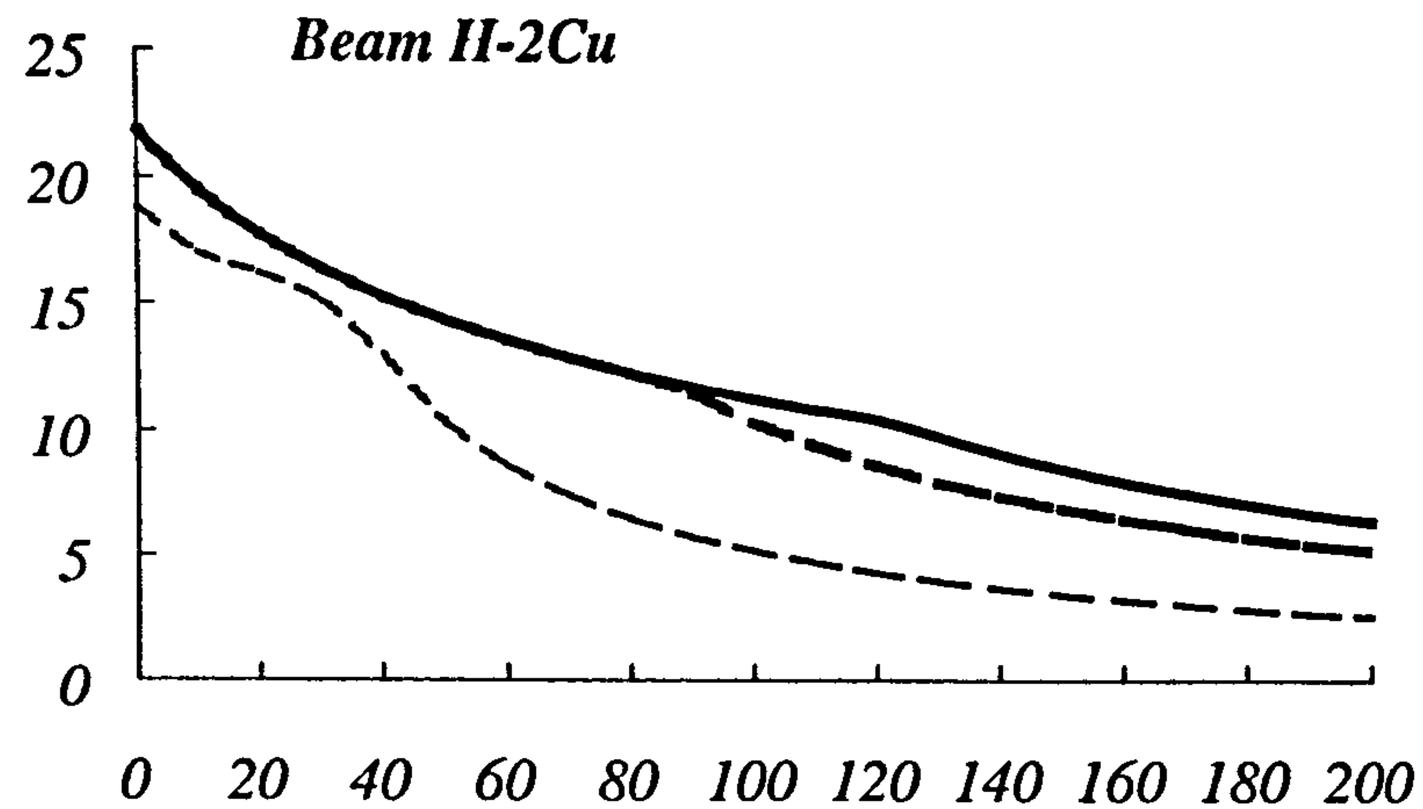

Fig. 6.36 Effect of E_p on the plate axial strain for beam *H-2Cu*.

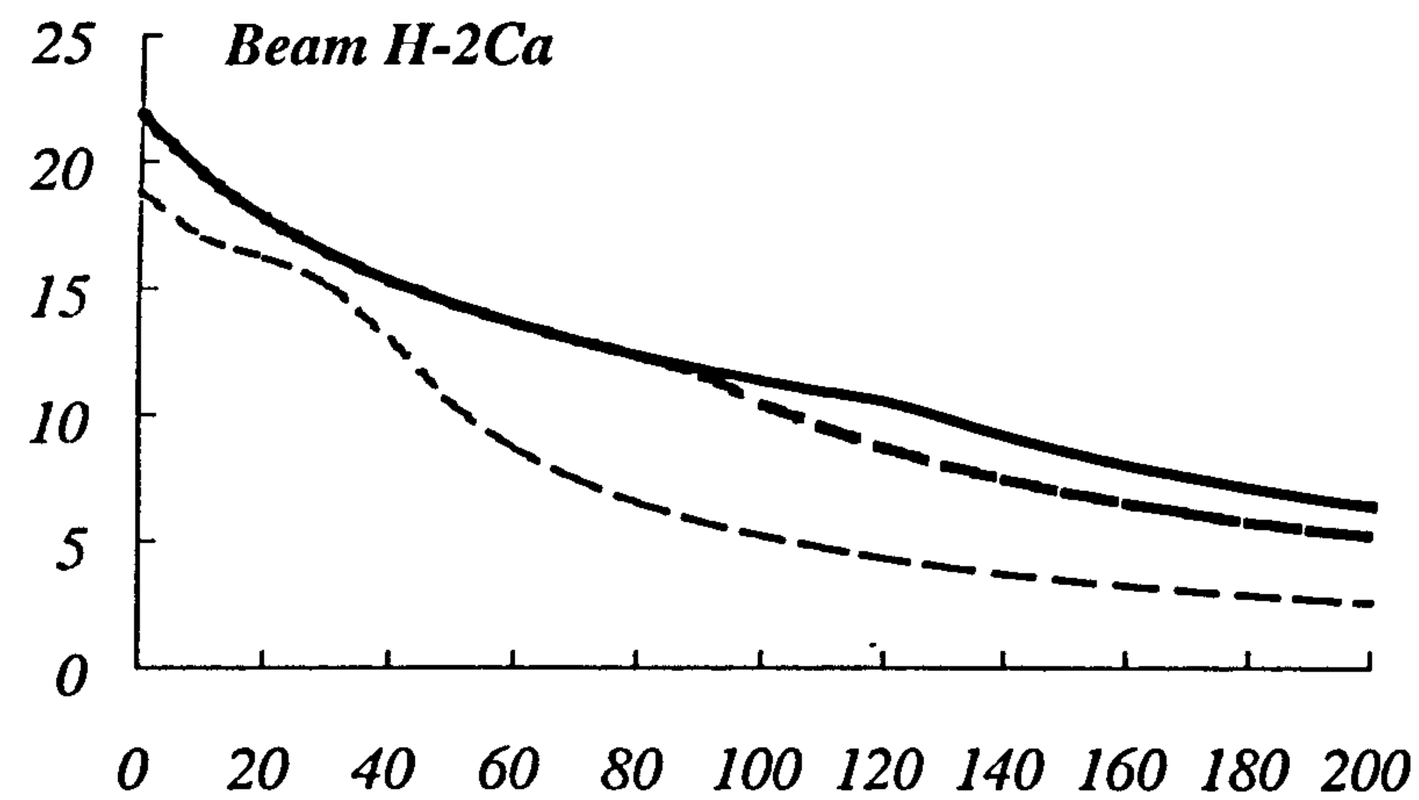

Fig. 6.37 Effect of E_p on the plate axial strain for beam *H-2Ca*.

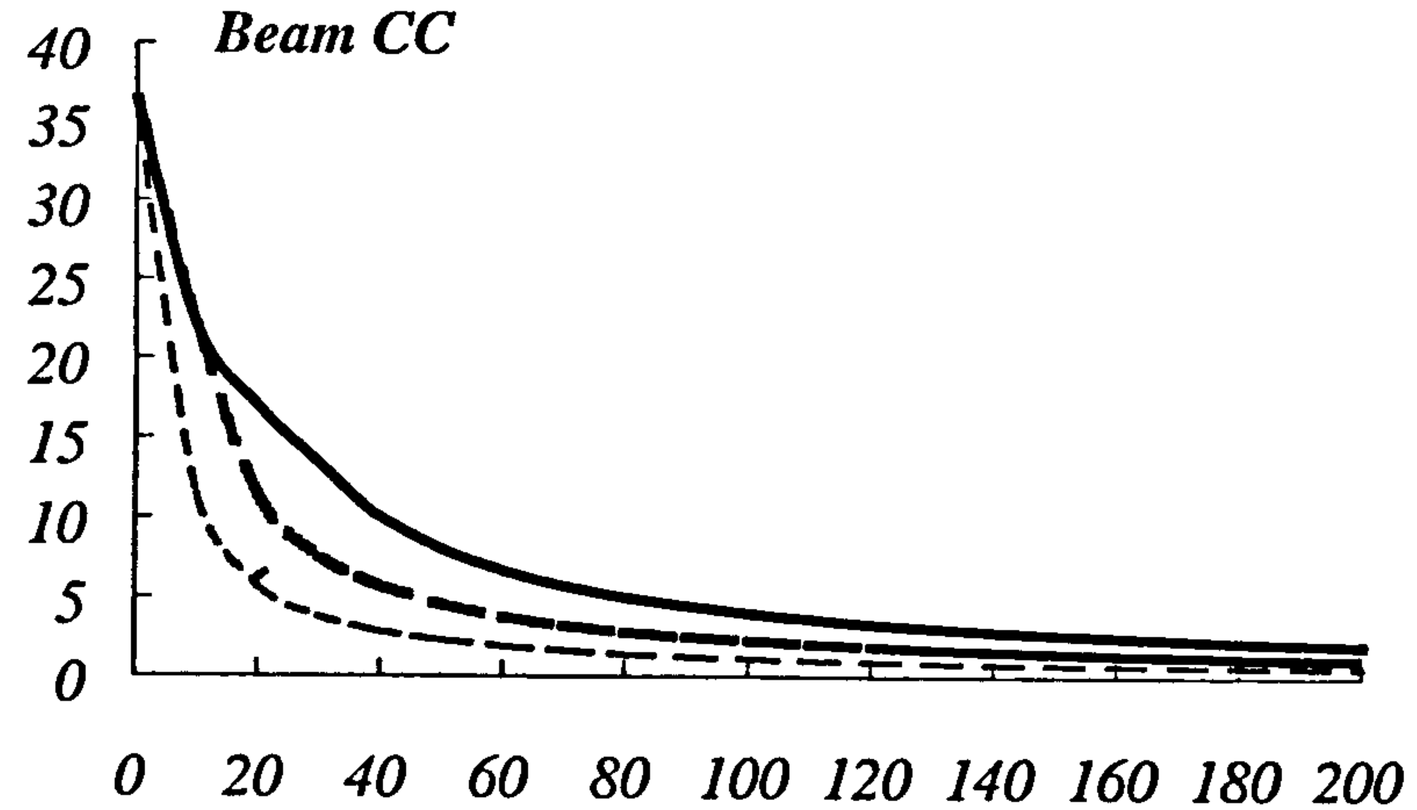

Fig. 6.38 Effect of E_p on the plate axial strain for beam *CC*.

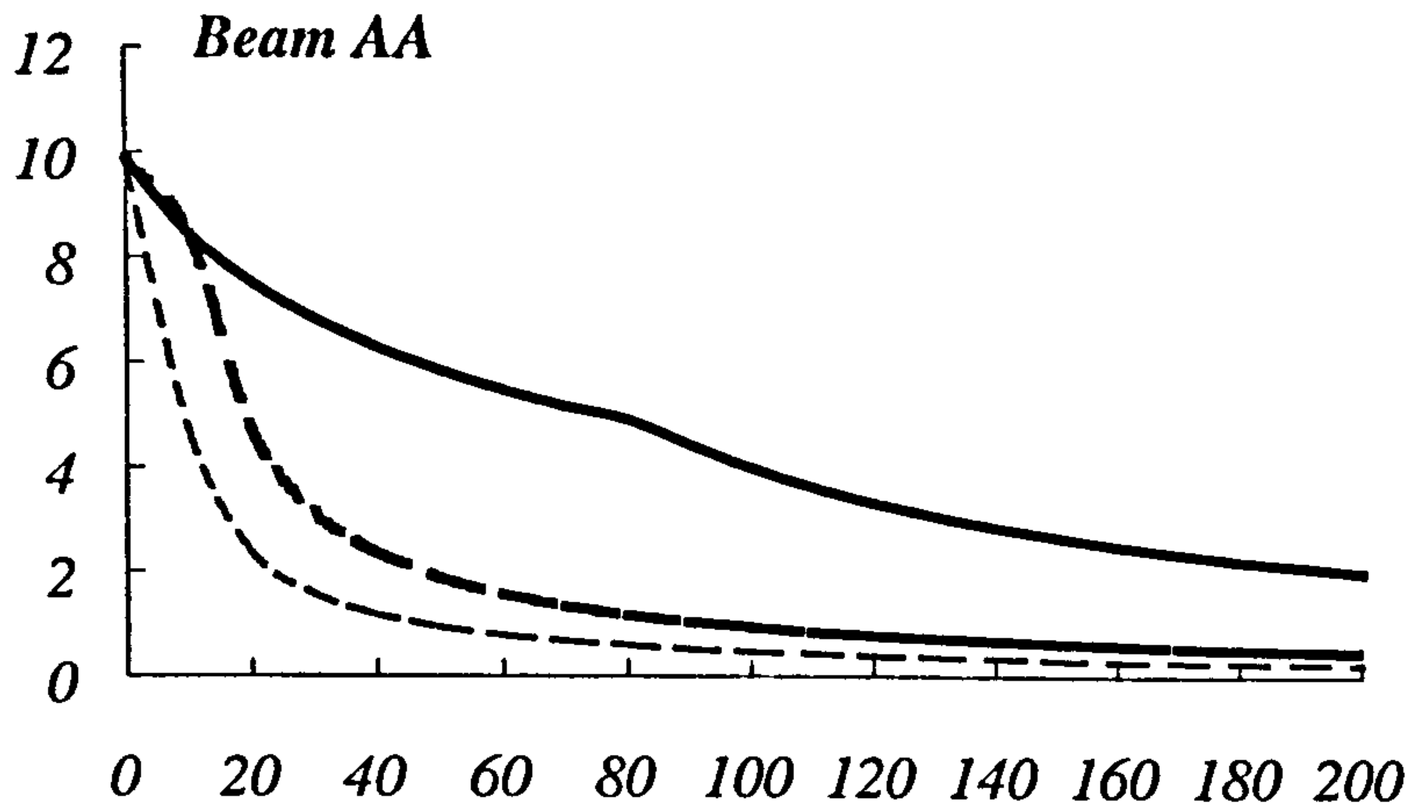

Fig. 6.39 Effect of E_p on the plate axial strain for beam *AA*.

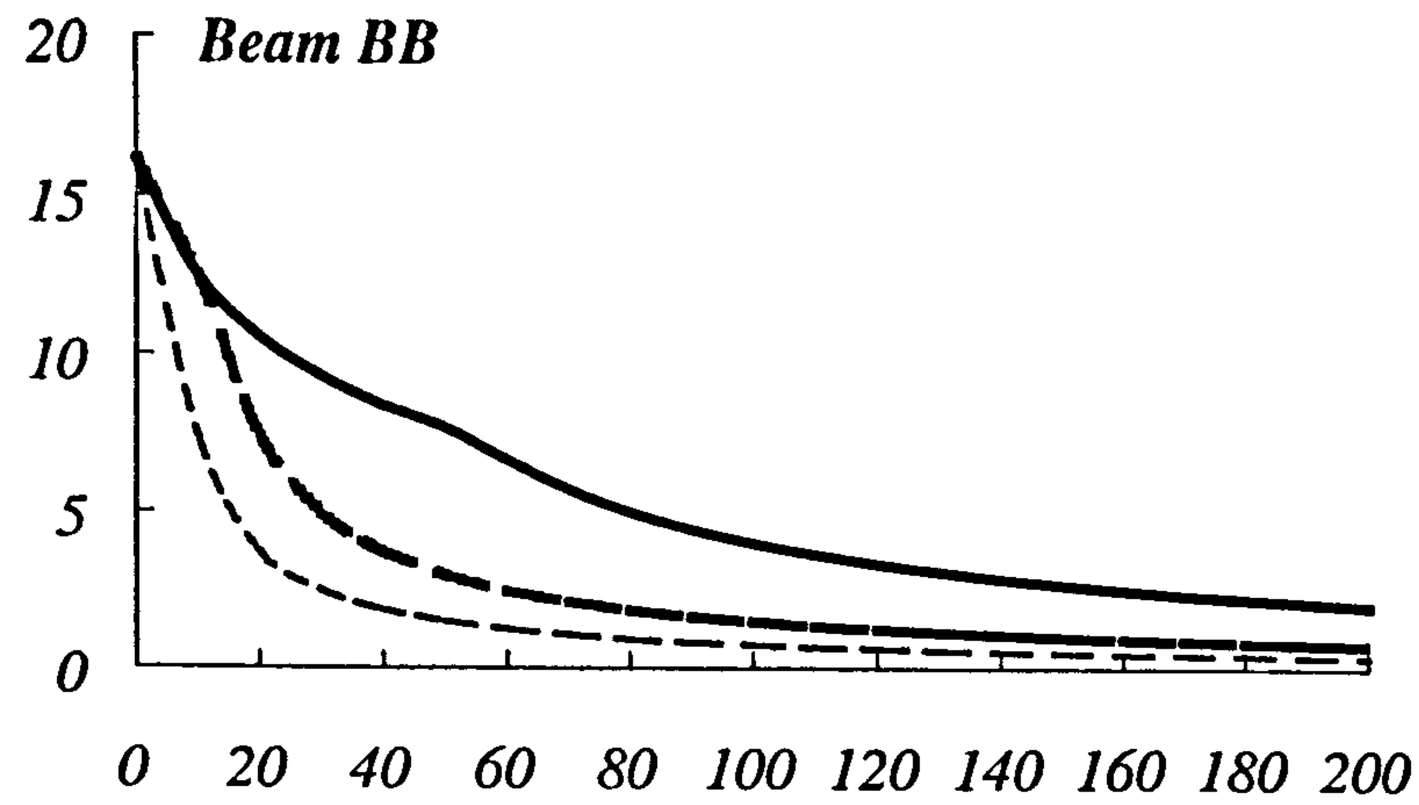

Fig. 6.40 Effect of E_p on the plate axial strain for beam *BB*.

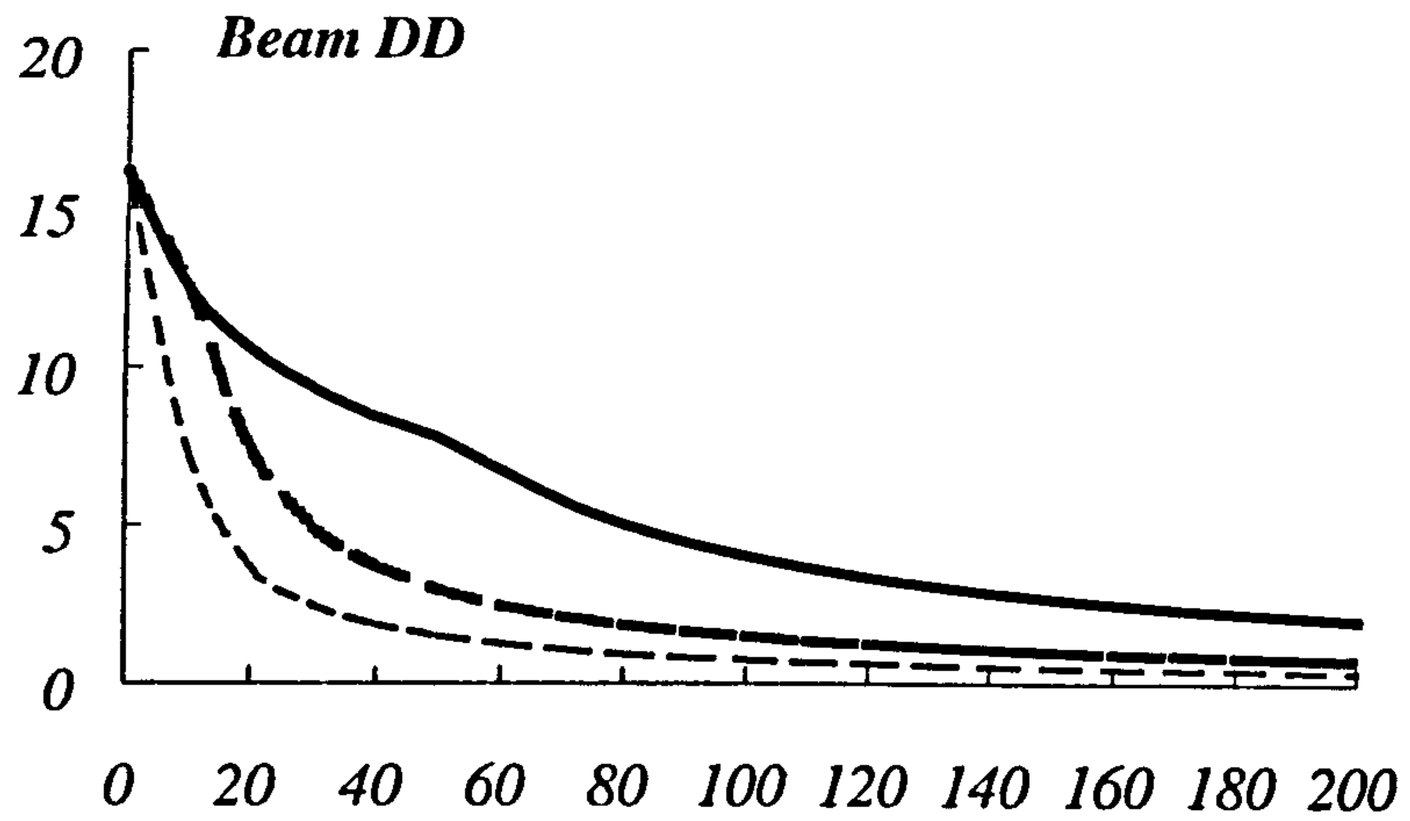

Fig. 6.41 Effect of E_p on the plate axial strain for beam *DD*.

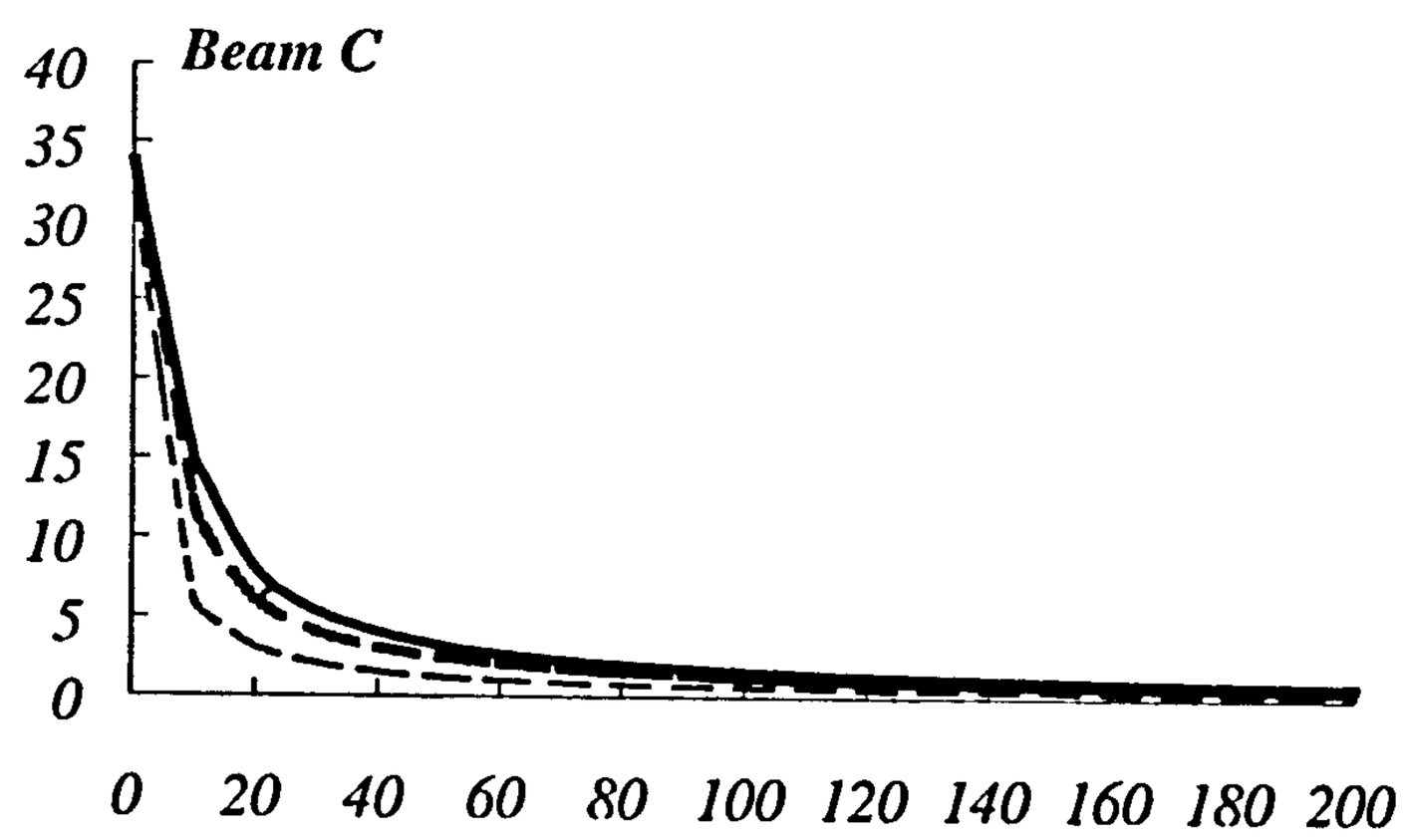

Fig. 6.42 Effect of E_p on the plate axial strain for beam *C*.

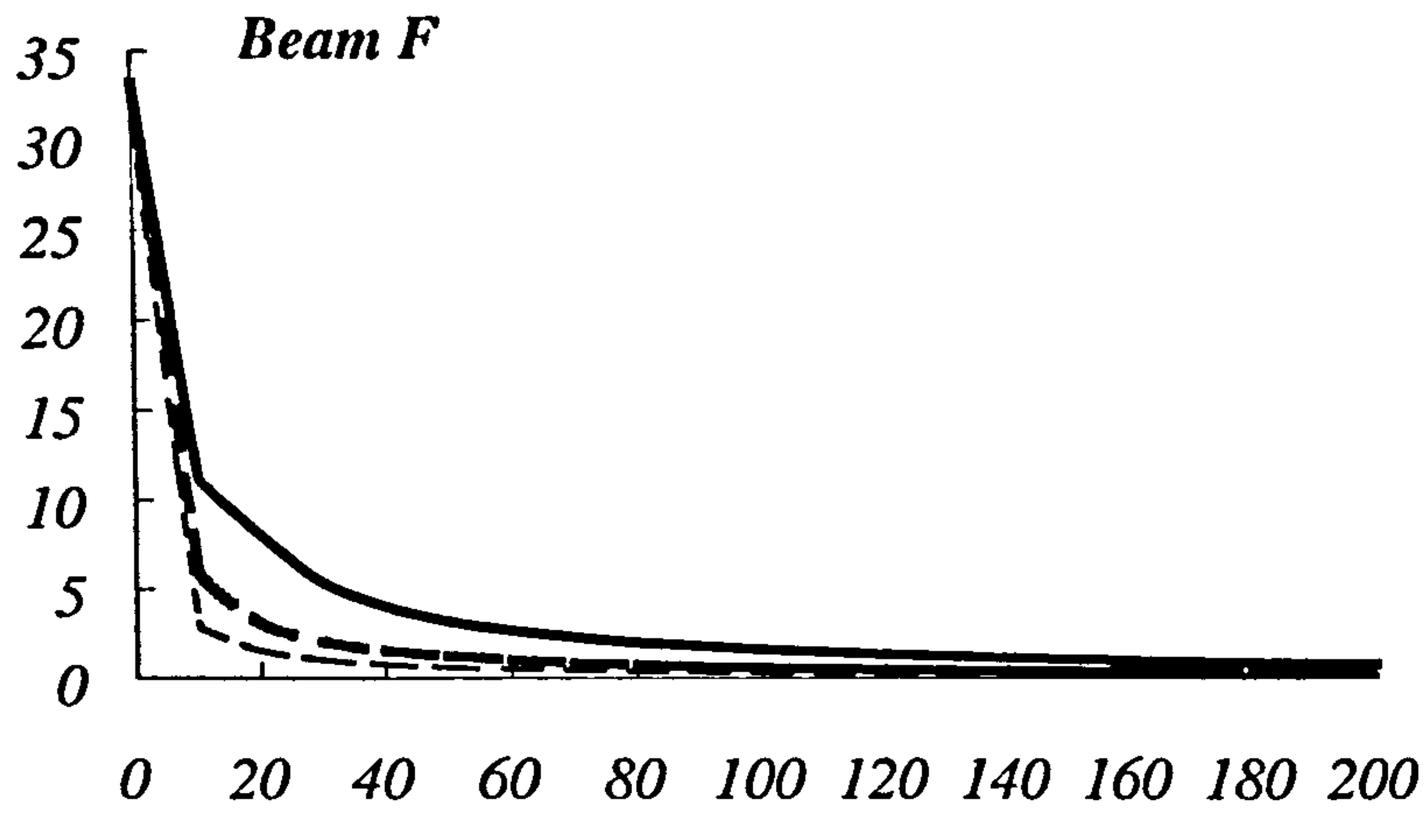

Fig. 6.43 Effect of E_p on the plate axial strain for beam *F*.

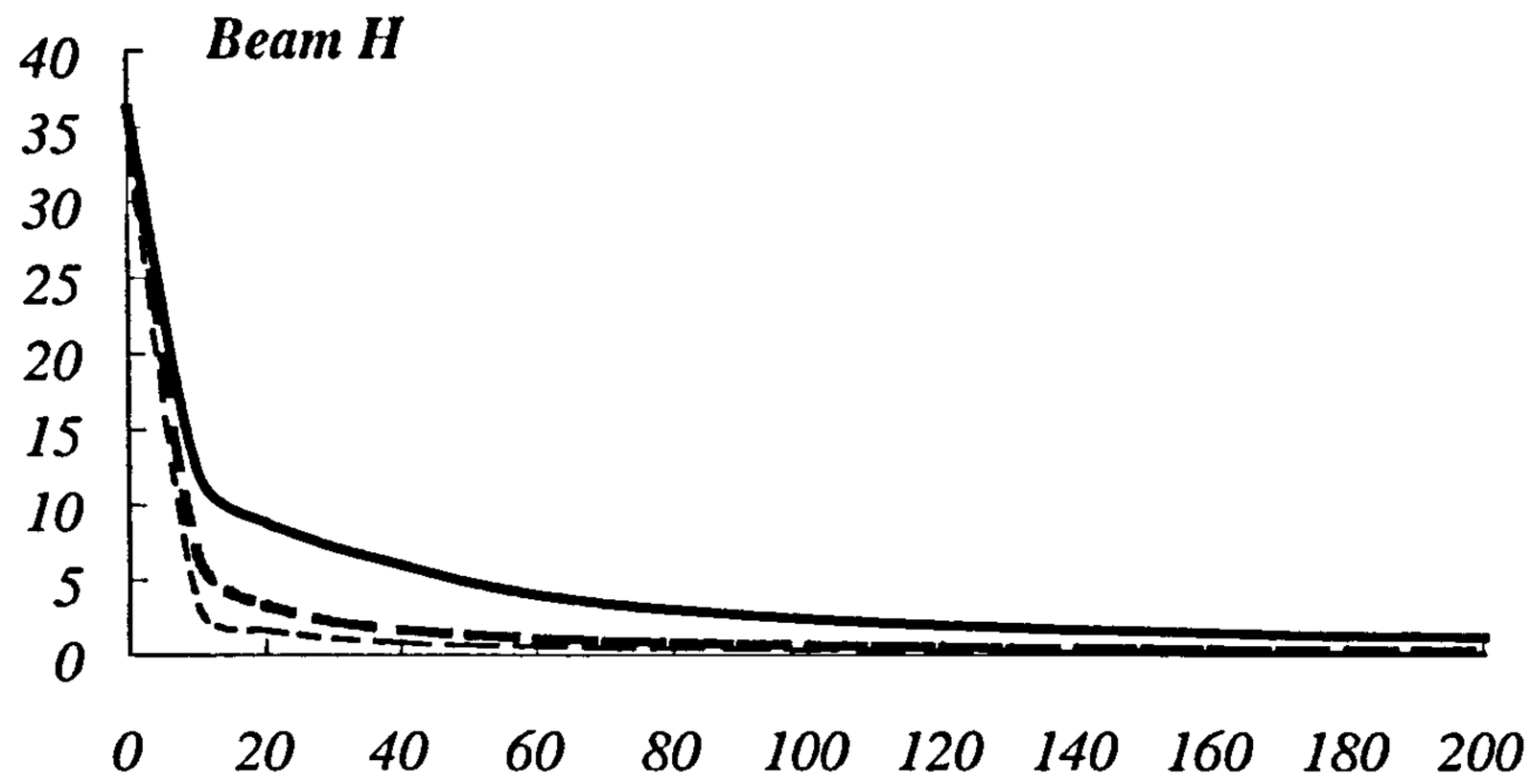

Fig. 6.44 Effect of E_p on the plate axial strain for beam *H*.

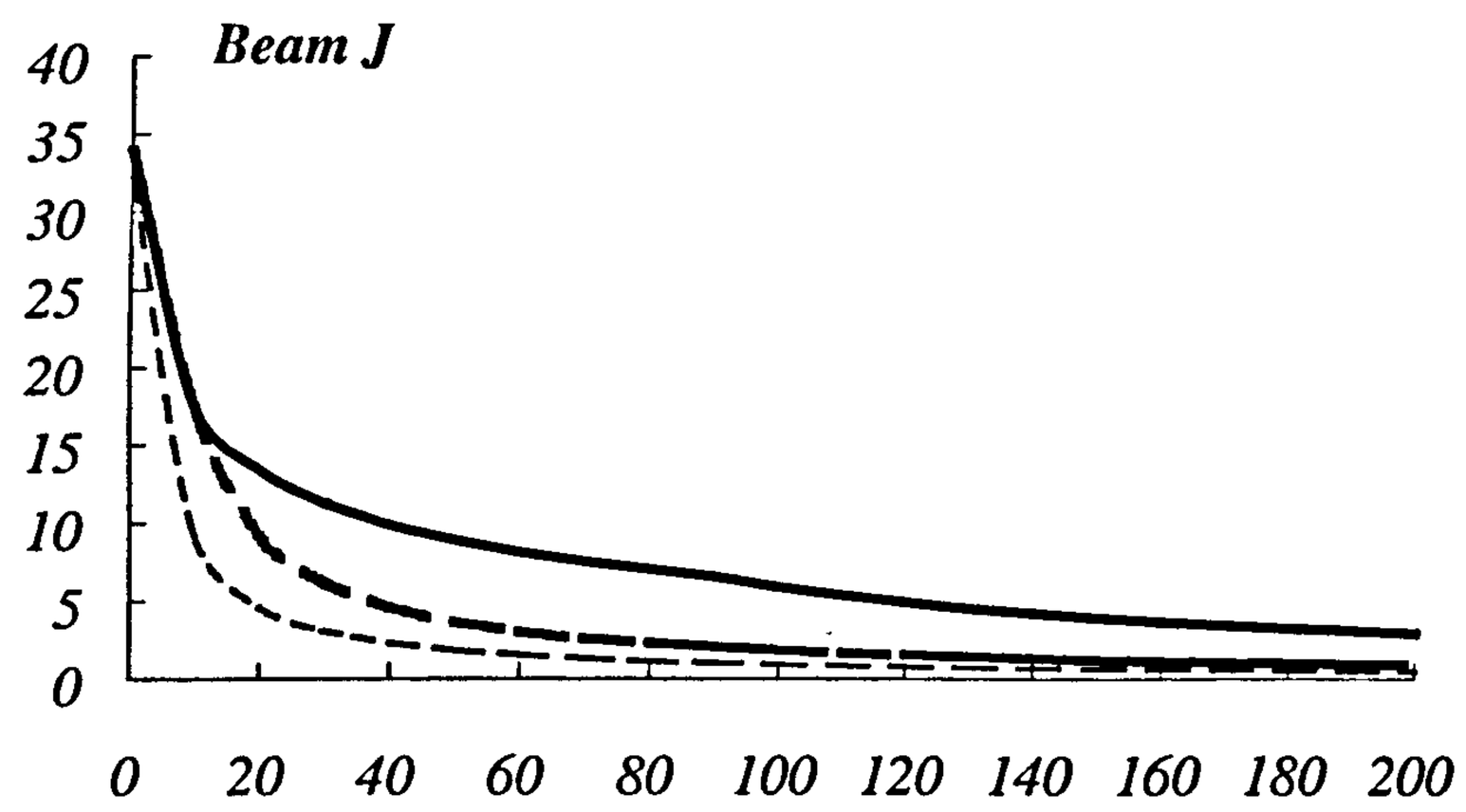

Fig. 6.45 Effect of E_p on the plate axial strain for beam *J*.

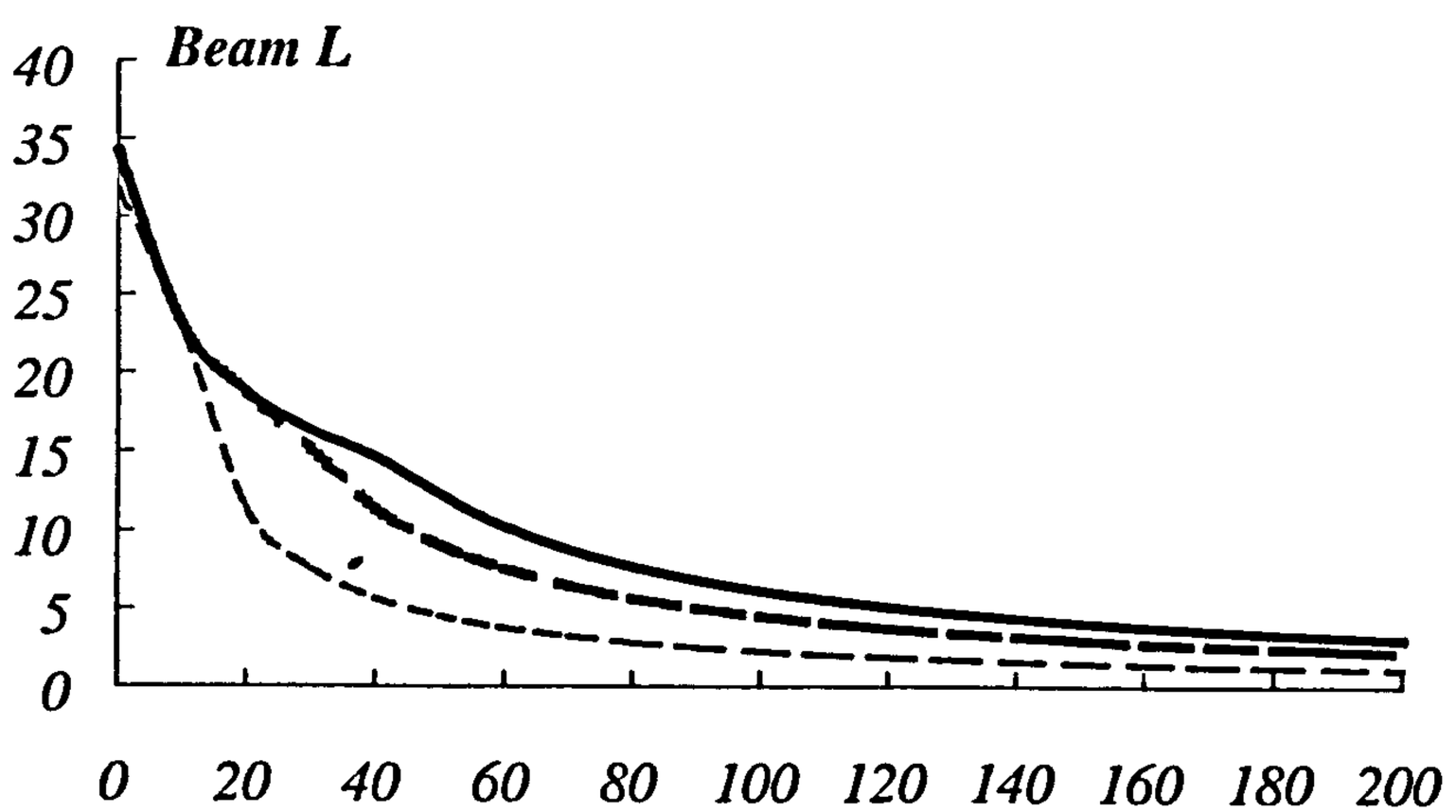

Fig. 6.46 Effect of E_p on the plate axial strain for beam *L*.

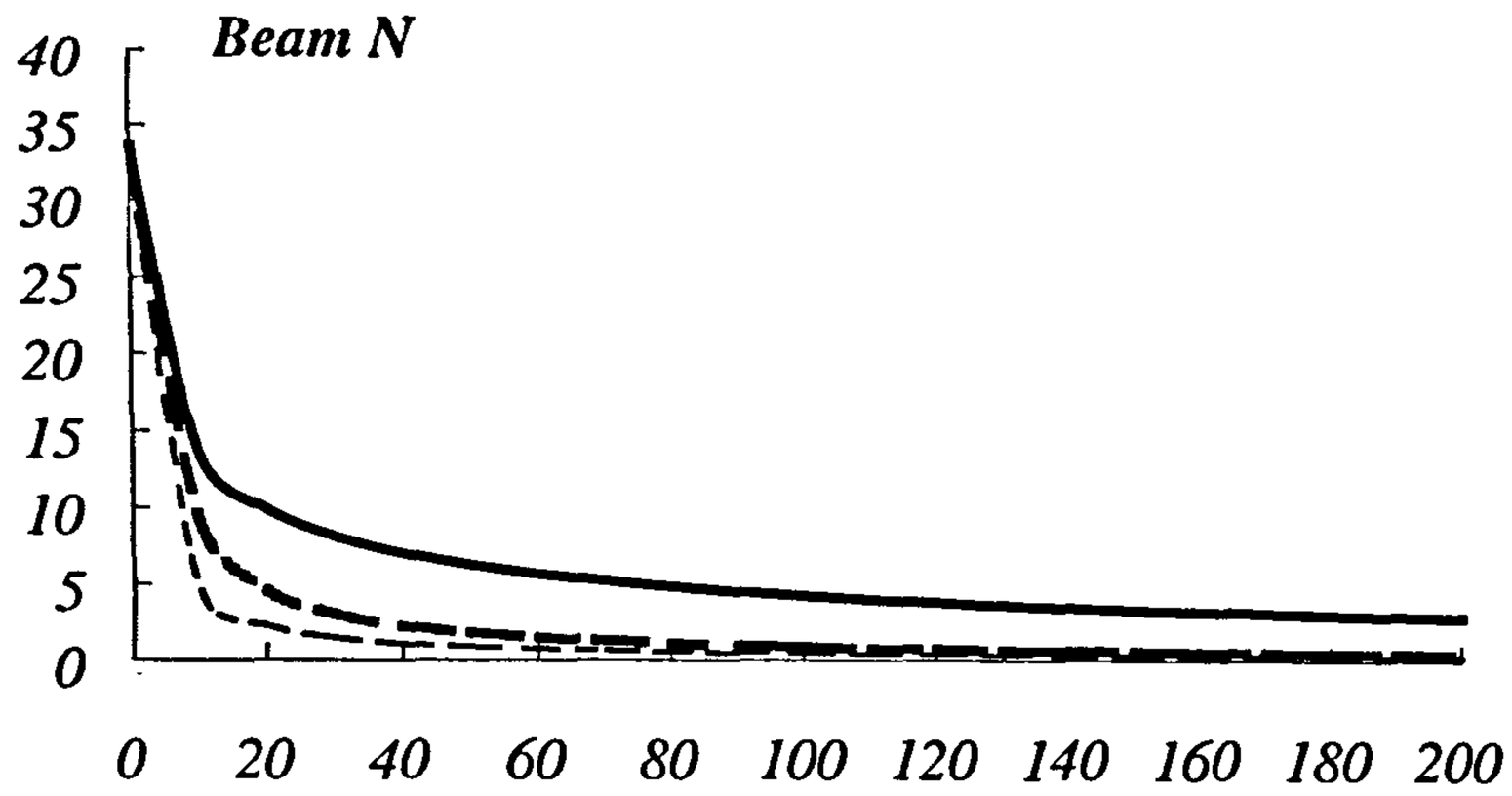

Fig. 6.47 Effect of E_p on the plate axial strain for beam *N*.

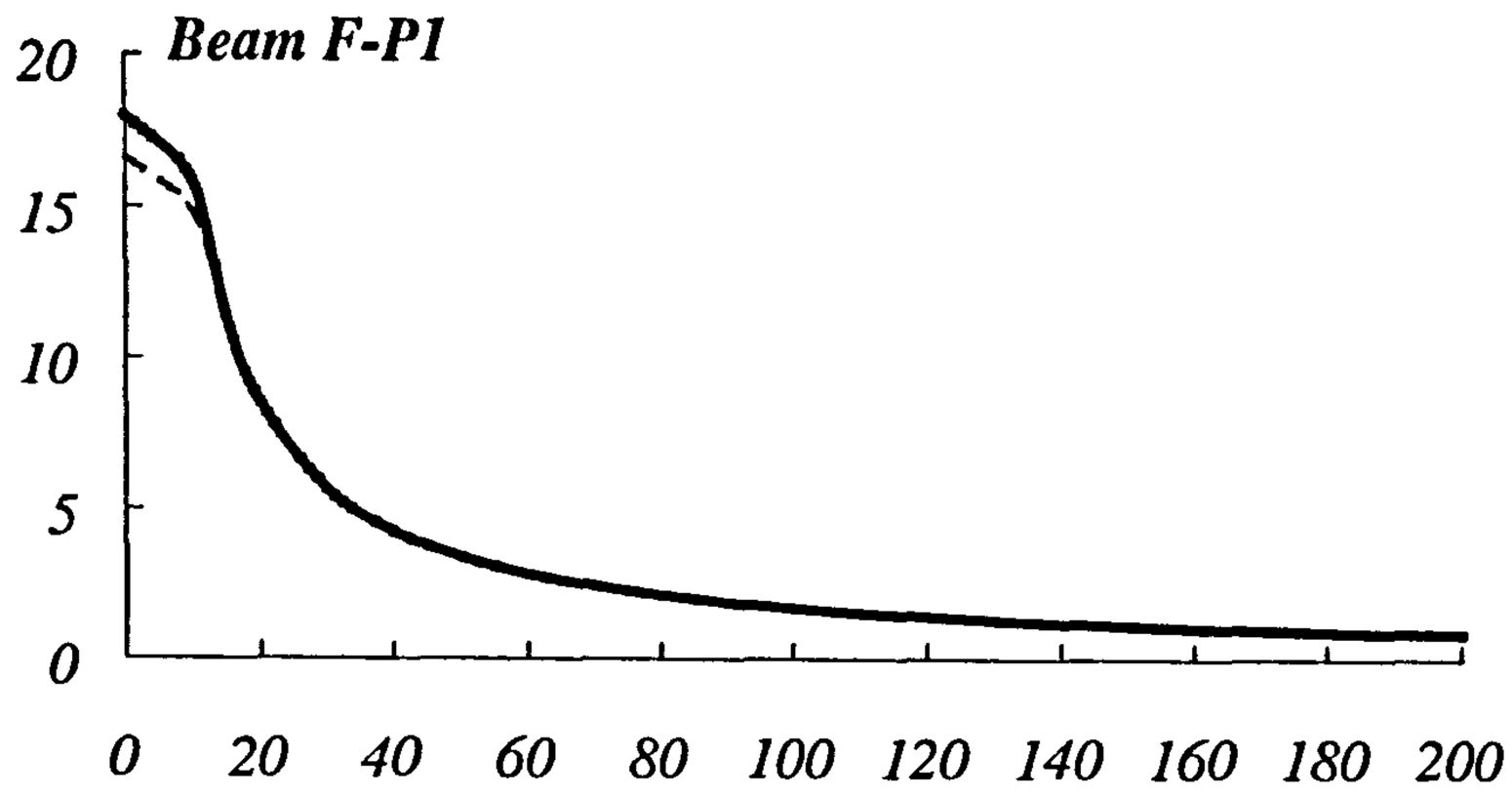

Fig. 6.48 Effect of E_p on the plate axial strain for beam *F-P1*.

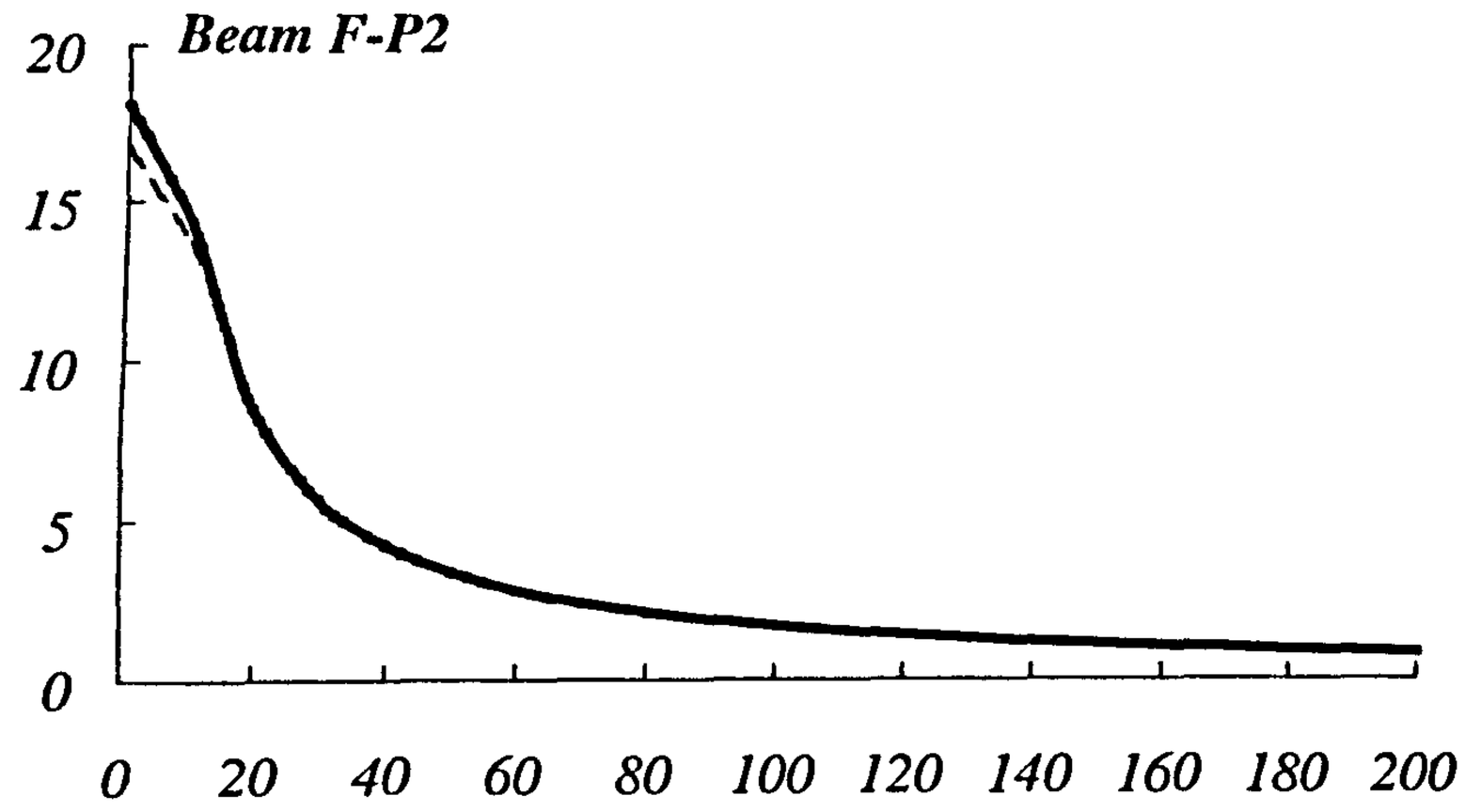

Fig. 6.49 Effect of E_p on the plate axial strain for beam *F-P2*.

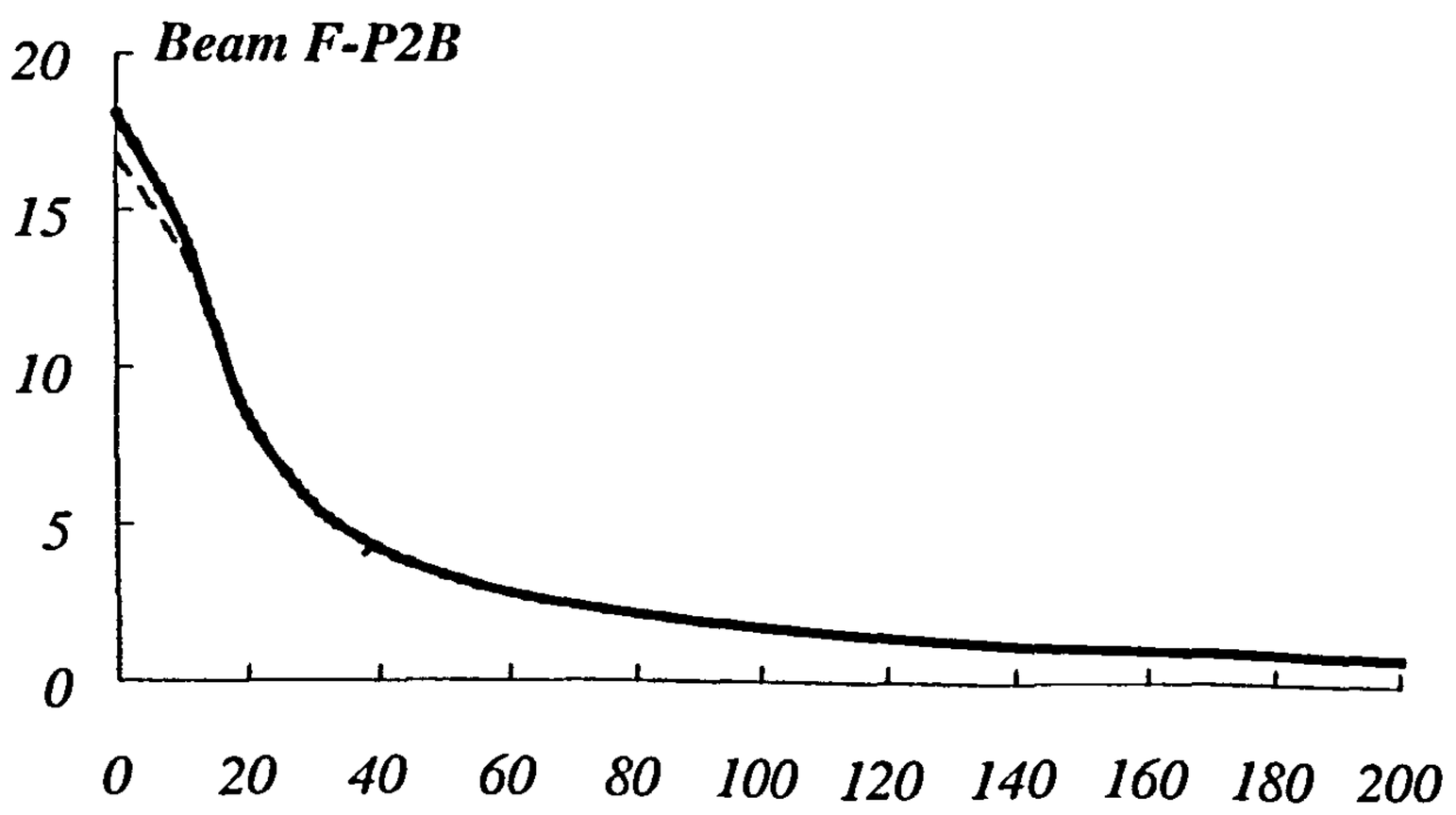

Fig. 6.50 Effect of E_p on the plate axial strain for beam *F-P2B*.

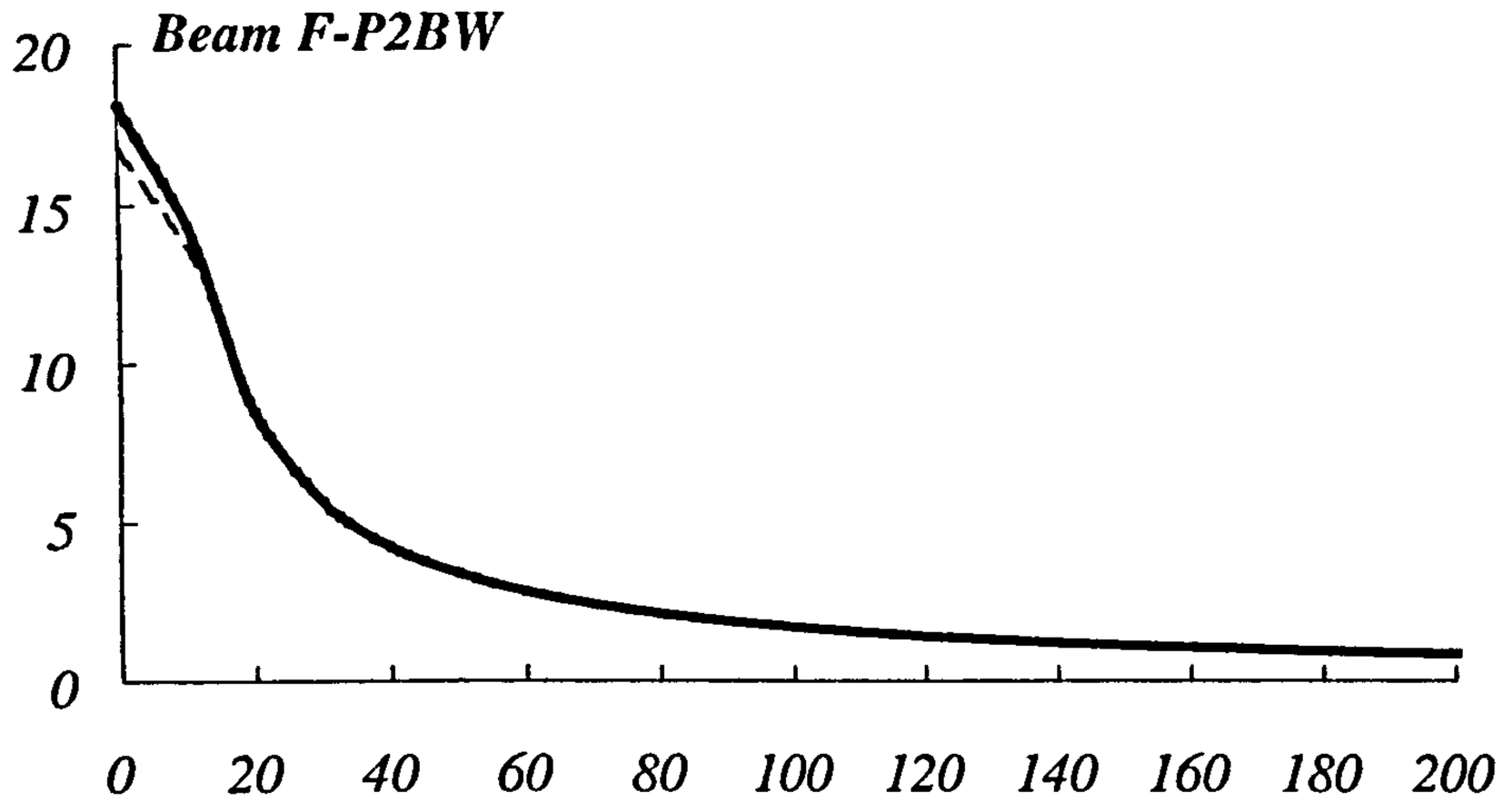

Fig. 6.51 Effect of E_p on the plate axial strain for beam *F-P2BW*.

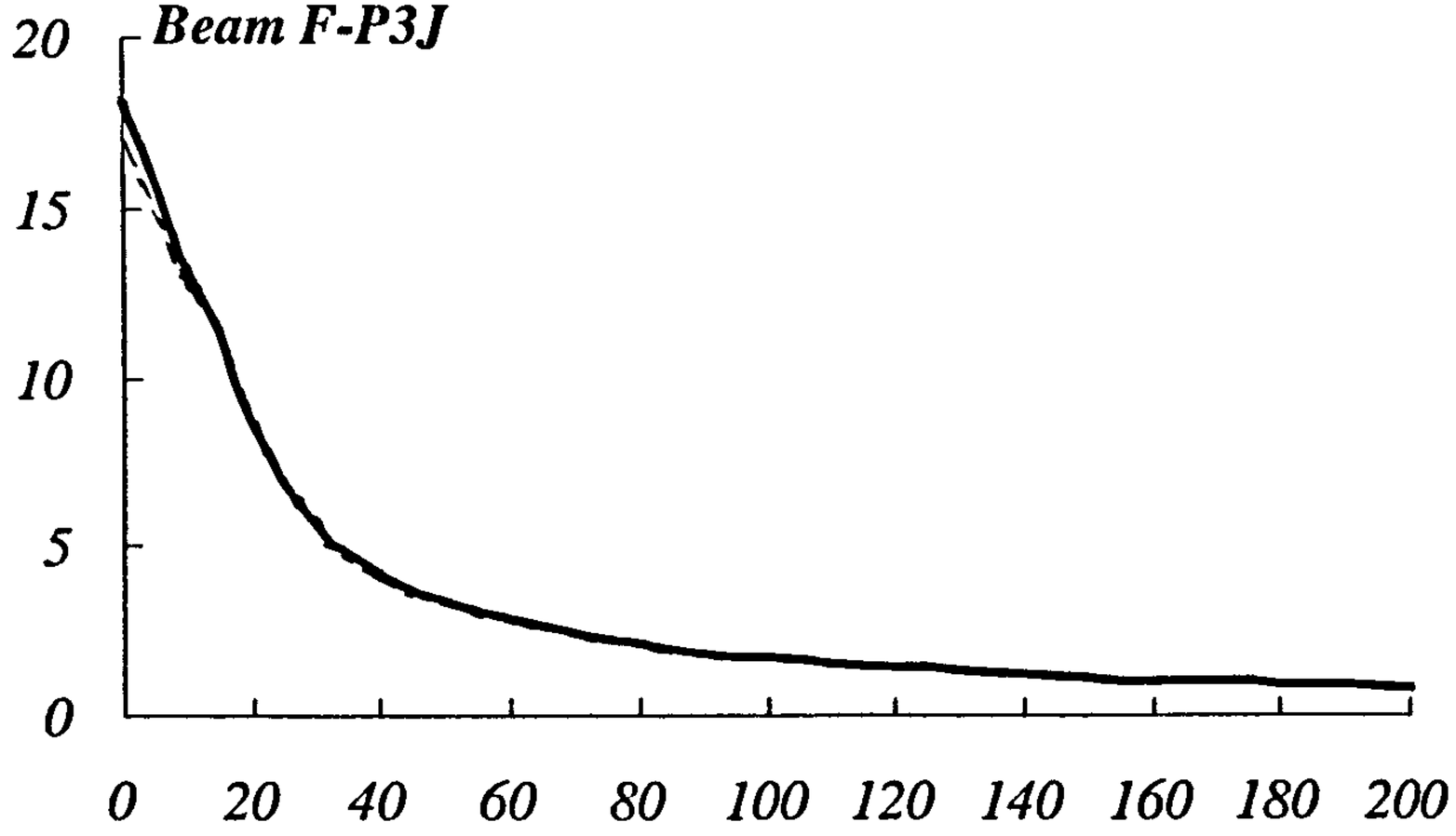

Fig. 6.52 Effect of E_p on the plate axial strain for beam *F-P3J*.

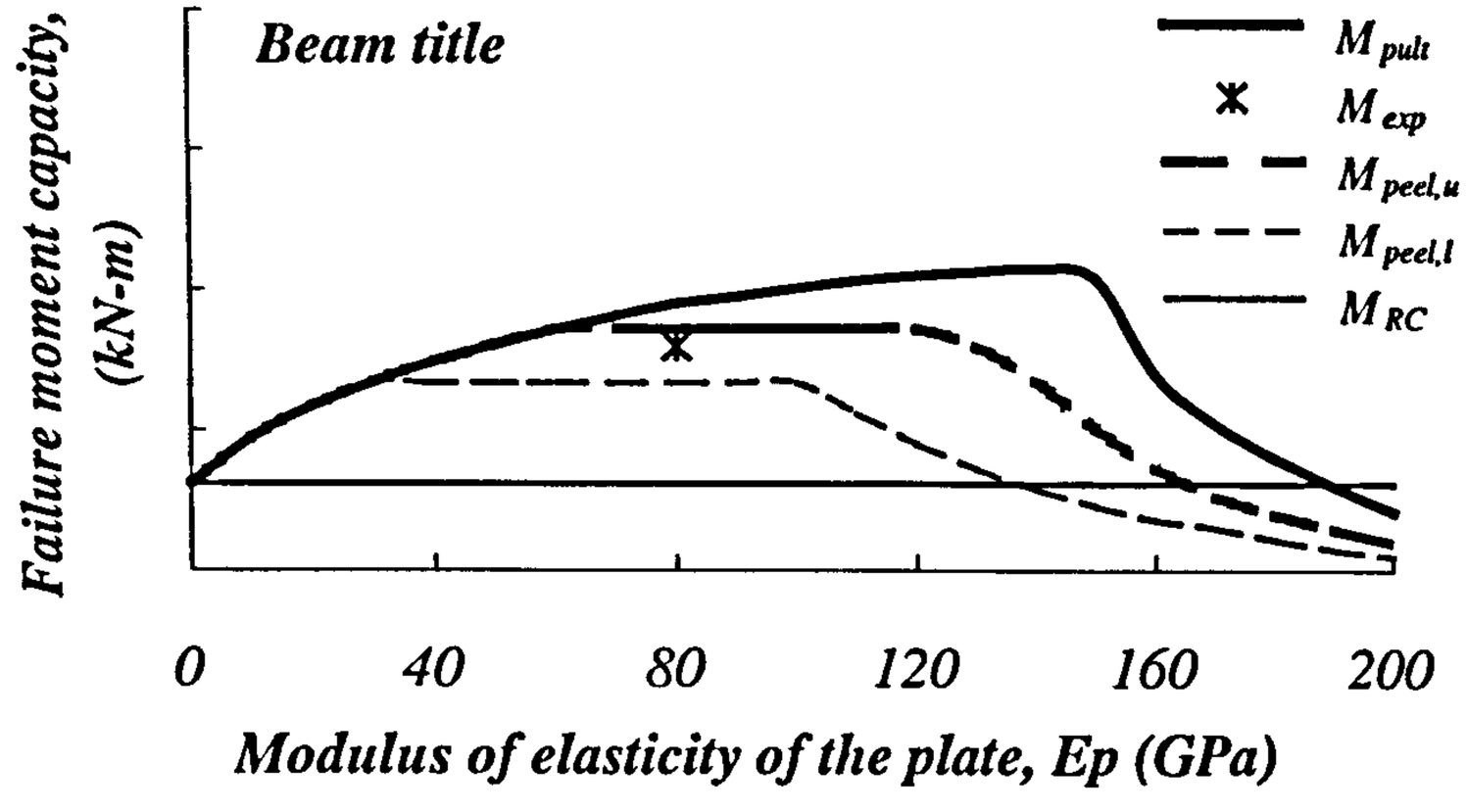

Fig. 6.53 Effect of increasing the plate modulus of elasticity, E_p, on the failure moment capacities of the plated beams (typical legends for Figs 6.54 to 6.74).

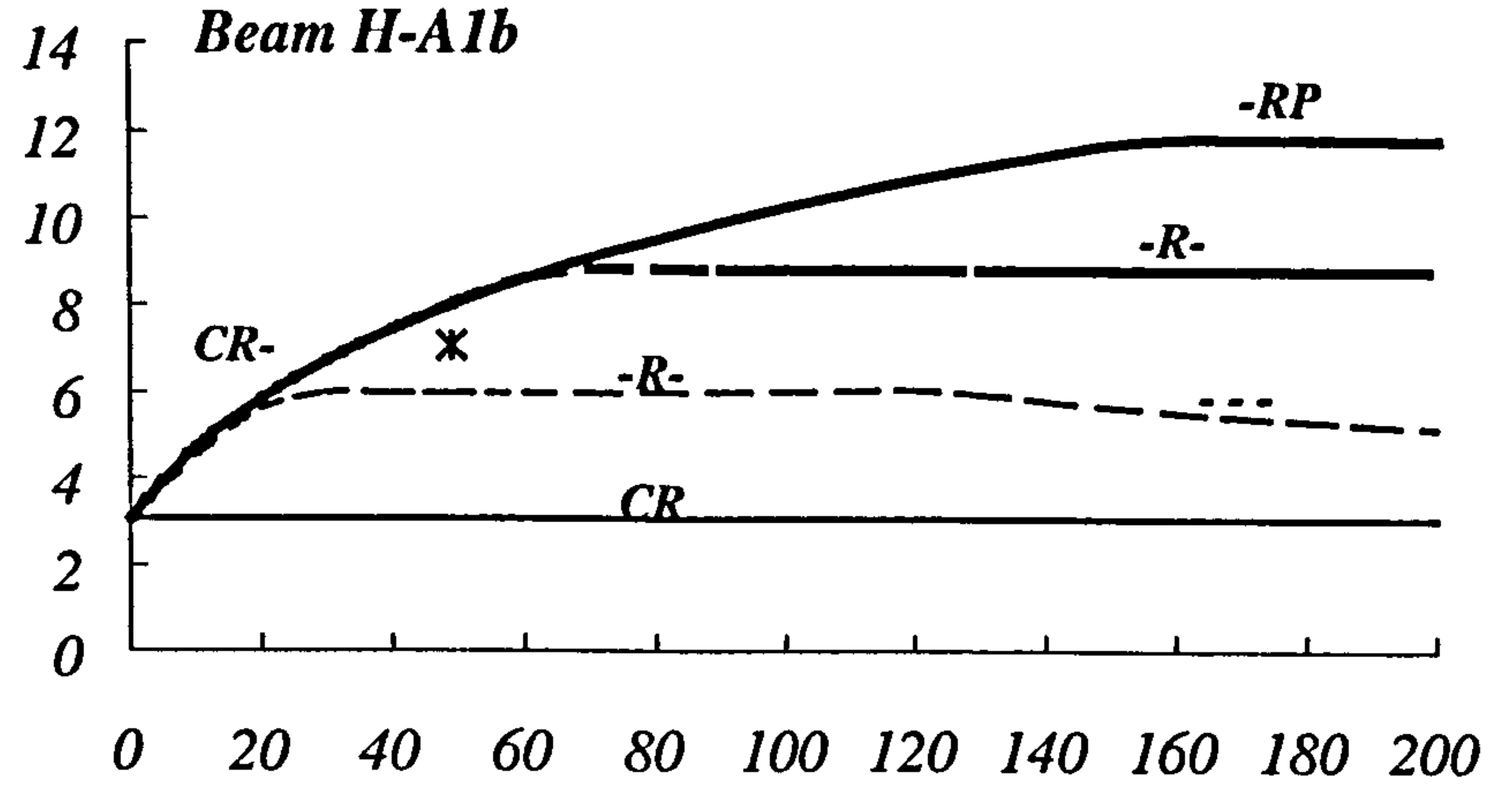

Fig. 6.54 Effect of E_p on failure moments for beam *H-A1b*.

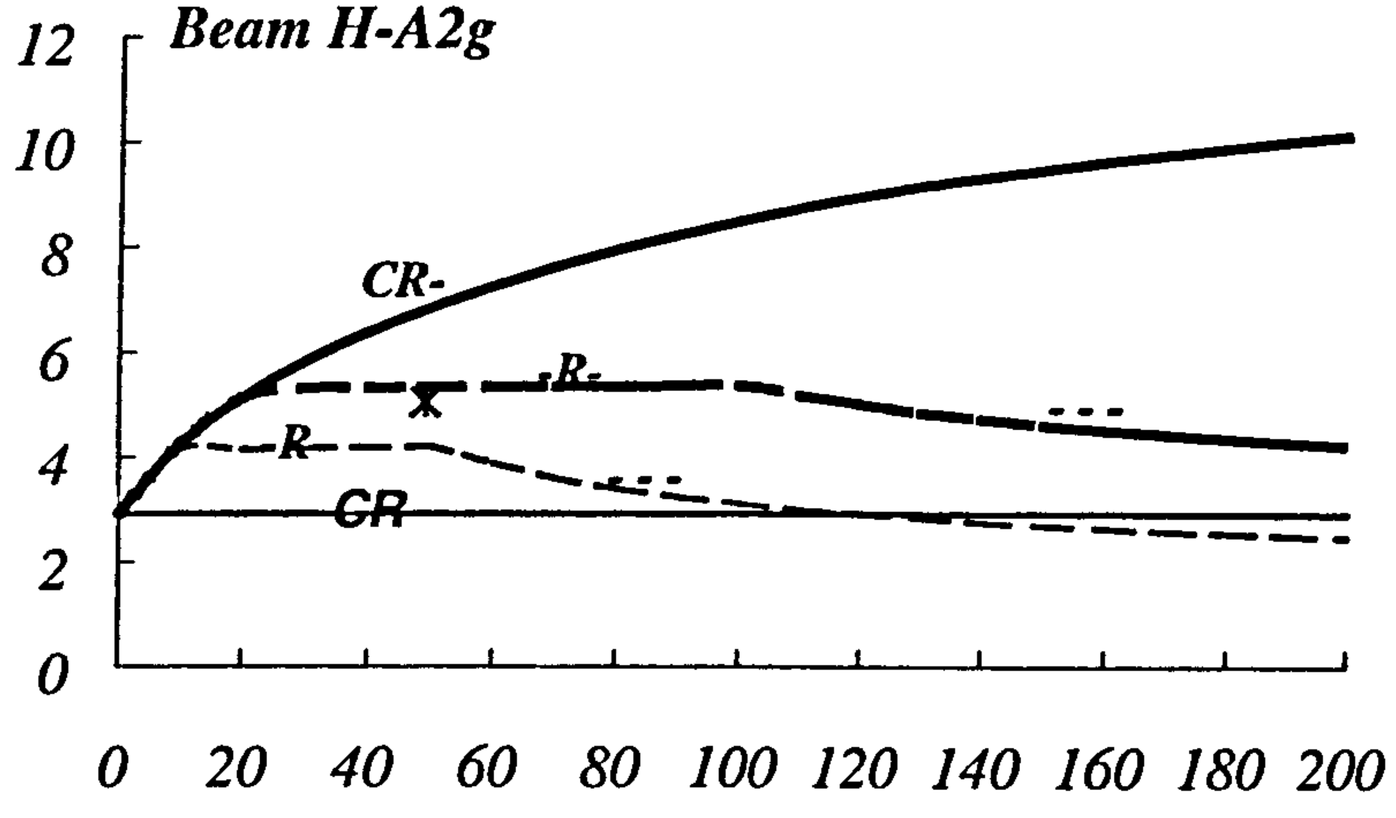

Fig. 6.55 Effect of E_p on failure moments for beam *H-A2g*.

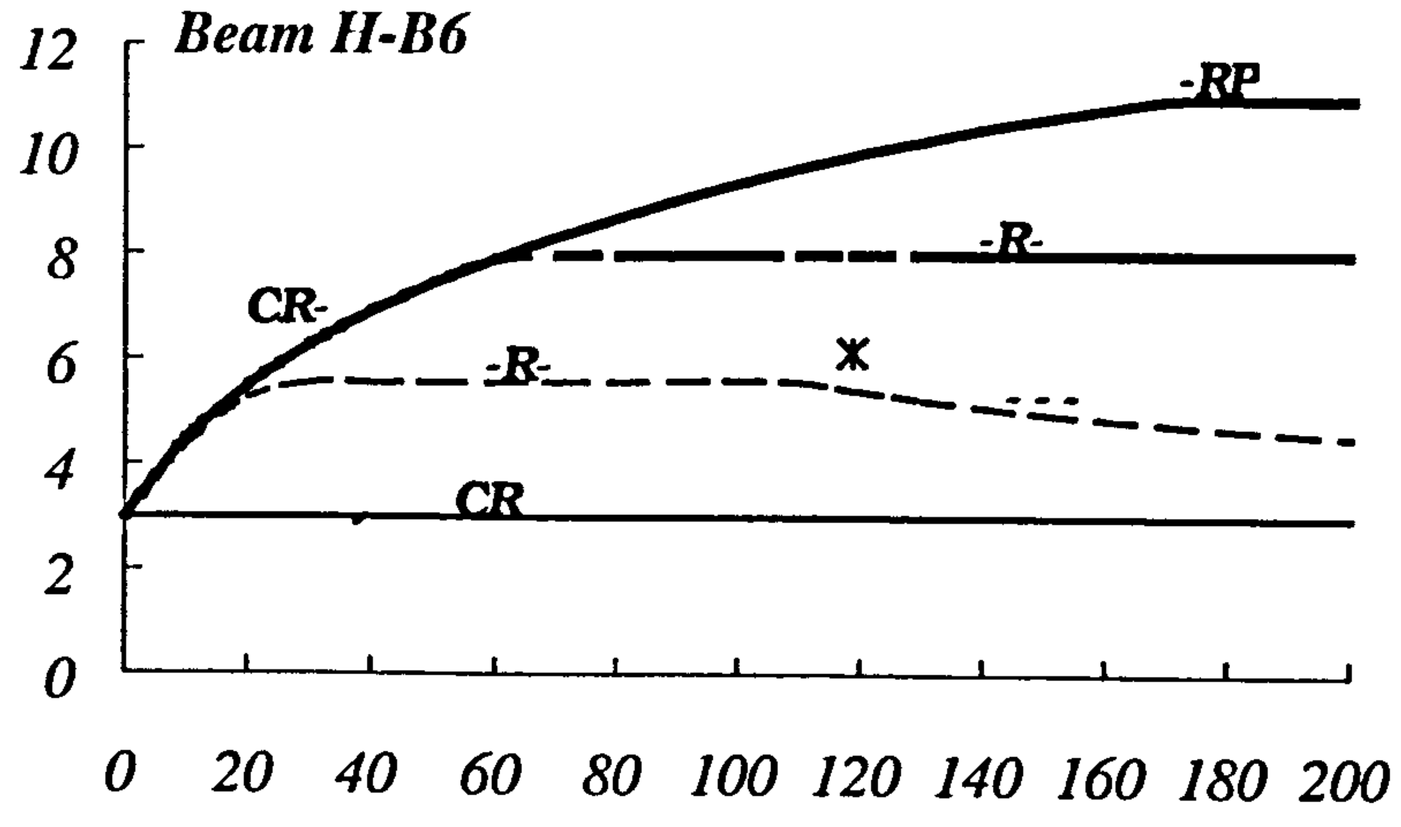

Fig. 6.56 Effect of E_p on failure moments for beam *H-B6*.

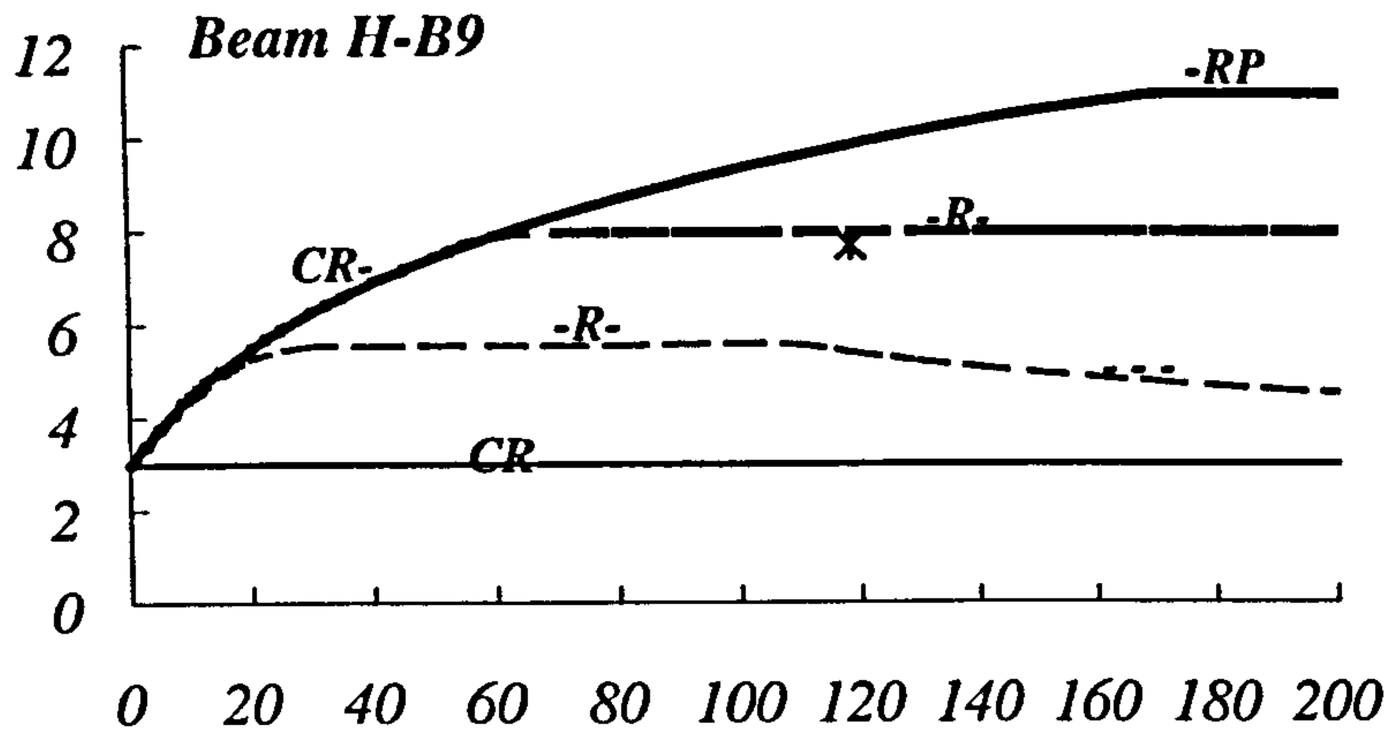

Fig. 6.57 Effect of E_p on failure moments for beam *H-B9*.

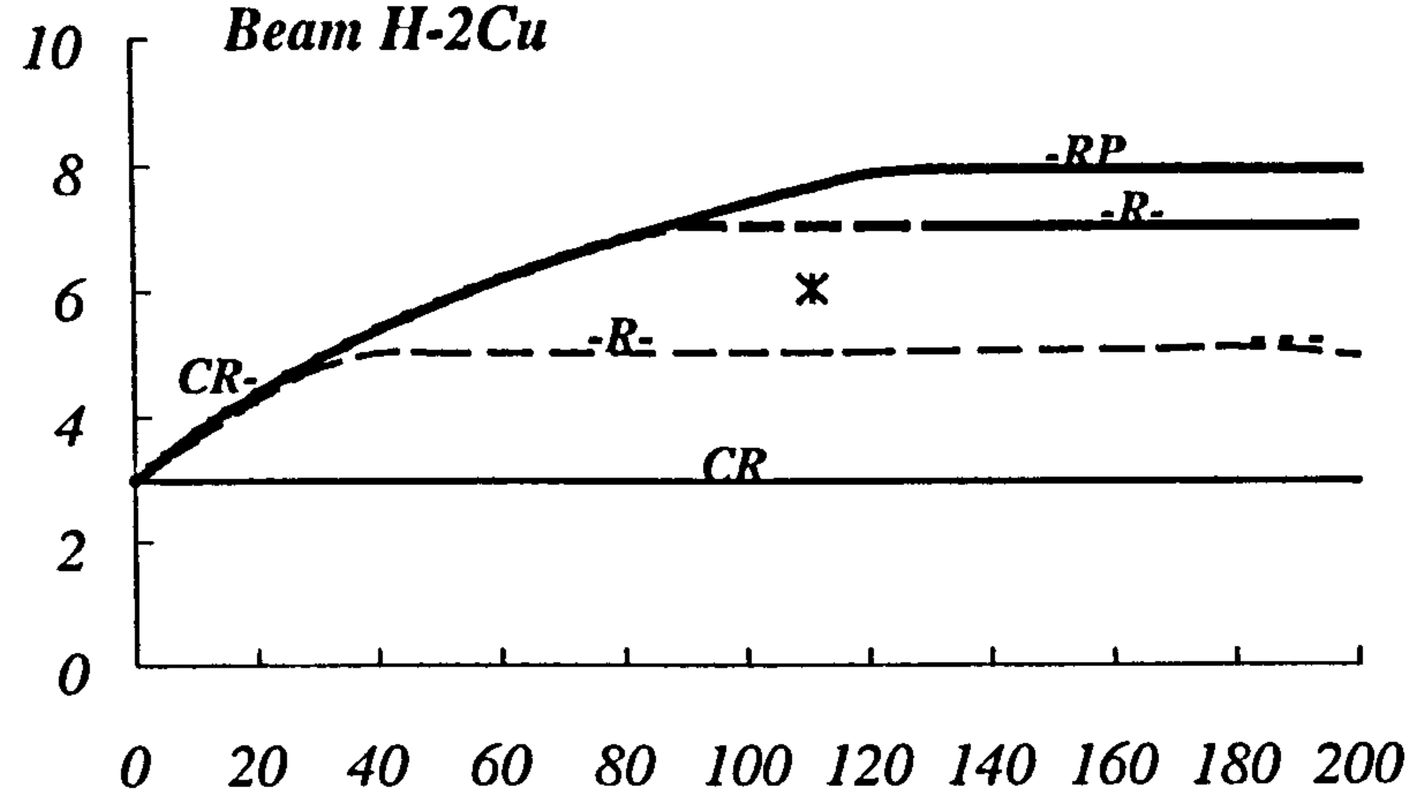

Fig. 6.58 Effect of E_p on failure moments for beam *H-2Cu*.

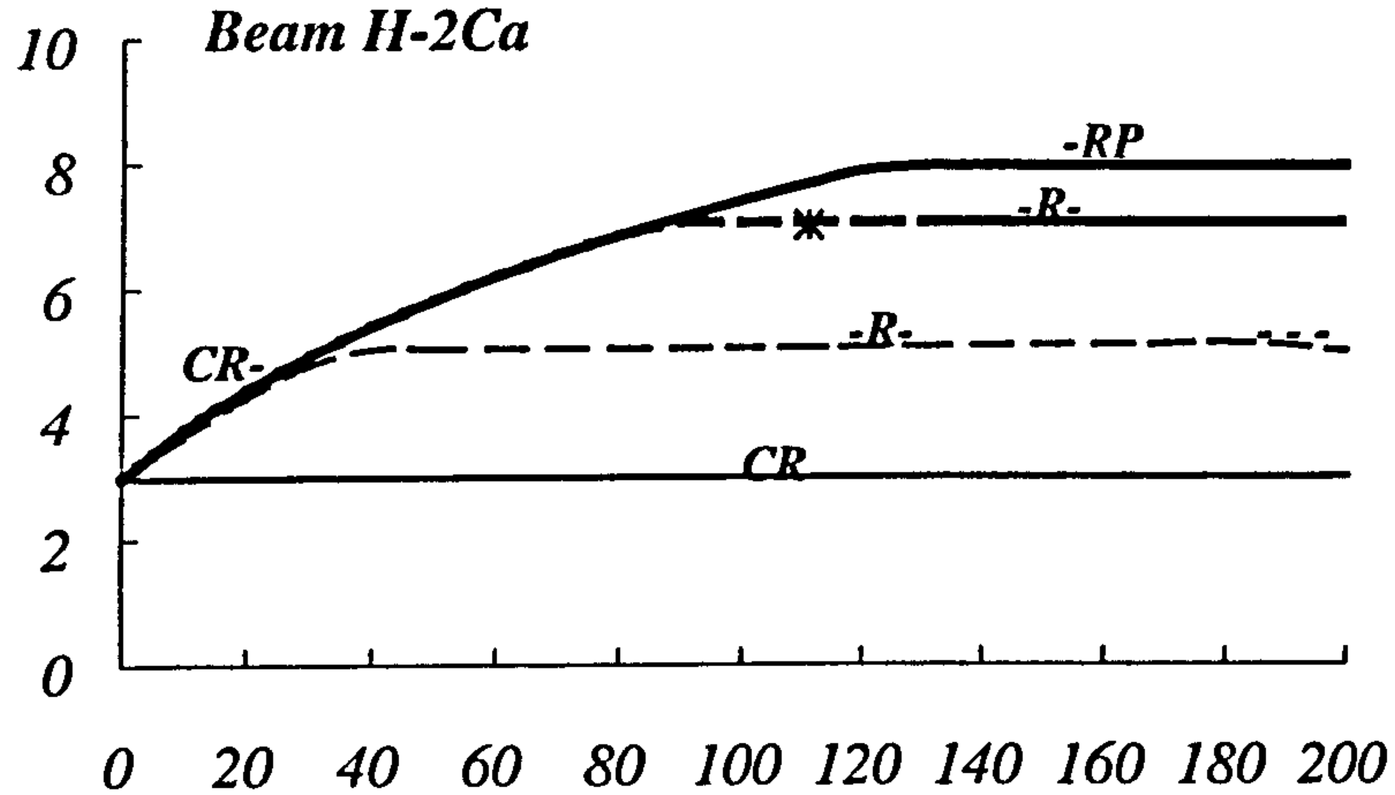

Fig. 6.59 Effect of E_p on failure moments for beam *H-2Ca*.

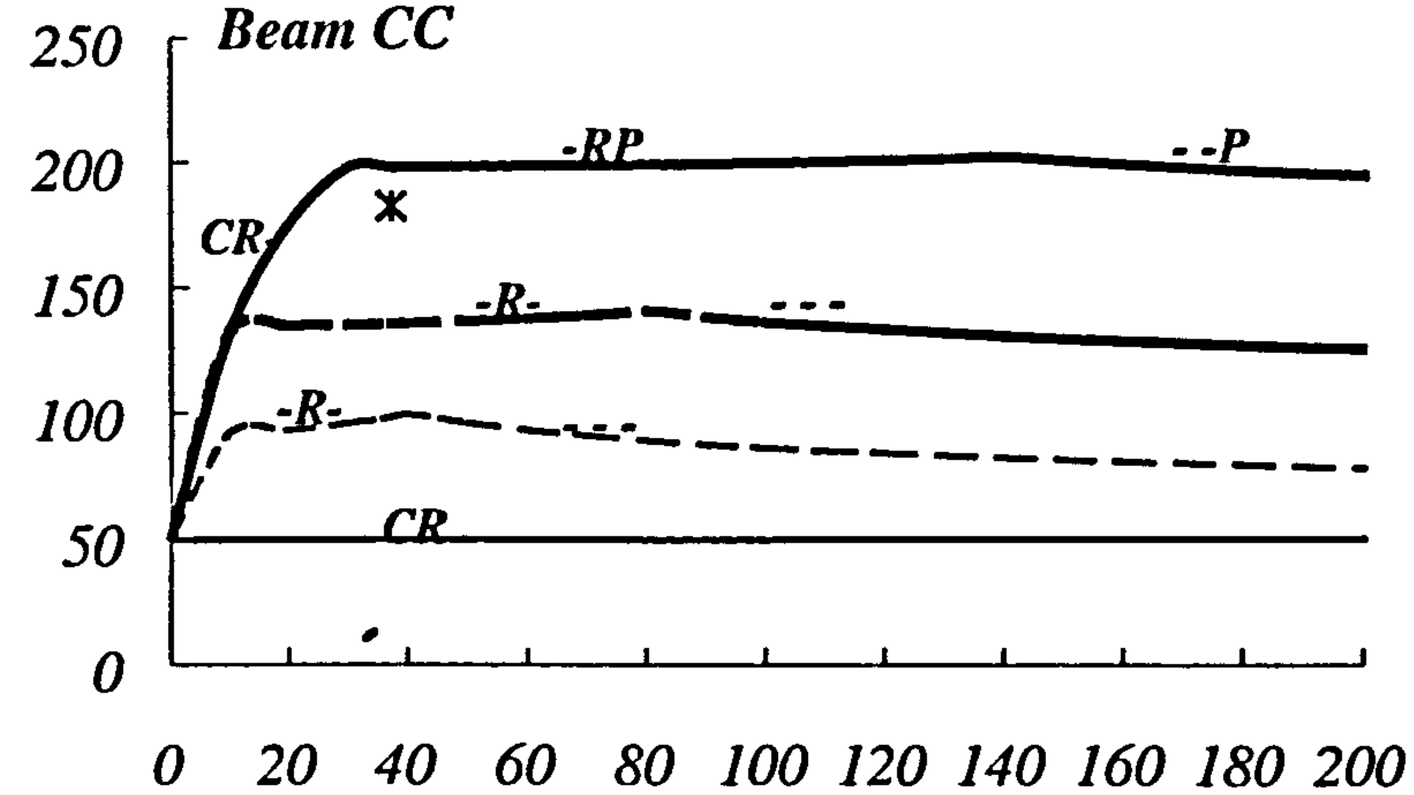

Fig. 6.60 Effect of E_p on failure moments for beam *CC*.

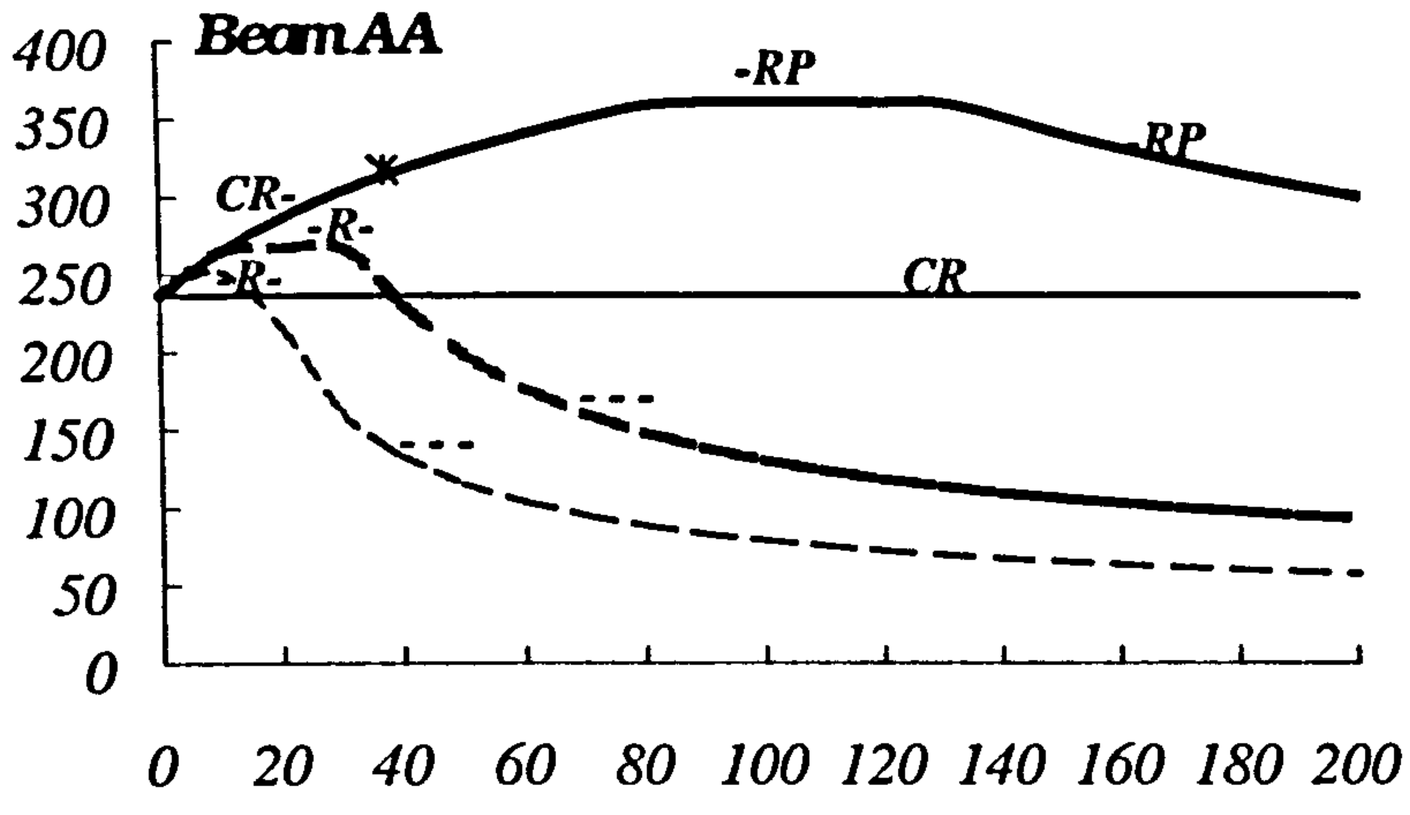

Fig. 6.61 Effect of E_p on failure moments for beam *AA*.

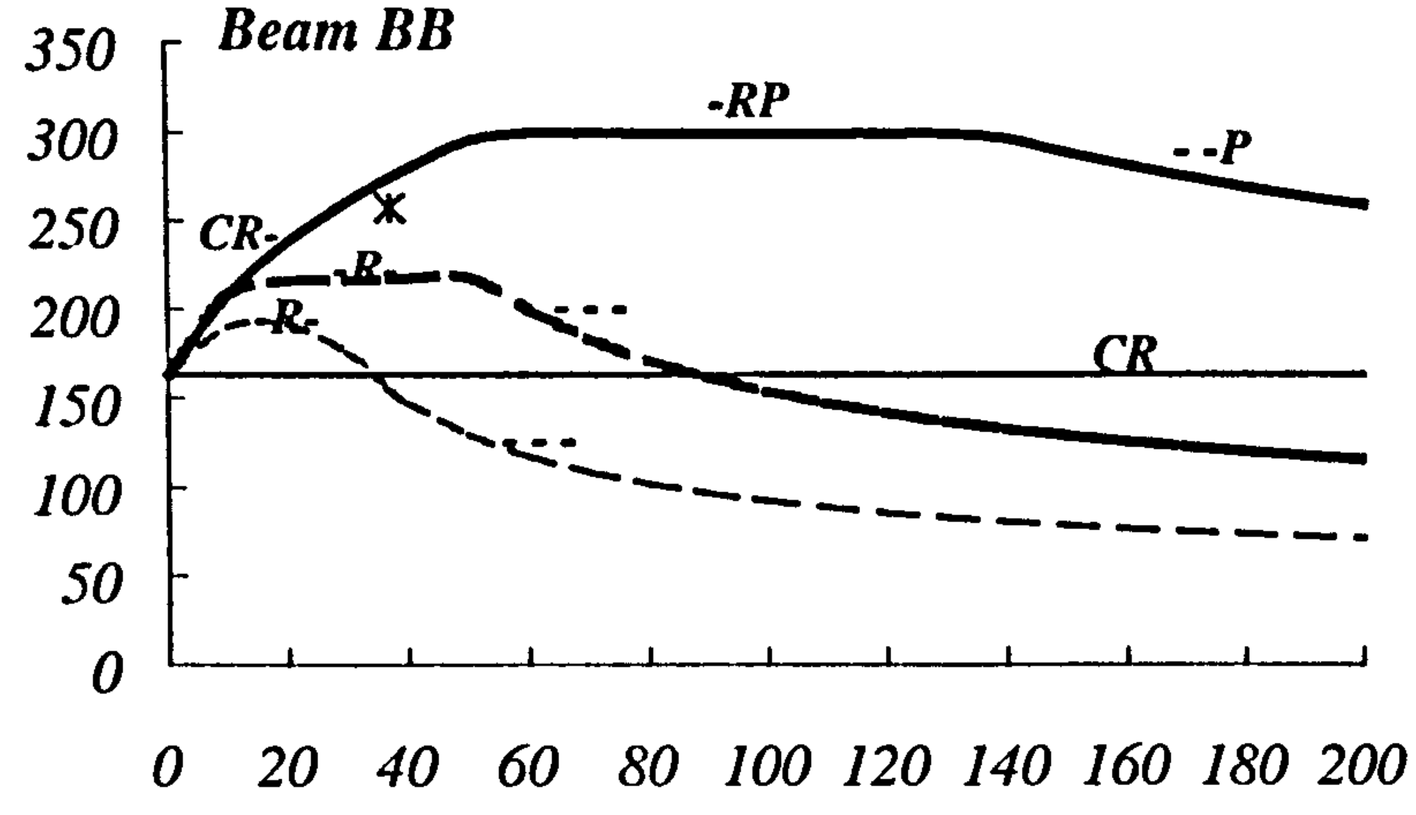

Fig. 6.62 Effect of E_p on failure moments for beam *BB*.

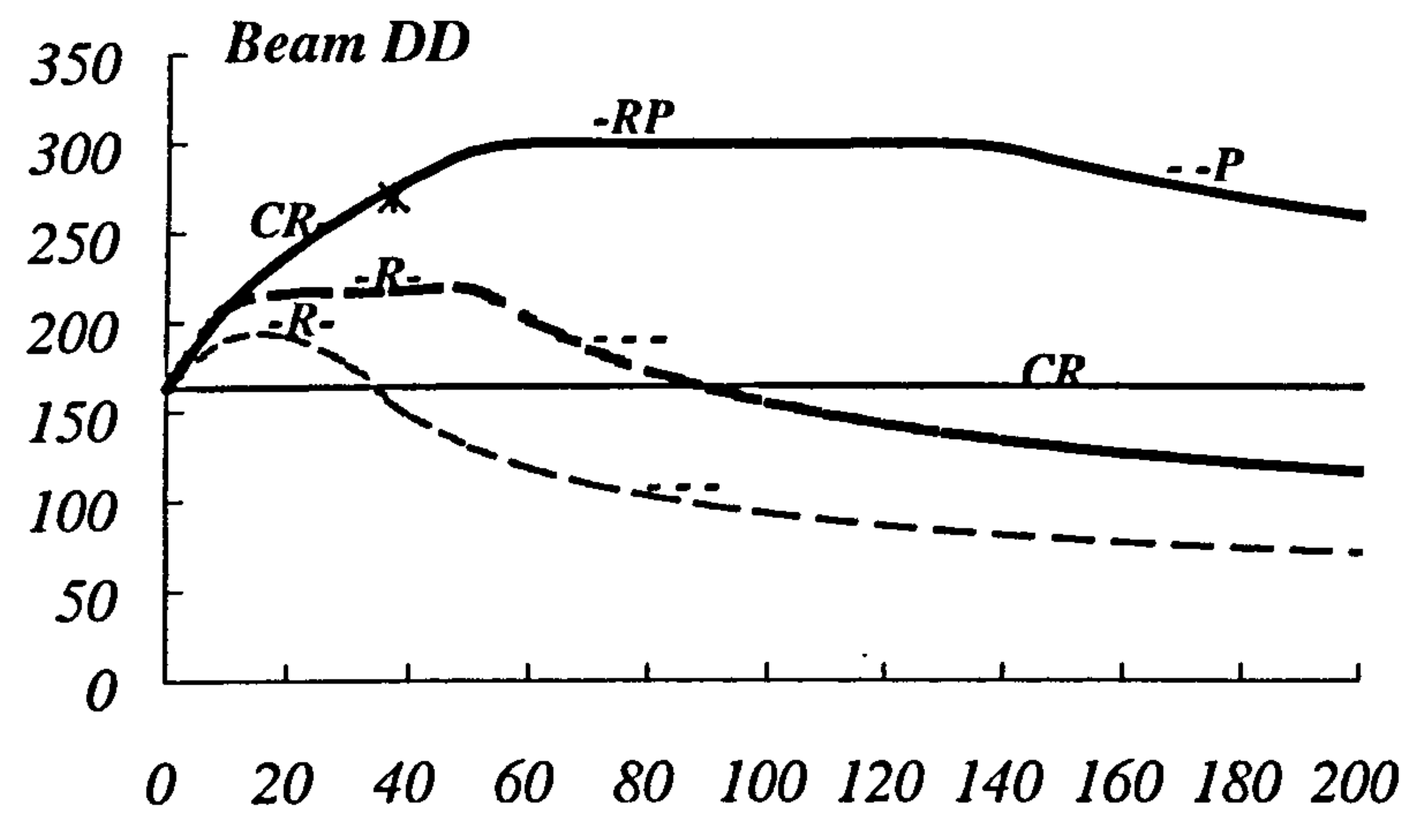

Fig. 6.63 Effect of E_p on failure moments for beam *DD*.

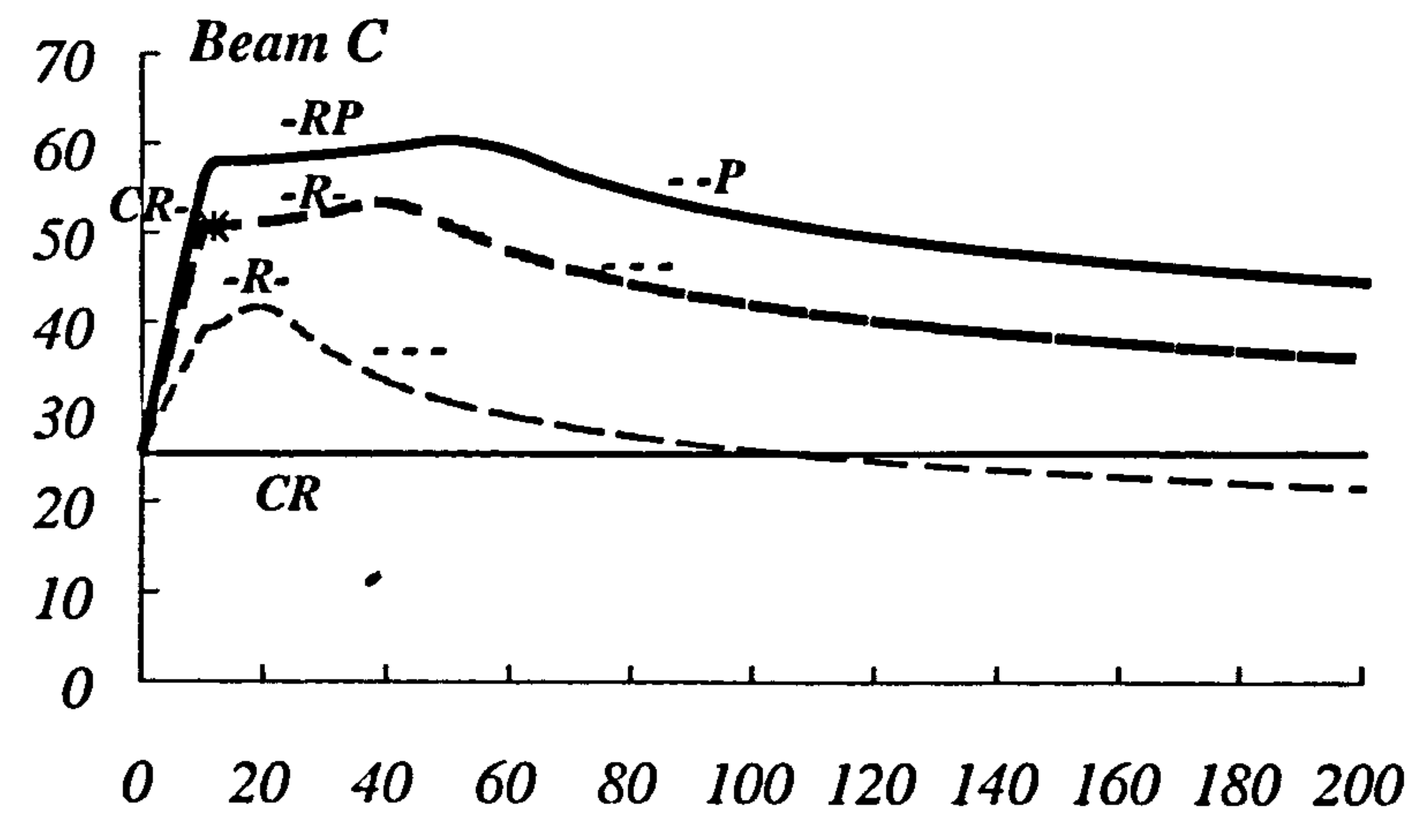

Fig. 6.64 Effect of E_p on failure moments for beam *C*.

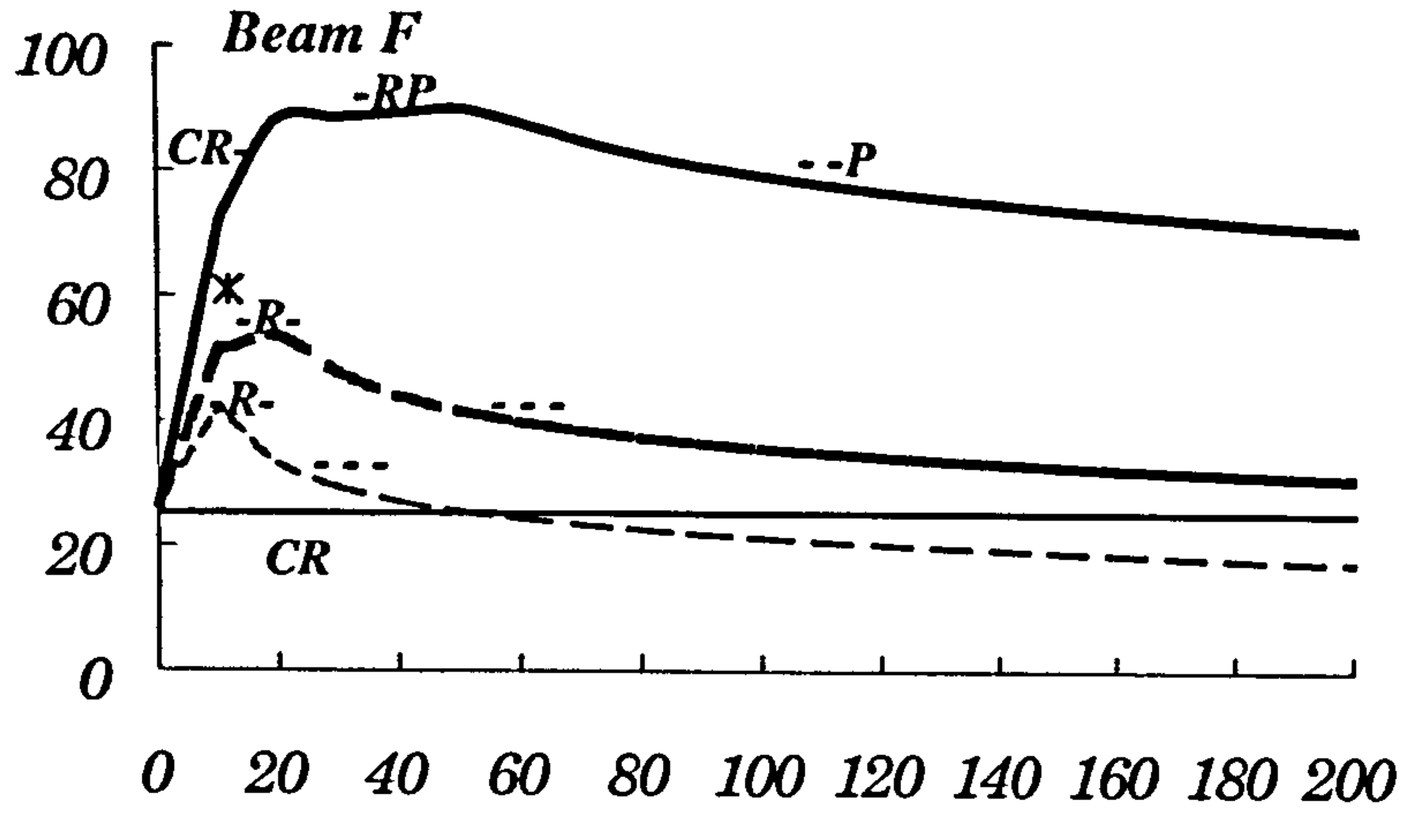

Fig. 6.65 Effect of E_p on failure moments for beam *F*.

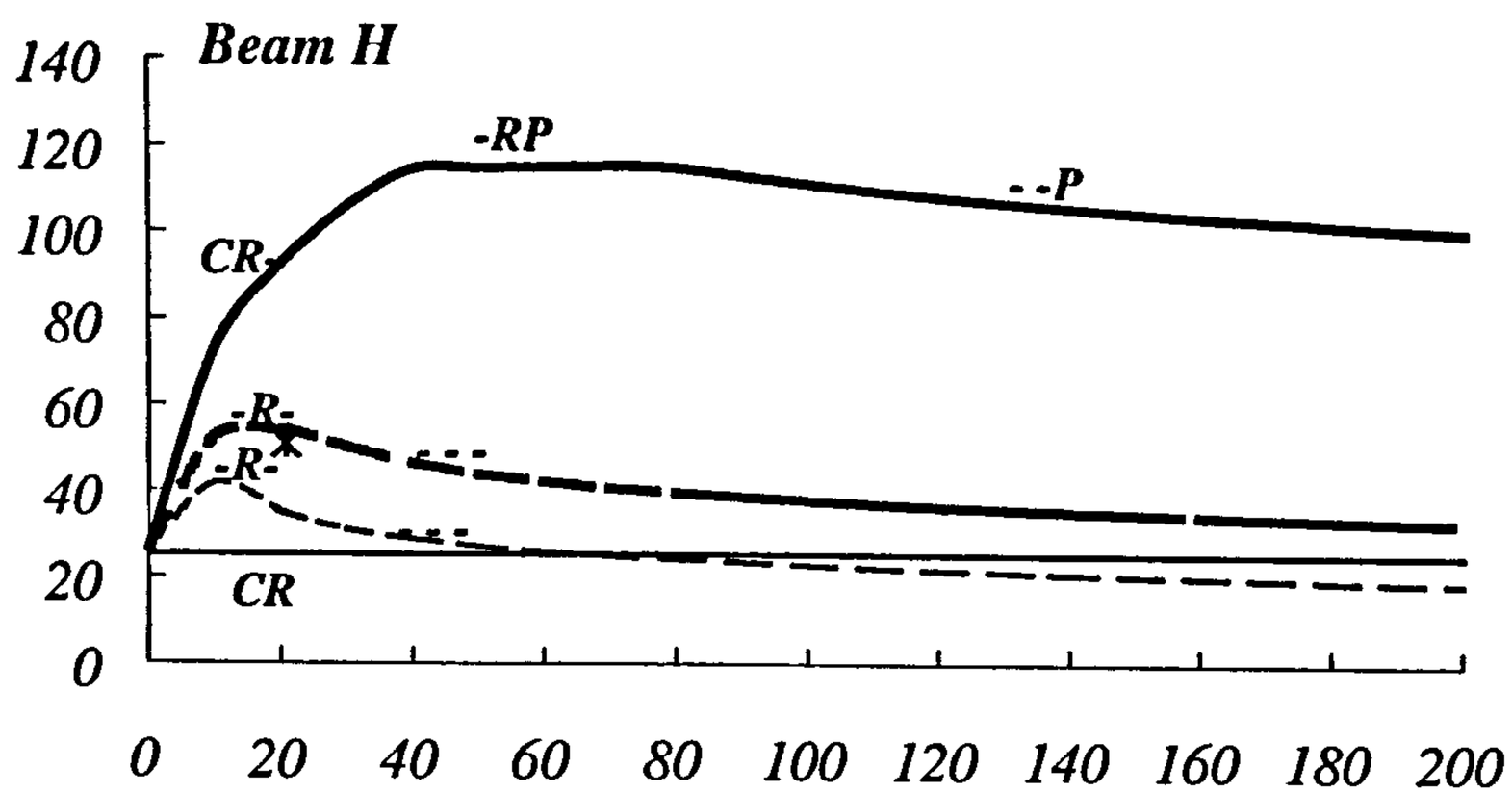

Fig. 6.66 Effect of E_p on failure moments for beam *H*.

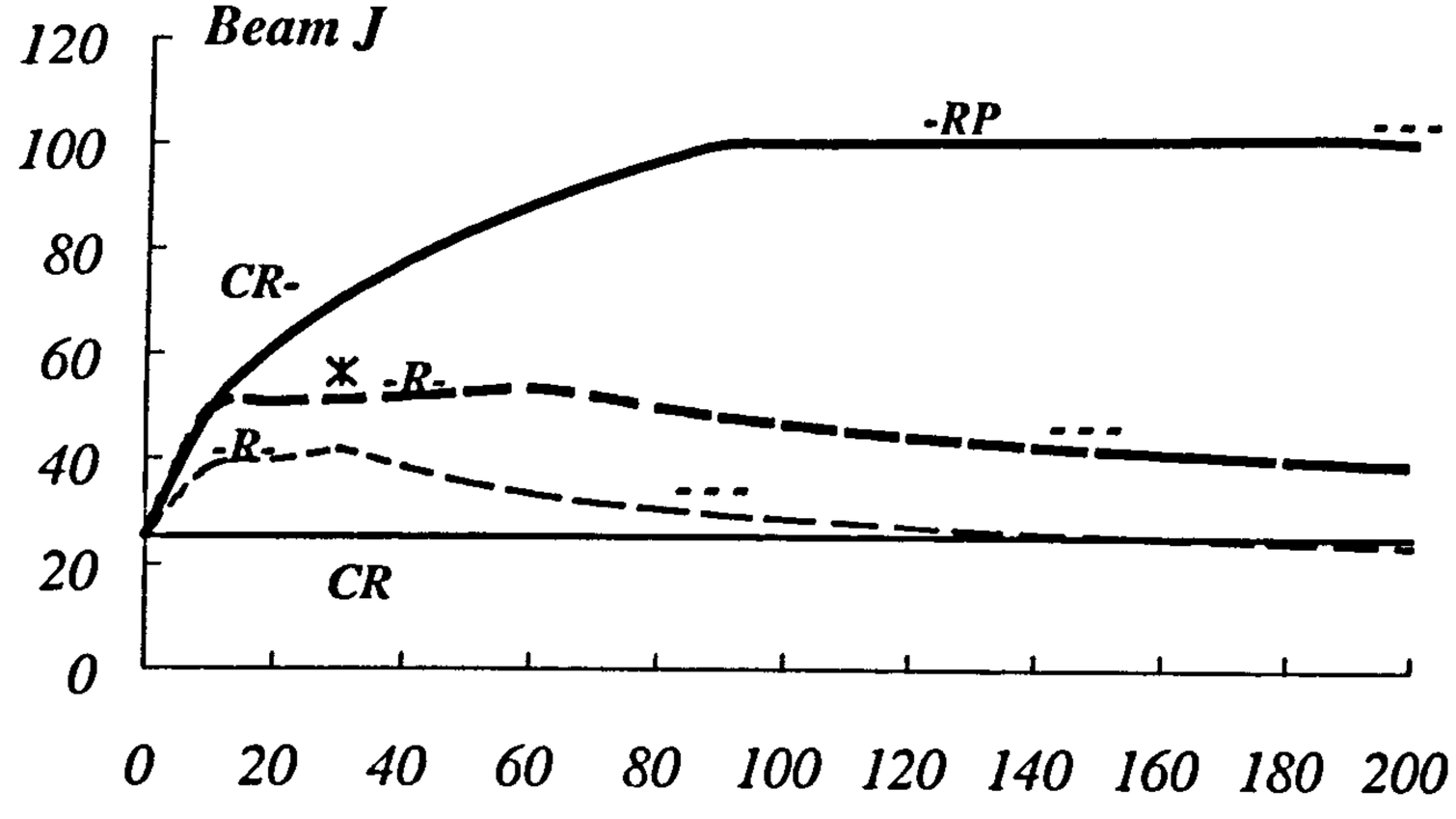

Fig. 6.67 Effect of E_p on failure moments for beam *J*.

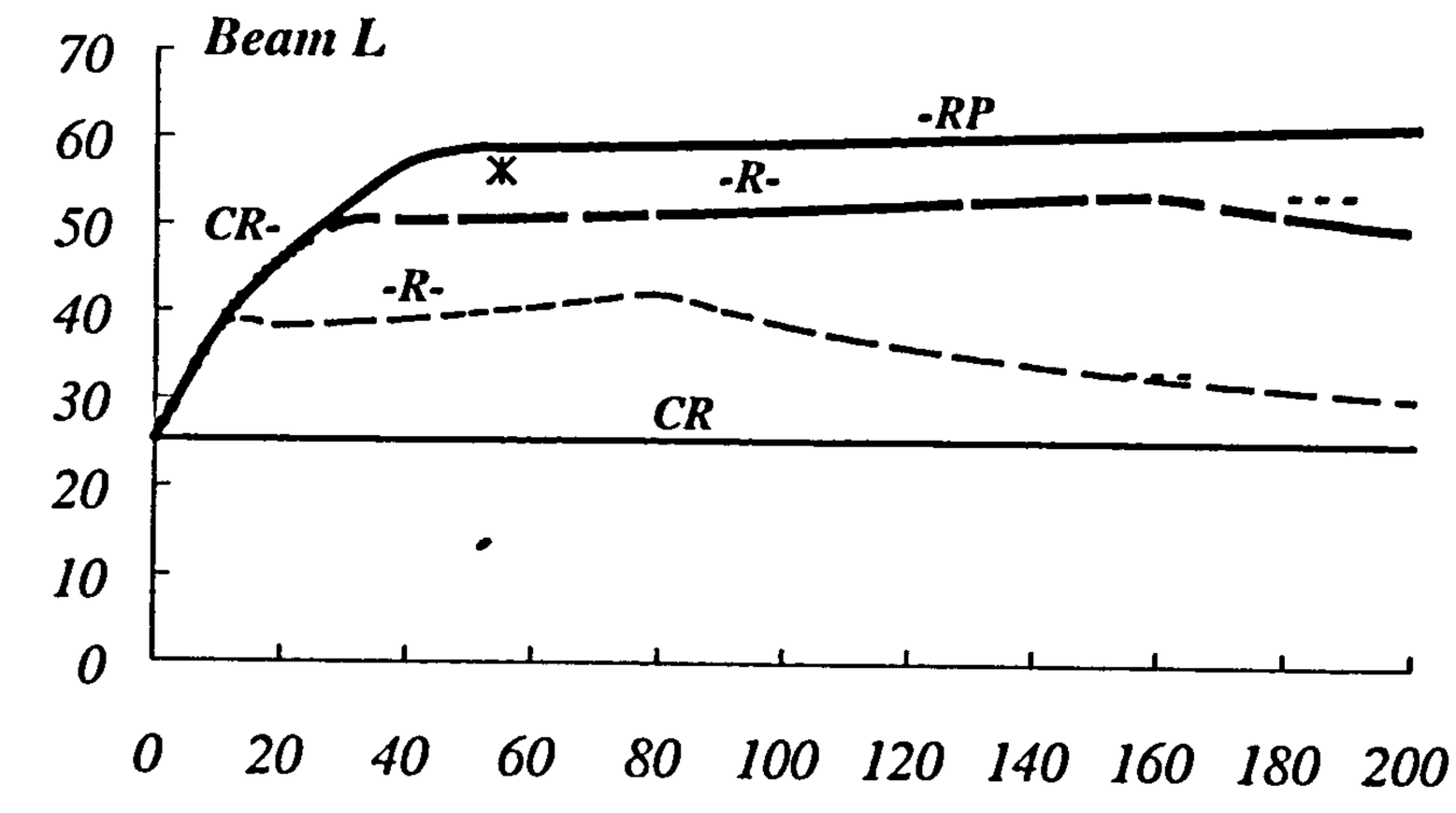

Fig. 6.68 Effect of E_p on failure moments for beam *L*.

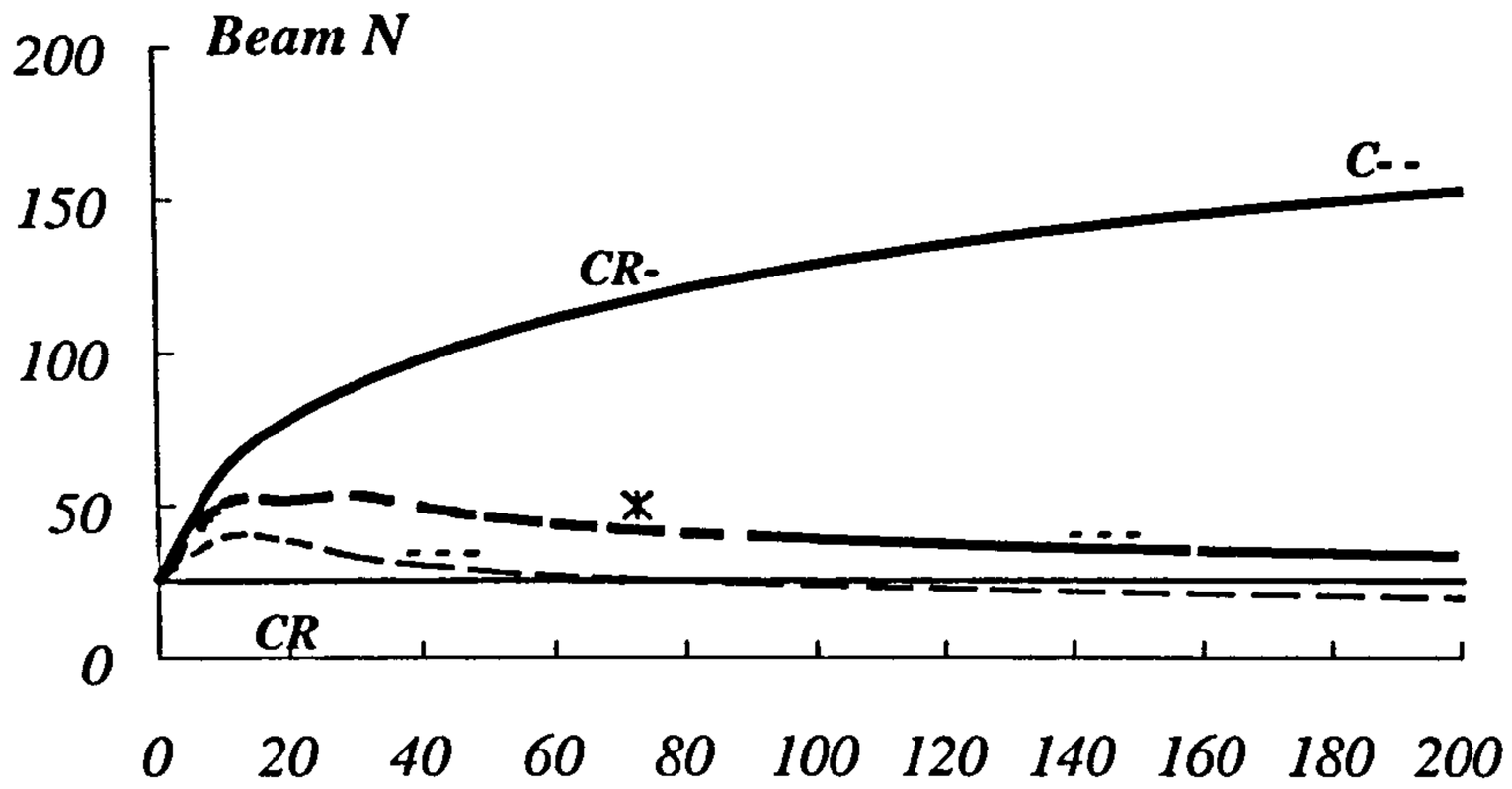

Fig. 6.69 Effect of E_p on failure moments for beam *N*.

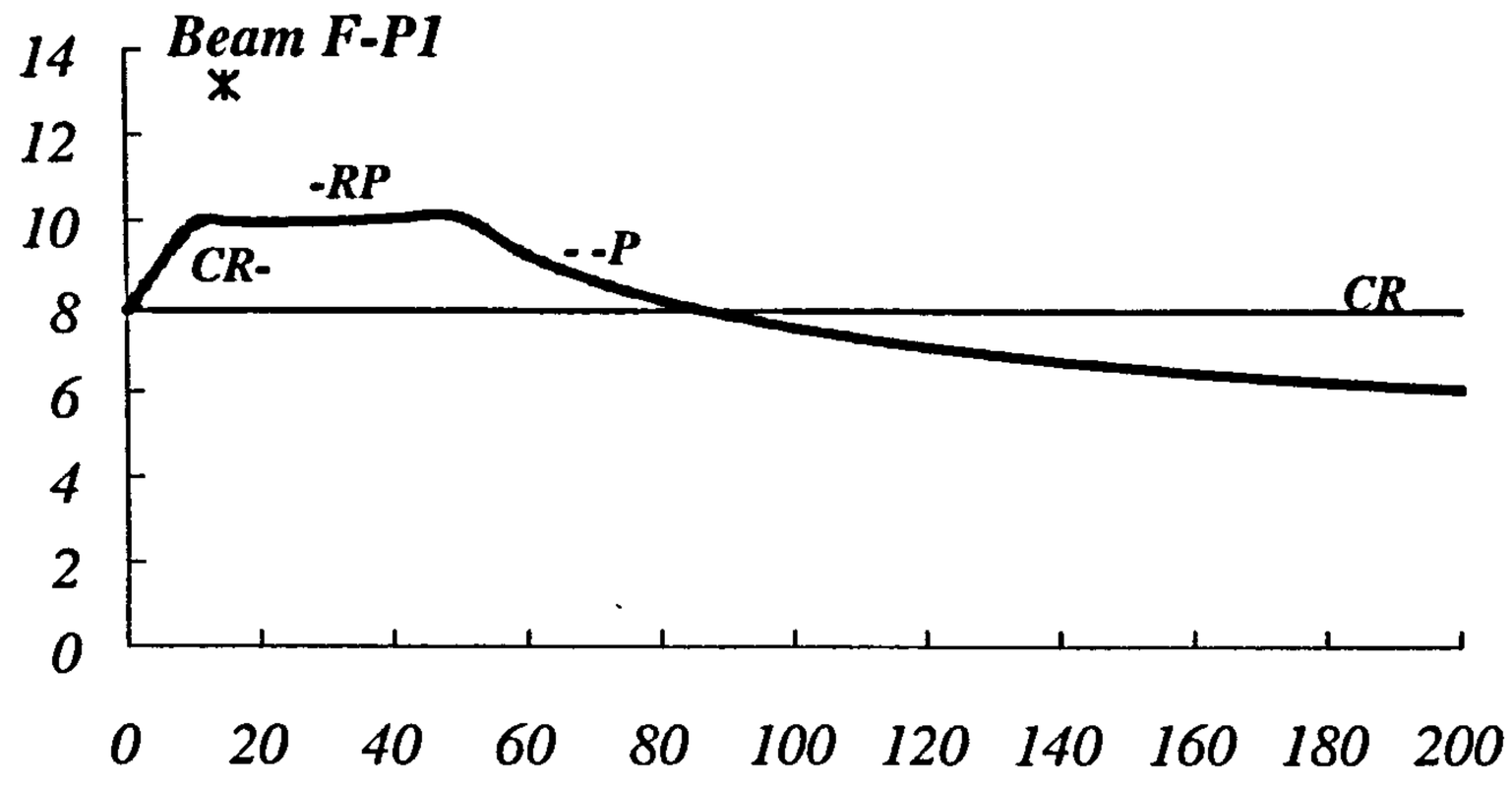

Fig. 6.70 Effect of E_p on failure moments for beam *F-P1*.

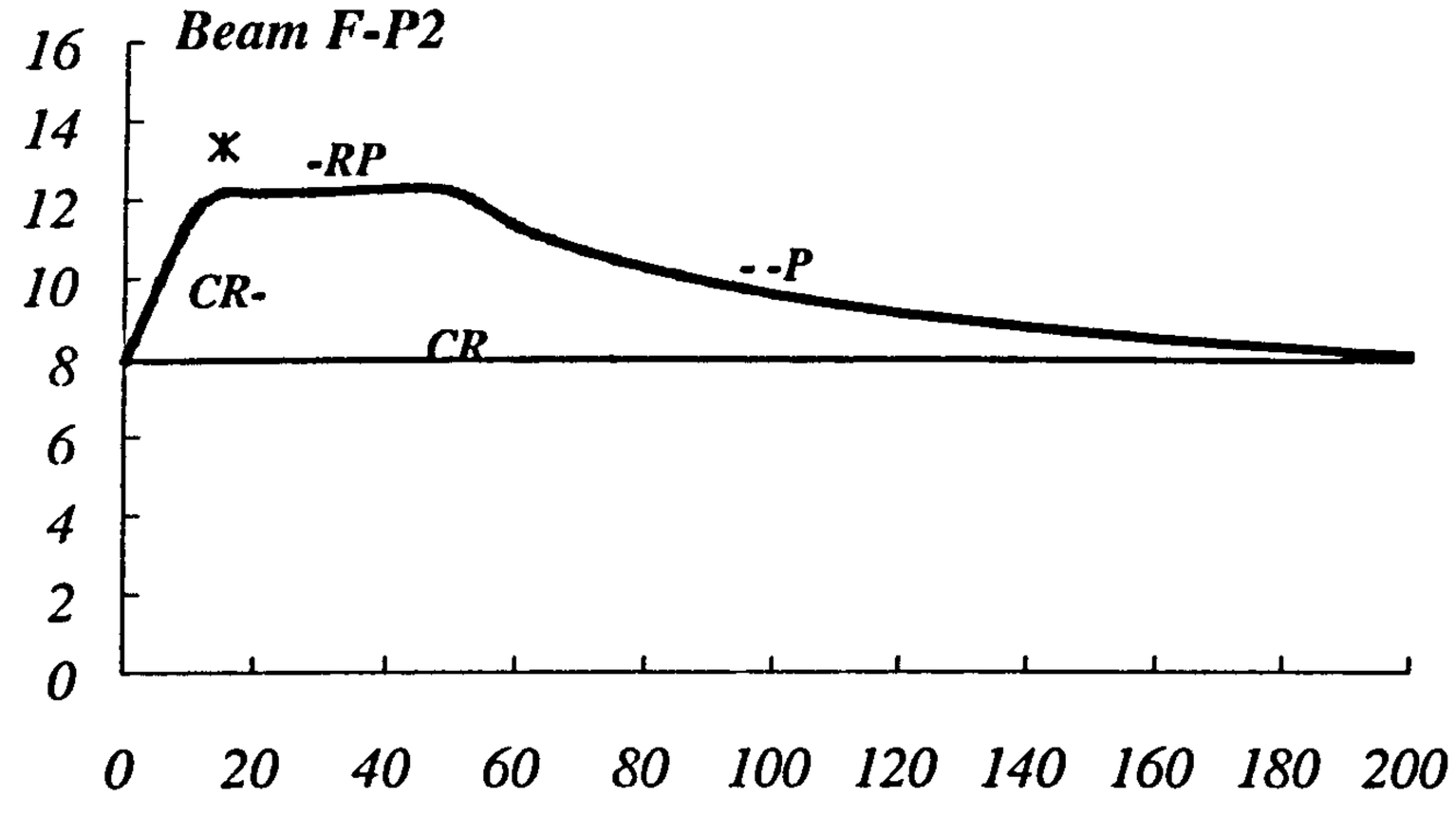

Fig. 6.71 Effect of E_p on failure moments for beam *F-P2*.

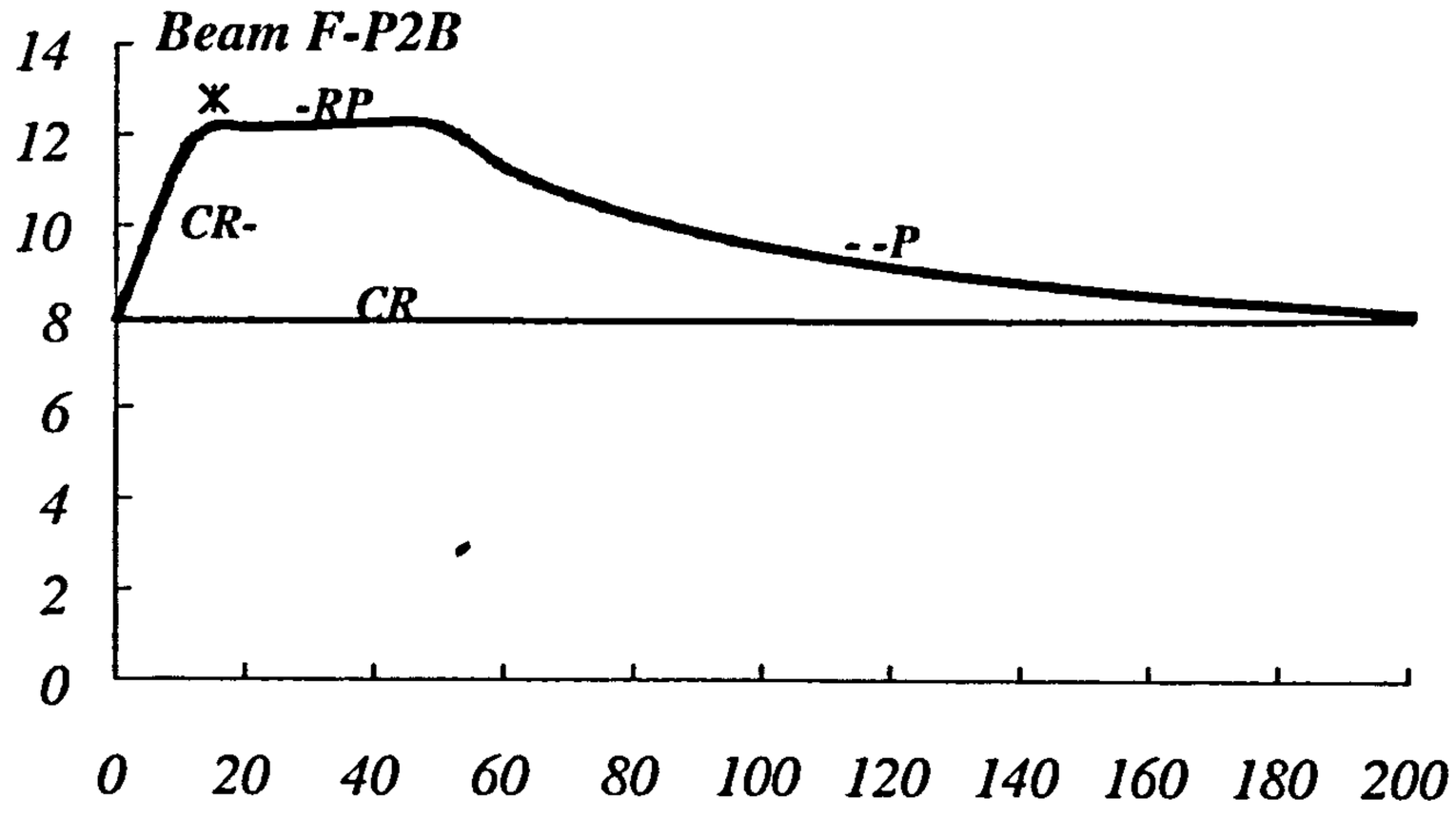

Fig. 6.72 Effect of E_p on failure moments for beam *F-P2B*.

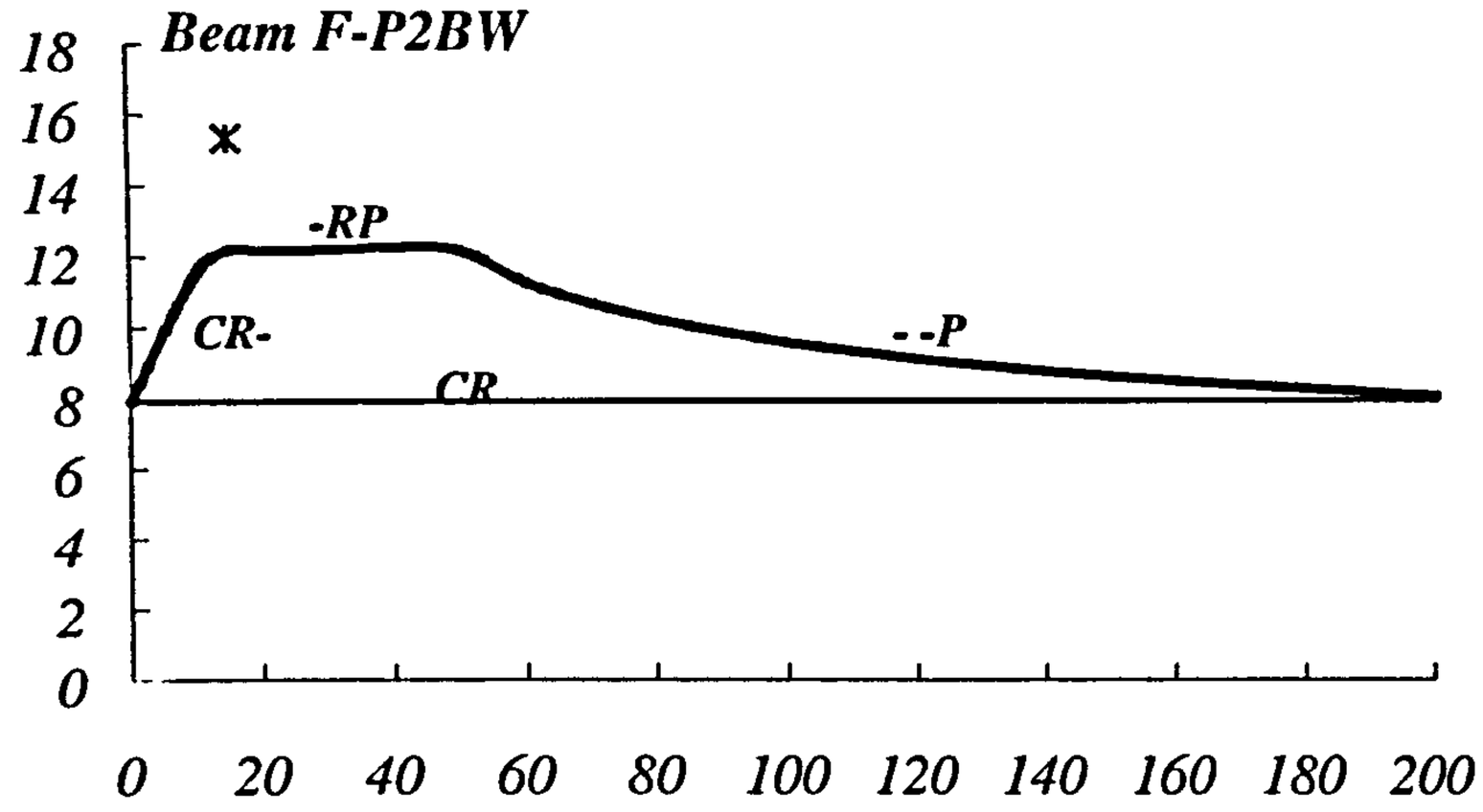

Fig. 6.73 Effect of E_p on failure moments for beam *F-P2BW*.

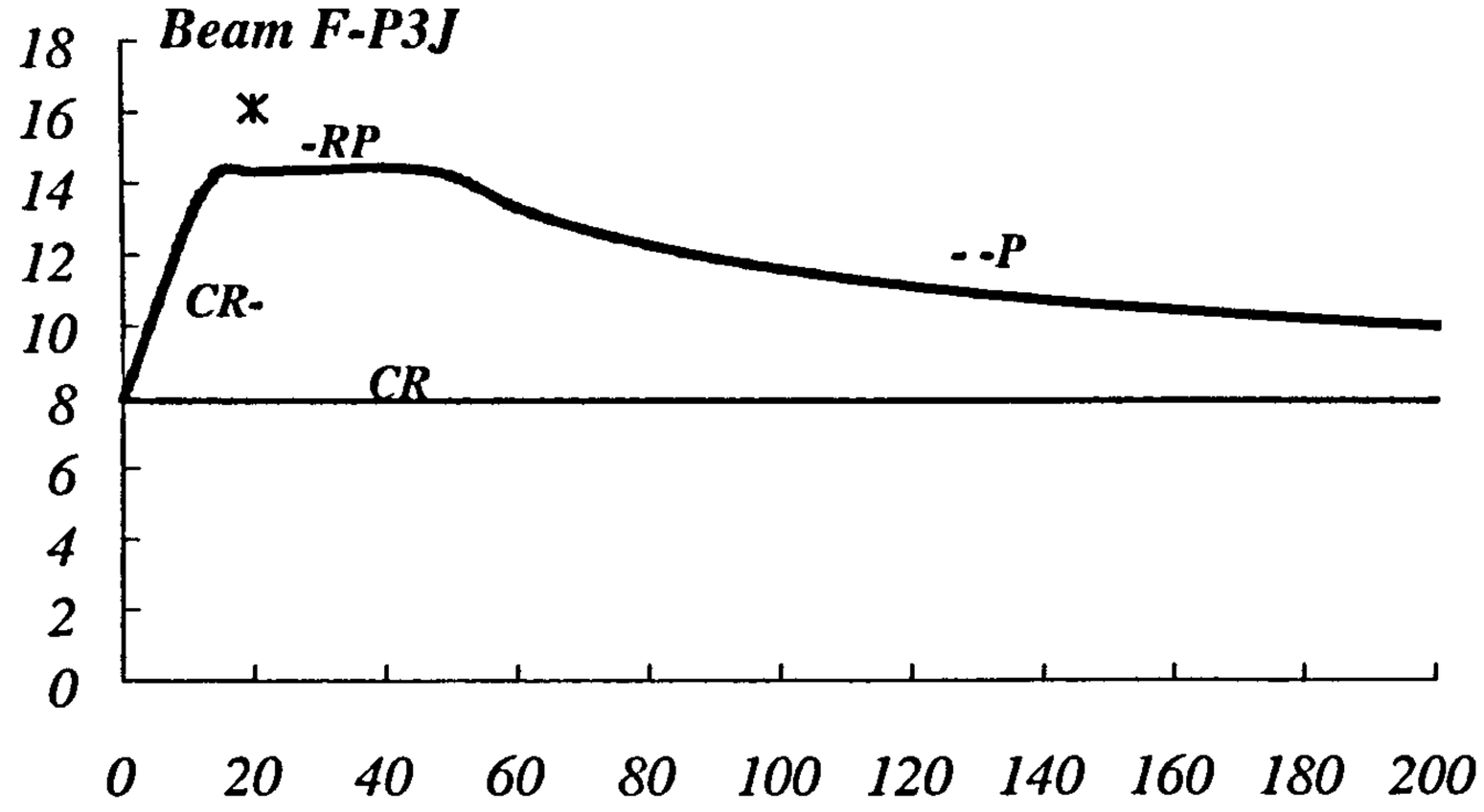

Fig. 6.74 Effect of E_p on failure moments for beam *F-P3J*.

Chapter 7

CRITICAL MODULI OF ELASTICITY FOR THE FRP PLATE

Chapter 7

CRITICAL MODULI OF ELASTICITY FOR THE FRP PLATE

7.1 INTRODUCTION

The purpose of this chapter is to develop the appropriate procedures for predicting the critical values of moduli of elasticity for externally bonded FRP plates which control the changes in the mode(s) of failure for a plated beam, hence, influencing its flexural load bearing capacity.

Details of the formulations for determining the key values of the plate moduli of elasticity, ***Ep***, which distinguish between the full bond and the plate peeling behaviour, will be presented. Simple means of determining the underlying types of failure (i.e. as to whether brittle or ductile), will also be addressed.

7.2 GENERAL

Structural designers face largely limited choices as regards specifying various characteristics of reinforced concrete beams which are in need of strengthening. The beam dimensions, configurations, the area of embedded bars and their arrangements, plus the characteristics of concrete and steel (such as their strengths) are already fixed in practical strengthening occasions and may not be altered. It, then, follows that the only parameters which are under the control of the designer are related to various external plate characteristics such as

1- the position, length, width, and thickness of the externally bonded plate,

2- the type of material (such as steel, carbon fiber reinforced plastics (CFRP), or glass fiber reinforced plastics (GFRP)) to be used for the plate,

3- the ultimate strength and modulus of elasticity for the plate material, and

4- the tensile and shear strength, shear modulus, and the thickness of the adhesive material (i.e. the epoxy glue).

7.3 CRITICAL MODULI OF ELASTICITY

In the previous chapter, it was shown that the magnitude of modulus of elasticity for the external FRP plate has a very significant influence as regards the determination of various modes of failure and associated flexural load bearing capacities relating to plated beams. Moreover, the behaviour of the composite beam was classified in terms of two types: (1) ductile (under-reinforced), or (2) brittle (over-reinforced), according to the key values of the plate moduli of elasticity, ***Ep,*** at points A ($E_{(A)}$) (in Figure 7.1) and C ($E_{(C)}$) as shown in Figure 7.6.

The minimum value of these two key ***Ep***-values is believed to determine the beam classification following which all the other critical points relating to changes in the mode of failure may, then, be determined. If $E_{(A)}$ at point A is lower than the corresponding value of $E_{(C)}$ at point C, then, the behaviour of plated beam will be of an under-reinforced type, otherwise the plated beam may be classified as an over-reinforced element. The underlying reason for this type of classification is based on the finding (to be discussed later) that the more the area of the externally bonded plate is, the less will be the magnitude of $E_{(C)}$, while the higher would be the associated

value of $E_{(A)}$ and, hence, the greater the possibility for the occurrence of the brittle mode *C- -* (which is a typical one for an over-reinforced unplated section).

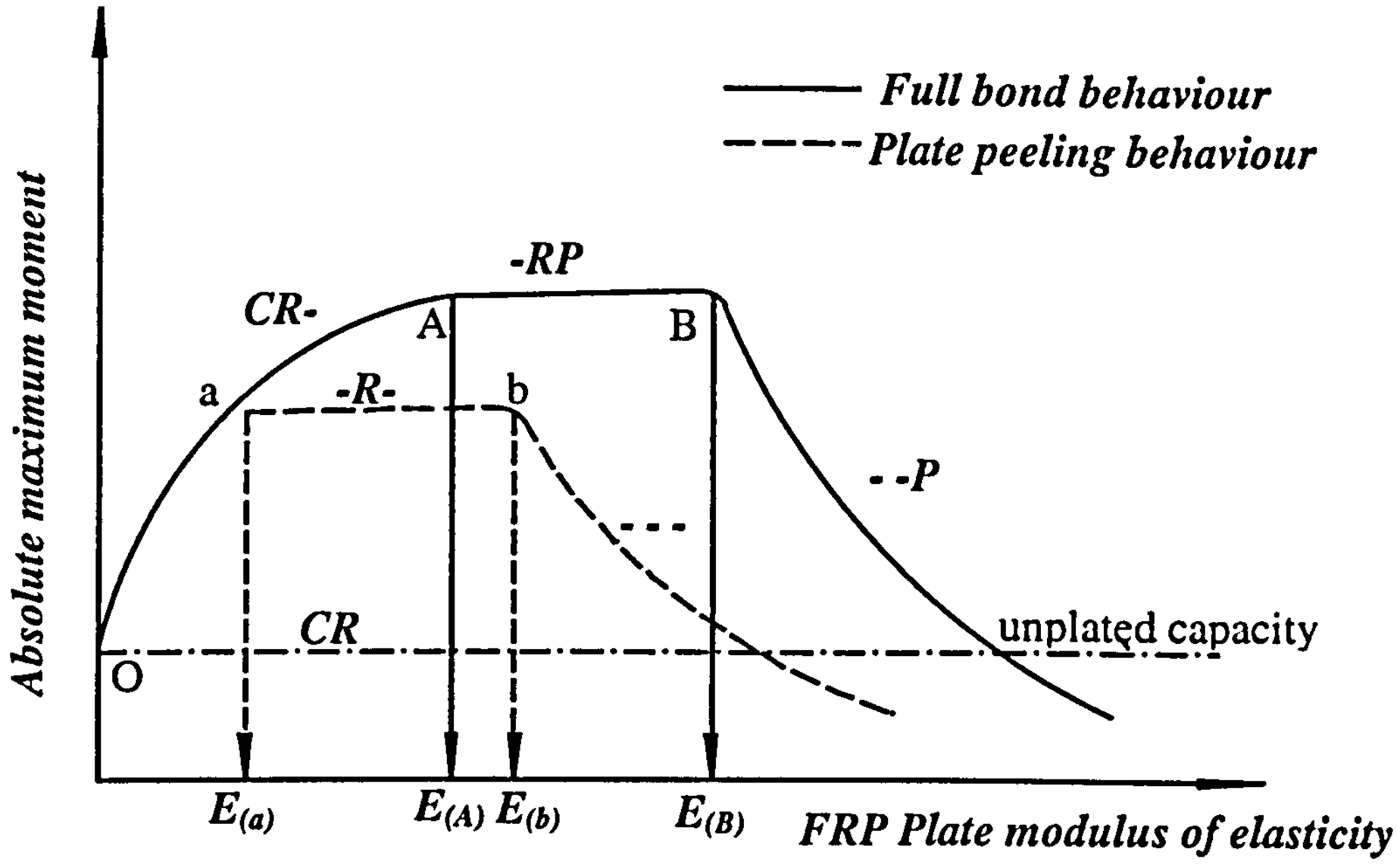

Fig. 7.1 Various modes of failure for an under-reinforced plated beam

In the following sections, such critical values of the plate moduli of elasticity will be formulated in a closed-form, hence, enabling one to have a simple means of predicting variations in the modes of failure associated with changes in the magnitude of modulus of elasticity for the externally bonded FRP plate.

7.3.1 Moduli of Elasticity for Under-Reinforced Plated Beams

Figure 7.1 presents the influence of variations in the magnitude of the FRP plate modulus of elasticity on the corresponding values of flexural load bearing capacity for typical under-reinforced plated beam designs as discussed in Chapter 6. This figure shows changes in the modes of failure for plated beams for those cases when the externally bonded plate acts as fully bonded to the concrete beam (path O-A-B), and also for cases when the composite beam fails prematurely, due to the plate peeling phenomenon (path O-a-b).

The plot for the flexural load bearing capacity of unplated beam is also shown for comparison, and it is not surprising that for diminishing values of the plate modulus of elasticity (approaching zero), the flexural load bearing capacity of the plated beam approaches the corresponding one for an unplated section.

7.3.1.1 Minimum Value of E_P for the Mode -RP (Point A)

For the initial mode of failure ***CR-***, when the axial plate stress first reaches the corresponding plate ultimate strength, f_{pu}, while the axial strain in the embedded bars, ε_s, is still larger than the corresponding yield strain for steel, ε_{sy}, then, the mode of failure ***CR-*** will be followed by the ***-RP*** mode: this will happen for those values of plate modulus of elasticity $E_{(A)}$ (point A, Figure 7.1) in connection with under-reinforced plated beams.

For the critical values of $E_{(A)}$, both the embedded bars and the plate are fully stressed, and the maximum concrete compressive strain, ε_o, is very nearly equal to the crushing value (i.e. $\varepsilon_o \cong 0.0035$) - see Figure 7.2.

Equation (7.1) expresses the equilibrium condition for the forces, corresponding to the plate modulus of elasticity $E_{(A)}$, making use of the relationship defining the value of concrete compression force (i.e. Equation (B.50) derived in Appendix B).

$$A_s f_y + A_p f_{pu} = A'_s E_s \varepsilon_o (1 - \frac{d'}{y_A}) + y_A b (\frac{\beta}{\varepsilon_o}) [\frac{E_c \beta}{6} + 0.67 f_{cu} (\frac{\varepsilon_o}{\beta} - \frac{2}{3})] \quad (7.1)$$

which may be re-written as

$$y_A^2 b (\frac{\beta}{\varepsilon_o}) [\frac{E_c \beta}{6} + 0.67 f_{cu} (\frac{\varepsilon_o}{\beta} - \frac{2}{3})] + y_A (A'_s E_s \varepsilon_o - A_s f_y - A_p f_{pu}) - A'_s E_s \varepsilon_o d' = 0 \quad (7.2)$$

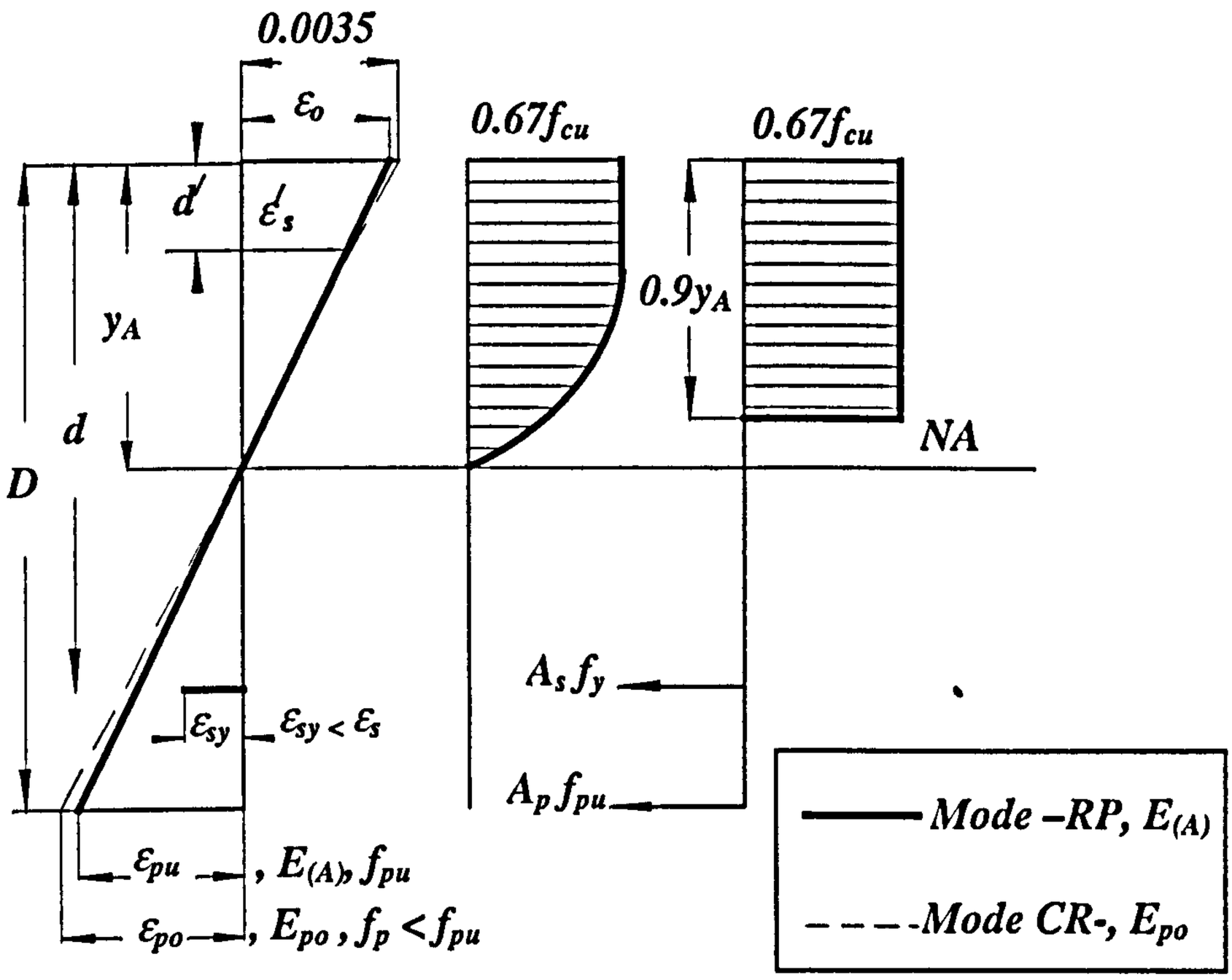

Fig. 7.2 Transition from the Mode *CR*- to the Mode -*RP*

The depth of neutral axis, y_A, may be determined from the above equation, while from the assumed strain distribution, as shown in Figure 7.2, one may arrive at the following:

$$\frac{\varepsilon_{pu}}{D-y_A} = \frac{0.0035}{y_A}$$

with

$$\varepsilon_{pu} = \frac{0.0035}{y_A}(D - y_A)$$

It follows that, the critical value of plate modulus of elasticity at point A, $E_{(A)}$, is

$$E_{(A)} = \frac{f_{pu}}{\varepsilon_{pu}} = \frac{f_{pu}}{0.0035}\frac{y_A}{(D-y_A)} \qquad (7.3)$$

If the influence of the embedded steel bars in the compression side is ignored, and the simplified stress block for concrete as that recommended by BS8110 (1985) is assumed (Figure 7.2), Equation (7.1) may be written as

$$A_s f_y + A_p f_{pu} = 0.9 y_A b \; x 0.67 f_{cu}$$

so that

$$y_A = \frac{A_s f_y + A_p f_{pu}}{0.67 f_{cu} 0.9 b}$$

The critical value of the plate modulus of elasticity, $E_{(A)}$, may, then, be determined by a very simple closed-form relationship:

$$E_{(A)} = \frac{f_{pu}}{\varepsilon_{pu}} = \frac{f_{pu}(A_s f_y + A_p f_{pu})}{0.0035(0.9x0.67 f_{cu} bD - A_s f_y - A_p f_{pu})} \qquad (7.4)$$

7.3.1.2 Minimum Value of E_P for the Mode - -P (Point B, Under-Reinforced)

In Chapter 6, it was shown that in the ductile mode ***–RP***, the axial strains in the plate and the embedded steel bars are reduced with the associated increasing values of E_p. At a certain value of E_p ($E_{(B)}$ in Figure 7.1), the axial strain in the embedded bars will be reduced to that equal to yield strain (i.e. $\varepsilon_s \equiv \varepsilon_{sy}$) and, then, the failure of the beam will be due to plate rupture in the absence of associated large deformations (i.e. the brittle - -*P* mode takes place).

The conditions corresponding to the critical value of $E_{(B)}$ are that the embedded bars experience yield (i.e. their axial stresses are equal to f_y) and that the axial plate stress is at its maximum possible level ($=f_{pu}$), while the associated values of concrete

stresses and strains are not critical – see Figure 7.3: the following relationships may, therefore, be derived

$$\frac{\varepsilon_{sy}}{d-y_B}=\frac{\varepsilon_{pu}}{D-y_B}=\frac{\varepsilon_s'}{y_B-d'}$$

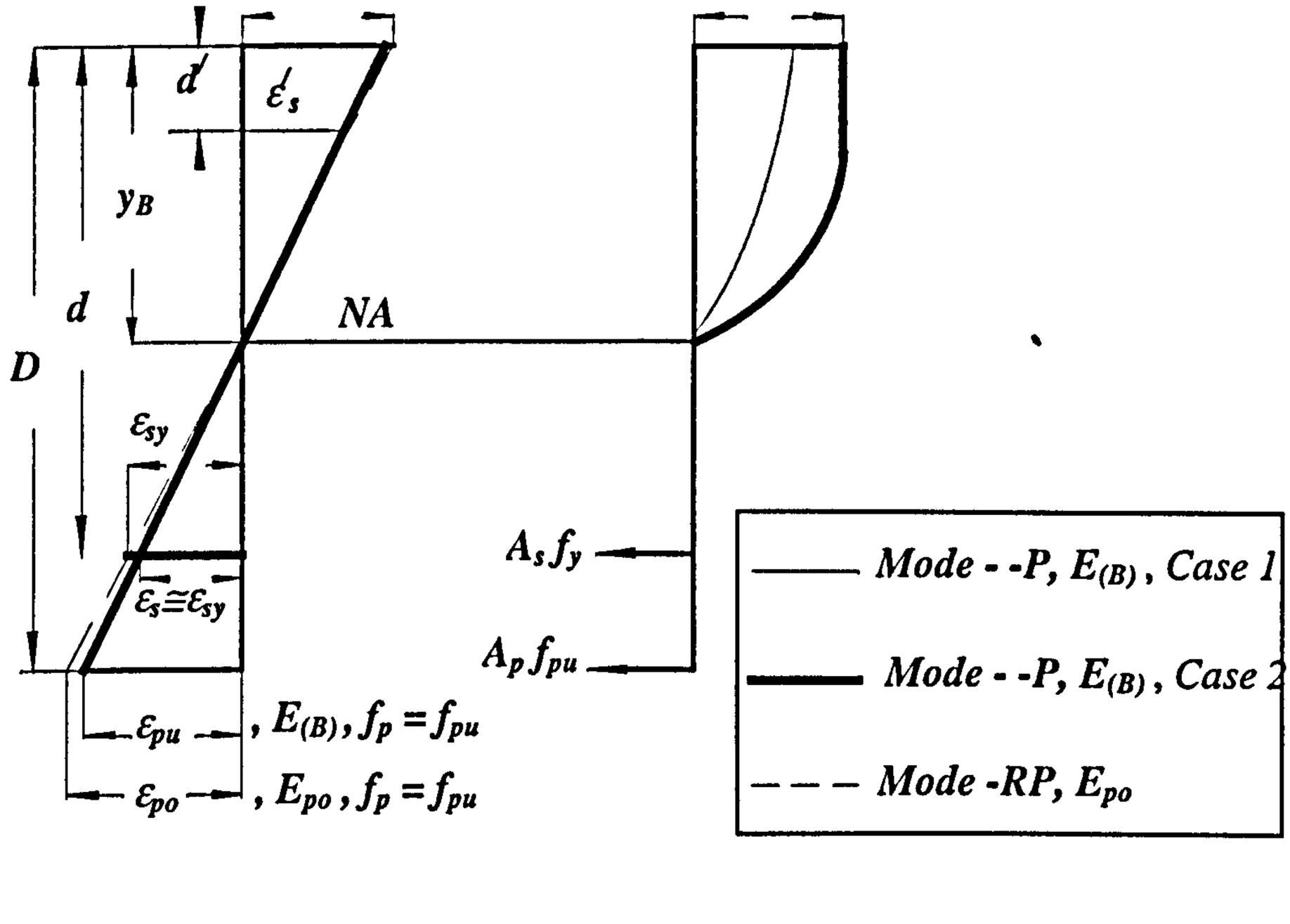

Fig. 7.3 Transition from the Mode -*RP* to the Mode - -*P*

Since the concrete is not in the crushing state, there will be two cases to be considered as regards the total value of concrete compression force – see the discussion in Appendix B. The first case corresponds to those instances when the maximum concrete stress is less than $0.67f_{cu}$, in which case the total compression force may be expressed by the following equation - see Appendix B, Equation (B.53)

$$F_c = A_s' E_s \varepsilon_s \frac{y-d'}{d-y} + \frac{bE_c}{2}\left(\frac{\varepsilon_s}{d-y}\right)y^2 + \frac{bK_1}{3}\left(\frac{\varepsilon_s}{d-y}\right)^2 y^3 \qquad (7.5)$$

where

$$K_1 = \frac{0.67 f_{cu} - E_c \beta}{\beta^2}$$

In the second case, on the other hand, the maximum concrete stress becomes equal to $0.67f_{cu}$, but the corresponding maximum concrete compressive strain will be less than 0.0035 although greater than β: the total concrete compression force, F_c, may, then, be expressed by the following Equation - see Appendix B, Equation (B.40) .

$$F_c = A'_s E_s \varepsilon_s \frac{y-d'}{d-y} + 0.67 f_{cu} b\left(y + \frac{\beta}{\varepsilon_s} y - \frac{\beta}{\varepsilon_s} d \right) + \frac{bE_c}{2} \frac{\beta^2}{\varepsilon_s}(d-y) + \frac{bK_1}{3} \frac{\beta^3}{\varepsilon_s}(d-y) \quad \textbf{(7.6)}$$

For both cases (1) and (2), the equilibrium equation of section forces may be used to determine the depth of neutral axis y_B (as explained in the following sections), with the total tension force, F_T, given by

$$F_T = A_s f_y + A_p f_{pu}$$

7.3.1.2.1 Case 1

The equilibrium equation for section forces corresponding to *case 1* is

$$A_s f_y + A_p f_{pu} = A'_s E_s \varepsilon_s \frac{y_{B1} - d'}{d - y_{B1}} + \frac{bE_c}{2} \left(\frac{\varepsilon_s}{d - y_{B1}}\right) y_{B1}^2 + \frac{bK_1}{3} \left(\frac{\varepsilon_s}{d - y_{B1}}\right)^2 y_{B1}^3$$

Multiply the above equation by $(d - y_{B1})^2$, to get

$$(A_s f_y + A_p f_{pu})(d - y_{B1})^2 = A'_s E_s \varepsilon_s (y_{B1} - d')(d - y_{B1}) +$$

$$\frac{bE_c \varepsilon_s}{2}(d - y_{B1}) y_{B1}^2 + \frac{bK_1 \varepsilon_s^2}{3} y_{B1}^3$$

$$y_{B1}^3[K_2 - K_E] + y_{B1}^2[K_E d - K' - K_T] + y_{B1}[K'(d + d') + 2K_T d] - (K' dd' + K_T d^2) = 0 \quad \textbf{(7.7)}$$

where

$$K_2 = \frac{bK_1 \varepsilon_s^2}{3}, \; K_1 = \frac{0.67 f_{cu} - E_c \beta}{\beta^2}, \; K_E = \frac{bE_c \varepsilon_s}{2}, \; K' = A'_s E_s \varepsilon_s \text{ and}$$

$$K_T = (A_s f_y + A_p f_{pu})$$

By solving Equation (7.7) (using a trial and error method), the neutral axis depth, y_{B1}, may be determined. The associated maximum value of concrete compressive strain, ε_o, is given by

$$\varepsilon_o = \varepsilon_{sy} \frac{y_{B1}}{d - y_{B1}} \qquad (7.8)$$

If the maximum concrete strain ε_o is less than β (where, $\beta = 2.44 \times 10^{-4} \sqrt{f_{cu}}$), then, the initially assumed stress distribution over the section is valid, and the so-calculated neutral axis depth is the correct one. However, if ε_o turns out to be more than β, the depth of neutral axis should be calculated according to the following procedure for *case 2*.

7.3.1.2.2 Case 2

The equilibrium equation for section forces in the *case 2*, is

$$A_s f_y + A_p f_{pu} = A_s' E_s \varepsilon_s \frac{y_{B2} - d'}{d - y_{B2}} + 0.67 f_{cu} b (y_{B2} + \frac{\beta}{\varepsilon_s} y_{B2} - \frac{\beta}{\varepsilon_s} d) + \frac{bE_c}{2} \frac{\beta^2}{\varepsilon_s} (d - y_{B2}) + \frac{bK_1}{3} \frac{\beta^3}{\varepsilon_s} (d - y_{B2})$$

$$(A_s f_y + A_p f_{pu})(d - y_{B2}) = A_s' E_s \varepsilon_s (y_{B2} - d')(d - y_{B2}) + 0.67 f_{cu} by (d - y_{B2}) + [\frac{bE_c}{2} \frac{\beta^2}{\varepsilon_s} + \frac{bK_1}{3} \frac{\beta^3}{\varepsilon_s} - 0.67 f_{cu} b \frac{\beta}{\varepsilon_s}](d - y_{B2})^2$$

$$K_T (d - y_{B2}) = K' (y_{B2} - d')(d - y_{B2}) + K_f y (d - y_{B2}) + K_3 (d - y_{B2})^2$$

where

$$K_3 = [\frac{bE_c}{2} \frac{\beta^2}{\varepsilon_s} + \frac{bK_1}{3} \frac{\beta^3}{\varepsilon_s} - 0.67 f_{cu} b \frac{\beta}{\varepsilon_s}] \text{ and } K_f = 0.67 f_{cu} by$$

which may be written as;

$$y_{B2}^2[K_3 - K' - K_f] + y_{B2}[d(K' + K_f - 2K_3) + K'd' + K_T] + d[K_3 d - K'd' - K_T] = 0$$

By solving the above equation, the depth of neutral axis, y_{B2}, may be determined and, then, the maximum compressive strain in concrete may be calculated as in *Case 1* (Equation (7.8)) to ensure that it is more than β.

Using the appropriate value of y_B (either from *Case 1* or *Case 2*), the minimum value of $E_{(B)}$ for the mode **- -*P*** to be initiated may, then, be calculated as follows:

$$\frac{\varepsilon_{pu}}{D - y_B} = \frac{\varepsilon_{sy}}{d - y_B}$$

and

$$\varepsilon_o = \frac{f_y}{E_s}\frac{(D - y_B)}{(d - y_B)}$$

with

$$E_{(B)} = \frac{f_{pu}}{\varepsilon_{pu}} = \frac{(d - y_B)}{(D - y_B)}\frac{f_{pu}}{f_y}E_s \qquad (7.9)$$

7.3.1.3 Minimum Value of E_p for the Mode -R- (Point a)

For the failure mode ***CR-***, if the plate axial stress first reaches the plate peeling stress, and if there are no arrangements to prevent occurrence of such premature peeling (such as implementation of plate end anchorages), while the axial strain in the embedded bars, ε_s, is still larger than the yield strain for steel, ε_{sy}, then, the mode of failure will change from ***CR-*** to the ***-R-*** mode, and this will happen at the critical value of the plate modulus of elasticity $E_{(a)}$ - see point a in Figure 7.1, or Figure 7.6.

The conditions associated with the critical value of plate modulus of elasticity, $E_{(a)}$, are that the embedded bars are fully stressed, that the plate axial stress is equal to the peeling value, σ_s, and that the maximum concrete compressive strain is very nearly equal to the crushing value (i.e. $\varepsilon_o \cong 0.0035$): under these conditions, the mode of failure will be changed from concrete crushing to that of plate peeling – see Figure 7.4.

Following the same procedures as those used for the determination of the value of $E_{(A)}$, the depth of neutral axis, y_a, may be determined from the following

$$y_a^2 b(\frac{\beta}{\varepsilon_o})[\frac{E_c \beta}{6} + 0.67 f_{cu}(\frac{\varepsilon_o}{\beta} - \frac{2}{3})] + y_a(A_s' E_s \varepsilon_o - A_s f_y - A_p \sigma_s) - A_s' E_s \varepsilon_o d' = 0$$

and, based on the strain distribution in Figure 7.4

$$\frac{\varepsilon_{pel}}{D - y_a} = \frac{0.0035}{y_a}$$

The magnitude of critical axial plate strain, ε_{pel}, which causes the transfer from the ***CR-*** mode to the ***-R-*** mode, will be

$$\varepsilon_{pel} = \frac{0.0035}{y_a}(D - y_a)$$

while, the minimum plate modulus of elasticity, $E_{(a)}$, for the mode ***-R-*** at the critical point a, in Figure 7.1, may be determined from

$$E_{(a)} = \frac{\sigma_s}{\varepsilon_{pel}} = \frac{\sigma_s}{0.0035}\frac{y_a}{(D - y_a)} \qquad \textbf{(7. 10)}$$

Ignoring the influence of the steel bars in the compression side, and using a simplified stress block for concrete as that recommended by BS8110 (1985) (Figure 7.4)

$$y_a = \frac{A_s f_y + A_p \sigma_s}{0.67 f_{cu} 0.9b}$$

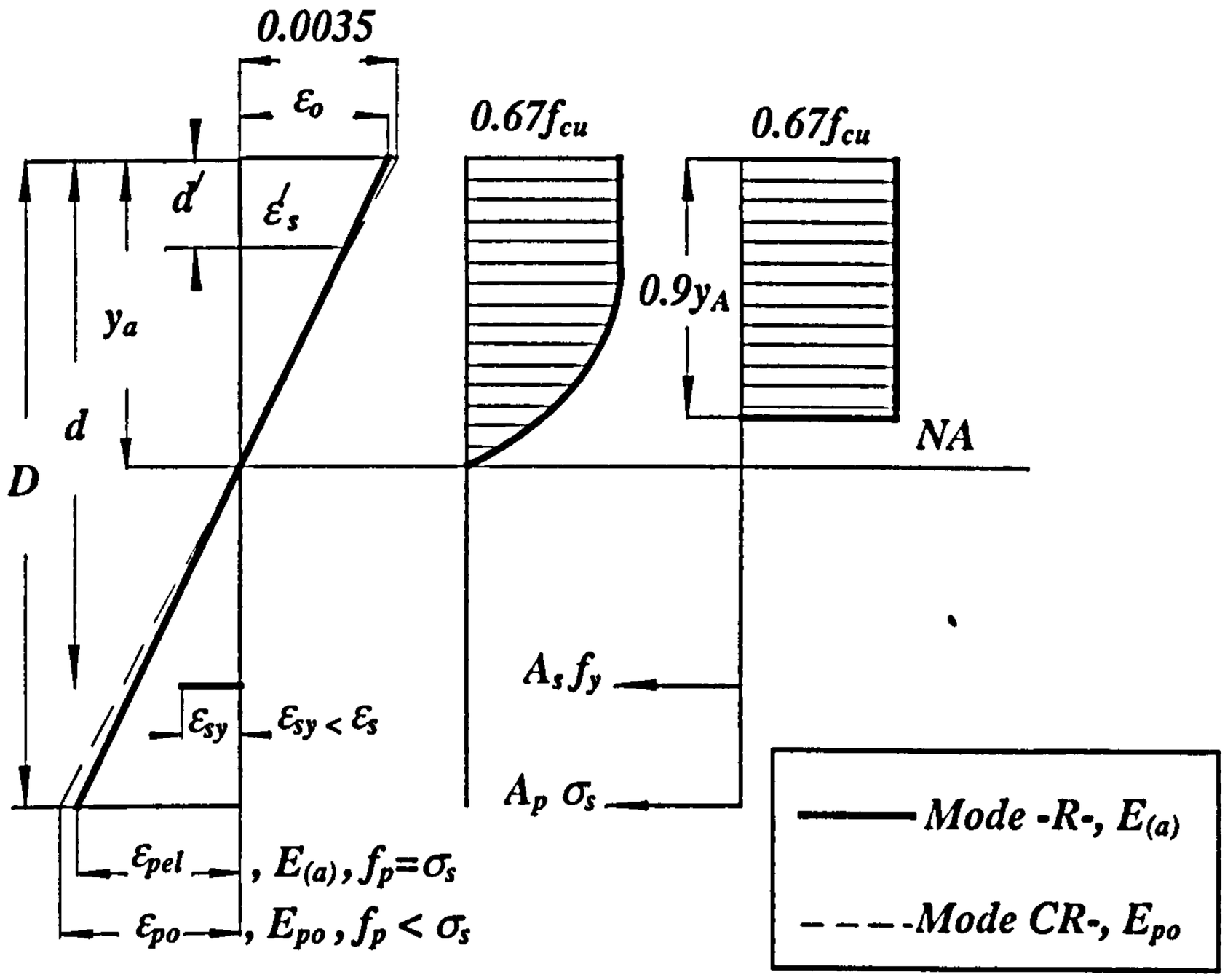

Fig. 7.4 Transition from the Mode *CR*- to the Mode -*R*-

Under such conditions, therefore, the critical plate modulus of elasticity, $E_{(a)}$, may be determined by the following simple formula

$$E_{(a)} = \frac{\sigma_s}{\varepsilon_{pel}} = \frac{\sigma_s (A_s f_y + A_p \sigma_s)}{0.0035(0.9x0.67 f_{cu} bD - A_s f_y - A_p \sigma_s)} \qquad (7.11)$$

7.3.1.4 Minimum Value of E_p for the Mode - - - (Point b, Under-Reinforced)

In Chapter 6, it was shown that in the ductile mode –*R*-, increasing the magnitude of E_p reduces the axial strains in the plate and the embedded steel bars. At a certain value of E_p (corresponding to $E_{(b)}$ in Figure 7.1), the strain in the embedded bars will be sufficiently reduced to be equal to the yield value (i.e. $\varepsilon_s \cong \varepsilon_{sy}$) and, then, the failure

may be attributed to the plate peeling, occurring in the absence of associated large deformations (i.e. the brittle - - - mode).

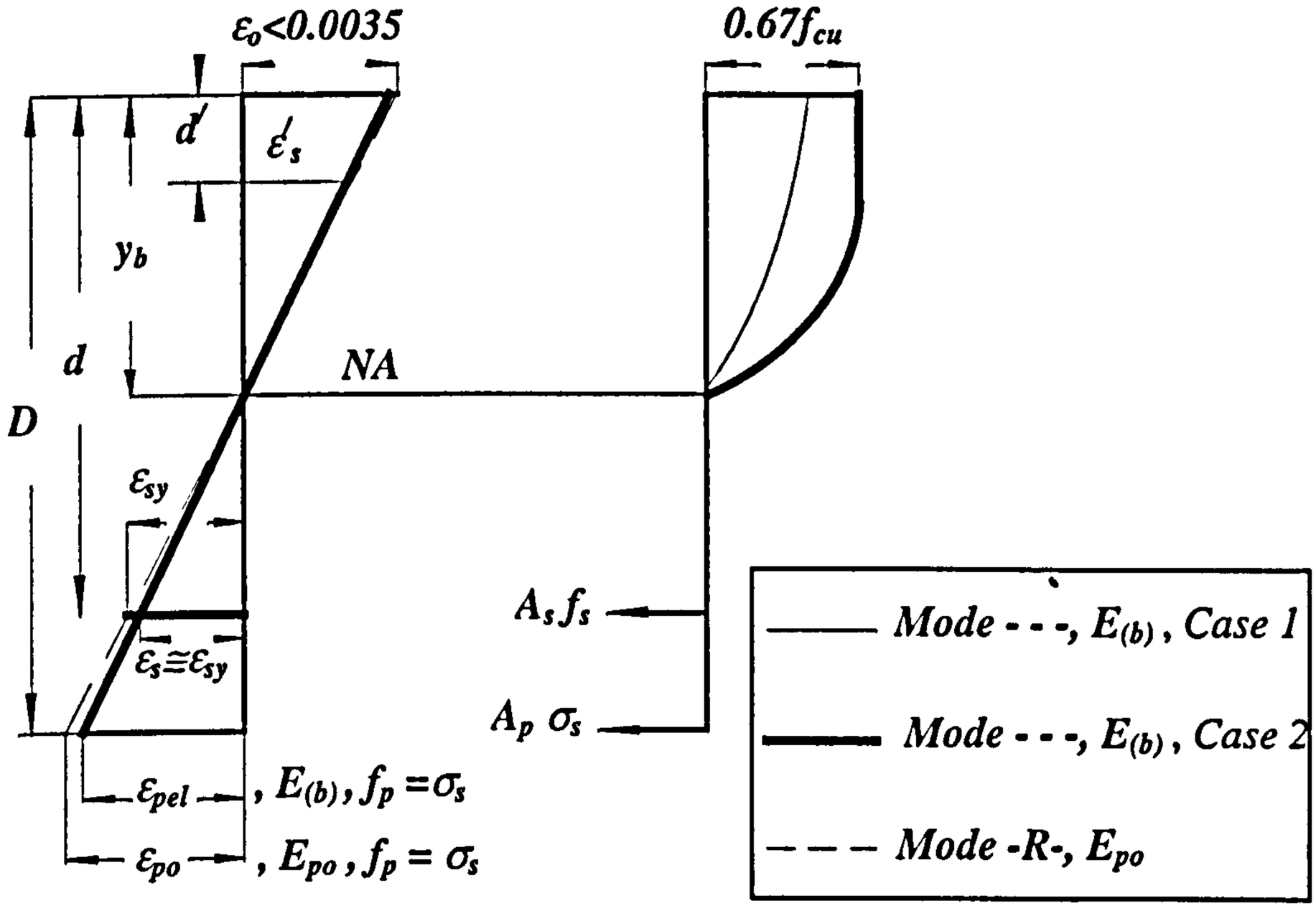

Fig. 7.5 Transition from the Mode -*R*- to the Mode - - -

Under these conditions, for the critical value of $E_{(b)}$, the axial strains in the embedded bars are just equal to that of yield for steel, ε_{sy}, and the corresponding plate axial stress will be equal to the critical plate peeling stress, σ_s, while the values of stresses and strains in concrete will not be the critical ones – see Figure 7.5: in such cases, the following hold

$$\frac{\varepsilon_{sy}}{d - y_b} = \frac{\varepsilon_{pel}}{D - y_b} = \frac{\varepsilon_s'}{y_b - d'} \qquad \textbf{(7.12)}$$

Since the concrete is not in the crushing state, two distinctly different cases should be considered for the determination of total concrete compression force – see the discussions in section (7.3.1.2), leading to Equations (7.5) and (7.6).

For both cases, the equilibrium equation for section forces should be used in order to determine the depth of neutral axis, y_b (to be discussed in the following sections), with the total tension force given by

$$F_T = A_s f_y + A_p \sigma_s \qquad \textbf{(7. 13)}$$

7.3.1.4.1 Case 1

The equilibrium equation relating to section forces for *Case 1* is

$$A_s f_y + A_p \sigma_s = A_s' E_s \varepsilon_s \frac{y_{b1} - d'}{d - y_{b1}} + \frac{bE_c}{2}\left(\frac{\varepsilon_s}{d - y_{b1}}\right) y_{b1}^2 + \frac{bK_1}{3}\left(\frac{\varepsilon_s}{d - y_{b1}}\right)^2 y_{b1}^3$$

Multiply the above equation by $(d - y_{b1})^2$, to get

$$(A_s f_y + A_p \sigma_s)(d - y_{b1})^2 = A_s' E_s \varepsilon_s (y_{b1} - d')(d - y_{b1}) + \frac{bE_c \varepsilon_s}{2}(d - y_{b1}) y_{b1}^2 + \frac{bK_1 \varepsilon_s^2}{3} y_{b1}^3$$

$$y_{b1}^3[K_2 - K_E] + y_{b1}^2[K_E d - K' - K_T] + y_{b1}[K'(d + d') + 2K_T d] - (K' dd' + K_T d^2) = 0 \qquad \textbf{(7. 14)}$$

where

$K_2 = \frac{bK_1 \varepsilon_s^2}{3}$, $K_1 = \frac{0.67 f_{cu} - E_c \beta}{\beta^2}$, $K_E = \frac{bE_c \varepsilon_s}{2}$, $K' = A_s' E_s \varepsilon_s$ and

$K_T = (A_s f_y + A_p \sigma_s)$

By solving equation (7.14), using a method of trial and error, the depth of neutral axis, y_{b1}, may be determined. The corresponding maximum value of concrete compressive strain, ε_o, may be calculated from the following

$$\varepsilon_o = \varepsilon_{sy} \frac{y_{b1}}{d - y_{b1}} \qquad \textbf{(7. 15)}$$

If the so-obtained value of maximum concrete strain, ε_o, is found to be less than β (where, $\beta = 2.44\times10^{-4}\sqrt{f_{cu}}$), then, the assumed stress distribution is considered to be a valid one, and the predicted depth of neutral axis is assumed to be correct. However, if ε_o is found to be more than β, the correct value of the depth of neutral axis should be calculated following the procedure presented in the next section (*Case 2*).

7.3.1.4.2 Case 2

The equilibrium equation of section forces for this case is

$$A_s f_y + A_p \sigma_s = A_s' E_s \varepsilon_s \frac{y_{b2} - d'}{d - y_{b2}} + 0.67 f_{cu} b (y_{b2} + \frac{\beta}{\varepsilon_s} y_{b2} - \frac{\beta}{\varepsilon_s} d) + \frac{bE_c}{2} \frac{\beta^2}{\varepsilon_s} (d - y_{b2}) + \frac{bK_1}{3} \frac{\beta^3}{\varepsilon_s} (d - y_{b2})$$

After multiplying by $(d - y_{b2})$ and rearranging, one gets

$$(A_s f_y + A_p \sigma_s)(d - y_{b2}) = A_s' E_s \varepsilon_s (y_{b2} - d')(d - y_{b2}) + 0.67 f_{cu} by(d - y_{b2}) + [\frac{bE_c}{2} \frac{\beta^2}{\varepsilon_s} + \frac{bK_1}{3} \frac{\beta^3}{\varepsilon_s} - 0.67 f_{cu} b \frac{\beta}{\varepsilon_s}](d - y_{b2})^2$$

or

$$K_T(d - y_{b2}) = K'(y_{b2} - d')(d - y_{b2}) + K_f y(d - y_{b2}) + K_3(d - y_{b2})^2$$

where

$$K_3 = [\frac{bE_c}{2} \frac{\beta^2}{\varepsilon_s} + \frac{bK_1}{3} \frac{\beta^3}{\varepsilon_s} - 0.67 f_{cu} b \frac{\beta}{\varepsilon_s}] \quad \text{and} \quad K_f = 0.67 f_{cu} by \quad K' = A_s' E_s \varepsilon_s ,$$

and, $K_T = (A_s f_y + A_p \sigma_s)$

One, finally, arrives at the following

$$y_{b2}^2[K_3 - K' - K_f] + y_{b2}[d(K' + K_f - 2K_3) + K'd' + K_T] + d[K_3 d - K'd' - K_T] = 0$$

By solving the above equation, the depth of neutral axis, y_{b2}, may be determined and, then, the corresponding value of maximum compressive strain in concrete may be calculated as in the first case, using equation (7.15), to ensure that it is more than β.

Using the appropriate value of y_b (as determined from either *Case 1* or *Case 2*), the minimum critical value of $E_{(b)}$, for initiation of the mode - -P, may be estimated as follows

$$\frac{\varepsilon_{pel}}{D-y_b} = \frac{\varepsilon_{sy}}{d-y_b}$$

and

$$\varepsilon_{pel} = \frac{f_y}{E_s}\frac{(D-y_b)}{(d-y_b)}$$

with

$$E_{(b)} = \frac{\sigma_s}{\varepsilon_{pel}} = \frac{(d-y_b)}{(D-y_b)}\frac{\sigma_s}{f_y}E_s \qquad \textbf{(7. 16)}$$

7.3.2 Critical Values of the Moduli of Elasticity for Over-Reinforced Plated Beams

Figure 7.6 presents the influence of variations in the magnitude of modulus of elasticity for the FRP plate on the corresponding modes of failure for over-reinforced plated beams (as discussed in Chapter 6).

The figure presents the variations in the flexural modes of failure for the plated beam if the external bonded plate acts as fully bonded to concrete up to beam's failure (path O-C-D), and also covers those cases when the beam experiences premature failure due

to plate peeling (path O-C-d). If there are no provisions made to prevent the occurrence of plate peeling, and if the plate peeling stress is relatively low (i.e. lower than that for the mode *C- -*, at point C), then, the composite beam would follow the path O-a-b as an under-reinforced member - as fully discussed earlier in this chapter.

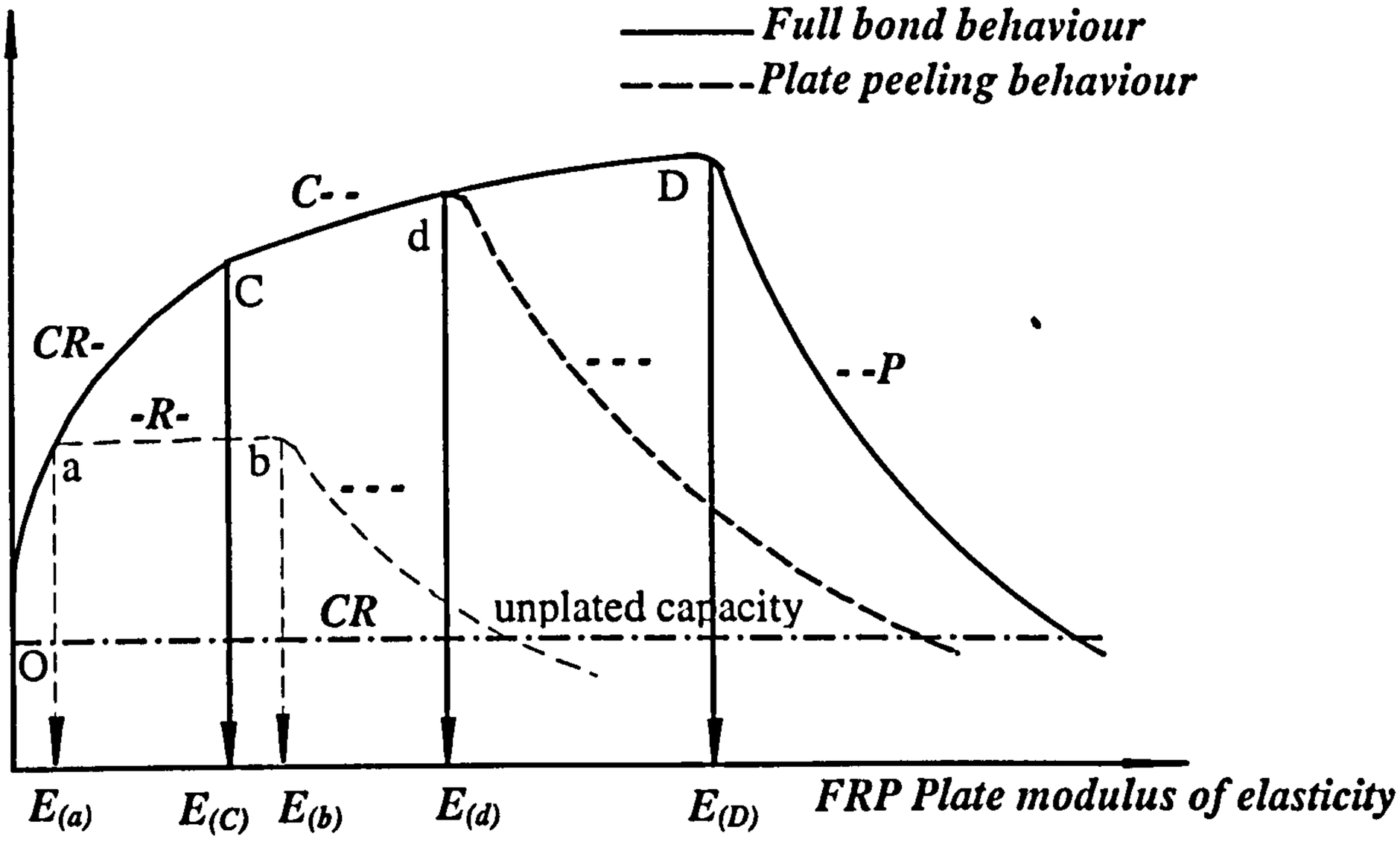

Fig. 7.6 Various failure modes for an over-reinforced plated beam

7.3.2.1 Minimum Value of E_p for the Mode C- - (Point C)

Starting with the primary mode *CR-*, in connection with which the axial strain in the embedded bars is reduced, and the axial stress in the plate is increased as the plate modulus of elasticity increases, with the strain in the embedded bars reducing in magnitude to that of yield for steel first (i.e. $\varepsilon_s \cong \varepsilon_{sy}$) with the stress in the plate not reaching the ultimate strength for FRP material (i.e. $f_p < f_{pu}$), then, the failure mode will change to the brittle mode *C- -*: this will happen at the critical value of plate modulus of elasticity $E_{(C)}$, with the beam being referred as an over-reinforced element.

Associated with the critical parameter $E_{(C)}$, is the maximum concrete compressive strain equal to the crushing value ($\varepsilon_o = 0.0035$), and the embedded bars are assumed to just experience yielding (i.e. $f_s = f_{sy}$), with the plate axial stress being lower than the ultimate value – see Figure 7.7.

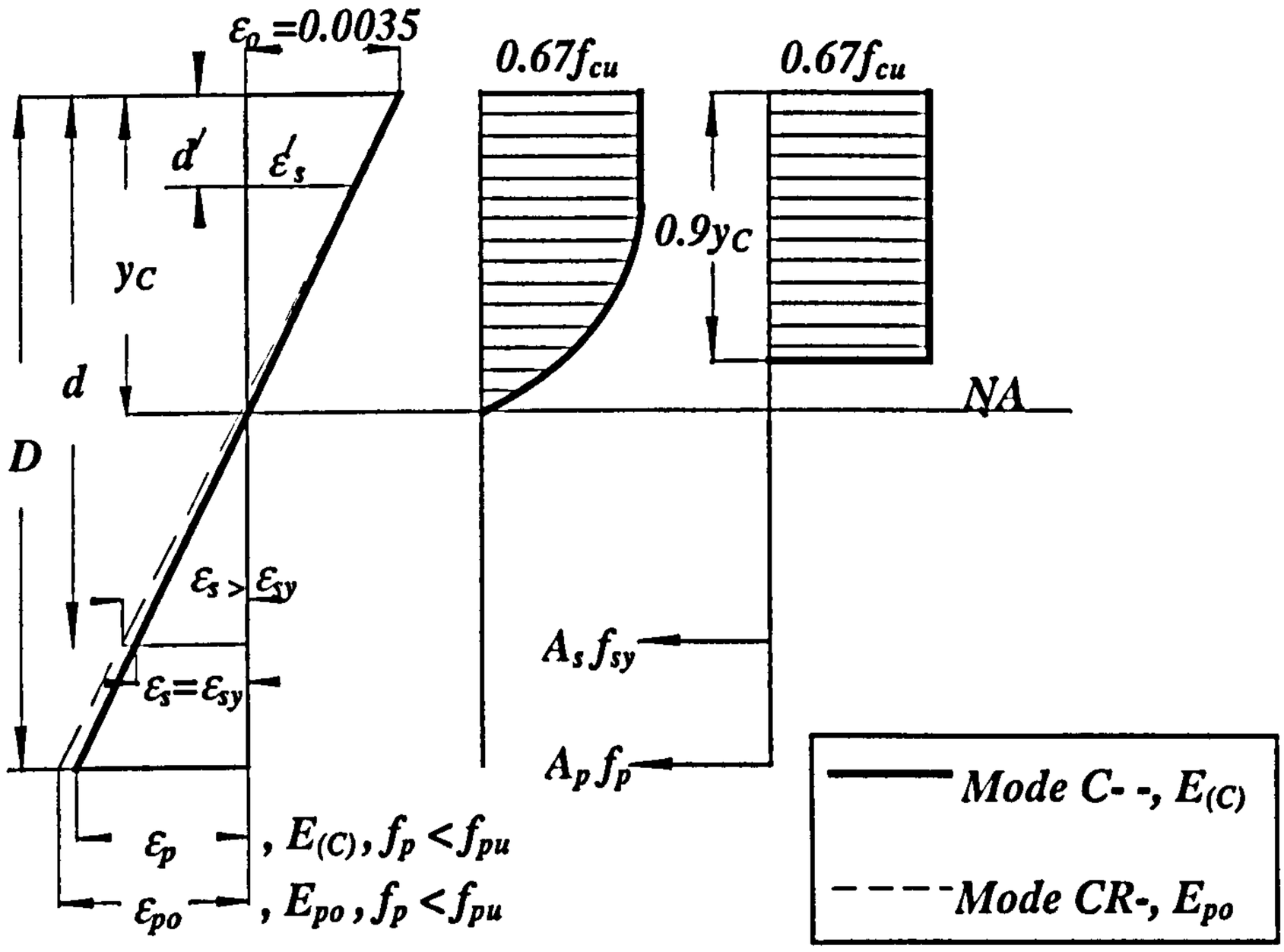

Fig. 7.7 Transition from the Mode *CR-* to the Mode *C- -*

From Figure 7.7, the following relations hold:

$$\frac{\varepsilon_{sy}}{D - y_C} = \frac{\varepsilon_o}{y_C} \text{ where, } \varepsilon_{sy} = \frac{f_y}{E_s}$$

and, the neutral axis depth, y_c, is given by

$$y_C = \frac{\varepsilon_o d}{(\varepsilon_o + \frac{f_y}{E_s})}$$

Considering the equilibrium condition for section forces, with Equation (B.50) (derived in Appendix B) giving the total concrete compression force in the crushed state, then

$$A_s f_y + A_p E_{(C)} \frac{D - y_C}{y_C} \varepsilon_o = A'_s E_s \varepsilon_o (1 - \frac{d'}{y_C}) + y_C b (\frac{\beta}{\varepsilon_o}) [\frac{E_c \beta}{6} + 0.67 f_{cu} (\frac{\varepsilon_o}{\beta} - \frac{2}{3})]$$

or

$$E_{(C)} = \frac{A'_s E_s \varepsilon_o (1 - \frac{d'}{y_C}) + y_C b (\frac{\beta}{\varepsilon_o}) [\frac{E_c \beta}{6} + 0.67 f_{cu} (\frac{\varepsilon_o}{\beta} - \frac{2}{3})] - A_s f_y}{A_p (\frac{D}{y_C} - 1) \varepsilon_o} \qquad (7.17)$$

Adopting the concept of simplified compression stress block for concrete (Figure 7.7)

$$E_{(C)} = \frac{0.0035 A'_s E_s (1 - \frac{d'}{y_C}) + 0.9 y_C 0.67 f_{cu} b - A_s f_y}{0.0035 A_p (\frac{D}{y_C} - 1)} \qquad (7.18)$$

7.3.2.2 Minimum Value of E_p for the Mode - -P (Point D, Over-Reinforced)

In Chapter 6, it has been shown that for the brittle mode ***C- -***, as the plate modulus of elasticity E_p is increased, the axial stress in the plate is increased while the axial strains in the plate and the embedded bars are reduced. At a certain value of E_p ($E_{(D)}$ in Figure 7.6), the plate axial stress reaches the ultimate value and, then, the brittle **FRP** plate will be the critical element causing failure, with the failure not being controlled by the crushing of concrete.

At the critical value of $E_{(D)}$, the maximum concrete compressive strain will just be at the crushing level (*i.e.* $\varepsilon_o \cong 0.0035$), and the plate axial stress reaches the rupture stress f_{pu}, while the stresses in the embedded steel bars will be lower than the yield value (or they may even be in compression if y_D>d) – see Figure 7.8.

i.e.

$$\frac{\varepsilon_o}{y_D} = \frac{\varepsilon_{pu}}{D - y_D} = \frac{\varepsilon_s'}{y_D - d'} = \frac{\varepsilon_s}{d - y_D} \text{ if } d > y_D$$

or

$$\frac{\varepsilon_o}{y_D} = \frac{\varepsilon_s}{y_D - d} \text{ if } d < y_D$$

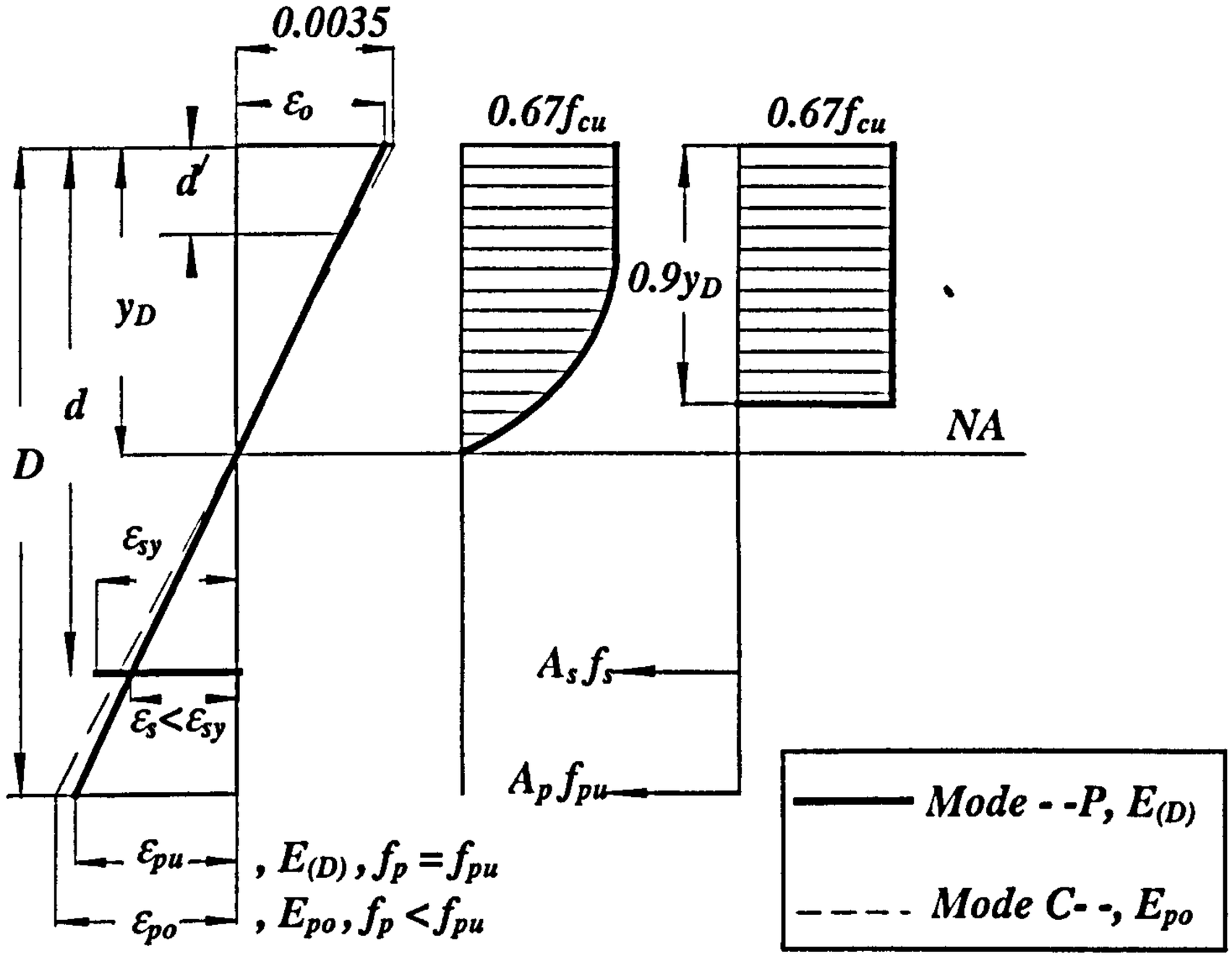

Fig. 7.8 Transition from the Mode *C*- - to the Mode - -*P*

Using the equilibrium condition for section forces as given by Equation (B.50) for the concrete compression force (see Appendix B), if $d > y_D$ (i.e. with the main embedded bars in tension)

$$A_s E_s \varepsilon_o \left(\frac{d - y_D}{y_D}\right) + A_p f_{pu} = A_s' E_s \varepsilon_o \left(\frac{y_D - d'}{y_D}\right) + y_D b \left(\frac{\beta}{\varepsilon_o}\right)\left[\frac{E_c \beta}{6} + 0.67 f_{cu}\left(\frac{\varepsilon_o}{\beta} - \frac{2}{3}\right)\right]$$

and, if $d < y_D$ (i.e. with the main embedded bars in compression)

$$A_p f_{pu} = A_s E_s \varepsilon_o (\frac{y_D - d}{y_D}) + A'_s E_s \varepsilon_o (\frac{y_D - d'}{y_D}) +$$
$$y_D b (\frac{\beta}{\varepsilon_o}) [\frac{E_c \beta}{6} + 0.67 f_{cu} (\frac{\varepsilon_o}{\beta} - \frac{2}{3})]$$

which gives the same equation. Multiply the above equation by y_D, to get

$$y_D^2 b (\frac{\beta}{\varepsilon_o}) [\frac{E_c \beta}{6} + 0.67 f_{cu} (\frac{\varepsilon_o}{\beta} - \frac{2}{3})] + A_s E_s \varepsilon_o (y_D - d) - A_p f_{pu} y_D$$
$$+ A'_s E_s \varepsilon_o (y_D - d') = 0$$

which may be written as

$$y_D^2 [\frac{E_c \beta}{6} + 0.67 f_{cu} (\frac{\varepsilon_o}{\beta} - \frac{2}{3})] b (\frac{\beta}{\varepsilon_o}) + y_D [E_s \varepsilon_o (A_s + A'_s) - A_p f_{pu}]$$
$$- E_s \varepsilon_o (A'_s d' + A_s d) = 0$$

where, ε_o=*0.0035* and $\beta = 2.44 x 10^{-4} \sqrt{f_{cu}}$

Solving this equation for y_D, then

$$\frac{\varepsilon_{pu}}{D - y_D} = \frac{0.0035}{y_D}$$

and

$$E_{(D)} = \frac{f_{pu}}{\varepsilon_{pu}} = \frac{f_{pu}}{0.0035} \frac{y_D}{(D - y_D)} \qquad \textbf{(7. 19)}$$

7.3.2.3 Minimum Value of E_p for the Mode - - - (Point d, Over-Reinforced)

With no provisions made to prevent the occurrence of plate peeling (such as plate end anchoring) and when (with corresponding increases in the plate modulus of elasticity in the mode *C- -*) the axial stress in the plate reaches the plate peeling stress, the failure will be controlled by the plate peeling rather than the crushing of concrete.

This will happen at the critical value of $E_{(d)}$ at point d in Figure 7.6, provided that the corresponding plate peeling stress remains less than the ultimate strength for FRP.

At this critical value of $E_{(d)}$, the maximum concrete compressive strain is just less than the crushing value (*i.e.* $\varepsilon_o \cong 0.0035$), and the plate axial stress reaches the plate peeling stress, σ_s, while the stresses in the embedded bars will be lower than the yield strength for steel (or they may even be in compression if $y_d > d$) - see Figure 7.9. Under such conditions, one gets

$$\frac{\varepsilon_o}{y_d} = \frac{\varepsilon_{pel}}{D - y_d} = \frac{\varepsilon_s'}{y_d - d'} = \frac{\varepsilon_s}{d - y_d} \quad \text{if } d > y_d$$

or

$$\frac{\varepsilon_o}{y_D} = \frac{\varepsilon_s}{y_D - d} \quad \text{if } d < y_d$$

Using the equilibrium condition for section forces, and using Equation (B.50) in Appendix B for estimating the magnitude of the concrete compression force, if $d > y_d$ (i.e. with the main bars in tension), then

$$A_s E_s \varepsilon_o \left(\frac{d - y_d}{y_d}\right) + A_p \sigma_s = A_s' E_s \varepsilon_o \left(\frac{y_d - d'}{y_d}\right) + y_d b \left(\frac{\beta}{\varepsilon_o}\right)\left[\frac{E_c \beta}{6} + 0.67 f_{cu}\left(\frac{\varepsilon_o}{\beta} - \frac{2}{3}\right)\right]$$

And, if $d < y_d$ (i.e. with the main bars in compression)

$$A_p \sigma_s = A_s E_s \varepsilon_o \left(\frac{y_d - d}{y_d}\right) + A_s' E_s \varepsilon_o \left(\frac{y_d - d'}{y_d}\right) + y_d b \left(\frac{\beta}{\varepsilon_o}\right)\left[\frac{E_c \beta}{6} + 0.67 f_{cu}\left(\frac{\varepsilon_o}{\beta} - \frac{2}{3}\right)\right]$$

which gives the same equation. Multiply the above equation by y_d, to get

$$A_s E_s \varepsilon_o (y_d - d) + A'_s E_s \varepsilon_o (y_d - d') - A_p \sigma_s y_d +$$

$$y_d^2 b(\frac{\beta}{\varepsilon_o})[\frac{E_c \beta}{6} + 0.67 f_{cu}(\frac{\varepsilon_o}{\beta} - \frac{2}{3})] = 0$$

$$y_d^2[\frac{E_c \beta}{6} + 0.67 f_{cu}(\frac{\varepsilon_o}{\beta} - \frac{2}{3})] b(\frac{\beta}{\varepsilon_o}) + y_d[E_s \varepsilon_o (A_s + A'_s) - A_p \sigma_s]$$

$$- E_s \varepsilon_o (A'_s d' + A_s d) = 0$$

where, ε_o=*0.0035* and $\beta = 2.44x10^{-4}\sqrt{f_{cu}}$.

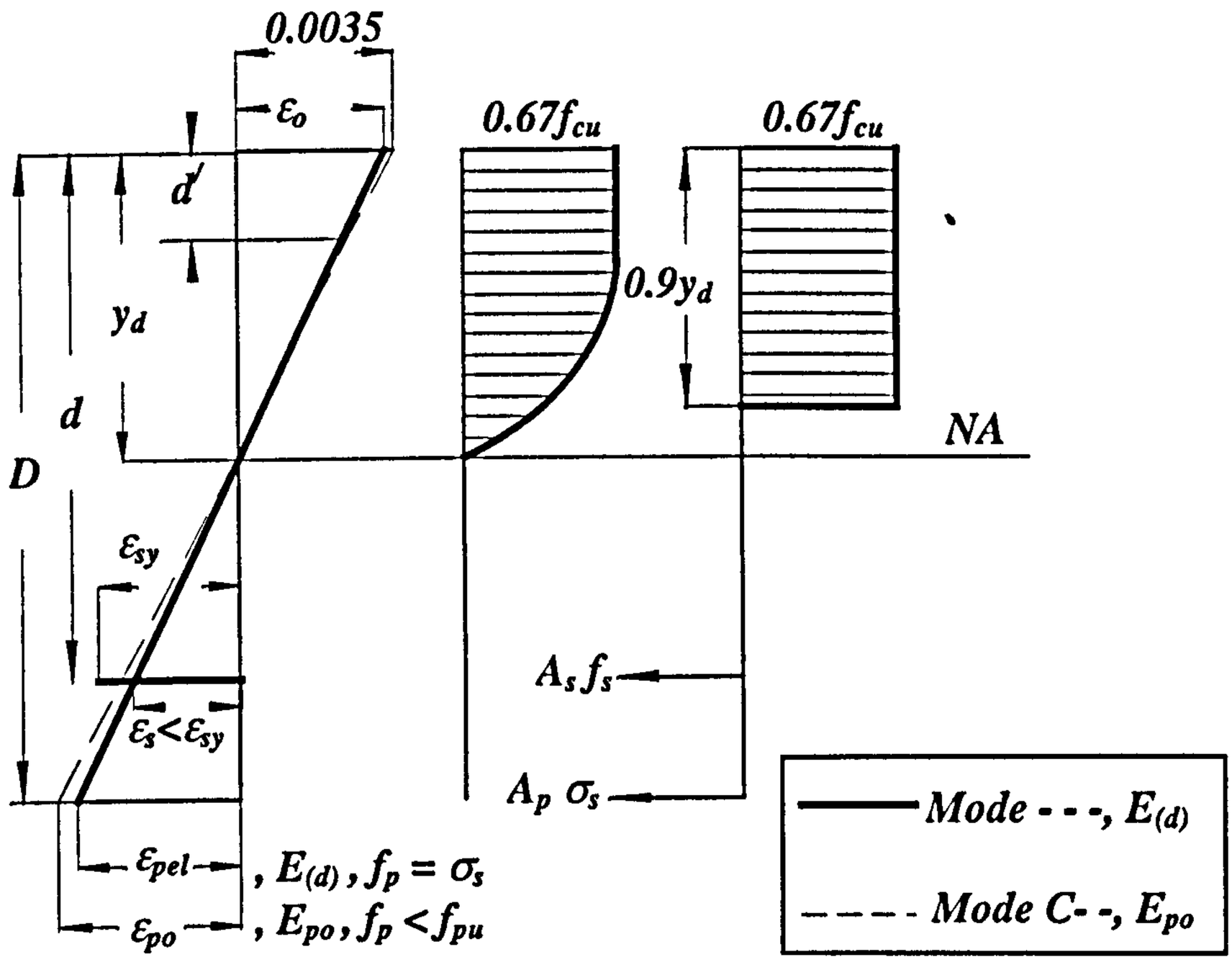

Fig. 7.9 Transition from the Mode *C*- - to the Mode - - -

Solving this equation for y_d, then

$$\frac{\varepsilon_{pel}}{D - y_d} = \frac{0.0035}{y_d}$$

and

$$E_{(d)} = \frac{\sigma_s}{\varepsilon_{pel}} = \frac{\sigma_s}{0.0035}\frac{y_d}{(D - y_d)} \qquad \textbf{(7. 20)}$$

7.3.3 Determining the General Behaviour

In order to determine the maximum value of E_p for the primary mode ***CR-*** associated with over- and/or under-reinforced beams with externally bonded FRP plates, the two values of moduli of elasticity $E_{(A)}$ and $E_{(C)}$ for the plate as given by Equations (7.4) and (7.18), respectively, need to be calculated, with the minimum of them determining the type of behaviour at the critical points of mode transition to the successor mode of failure. If $E_{(A)}$ is found to be less than $E_{(C)}$, then, the successor mode of failure (after the primary mode ***CR-***) will be the ductile mode ***-RP***, and the upgraded beam will be under-reinforced (Figure 7.1). On the other hand, if the predicted value of $E_{(C)}$ is found to be less than the corresponding value of $E_{(A)}$, then, the next failure mode will be the brittle one ***C- -***, and the beam will, then, be classified as an over-reinforced one – Figure 7.6.

The underlying reason for these over- and/or under-reinforced classification for the plated beams, may be explained by studying the two simplified (but accurate) methods for calculating the values of both $E_{(A)}$ and $E_{(C)}$ (as predicted by Equations (7.3), (7.4), (7.17) and (7.18)), bearing in mind that the unplated beam is always assumed to be under-reinforced.

A careful examination of these equations, suggests that all the section parameters (such as the beam configuration and material characteristics) affect the behaviour of the beam, and determine as to which mode of failure will be the dominant one at a certain critical value of E_p: these parameters are as follows:

1- the total area of steel bars, their depth, yield stress, and modulus of elasticity,

2- the plate cross-section area, and ultimate strength, and

3- the concrete cross-section dimensions, compressive strength, and modulus of elasticity.

As regards the area of externally bonded plate, the larger the area of the plate is in the simplified equations, the higher will be the value of $E_{(A)}$ and the lower is the magnitude of $E_{(C)}$: in other words, the higher will be the possibility of occurrence for the brittle mode of failure ***C- -***. In the failure mode ***C- -***, the failure is due to crushing of concrete in a sudden fashion prior to the yielding of the embedded steel bars, and it happens without associated noticeable deformations - i.e. it is an over-reinforced type of failure.

On the other hand, the lower the area of the plate is, the lower will be the value of $E_{(A)}$ with a higher associated critical modulus of elasticity $E_{(C)}$ being predicted, leading to the occurrence of the ductile mode ***-RP*** as the successor mode. The failure in this mode (i.e. ***-RP***) will be initiated in the plate (i.e. by plate rupture) associated with large deformations and curvatures – i.e. the failure mode will be of an under-reinforced type, with the corresponding unplated beams failing due to crushing of concrete.

7.4 VERIFICATION OF THE DERIVED FORMULAE FOR THE CRITICAL VALUES OF E_P FOR THE FRP PLATE

In this section, the proposed closed-form formulae for determining the critical values of the plate moduli of elasticity associated with various failure modes, will be checked against results based on numerical (i.e. theoretical) parametric studies, using the same

group of twenty one beams designs which were previously used in the theoretical parametric studies as discussed in Chapter 6.

In Table (7.1), the numerical results relating to the predicted critical values of $E_{(A)}$, $E_{(B)}$, $E_{(C)}$ and $E_{(D)}$ associated with the full bond behaviour are compared with the critical values based on the numerical parametric studies (Ref. Chapter 6), where the changes in the failure modes with increasing values of the plate moduli of elasticity were fully reported. Tables (7.2) and (7.3) show similar comparisons for the lower and upper bound peeling moments, respectively, for the corresponding partially bonded behaviour, and present a comparison of the critical values of $E_{(a)}$, $E_{(b)}$ and $E_{(d)}$ based on the closed-form formulae (as derived in the previous sections) with the corresponding critical values as obtained from the numerical parametric studies.

In these tables, the predicted 2nd mode of failure (as the successor to the primary mode ***CR-***) is shown in column (3), and is determined according to the lower value of $E_{(A)}$ (column (1)) and $E_{(C)}$ (column (2)) in Table (7.1), or the lower value of $E_{(a)}$ (column (1)) and $E_{(C)}$ (column (2)) in Tables (7.2) and (7.3). If $E_{(C)}$ is the lower value, then, the predicted 2nd mode of failure will be the ***C- -*** mode, corresponding to the value of $E_{(B)}$ in column (4) (or $E_{(b)}$ if partial bond behaviour, as in Tables (7.2) and (7.3), is not applicable as the section is classified as an over-reinforced one – see Fig. 7.6). On the other hand, if $E_{(C)}$ is the higher value, then, the predicted 2nd mode of failure in column (4) is either the ***–RP*** mode (if compared with $E_{(A)}$ for full bond behaviour in Table (7.1)) or the ***-R-*** mode (if compared with $E_{(a)}$ for partial bond behaviour in Tables (7.2) and (7.3)). In this case, the critical value $E_{(D)}$ or $E_{(d)}$ in column (5) is not applicable as the section is classified as an under-reinforced one – see Fig. 7.1. The

predicted 2nd mode of failure in column (3) should be compared with that resulting from the numerical parametric studies and shown in column (7). The critical value of the plate modulus of elasticity $E_{(A)}$ or $E_{(C)}$, where the mode of failure is changed from the primary mode ***CR-*** to the successor mode, is either the ***–RP*** mode (if under-reinforced section) or the ***C- -*** mode (if over-reinforced section), respectively, as suggested by the numerical parametric studies (shown in column (6)), and should be compared with the corresponding lower value of those given in columns (1) and (2). Because the numerical parametric studies were carried out with an interval of 10 GPa for the plate modulus of elasticity, the exact critical value is not available, and only the range over which the mode change–over happens (e.g. 140-150 GPa) is shown. Similar results, for the partial bond behaviour, are shown in Tables (7.2) and (7.3). Finally, the lower value (as predicted by the proposed closed-form formulae) presented in columns (4) and (5) should be compared with the corresponding value in column (8).

A careful examination of such results strongly suggest that the proposed closed-form formulae successfully predict such critical values for the moduli of elasticity and the corresponding modes of failure although (in some cases) certain results may not be compared because the numerical parametric studies were carried out covering a limited (but practical) range of moduli of elasticity for FRP $10 < E_p < 200$ GPa which do not cover the whole range of values for this parameter as is predictable using closed-form solutions. For certain cases, such closed-form solutions predict values of the critical moduli of elasticity as high as 5047 GPa: such values are outside the current manufacturing limits for FRP materials and are of not much practical concern.

In other words, such extreme changes of failure modes for certain beam designs (although theoretically possible) do not happen in practice.

Based on the results presented in Tables (7.1), (7.2) and (7.3), it is concluded that the proposed closed-form formulae relating to the critical values of the plate moduli of elasticity are, indeed, correct, and these formulae may be considered as being generally reliable. In the following section, certain design parameters will be studied, using the presently proposed closed-form formulae, and the effect of each individual parameter on the critical values of the plate modulus of elasticity and, hence, the modes of failure, will be examined.

7.5 MAIN PARAMETERS AFFECTING THE BEHAVIOUR OF A FRP PLATED BEAM

Studying the changes in the mode(s) of failure due to variations in other parameters such as the total area of embedded steel bars, concrete compressive strength, etc., as one changes the value of Young's modulus for the FRP plate, E_p, is very complicated and, for the present purposes, the subsequent brief discussion will be limited to the most important (i.e. first order) factors. As the variations in the Young's modulus for steel bars are very limited in practice, changes in this parameter will not be considered in what follows.

Beam	Predicted (based on the equations derived in chapter 7)					Numerical parametric study (10 GPa intervals for E_p)		
	$E_{(A)}$ *GPa* *(1)*	$E_{(C)}$ *GPa* *(2)*	2nd mode of failure (3)	$E_{(B)}$ *GPa* *(4)*	$E_{(D)}$ *GPa* *(5)*	$E_{(A)}$ or $E_{(C)}$ *GPa* *(6)**	2nd mode of failure (7)	$E_{(B)}$ or $E_{(D)}$ *GPa* *(8)**
H-A1b	149	594	***-RP***	*368*	*URS*	150-160	***-RP***	200+
H-A2g	262	382	***-RP***	*342*	*URS*	200+	***NA***	200+
H-B6	161	478	***-RP***	*335*	*URS*	170-180	***-RP***	200+
H-B9	161	478	***-RP***	*335*	*URS*	170-180	***-RP***	200+
H-2Cu	119	1082	***-RP***	*448*	*URS*	120-130	***-RP***	200+
H-2Ca	119	1082	***-RP***	*448*	*URS*	120-130	***-RP***	200+
CC	26	427	***-RP***	143	*URS*	20-30	***-RP***	140-150
AA	77	234	***-RP***	135	*URS*	80-90	***-RP***	130-140
BB	51	312	***-RP***	138	*URS*	50-60	***-RP***	130-140
DD	51	312	***-RP***	138	*URS*	50-60	***-RP***	130-140
C	10	210	***-RP***	56	*URS*	10-20	***-RP***	50-60
F	18	104	***-RP***	54	*URS*	10-20	***-RP***	50-60
H	36	117	***-RP***	79	*URS*	30-40	***-RP***	70-80
J	83	313	***-RP***	196	*URS*	80-90	***-RP***	190-200
L	41	785	***-RP***	*217*	*URS*	40-50	***-RP***	200+
N	-7,840	156	***C- -***	*ORS*	*5047*	140-150	***C- -***	200+
F-P1	10	506	***-RP***	50	*URS*	10-20	***-RP***	40-50
F-P2	12	252	***-RP***	49	*URS*	10-20	***-RP***	40-50
F-P2B	12	252	***-RP***	49	*URS*	10-20	***-RP***	40-50
F-P2BW	12	252	***-RP***	49	*URS*	10-20	***-RP***	40-50
F-P3J	14	167	***-RP***	48	*URS*	10-20	***-RP***	40-50

Table 7.1 Critical values of E_p and modes of failure (full bond behaviour)

Notes

URS = Under- Reinforced Section: $E_{(D)}$ is not applicable (Figure 7.1).

ORS = Over-Reinforced Section: $E_{(B)}$ is not applicable (Figure 7.6).

200+ = Value higher than the maximum of the studied range (i.e. higher than 200 GPa).

NA = Not Available.

* :n - (n+10) = Value of E_p (where the mode is changed) lies between n and (n+10) GPa.

Beam	Predicted (based on the equations derived in chapter 7)					Numerical parametric study (10 GPa intervals for E_p)		
	$E_{(a)}$ *GPa* *(1)*	$E_{(C)}$ *GPa* *(2)*	2nd mode of failure (3)	$E_{(b)}$ *GPa* *(4)*	$E_{(d)}$ *GPa* *(5)*	$E_{(a)}$ or $E_{(C)}$ *GPa* *(6)**	2nd mode of failure (7)	$E_{(b)}$ or $E_{(d)}$ *GPa* *(8)**
H-A1b	62	594	**-R-**	*235*	*URS*	60-70	**-R-**	200+
H-A2g	22	382	**-R-**	*121*	*URS*	20-30	**-R-**	100-110
H-B6	60	478	**-R-**	*203*	*URS*	60-70	**-R-**	200+
H-B9	60	478	**-R-**	*203*	*URS*	60-70	**-R-**	200+
H-2Cu	85	1082	**-R-**	*364*	*URS*	80-90	**-R-**	200+
H-2Ca	85	1082	**-R-**	*364*	*URS*	80-90	**-R-**	200+
CC	10	427	**-R-**	81	*URS*	10-20	**-R-**	80-90
AA	11	234	**-R-**	33	*URS*	10-20	**-R-**	30-37.2
BB	12	312	**-R-**	51	*URS*	10-20	**-R-**	50-60
DD	12	312	**-R-**	51	*URS*	10-20	**-R-**	50-60
C	7	210	**-R-**	46	*URS*	0-10	**-R-**	40-50
F	4	104	**-R-**	22	*URS*	0-10	**-R-**	20-30
H	4	117	**-R-**	23	*URS*	0-10	**-R-**	20.7-30
J	11	313	**-R-**	65	*URS*	10-20	**-R-**	60-70
L	28	785	**-R-**	*169*	*URS*	20-30	**-R-**	160-170
N	5	156	**-R-**	*25*	*URS*	0-10	**-R-**	30-40
F-P1	12	506	**-RP↑**	50	*URS*	10-20	**-RP↑**	40-50
F-P2	12	252	**-RP↑**	49	*URS*	10-20	**-RP↑**	40-50
F-P2B	12	252	**-RP↑**	49	*URS*	10-20	**-RP↑**	40-50
F-P2BW	12	252	**-RP↑**	49	*URS*	10-20	**-RP↑**	40-50
F-P3J	14	167	**-RP↑**	48	*URS*	10-20	**-RP↑**	40-50

Table 7.2 Critical values of E_p and modes of failure (partial bond behaviour, $\sigma_{s(max)}$)

<u>Notes</u>

URS = Under- Reinforced Section: $E_{(d)}$ is not applicable (Figure 7.1).

200+ = Value higher than the maximum of the studied range (i.e. higher than 200 GPa).

↑ = $\sigma_{s(max)}$ is higher than the ultimate strength of the plate (full bond behaviour).

* :n - (n+10) = Value of E_p (where the mode is changed) lies between n and (n+10) GPa.

Beam	Predicted (based on the equations derived in chapter 7)					Numerical parametric study (10 GPa intervals for E_p)		
	$E_{(a)}$ *GPa* *(1)*	$E_{(C)}$ *GPa* *(2)*	2nd mode of failure (3)	$E_{(b)}$ *GPa* *(4)*	$E_{(d)}$ *GPa* *(5)*	$E_{(a)}$ or $E_{(C)}$ *GPa* *(6)**	2nd mode of failure (7)	$E_{(b)}$ or $E_{(d)}$ *GPa* *(8)**
H-A1b	21	594	**-R-**	*117*	*URS*	20-30	**-R-**	120-130
H-A2g	9	382	**-R-**	*60*	*URS*	0-10	**-R-**	50-60
H-B6	20	478	**-R-**	*101*	*URS*	20-30	**-R-**	100-110
H-B9	20	478	**-R-**	*101*	*URS*	20-30	**-R-**	100-110
H-2Cu	31	1082	**-R-**	*182*	*URS*	30-40	**-R-**	180-190
H-2Ca	31	1082	**-R-**	*182*	*URS*	30-40	**-R-**	180-190
CC	4	427	**-R-**	41	*URS*	0-10	**-R-**	40-50
AA	5	234	**-R-**	16	*URS*	0-10	**-R-**	10-20
BB	5	312	**-R-**	26	*URS*	0-10	**-R-**	20-30
DD	5	312	**-R-**	26	*URS*	0-10	**-R-**	20-30
C	3	210	**-R-**	23	*URS*	0-10	**-R-**	20-30
F	1	104	**-R-**	11	*URS*	0-10	**-R-**	0-11.7
H	1	117	**-R-**	11	*URS*	0-10	**-R-**	10-20
J	4	313	**-R-**	32	*URS*	0-10	**-R-**	30.3-40
L	10	785	**-R-**	*85*	*URS*	10-20	**-R-**	80-90
N	2	156	**-R-**	12	*URS*	0-10	**-R-**	10-20
F-P1	10	506	**-RP↑**	50	*URS*	10-20	**-RP↑**	40-50
F-P2	12	252	**-RP↑**	49	*URS*	10-20	**-RP↑**	40-50
F-P2B	12	252	**-RP↑**	49	*URS*	10-20	**-RP↑**	40-50
F-P2BW	12	252	**-RP↑**	49	*URS*	10-20	**-RP↑**	40-50
F-P3J	14	167	**-RP↑**	48	*URS*	10-20	**-RP↑**	40-50

Table 7.3 Critical values of E_p and modes of failure (partial bond behaviour, $\sigma_{s(min)}$)

Notes

URS = Under- Reinforced Section: $E_{(d)}$ is not applicable (Figure 7.1).

200+ = Value higher than the maximum of the studied range (i.e. higher than 200 GPa).

↑ = $\sigma_{s(min)}$ is higher than the ultimate strength of the plate (full bond behaviour).

* :n - (n+10) = Value of E_p (where the mode is changed) lies between n and (n+10) GPa.

7.5.1 Concrete Compressive Strength

From Equations (7.4) and (7.18), it is clear that the higher the concrete compressive strength, the lower will be the predicted values of $E_{(A)}$ and $E_{(a)}$ (assuming that all the other parameters remain unchanged), and the higher will be the value of $E_{(C)}$. It, then, follows that high values of concrete compressive strength reduce the magnitudes of $E_{(A)}$ (and $E_{(a)}$) with $E_{(C)}$ increasing: this, then, increases the possibility for the successor mode to be ***-RP***. Under such conditions, increases in the concrete compressive strength will cause the successor mode to be initiated at relatively low values of plate modulus of elasticity.

It is also, perhaps, worth mentioning that the effect of changes in the width of the concrete beam on the behaviour of the plated member is similar to that of the concrete compressive strength.

7.5.2 Plate Ultimate Strength and Yield Strength for the Embedded Bars

Based on the proposed closed-form formulations, it may be deduced that increasing either the plate ultimate strength or the yield strength of the embedded bars leads to the critical value of the plate modulus of elasticity $E_{(A)}$ (for the initiation of the ductile mode ***-RP***) to be of a relatively higher value, while the corresponding critical value of plate modulus of elasticity $E_{(C)}$ (for the initiation of the brittle mode ***C-*** **-**) will be lower in magnitude, as the yield strength of embedded bars increases, although it will not be affected by changes in the ultimate strength of the plate.

This observation, therefore, suggests that occurrence of the brittle mode *C- -* is the most probable one associated with relatively large values for the yield strength of the reinforcing steel bars and/or relatively large values of the ultimate strength for the externally bonded **FRP** plate.

7.5.3 Total Area of Reinforcing Bars

It is also obvious that, using main embedded bars with large total cross section areas will increase the possibility of occurrence for the brittle mode of failure *C- -*, and reduce the possibility of the ductile mode *–RP* to be initiated.

The influence of changes in the total area of reinforcing bars on the behaviour of plated beams is, generally, similar to that for the corresponding unplated beams.

7.6 SUMMARY AND CONCLUSIONS

Closed-form formulae have been developed for determining the variations in the modes of failure for a FRP plated beam associated with changes in the magnitude of Young's modulus for the FRP material. The critical values of moduli of elasticity for FRP plates, at which changes in the failure modes are initiated, are also critically addressed: the following steps should, therefore, be followed (in conjunction with Figures 7.1 and 7.6), for determining these critical values of plate moduli of elasticity:

A- If the plate peeling stress is higher than the ultimate strength of the plate, or if there are certain design arrangements which ensure that the plate peeling will not happen (such as presence of plate end anchorages), then:

1- Calculate y_A and $E_{(A)}$ from the following:

$$y_A^2 b(\frac{\beta}{\varepsilon_o})[\frac{E_c\beta}{6}+0.67 f_{cu}(\frac{\varepsilon_o}{\beta}-\frac{2}{3})]+ y_A(A_s' E_s \varepsilon_o - A_s f_y - A_p f_{pu}) - A_s' E_s \varepsilon_o d' = 0$$

and

$$E_{(A)} = \frac{f_{pu}}{\varepsilon_{pu}} = \frac{f_{pu}}{0.0035}\frac{y_A}{(D-y_A)}$$

2- Calculate y_C and $E_{(C)}$ from the following:

$$y_C = \frac{\varepsilon_o d}{(\varepsilon_o + \frac{f_y}{E_s})}$$

$$E_{(C)} = \frac{A_s' E_s\ \varepsilon_o (1-\frac{d'}{y_C}) + y_C b(\frac{\beta}{\varepsilon_o})[\frac{E_c\beta}{6}+0.67 f_{cu}(\frac{\varepsilon_o}{\beta}-\frac{2}{3})] - A_s f_y}{A_p(\frac{D}{y_C}-1)\varepsilon_o}$$

3- If $E_{(C)} < E_{(A)}$, then, the plated beam is an over-reinforced type, and the next mode of failure, following the primary mode ***CR-***, will be the brittle one ***C- -***; being initiated at the critical plate modulus of elasticity $E_{(C)}$.

4- If $E_{(C)} > E_{(A)}$, then the plated beam is of an under-reinforced type, and the subsequent mode of failure, following the primary mode ***CR-***, will be the ductile one ***-RP***; being initiated at the critical value of plate modulus of elasticity $E_{(A)}$.

5- For an over-reinforced plated beam (i.e. the beam with $E_{(C)} < E_{(A)}$), calculate y_D and $E_{(D)}$ from the following:

$$y_D^2[\frac{E_c\beta}{6}+0.67 f_{cu}(\frac{\varepsilon_o}{\beta}-\frac{2}{3})]b(\frac{\beta}{\varepsilon_o}) + y_D[E_s\ \varepsilon_o(A_s+A_s') - A_p f_{pu}] -$$
$$E_s\ \varepsilon_o(A_s' d' + A_s d) = 0$$

$$E_{(D)} = \frac{f_{pu}}{\varepsilon_{pu}} = \frac{f_{pu}}{0.0035}\frac{y_D}{(D-y_D)}$$

6- For an under-reinforced plated beam (i.e. the beam with $E_{(C)} > E_{(A)}$), on the other hand, calculate y_B and ε_o from the following:

$$y_B^2[K_3 - K' - K_f] + y_B[d(K' + K_f - 2K_3) + K'd' + K_T] + d[K_3 d - K'd' - K_T] = 0$$

and

$$\varepsilon_o = \varepsilon_{sy} \frac{y_B}{d - y_B}$$

where

$$K_1 = \frac{0.67 f_{cu} - E_c \beta}{\beta^2}, \qquad K_2 = \frac{bK_1 \varepsilon_s^2}{3}, \; K_E = \frac{bE_c \varepsilon_s}{2}, \quad ,$$

$K' = A_s' E_s \varepsilon_s$ and $K_T = (A_s f_y + A_p f_{pu})$

7- If $\varepsilon_o < \beta$, then, y_B should be recalculated by

$$y_B^3[K_2 - K_E] + y_B^2[K_E d - K' - K_T] + y_B[K'(d + d') + 2K_T d] - (K'dd' + K_T d^2) = 0$$

where

$$K_3 = [\frac{bE_c}{2}\frac{\beta^2}{\varepsilon_s} + \frac{bK_1}{3}\frac{\beta^3}{\varepsilon_s} - 0.67 f_{cu} b \frac{\beta}{\varepsilon_s}] \text{ and } K_f = 0.67 f_{cu} by$$

8- Finally, $E_{(B)}$ is given by:

$$E_{(B)} = \frac{f_{pu}}{\varepsilon_{pu}} = \frac{(d - y_B)}{(D - y_B)} \frac{f_{pu}}{f_y} E_s$$

B- If the plate peeling stress is found to be lower than the plate ultimate strength, and the beam experiences premature peeling, the type of behaviour (i.e. the corresponding changes in the failure modes) and the critical values of moduli of elasticity for the plate may be determined as follows:

1- Calculate y_a and $E_{(a)}$, using

$$y_a^2 b(\frac{\beta}{\varepsilon_o})[\frac{E_c\beta}{6}+0.67 f_{cu}(\frac{\varepsilon_o}{\beta}-\frac{2}{3})]+ y_a(A_s' E_s \varepsilon_o - A_s f_y - A_p \sigma_s) - A_s' E_s \varepsilon_o d' = 0$$

$$E_{(a)} = \frac{\sigma_s}{\varepsilon_{pel}} = \frac{\sigma_s}{0.0035}\frac{y_a}{(D-y_a)}$$

2- Calculate y_d and $E_{(d)}$ from:

$$y_d^2[\frac{E_c\beta}{6}+0.67 f_{cu}(\frac{\varepsilon_o}{\beta}-\frac{2}{3})]b(\frac{\beta}{\varepsilon_o})+ y_d[E_s\ \varepsilon_o(A_s+A_s') - A_p\sigma_s] -$$
$$E_s\ \varepsilon_o(A_s' d' + A_s d) = 0$$

$$E_{(d)} = \frac{\sigma_s}{\varepsilon_{pel}} = \frac{\sigma_s}{0.0035}\frac{y_d}{(D-y_d)}$$

3- If $E_{(d)} > E_{(a)}$, then, the plated beam is categorised as an as under-reinforced one, and the subsequent mode of failure following the primary mode *CR-* will be the ductile mode *-R-*; being initiated at the critical value of plate modulus of elasticity $E_{(a)}$. For such a beam, the brittle failure mode - - -, then, initiates at the critical value of plate modulus of elasticity $E_{(b)}$, which may be predicted as follows

$$y_b^2[K_3 - K' - K_f]+ y_b[d(K'+K_f-2K_3)+K'd'+K_T]+$$
$$d[K_3 d - K' d' - K_T] = 0$$

where $K' = A_s' E_s \varepsilon_s$, $K_f = 0.67 f_{cu} b y$, $K_T = (A_s f_y + A_p \sigma_s)$,

$$K_3 = [\frac{bE_c}{2}\frac{\beta^2}{\varepsilon_s}+\frac{bK_1}{3}\frac{\beta^3}{\varepsilon_s}-0.67 f_{cu} b\frac{\beta}{\varepsilon_s}] \text{ and } K_1 = \frac{0.67 f_{cu} - E_c\beta}{\beta^2}$$

with

$$\varepsilon_o = \varepsilon_{sy}\frac{y_b}{d-y_b}$$

If $\varepsilon_o < \beta$, y_b should be recalculated by

$$y_b^3[K_2 - K_E]+ y_b^2[K_E d - K' - K_T]+ y_b[K'(d+d')+2K_T d] -$$
$$(K' dd' + K_T d^2) = 0$$

where

$$K_2 = \frac{bK_1\varepsilon_s^2}{3} \text{ and } K_E = \frac{bE_c\varepsilon_s}{2}$$

Finally, $E_{(b)}$ is predicted from

$$E_{(b)} = \frac{\sigma_s}{\varepsilon_{pel}} = \frac{(d - y_b)}{(D - y_b)} \frac{\sigma_s}{f_y} E_s$$

4- If $E_{(d)} < E_{(a)}$, then, the plated beam will behave as an over-reinforced one, and the brittle mode - - - will follow, initiated at the critical value of plate modulus of elasticity $E_{(d)}$.

Chapter 8

SIMPLE PROCEDURE(S) FOR PREDICTING THE PEELING LOAD OF STEEL AND/OR FRP PLATED BEAMS

Chapter 8

SIMPLE PROCEDURE(S) FOR PREDICTING THE PEELING LOAD OF STEEL AND/OR FRP PLATED BEAMS

8.1 INTRODUCTION

In this chapter, simple procedure(s) will be developed for predicting the premature plate peeling load of steel and/or FRP plated beams. The results based on the proposed straightforward formulations will be checked against a large number of experimental results for large and/or small scale beams strengthened with steel and/or FRP plates, covering a wide range of beam design parameters: using numerical examples, it will be demonstrated that the simple proposed formulations (which are amenable to hand calculations, using a pocket calculator) lead to results which reasonably enjoy the same level of accuracy as those based on the more involved iterative method.

8.2 SIMPLE PROCEDURE(S) FOR PREDICTING THE PLATE PEELING LOAD CAPACITY

Unlike the ultimate limit state design for under-reinforced sections, premature plate peeling failure usually takes place with the embedded steel bars experiencing elastic deformations and/or when the maximum strain in concrete is below the crushing value. Under such conditions, no closed-form formulae for determining the depth of neutral axis (by resorting to equilibrium conditions) exist: estimating the upper and/or lower bound plate peeling loads is, therefore, not a straightforward procedure, and calculating the depth of neutral axis involves the use of iterative procedures. Establishing simple design procedures (which enjoy an acceptable level of accuracy),

however, is highly desirable for use in practice. In the presently proposed plate peeling theory, the load bearing capacity of the plated member is controlled by the axial stress in the plate. Once the depth of neutral axis plus the corresponding plate axial strain are known, the bending strains and stresses across the beam section may be determined, using which the overall flexural load capacity may be predicted.

In what follows, a simple procedure will be proposed for obtaining reasonable estimates of the depth of neutral axis, following which the prediction of the plate peeling moment will be rather straightforward, being obtained by summing up the moments, due to tensile and compressive forces, about the neutral axis. To this end, two alternative methods for calculating the concrete compressive force and, hence, the resulting moment will be adopted. Both of these methods will be based on closed-form formulations, with one representing the stress-strain relationship for concrete as that recommended by BS8110 (1985) (i.e. the same mathematical model as previously used in the iterative method), while the second method approximates the distribution of compressive stresses in concrete as being uniform.

To check the accuracy of the final numerical results based on the simple closed-form formulations, such results will be compared with the corresponding data based on the iterative procedure, and also extensive associated experimental data reported by others. The specimen details used in these comparisons will be those for beams 1-58 with FRP plates, and also the design details for beams 59-169 with steel plates, as fully discussed in Chapter 3. In what follows, the term "accurate" results refers to those results based on the iterative analysis (as described in appendix A) with the concrete stress-strain relationship as that recommended by BS8110 (1985).

8.2.1 Predicting the depth of neutral axis

Unlike an unplated beam in which failure happens due to over-stressing of steel and/or over-straining of concrete, premature plate peeling failure usually takes place at rather low levels of external loads and axial stresses (and, hence, strains) in the plate. Under such low levels of tension in the plate and the embedded bars, it is reasonable to assume that low levels of concrete compression force with associated low levels of concrete stresses (and strains) exist. For the premature plate peeling modes of failure, therefore, due to low levels of plate axial strains, the bending strains throughout the entire critical beam section (directly under the point load nearest to the support) would be relatively small. It is, then, appropriate to assume (for simplicity) a linear stress (and strain) distribution for concrete in compression. Based on this assumption, a reasonable value for the depth of neutral axis may be determined. The final distribution of stresses in concrete may, then, be calculated, according to the stress-strain relationships as recommended by BS8110 (1985). Figure 8.1 presents the assumed linear stress (and strain) distributions throughout the entire plated (and cracked) section.

From Figure 8.1, the following relations for bending strains may be derived:

$$\frac{\varepsilon_p}{D-y} = \frac{\varepsilon_s}{d-y} = \frac{\varepsilon_s'}{y-d'} = \frac{\varepsilon_c}{y}$$

$$\varepsilon_s = \varepsilon_c \frac{d-y}{y},\ \varepsilon_s' = \varepsilon_c \frac{y-d'}{y} \text{ and } \varepsilon_p = \varepsilon_c \frac{D-y}{y}$$

while, for the corresponding stresses

$$f_c = E_c \varepsilon_c,$$

$$f_s = E_s \varepsilon_s = E_s \varepsilon_c \frac{d-y}{y},$$

$$f'_s = E_s\,\varepsilon'_s = E_s\varepsilon_c\frac{y-d'}{y} \text{ and}$$

$$f_p = E_p\varepsilon_p = E_p\varepsilon_c\frac{D-y}{y}$$

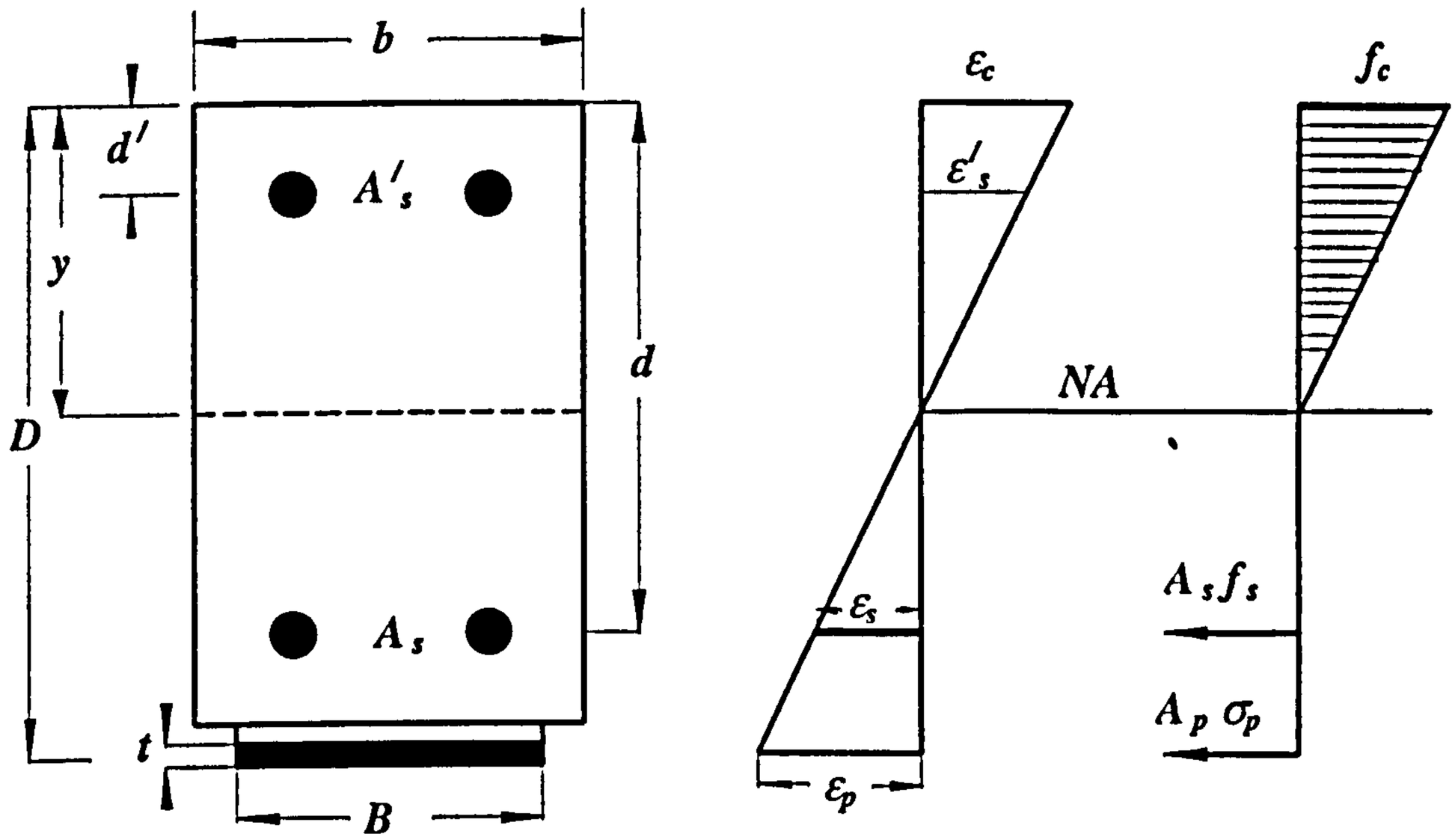

Fig. 8.1 Linear strain and stress distributions in concrete.

From the equilibrium condition, $F_c = F_t$, where

$$F_t = A_s E_s \varepsilon_c \frac{d-y}{y} + A_p E_p \varepsilon_c \frac{D-y}{y}$$

and

$$F_c = \frac{byE_c\varepsilon_c}{2} + A'_s E_s \varepsilon_c \frac{y-d'}{y}$$

so that

$$\frac{byE_c}{2}\varepsilon_c + A'_s E_s \varepsilon_c \frac{y-d'}{y} = A_s E_s \varepsilon_c \frac{d-y}{y} + A_p E_p \varepsilon_c \frac{D-y}{y}$$

multiplying the above equation by $\frac{y}{b\,d^2 E_c \varepsilon_c}$, and assuming $\alpha_{sc} = \frac{E_s}{E_c}$ with $\alpha_{pc} = \frac{E_p}{E_c}$,

then

$$\frac{1}{2}\left(\frac{y}{d}\right)^2 + \frac{A'_s}{bd}\alpha_{sc}\left(\frac{y}{d} - \frac{d'}{d}\right) = \frac{A_s}{bd}\alpha_{sc}\left(1 - \frac{y}{d}\right) + \frac{A_p}{bd}\alpha_{pc}\left(\frac{D}{d} - \frac{y}{d}\right)$$

Assuming: $X=\frac{y}{d}$, $\rho_s=\frac{A_s}{bd}$, $\rho'_s=\frac{A'_s}{bd}$ and $\rho_p=\frac{A_p}{bd}$, the above equation may be rewritten as

$$\frac{1}{2}X^2+\rho'_s\alpha_{sc}\left(X-\frac{d'}{d}\right)=\rho_s\alpha_{sc}(1-X)+\rho_p\alpha_{pc}\left(\frac{D}{d}-X\right)$$

$$\frac{1}{2}X^2+X\left(\rho'_s\alpha_{sc}+\rho_s\alpha_{sc}+\rho_p\alpha_{pc}\right)-\left(\rho'_s\alpha_{sc}\frac{d'}{d}+\rho_s\alpha_{sc}+\rho_p\alpha_{pc}\frac{D}{d}\right)=0$$

which leads to

$$X=-\left(\rho'_s\alpha_{sc}+\rho_s\alpha_{sc}+\rho_p\alpha_{pc}\right)+\sqrt{\left(\rho'_s\alpha_{sc}+\rho_s\alpha_{sc}+\rho_P\alpha_{pc}\right)^2+2\left(\rho'_s\alpha_{sc}\frac{d'}{d}+\rho_s\alpha_{sc}+\rho_p\alpha_{pc}\frac{D}{d}\right)}$$

with the depth of neutral axis, y, given by the following closed-form formula

$$y=d\left(-\left(\alpha_{sc}(\rho'_s+\rho_s)+\rho_p\alpha_{pc}\right)+\sqrt{\left(\alpha_{sc}(\rho'_s+\rho_s)+\rho_P\alpha_{pc}\right)^2+2\left(\alpha_{sc}\left(\rho'_s\frac{d'}{d}+\rho_s\right)+\rho_p\alpha_{pc}\frac{D}{d}\right)}\right) \quad \textbf{(8.1)}$$

In order to check the accuracy of the above derivations, and to assess the implications of assuming a linear stress distribution for concrete in compression, the depth of neutral axis for the previously discussed 111 steel plated beam designs (i.e. beams 59-169) have been calculated (according to the above simple formula). Such estimated depths of neutral axis were, then, compared with the corresponding ones obtained via the more involved iterative technique in which a rather sophisticated form of stress-strain relationship (as recommended by BS8110 (1985)) was adopted. Figure 8.2 presents the encouraging correlations between the simplified and the more accurate methods for estimating the depth of neutral axis of the 111 steel plated beams, where the correlation factor is found to be 0.985. It should be noted that the iterative procedure included (unlike the simplified version) the effect of concrete in tension,

with the simplified procedure being developed for a cracked section, with the presence of concrete tension below the neutral axis ignored.

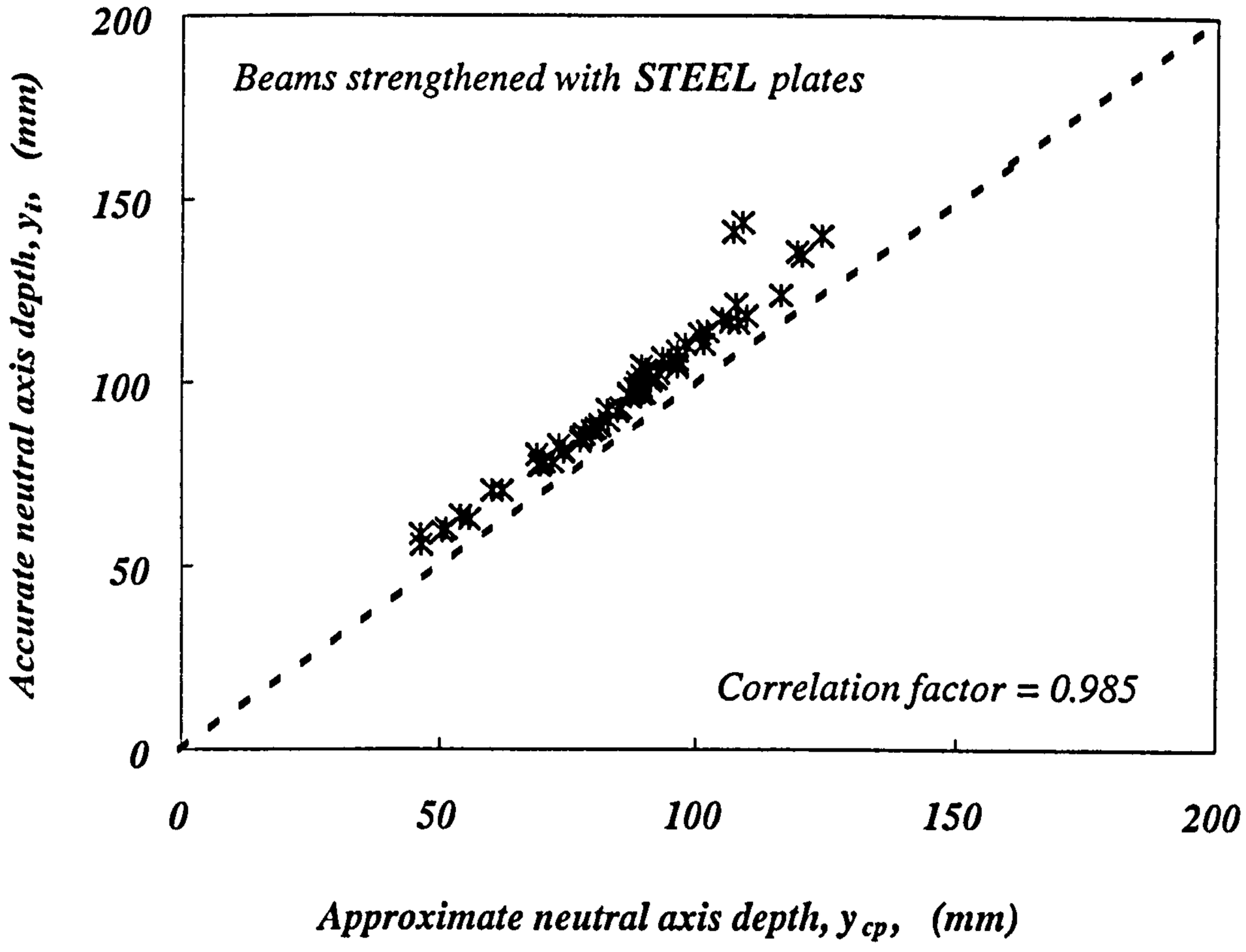

Fig. 8.2 Correlations between the results based on the approximate and the iterative procedures for calculating the depth of neutral axis for beams 59-169, which were strengthened with steel plates.

An examination of the results in Figure 8.2 suggests that, for all the data points, the results based on the more accurate iterative procedure are located slightly over the 45° line: neglecting tension in concrete in the simplified procedure is believed to have reduced the total tension and, hence, the total concrete compression force, with this being instrumental in reducing the area (i.e. the depth) of the concrete compression zone. Indeed, the rather small disagreements between the results based on these alternative approaches, may be primarily attributed to the neglect of concrete tension in the simplified approach, rather than it being as a result of the assumed linear stress distribution for concrete in compression.

The situation for FRP plates is, however, not exactly the same as that when steel plates are used; the underlying reason being that (unlike steel for which the modulus of elasticity remains fairly the same) FRP plates are currently manufactured with widely varying moduli of elasticity with their Young's modulus being generally lower than that of steel. It, then, follows that, for the same plate peeling stress, larger (compared to steel) axial strains are to be induced in the FRP plates. As shown in Chapter 6, however, for premature modes of failure, reducing the axial strains in the plate (e.g. by using plates with higher moduli of elasticity) leads to reductions in the bending strains across the entire beam section. For relatively larger beam strains, there would be more deviations from the assumed linear concrete stress distribution in compression with this being the underlying assumption for the proposed simplified approach. Such deviations from the linear stress distribution are expected to lead to significant deviations from the exact solution, in the estimates of depth of neutral axis associated with the simplified approach. Figure 8.3 shows the correlations between the results based on the simplified and the iterative approaches for calculating the depth of neutral axis, for 58 reinforced concrete beams strengthened with external FRP plates, covering a wide range of values for the modulus of elasticity (from 10.3 to 118.5 *GPa*). Similar to steel plated beams, a high correlation factor of 0.989 is still obtained, although, the results in Figure 8.3 give a relatively larger scatter (compared to steel plated beams).

It is interesting to note that, although the so-obtained values for the depth of neutral axis based on the simplified method are (unlike the iterative procedure) not dependant on the magnitude of the axial stress in the plate, $\sigma_{s(\min)}$, the reasonable correlations

between the results based on these two approaches, as shown in Figures 8.2 and 8.3, are still encouraging.

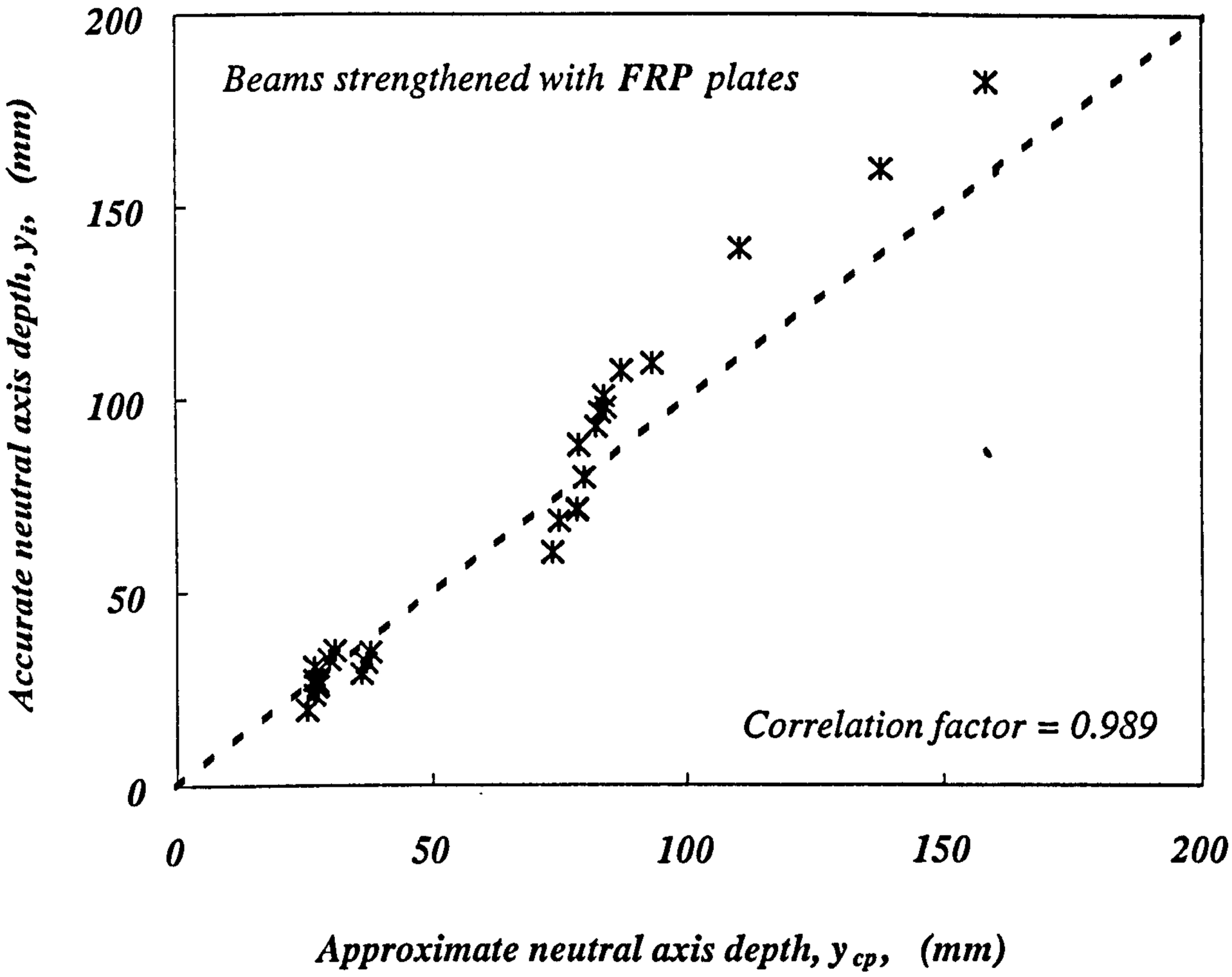

Fig. 8.3 Correlations between the approximate and the accurate values for the neutral axis depth for beams strengthened with FRP plates.

8.2.2 Calculating the plate peeling moment

In what follows, two alternative simplified methods will be developed for calculating the plate peeling moments. In both methods, the tension force in concrete will be neglected for simplicity. In the first method, the stress-strain relationship for concrete as recommended by BS8110 (1985) will be adopted, and the bending moment will be estimated using a parabolic stress distribution for concrete in compression. In the second method, the concrete stress distribution will be assumed to be given by a uniform stress block. In both methods, the maximum concrete strain will be

$$\varepsilon_c = \varepsilon_p \frac{y}{D-y} \leq 0.0035 \tag{8.2}$$

where

$$\varepsilon_p = \frac{\sigma_{s(\min)}}{E_p}$$

and, the tensile stresses in the embedded steel bars will be

$$f_s = \sigma_p \frac{d-y}{D-y} \frac{E_s}{E_p} \leq f_y$$

while, the stresses in the steel bars in compression are

$$f'_s = \sigma_p \frac{y-d'}{D-y} \frac{E_s}{E_p} \leq f_y$$

8.2.2.1 Parabolic stress distribution for concrete

Here, there are two cases to be considered (Figure 8.4), depending on the magnitude of the maximum strain in concrete as given by Equation (8.2). If the maximum concrete strain is lower than β (case 1), then, the moment resulting from the concrete compressive stresses may be derived as follows:

$$M_c = b\int_0^y f_{cz}\, z dz$$

$$M_c = b\int_0^y \left(E_c \varepsilon_z + \frac{0.67 f_{cu} - E_c \beta}{\beta^2} \varepsilon_z^2 \right) z dz$$

$$M_c = y^2 b \left(\frac{E_c \varepsilon_c}{3} + \frac{0.67 f_{cu} - E_c \beta}{4\beta^2} \varepsilon_c^2 \right)$$

where $\beta = 2.44 \times 10^{-4} \sqrt{f_{cu}}$

With $\sigma_p = \sigma_{s(\min)}$, then, the simplified lower bound plate peeling moment, M_{peel-p}, will be

$$M_{peel-p} = y^2 b\left(\frac{E_c \varepsilon_c}{3} + \frac{0.67 f_{cu} - E_c \beta}{4\beta^2}\varepsilon_c^2\right) + A'_s f'_s (y - d') + A_s f_s (d - y) + A_p \sigma_{s(\min)} (D - y)$$

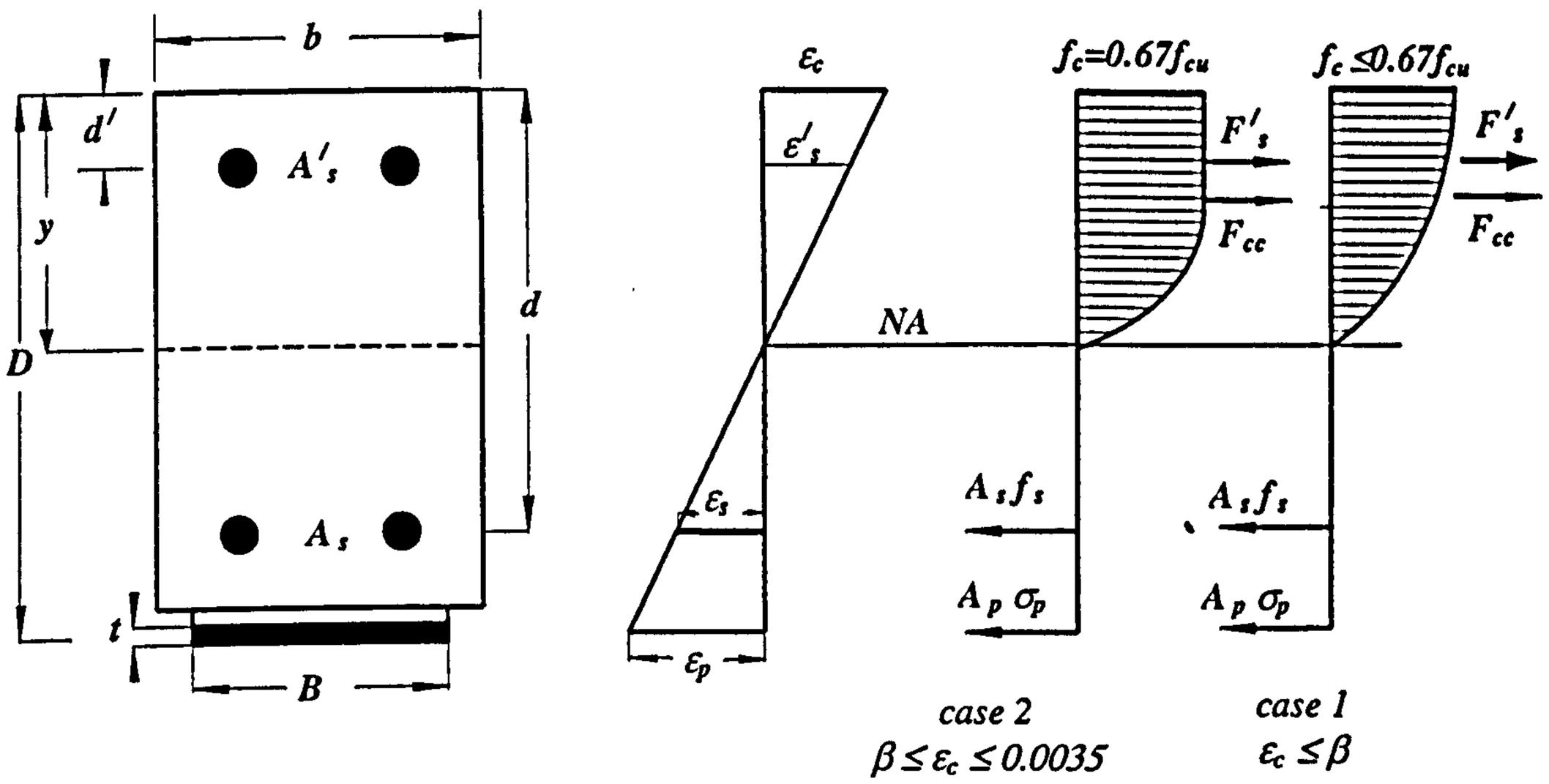

Fig. 8.4 Section strains, stresses, and dimensions after BS8110 (1985).

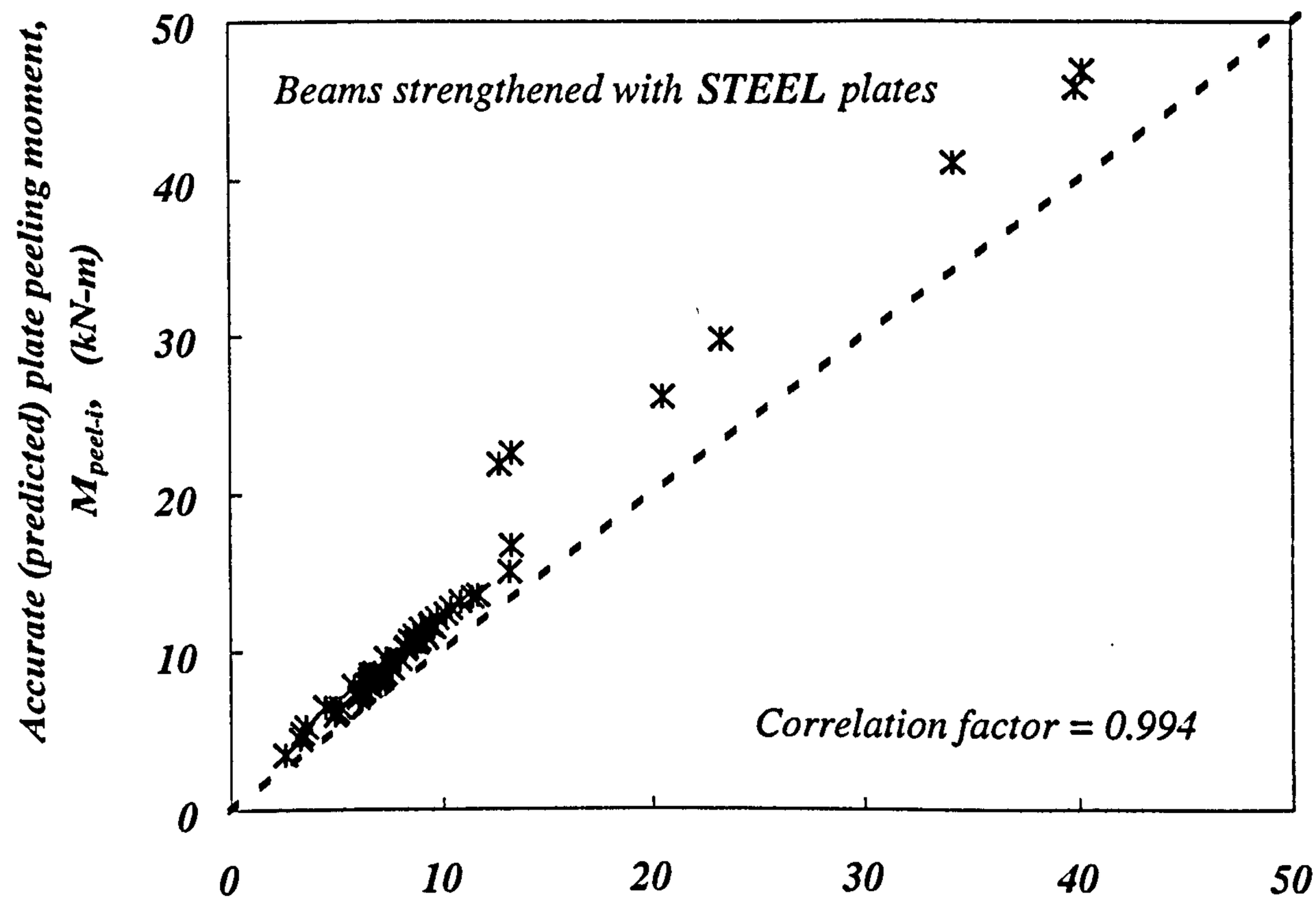

Fig. 8.5 Correlations between the proposed simple (parabolic) and the accurate values for the plate peeling moment for beams strengthened with steel plates.

Alternatively, if the maximum concrete strain is found to be larger than β (case 2), then, the moment resulting from the concrete compressive stresses may be derived as

$$M_c = 0.67 f_{cu} b(y - y_1)\left(y_1 + \frac{(y - y_1)}{2}\right) + b\int_0^{y_1} f_{cz} z dz$$

$$M_c = 0.335 f_{cu} b\left(y^2 - y_1^2\right) + y^2 b\left(\frac{E_c \varepsilon_c}{3} + \frac{0.67 f_{cu} - E_c \beta}{4}\right)$$

With $\sigma_p = \sigma_{s(\min)}$, the simplified lower bound plate peeling moment, M_{peel-p}, will be

$$M_{peel-p} = 0.335 f_{cu} b\left(y^2 - y_1^2\right) + y^2 b\left(\frac{E_c \varepsilon_c}{3} + \frac{0.67 f_{cu} - E_c \beta}{4}\right) + A_s' f_s'(y - d') + A_s f_s(d - y) + A_p \sigma_{s(\min)}(D - y)$$

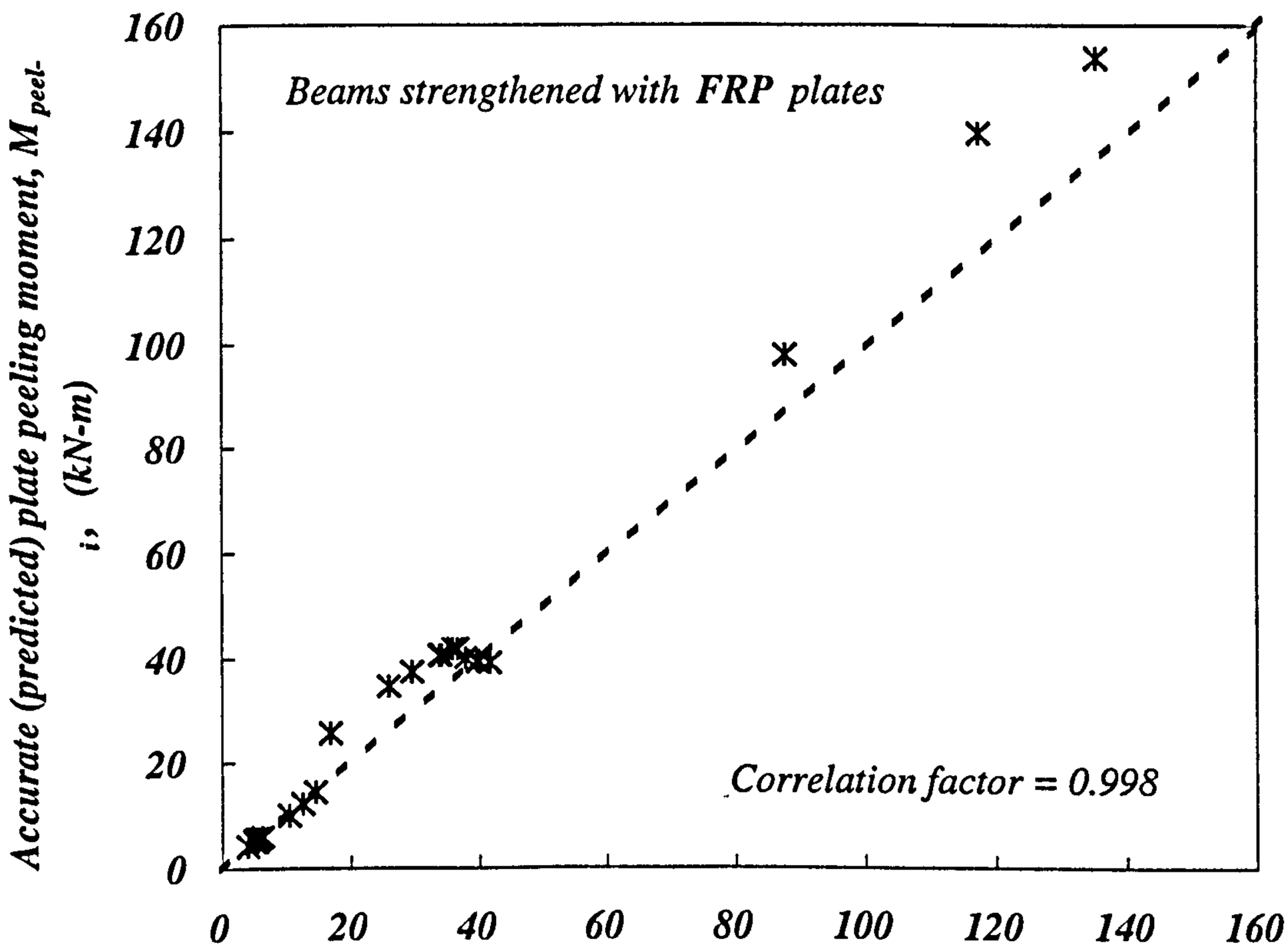

Fig. 8.6 Correlations between the proposed simple (parabolic) and the accurate values for the plate peeling moment for beams strengthened with FRP plates.

To check the validity of the above-simplified method, plate peeling moments for the previously mentioned 111 steel and 58 FRP plated beams were calculated, using both

the so-called accurate iterative method and also the above simplified procedure. Figures 8.5 and 8.6 show the encouraging correlations between the simplified and the iterative plate peeling moments for beams strengthened with steel and FRP plates, respectively.

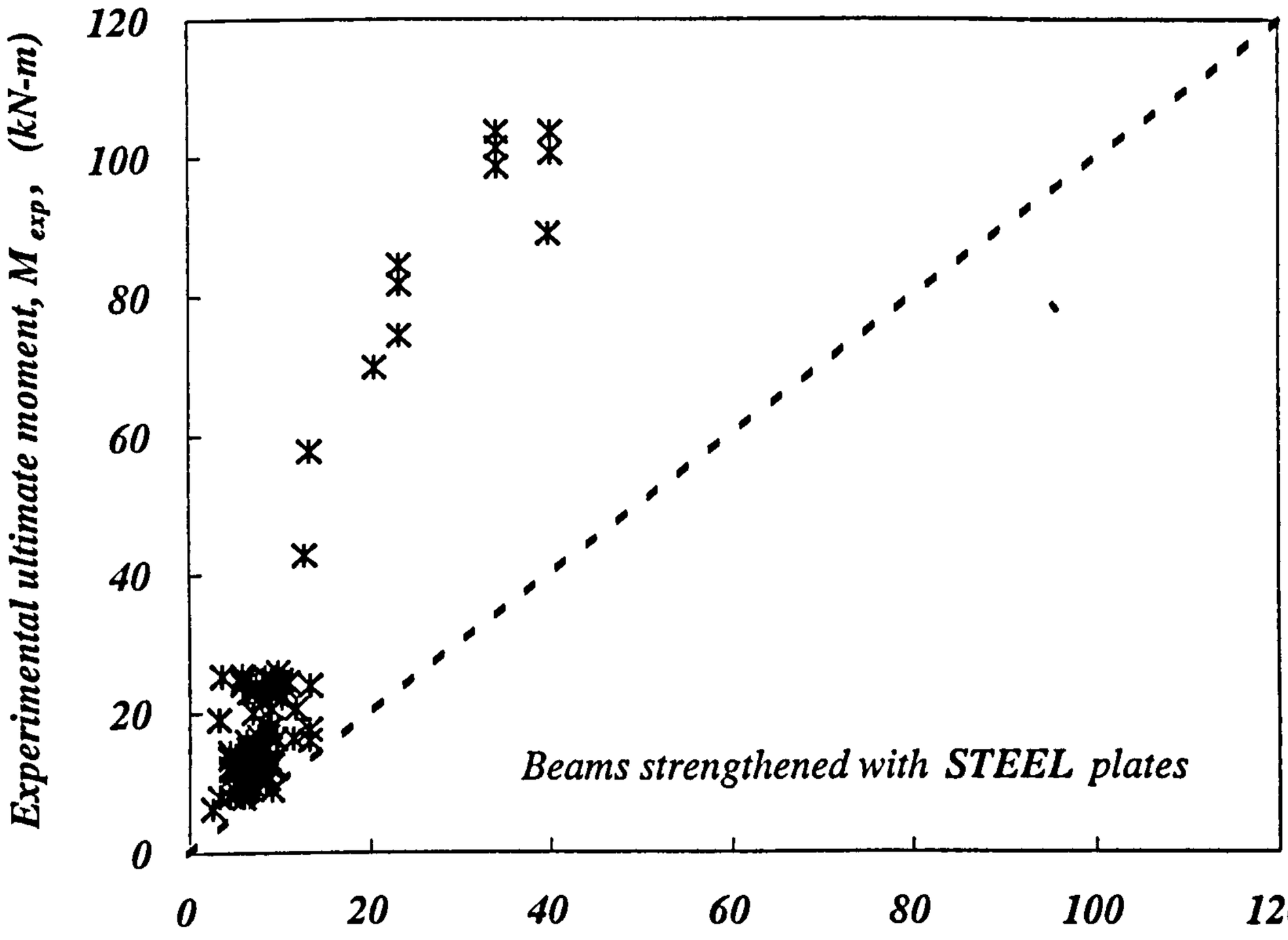

Fig. 8.7 Comparisons between the proposed simplified plate peeling moment (parabolic) and the corresponding experimental results for beams strengthened with steel plates.

Finally, Figures 8.7 and 8.8 compare the theoretical and experimental ultimate peeling moments for the 111 beams (i.e. beams 59-169) strengthened with steel plates, and the 58 FRP plated beams (i.e. beams 1-58), respectively. In both Figures 8.7 and 8.8, the simplified theoretical approach is found to predict conservative values for the lower bound plate peeling moment with almost all of the data points lying above the 45° lines. It should be noted that unlike Oehlers (1992) who has quoted both the initial and also the ultimate experimental peeling moments, all the other references have

only quoted a single value for the failure peeling moment in their tests which, for the present purposes, have been assumed to relate to ultimate (as opposed to initial) moments.

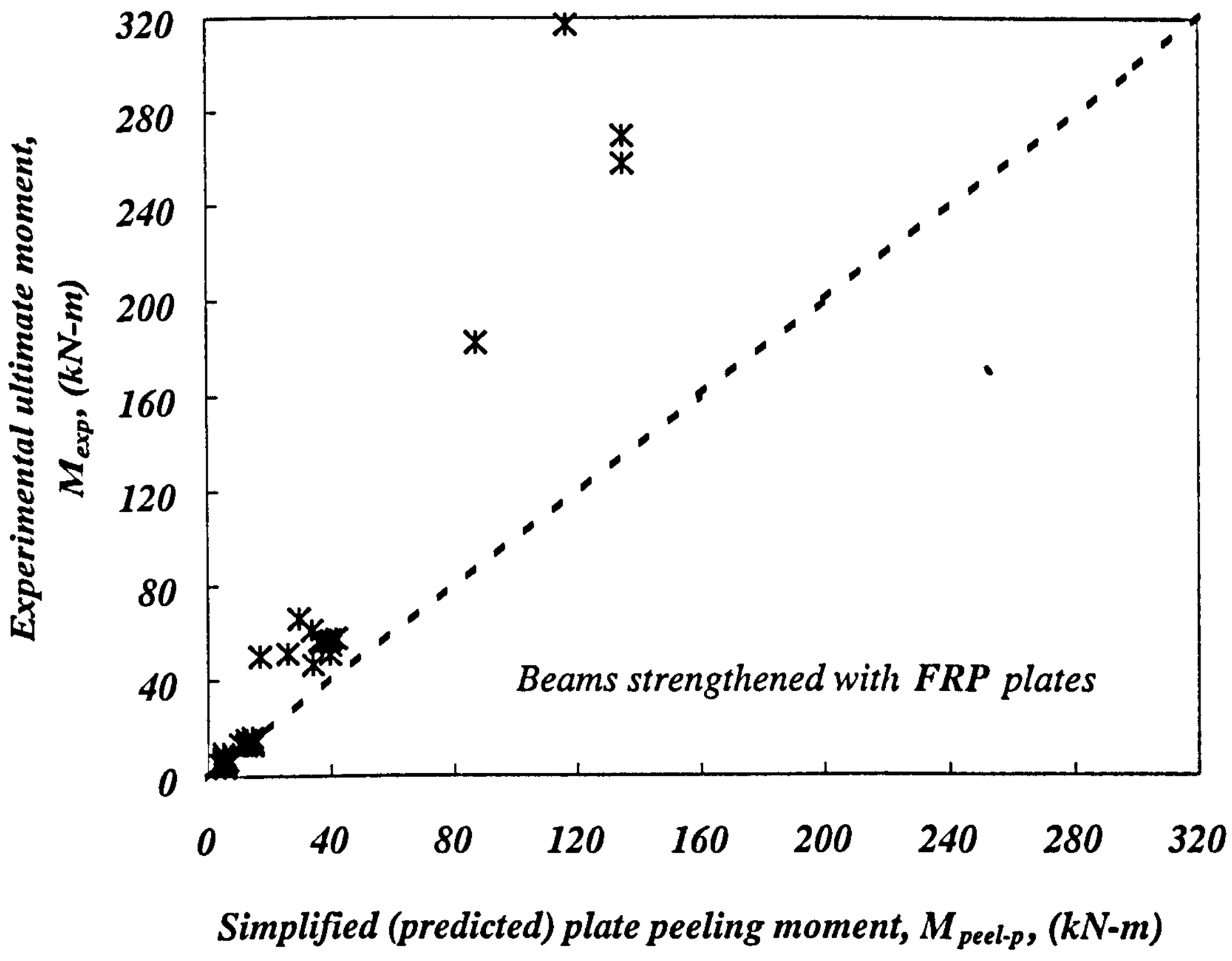

Fig. 8.8 Comparisons between the proposed simplified plate peeling moment (parabolic) and the corresponding experimental results for beams strengthened with FRP plates.

Moreover, comparison of Figures 8.7 and 8.9, on the one hand, and Figures 8.8, and 8.10, on the other (where, the results in Figures 8.9 and 8.10 are produced with the external plate peeling moments predicted using the more accurate iterative method) suggest that the predictions of lower bound plate peeling moment, based on both the iterative and the simplified procedures are, for all practical purposes, similar, with both of them leading to largely similar correlations with experimental data.

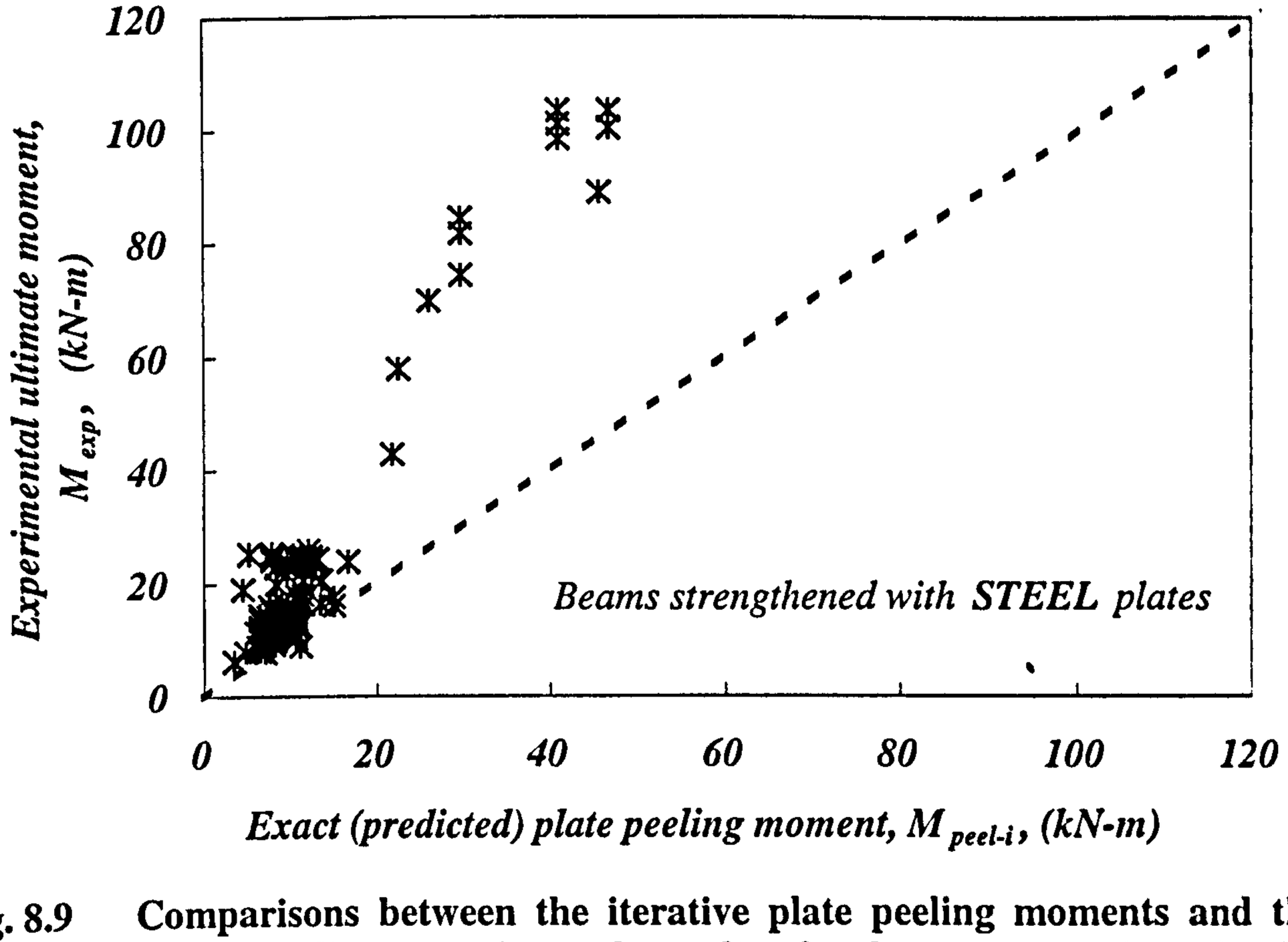

Fig. 8.9 **Comparisons between the iterative plate peeling moments and the corresponding experimental results, for beams strengthened with steel plates.**

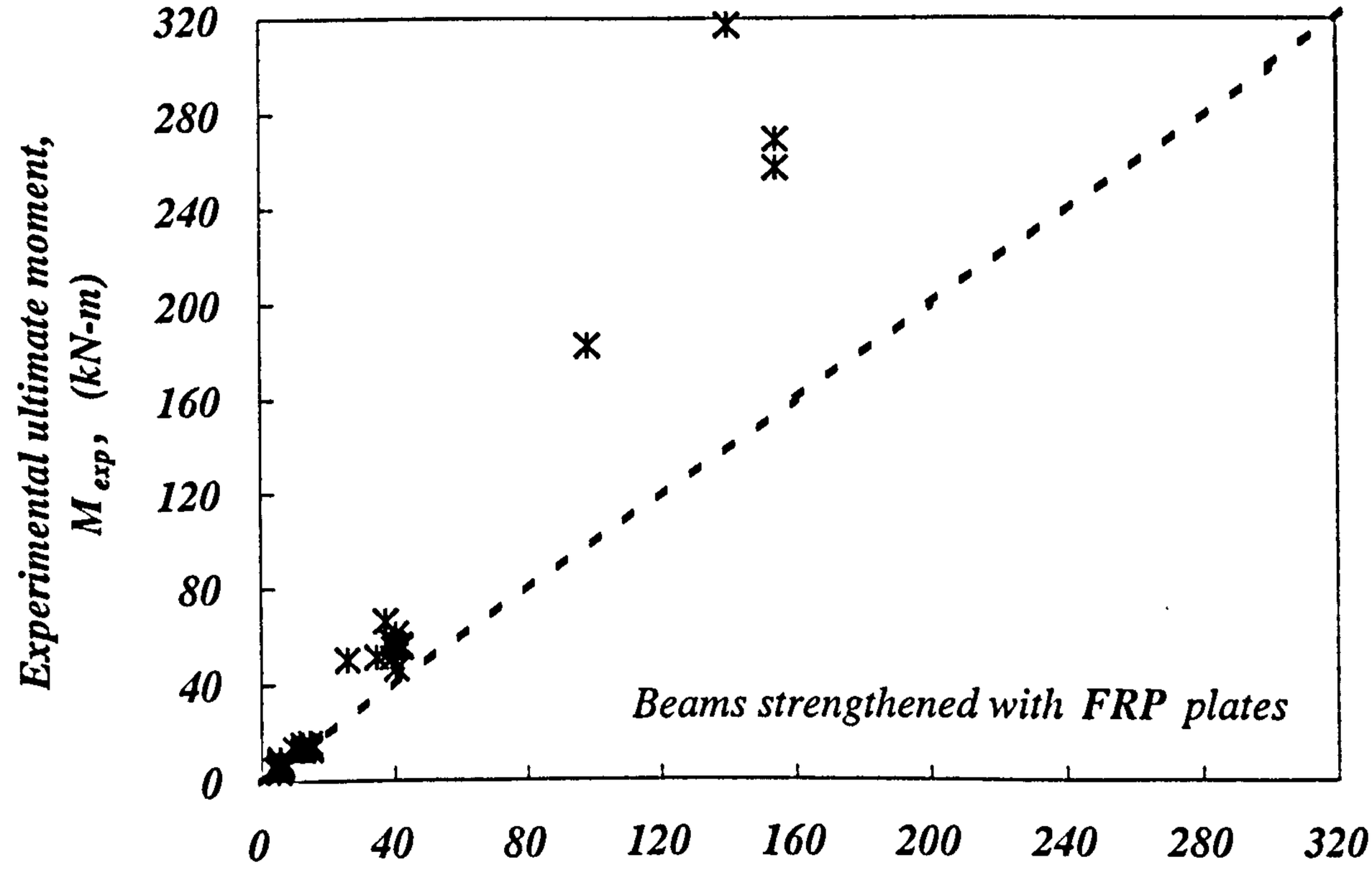

Fig. 8.10 **Comparisons between the iterative plate peeling moments and the corresponding experimental results, for beams strengthened with FRP plates.**

8.2.2.2 Uniform stress block approximation

The above straightforward method may be simplified further, as follows.

Here, the concrete parabolic compressive stress curve may be replaced by a uniform stress distribution block with the assumed uniform concrete stresses equal to the maximum one corresponding to the ultimate concrete strain in compression, Figure 8.11. The depth of neutral axis, y, may, then, be calculated as suggested in section 8.2.1 (Equation (8.1)). The parameter, a, in Figure 8.11 represents the depth of equivalent stress block, the resultant force of which is in balance with the other forces acting on the beam section (for equilibrium). The plate peeling moment may, then, be determined as follows:

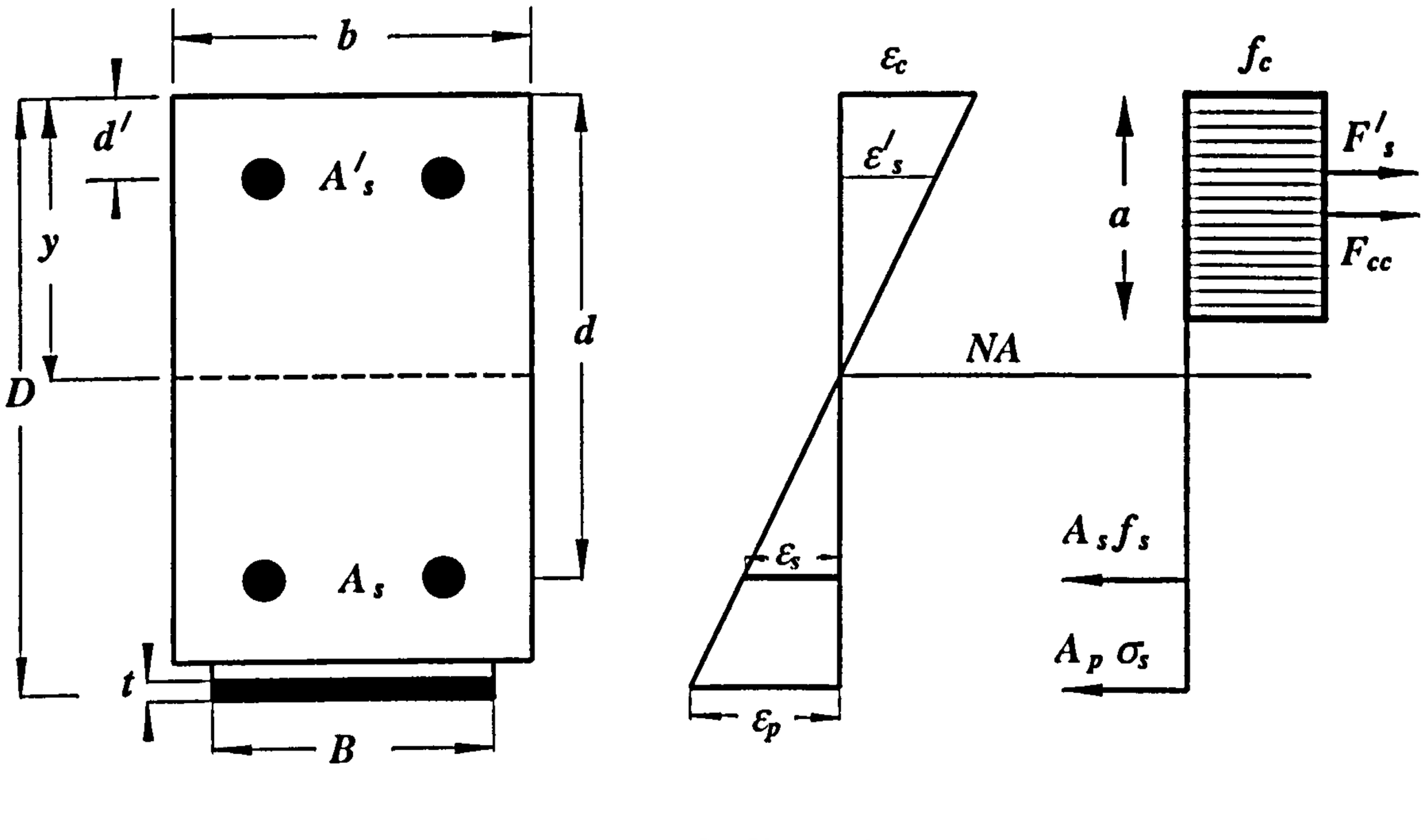

Fig. 8.11 Section strains, stresses, and dimensions (concrete uniform stress block).

1- Calculate the total compression force in concrete, as the difference between the total tension force (in the plate and the embedded bars) and the force in the compressed bars – i.e. $F_c = A_s f_s + A_p \sigma_{s(\min)} - A'_s f'_s$,

2- Calculate the maximum concrete stress, f_c, where

$$f_c = \begin{cases} 0.67 f_{cu} & , \quad \beta < \varepsilon_c \leq 0.0035 \\ E_c \varepsilon_c + \dfrac{0.67 f_{cu} - E_c \beta}{\beta^2} \varepsilon_c^2 , & \varepsilon_c \leq \beta \end{cases}$$

3- Calculate the depth of concrete compressive stress block, a, as

$$a = \frac{A_s f_s + A_p \sigma_{s(\min)} - A'_s f'_s}{f_c}$$

4- The plate peeling moment is

$$M = A_s f_s (d - a/2) + A_p \sigma_{s(\min)} (D - a/2) + A'_s f'_s (a/2 - d')$$

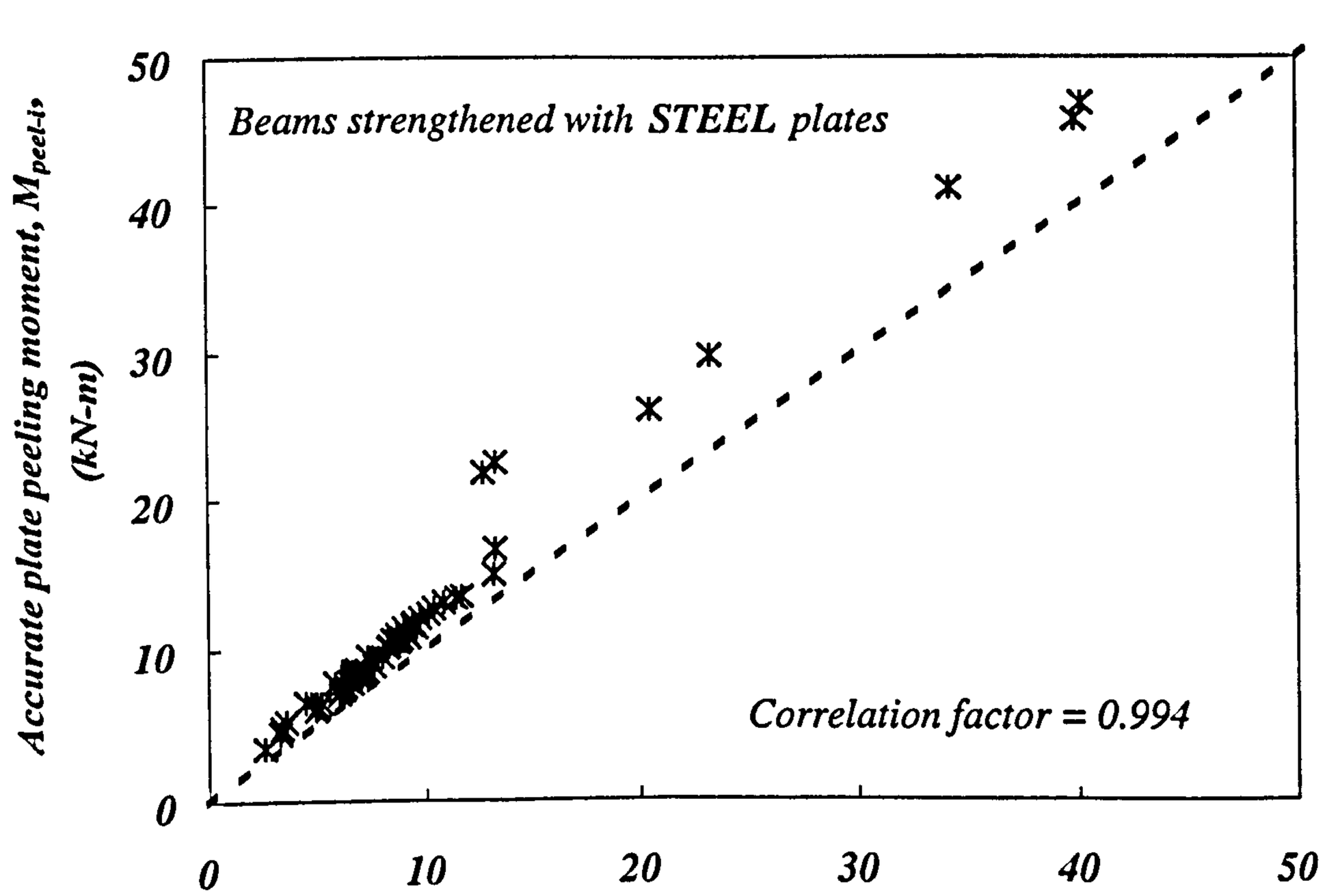

Fig. 8.12 Correlations between the simplified (uniform stress block) and the iterative values for the plate peeling moment for beams strengthened with steel plates.

Figure 8.12 presents the encouraging correlations between the results based on both the iterative and the above-simplified technique (i.e. uniform stress block approximation) for the 111 beams strengthened with steel plates: the correlation factor is 0.994. The similarity between the results in Figure 8.12 and Figure 8.5 is particularly noteworthy, with the uniform stress-block approach resulting in predictions which are, indeed, very similar to those based on a parabolic concrete stress distribution as adopted in the other (alternative) straightforward approach.

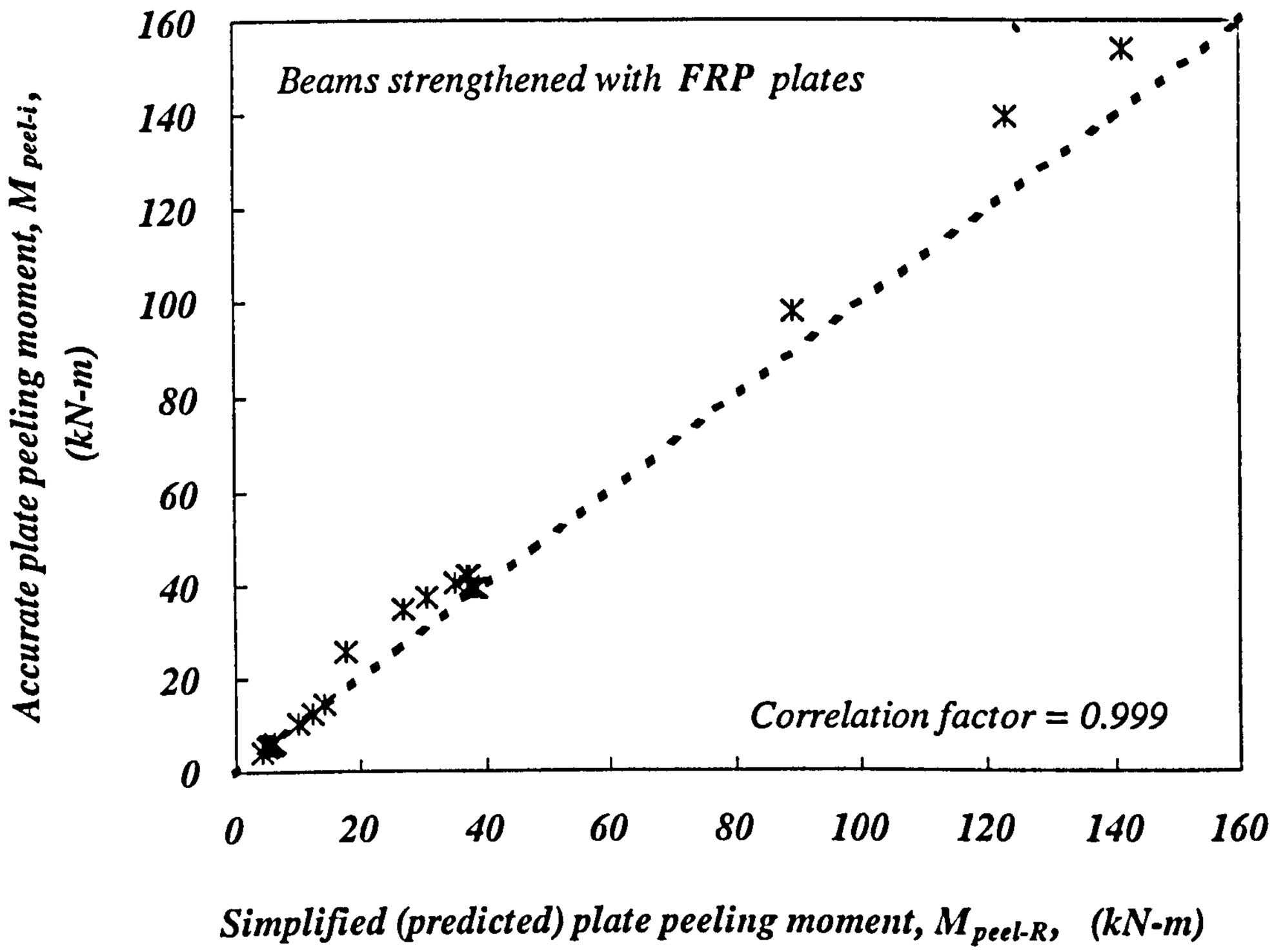

Fig. 8.13 Correlations between the simplified (uniform stress block) and the iterative values for the plate peeling moment for beams strengthened with FRP plates.

The presently proposed method is also applicable to beams strengthened with FRP plates. Figure 8.13 shows the encouraging correlations (for the 58 beams with external FRP plates) between results based on the proposed simplified uniform stress block and the iterative methods, where the correlation factor is 0.999. A comparison of the

results presented in Figure 8.13 and Figure 8.6 is also instructive: the results based on the concrete uniform stress block approach are (as a whole) similar to those based on the alternative simplified method which adopts a concrete parabolic stress distribution.

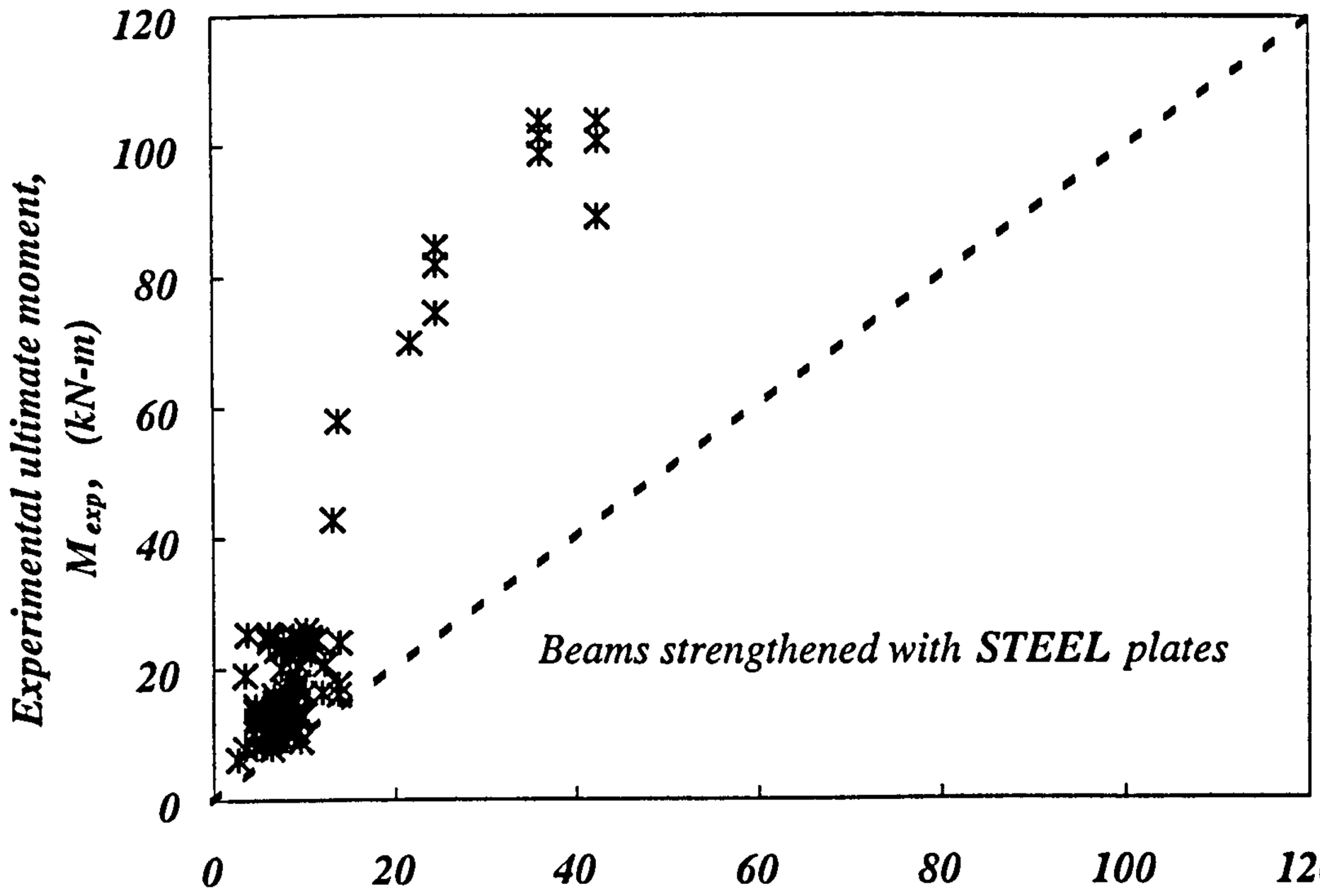

Fig. 8.14 Comparisons between the proposed simplified theoretical method (uniform stress block) and the corresponding experimental results for beams strengthened with steel plates.

Figures 8.14 and 8.15 present comparisons between the test data and the simplified theoretical predictions (based on the concrete uniform stress block) for the 111 steel plated and the 58 FRP plated beams, respectively: it is obvious that the presently proposed simple method successfully predicts safe values for the plate peeling moment with almost all of the data points lying above the 45° lines. It is also worth comparing Figures 8.14 and 8.15 with Figures 8.9 and 8.10, respectively, with the last two figures relating to cases where the plate peeling moment has been predicted using

the iterative method. It is clear that the predictions based on both the iterative and the simplified approaches are very similar.

In conclusion, both of the presently proposed simplified approaches are found to predict reasonable values for the lower bound plate peeling moments for both cases of steel- and/or FRP-plated beams, with the one adopting the concrete uniform stress block in compression involving less effort for arriving at the final solution.

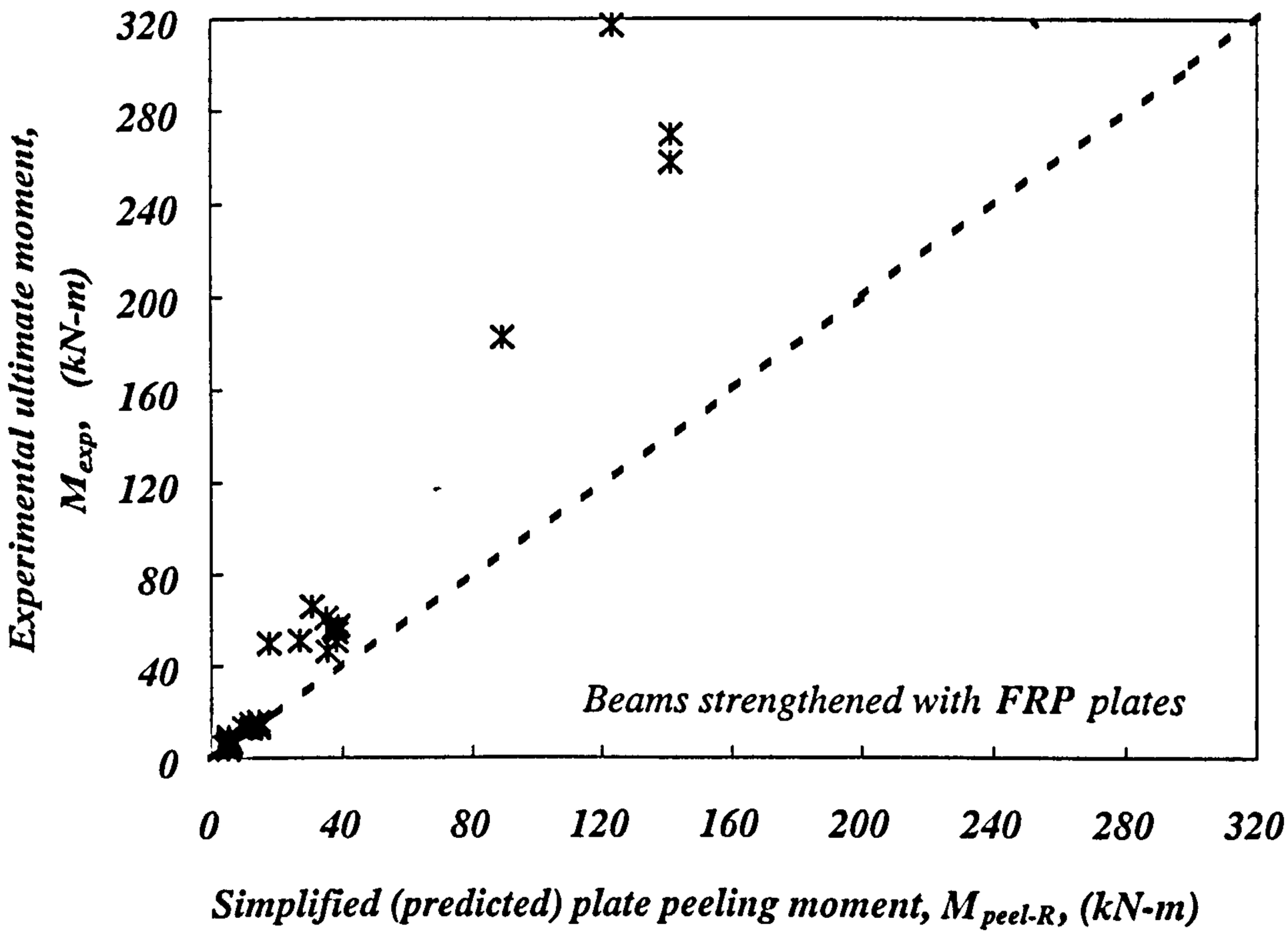

Fig. 8.15 Comparisons between the proposed simplified theoretical method (uniform stress block) and the corresponding experimental results for beams strengthened with FRP plates.

8.3 SUMMARY AND CONCLUSIONS

In this chapter, simplified (but reasonably accurate) methods for predicting the lower bound plate peeling moment of reinforced concrete beams strengthened with external steel and/or FRP plates have been developed. The proposed methods are

straightforward, being amenable to hand calculations, using a pocket calculator, hence, suitable for use in practice. With the depth of neutral axis predicted (assuming a linear stress distribution for concrete in compression), the final results for lower bound plate peeling moment have been found to be supported by those based on the more involved iterative procedure and also by extensive test data as reported by others, covering a wide range of beam design parameters. It is, perhaps, worth noting the very encouraging correlations achieved in terms of the neutral axis depth by both the iterative method (which is dependant on the magnitude of the plate axial stress) and the corresponding values based on the simplified method, with the results of the latter being independent of the plate axial stress.

With the depth of neutral axis determined, it has been demonstrated that the subsequent approximation of the concrete stress distribution in compression to a uniformly distributed type, leads to final predictions of plate peeling moment which are, indeed, reasonable, and good enough for practical applications. The following simple steps, should, then, be followed for predicting the lower bound plate peeling moment of reinforced concrete beams strengthened in flexure with external steel and/or FRP plates:

1- Calculate the depth of neutral axis for the plated beam, using

$$y = d\left(-\left(\alpha_{sc}(\rho'_s+\rho_s)+\rho_p\alpha_{pc}\right)+\sqrt{\left(\alpha_{sc}(\rho'_s+\rho_s)+\rho_p\alpha_{pc}\right)^2+2\left(\alpha_{sc}\left(\rho'_s\frac{d'}{d}+\rho_s\right)+\rho_p\alpha_{pc}\frac{D}{d}\right)}\right)$$

where

$$\rho_s=\frac{A_s}{bd},\ \rho'_s=\frac{A'_s}{bd},\ \rho_p=\frac{A_p}{bd},\ \alpha_{sc}=\frac{E_s}{E_c}\ \text{and}\ \alpha_{pc}=\frac{E_p}{E_c},$$

2- Calculate the minimum axial plate peeling stress, $\sigma_{s(\min)}$, as follows:

$$\sigma_{s(\min)} = 0.154 \frac{L_p h_1 b^2 \sqrt{f_{cu}}}{h' b_1 t \sum O_{bars}}$$ (for beams loaded prior to strengthening), or

$$\sigma_{s(\min)} = 0.154 \frac{L_p h_1 b^2 \sqrt{f_{cu}}}{h' b_1 t (\sum O_{bars} + b_1)}$$ (for beams strengthened before being loaded)

The plate axial strain, ε_p, is, then, given as

$$\varepsilon_p = \frac{\sigma_{s(\min)}}{E_p}$$

3- Calculate the stresses in the steel bars and concrete as follows:

the maximum concrete strain, $\varepsilon_c = \varepsilon_p \frac{y}{D-y} \leq 0.0035$,

the maximum concrete compressive stress

$$f_c = \begin{cases} 0.67 f_{cu} & , \quad \beta < \varepsilon_c \leq 0.0035 \\ E_c \varepsilon_c + \frac{0.67 f_{cu} - E_c \beta}{\beta^2} \varepsilon_c^2 & , \quad \varepsilon_c \leq \beta \end{cases}$$

and, the tensile stresses in the embedded steel bars are given by

$$f_s = \sigma_p \frac{d-y}{D-y} \frac{E_s}{E_p} \leq f_y$$

while, the axial stresses in the steel bars in compression, will be

$$f'_s = \sigma_p \frac{y-d'}{D-y} \frac{E_s}{E_p} \leq f_y$$

4- Calculate the depth of the concrete uniform stress block, a, as

$$a = \frac{A_s f_s + A_p \sigma_{s(\min)} - A'_s f'_s}{f_c}$$

5- The lower bound plate peeling moment is, finally, given by

$$M_{peel-R} = A_s f_s (d - a/2) + A_p \sigma_{s(\min)} (D - a/2) + A'_s f'_s (a/2 - d')$$

Chapter 9

SUMMARY AND CONCLUSIONS

Chapter 9

SUMMARY AND CONCLUSIONS

9.1 INTRODUCTION

One of the main objectives of this thesis was to develop a practical procedure, which is sufficiently reliable; to be used for designing externally plated beams against premature plate peeling failures. In addition, a key aim was to develop a model which is capable of predicting the load bearing capacity of either pre-cracked or uncracked (as cast) reinforced concrete beams (prior to external plating) which were subsequently strengthened with steel or FRP plates. Theoretical parametric studies were also to be carried out in order to quantify the influence of various first order plated beam design parameters on the plate peeling load. In particular, the effect of variations of the axial Young's modulus of the plate on various modes of failure and associated failure loads of the FRP plated beams, in the absence or presence of plate peeling failures, was to be examined in detail.

9.2 RESEARCH OVERVIEW

The research work carried out in this thesis may be divided into three main tasks, as follows:

1- Extensive literature review for gathering the necessary detailed and extensive experimental data plus a critical examination of the previously available methods for predicting the premature steel or FRP plate peeling failure load. To this end, various features of the previously available theories have been examined in some detail, with their shortcomings identified. Indeed, non (apart from one) of the

previous theoretical and/or semi-empirical models were found to be generally applicable and in almost all cases studied, major shortcomings were found: this was largely done by a comparison of their predictions with experimental data reported by others.

2- The teeth model of Zhang and Raoof, however, was found to be a promising one, and has, indeed, been extended to cases when external FRP (as opposed to steel) plates are used for upgrading R.C. beams.

3- Simple but, at the same time, reliable practical design procedures (based on an extended version of Raoof and Zhang's model in conjunction with the results of theoretical parametric studies) have been developed for predicting the flexural load bearing capacity of reinforced concrete beams strengthened with externally bonded FRP or steel plates, with the final numerical results supported by mainly large scale and extensive test data for both steel and FRP plated beams, covering a wide range of beam design parameters and external plating techniques.

9.2.1 Experimental Review and Critical Examination

The review of experimental studies relating to reinforced concrete beams strengthened with externally bonded steel and/or FRP plates has been extensive and very fruitful. The gathered experimental data included a wide range of beam designs relating to 58 FRP and 111 steel plated R.C. beams. In general, experimental works of others suggested that external plating increases the flexural stiffness, although some plated beams were found to have failed at loads lower than the flexural load bearing capacity of the corresponding unplated beams with the mode of failure being brittle. There did not, however, appear to be any conclusive explanation for this alarming experimental finding, considering that the external plate bonding technique has already been used

in practice for upgrading a large number of buildings and bridges, in a number of countries. A critical examination of the previously reported analytical methods suggested that they are relatively few in number, with most of them being based on a curve fitting exercise, involving a limited number of experimental data. The practical implications of various assumptions used in different approaches were critically examined, and the most promising approach for further research, was identified. The purely empirical approach for avoiding occurrence of plate peeling which involves restricting the ratio of plate width/thickness was examined: although promising for steel-plated beams, it was found not to be applicable to FRP plated R.C. beams.

In general, there appeared to be three distinctly different approaches to the plate-peeling problem. A semi-analytical model has been proposed by the group at King Fahd University: in this approach, using experimental results on steel plated R.C. beams, the normal and shear stresses in the adhesive layer at the end of the plate are predicted with these stresses being assumed to control the occurrence of premature plate peeling failures. In one case, by adjusting the capacity of the shear reinforcement according to a semi-empirical factor, it has been claimed that one can predict the peeling failure. In another case, it has been assumed that the plate peeling occurs due to excessive shear stresses in the adhesive layer at the end of the plate. However, a critical examination of both these methods revealed major numerical inconsistencies in the reported results.

In another approach (by Oehlers and his associates), it has been assumed that the plate-peeling failure occurs when the peeling stress in the adhesive layer due to the beam curvature reaches the maximum tensile strength of concrete. This assumption

and the subsequently proposed design formulations were also found to suffer from major shortcomings. The so-proposed design formulations were shown to give poor results as, in this approach, the predicted load bearing capacity for the plated beam was found to be too conservative (indeed, in most cases, even lower than the flexural capacity of the corresponding unplated R.C. beam). In other words, ironically, by using the external plating technique in order to strengthen a beam in flexure, this method was found to predict the failure load of the plated beam to be even lower than that the corresponding unplated R.C. beam!

The third approach (by Raoof & Zhang) has been based on assuming that the plate peeling failure occurs when the tensile stresses in the concrete cover at the point of fixity (just underneath the main reinforcing bars) to the cantilever (tooth) formed between two adjacent stabilised cracks, become equal to the concrete tensile strength. Based on this assumed mechanism of failure, and in view of variations in the spacings of stabilised cracks (by a factor of, say, 2), Raoof and Zhang have argued that a unique solution for the plate peeling load does not exist and an upper/lower bound approach must be adopted, with the lower bound solution being the safe one for design purposes. The predictions based on this method for steel plated beams have been shown by Raoof and Zhang to provide encouraging upper/lower bounds to an extensive set of large-scale experimental data reported by others, hence, confirming its general validity for steel-plated R.C. beams.

9.2.2 Model Development and Parametric Studies

Based on a critical examination of the previously available methods of analysis, Raoof and Zhang's approach was found to be the most promising one, and was,

therefore, adopted for further development. This approach was used to predict the load bearing capacity of FRP plated beams, addressing the cracking conditions (i.e. those cases involving cracked or uncracked R.C. beams prior to plating). A computer programme was written to deal with the problem, using an iterative technique with the capability to handle different cracking patterns. The final numerical results for 111 steel-plated and also 58 FRP plated R.C. beams were verified against mainly large scale experimental data. In all cases, the theoretical predictions were found to give encouraging upper/lower bound solutions to test data for R.C. beams with external FRP or steel plates which were either as cast or pre-cracked prior to plating. The effect of preloading prior to strengthening (which is more relevant to practical conditions, where structures are already cracked under service conditions) was also studied. Theoretical parametric studies (supported with experimental results) were also carried out, covering the influence of various parameters such as the plate width, thickness, and area. Extensive numerical results suggested that the previous practice by various researchers of testing as cast (i.e. uncracked) plated beams to predict the peeling behaviour of cracked beams (prior to plating) in actual structures does, indeed, provide conservative results for use in practice.

Guided by the outcome of the literature review, the need to carefully define the variations in the modes of failure for FRP plated beams with changes in the axial Young's modulus of the FRP plate was identified. Subsequent work suggested that, in general, there are two modes of failure which are exclusive to R.C. beams strengthened with FRP plates while another two different failure modes are exclusively associated with beams strengthened with steel plates, with four alternative modes of failure being common to both types (steel or FRP) of plated beams. In total,

therefore, eight different possible modes of failure for plated beams were identified as opposed to only two types of failure modes associated with unplated reinforced concrete beams. It was also possible to identify which of these different modes of failure is of the undesirable brittle type, with others being of a ductile nature. By resorting to equilibrium conditions for forces over the critical plated beam sections, it was possible to identify the range of FRP Young's moduli over which each mode of failure is operative and, indeed, a method was proposed for identifying the critical values of Young's modulus associated with which mode transitions take place. Very briefly, the effect of increasing the FRP modulus of elasticity on the flexural load bearing capacity, the strain distribution(s) across the plated section, and the depth of the neutral axis, were studied within each of the six possible modes of failure, for FRP plated beams, on an individual basis. Furthermore, the possible mode(s) of failure which are to follow each mode (as a result of increasing the value of FRP modulus of elasticity) were identified. It should be noted that the corresponding unplated R.C. beams were, in general, assumed to be under-reinforced in all cases of external plating. As mentioned previously, formulations were developed for determining the types of expected modes of failure. These studies identified two general types of behaviour for plated beams: either over- or under-reinforced. Based on the so-developed formulations for the critical values of moduli of elasticity for the FRP plate, brief theoretical parametric studies were also carried out in order to investigate the influence of other parameters (such as the area of the externally bonded plate, the concrete compressive strength, and the yield strength of the embedded bars and the external plate) on the failure load.

9.2.3 Design Procedure(s)

Simplified (but reasonably accurate) methods for predicting the lower bound plate peeling moment of reinforced concrete beams strengthened with external steel and/or FRP plates have been developed. The proposed methods are straightforward, being amenable to hand calculations, using a pocket calculator, hence, suitable for use in practice. With the depth of neutral axis predicted (assuming a linear stress distribution for concrete in compression), the final results for lower bound plate peeling moment have been found to be supported by those based on the more involved iterative procedure and also by extensive test data as reported by others, covering a wide range of beam design parameters. It is, perhaps, worth noting the very encouraging correlations achieved in terms of the neutral axis depth by both the iterative method (which is dependant on the magnitude of the plate axial stress) and the corresponding values based on the simplified method, with the results of the latter being independent of the plate axial stress.

With the depth of neutral axis determined, it has been demonstrated that the subsequent approximation of the concrete stress distribution in compression to a uniformly distributed type, leads to final predictions of plate peeling moment which are, indeed, reasonable, and good enough for most practical applications.

To verify the design approach, two methods of validation were adopted. The first method involved a comparison of the independent results (such as the depth of neutral axis and the plate peeling moment) of the proposed simplified procedures with the corresponding ones based on the more involved iterative method. In the second method, test data for 169 different plated R.C. beam designs (i.e. 58 and 111 beams

strengthened with external FRP and steel plates, respectively) were used for further verifications. This involved a comparison of the final numerical results based on the proposed simplified procedure(s) with the corresponding experimental data for all the aforementioned 169 beam designs, where, in all cases, the proposed design calculations were found to predict safe solutions, suitable for use in practice. It should be noted that the results based on the proposed design procedures are independent of the experimental and/or the numerical (i.e. the iterative) data. It is, however, encouraging that the results of both the simplified and the iterative methods were found to be largely in agreement

This design approach may be summarised as in the following five simple steps:

1- Calculate the depth of neutral axis, using a closed-form formula that is based on assuming a linear distribution of concrete stresses across the critical plated beam section.

2- Calculate the minimum peeling stress (and strain) of the externally bonded plate.

3- Calculate the strains (and hence stresses) across the beam critical section, using the above calculated depth of neutral axis in conjunction with the predicted minimum plate peeling axial strain. In doing so, use the more accurate non-linear formulae for calculating the concrete stresses corresponding to the maximum concrete strain in compression.

4- Calculate the depth of the stress block, which satisfies force equilibrium, by approximating the non-linear compressive stress distribution in concrete to a uniform stress block with the constant concrete stress assumed to be given by value as calculated in step 3

5- Calculate the plate peeling moment, as the sum of the moments associated with all the elemental forces about the neutral axis.

9.3 CONCLUSIONS

The following are the main conclusions:

1- Strengthening reinforced concrete beams using externally bonded plates may have an adverse effect on the load bearing capacity of the plated beams if one does not guard against the occurrence of plate peeling failure.

2- The well known and purely empirical approach of keeping the plate width/thickness ratio above 60 to avoid plate peeling failure is a reasonable one for preliminary design of steel plated beams. However, it is not generally valid when FRP plates are used.

3- The previously reported semi-empirical methods of analysis as proposed by various researchers, which are based on calibrating certain parameters by using experimental results are not, generally, reliable and would lead to unsafe design in certain circumstances, while, in others, these lead to overly conservative estimations of the beam load bearing capacity. Indeed, in certain circumstances, the so-estimated load bearing capacities would be lower than that even that of the corresponding unplated R.C. beam.

4- The previously available semi-empirical approaches provide no means of predicting the stresses or strains across the critical beam sections at failure neither are they capable of predicting the type of failure (i.e. as to whether brittle or ductile).

5- The presently proposed model enables one to identify the first order plated beam design parameters which control the final failure load. Once validated

against mainly large scale test data as reported by others, the present model has been used for theoretical parametric studies in order to study the influence of varying the magnitude of the modulus of elasticity for externally bonded FRP plates on the variations in the final modes of failure. Based on this study, the effects of other important beam design parameters have also been investigated.

6- The area of the plate, not the plate width/thickness ratio, has been identified to be the main factor (amongst others, such as the FRP modulus of elasticity) affecting the behaviour of FRP plated R.C. beams.

7- The common practice among various researchers of carrying out experimental studies on as cast (i.e. uncracked) R.C. beams in connection with which, the original (unplated) beams have not been preloaded prior to external plating, has been shown to be a conservative approach, resulting in a reduction in the failure load (c.f. pre-cracked plated R.C. beams).

8- As discussed in Chapter 5, eight different possible flexural modes of failure have been identified in connection with externally plated R.C. beams. Currently, there is a lack of accurate description (or identification) regarding the whole range of possible modes of failure, with the previous experimental studies on FRP plated R.C. beams suffering from a lack of systematic approach, covering all the possibilities. In the present work, therefore, an accurate classification of all the possible modes of failure has been proposed with a detailed quantitative treatment of the mode transitions as a function of changes in the FRP Young's modulus.

9- Purely experimental parametric studies (i.e. experimental comparisons) are suggested to be potentially misleading because of a general lack of a unique solution for the steel and/or FRP plate peeling phenomenon.

10- The proposed design procedure(s) are believed to be sufficiently accurate yet fairly simple (c.f. the lengthy iterative method) for use in practice.

9.4 RECOMMENDATIONS FOR FURTHER RESEARCH

The work reported in this thesis has gone some way to clarify certain critical areas of practical interest. Both, further experimental and theoretical research is, however, still needed in order to clarify the following issues:

1- Studying the effect of partial slippage between the externally bonded plate and the concrete beam on the failure mechanism and load: this factor will be of significance in relation to the predicted axial stresses in the plate in those cases when a thicker adhesive layer with lower values of shear modulus of rigidity is used. Ignoring the partial slippage between the plate and the R.C. beam is, however, likely to result in conservative predictions of failure load.

2- Further studies of providing plate end fixities, for avoiding occurrence of FRP or steel plate peeling failures, are needed. In this context, different types of end anchorages will have to be dealt with, resorting to largely experimental techniques. Although fairly effective in the case of steel plates, bolts can not be used for fixing the ends of FRP plates, and other options should be explored.

3- Detailed experimental investigation regarding the distribution of stresses within the adhesive layer along the length of the plate, located within the shear

span, in order to improve the presently proposed expressions for determining the effective length of the plate, is another issue which needs further work.

4- Analytical studies (to be supported with test data) similar to those presented in this thesis in relation to the variations in the modulus of elasticity for the FRP plate should be carried out, addressing the influence of variations of other main parameters affecting the behaviour of the plated beam (e.g. the plate area and ultimate strength, the area of embedded bars, and ultimate strength plus other characteristics of the adhesive material).

REFERENCES

REFERENCES

ACI Committee 318 (1983), Building Code Requirements for Reinforced Concrete (ACI 318-83). American Concrete Institute, Detroit.

Allen, A. H. (1988), Reinforced Concrete Design to BS8110. E. & F. N. Spon Ltd, London.

Arduini, M., and Nanni, A. (1997), "Parametric Study of Beams with Externally Bonded FRP Reinforcement", ACI Structural Journal, Volume 94, No. 5, September-October, 493-501.

Arockiasamy, M., and Dutta, P. K. (1996), "Retrofitting and Structural Repair with Advanced Polymer Matrix Composite Materials", Proceedings of the Sixth (1996) International Offshore and Polar Engineering Conference, Los Angeles, USA, May, 26-31.

Australian Standard 3600-1988 (1988:A), Concrete Structures-Commentary. Standards Association of Australia, Sydney, New South Wales, Australia.

Australian Standard 3600-1988 (1988:B), Concrete Structures. Standards Association of Australia, Sydney, New South Wales, Australia.

Baluch, M. H., Ziraba, Y. N., Azad, A. K., Sharif, A. M., Al-Sulaimani, G. J., and Basunbul, I. A. (1995), "Shear Strength of Plated RC Beams", Magazine of Concrete Research, 1995, Volume 47, No. 173, December, 369-374.

BJŐRN TÄUSTEN (1994), Plate Bonding: Strengthening of Existing Concrete Structures with Epoxy Bonded Plates of Steel or Fibre Reinforced Plastics. PhD thesis, LULEA University of Technology, Sweden.

Bortolottl, L. (1990), "Interdependence of Concrete Strength Parameters", ACI Materials Journal, Volume 87, No. 1, January-February, 25-26.

BS5400 (1990), British Standards Institute, Steel, Concrete and Composite Bridges. BSI, London, Part 4.

BS8110 (1985), British Standards Institute, Structural Use of Concrete. BSI, London.

Calder, A. J. J. (1979), "Exposure Tests on Externally Reinforced Concrete Beam - First Two Years", Supplementary Report 529, Transport & Road Research Laboratory, Crowthorn, U.K.

Calder, A. J. J. (1988), "Exposure Tests on Externally Reinforced Concrete Beam - Performance after Ten Years", Supplementary Report 129, Transport & Road Research Laboratory, Crowthorn, U.K.

Calder, A. J. J. (1989), "Exposure Tests on 3.5 m Externally Reinforced Concrete Beam - the First 8 Years", Supplementary Report 191, Transport & Road Research Laboratory, Crowthorn, U.K.

Carniero, F. L. L. B., and Barcellos, A. (1953), "Concrete Tensile Strength", RILEM Bulletin (Paris), No. 13, March, 97-123.

Davies, J. D., and Bose, D. K. (1968), "Stress Distribution in Splitting Tests", ACI Journal, August, 662-669.

Day, R. L., and Haque, M. N. (1993), "Correlation Between Strength of Small and Standard Concrete Cylinders", ACI Material Journal, Volume 90, No. 5, September-October, 452-462.

Garden, H. N. (1997), The Strengthening of Reinforced Concrete Members Using Externally Bonded Composite Materials (BL). PhD thesis, University of Surrey, Guildford, Surrey, United Kingdom.

Garden, H. N., Hollaway, L. C., and Thorne, A. M. (1997), "A Preliminary Evaluation of Carbon Fibre Reinforced Polymer Plates for Strengthening Reinforced Concrete Members", Proceedings of the Institution of Civil Engineers, Structures and Buildings, Volume 123, May, 127-142.

Garden, H. N., Hollaway, L. C., Thorne, A. M., and Parke, G. A. R. (1996), "A Parameter Study of the Strengthening of Reinforced Concrete Beams with Bonded Composites", Proceedings of The Third International Conference on Bridge Management, Inspection, Assessment, and Repair, J. E. Harding, G.A.R. Parke, and M.J. Ryall (eds.), E. & F. N. Spon, University of Surrey, Guildford, Surrey, United Kingdom, April, 400-408.

Geymayer, H. G. (1968), "Static Test of Reinforced Concrete beams: Development of Iterative Analysis Procedure and Tests of Beams Reinforced with Steel, Aluminium, and Fiber Glass, with and without Helical Compressive Reinforcement", Technical Report No. 6-818, U.S. Army Corps of Engineers, Waterways Experiment Station, Vicksburg, March.

Grieb, W. E., and Werner, G. (1962), "Comparison of the Splitting Tensile Strength of Concrete with Flexural and Compressive Strengths", PUBLIC ROADS, Volume 323, No. 5, December, 97-106.

Hamoush, S. A., and Ahmed, S. H. (1990), "Debonding of Steel Plate-Strengthened Concrete Beams", Journal of Structural Engineering, ASCE, Volume 116, No. 2, November, 356-371.

Handbook to British Standard BS8110 (1985), Structural Use of Concrete. Viewpoint Publications, 1987.

Hassanen, M. A. H., and Raoof, M. (2000:A), "R.C. Beams Upgraded with Externally Bonded Plates", Conference Proceedings of the 2000 Structures Congress entitled "Advanced Technology in Structural Engineering", American Society of Civil Engineers, May, 2000, Philadelphia, Pennsylvania, U.S.A., CD-ROM, "Topics in Timber, Composites and Concrete" session. ISBN 0-7844-0492-5.

Hassanen, M. A. H., and Raoof, M. (2000:B), "Simple Procedure(s) for Predicting the Peeling Load of Steel or FRP Plated R.C. Beams", Proceedings of the Concrete Communication Conference 2000, June, Birmingham, University of Birmingham, U.K., 165-185.

Hassanen, M. A. H., and Raoof, M. (2000:C), "Design Against Premature Peeling Failure of R.C. Beams With Externally Bonded Steel or FRP Plates", Submitted for publication, Magazine of Concrete Research.

Hollaway, L. (1997), Private Communication.

Jansze, W., Den Uijl, J., and Walraven, J. (1996), " Anchorage of Externally Bonded Steel Plates", Proceedings of Concrete in the Service of Mankind Congress, 'Concrete Repair, Rehabilitation and Protection', R.K. Dhir and M.R. Jones (eds.), E. &F. N. Spon, University of Dundee, Dundee, Scotland, June, 591-598.

Jones, R., Swamy, R. N., and Ang, T. H. (1982), "Under- and Over-reinforced Concrete Beams with Glued Steel Plates", The International Journal of Cement Composites and Lightweight Concrete, Volume 4, No. 1, February, 19-32.

Jones, R., Swamy, R. N., and Charif, A. (1988), "Plate Separation and Anchorage of Reinforced Concrete Beams Strengthened by Epoxy-Bonded Steel Plates", The Structural Engineer, Volume 66, No. 5/1, February, 85-94.

Jones, R., Swamy, R. N., Bloxham, J., and Bouderbalah, A. (1980), "Composite Behaviour of Concrete Beams with Epoxy Bonded External Reinforcement", The International Journal of Cement Composites, Volume 2, No. 2, May, 91-107.

Kent, D. C., and Park, R. (1971), "Flexural Members with Confined Concrete", Journal of Structural Division, ASCE, Volume 97, No. 7, 1969-1990.

Knott, J. F. (1973), Fundamentals of Fracture Mechanics. Butterworths, London.

Kong, F. K., and Evans, R. H. (1975), Reinforced and Prestressed Concrete. Thomas Nelson and Sons Ltd, Great Britain.

Lue, W. (1993), Strengthening of Post-Tensioned and Reinforced Concrete Beams Strengthened by Steel Plates. MSc thesis, University of Aldelaide, Aldelaide, Australia.

Lutuinen, V., Hurskainen, K., and Sakiso, K. (1996), "Road Bridges Strengthened by Epoxy Bonded Steel Plates", Proceedings of The Third International Conference on Bridge Management, Inspection, Assessment, and Repair, J.E. Harding, G.A.R. Parke, and M.J. Ryall (eds.), E. & F. N. Spon, University of Surrey, Guildford, Surrey, United Kingdom, April, 409-411.

Macdonald, M. D. (1982), "The Flexural Performance of 3.5 m Concrete Beams with Various Bonded External Reinforcement", Transport Research Laboratories (TRRL), Department of the Environment, Crowthorn, Suppl Report No. 728.

Malek, A. M., and Saadatmanaesh, H. (1998:A), "Analytical Study of Reinforced Concrete Beams Strengthened with Web Bonded Fibre Reinforced Plastic Plates or Fabrics", ACI Structural Journal, Vol. 95, No. 3, May - June, 343-352.

Malek, A. M., and Saadatmanesh, H. (1998:B), "Ultimate Shear Capacity of Reinforced Concrete Beams Strengthened with Web-Bonded Fibre-Reinforced Plastic Plates", ACI Structural Journal, Vol. 95, No. 4, July-August, 391-399.

Martin, L. H., Croxton, P. C. L., and Purkiss, J. A. (1989), Concrete Design to BS8110. Edward Arnold, London.

Martins, P. C. De Renzende, and Guimaräes, K. D. (1996), "The Behaviour of RC Beams Strengthened by Glued Plates or Grouted Additional Rebars", Proceedings of Concrete in the Service of Mankind Congress, 'Concrete Repair, Rehabilitation and Protection', R.K. Dhir and M.R. Jones (eds.), E. &F. N. Spon, University of Dundee, Dundee, Scotland, June, 599-604.

Meier, U., and Kaiser, H. (1991), "Strengthening of Structures with CFRP Laminates", Advanced Composites Materials in Civil Engineering Structures, ASCE, Proceedings of the Speciality Conference, Las Vegas, 224-232

Moloney, G. F. K. (1986), "The Repair and Strengthening of Reinforced Concrete Beams with Externally Bonded Mild Steel Plates", Thesis presented to the National University of Ireland at Cork, Ireland, in partial fulfilment of the requirements for the degree of Master of Engineering.

Moran, J. P. (1988), "Separation of Externally Bonded Steel Plates from Reinforced Concrete Beams in Flexural", Thesis presented to the National University of Ireland at Cork, Ireland, in partial fulfilment of the requirements for the degree of Master of Engineering.

Mosley, W. H., and Bungey, J. H. (1990), Reinforced Concrete Design. MacMillan Education, 4th edn.

Narrow, I., and Ullberg, E. (1963), "Correlation Between Tensile Splitting Strength and Flexural Strength of Concrete", Journal of the American Institute, Volume 60, No. 1, January, 27-37.

Nawy, E.G. (1992), "Cracking of Concrete: ACI and CEB Approaches", Proceedings of the International Conference on Advances on Concrete Technology, Molhotra, V.M. (ed.), Organised by CANMET, Athens, January, 199-238.

Nilsson, S. (1961), "The Tensile Strength of Concrete Determined by Splitting Tests on Cubes", RILEM Bulletin (Paris), June, 63-67.

Oehlers, D. J. (1992), "Reinforced Concrete Beams with Plates Glued to their Soffits", Journal of Structural Engineering, ASCE, Volume 118, No. 8, August, 2023-2038.

Oehlers, D. J. (1995), "Rules for Bonding Steel Plates to Existing Reinforced Concrete Slabs", Australian Civil Engineering Transactions, Volume CE37, No. 1, February.

Oehlers, D. J., and Ahmed, M. (1996), "Upgrading Reinforced Concrete Beams by Bolting Steel Side Plates", Proceedings of The Third International Conference on Bridge Management, Inspection, Assessment, and Repair, J.E. Harding, G.A.R. Parke, and M.J. Ryall (eds.), E. & F. N. Spon, University of Surrey, Guildford, Surrey, United Kingdom, April, 412-419.

Oehlers, D. J., and Bradford, M. A. (1995), Composite Steel and Concrete Structural Members: Fundamental Behaviour. Pergamon press, United Kingdom.

Oehlers, D. J., and Moran, J. P. (1990), "Premature Failure of External Plated Reinforced Concrete Beams", Journal of Structural Engineering, ASCE, Volume 116, No. 4, April, 978-995.

Oehlers, D. J., Mohamed, Ali M. S., and Weimin, Luo (1998), "Upgrading Continuous Reinforced Concrete Beams by Gluing Steel Plates to their Tension Faces", Journal of Structural Engineering, ASCE, Volume 124, No. 3, March, 224-232.

Oehlers, D. J., Wright, H. D., and Burnet, M. J. (1994), "Flexural strength of profiled beams", Journal of Structural Engineering, ASCE, Volume 120, No. 2, February 1992, 378-393.

Oluokun, F. A. (1991), "Prediction of Concrete Tensile Strength from its Compressive Strength: Evaluation of Existing Relations for Normal Weight Concrete", ACI Structural Journal, Volume 88, No. 3, May-June, 302-309.

Orr, D. M. F., and Kiely, G. (1990), "Strengthening Beams with Externally Bonded Flexural and Shear Reinforcement", IABSE Symposium on Mixed Structures Including New Materials, Brussels, Belgium, September, 271-273.

Quantrill, R. J., Hollaway, L. C., and Thorne, A. M. (1996:A), "Experimental and Analytical Investigation of FRP Strengthened Beam Response: Part I", Magazine of Concrete Research, Volume 48, No. 177, December, 331-342.

Quantrill, R. J., Hollaway, L. C., and Thorne, A. M. (1996:B), "Prediction of the Maximum Plate End Stresses of FRP Strengthened Beams: Part II", Magazine of Concrete Research, Volume 48, No. 177, December, 343-351.

Raoof, M., and Hassanen, M. A. H. (1998:A), "Premature Plate Peeling Failure in R.C. Beams Strengthened by External Plates", Proceedings of Fifth International Exhibition & Conference For Building & Construction, Inter Build 98, Cairo, Egypt, June, 631-640.

Raoof, M., and Hassanen, M. A. H. (1998:B), "Peeling Failure of External Plates in Steel/Concrete Composite Beams", Proceedings of Fifth Pacific Structural Steel Conference (PSSC), Seoul, Korea, October, Vol. 2, 967-972.

Raoof, M., and Hassanen, M. A. H. (1999), "Reinforced Concrete Beams with Externally Bonded FRP Plates", 1st International Conference on Advances in Structural Engineering and Mechanics, ASEM 1999, Seoul, Korea, August, Vol. 2, 1343-1348.

Raoof, M., and Hassanen, M. A. H. (2000:A), "Reinforced Concrete Beams Upgraded with Externally Bonded Steel or FRP Plates", Proceedings of Fourth International Conference on Bridge Management, M.J. Ryall, G.A.R. Parke and J.E. Harding (eds.), Thomas Telford, University of Surrey, Guilford, Surrey, April, 508-515.

Raoof, M., and Hassanen, M. A. H. (2000:B), "Peeling Failure of R.C. Beams with FRP or Steel Plates Glued to Their Soffits", Proceedings of the Institution of Civil Engineers, Structures and Buildings, Vol. 140, August, 291-305.

Raoof, M., and Zhang, S. (1997), "An Insight into the Structural Behaviour of R.C. Beams with Externally Bonded Plates", Proceedings of the Institution of Civil Engineers, Structures and Buildings, Vol. 122, November, 477-492.

Raoof, M., El-Rimawi, J.A., and Hassanen, M. A. H. (2000), "Theoretical and Experimental Study on Externally Plated R.C. Beams", Engineering Structures, Vol. 22, No. 1, January, 85-101.

Raoof, M., and Zhang, S. (1996:A), "Peeling failure of Reinforced Concrete Beams with Externally bonded Steel Plates", Proceedings of The Third International Conference on Bridge Management, Inspection, Assessment, and Repair, J.E. Harding, G.A.R. Parke, and M.J. Ryall (eds.), E. & F. N. Spon, University of Surrey, Guildford, Surrey, United Kingdom, April, 420-428.

Raoof, M., and Zhang, S. (1996:B), "Analysis of Plate Peeling Failure of RC Beams with External Bonded Plates", Proceedings of Concrete in the Service of Mankind Congress, 'Concrete Repair, Rehabilitation and Protection', R.K. Dhir and M.R. Jones (eds.), E. & F. N. Spon, University of Dundee, Dundee, Scotland, June, 605-614.

Raphael, J. M. (1984), "Tensile Strength of Concrete", ACI Journal, March-April, 158-165.

Reynolds, C. E., and Steedman, J. C. (1992), Design of Reinforced Concrete Buildings. E. & F. N. Spon Ltd, London.

Ritchie P., A., David, A. T., Lr-Wu, and Connelly, G. M. (1991), "External Reinforcement of Concrete Beams Using Fiber Reinforcement Plastics", ACI Structural Journal, Volume 88, No. 4, July-August, 490-500.

Roberts, T. M. (1988), "Plate Separation and Anchorage of Reinforced Concrete Beams Strengthened by Epoxy Bonded Steel Plates", (correspondence). The Structural Engineer, Volume 67, No. 12/21, June, 187-188.

Roberts, T. M. (1989), "Approximate Analysis of Shear and Normal Stress Concentrations in the Adhesive Layer of Plated RC Beams", The Structural Engineer, Volume 67, No. 12/20, June, 229-233.

Roberts, T. M., and Haji-Kazemi, H. (1989), "A Theoretical Study of the Behaviour of Reinforced Concrete Beams Strengthened by Externally Bonded Steel Plates", Proceedings of the Institution of Civil Engineers, Part 2, No. 87, March, 39-55.

Saadatmanesh, H., and Ehsani, M. R. (1990), "Fibre Composition Plates Can Strengthen Concrete Beams", Concrete International, Volume 12, No. 3, 65-71.

Saadatmanesh, H., and Ehsani, M. R. (1991), "RC Beams Strengthened with GFRP Plates, I: Experimental Study", Journal of Structural Engineering, ASCE, Volume 117, No. 11, November, 3417-3433.

Sharif, A., Al-Sulaimani, G. J., Basunbul, I. A., Baluch, M. H., and Ghaleb, B. N. (1994), "Strengthening of Initially Loaded Reinforced Concrete Beams Using FRP Plates", ACI Structural Journal, Volume 91, No. 2, March-April, 160-168.

Swamy, R. N., Hobbs, B., and Roberts, M. (1995), "Structural Behaviour of Externally Bonded Steel Plated RC Beams after Long-Term Exposure", The Structural Engineer, Volume 73, No. 16/15, August, 255-261.

Swamy, R. N., Jones, R., and Bloxham, J. W. (1987), "Structural Behaviour of Reinforced Concrete Beams Strengthened by Epoxy-Bonded Steel Plates", The Structural Engineer, Volume 65A, No. 2, February, 59-68.

Swamy, R. N., Jones, R., and Charif, A. (1989), "The Effect of External Plate Reinforcement on the Strengthening of Structurally Damaged RC Beams", The Structural Engineer, Volume 67, No. 3/7, February, 45-59 and 56.

Triantafillou, T. C., and Gibson, L. G. (1989), "Debonding in Foam-Core Sandwich Panels", Materials and Structures, Volume 22, 64-69.

Triantafillou, T. C., and Plevris, N. (1992), "Strengthening of RC Beams with Epoxy-Bonded Fibre-Composite Materials", Materials and Structures, Volume 25, No. 25, 201-211.

Watstein, B., and Parsons, D. E. (1943), "Width and Spacing of Tensile Cracks in Reinforced Concrete Cylinders", *J. Res. Natl. Bur. Standards*, Vol. 31, No. RP545, July, 1-24.

Wei, An, Saadatmanesh, H., and Ehsani, M. R. (1991), "RC Beams Strengthened with GFRP Plates, II: Analysis and Parametric Study", Journal of Structural Engineering, ASCE, Volume 117, No. 11, November, 3434-3455.

Wright, P. J. F. (1955), "Comments on an Indirect Tensile Test on Concrete Cylinders", Magazine of Concrete Research, Volume 47, July, 87-96.

Zhang, S., Raoof, M., and Wood, L. A. (1995), "Prediction of Peeling Failure of Reinforced Concrete Beams with Externally Bonded Plates", Proceedings of the Institution of Civil Engineers, Structures and Buildings, Volume 110, August, 257-268.

Ziraba, Y. N., Baluch, M. H., Basunbuli. A., Sharif, A. M., Azad, A. K., and Al-Sulaimani, G. J. (1994), "Guidelines Toward the Design of Reinforced Concrete Beams with External Plates", ACI Structural Journal, Volume 91, No. 6, 639-646.

Appendix A

COMPUTER PROGRAMME

Appendix A

COMPUTER PROGRAMME

A.1 GENERAL

This appendix explains the assumptions and methods of calculating various flexural load bearing capacities of externally plated and/or unplated R.C. beams. It also presents the listing for the source file of the FORTRAN-77 (release 9.0 for HP-UX system) computer programme developed for analysing the stresses and strains in the critical sections of plated and unplated R.C. beams.

A.2 TYPES OF FLEXURAL LOAD BEARING CAPACITIES

All the flexural load bearing capacities refer to the predicted or experimental bending moments at the critical beam section under the external point load nearest to the support with the beam subject to symmetrical four-point loading. There are two main types of predicted beam flexural capacities as calculated by the computer programme:

1. Beam capacities based on the assumption of full bond between the plate and concrete up to total failure: the plated and unplated beam capacities, M_{pult} and M_{RC}, respectively, are based on this assumption.
2. Beam capacities controlled by the occurrence of premature peeling initiated at the end of the plate: the lower and upper bound plate peeling capacities, $M_{peel,l}$ and $M_{peel,u}$, respectively. Obviously, in such cases, a full bond behaviour is assumed up to the sudden occurrence of fully brittle premature plate peeling.

In addition, two separate cases relating to the cracking conditions at the time of strengthening by external plating are considered when estimating the lower and upper bound peeling moments:

1. The lower and upper bound peeling moments for uncracked plated beams, $M_{peel-1,l}$ and $M_{peel-1,u}$, respectively, and

2. The lower and upper bound peeling moments for cracked (prior to plating) R.C. beams, $M_{peel-2,l}$ and $M_{peel-2,u}$, respectively.

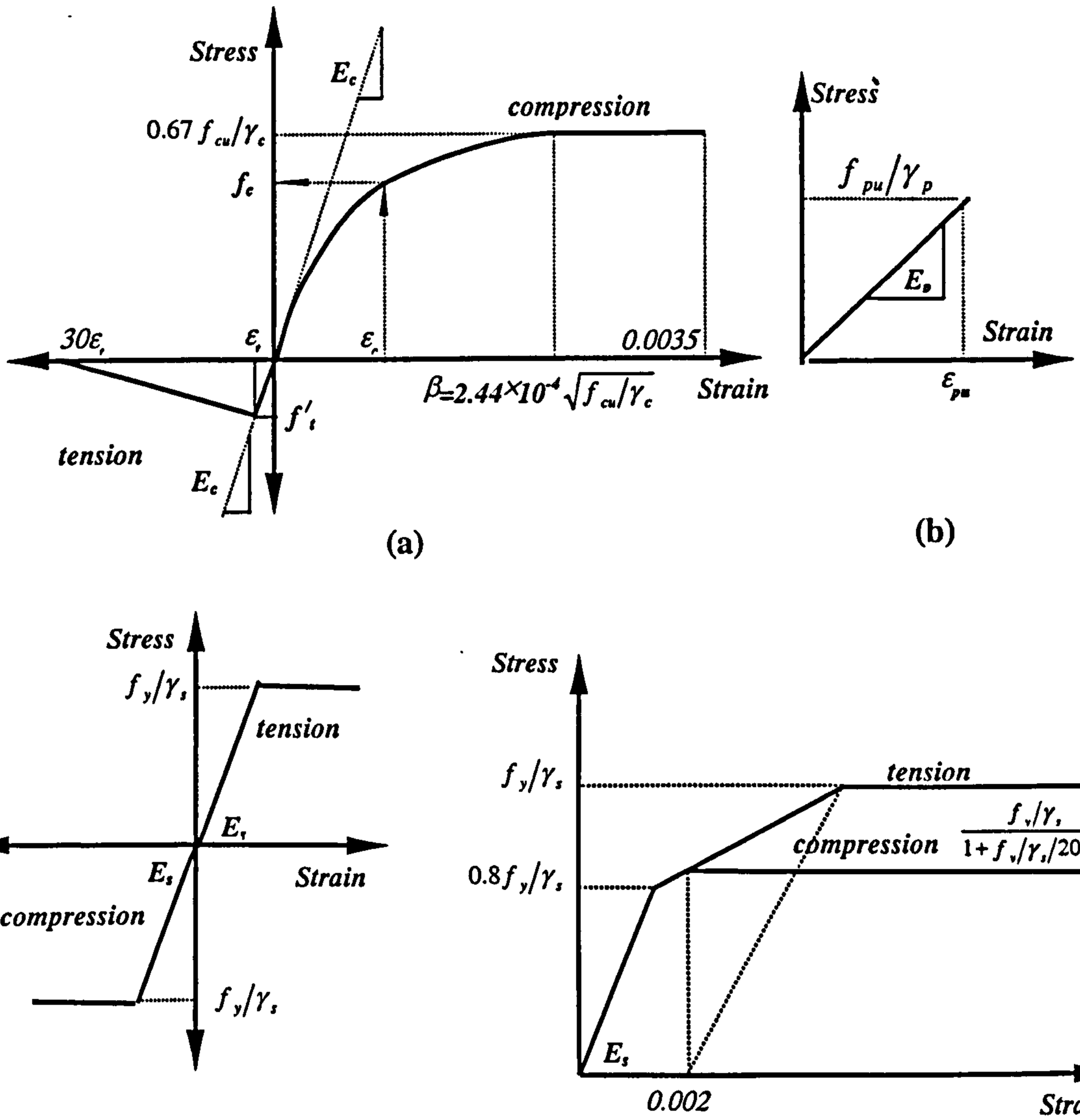

Fig. A.1 Assumed stress-strain relationships: (a) for concrete after BS8110 (1985), (b) for FRP material, (c) bi-linear for steel after BS8110 (1985), and (d) tri-linear for steel after BS5400 (1990).

The following are the main assumptions for calculating the flexural load bearing capacities of plated and unplated beams:

- Plane sections remain plane after bending.
- For all the flexural load capacities, the stress-strain relationships shown in Figure A.1 are assumed, whenever applicable.
- The material partial safety factors, γ_m, as recommended by BS8110 (1985) are used for calculating only the unplated beam flexural capacity M_{RC} (i.e. $\gamma_c = 1.5$ for concrete, $\gamma_s = 1.15$ for steel, and $\gamma_p = 1.15$ for FRP).
- The material partial safety factors, γ_m, are considered to be equal to 1.0 for all the other flexural load capacities.

A.3 ESTIMATING THE EFFECTIVE LENGTH OF THE BONDED PLATE

For the sake of flexibility and to enable further research, the computer programme offers various options for determining the plate peeling stresses and moments, as regards the choice for the portion of the length of the plate within the critical shear span:

1- The plate length may be equal to the actual one,

2- The plate length may be equal to the effective one,

3- The plate length may be equal to the minimum of the actual and the effective ones, and

4- The plate length may be equal to the minimum (or the maximum) spacing between two adjacent stabilised cracks with the critical beam section located at a distance equal to this crack spacing as measured from the end of the plate.

The critical beam section for options 1-3 is located immediately under the external point load nearest to the support. All the numerical results presented in this thesis, are, indeed, based on option 3.

The stabilised crack spacing is a critical parameter for calculating the plate peeling stresses. One of the parameters that influence the magnitude of the stabilised crack spacing is the bond strength between the plate and concrete. Different values for the bond strength may be assumed in the computer programme, with the subsequent estimates of effective plate length depending on the so-obtained values of stabilised crack spacing(s).

A.4 GENERAL REMARKS

- The computer programme is based on an iteration technique to determine the depth of neutral axis in order to satisfy the equilibrium condition. The iterations start with a reasonable initial value for the depth of neutral axis and a constant value for the plate axial strain(s) (for calculating the plate peeling moments) or a constant value of 0.0035 for the maximum concrete compressive strain (for calculating the full bond capacity of plated and unplated sections).
- The position of the neutral axis is updated, depending on the results for equilibrium. The strains (and stresses) across the section are calculated. The section forces may, then, be recalculated and the equilibrium condition is checked again, with the whole process repeated until equilibrium is satisfied.

- For the plate peeling, if equilibrium can not be achieved with the maximum concrete compressive strain being less than the crushing value (i.e. 0.0035), then, the initially assumed constant value for the plate axial tensile strain should be slightly reduced until equilibrium is satisfied, with the maximum concrete compressive strain being less than the crushing value.
- For the full bond capacity of FRP plated beams, if equilibrium can not be achieved while assuming the plate axial tensile strain to be less than the ultimate value, then, the failure is assumed to be due to plate rupture, and the maximum concrete compressive strain should, then, be sufficiently reduced (from the crushing value) until the equilibrium condition is satisfied.

A.5 LIST OF THE PROGRAMME

```
CCCCCCCCCCCCCCCCCCCCCCCCCCCCCCCCCCCCCCCCCCCCCCCCCCCCCCCCCCCCCCCCCCCCCCCCCC
C       THIS PROGRAM IS WRITTEN BY MAHMOUD A. H. HASSANEN                   C
C       CIVIL & BUILDING ENGINEERING DEPARTMENT                             C
C       LOUGHBOROUGH UNIVERSITY                                             C
CCCCCCCCCCCCCCCCCCCCCCCCCCCCCCCCCCCCCCCCCCCCCCCCCCCCCCCCCCCCCCCCCCCCCCCCCC
          DOUBLE PRECISION O,HSC,HST,HH,H1,FCU,EC,FY,ES,BP,TP,FP,EP,
      *   PEXP,EXPM,AC,PI,FT,U,S,AE,AP,AT,PSL,PSU,PSX,PRNL,PRNU,PRNX,
      *   LP,LO,LPA,LPMIN,D,DRFT,XX,BML,BMU,BMX,DT,NAXL,NAXU,NAXX,RSL,
      *   RSU,RSX,RRNL,RRNU,RRNX,CSL,CSU,CSX,CRNL,CRNU,CRNX,TA,BOND,
      *   PRNM,PRNP,PRNN,BMM,BMP,BMN,PSM,PSP,PSN,RSM,RSP,RSN,RRNM,
      *   RRNP,RRNN,CSM,CSP,CSN,CRNM,CRNP,CRNN,NAXM,NAXP,NAXN
          INTEGER  B,T,NBC,NBT,I,NCR,DC,II,JJ
          CHARACTER *5 RFT,FPMX,FPMU,FPML,FPMM,FPMP,FPMN
          CHARACTER *6 SCNM,TYPE
          CHARACTER *7 STATUS, CRACKS, BARCURV, LPEFORACT,
      *   CONCRETE,PLTCURV
          CHARACTER *12 OUTFILE, DATAFILE, START
          CHARACTER *1 CASE
          CHARACTER *133 TITL
          CHARACTER *485 HEAD
          CHARACTER *5 RUNCASE, FRPBOND
CCCCCCCCCCCCCCCCCCCCCCCCCCCCCCCCCCCCCCCCCCCCCCCCCCCCCCCCCCCCCCCCCCCCCCCCCC
C       NEXT ARE THE ACCEPTABLE PARAMETERS FOR THE INPUT VARIABLES          C
C       CASE      = PLATE LENGTH= EFFECT, ACTUUAL, CRACK, DUBLE-CRACK       C
C       CRACKS    = UNCRAKD/PRECRKD :CRACKED/UN-C. PRIOR TO PLATING         C
C       BARCURV   = BILINER/TRILNER :Bi/Tri-LINEAR, BAR MATERIAL            C
C       PLTCURV   = BILINER/TRILNER :Bi/Tri-LINEAR, PLATE MATERIAL          C
C       LPEFORACT= LPEFORA/LPEONLY :Min of Effect./Act. or Eff.             C
C       CONCRETE = CONCTOK/NOCONCT :Use/Ignore Conc. in Tension             C
C       FRPBOND   = RTFCU/U0.8N/U3.0N/U6.0N : Bond bet.Plt & Conc.          C
CCCCCCCCCCCCCCCCCCCCCCCCCCCCCCCCCCCCCCCCCCCCCCCCCCCCCCCCCCCCCCCCCCCCCCCCCC
C       START IS A FILE THAT INCLUDES NAMES OF INPUT/OUTPUT DATA            C
```

```
C       FILES AND THE ABOVE CONTROLLING PARAMETERS FOR REFERENCES  C
        READ (*,*) START
        OPEN (UNIT=11, FILE=START , STATUS='UNKNOWN')
        READ(11,*) DATAFILE
        READ(11,*) OUTFILE
        READ(11,*) CASE
        READ(11,*) CRACKS
        READ(11,*) BARCURV
        READ(11,*) PLTCURV
        READ(11,*) LPEFORACT
        READ(11,*) CONCRETE
        READ(11,*) FRPBOND
        CLOSE (11)
111     IF (((CASE.EQ.'C').OR.(CASE.EQ.'D')).OR.((CASE.EQ.'E').OR.
     *  (CASE.EQ.'A'))) THEN
          IF (CASE.EQ.'E') WRITE (*,*) START
        ELSE
          GO TO 10001
        END IF
C       HEARDER IS A FILE THAT CONTAINS CERTAIN TWO LINES HEADING  C
        OPEN (UNIT=66, FILE='HEADER' , STATUS='UNKNOWN')
        OPEN (UNIT=77, FILE=DATAFILE , STATUS='UNKNOWN')
        OPEN (UNIT=88, FILE= OUTFILE , STATUS='UNKNOWN')
        READ (66,19)HEAD
        WRITE(88,19)HEAD
        WRITE (88,20) START,DATAFILE,OUTFILE,CASE,CRACKS,BARCURV,
     *  PLTCURV,CONCRETE,FRPBOND
        READ (66,19)HEAD
        WRITE(88,19)HEAD
        CLOSE (66)
        CLOSE (88)
        II=3
        DO 4 I= 1 , 5
           READ(77,17)TITL
4       CONTINUE
100     READ(77,1996)SCNM,B,T,NBC,DC,HSC,NBT,DT,HST,HH,H1,FCU,EC,
     *  FY,ES, BP,TP,LO,LPA,FP,EP,PEXP,TYPE,TA
        IF (SCNM.EQ."ENDOFF")   GO TO 9999
        IF (BP.EQ.0.0) BP=0.0000001
        IF (FP.EQ.0.0) FP=0.0000001
        IF (FCU.EQ.0.0) FCU=0.0001
        PI=3.141592654
        FT=0.36*SQRT(FCU)
        O=NBT*DT*PI
        IF (FRPBOND.EQ.'RTFCU') BOND=0.28*SQRT(FCU)
        IF (FRPBOND.EQ.'U0.8N') BOND=0.8
        IF (FRPBOND.EQ.'U3.0N') BOND=3.0
        IF (FRPBOND.EQ.'U6.0N') BOND=6.0
        IF (TYPE.EQ.' STEEL') THEN
           IF (CRACKS.EQ.'UNCRAKD') U=0.28*SQRT(FCU)*(O + BP )
           IF (CRACKS.EQ.'PRECRKD') U=0.28*SQRT(FCU)* O
        ELSE
           IF (CRACKS.EQ.'UNCRAKD') U=0.28*SQRT(FCU)*O + BOND*BP
           IF (CRACKS.EQ.'PRECRKD') U=0.28*SQRT(FCU)*O
        END IF
        D=T+TA+TP/2.0
        S=D/2.0
        AE=2.0*H1*B
        AP=BP*TP
        AT=NBT*DT*DT*PI/4.0
        AC=NBC*DC*DC*PI/4.0
```

```
      EC=EC*1000.0
      ES=ES*1000.0
      EP=EP*1000.0
      HST=HST+TP/2.0+TA
      EXPM=PEXP*LO/1000.0
      IF ((LO.EQ.9999).AND.(LPA.EQ.8888)) EXPM=PEXP
      DRFT=T-H1
      XX=1
      WRITE (*,*) 'OUTPUT FOR SEC.   ',SCNM
      CALL PSTRN (FP,EP,AE,FT,U,BP,LPA,B,HH,TP,PSL,PSU,PRNL,PRNU
     *   ,CASE,LP,LO,NCR,TYPE,FY,ES,EC,FCU,AT,AP,SCNM,LPEFORACT,
     *   PLTCURV,FRPBOND,LPMIN)
      RUNCASE='LOWER'
      CALL FORCS (FY,ES,FCU,EC,FT,FP,EP,PRNL,S,B,HST,HSC,D,AC,
     *   AT,AP,BML,PSL,LO,LPA,LP,XX,STATUS,CASE,RUNCASE,RSL,RRNL,
     *   CSL,CRNL,TYPE,RFT,TP,TA,CONCRETE,BARCURV,PLTCURV)
      FPML=RFT
      NAXL=D-S
      IF (STATUS.EQ.'FAILURE') THEN
           WRITE(88,*)SCNM,'.......',STATUS,'..IN LOWER LIMIT'
           GO TO 9999
      END IF
      XX=0.001
      LP=2.0*LP
      RUNCASE='UPPER'
      CALL FORCS FY,ES,FCU,EC,FT,FP,EP,PRNU,S,B,HST,HSC,D,AC,AT,AP,
     *   BMU,PSU,LO,LPA,LP,XX,STATUS,CASE,RUNCASE,RSU,RRNU,
     *   CSU,CRNU,TYPE,RFT,TP,TA,CONCRETE,BARCURV,PLTCURV)
      LP=LP/2.0
      FPMU=RFT
      NAXU=D-S
      IF (STATUS.EQ.'FAILURE') THEN
         WRITE(88,*)SCNM,'.........',STATUS,'..IN UPPER LIMIT'
         GO TO 9999
      END IF
      RUNCASE='MXMUM'
      XX=1
      CALL FORCS FY,ES,FCU,EC,FT,FP,EP,PRNX,S,B,HST,HSC,D,AC,AT,AP,
     *   BMX,PSX,LO,LPA,LP,XX,STATUS,CASE,RUNCASE,RSX,RRNX,
     *   CSX,CRNX,TYPE,RFT,TP,TA,CONCRETE,BARCURV,PLTCURV)
      FPMX=RFT
      NAXX=D-S
      IF (STATUS.EQ.'FAILURE') THEN
         WRITE(88,*)SCNM,'.........',STATUS,'..IN MXMUM LIMIT'
         GO TO 9999
      END IF
      RUNCASE='MINUM'
      XX=1
      CALL FORCS(FY,ES,FCU,EC,FT,FP,EP,PRNM,S,B,HST,HSC,D,AC,AT,AP,
     *   BMM,PSM,LO,LPA,LP,XX,STATUS,CASE,RUNCASE,RSM,RRNM,
     *   CSM,CRNM,TYPE,RFT,TP,TA,CONCRETE,BARCURV,PLTCURV)
      FPMM=RFT
      NAXM=D-S
      IF (STATUS.EQ.'FAILURE') THEN
         WRITE(88,*)SCNM,'.........',STATUS,'..IN MXMUM LIMIT'
         GO TO 9999
      END IF
      RUNCASE='BSUNP'
      XX=1
      CALL FORCS FY,ES,FCU,EC,FT,FP,EP,PRNN,S,B,HST,HSC,D,AC,AT,AP,
     *   BMN,PSN,LO,LPA,LP,XX,STATUS,CASE,RUNCASE,RSN,RRNN,
```

```
*    CSN,CRNN,TYPE,RFT,TP,TA,CONCRETE,BARCURV,PLTCURV)
     FPMN=RFT
     NAXN=D-S
     IF (STATUS.EQ.'FAILURE') THEN
        WRITE(88,*)SCNM,'.........',STATUS,'..IN MXMUM LIMIT'
        GO TO 9999
     END IF
     RUNCASE='BSPTD'
     XX=1
     CALL FORCS FY,ES,FCU,EC,FT,FP,EP,PRNP,S,B,HST,HSC,D,AC,AT,AP,
*    BMP,PSP,LO,LPA,LP,XX,STATUS,CASE,RUNCASE,RSP,RRNP,
*    CSP,CRNP,TYPE,RFT,TP,TA,CONCRETE,BARCURV,PLTCURV)
     FPMP=RFT
     NAXP=D-S
     IF (STATUS.EQ.'FAILURE') THEN
        WRITE(88,*)SCNM,'.........',STATUS,'..IN MXMUM LIMIT'
        GO TO 9999
     END IF
     IF (BMU.GT.BMX) BMU=BMX
     OPEN (UNIT=88, FILE= OUTFILE  , STATUS='UNKNOWN')
     DO 620 JJ = 1 , II
     READ (88,19) HEAD
620  CONTINUE
     WRITE (88,2996)SCNM,BMX,EXPM,BMU,BML,FPMX,FPMU,FPML,D,DRFT,
   *  NAXX,NAXU,NAXL,PSX,PSU,PSL,PRNX,PRNU,PRNL,RSX,RSU,RSL,RRNX,
   *  RRNU,RRNL,CSX,CSU,CSL,CRNX,CRNU,CRNL,LPMIN,LP,
   *  SCNM,BMM,EXPM,BMP,BMN,FPMM,FPMP,FPMN,D,DRFT,
   *  NAXM,NAXP,NAXN,PSM,PSP,PSN,PRNM,PRNP,PRNN,RSM,RSP,RSN,RRNM,
   *  RRNP,RRNN,CSM,CSP,CSN,CRNM,CRNP,CRNN
     II=II+1
     CLOSE (88)
     GO TO 100
17   FORMAT(A133)
18   FORMAT(A47)
19   FORMAT(A485)
20   FORMAT(A10,2A14,A5,5A10)
1996 FORMAT(A6,4I6,F6.1,I6,10F6.1,2I6,3F6.1,A6,F6.1)
2996 FORMAT(A6,4F8.2,3A4,8F8.2,3F8.5,3F8.2,3F8.5,3F8.2,3F8.5,
   * 2F8.1,'  ',A6,4F8.2,3A4,8F8.2,3F8.5,3F8.2,3F8.5,3F8.2,3F8.5)
9999 CLOSE (77)
10001 END
CCCC  END OF THE MAIN PROGRAMME
CCCCCCCCCCCCCCCCCCCCCCCCCCCCCCCCCCCCCCCCCCCCCCCCCCCCCCCCCCCCCCCCCCCCCCCCCCC
      SUBROUTINE PSTRN (F,E,AE,FT,U,BP,LPA,B,HH,TP,PSL,PSU,PRNL,
   *  PRNU,CASE,LP,LO,NCR,TYPE,FY,ES,EC,FCU,AT,AP,SCNM,LPEFORACT,
   *  PLTCURV,FRPBOND,LPMIN)
      CHARACTER *7  STATUS, PLTCURV, LPEFORACT
      CHARACTER *1  CASE
      CHARACTER *5  FRPBOND
      CHARACTER *6  SCNM,TYPE
      DOUBLE PRECISION F,E,AE,FT,U,BP,LPA,HH,TP,PSL,PSU,PRNL,
   *  PRNU,LPMIN,LPAA,LP,FY,ES,EC,FCU,AT,AP,LO
      REAL AA,BB,CC,DD
      INTEGER B,NCR,SF
CCCCCCCCCCCCCCCCCCCCCCCCCCCCCCCCCCCCCCCCCCCCCCCCCCCCCCCCCCCCCCCCCCCCCCCCCCC
C     NEXT VALUES ARE FOR THE EQUATION
C     LPAA=(AA-BB*LPMIN)LPMIN IF LPMIN =< DD
C     LPAA=CC*LPMIN           IF LPMIN >  DD
C     WHERE AA,BB,CC,DD FOR MATERIAL AND BOND STRESS
CCCCCCCCCCCCCCCCCCCCCCCCCCCCCCCCCCCCCCCCCCCCCCCCCCCCCCCCCCCCCCCCCCCCCCCCCCC
      LPMIN=AE*FT/(U)
```

```
IF (TYPE.EQ.' FRP   ')  THEN
   IF (FRPBOND.EQ.'RTFCU') THEN
         AA=24.0
         BB=0.5
         CC=4.0
         DD=40.0
   END IF
   IF (FRPBOND.EQ.'U0.8N') THEN
         AA=11.6
         BB=0.17
         CC=2.0
         DD=56.5
         END IF
         IF (FRPBOND.EQ.'U3.0N') THEN
               AA=34.6
               BB=0.87
               CC=5.0
               DD=34.0
         END IF
         IF (FRPBOND.EQ.'U6.0N') THEN
               AA=89.0
               BB=3.5
               CC=8.5
               DD=23.0
         END IF
      ELSE
C     CASES OF STEEL PLATES ONLY
            AA=21.0
            BB=0.25
            CC=3.0
            DD=72
END IF
IF (LPMIN.LE.DD) THEN
         LPAA=(AA-BB*LPMIN)*LPMIN
ELSE
         LPAA=CC*LPMIN
END IF
IF (CASE.EQ.'A') THEN
    IF (LPA.EQ.8888) THEN
        LP=LPAA
    ELSE
        LP=LPA
    END IF
    SF=2.0
END IF
IF (CASE.EQ.'E')  THEN
   SF=2.0
   IF (LPEFORACT.EQ.'LPEONLY') THEN
      LP=LPAA
   ELSE
      IF (LPA.GT.LPAA) THEN
          LP=LPAA
      ELSE
          LP=LPA
      END IF
   END IF
   IF (LPA.EQ.8888) LP=LPAA
END IF
IF (CASE.EQ.'C') THEN
    LP=LPMIN
    SF=4.0
```

```
END IF
IF (CASE.EQ.'D') THEN
    LP=2.0*LPMIN
    SF=4.0
END IF
NCR=LP/LPMIN
PSL=LPMIN*FT*LP*B/(6.0*HH*TP*BP)
PSU=SF*PSL
IF (PSL.GT.F) THEN
    PSL=F
END IF
IF (PSU.GT.F) THEN
    PSU=F
END IF
      STATUS='TENSION'
      CALL STLSTRN (F,E,PSL,PRNL,STATUS,TYPE,PLTCURV)
      CALL STLSTRN (F,E,PSU,PRNU,STATUS,TYPE,PLTCURV)
      RETURN
      END
C     END OF SUBROTUINE PSTRN
CCCCCCCCCCCCCCCCCCCCCCCCCCCCCCCCCCCCCCCCCCCCCCCCCCCCCCCCCCCCCCCCCCCCCCC
      SUBROUTINE FORCS FY,ES,FCU,EC,FT,FP,EP,PLTSTRN,S,B,HST,HSC,D,
     *  AC,AT,AP,BM,PLTSTRS,LO,LPA,LP,XX,STATUS,CASE,
     *  RUNCASE,TSSTRS,TSSTRN,CONCSTRS,CNSTRN,TYPE,RFT,TP,TA,
     *  CONCRETE,BARCURV,PLTCURV)
      DOUBLE PRECISION S,HST,PLTSTRN,D,HSC,CSSTRN,CNSTRN,FCC,MCC,
     *  FTC,MTC,FY,ES,FT,CSSTRS,AC,FCS,MCS,TSSTRS,AT,FTS,MTS,FP,EP,
     *  PLTSTRS,AP,FCU,EC,BM,TSSTRN,FPT,MPT,CC,TT,VV,STRNCC,CONCSTRS,
     *  STRNTC,XX,NET,PREV,LO,LPA,LP,LMTSTRN,TP,TA
      INTEGER I,N,B,MM
      CHARACTER *5 RFT
      CHARACTER *1 CASE
      CHARACTER *7 STATUS,CONCRETE,BARCURV,PLTCURV
      CHARACTER *5 RUNCASE
      CHARACTER *6 TYPE
      IF ((RUNCASE.EQ.'BSUNP').OR.(RUNCASE.EQ.'BSPTD')) THEN
          LMTSTRN=FP/EP/1.15
      ELSE
          LMTSTRN=FP/EP
      END IF
      PREV=0.0
      MM=1
222   IF ((RUNCASE.NE.'LOWER').AND.(RUNCASE.NE.'UPPER')) THEN
        CNSTRN=0.0035
        PLTSTRN=CNSTRN*S/(D-S)
        IF (TYPE.EQ.' FRP  ') THEN
          IF ((RUNCASE.EQ.'MINUM').OR.(RUNCASE.EQ.'BSUNP')) GO TO 7
          IF (PLTSTRN.GT.LMTSTRN) THEN
              PLTSTRN=LMTSTRN
              IF (MM.EQ.1) S=D*PLTSTRN/(PLTSTRN+CNSTRN)
              CNSTRN=PLTSTRN*(D-S)/S
        END IF
      END IF
    ELSE
      CNSTRN=PLTSTRN*(D-S)/S
      IF (CNSTRN.GT.0.0035) THEN
          CNSTRN=0.0035
          IF (MM.EQ.1)  S=D*PLTSTRN/(PLTSTRN+CNSTRN)
      END IF
      PLTSTRN=CNSTRN*S/(D-S)
    END IF
```

```
7       CSSTRN=PLTSTRN*(D-S-HSC)/S
        TSSTRN=PLTSTRN*(S-HST)/S
        IF ((RUNCASE.EQ.'BSPTD').OR.(RUNCASE.EQ.'BSUNP')) THEN
          IF (CNSTRN.GE.0.00349999) THEN
              IF (TSSTRS.GE.(FY/1.15) THEN
                  IF (PLTSTRS.LT.FP/1.15)    RFT=' CR- '
                  IF (PLTSTRS.GE.(FP/1.15)) RFT=' CRP '
              ELSE
                  IF (PLTSTRS.LT.FP/1.15)    RFT=' C-- '
                  IF (PLTSTRS.GE.(FP/1.15)) RFT=' C-P '
              END IF
          ELSE
              IF (TSSTRS.GE.(FY/1.15) THEN
                  IF (PLTSTRS.LT.FP/1.15)    RFT=' -R- '
                  IF (PLTSTRS.GE.(FP/1.15)) RFT=' -RP '
              ELSE
                  IF (PLTSTRS.LT.FP/1.15)    RFT=' --- '
                  IF (PLTSTRS.GE.(FP/1.15)) RFT=' --P '
              END IF
          END IF
        ELSE
          IF (CNSTRN.GE.0.00349999) THEN
              IF (TSSTRS.GE.(FY)) THEN
                  IF (PLTSTRS.LT.FP)          RFT=' CR- '
                  IF (PLTSTRS.GE.(FP))        RFT=' CRP '
              ELSE
                  IF (PLTSTRS.LT.FP)          RFT=' C-- '
                  IF (PLTSTRS.GE.(FP))        RFT=' C-P '
              END IF
          ELSE
              IF (TSSTRS.GE.(FY)) THEN
                  IF (PLTSTRS.LT.FP)          RFT=' -R- '
                  IF (PLTSTRS.GE.(FP))        RFT=' -RP '
              ELSE
                  IF (PLTSTRS.LT.FP)          RFT=' --- '
                  IF (PLTSTRS.GE.(FP))        RFT=' --P '
              END IF
            END IF
        END IF
        FCC=0.0
        MCC=0.0
        FTC=0.0
        MTC=0.0
        STATUS='COMPRES'
        CALL STLSTRS (FY,ES,CSSTRN,CSSTRS,STATUS,TYPE,BARCURV,
     *  RUNCASE)
        FCS=CSSTRS*AC
        MCS=FCS*(D - S - HSC)
        STATUS='TENSION'
        CALL STLSTRS (FY,ES,TSSTRN,TSSTRS,STATUS,TYPE,BARCURV,
     *  RUNCASE)
        FTS=TSSTRS*AT
        MTS=FTS*(S - HST)
        STATUS='TENSION'
        CALL STLSTRS (FP,EP,PLTSTRN,PLTSTRS,STATUS,TYPE,PLTCURV,
     *  RUNCASE)
        IF ((RUNCASE.EQ.'MINUM').OR.(RUNCASE.EQ.'BSUNP')) PLTSTRS=0.0
        FPT=PLTSTRS*AP
        MPT=FPT*S
        N=100
        DO  10  I=1 , N
```

```
            STRNCC=(I-0.5)*CNSTRN/N
            STATUS="COMPRESS"
            CALL CNCSTRS (FCU,EC,FT,STRNCC,CONCSTRS,STATUS,
     *      RUNCASE)
            IF (STATUS.EQ.'FAILURE') THEN
                 WRITE(*,*)STATUS, I
                 GO TO  666
            END IF
            FCC=FCC+CONCSTRS*B*(D-S)/N
            MCC=MCC+CONCSTRS*B*(((D-S)/N)**2)*(I-0.5)
            STRNTC=(I-0.5)*PLTSTRN*((S-TA-TP/2)/S)/N
            STATUS="TENSION"
            CALL CNCSTRS (FCU,EC,FT,STRNTC,CONCSTRS,STATUS,
     *      RUNCASE)
            IF (CONCRETE.EQ.'NOCONCT') CONCSTRS=0.0
            FTC=FTC+CONCSTRS*B*(S-TA-TP/2)/N
            MTC=MTC+CONCSTRS*B*(((S-TA-TP/2)/N)**2)*(I-0.5)
10          CONTINUE
            CC=FCC+FCS
            TT=FTC+FTS+FPT
            NET=CC-TT
            VV=SQRT((NET/TT)**2)
            IF (VV.LT.0.00001) THEN
                  GO TO 555
            ELSE
                   IF (CC.GT.TT) THEN
                      IF (PREV.LT.0.0) THEN
                          S=S-1.1*XX
                          XX=XX/10.0
                      END IF
                      S=S+XX
                   ELSE
                      IF (PREV.GT.0.0) THEN
                          S=S+1.1*XX
                          XX=XX/10.0
                      END IF
                      S=S-XX
                   END IF
            PREV=NET
            MM=MM+1
            GO  TO 222
            END IF
555         BM=(MCC+MCS+MTC+MTS+MPT)/1000000.0
            STATUS='COMPRES'
            CALL CNCSTRS (FCU,EC,FT,CNSTRN,CONCSTRS,STATUS,
          *  RUNCASE)
            IF (RUNCASE.NE.'MXMUM') THEN
                IF (LPA.NE.8888) THEN
                   IF ((CASE.EQ.'C').OR.(CASE.EQ.'D')) THEN
                       BM=BM*LO/(LO-LPA+LP)
                   END IF
                END IF
            END IF
666         RETURN
            END
C           END OF SUBROTUINE FORCES
CCCCCCCCCCCCCCCCCCCCCCCCCCCCCCCCCCCCCCCCCCCCCCCCCCCCCCCCCCCCCCCCCCCCCCCCCCC
            SUBROUTINE STLSTRN (F,E,STRS,STRN,STATUS,TYPE,CURV)
            DOUBLE PRECISION F,E,STRS,STRN,YLD,COM,DIF,E2,TNSNSTRN
            CHARACTER *7 STATUS,CURV
            CHARACTER *6 TYPE
```

```
YLD=0.8*F
COM=F/(1.0+F/2000.0)
DIF=0.002 - YLD/E
E2=(COM - YLD)/DIF
TNSNSTRN=YLD/E+(F-YLD)/E2
IF (TYPE.EQ.' FRP  ') THEN
   STRN=STRS/E
ELSE
  IF (CURV.EQ.'BILINER') THEN
     STRN=STRS/E
  ELSE
      IF (STRS.LT.YLD) THEN
         STRN=STRS/E
      ELSE
         IF (STRS.LT.COM) THEN
            STRN=YLD/E+(STRS - YLD)/E2
         ELSE
            IF (STATUS.EQ.'COMPRES') THEN
               STRN=0.002
            ELSE
               IF (STRS.LT.F) THEN
                  STRN=YLD/E+(STRS - YLD)/E2
               ELSE
                  STRN=TNSNSTRN
               END IF
            END IF
         END IF
      END IF
  END IF
END IF
         RETURN
         END
C        END OF SUBROYUINE STLSTRN
CCCCCCCCCCCCCCCCCCCCCCCCCCCCCCCCCCCCCCCCCCCCCCCCCCCCCCCCCCCCCCCCCCCCCCCCCC
         SUBROUTINE STLSTRS (F,E,STRN,STRS,STATUS,TYPE,CURV,
     *   RUNCASE)
         DOUBLE PRECISION F,E,STRN,STRS,YLD,COM,E2,YLDSTRN,TNSNSTRN,
     *   DIF,FOS
         CHARACTER *7 STATUS,CURV
         CHARACTER *6 TYPE
         CHARACTER *5 RUNCASE
         FOS=1.0
         IF ((RUNCASE.EQ.'BSUNP').OR.(RUNCASE.EQ.'BSPTD')) FOS=1.15
         YLD=0.8*F/1.15
         COM=(F/FOS)/(1.0+(F/FOS)/2000.0)
         DIF=0.002 - YLD/E
         E2=(COM - YLD)/DIF
         YLDSTRN=YLD/E
TNSNSTRN=YLD/E+(F/FOS-YLD)/E2
IF (TYPE.EQ.' FRP  ') THEN
      STRS=STRN*E
      IF (STRS.GT.F/FOS) STRS=F/FOS
ELSE
      IF (CURV.EQ.'BILINER')THEN
         STRS=STRN*E
         IF (STRS.GT.F/FOS) STRS=F/FOS
      ELSE
         IF (STRN.LT.YLDSTRN) THEN
           STRS=STRN*E
         ELSE
           IF (STRN.LT.0.002) THEN
```

```
            STRS=YLD+(STRN - YLDSTRN)*E2
          ELSE
            IF (STATUS.EQ.'COMPRES') THEN
               STRS=COM
            ELSE
               IF (STRN.LT.TNSNSTRN) THEN
                STRS=YLD+(STRN - YLDSTRN)*E2
               ELSE
                STRS=F/FOS
               END IF
            END IF
          END IF
       END IF
    END IF
          END IF
          RETURN
          END
C         END OF SUBROUTINE STLSTRS
CCCCCCCCCCCCCCCCCCCCCCCCCCCCCCCCCCCCCCCCCCCCCCCCCCCCCCCCCCCCCCCCCCCCCCCCCC
          SUBROUTINE CNCSTRS (F,E,FT,STRN,STRS,STATUS,RUNCASE)
          DOUBLE PRECISION F,E,FT,STRN,STRS,CRUSH,TNSTRN,BISTRN,
      *   BITA,LMTSTRN
          CHARACTER *7 STATUS
          CHARACTER *5 RUNCASE
C         STRESS = EC X STRAIN + BITA X STRAIN^2  (PARABOLIC EQN.)
          IF ((RUNCASE.EQ.'BSUNP').OR.(RUNCASE.EQ.'BSPTD')) THEN
             CRUSH=0.67*F/1.5
             IF (E.EQ.0.0) E=5.5*1000.0*SQRT(F/1.5)
             BISTRN=2.4/10000.0*SQRT(F/1.5)
             BITA=(CRUSH - E*BISTRN)/(BISTRN**2.0)
             IF (STATUS.EQ."TENSION") THEN
             STRS=0.0
          ELSE
             IF (STRN.LT.BISTRN) THEN
                 STRS=E*STRN+BITA*STRN**2.0
             ELSE
                IF (STRN.LE.0.0035) THEN
                 STRS=CRUSH
                ELSE
                 STATUS="FAILURE"
                END IF
             END IF
          END IF
       ELSE
          CRUSH=0.67*F
          TNSTRN=FT/E
          BISTRN=2.44/10000.0*SQRT(F)
          LMTSTRN=30.0*TNSTRN
          BITA=(CRUSH - E*BISTRN)/(BISTRN**2.0)
          IF (STATUS.EQ."TENSION") THEN
             IF (STRN.LT.TNSTRN) THEN
                STRS=E*STRN
             ELSE
                IF (STRN.LT.LMTSTRN) THEN
                   STRS=FT*(LMTSTRN - STRN)/(29*TNSTRN)
                ELSE
                   STRS=0.0
                END IF
             END IF
          ELSE
             IF (STRN.LT.BISTRN) THEN
```

```
                  STRS=E*STRN+BITA*STRN**2.0
               ELSE
                  IF (STRN.LE.0.0035) THEN
                     STRS=CRUSH
                  ELSE
                     STATUS="FAILURE"
                  END IF
               END IF
            END IF
         END IF
         RETURN
         END
C        END OF SUBROUTINE CNCSTRS
C        END OF PROGRAMME
CCCCCCCCCCCCCCCCCCCCCCCCCCCCCCCCCCCCCCCCCCCCCCCCCCCCCCCCCCCCCCCCCCCCCCCCCCCCCCC
```

Appendix B

COMPRESSION FORCES IN CRUSHED AND UNCRUSHED CONCRETE SECTIONS

Appendix B

COMPRESSION FORCES IN CRUSHED AND UNCRUSHED CONCRETE SECTIONS

B.1 GENERAL

The flexural failure for an unplated beam either happens due to the crushing of concrete after the internal reinforcing steel bars have yielded (ductile failure for under-reinforced sections), or before yielding of the embedded steel bars (brittle failure for over-reinforced sections).

The plated beam, on the other hand, exhibits certain other flexural modes of failure associated with which the strains and/or stresses in the concrete in compression are not the determining (critical) factors. For a certain number of such modes of failure (when the failure is due to plate peeling), the plated beam may have either steel or FRP plates, while some of the other modes of failures (due to plate rupture) are associated with composite beams upgraded with only FRP plates: a full explanation for this classification is given in Chapter 5.

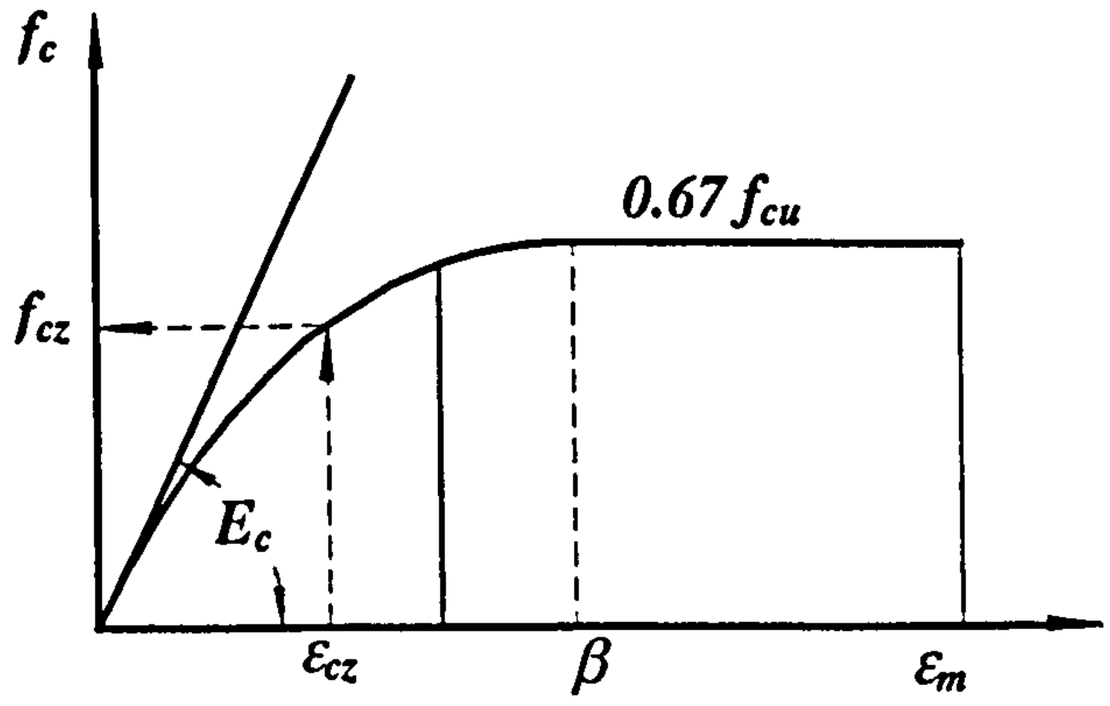

Fig. B.1 Stress-strain relationship for concrete in compression after BS5400 (1990).

In this appendix, formulations will be presented for calculating the magnitude of total compressive force and moment for both those cases of beam failures due to either the crushing of concrete or when no concrete crushing takes place as in those instances in which failure is due to plate rupture and/or end plate peeling.

The stress-strain relationship for concrete in compression, as used here, is based on the one recommended by BS5400 (1990) as shown in Figure B.1, with $\beta = \eta_b \sqrt{f_{cu}}$ and $\varepsilon_m = 0.0035$, where $\eta_b = 2.44 \times 10^{-4}$.

The formula adopted for calculating the concrete compressive stress, f_c, corresponding to a certain level of concrete strain, ε_c, in Equation (B.1) (given below), is based on the relationship presented in Fig. B.1, which is defined by the following

1- $f_c = 0$ and $\frac{df_c}{d\varepsilon_c} = E_c$, $at \quad \varepsilon_c = 0$

2- $f_c = 0.67 f_{cu}$, $at \quad \varepsilon_c = \beta = 2.44 \times 10^{-4} \sqrt{f_{cu}}$

with the final relations expressed as

$$f_c = \begin{cases} 0.67 f_{cu} & , \quad \beta < \varepsilon_c \leq 0.0035 \\ E_c \varepsilon_c + \dfrac{0.67 f_{cu} - E_c \beta}{\beta^2} \varepsilon_c^2 & , \quad \varepsilon_c \leq \beta \end{cases} \qquad \textbf{(B.1)}$$

where, E_c is the modulus of elasticity for concrete, and if E_c is not experimentally obtained, it may be estimated using BS8110 (1985) recommended formula $E_c = 5.5\sqrt{f_{cu}/\gamma_m}$, where f_{cu} = concrete cube strength in MPa, and the units of E_c are in kN/mm^2. γ_m is the material partial safety factor, and it will be assumed to be

equal to 1.0 when calculating the absolute maximum moment capacity, M_{pult}, the absolute minimum moment capacity, M_{min}, and the upper and lower bound peeling moment capacities, $M_{peel,l}$ and $M_{peel,u}$, respectively, while it will be assumed to be equal to 1.5 (as recommended by BS8110 (1985)), when calculating the plated and unplated section design capacities in flexure, M_{pltd} and M_{RC}, respectively.

In the absence of any experimental data, most of the national and/or international codes of practice relate the concrete modulus of elasticity to the square root of the concrete compressive strength, as in the following equation, where the factor η_e differs from one code to another.

$$E_c = \eta_e \sqrt{f_{cu}} \qquad \textbf{(B.2)}$$

B.2 COMPRESSION FORCES ASSOCIATED WITH CRUSHED CONCRETE

Figure B.2 shows the stresses and strains in the portion of concrete in compression, with steel bars in compression present, when the section fails due to the concrete crushing with the maximum concrete strain at the top fibre, ε_o, equal to the crushing value, ε_m.

The total compression force acting on the section, F_c, consists of the compression force in the steel bars, F_s', and the compression forces in the concrete, F_{cc1} and F_{cc2}: using Figure B.2, the following relations may be derived

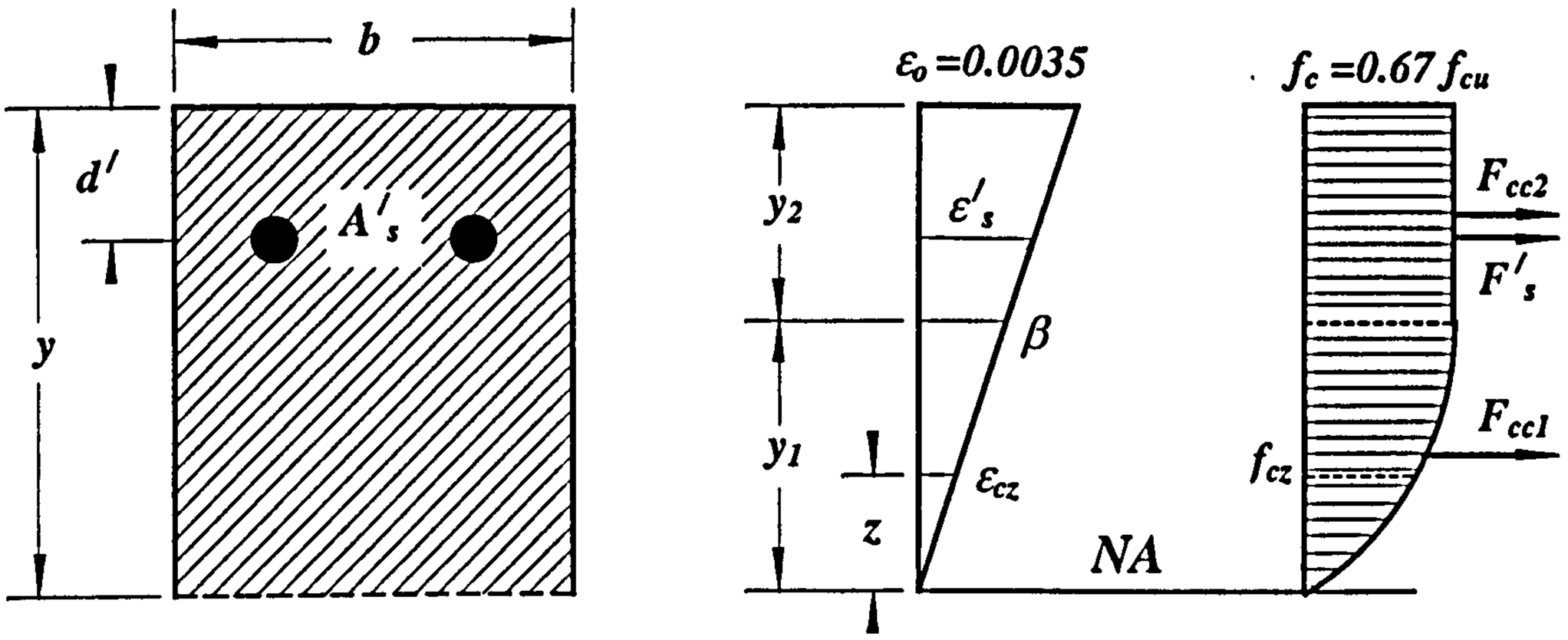

Fig. B.2 Section compression stresses, strains and dimensions.

$$\frac{\varepsilon_o}{y} = \frac{\beta}{y_1} = \frac{\varepsilon'_s}{y-d'} = \frac{\varepsilon_{cz}}{z} \tag{B.3}$$

$$\varepsilon'_s = \frac{y-d'}{y}\varepsilon_o, \qquad \varepsilon_{cz} = \frac{z}{y}\varepsilon_o \tag{B.4}$$

$$y_1 = \frac{\beta}{\varepsilon_o} y \ = \eta_1 y \ \text{ where } \eta_1 = \frac{\beta}{\varepsilon_o} \tag{B.5}$$

$$y_2 = y - y_1 = (1 - \frac{\beta}{\varepsilon_o})\, y$$

with

$$\eta_2 = \left(1 - \frac{\beta}{\varepsilon_o}\right) = \left(1 - \frac{\beta}{0.0035}\right) \tag{B.6}$$

If one assumes the recommended values of $\varepsilon_o = \varepsilon_m = 0.0035$, and

$\beta = 2.44\times10^{-4}\sqrt{f_{cu}}$ (after BS8110 (1985)), then

$$\eta_1 = \frac{2.44\times10^{-4}\sqrt{f_{cu}}}{0.0035} = 0.0697\sqrt{f_{cu}}$$

and

$$\eta_2 = \left(1 - 0.0697\sqrt{f_{cu}}\right) \tag{B.7}$$

From Figure B.2

$$F_c = F'_s + F_{cc1} + F_{cc2}\,; \tag{B.8}$$

$$F'_s = A'_s f'_s = A'_s E_s \varepsilon'_s$$
$$= A'_s E_s \varepsilon_o \frac{y - d'}{y} = A'_s E_s \varepsilon_o (1 - d'/y) \quad \textbf{(B.9)}$$

$$F_{cc2} = 0.67 f_{cu}\, b\, y_2 = 0.67 f_{cu}\, b\, \eta_2 y \quad \textbf{(B.10)}$$

$$F_{cc1} = b\int_0^{y_1} f_{cz} dz = b\int_0^{y_1} \left[E_c \varepsilon_{cz} + \frac{0.67 f_{cu} - E_c \beta}{\beta^2} \varepsilon_{cz}^2 \right] dz$$
$$= b\int_0^{y_1} \left[E_c \frac{\varepsilon_o}{y} z + \left(\frac{0.67 f_{cu} - E_c \beta}{\beta^2} \right) \left(\frac{y_1}{y} \right)^2 z^2 \right] dz$$
$$= yb \left[\frac{E_c \varepsilon_o}{2} \left(\frac{y_1}{y} \right)^2 + \left(\frac{0.67 f_{cu} - E_c \beta}{3\beta^2} \right) \left(\frac{y_1}{y} \right)^3 \varepsilon_o^2 \right]$$
$$= yb \left[\frac{E_c \varepsilon_o}{2} \eta_1^2 + \left(\frac{0.67 f_{cu} - E_c \beta}{3\beta^2} \right) \eta_1^3 \varepsilon_o^2 \right] \quad \textbf{(B.11)}$$
$$= yb \eta_1 \left[\frac{E_c \beta}{2} + \left(\frac{0.67 f_{cu} - E_c \beta}{3} \right) \right]$$
$$= yb \eta_1 \left[\frac{E_c \beta}{6} + \frac{0.67 f_{cu}}{3} \right]$$

The total compression force, F_c, then, is

$$F_c = A'_s E_s \varepsilon_o \left(1 - \frac{d'}{y} \right) + 0.67 f_{cu}\, b \eta_2 y + yb \eta_1 \left(\frac{E_c \beta}{6} + \frac{0.67 f_{cu}}{3} \right) \quad \textbf{(B.12)}$$

or

$$F_c = A'_s E_s \varepsilon_o \left(1 - \frac{d'}{y} \right) + 0.67 f_{cu}\, b \left(1 - \frac{\beta}{\varepsilon_o} \right) y + yb \left(\frac{\beta}{\varepsilon_o} \right) \left(\frac{E_c \beta}{6} + \frac{0.67 f_{cu}}{3} \right) \quad \textbf{(B.13)}$$

which, may be expressed as

$$F_c = A'_s E_s \varepsilon_o \left(1 - \frac{d'}{y} \right) + yb \left(\frac{\beta}{\varepsilon_o} \right) \left(\frac{E_c \beta}{6} - \frac{2}{3} 0.67 f_{cu} \right) + 0.67 f_{cu}\, yb$$
$$= A'_s E_s \varepsilon_o \left(1 - \frac{d'}{y} \right) + yb \left(\frac{\beta}{\varepsilon_o} \right) \left[\frac{E_c \beta}{6} - \frac{2}{3} 0.67 f_{cu} + 0.67 f_{cu} \left(\frac{\varepsilon_o}{\beta} \right) \right] \quad \textbf{(B.14)}$$
$$= A'_s E_s \varepsilon_o \left(1 - \frac{d'}{y} \right) + yb \left(\frac{\beta}{\varepsilon_o} \right) \left[\frac{E_c \beta}{6} + 0.67 f_{cu} \left(\frac{\varepsilon_o}{\beta} - \frac{2}{3} \right) \right]$$

The above equation may now be used, if the modulus of elasticity for concrete is obtained experimentally. If the modulus of elasticity is not experimentally determined, then, it may be related to the concrete compressive strength using Equation (B.2), and

$$
\begin{aligned}
F_c &= A'_s E_s \varepsilon_o \left(1-\frac{d'}{y}\right) + yb\left(\frac{\beta}{\varepsilon_o}\right)\left[\frac{E_c\beta}{6}+0.67 f_{cu}\left(\frac{\varepsilon_o}{\beta}-\frac{2}{3}\right)\right] \\
&= A'_s E_s \varepsilon_o \left(1-\frac{d'}{y}\right) + 0.67 f_{cu}\, yb\left[1+\frac{\beta}{\varepsilon_o}\left(\frac{\eta_e\eta_b}{4}-\frac{2}{3}\right)\right] \\
&= A'_s E_s \varepsilon_o \left(1-\frac{d'}{y}\right) + 0.67 f_{cu}\, yb\left[1+\frac{\eta_b\sqrt{f_{cu}}}{\varepsilon_o}\left(\frac{\eta_e\eta_b}{4}-\frac{2}{3}\right)\right] \\
&= A'_s E_s \varepsilon_o \left(1-\frac{d'}{y}\right) + 0.67 f_{cu}\, yb\,\alpha_{f_{cu}}
\end{aligned}
\qquad \textbf{(B.15)}
$$

where

$$
\alpha_{f_{cu}} = \left[1+\frac{\eta_b\sqrt{f_{cu}}}{\varepsilon_o}\left(\frac{\eta_b\eta_e}{4}-\frac{2}{3}\right)\right] \qquad \textbf{(B.16)}
$$

It is clear that $\alpha_{f_{cu}}$ depends only on the concrete compressive strength. Following BS5400 (1990) and BS8110 (1985), $\eta_e = 5.5$, $\eta_b = 2.44\times10^{-4}$, and $\varepsilon_o = \varepsilon_m = 0.0035$; and the above equation may be re-written as

$$
\begin{aligned}
\alpha_{f_{cu}} &= \left[1+\frac{2.44\times10^{-4}\sqrt{f_{cu}}}{0.0035}\left(\frac{5500\times2.44\times10^{-4}}{4}-0.667\right)\right] \\
&= \left[1+\frac{2.44\times10^{-4}\sqrt{f_{cu}}}{0.0035}(-0.3311667)\right] \\
&= \left(1-\frac{\sqrt{f_{cu}}}{43.1}\right)
\end{aligned}
\qquad \textbf{(B.17)}
$$

From Equations (B.15) and (B.17), the concrete parabolic stress distribution located above the neutral axis may be represented by an equivalent rectangular stress block as

shown in Figure B.3, with the same maximum value of stress equal to $0.67 f_{cu}$, but with a reduced height of $y\alpha_{f_{cu}}$.

As the factor $\alpha_{f_{cu}}$ only depends on the concrete compressive strength (or even, generally, on ε_m, β, f_{cu} and E_c), from Equation (B.15) it is clear that the total compression force acting on the section will increase by increasing the neutral axis depth, y, if the section is to fail in any of the modes of failure associated with which crushing of concrete takes place.

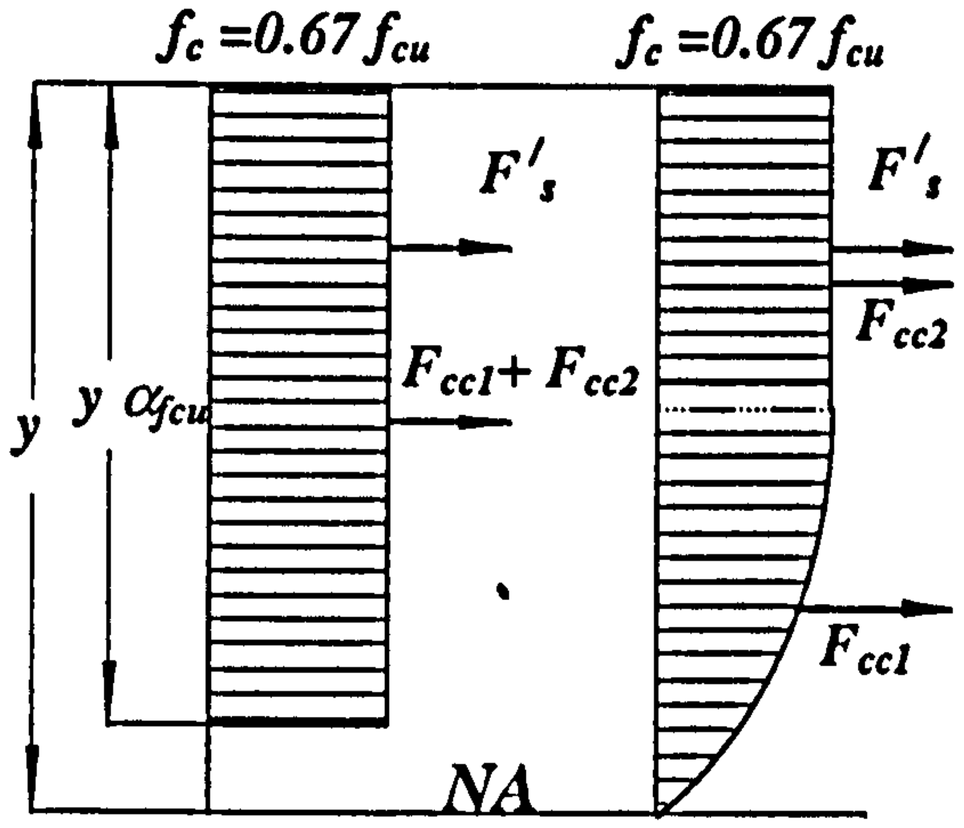

Fig. B.3 Equivalent stress block.

This increase in the compression force leads to similar increases in the magnitude of total tensile force in order to maintain equilibrium of forces over the whole section.

B.3 COMPRESSION FORCES ASSOCIATED WITH UNCRUSHED CONCRETE

For the section which does not experience concrete crushing, there are two possible cases to be considered. The first case relates to those sections with maximum concrete stress being less than $0.67 f_{cu}$ and subjected only to a parabolic stress distribution (i.e. the maximum strain ε_o is less than β). The second case, on the other hand, relates to sections subjected to a maximum concrete compressive stress $0.67 f_{cu}$

associated with which there is a maximum concrete strain, ε_o, less than the crushing value, ε_m, but higher than β (see Figure B.1).

B.3.1 Maximum Concrete Compressive Strain Less Than β

In this case, the concrete stress distribution is parabolic throughout the entire region in compression, and may be expressed by the following

$$f_{cz} = E_c \varepsilon_{cz} + \frac{0.67 f_{cu} - E_c \beta}{\beta^2} \varepsilon_{cz}^2 \qquad \textbf{(B.18)}$$

$$f_{cz} = E_c \varepsilon_{cz} + k_1 \varepsilon_{cz}^2 \qquad \textbf{(B.19)}$$

where

$$K_1 = \frac{0.67 f_{cu} - E_c \beta}{\beta^2} \qquad \textbf{(B.20)}$$

Figure B.4 shows the compressive stresses and strains of concrete and the associated steel bars, when the section fails due to plate rupture or plate peeling associated with which the maximum concrete strain is less than the crushing value.

From Figure B.4, the following relations may be derived

$$\frac{\varepsilon_p}{D-y} = \frac{\varepsilon_s}{d-y} = \frac{\varepsilon_s'}{y-d'} = \frac{\varepsilon_{cz}}{z} \qquad \textbf{(B.21)}$$

The total compressive force, F_c, acting on the section, consists of the compression force in the steel bars, F_s', and the compression force in the concrete, F_{cc}:

$$F_c = F_s' + F_{cc} \qquad \textbf{(B.22)}$$

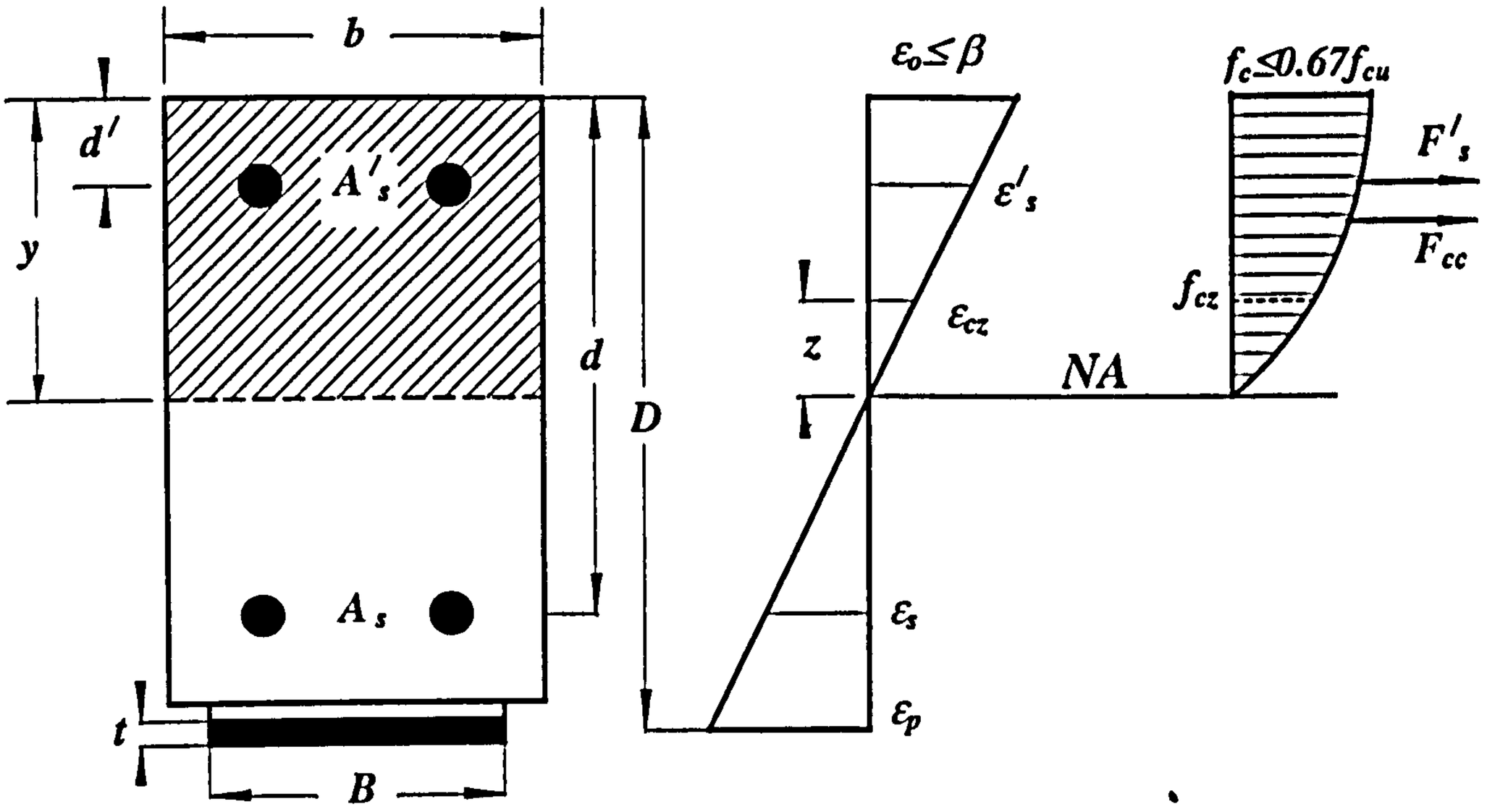

Fig. B.4 Section strains, stresses and dimensions (Case 1).

The total force in the embedded steel bars in compression, is

$$F'_s = A'_s f'_s = A'_s E_s \varepsilon'_s$$
$$= A'_s E_s \varepsilon_p \frac{y-d'}{D-y} \qquad \textbf{(B.23)}$$

and, if expressed in terms of the axial strains in the embedded bars, then

$$F'_s = A'_s E_s \varepsilon_s \frac{y-d'}{d-y} \qquad \textbf{(B.24)}$$

The compression force in concrete is

$$F_{cc} = b\int_0^y f_{cz} dz = b\int_0^y \left(E_c \varepsilon_{cz} + K_1 \varepsilon_{cz}^2\right) dz$$
$$= b\int_0^y \left[E_c \frac{\varepsilon_p}{D-y} z + K_1 \left(\frac{\varepsilon_p}{D-y}\right)^2 z^2 \right]^2 dz \qquad \textbf{(B.25)}$$
$$= \frac{bE_c}{2}\left(\frac{\varepsilon_p}{D-y}\right) y^2 + \frac{bK_1}{3}\left(\frac{\varepsilon_p}{D-y}\right)^2 y^3$$

If the above equation is expressed in terms of the axial strains in the embedded steel bars

$$F_{cc} = \frac{bE_c}{2}\left(\frac{\varepsilon_s}{d-y}\right)y^2 + \frac{bK_1}{3}\left(\frac{\varepsilon_s}{d-y}\right)^2 y^3 \qquad \textbf{(B.26)}$$

The total compression force, F_c, then, is

$$F_c = A_s' E_s \varepsilon_p \left(\frac{y-d'}{D-y}\right) + \frac{bE_c}{2}\left(\frac{\varepsilon_p}{D-y}\right)y^2 + \frac{bK_1}{3}\left(\frac{\varepsilon_p}{D-y}\right)^2 y^3 \qquad \textbf{(B.27)}$$

If the above equation is expressed in terms of the axial strains in the embedded steel bars, one gets

$$F_c = A_s' E_s \varepsilon_s \left(\frac{y-d'}{d-y}\right) + \frac{bE_c}{2}\left(\frac{\varepsilon_s}{d-y}\right)y^2 + \frac{bK_1}{3}\left(\frac{\varepsilon_s}{d-y}\right)^2 y^3 \qquad \textbf{(B.28)}$$

with K_1 as defined by Equation (B.20).

B.3.2 Maximum Concrete Compressive Strain More Than β

In this case, the concrete stress distribution consists of a combination of parabolic and uniform distribution parts, and may be expressed by the following

$$f_c = \begin{cases} 0.67 f_{cu} & , \quad \beta < \varepsilon_c \le 0.0035 \\ E_c\varepsilon_c + \dfrac{0.67 f_{cu} - E_c\beta}{\beta^2}\varepsilon_c^2 & , \quad \varepsilon_c \le \beta \end{cases}$$

or $f_{cz} = E_c\varepsilon_{cz} + k_1\varepsilon_{cz}^2 \quad , \quad \varepsilon_{cz} \le \beta$

where

$$K_1 = \frac{0.67 f_{cu} - E_c\beta}{\beta^2}$$

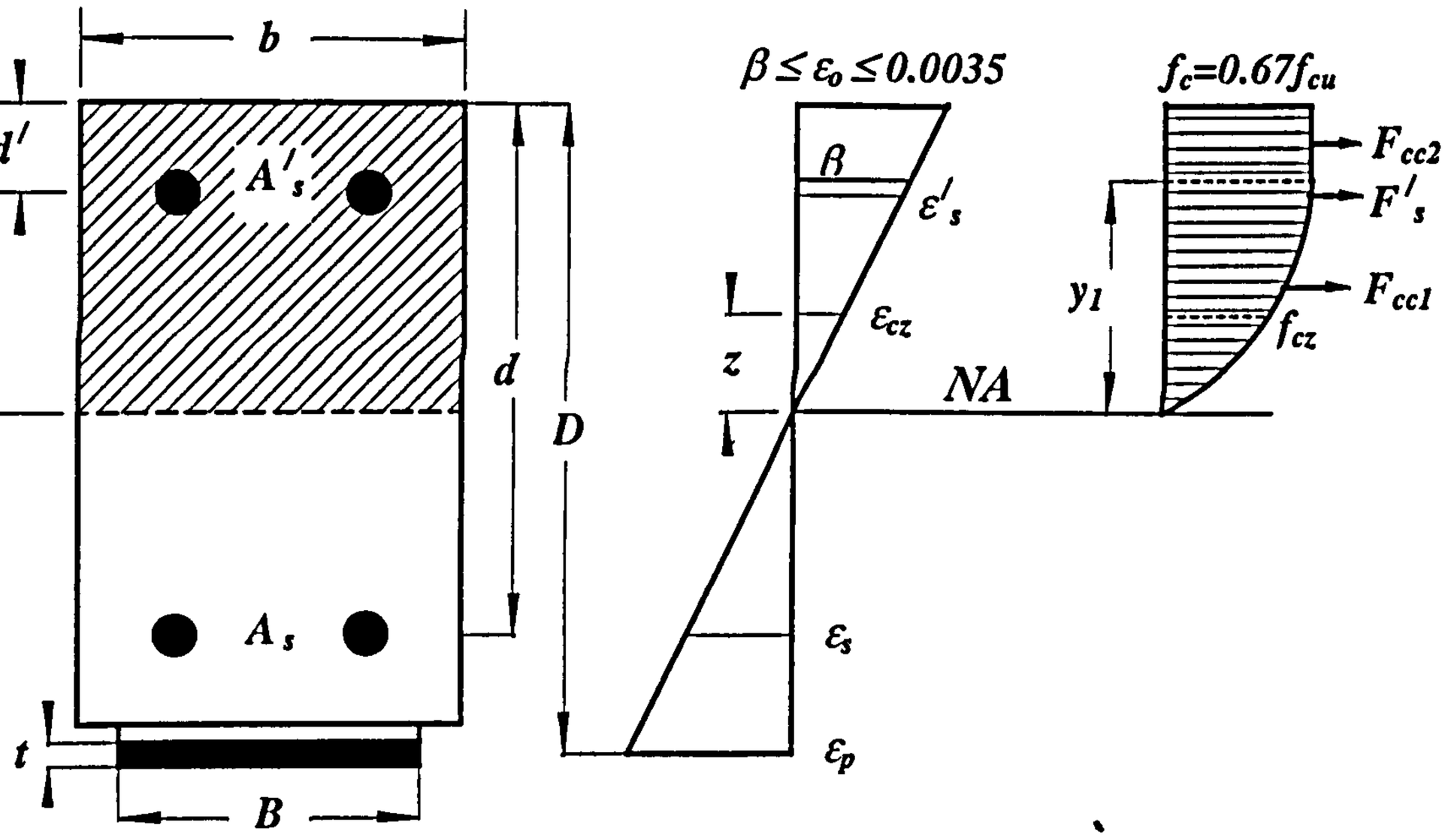

Fig. B.5 Section strains, stresses and dimensions (Case 2).

From Figure B.5, the following relations may be derived

$$\frac{\varepsilon_p}{D-y}=\frac{\varepsilon_s}{d-y}=\frac{\varepsilon_s'}{y-d'}=\frac{\varepsilon_{cz}}{z} \tag{B.29}$$

$$\begin{aligned} y_1 &= \frac{\beta}{\varepsilon_p}(D-y) \\ &= \frac{\beta}{\varepsilon_s}(d-y) \end{aligned} \tag{B.30}$$

$$\begin{aligned} y_2 &= y-y_1 \\ &= y-\frac{\beta}{\varepsilon_p}(D-y) \\ &= y-\frac{\beta}{\varepsilon_s}(d-y) \end{aligned} \tag{B.31}$$

The total compression force, F_c, acting on the section, consists of the compression force in the steel bars, F_s', and the compression forces in the concrete, F_{cc1} and F_{cc2}, where

$$F_c = F_s' + F_{cc1} + F_{cc2} \tag{B.32}$$

The compression force in the embedded steel bars, F'_s, will be

$$F'_s = A'_s f'_s = A'_s E_s \varepsilon'_s = A'_s E_s \varepsilon_p \frac{y-d'}{D-y} \tag{B.33}$$

If the above equation is expressed in terms of the axial strains in the embedded steel bars

$$F'_s = A'_s E_s \varepsilon_s \frac{y-d'}{d-y} \tag{B.34}$$

and, the concrete compression force, F_{cc2}, is

$$\begin{aligned} F_{cc2} &= 0.67 F_{cu} b y_2 = 0.67 f_{cu} b \left(y + \frac{\beta}{\varepsilon_s} y - \frac{\beta}{\varepsilon_s} d \right) \\ &= 0.67 f_{cu} b \left(y + \frac{\beta}{\varepsilon_p} y - \frac{\beta}{\varepsilon_p} D \right) \end{aligned} \tag{B.35}$$

If the above equation is expressed in terms of the axial strains in the embedded steel bars, one arrives at the following

$$F_{cc2} = 0.67 f_{cu} b \left(y + \frac{\beta}{\varepsilon_s} y - \frac{\beta}{\varepsilon_s} d \right) \tag{B.36}$$

while, the force, F_{cc1}, is

$$\begin{aligned} F_{cc1} &= b \int_0^{y_1} f_{cz} dz = b \int_0^{y_1} \left(E_c \varepsilon_{cz} + K_1 \varepsilon_{cz}^2 \right) dz \\ &= b \int_0^{y_1} \left[E_c \frac{\varepsilon_p}{D-y} z + K_1 \left(\frac{\varepsilon_p}{D-y} \right)^2 z^2 \right] dz \\ &= \frac{bE_c}{2} \left(\frac{\varepsilon_p}{D-y} \right) y_1^2 + \frac{bK_1}{3} \left(\frac{\varepsilon_p}{D-y} \right)^2 y_1^3 \\ &= \frac{bE_c}{2} \frac{\beta^2}{\varepsilon_p} (D-y) + \frac{bK_1}{3} \frac{\beta^3}{\varepsilon_p} (D-y) \end{aligned} \tag{B.37}$$

Again, if the above equation is expressed in terms of the axial strains in the embedded steel bars, one gets

$$F_{cc1} = \frac{bE_c}{2}\frac{\beta^2}{\varepsilon_s}(d-y) + \frac{bK_1}{3}\frac{\beta^3}{\varepsilon_s}(d-y) \qquad \textbf{(B.38)}$$

The total compression force, F_c, is, then, given by

$$F_c = A_s' E_s \varepsilon_p \left(\frac{y-d'}{D-y}\right) + 0.67 f_{cu} b \left(y + \frac{\beta}{\varepsilon_p} y - \frac{\beta}{\varepsilon_p} D\right) + \frac{bE_c}{2}\frac{\beta^2}{\varepsilon_p}(D-y) + \frac{bK_1}{3}\frac{\beta^3}{\varepsilon_p}(D-y) \qquad \textbf{(B.39)}$$

and, if the above equation is expressed in terms of the axial strains in the embedded steel bars:

$$F_c = A_s' E_s \varepsilon_s \left(\frac{y-d'}{d-y}\right) + 0.67 f_{cu} b \left(y + \frac{\beta}{\varepsilon_s} y - \frac{\beta}{\varepsilon_s} d\right) + \frac{bE_c}{2}\frac{\beta^2}{\varepsilon_s}(d-y) + \frac{bK_1}{3}\frac{\beta^3}{\varepsilon_s}(d-y) \qquad \textbf{(B.40)}$$

If one assumes the BS8110 (1985) recommendations for estimating the values of E_c and β, one arrives at the following

$$F_c = A_s' E_s \varepsilon_p \left(\frac{y-d'}{D-y}\right) + 0.67 f_{cu} b \left[y - \frac{\beta}{3\varepsilon_p}(D-y)\right] \qquad \textbf{(B.41)}$$

and, if the above equation is expressed in terms of the axial strains in the embedded steel bars

$$F_c = A_s' E_s \varepsilon_s \left(\frac{y-d'}{d-y}\right) + 0.67 f_{cu} b \left[y - \frac{\beta}{3\varepsilon_s}(d-y)\right] \qquad \textbf{(B.42)}$$

B.4 THE COMPRESSION MOMENT

The total moment of the compression forces about the neutral axis, associated with the crushed concrete type of failure, may now be calculated as in the following;

$$M_c = M_s' + M_{cc1} + M_{cc2}; \qquad \textbf{(B.43)}$$

$$M'_s = A'_s f'_s(y-d') = A'_s E_s \varepsilon'_s (y-d')$$
$$= A'_s E_s \varepsilon_o \frac{y-d'}{y}(y-d') = A'_s E_s \varepsilon_o y\left(1-\frac{d'}{y}\right)^2 \quad \textbf{(B.44)}$$

$$M_{cc2} = 0.67 f_{cu}\, b\, y_2\left(y-\frac{y_2}{2}\right) = 0.67 f_{cu}\, b\left(1-\frac{\beta}{\varepsilon_o}\right) y\left[y-\frac{y}{2}\left(1-\frac{\beta}{\varepsilon_o}\right)\right]$$
$$=0.67 f_{cu} b \frac{y^2}{2}\left(1-\frac{\beta}{\varepsilon_o}\right) = 0.67 f_{cu} b \frac{y^2}{2}\left[1-\left(\frac{\beta}{\varepsilon_o}\right)^2\right] \quad \textbf{(B.45)}$$

$$M_{cc1} = b\int_0^{y_1} f_c z\, dz = b\int_0^{y_1}\left[E_c \varepsilon_{cz} z + \left(\frac{0.67 f_{cu} - E_c \beta}{\beta^2}\right)\varepsilon_{cz}^2 z\right] dz$$
$$= b\int_0^{y_1}\left[E_c \frac{\varepsilon_o}{y} z^2 + \left(\frac{0.67 f_{cu} - E_c \beta}{\beta^2}\right)\left(\frac{\varepsilon_o}{y}\right)^2 z^3\right] dz$$
$$= y^2 b\left[\frac{E_c \varepsilon_o}{3}\left(\frac{y_1}{y}\right)^3 + \left(\frac{0.67 f_{cu} - E_c \beta}{\beta^2}\right)\left(\frac{y_1}{y}\right)^4 \varepsilon_o^2\right]$$
$$= y^2 b\left[\frac{E_c \varepsilon_o}{3}\left(\frac{\beta}{\varepsilon_o}\right)^3 + \left(\frac{0.67 f_{cu} - E_c \beta}{4\beta^2}\right)\left(\frac{\beta}{\varepsilon_o}\right)^4 \varepsilon_o^2\right] \quad \textbf{(B.46)}$$
$$= y^2 b\left(\frac{\beta}{\varepsilon_o}\right)^2\left[\frac{E_c \beta}{3} + \left(\frac{0.67 f_{cu} - E_c \beta}{4}\right)\right]$$
$$= y^2 b\left(\frac{\beta}{\varepsilon_o}\right)^2\left(\frac{E_c \beta}{12} + \frac{0.67 f_{cu}}{4}\right)$$

The total compression moment, M_c, is, then, given as

$$M_c = A'_s E_s \varepsilon_o\left(1-\frac{d'}{y}\right)^2 y + \frac{0.67 f_{cu} b y^2}{2}\left[1-\left(\frac{\beta}{\varepsilon_o}\right)^2\right] + \left(\frac{\beta}{\varepsilon_o}\right)^2\left(\frac{E_c \beta}{12} + \frac{0.67 f_{cu}}{4}\right) b y^2 \quad \textbf{(B.47)}$$

which may be expressed as

$$M_c = A'_s E_s \varepsilon_o\left(1-\frac{d'}{y}\right)^2 y + \left[\frac{0.67 f_{cu}}{2} + \left(\frac{\beta}{\varepsilon_o}\right)^2\left(\frac{E_c \beta}{12} - \frac{0.67 f_{cu}}{4}\right)\right] b y^2 \quad \textbf{(B.48)}$$

If one assumes the recommended values of $\varepsilon_o = \varepsilon_m = 0.0035$, $\beta = 2.44\times10^{-4}\sqrt{f_{cu}}$

and $E_c = 5500\sqrt{f_{cu}}$ (after BS8110 (1985))

$$M_c = A'_s E_s \varepsilon_o \left(1 - \frac{d'}{y}\right)^2 y + \frac{0.67 f_{cu} b}{2}\left(1 - \frac{f_{cu}}{1234}\right) y^2 \qquad \textbf{(B.49)}$$

B.5 CONCLUSIONS

1- If the plated section is to fail in any of the failure modes which are due to the concrete crushing, then:

a- The total compression force in the concrete crushed section is

$$F_c = A'_s E_s \varepsilon_m \left(1 - \frac{d'}{y}\right) + yb\left(\frac{\beta}{\varepsilon_m}\right)\left[\frac{E_c \beta}{6} + 0.67 f_{cu}\left(\frac{\varepsilon_m}{\beta} - \frac{2}{3}\right)\right] , \qquad \textbf{(B.50)}$$

or

$$F_c = A'_s E_s \varepsilon_m \left(1 - \frac{d'}{y}\right) + 0.67 f_{cu}\, yb\, \alpha_{f_{cu}} \qquad \textbf{(B.51)}$$

where

$$\alpha_{f_{cu}} = \left[1 + \frac{\eta_b \sqrt{f_{cu}}}{\varepsilon_m}\left(\frac{\eta_b \eta_e}{4} - \frac{2}{3}\right)\right], \; E_c = \eta_e \sqrt{f_{cu}} \quad \text{and} \; \beta = \eta_b \sqrt{f_{cu}}$$

and, based on the BS5400 (1990) and BS8110 (1985) values of

$\eta_b = 2.44 \times 10^{-4}$, $\eta_e = 5.5$ and $\varepsilon_m = 0.0035$

then

$$\alpha_{f_{cu}} = \left(1 - \frac{\sqrt{f_{cu}}}{43.1}\right)$$

b- The total compression and tension forces will increase, if the neutral axis depth is increased.

2- When the failure mode is not due to the concrete crushing, there would be two possible cases of compression stress distribution for concrete to be considered. The first case corresponds to when the maximum concrete stress is less than

$0.67f_{cu}$ and the stress distribution will be parabolic all along the portion of concrete in compression - (see Figure B.4). In this case, the maximum concrete strain, ε_o, will be less than β.

The second case occurs when the maximum concrete stress is equal to $0.67f_{cu}$, but the maximum strain in concrete is less than the crushing value, $\varepsilon_m = 0.0035$.

In this case, a portion of the stress distribution will be of a parabolic form, while the other portion will be equivalent to a uniform compression stress block - see Figure (B.5). In this case, the maximum concrete strain, ε_o, will be less than the crushing value (i.e. $\varepsilon_o < 0.0035$), but more than β.

a- The total compression force, F_c, for the Case 1 ($\varepsilon_o \leq \beta$), is

$$F_c = A'_s E_s \varepsilon_p \left(\frac{y-d'}{D-y}\right) + \frac{bE_c}{2}\left(\frac{\varepsilon_p}{D-y}\right)y^2 + \frac{bK_1}{3}\left(\frac{\varepsilon_p}{D-y}\right)^2 y^3 \qquad \textbf{(B.52)}$$

If the above equation is expressed in terms of the axial strains in the embedded steel bars, then

$$F_c = A'_s E_s \varepsilon_s \left(\frac{y-d'}{d-y}\right) + \frac{bE_c}{2}\left(\frac{\varepsilon_s}{d-y}\right)y^2 + \frac{bK_1}{3}\left(\frac{\varepsilon_s}{d-y}\right)^2 y^3 \qquad \textbf{(B.53)}$$

where, $K_1 = \dfrac{0.67f_{cu} - E_c\beta}{\beta^2}$

b- The total compression force, F_c, for Case 2 ($\beta \leq \varepsilon_o < 0.0035$), is

$$F_c = A'_s E_s \varepsilon_p \left(\frac{y-d'}{D-y}\right) + 0.67f_{cu}b\left(y + \frac{\beta}{\varepsilon_p}y - \frac{\beta}{\varepsilon_p}D\right) + \frac{bE_c}{2}\frac{\beta^2}{\varepsilon_p}(D-y) + \frac{bK_1}{3}\frac{\beta^3}{\varepsilon_p}(D-y) \qquad \textbf{(B.54)}$$

and, if the above equation is expressed in terms of the axial strains in the embedded steel bars, the following holds

$$F_c = A_s' E_s \varepsilon_s \left(\frac{y-d'}{d-y} \right) + 0.67 f_{cu} b \left(y + \frac{\beta}{\varepsilon_s} y - \frac{\beta}{\varepsilon_s} d \right) + \frac{bE_c}{2} \frac{\beta^2}{\varepsilon_s} (d-y) + \frac{bK_1}{3} \frac{\beta^3}{\varepsilon_s} (d-y) \quad \textbf{(B.55)}$$

If one assumes the recommendations by BS8110 (1985) for E_c and β, the following holds

$$F_c = A_s' E_s \varepsilon_p \left(\frac{y-d'}{D-y} \right) + 0.67 f_{cu} b \left[y - \frac{\beta}{3\varepsilon_p} (D-y) \right] \quad \textbf{(B.56)}$$

and, if the above equation is expressed in terms of the axial strains in the embedded steel bars, one arrives at the following

$$F_c = A_s' E_s \varepsilon_s \left(\frac{y-d'}{d-y} \right) + 0.67 f_{cu} b \left[y - \frac{\beta}{3\varepsilon_s} (d-y) \right] \quad \textbf{(B.57)}$$